



In the name of God

*Proceeding of the 15th Iranian Physical
Chemistry Conference*

University of Tehran, Tehran, Iran
September 3-6, 2012



Organizer:



University of Tehran



Iranian Chemical Society



Scientific Chairman: Dr. Ali Maghari

Executive Chairman: Dr. Hassan Behnejad

Scientific Committee:

Dr. A. Maghari
Dr. Gh. Islampour
Dr. H. Eslami
Dr. H. Behnejad
Dr. Gh. Parsafar
Dr. A. H. Pakiari
Dr. S. Khoei
Dr. S. Jalili
Dr. A. Rostami
Dr. H. Mahdavi
Dr. F. Shemirani
Dr. H. Sabzian
Dr. A. Jalili
Dr. A. Shafiei
Dr. Z. Jamshidi
Dr. A. Mohajeri
Dr. S. H. Mousavipour
Dr. S. Yaganegi

Organizing Committee:

Dr. H. Behnejad
Dr. A. Shayesteh
Dr. M. Hamzehloo
Mr. A. Rafi Dargahi



List of Referees:

Dr. Ashasi, H.	Dr. Khoei, S.
Dr. Azizi, Kh.	Dr. Maghari, A.
Dr. Behnejad, H.	Dr. Mahdavi, H.
Dr. Bordbar, A.	Dr. Mahjani, M. Gh.
Dr. Bordbar, M. M.	Dr. Mohajeri, A.
Dr. Dahestani, M.	Dr. Mousavipour, S. H.
Dr. Ebrahimi, A.	Dr. Najafi, b.
Dr. Eslami, H.	Dr. Nasehzadeh, A.
Dr. Fakhraei, S.	Dr. Nourizadeh, S.
Dr. Farrokhnia, M.	Dr. Pakiari, H. A.
Dr. Farzi, N.	Dr. Parsafar, Gh.
Dr. Foroutan, M.	Dr. RashidiRanjbar, P.
Dr. Ghannadzadeh, H.	Dr. Refati, A. A.
Dr. Gharibi, H.	Dr. Rezaei, M.
Dr. Ghatee, H.	Dr. Rostami, A.
Dr. Gholami, M. R.	Dr. Sabet, A.
Dr. Goharshadi, E.	Dr. Sabouri, A. A.
Dr. Habibi, A.	Dr. Sabzian, H.
Dr. Habibi, M. H.	Dr. Sadeghi, R.
Dr. Habibi, S. M.	Dr. Shayesteh, A.
Dr. Hadipour, N.	Dr. SoleymanNejad, M.
Dr. Hashemianzadeh, M.	Dr. Shemirani, F.
Dr. Hamedanian, M.	Dr. Shafiei, A.
Dr. Illukhani, H.	Dr. Tabrizchi, M.
Dr. Islampour, Gh.	Dr. Tafazzoli, M.
Dr. Jafarian, M.	Dr. Yeganegi, S.
Dr. Jalili, A. H.	Dr. Zafarani, M. T.
Dr. Jamshidi, Z.	Dr. Zargam, N.
Dr. Karimi, M. H.	Dr. Zeini, A.
Dr. Keshavarzi, E.	



Table of Content

Invited Lecturer	1
Oral Session	9
Poster Session	294
Applied Chemistry	295
Computational Chemistry	447
Classical & Statistical Thermodynamics	1434
Electrochemistry	1807
Chemical Kinetics	2040
Nanochemistry	2284
Quantum Mechanics & Spectroscopy	3519
Surface Chemistry	3722



Invited Lecturer

15th Physical Chemistry Conference



Tautomerism and Dichroism in Anisotropic Media

A.Ghanadzadeh Gilani

Department of Chemistry, University of Guilan, Rasht, Iran

E-mail: aggilani@guilan.ac.ir

Keywords: Tautomerism / Azo dyes / Liquid crystals / Dichroism

Azoquinolin compounds are well known to be in equilibrium with other *tautomeric forms*. It is described by the intra-molecular proton transfer between the phenol and imine groups in ground and/or excited state. Nature and position of the substituents of the molecule play a significant role on the tautomeric equilibrium, and thus on photo-physical properties.

Since the azo group is an electron acceptor. The hydrazone tautomer is favored by electron withdrawing substituents, like NO₂, because the imino group is an electron donor. Further stabilization of the hydrazone tautomer is achieved with intra- or intermolecular hydrogen bonding.

It is due to the large differences in the dipole moments and electron donor and acceptor properties of each tautomer. Generally, the equilibrium is influenced strongly by the properties of the solvent. The hydrazone tautomer is promoted by an increase in the polarity of the media. Both tautomers can be detected from the visible absorption spectra. The differences between the absorption spectra of the tautomeric compounds can be used to distinguish them.

The anisotropic solvation characteristic of azoquinolins (Fig. 1) in polar nematic liquid crystals was investigated. The azoquinolin dyes in the polar nematic hosts show an

anomalous behavior. From the spectral data (Fig. 2), the influence of anisotropic environment on the solvation of the compound is complicated. However, the spectral behavior of azoquinolins in nematic solvent should have multiple origins, and several interactions contribute to some extent.

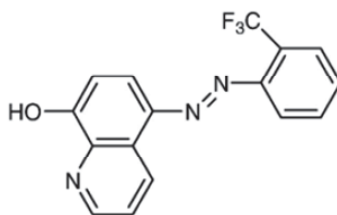


Fig. 1 o-azoquinolin dye

For the dye, the azo form is almost entirely dominated in polar nematic host, while the compound remains dominantly in hydrazone form in dipolar aprotic solvents such as acetonitrile.

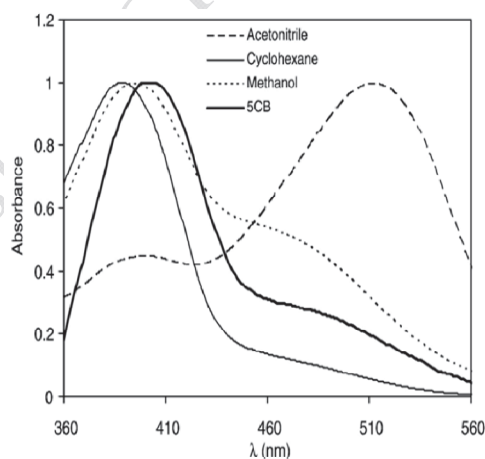


Fig. 2 Visible absorption spectra of o-azoquinolin in liquid and liquid crystalline solutions

It should be concluded that, the spectral changes in nematic host depends on several factors such as solvent polarity, viscosity, molecular packing, polarizability and host rigidity.

The polarized absorptions spectra of the compounds were recorded in parallel-aligned liquid crystal cells and their dichroic ratios were obtained. The dichroic ratios ($R = A_{\parallel} / A_{\perp}$) of the dyes dissolved in the nematic host were calculated from the absorption of light polarized parallel (A_{\parallel}) and perpendicular (A_{\perp}) to the liquid crystal alignment (Fig. 3).

According to the dichroism results obtained in the present work the dichroic ratios R of the dyes are larger than one. This means that the absorption bands for these dyes could be considered as parallel transition (i.e. $\pi - \pi^*$).

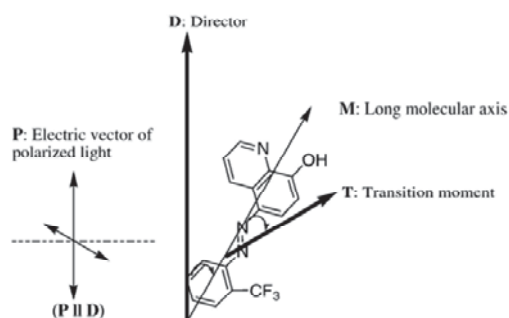


Fig. 3

References:

- [1] A. Ghanadzadeh Gilani, E. Moradi, S. Binay, M. Moghadam, *Spectrochim. Acta A* 2012, 87, 112
- [2] A. Ghanadzadeh Gilani, M. Moghadam, M.S. Zakerhamidi, E. Moradi, *Dyes Pigm.* 2012, 92, 1320
- [3] A. Ghanadzadeh Gilani, M.R. Yazdanbakhsh, N. Mahmoodi, M. Moghadam, E. Moradi, *J. Mol. Liq.* 2008, 139, 72.



Nanoporous Materials and Its Applications

Alireza Badii

School of chemistry, College of Science, University of Tehran, Iran¹

Order forms of nanoporous materials have been synthesized in a variety of hexagonal, cubic, and lamellar phases through the reaction of inorganic species in the presence of surfactant self-assemblies as supramolecular templates [1]. These materials have attracted vast interest because of their potential application as catalysts [2-5], solid phase microextraction (SPME) [6, 7], metal scavengers [8], preconcentration of metals [9, 10] and in the modified electrodes [11-13]. Up to now, the synthesis pathways, which rely on the competition between hydrophilic and hydrophobic entities are not full understood. They involve interfacial chemistry that is studied here in the purpose to i) improvement the quality of the material, ii) find novel routes for metal functionalization and iii) modify the hydrophobicity of the surface. The materials were characterized using various techniques: elemental analysis, atomic absorption, nitrogen adsorption-desorption, ion chromatography, XRD, FT-IR, UV-visible and solid state NMR.

Taking advantage of the electrostatic interface between the silanolate groups and surfactant head groups in the as-synthesis form of MTS, cobalt (III) complexes were directly ion exchanged with surfactant in ethanol solution. The adsorbed complex is either in pure electrostatic interaction with the surface or grafted at the surface within the channels depending on the nature of the complex. This method provides a novel post-synthesis metal modification route that preserves the channel structure and, saves a calcination step in comparison with other synthesis routes [14-16].



A new analytical method to titrate the silanolate groups on the surface of MTS has been proposed which allows to measure surface charge density (SCD). This method has been used to evidence the effect of the surfactant counterion on SCD. We have also shown that a higher lyotropic character of the anions favours long range order of the mesostructure. Therefore, the well accepted $\{S^+, I^-\}$ generic pathway should be better referred as to $\{S^+, m X^-, (1-m) I^-\}$ [16-19].

Direct displacement of surfactant by the silylating agent has been shown to take place on the as-synthesized form of MTS. Total or partial silylation of the surface is obtained depending of the silylating agent. A mixture of chloromethylsilane in hexamethyldisiloxane leads to full coverage of trimethylsilyl groups and to a highly hydrophobic surface. Hexamethyldisilazane silylates with almost no displacement of the surfactant. A subsequent removal of the latter leaves behind hydrophilic islands of the size of the ammonium head. Cation exchange can be performed in these islands at pH up to 10 without structure collapse [20-21].

A new approach to produce the nano-layered silica using very low surfactant concentration was provided. This method is safe and cheap with too high yield of the product to the template without necessity to recovery of surfactant. The effect of temperature, crystallization time and co-surfactant concentration on phase formation was studied. The result of this part of research was proofed in US patent No. 13034357 [22].

References

- [1] Beck J.S. *et al.*, *J. Am. Chem. Soc.* 1992, 114, 10834.
- [2] D. Trong On D *et al.*, *Appl. Catal. A: Gen.* 2001, 222, 299.
- [3] Gholami J, Badiei A, Abbasi A and Mohammadi Ziarani G *Chin. J. Catal.* 2012, 33, 1347.
- [4] Badiei A, Gholami J, Khaniani Y, *E-J. Chem.* 2009, 6, S324.



- [5] Darabi H R, Aghapoor K, Mohsenzadeh F, Taala F, Asadollahnejad N, Badiei A *Catal. Let.* 2009, 133, 84.
- [6] Hashemi P, Shamizadeh M, Badiei A, Ghiasvand A R, Azizi K *Chromatographia* 2009, 70, 1147.
- [7] Hashemi P, Shamizadeh M, Badiei A, Poor P Z, Ghiasvand A R, Yarahmadi A *Anal. Chem. Acta.* 2009, 646, 1.
- [8] Bibby A and Mercier L *Chem. Mater.* 2002, 14, 1591.
- [9] Gangali M R, Hajiagha Babaei L, Badiei A, Mohammadi Ziarani G and Tarlani A *Anal. Sci.* 2004, 20, 725.
- [10] Ganjali M R, Daftari A, Hajiagha Babaei L, Badiei A, Saberyan K, Mohammadi Ziarani G and Moghimi A *Water, Air, Soil Pollut.* 2006, 173, 71.
- [11] Javanbakht M, Badiei A, Ganjali M R, Norouzi P, Hasheminasab A and Abdouss M *Anal. Chim. Acta.* 2007, 601, 172.
- [12] Javanbakht M, Khoshsafar H, Ganjali M R, Badiei A, Norouzi P and Hasheminasab A *Current Anal. Chem.* 2009, 5, 35.
- [13] Javanbakht M, Divsar F, Badiei A, Fatollahi F, Khaniani Y, Ganjali M R, Norouzi P, Chaloosi M, and Ziarani G M *Electrochim. Acta* 2009, 54, 5381.
- [14] Béland F., Badiei A., Ronning M., Nicholson D., and Bonneviot L., *Phys. Chem. Chem. Phys. (PCCP)*, 1999, 1, 605.
- [15] Zarabadi-poor, P., Badiei A., Fahlman B. D., Arab P., Mohammadi Ziarani G., *Ind. Eng. Chem, Res.*, 50, 2011, 10036.
- [16] Badiei A.; Bonneviot L., *Inorg. Chem.*, 1998, 37, 4142
- [17] Bonneviot L., Badiei A., and Crowther N., US 2317056, 2004. (US Patent).
- [18] Badiei A.; Cantournet S., Morin M., and Bonneviot L., *Langmuir*, 1998, 14, 7087.



- [19] Reinert P., B. Garcia, C. Morin, A. Badiei, P. Perriat, O. Tillement, L. Bonneviot, *Nanotechnology in mesostructure Materials Stud. Sur. Sci.Catal.*, 2003, 146, 133.
- [20] Bonneviot L., M. Morin, and A. Badiei, US 0133868, 2003. (US Patent).
- [21] Badiei A., L. Bonneviot, N. Crowther G. Mohammadi Ziarani, *J. Organomet. Chem.*, 2006, 691, 5923.
- [22] Badiei A., Khaniani Y., Mohammadi Ziarani G., US 13/034,357, 2011, (US Patent).



Oral Session



Dynamics and Diffusion of N₂ and O₂ in Zeolite Li-LSX Studied by Molecular Dynamics Simulations

M. H. Kowsari^{*a,b}, Mahdiyeh Bamdad^b, and Mahmud Ashrafizaadeh^b

^a Department of Chemistry, Institute for Advanced Studies in Basic Science (IASBS), Zanjan, 45137-66731, Iran.

^b Department of Mechanical Engineering and Sheikh Bahaei National High-Performance Computing Center, Isfahan University of Technology, Isfahan, 84156-83111, Iran. (E-mail: mohammad.kowsari@gmail.com)

Keywords: Zeolite Li-LSX, Molecular Dynamics (MD), Diffusion, Mean Square Displacement

Introduction:

Studying the dynamics behavior of molecules inside the pores of zeolites is a central feature to control the performance of these materials in many industrial applications. For example, the differences in diffusion coefficients of the guest species in the pore media basically control of separation procedure. Previous researches show that zeolite Li-LSX, with [Li₉₆ Si₉₆ Al₉₆ O₃₈₄] formula unit, is suitable for selectively adsorbs nitrogen over oxygen [1]. Thus, this zeolite can be used for effective separation of N₂ from air, and for O₂ production in the chemical industry.

In this work, the dynamics and the self-diffusion coefficients of N₂ and O₂, both as pure species and as air binary mixtures, in two designed states of zeolite Li-LSX, were studied by MD simulations. The main purpose of this study is to compare the mean square displacement (MSD) and diffusion of N₂ and O₂ in zeolite Li-LSX. We also determine the effect of temperature, loading, and Li III situation on the dynamics of guest species inside of the Li-LSX framework.

Computational Details and Methodology:

Extensive *NVT* and *NVE* MD simulations are carried out by DL_POLY program to study the dynamics and the diffusion of N₂ and O₂ at different loading in 2×2×2 replica of the cubic unit cell (*Fd-3*) of Li-LSX for several temperatures between 260 and 700 K. The

intermolecular interactions were employed using Lennard–Jones (12–6) and coulombic potentials by the reported parameters in Ref. [2]. Except of Li III cationic sites, which are considered in both of fixed and mobile form in the simulations, other atoms of zeolite are fixed at the crystallographic coordinates obtained by Lobo [3]. The gas molecules were modeled as rigid sites and inserted randomly in the pores using of Mercury program. Periodic boundary conditions were employed and the equations of motion were integrated using the Verlet leapfrog scheme. The time step of the simulations was 1 fs and cutoff distance of $R_{\text{cutoff}} = 20 \text{ \AA}$. The electrostatic interactions were calculated using the Ewald summation method. The final MSD results for N_2/O_2 were obtained by ensemble–averaging from 350 ps of five *NVE* runs in each case. The self-diffusion coefficient of particle i is obtained from the slope of the MSD plot versus time using Einstein relation.

Results and Discussions:

Simulated MSDs are compared for the gases of binary mixtures inside of zeolite Li-LSX in Figure 1. The calculated diffusion coefficients of gases from the Einstein relation at different temperatures and conditions are also reported in Table 1. O_2 illustrates faster dynamics than N_2 inside the zeolite. Our results show that the MSD and diffusion of N_2 increase in the presence of mobile Li III cations in the simulations. This is a result of the strong interaction of the quadrupole moment of N_2 molecules by the electric field associated with the Li cations of the Li-LSX lattice.

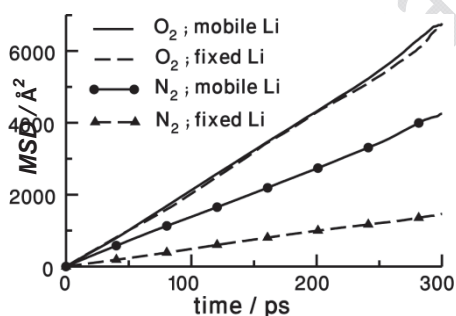


Table 1. Simulated diffusion coefficients, D_i , (in $10^{-8} \text{ m}^2\text{s}^{-1}$), at different temperatures for O_2 and N_2 , as binary mixtures and as single species, in LiLSX framework using of fixed Li III (with the diffusion

Figure 1. The calculated MSDs for O₂ and N₂ as air binary mixtures in LiLSX at 400K for two forms of Li III cations in the simulations.

Summary and Conclusions:

MD simulations are used to study the dynamics and diffusion of N₂ and O₂ in Li-LSX zeolite at different loadings, temperatures, and the fixed or mobile situations of Li cationic sites. We find that the Li III cationic sites have an important role in the dynamics and diffusion of N₂ molecules. Further research is planned to study the activation energy for diffusion process of gases and more description of the dynamics of guests in Li-LSX zeolite.

Acknowledgement:

Financial support of the Aviation Industries and the ministry of science and the computational support of National High-Performance Computing Center of the Isfahan University of Technology are acknowledged.

References

- [1] R. K. Agha, G. De Weireld, and M. Frère; *Adsorption*; 11, 179–182, 2005.
- [2] K. Watanabe, N. Austin, and M. R. Stapleton; *Mol. Simul.*; 15, 197–221, 1995.
- [3] M. Feuerstein and R. F. Lobo; *Chem. Mater.*; 10, 2197–2204, 1998.

$T /$ K	D_{N_2} ; in mix (N ₂ /O ₂) (16:4)/uc	D_{O_2} ; in mix (N ₂ /O ₂) (16:4)/uc	D_{N_2} ; pure (loading 16/uc)	D_{O_2} ; pure (loading 4/uc)
29 8	0.11,(1.01)	2.77,(2.76)	-----,(0.98)	3.00,(3.34)
40 0	0.82,(2.27)	3.70,(3.65)	0.71,(2.56)	4.26,(4.35)
50 0	1.80,(3.41)	3.95,(3.97)	1.93,(3.35)	4.62,(4.91)
60 0	2.92,(4.50)	4.39,(4.47)	2.76,(4.13)	6.00,(5.59)
70 0	3.67,(4.84)	4.92,(5.39)	3.95,(4.63)	6.60,(7.62)



Vapor-liquid interfacial properties of ionic liquids

A. Maghari and F. Ziamajidi

Department of Physical Chemistry, University of Tehran, Tehran, Iran

ziamajidi@khayam.ut.ac.ir

Introduction:

Ionic liquids are essentially molten salts composed entirely of a mixture of anions and cations with a melting temperature below the boiling temperature of water. These are rapidly gaining interest as replacements for traditional organic solvents used in chemical processes. They have the ability to dissolve an enormous range of inorganic, organic, and polymeric materials at very high concentrations, are noncorrosive, and have low viscosities and no significant vapor pressures. In this work, we developed a new version of SAFT EOS to describe the behavior of vapor-liquid interfacial properties of ionic liquids using a density functional theory (DFT). We have calculated the surface tension as well as interfacial surface thickness with use of three methods, including the common intersection method (CIM), Winkelmann method and inversion method. The calculated results are also compared with experimental data and show that these methods are given satisfactory predictions the surface thickness and its corresponding surface tension at various temperature.

Method:

The fluid in the surface region is assumed an inhomogeneous one. In the vertical direction of the surface, density gradient $\rho(z)$ is changed with z and is usually approximated using the hyperbolic tangent function imposed by the van der Waals theory of capillarity:

$$\rho(z) = \frac{1}{2}(\rho^l + \rho^v) - \frac{1}{2}(\rho^l - \rho^v) \tanh\left[\frac{2(z-z_0)}{\delta}\right]$$

(1)

where δ is surface thickness, ρ^l and ρ^v are liquid and vapor densities, respectively. The surface tension can be expressed as follows:

$$\gamma = \int_{-\infty}^{+\infty} [p - p[\rho_0(z)]] dz \quad (2)$$

where p is normal pressure, $p[\rho_0(z)]$ is the tangential pressure tensor that can be calculated from the density in every layer by the EOS.

From Eq. (1), it can be seen that the density profile $\rho(z)$ depends on the surface thickness δ .

Winkelman used the following expression to estimate the surface thickness [1]:

$$\delta = - \frac{\rho^l - \rho^v}{\left(\frac{d\rho}{dz} \right)_{z=z_0}} \quad (3)$$

Furthermore, Maghari et al. [2,3] have presented a novel approach, named common intersection method (CIM) based upon the characteristic of an intersection point on the isotherms of the density profile versus density. Moreover, they introduced an inversion method to predict the surface thickness from the surface tension experimental data.

In this work, the surface thicknesses of some ionic liquids obtained from these methods, are used for calculating of surface tension by DFT approach and modified SAFT BACK EOS.

Results and discussion:

The behavior of surface tension and surface thickness versus temperature for hexyl-3-methylimidazolium tetra fluor borate (as an example of ionic liquid) are shown in Figs 1

and 2, respectively. Surface tension decreases with increasing temperature, whereas surface thickness increases with increasing temperature. The results presented indicate that within the -3-methylimidazolium family the increase in the cation alkyl chain length reduces the surface tension values.

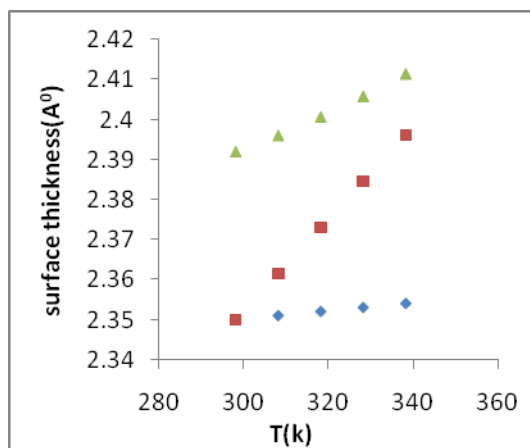


Fig. 1. Surface thickness of [Hmim][BF₄] from 293 to 342 K. with DFT method: ♦, Inversion,

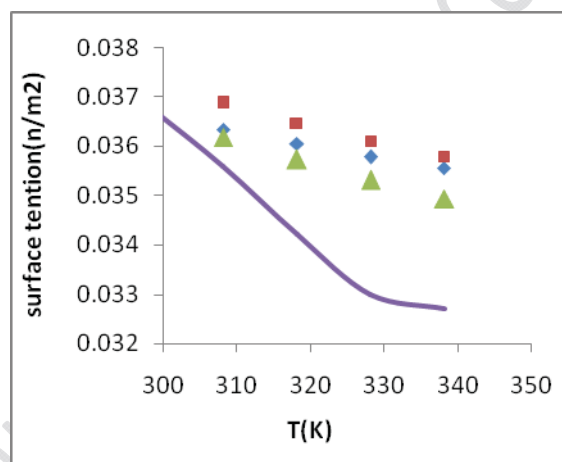


Fig. 2. Surface tension of [Hmim][BF₄] from 293 to 342 K. with different methods: ♦, Inversion, □, GCMC, ▲, DFT.

Reference:

- [1] J. Winkelmann, *J Phys. Condens. Matter*, **13** (2001) 4739.
- [2] A. Maghari and M. Najafi, 2009, *J. Stat. Mech*, (2009) PO5003.
- [3] A. Maghari and M. Najafi, *J. Stat. Mech*, (2009) PO2041.



Molecular Dynamics Simulation of an Amine-Functionalized Imidazolium-Based Ionic Liquid

M. H. Kowsari* and M. Aziznezhad

Department of Chemistry, Institute for Advanced studies in Basic Sciences (IASBS), Zanjan, 45137-66731, Iran
(E-mail: mohammad.kowsari@gmail.com; mohammadaziznezhad@gmail.com)

Key words: Molecular dynamics, Ionic liquid, CO₂ capture, Transport properties.

Introduction:

Rising of unexpected emission of carbon dioxide (CO₂) in the atmosphere is one of the great challenges in this world. Recent studies show that the Ionic liquids (ILs) can be used as the suitable liquid absorbents in the capture of CO₂ from its production places and prior to atmospheric release. However, this sequestration and capturing capacity can be improved by introducing basic character in the ILs. Functionalization of ILs with a suitable moiety (like amine) may be implied in this regard. As the first stage of drawing CO₂ capture process in ILs, in this work we investigate the structure and properties of the pure IL 1-(3-aminopropyl)-3-methyl-imidazolium tris(pentafluoroethyl)trifluorophosphate, ([apmim][FEP]) as the proper absorbent candidate, with molecular dynamics (MD) simulation. The purpose of this work is to provide clear microscopic picture of this IL in pure state and determine the role of amine functionalized cations and perfluorinated anions on the properties of ILs. Finally we will use the simulation results of pure ionic liquids as the initial point for simulating of CO₂ capture in this ionic media in nearly future.

Computational methods:

The force field parameters used in this work for the [apmim]⁺ cation and the [FEP]⁻ anion is reported by Maginn *et al.* [1,2]. The simulations were done in constant pressure and temperature (*NpT*) ensemble with the Nosé–Hoover thermostat/barostat algorithm as implemented in the DL_POLY 2.18 package [3]. The simulation box consists of 150 ion pairs of [apmim][FEP]. Periodic boundary conditions were used, and the equations of motion were integrated using the *Verlet leapfrog* scheme. In all simulations, pressure, time step, and cutoff

distance were fixed at 1 atm, 0.001 ps and 17 Å, respectively. After equilibration of system in several steps up to desired temperatures (300, 400, and 500 K), generally the production runs with ~7.5 ns trajectory time length used for data collecting and analysis.

Results and discussion:

We compute the radial distribution functions (RDFs), mean-square displacements (MSDs), velocity autocorrelation functions (VACFs), and diffusion coefficients of ionic species in this ionic liquid. Some of calculated properties are summarized for example in Figure 1. The diffusion coefficients of ions are calculated from the slope of mean square displacement plots, and the electrical conductivity from the Nernst-Einstein formulas. Simulation results are in agreement with experiment in predicting relative trends of properties and determining the role of the amine functionalized imidazolium-based cation and perfluorinated [FEP]⁻ anion on the dynamics and transport behavior of this task specific ionic liquid compared with common ILs.

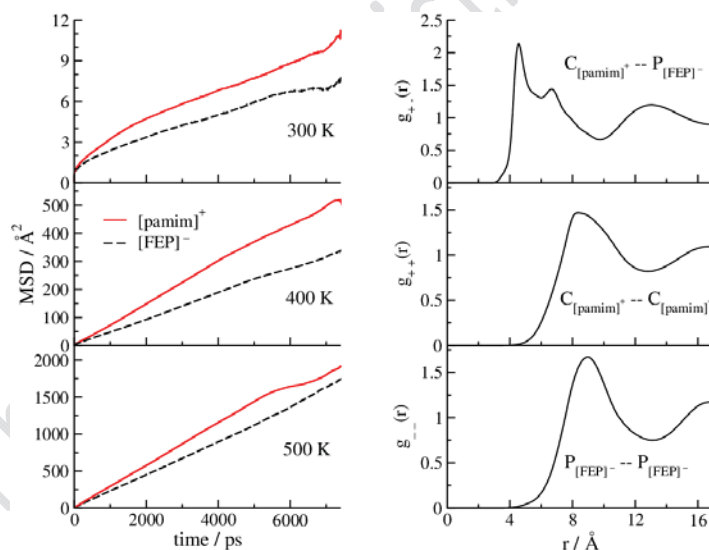


Figure 1: The calculated MSDs of ions at different temperatures (left), and the RDFs for the key atomic sites of the cation-anion, cation-cation, and the anion-anion from the simulation of [pamim][FEP] at 400 K (right).

Acknowledgments:

The financial support of this work by Iran National Science Foundation and computational



support of IASBS is gratefully acknowledged.

References:

- [1] K. E. Gutowski and E. J. Maginn; *J. Am. Chem. Soc.*; 130, 14690–14704, 2008.
- [2] X. Zhang, F. Huo, Z. Liu, W. Wang, W. Shi, and E. J. Maginn; *J. Phys. Chem. B*; 113, 7591–7598, 2009.
- [3] http://www.cse.clrc.ac.uk/msi/software/DL_POLY/.



Molecular Dynamics Simulations Studies of surfactant -Wrapped Single -Walled Carbon Nanotubes surface

M. Foroutan*, M. Fatemi

Department of Physical Chemistry, School of Chemistry, College of Science, University of Tehran, Tehran,
Iran, m.fatemi@khayam.ut.ac.ir

Keywords: Molecular Dynamics (MD) Simulation, Carbon Nanotubes (CNT), Triton X100 Surfactant, Radius of Gyration (R_g).

Introduction :

We used a molecular dynamics (MD) simulation approach to probe the behaviors of the carbon nanotubes (CNT) with Triton X100 surfactant. So we assess nanotubes in different temperatures and diameter, according as the result of our simulations; the strong intermolecular interaction between CNT and TX100 that cannot be influenced by the temperature in the range we reported, and with an increase in nanotubes diameter, the interaction energy is increased.

Computational Procedure:

MD simulations were performed in the Tinker molecular modeling package (version 5.0)[1], using the AMBER99 force field, we used the (5,5), (6,6), (9,9), and (10,10) CNTs armchair with a length of about 25 Å. The diameter of CNTs ranges from 6.68 to 13.46 Å. Using a canonical ensemble (constant NVT), the velocity form of Verlet algorithm method and the Nose-Hoover thermostat algorithm were used to integrate the equations of motion with a time step of 1.0 fs. Non-bonded van-der-Waals interactions were modeled by a Lennard-Jones potential with a cut-off distance of 1.2 nm. Our simulation is related to the behavior of the TX100 when they are close to the CNT in an “ideal” poor solvent.

Results and Discussion:

Figure 1 and 2 represent the snapshots of CNT wrapped by the TX100. As figure 3 shows; with an increase in CNT diameter, the interaction energy is increased[2], because the surface

contact area between them increases accordingly, As Figure 4 shows; the attractive interaction of the TX100 with the CNT increasing only slightly with increasing temperature. Thus, the temperature dependence of the interaction energies can be considered negligible. As figure 5 shows, the radius of gyration (R_g) values of TX100 molecules increasing and show a fluctuation as the flexible hydrophilic polyethylene oxide chains wrap around the CNTs. As figure 6 shows, the R_g of TX100, when interaction with CNTs is higher than without CNTs, is caused by the intermolecular energy between TX100 and CNTs, which directly gives rise to the strong π - π interactions [3] with the nanotube surface, called “ π -stacking”[4] are responsible for the strong tendency of nanotubes to “stick together”, which is a major obstacle to their processing.

Conclusion:

Our simulation results showed that, the CNTs with larger diameter are suggested as better candidates compared to smaller CNTs in diameter for nanocomposite reinforcement applications, and the higher temperature and consequently higher kinetic energy does not have any significant effect on the total TX100 size.

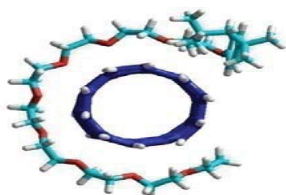


Fig. 1. Front view snapshot for a (5, 5) CNT Wrapping by

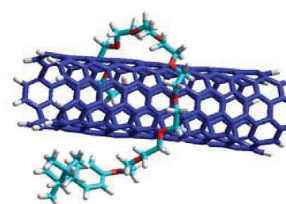


Fig. 2. Side view snapshot for a

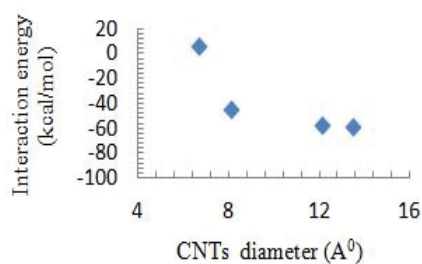


Fig. 3. Interaction energy as a function of CNT diameter at 300

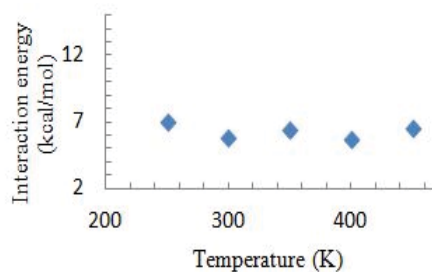


Fig. 4. Interaction energy as a function of temperature for CNTs.

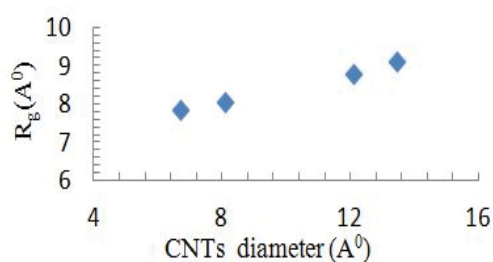


Fig.5. Change of $\langle R_g \rangle$ of the surfactant after the interaction with different CNTs in diameter.

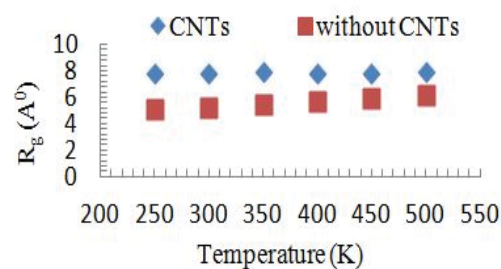


Fig.6. Change of $\langle R_g \rangle$ of TX100 after the interaction with and without CNTs as a function of temperature.

References:

- [1] Won, C. Y.; Joseph, S.; Aluru, N. R. J. Chem. Phys. **2006**, 125, 114701.
- [2] Jamie S. Quinton.; Adam J. Blanch.; Claire E. Lenehan. J. Phys. Chem. B **2010**, 114, 9805–9811.
- [3] Chen, R. J.; Zhang, Y.; Wang, D.; Dai, H. J. Am. Chem. Soc. **2001**, 123, 3838.
- [4] Tan, Y.; Resasco, D. E. J. Phys. Chem. B **2005**, 109, 14454.



Study of the Imidazolium-Based [Tf₂N⁻] Ionic Liquids by Molecular Dynamics Simulations

M. H. Kowsari^{*a}, M. Fakhraee^b, and B. Najafi^b

^a Department of Chemistry, Institute for Advanced Studies in Basic Science (IASBS), Zanjan,
45137-66731, Iran.

^b Department of Chemistry, Isfahan University of Technology, Isfahan, 84156-83111, Iran.
(E-Mail: mohammad.kowsari@gmail.com; fakhraee.mostafa1@gmail.com)

Key words: Imidazolium salts, Ionic liquids, Molecular dynamics, Simulation, Diffusion

Introduction:

Ionic liquids (ILs) are green liquid salts composed of organic cations and organic or inorganic anions. A combination of different anions and cations in ILs will lead to an infinitely large number of compounds with different properties. Some physical and chemical properties of ILs can be tailored by the selection of suitable cations, anions and substituent groups on the ions. Consequently, to design new ILs for specific tasks, it is very important to understand the relationship between the ionic structures and the fundamental properties of ILs [1].

In this work, atomistic molecular dynamics (MD) simulations have been used to study of the diverse thermodynamic quantities, structural features, dynamical behavior, and transport properties of four ionic liquids based on the imidazolium cation ([bmmim]⁺: 1-butyl-2,3-dimethyl-imidazolium, [pamim]⁺: 1-(3-aminopropyl)-3-methyl-imidazolium, [bmim]⁺: 1-butyl-3-methyl-imidazolium, and [mim]⁺: 1-methyl-imidazolium) and bis(trifluoromethane-sulfonyl)imide, (CF₃SO₂)₂N⁻ (also known as [Tf₂N]⁻) anion. The main purpose of these simulations is to compare the thermodynamic quantities (see Table 1), the mean square displacements (MSDs), transport coefficients, and the radial distribution functions (RDFs) of ILs. Finally, we determine the effects of alkyl / functional substituent groups of imidazolium cations on the properties of these ILs.

Computational methods:

MD Simulations of the four ILs were carried out with at least 5000 atoms (125–180 ion pairs) in the simulation cell at 298, 400, 450, 500, and 600 K. In all simulations via DL-POLY 2.18 software [2], pressure, time step, and cutoff distance were fixed at 1 atm, 0.001 ps and 16.5 Å, respectively. Periodic boundary conditions were employed, and the equations of motion were integrated using the *Verlet leapfrog* scheme. For each ionic liquid, all simulations were performed in the isothermal–isobaric (NpT) ensemble at five different temperatures during 5 ns to reach the equilibration of the system. To calculate the properties which are mentioned above, each of the equilibrated system was studied in the NpT ensemble with the long simulation run for 7.5 ns.

Results and discussion:

Some of calculated thermodynamic properties are summarized for example in Table 1. The diffusion coefficients of ions are calculated from the slope of mean square displacement plots, the electrical conductivity from the Nernst-Einstein formulas, and the viscosity from the Stokes-Einstein relation. Simulation results are in agreement with experiment in predicting relative trends of properties and determining the role of the substituted cation structure on the dynamics, thermodynamics, and transport behavior of this family of ionic liquids. Radial distribution functions of different atomic sites were also calculated at 400 K.

Table 1. The calculated internal energy of vaporization (ΔU_m^{vap}), enthalpy of vaporization (ΔH_m^{vap}), molar volume (V_m), and cohesive energy density (c) from simulations of 4 ILs at two temperatures.

[X][Tf ₂ N] ILs	T	ΔU_m^{vap}	ΔH_m^{vap}	V_m	c
[X] ⁺	(K)	(kJ/mol)	(kJ/mol)	(cm ³ /mol)	(J/cm ³)
[bmmim] ⁺	400	179.030	182.360	310.325	576.91
	500	161.631	165.791	331.301	487.90
[pamim] ⁺	400	214.412	217.742	280.749	763.71
	500	190.804	194.228	300.429	635.11



[bmim] ⁺	400	117.826	121.156	301.321	391.03
	500	93.240	97.400	322.653	288.98
[mim] ⁺	400	80.211	80.211	218.434	351.96
	600	32.166	37.154	245.332	131.11

Conclusions:

we determine the effects of changing the substituent groups of imidazolium cations on a wide range of properties of 4 imidazolium-based ILs. The trends in the MSD, diffusion coefficient, and electrical conductivity of studied systems are: [bmim][Tf₂N] > [pamim][Tf₂N] >

[bmmim][Tf₂N] > [mim][Tf₂N]. The trends in the $\Delta U_{\text{m}}^{\text{exp}}$, $\Delta H_{\text{m}}^{\text{exp}}$ and cohesive energy

density in these series of ILs are: [pamim][Tf₂N] > [bmmim][Tf₂N] > [bmim][Tf₂N] > [mim][Tf₂N].

References:

- [1] M. H. Kowsari, S. Alavi, B. Najafi, K. Gholizadeh, E. Dehghanpisheh, and F. Ranjbar; *Phys. Chem. Chem. Phys.*; 13, 8826-8837, 2011.
- [2] W. Smith and T. R. Forester, and I. T. Todorov, the DL_POLY molecular simulation package, v. 2.18, Daresbury Laboratory, UK, 2007.



Interaction of Neutral and Ionic Metal Clusters with Noble Gas Atoms; Theoretical Investigation

Z. Jamshidi* and M. Fakhraei Far

Chemistry and Chemical Engineering Research Center of Iran, Tehran, Iran

jamshidi@ccerci.ac.ir

Introduction:

The interactions between noble metals and noble gas atoms have become of great interest in theoretical and experimental investigations due to their respective noble characters. In recent years many effort has been expanded to prepare and characterize the systems in which a noble metal like Au, Ag, and Cu is bound to a noble gas. During the last few years, noble metal clusters have attracted great attention in basic science due to their unique physical and chemical properties. These metals clusters play an important role in several high technology fields such as nanoelectronic and nanomaterials. Most of the experimental works have been investigated the structure, electronic and optical properties of metal cluster in embedding rare gas matrix. However there has been rarely attention on the interaction of metal clusters with noble gas atoms. In the present work, calculation have been carried out in $M_n^+ - Rg$ complexes (M = Cu, Ag and Au; Rg = Kr, Xe and Rn; $v = 0$ and ± 1) and the nature of M-Rg bond has been investigated based on NBO, QTAIM, and EDA analysis.

Method of Calculation:

The interaction of trimer metal clusters with noble gas atoms calculated at DFT-CAM-B3LP/aug-cc-pVDZ-PP and MP2/aug-cc-pVDZ-PP level of theory, using the Gaussian 03 and 09 suites of programs. The interaction energy is defined as the difference between the energy of a complex and sum of the energies of its components, and interaction energies were corrected for the basis set superposition error. To reveal the nature of bonds, the NBO, QTAIM, and EDA analyses were carried out on CAM-B3LYP structures.

Result and Discussion:

The symmetry of optimized structure for anionic and cationic trimer corresponds to $D_{\infty h}$ and D_{3h} point groups, respectively. Neutral gold trimer have C_{2v} and D_{3h} symmetry (in agreement with the Jahn-Teller effect). The optimized geometry for the lowest-lying isomers of M_3^v ($v = 0$ and ± 1) complexes with rare gas atoms have been displayed in Figure 1. The equilibrium bond lengths and binding energies have been obtained for these complexes. According to Figure 2, for same metal, the values of interaction energies for the rare gases have the order of $Rn > Xe > Kr$, and also the corresponding values for gold complexes are higher than copper and silver complexes. As a matter of fact, these results were obtained for all of the $M_3^v - Rg$ complexes.

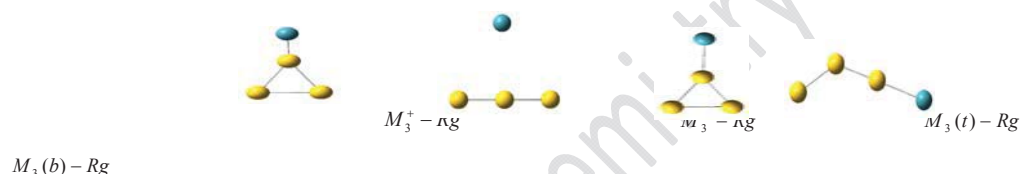


Figure 1: Geometrical structure of neutral and ionic coinage metal clusters and their complexes. The higher electron affinity (EA) of cationic complexes than neutral and anionic complexes leads to higher binding energies for cationic complexes than $M_3^- - Rg$ and $M_3 - Rg$.

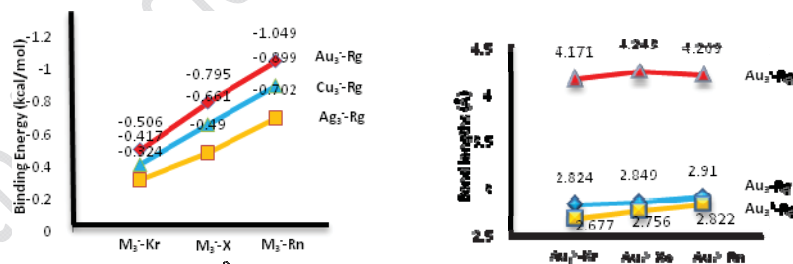


Figure 2: Binding energy (kcal mol^{-1}) and equilibrium bond lengths (\AA) for $M_3^v - Rg$ complexes

NBO analysis has been held on optimized CAM-B3LYP structures. Obviously, the positive natural charge (NPA) of Rg atoms in the same metal complexes increases through Kr to Rn. This indicates a substantial amount of charge transfer from Rg to M_3 clusters. However, for



same Rg atoms complexes with different metals, q^{Rg} has the order of $q_{Au_3-Rg}^{Rg} > q_{Cu_3-Rg}^{Rg} > q_{Ag_3-Rg}^{Rg}$. The QTAIM analysis, based on the bond critical point properties, revealed that cationic and neutral complexes had both electrostatic ($\nabla^2\rho(r) > 0$) and covalent ($H(r) < 0$) characters, simultaneously. While, for anionic complexes, both $\nabla^2\rho(r)$ and $H(r)$ are positive and these bonds are electrostatic in nature.

References:

- [1] X. Tong, C. Yang, M. Wang, X. Ma and D. Wang, *J. Chem. Phys.* **2011**, 134, 024306.
- [2] T. Zeng, M. Klobukowski, *J. Chem. Phys. A* **2008**, 112, 5236.
- [3] A. H. Pakiari, Z. Jamshidi, *J. Phys. Chem. A* **2008**, 112, 7969.
- [4] A. H. Pakiari, Z. Jamshidi, *J. Phys. Chem. A* **2010**, 114, 9212.



Theoretical investigation of the effects of solvent on the $1^1B_u \rightarrow 2^1A_g$ internal conversion decay in octatetraene

M. Miralinaghi^{a*}, A. Khavaninzadeh^b, and R. Islampour^b

^a Department of Chemistry, Varamin-Pishva Branch, Islamic Azad University, Varamin, Iran

^b Department of Chemistry, Tarbiat Moallem University, 49 Mofateh Avenue, Tehran, Iran

Email: msmiralinaghi@gmail.com

Key words: Duschinsky parameter, Internal conversion, Phase-dependency

Introduction:

The *all-trans*-1,3,5,7-octatetraene has two close-lying lowest singlet excited electronic states -the ionic 1^1B_u electronic state, and the covalent 2^1A_g electronic state which lies lower than the 1^1B_u state. In condensed phases, excitation to 1^1B_u state is typically followed by fast relaxation to the 2^1A_g state, which is responsible for the red-shifted fluorescence emission spectra.

It is the purpose of this article to calculate and compare the internal conversion decay rate constants of the *all-trans*-1,3,5,7-octatetraene (hereafter, simply referred to as "octatetraene") in the condensed and gas phases.

Theory:

The Internal conversion decay is due to the breakdown of the Born-Oppenheimer approximation. The general expressions we previously derived for calculating the internal



conversion rate constants between two displaced-distorted-rotated adiabatic potential energy surfaces have been used to determine the decay rate constants for $1^1B_u \leftrightarrow 2^1A_g$ internal conversions of octatetraene in which the coupling between the 1^1B_u and 2^1A_g occurs by the non-totally symmetric b_u modes. A recipe that allows one to estimate the Duschinsky parameters from the relative intensities of vibronic bands in absorption-emission spectra are also developed.

Results and discussion:

The phase-dependency of the zero-zero energy gap, frequencies of totally symmetric accepting modes, and Huang-Rhys factors for the $1^1B_u \leftrightarrow 2^1A_g$ internal conversion guided us to estimate the associated decay time in free jet expansions, static gas, and *n*-octane and *n*-hexane matrices.

Following table indicates that in the low temperature limit $1^1B_u \leftrightarrow 2^1A_g$ internal conversion takes place more efficiently in the condensed phase than in the gas phase.

Table1. Decay time constant associated with $1^1B_u \leftrightarrow 2^1A_g$ internal conversion

for octatetraene in different phases

$1^1B_u \leftrightarrow 2^1A_g$	$\tau_{IC} = 1/k_{IC}$	zero-zero energy gap (cm^{-1})
free jet expansions	1.65 (ps)	6604
static gas	2.36 (ps)	6574
<i>n</i> -octane	232.22 (fs)	3522
<i>n</i> -hexane	290.12 (fs)	3388



These results are in consistent with the ratio $(1^1B_u \rightarrow 1^1A_g) / (2^1A_g \rightarrow 1^1A_g)$ of integrated fluorescence intensity that was experimentally estimated to be ~ 16.6 in the gas phase [1] and 0.1 ± 0.05 in acetonitrile solution [2]. The internal conversion in acetonitrile solution at 293 K was estimated to be 400 fs [2]. In addition, we found that a 3-mode model consisting of promoting mode ν_{38} (of symmetry b_u , which is composed of CC double-bond stretches, CH₂ scissors, and CH in-plane bends [3]), which has the highest vibronic coupling and two totally symmetric accepting modes ν_6 (consisting of in-phase CC double-bond stretches, CH₂ scissors, and CH in-plane bends [3]) and ν_{12} (consisting of the in-phase CC single-bond stretches and CH in-plane bends [3]) could be considered as the minimal models for the $1^1B_u \rightleftharpoons 2^1A_g$ internal conversion both in condensed and in gas phase. Moreover, it has been found that distortions of vibrational modes to some extent increase the decay rate constant of this transition in gas phase, and have minor effect on the rate in condensed phase.

Conclusion:

Our calculations show that in the low temperature limit the $1^1B_u \rightleftharpoons 2^1A_g$ internal conversion takes place on a 232-290 fs time scale in condensed phase and 2 ps in gas phase.

References:

- [1] Bouwman, W. G.; Jones, A. C.; Phillips, D.; Thibodeau, P.; Friel, C.; Christensen, R. L. *J. Phys. Chem.* **1990**, *94*, 7429.
- [2] Ohta, K.; Naitoh, Y.; Tominaga, K.; Yoshihara, K. *J. Phys. Chem. A*, **2001**, *105*, 3973.
- [3] Yoshida, H.; Tasumi, M. *J. Chem. Phys.* **1988**, *89*, 2803-2809.



Interaction of Highly Reactive Molecules C_4H_4 , $C(CH_2)_3$ and $(C_3H_3)^-$ with η^5 -Cyclopentadienyl Metal Complexes $(\eta^5-C_5H_5)M$. A Theoretical Study

Ali H. Pakiari^{a*}, Masoumeh Mousavi^b

^{a,b} Chemistry Department, College of Science, Shiraz University, 71454 Shiraz (Iran)

E-mail: pakiariah@gmail.com

Keywords: Energy decomposition analysis (EDA), Natural orbitals for chemical valence (NOCV), Trimethylenemethane (TMM), Sandwich complexes

Introduction:

Delocalized π -hydrocarbyl ligands cyclobutadiene, C_4H_4 , (Cb), trimethylenemethane, $C(CH_2)_3$, (TMM), and cyclopropenyl (C_3H_3) belong to the fundamentally important species that for a long time have been considered as prototypical reactive intermediates which are too unstable to isolate under usual experimental conditions. A common feature for these reactive intermediates is that coordinated forms of them behave as if they are aromatic species, although they do not satisfy the simple Hückel criterion for aromaticity ($4n+2$ π electron) in their free state.

The purpose of this study is the elucidation of bonding interaction between this group of ligands and a selected series of η^5 -cyclopentadienyl metal complexes $(\eta^5-C_5H_5)M$ with $M=Co, Rh$, in complexes $[CpM-Cb]$, $[CpM-TMM]$, and $[CpM-C_3H_3]^+$.

Method:

Full geometry optimization has been performed at the framework of the DFT level, at the BP86 level of theory, being embedded in Gaussian 09 program. The basis sets for all atoms have a triple- ζ quality augmented with two sets of polarization functions, def2-TZVPP. The core electrons are approximated by the effective core potentials (ECP). To describe the nature of bonding interactions we use energy decomposition analysis on natural orbitals for chemical valence (EDA-NOCV) [1] implemented in ADF2009 package. Therefore, the second set of geometry optimization is carried out at BP86/TZ2P+ level with ADF package.



Results and Discussion:

Energy information origination from EDA-NOCV analysis, shows that in complexes CpM-Cb, CpM-TMM and [CpM-C₃H₃]⁻ (M=Co, Rh), the heterolytic fragmentation, CpCo⁺² and TMM⁻²/Cb⁻², corresponding to the ionic view, is accompanied by the a higher price in terms of energy compared to the homolytic fragmentation, CpCo^{↑↑} and TMM^{↑↓}/Cb^{↑↓}, corresponding to the covalent view. For example in CpCo-Cb complex, while the orbital interaction ΔE_{orb} of neutral species generates -189.9 kcal/mol stabilization, the ΔE_{orb} of doubly charged framework of CpCo⁺² and Cb⁻² rises to -347.8 kcal/mol. The values of dissociation energies also show that heterolytic (ionic) dissociation of CpCo-Cb (De= -706.2 kcal/mol) is almost six times more endothermic; i. e., less favorable, than the homolytic (covalent) dissociation (De=-127.6 kcal/mol). The same trend is observed for the interaction energy ΔE_{int} of the charged fragments (-723.2 kcal/mol) compared to the neutral ones (-128.6 kcal/mol).

Conclusion:

The bonding interactions in complexes CpM-Cb, CpM-TMM, and [CpM-C₃H₃]⁻ have been analyzed by charge and energy decomposition EDA-NOCV and MO analyses. A common feature for these reactive intermediates is that coordinated forms of them behave as if they are aromatic species, although they do not satisfy the simple Hückel criterion for aromaticity (4n+2 π electron) in their free state. There seems to be a general notion that the rich chemistry of these reactive molecules concerns the formation of a dianionic 6- π electron donor ligand (Cb⁻²/TMM⁻²) and satisfaction of Hückel's 4n+2 rule, through interaction with metal based fragments. In contrast to this common belief, EDA-NOCV analysis shows that the origin of this behavior lies in the strong covalent bonding interaction between the valence d $_{\pi}$ orbitals of the metal atom and p $_{\pi}$ orbitals of the ligand.

Reference:

- [1] (a) M. P. Mitoraj, A. Michalak, T. Ziegler, *J. Chem. Theory Comput.* **2009**, 5, 962; (b) A. Michalak, M. P. Mitoraj, T. Ziegler, *J. Phys. Chem. A* **2008**, 112, 1933; (c) M. Mitoraj, A. Michalak, *J. Mol. Model.* **2008**, 14, 681; (d) M. p. Mitoraj, A. Michalak, *Organometallics* **2007**, 26, 6576; (e) M. Mitoraj, A. Michalak, *J. Mol. Model.* **2007**, 13, 347.



Calculation of Absorption and Fluorescence Spectra of Large Polyatomic Molecules

A. Khavaninzadeh ^{*a}, M. Miralinaghi ^b, and R. Islampour ^a

^a Department of Chemistry, Tarbiat Moallem University, 49 Mofateh Avenue, Tehran, Iran

^b Department of Chemistry, Varamin-Pishva Branch, Islamic Azad University, Varamin, Iran

Email: a_khavaninzadeh@yahoo.com

Key words: *all-trans*-1,3,5,7-Octatetraene, Condon vibronic structure, Normal fluorescence, Absorption spectra.

Introduction:

The linear polyenes are a class of molecules whose spectroscopy, photophysics, and photochemistry have been a subject of active research, and are excellent candidates for illustrating the theory of non-Condon vibronic transitions. From various spectroscopic observations, it has been revealed that the linear (*all-trans*-)polyenes with four or more double bonds have two close-lying lowest singlet excited electronic states: the ionic 1^1B_u electronic state, and the covalent 2^1A_g electronic state which lies lower than the 1^1B_u state. The transition from the ground state 1^1A_g to 1^1B_u state is strongly dipole allowed which leads to well-resolved absorption spectra, whereas to the 2^1A_g state is symmetrically forbidden but vibronically allowed. In this study we present a general approach for

calculating the Condon vibronic structure observed in electronic absorption and fluorescence spectra of *all-trans*-1,3,5,7-octatetraene.

Theory:

1. *Absorption spectra:* For a molecular electronic absorption process in an isotropic medium, in which the transitions occur from the statistically equilibrated ground $\Phi_g(\mathbf{r}, \mathbf{Q})\chi_v(\mathbf{Q})$ to the manifold of all final excited $\Phi_e(\mathbf{r}, \mathbf{Q}')\chi_{v'}(\mathbf{Q}')$ adiabatic vibronic states, the thermally averaged absorption cross section $\alpha(\omega, T)$ is obtained as

$$\alpha(\omega, T) = \frac{4\pi\omega}{3\hbar c} \text{Re} \int_0^\infty dt \exp[i(\Omega_{eg} - \omega)t - \gamma_{eg}t] g_a(t)$$

(1)

where c is the speed of light, Ω_{eg} is $0-0'$ transition angular frequency, γ_{eg} is the width of vibronic band, and $g_a(t)$ is the time correlation function. Evaluation of $g_a(t)$ gives

$$g_a(t) = 2^N \bar{g}_a(t) (\det \Gamma^{-1} \Gamma'^{-1} \mathbf{T} \mathbf{T}' \mathbf{W}_1 \mathbf{W}_2)^{-1/2} \exp(-\mathbf{D}^T \mathbf{W}_3^{-1} \mathbf{D})$$

(2) where N is number of independent harmonic oscillators, $\Gamma(\Gamma')$ is $N \times N$ diagonal matrix of reduced frequency $\omega_j(\omega'_j)/\hbar$, $\mathbf{T}, \mathbf{T}', \mathbf{A}, \mathbf{A}'$ are $N \times N$ diagonal matrices that their

elements are defined as $T_j = (1 + \bar{\nu}_j)^2 - \bar{\nu}_j^2 \exp(-2i\omega_j t)$, $T'_j = 1 - \exp(2i\omega'_j t)$,

$A_j = \frac{(1 + \bar{\nu}_j) - \bar{\nu}_j \exp(-i\omega_j t)}{(1 + \bar{\nu}_j) + \bar{\nu}_j \exp(-i\omega_j t)}$, $A'_j = \frac{1 - \exp(i\omega'_j t)}{1 + \exp(i\omega'_j t)}$, respectively; $\bar{\nu}_j = [\exp(\hbar\omega_j/kT) - 1]^{-1}$ is the

mean occupation number, $\mathbf{W}_1 = \Gamma \mathbf{A} + \Gamma' \mathbf{A}'$, $\mathbf{W}_2 = \Gamma \mathbf{A}^{-1} + \Gamma' \mathbf{A}'^{-1}$, $\mathbf{W}_3 = \Gamma'^{-1} \mathbf{A}'^{-1} + \Gamma^{-1} \mathbf{A}^{-1}$, \mathbf{D} is the column vector whose components are the shift of the equilibrium nuclear configuration of

the excited respect to that of the ground electronic state. For the dipole-allowed electronic transition $\bar{g}_a(t) \approx |\mu_{ge}(\mathbf{0})|^2$ in which $\mu_{ge}(\mathbf{0})$ is the electronic transition dipole moment at the equilibrium configuration of the ground electronic state.

2. *Normal fluorescence*: The fluorescence intensity from the statistically equilibrated excited $\Phi_e(\mathbf{r}, \mathbf{Q}') \chi_v(\mathbf{Q}')$ to the manifold of all ground $\Phi_g(\mathbf{r}, \mathbf{Q}) \chi_v(\mathbf{Q})$ adiabatic states can be written as

$$w(\omega, T) = \frac{4\omega^3}{3\hbar c^3 \pi} \operatorname{Re} \int_0^\infty dt \exp[i(\Omega_{eg} - \omega)t - \gamma_{eg}t] g_e(t) \quad (3)$$

where the expression for $g_e(t)$ is similar to that of $g_a(t)$.

Results and discussion:

Absorption $1^1A_g \rightarrow 1^1B_u$ and fluorescence $1^1B_u \rightarrow 1^1A_g$ spectra of octatetraene have been calculated using equations (1) and (3), respectively in the 35053-42553 cm^{-1} region by including all b_u and active a_g totally symmetric modes at both jet-cooled and room temperature. A mirror image relationship exists between fluorescence and absorption spectra. The intensity of all vibronic bands are calculated relative to that of 0-0' band.

Conclusion:

Our calculations show that there is a good agreement between the vibronic structure of spectra calculated in this work and those obtained experimentally [1, 2, 3].

References:

- [1] Gavin, Jr., R. M.; Weisman, C.; McVey, J. K. and Rice, S. A. *J. Chem. Phys.* 1978, **68**, 522-529.



- [2] Leopold, D. G.; Vaida, V.; Granville, M. F. *J. Chem. Phys.* 1984, **81**, 4210-4217.
- [3] Bouwman, W. G.; Jones, A. C.; Phillips, D.; Thibodeau, P.; Friel, C. and Christensen, R. L. *J. Phys. Chem.* 1990, **94**, 7429-7434.

15th Physical Chemistry Conference



Potential Energy Surfaces of He-CS₂, Ne-CS₂ and Ar-CS₂ Dimers : Second Virial Coefficient and Vibrational Energy Levels

M. Tozihi^{a*}, H. Farrokhpour^b

^{a,b} Chemistry Department, Isfahan University of Technology, Isfahan, Iran

(Email^a: mtozihi@gmail.com; m.tozihi@ch.iut.ac.ir); (Email^b: farrokhphossein@gmail.com)

Keywords: potential energy surface, CCSD(T), SAPT, second virial coefficient, Vibrational levels.

Introduction:

There are numerous experimental data on the relaxation of the CS₂ molecule by a variety of bath rare gases^[1,2] which their interpretation needs to have an accurate potential energy surface for the interaction of CS₂ with the bath gas. The only report on the interaction of CS₂ with the rare gases is related to the work of Bruhel *et al.*^[3] In the present work, the potential energy surface (PES) of CS₂-Ar, CS₂-Ne and CS₂-He are calculated using ab initio method. The interaction second Virial coefficient (B₁₂) of the considered complexes are calculated using their calculated PES. In addition, the vibrational energy levels of the most stable configuration of each complex are also calculated.

Method :

The dimer geometry is described by two variables (R , θ) where R is the center of mass separation between the rare gas and CS₂, and θ is the angle between the vector \mathbf{R} and CS₂ axis. The interaction energy, on a regular grid of ten angular orientations: $\theta=0^\circ(10)90^\circ$, and radial separations: $R=2.5(0.1)15$ Å, were calculated at the CCSD(T)/aug-cc-pVDZ level of theory plus a set of $3s3p2d1f1g$ bond function considering the BSSE correction. All of the calculations have been performed using GASSIAN 09. In addition, the symmetry adapted perturbation theory (SAPT) calculations with the same basis set were also performed on the most stable configuration ($\theta=90^\circ$) of each complex for comparing with the CCSD(T) results.

Result and discussion:

The calculated points on the CS₂-rare gas PES were fitted globally to an analytical model potential.^[4,5] Fig1 shows comparison between the calculated potential and the results obtained from the global fitting for Ar-CS₂ complex. The values of the isotropic dipole-dipole (C₆) and dipole-quadrupole dispersion (C₈) coefficients of each complex were obtained from its calculated CCSD(T) potential energy surface.

We have also calculated the B_{12} of each complex (Fig 2) from its calculated angle-dependent potential.

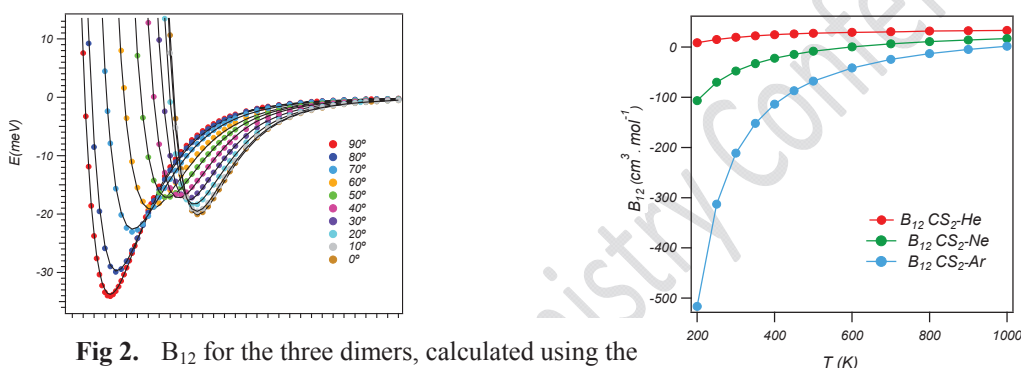


Fig 2. B_{12} for the three dimers, calculated using the

potential energy of CS₂-Ar

solid lines represent the fit.

computed potential energy surfaces in this work.

The calculated potential of the most stable configuration ($\theta=0^\circ, 90^\circ$) of each complex was used in the LEVEL 8.0 program to determine the vibrational energy levels and the spectroscopic constants.

Table 1. The spectroscopic parameters (vibrational frequency, unharmonicity) for the He, Ne and Ar- CS₂ complexes (T-shape and linear geometry) calculated in this work.

	Ar-CS ₂ ($\theta=90^\circ$)	Ar-CS ₂ ($\theta=0^\circ$)	Ne-CS ₂ ($\theta=90^\circ$)	Ne-CS ₂ ($\theta=0^\circ$)
ω_e (cm ⁻¹)	39.465	31.554	32.894	27.323
$\omega_e x_e$	1.3637	1.5452	2.8442	2.4872
$\omega_e y_e$	-0.025106	-0.03044	0.01227	-0.1233
$\omega_e z_e$	0.001453	0.0027896	0.0020424	-

Conclusion:

In this work, the potential energy surfaces of the He-CS₂, Ne-CS₂ and Ar-CS₂ van der Waals complexes were calculated applying CCSD(T)/aug-cc-pVDZ-333211 level of theory. Finally



B₁₂ for each complex, vibrational levels and the spectroscopic constants of the most stable configuration were calculated by using of LEVEL 8.0 program.

Reference:

- [1] J. E. Dove, H. Hilppler, J. Chem. Phys. 1985, 82, 1907.
- [2] M. Heymann, H. Hippler, H. J. Plach, J. Troe, J. Chem. Phys. 1987, 87, 3867.
- [3] M. Bruhel, G. C. Schatz, J. Phys. Chem 1988, 92, 7223.
- [4] R. Bukowski, J. Sadlej, P. Jankowski, K. Szalewicz, S. A. Kucharski, H. L. Williams, B. M. Rice, J chem phys 1999, 110, 3785.
- [5] G. Murdachaew, A. Misquitta, R. Bukowski, K. Szalewicz, J chem phys 2001, 114, 764.



Effect of copper oxide formation on the kinetics and mechanism of oxygen reduction reaction on copper

A. Arab^{a*}, F. Gopal^b

^aDepartment of Physical Chemistry, Faculty of Chemistry, Semnan University, Semnan, Iran

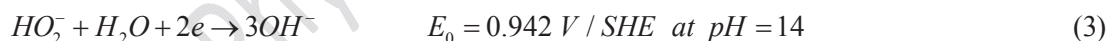
^bDepartment of Chemistry, Sharif University of Technology, Tehran, Iran

Email: r.arab2010@gmail.com

Keywords: Oxygen reduction, Copper, Copper oxide, Alkaline solution, Cyclic Voltammetry

Introduction:

Oxygen Reduction Reaction (ORR) has become one of the most extensively studied electrochemical reactions due to interest for the development of polymer electrolyte fuel cells [1]. In aqueous alkaline solutions, oxygen reduction is a multi-electron reaction that may proceed according to different pathways (Eqs. 1-3)



The situation becomes more complicated if the electrocatalyst happens to be non-noble transition metals where the formation and involvement of the oxide layers even further complicate the mechanism [2, 3]. In this work ORR was studied on copper in 1M NaOH solution in a wide range of potential and effect of copper oxide formation has been investigated on the kinetics and mechanism of ORR.

Materials and methods:

Sodium hydroxide used in this work was analytical grade Merck product and oxygen was 99.9% pure provided by a local supplier. Water was deionized and distilled and subsequently de-oxygenated by purging with nitrogen (99.99%). Cylindrical copper of 99.99% purity was placed in Teflon holder exposing circular areas of 0.283 cm². Experiments were conducted in a conventional thermostated three electrode cell with copper forming the working electrode. Its potential was monitored against a glass frit separated SCE and a large platinum plate forming the counter electrode. The cell was powered by a VoltaLab PGZ100 Potentiostat/Galvanostat run by a PC through its commercial software's.

Results and discussion:

Fig. 1 shows current-potential curves for ORR on copper in O₂ saturated 1M NaOH solution at 27 °C obtained over a range of rotation rates (200–1000 rpm) where 5 minutes time delay at open circuit potential employed between voltammograms. The kinetic analysis of curves has been carried out using the Koutecky-Levich Eq.

$$\frac{1}{j} = \frac{1}{nFkC_{O_2}} + \frac{1}{0.62nFD_{O_2}^{2/3} \nu^{-1/6} C_{O_2} \omega^{1/2}} \quad (4)$$

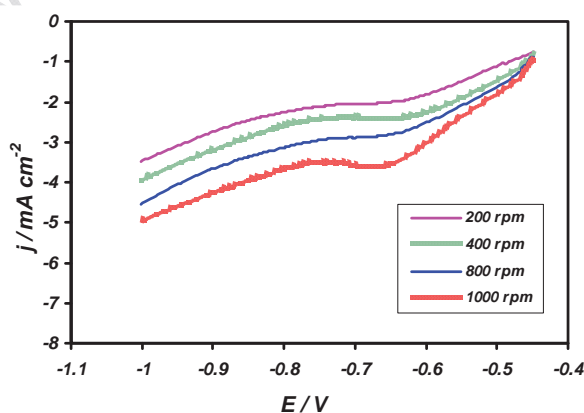




Fig. 1. Current-potential curves for ORR on copper rotating-disc electrode in O₂ saturated 1M NaOH solution at 27 °C with 5 minutes time delay at open circuit potential between consecutive cycles. Potential sweep rate is 40 mV/s.

Conclusions:

On the basis of the experimental findings it is concluded that direct oxygen reduction is accompanied by the electrochemical reductions of copper oxides which formed during time delay at open circuit potential. The number of electrons transferred per O₂ molecule obtained on different copper surface is close to 4 on oxide free copper surface and gradually decreases to 2 when the oxide layers cover the copper surface. Also calculation of rate constant of oxygen reduction on copper surface, demonstrated a faster kinetic of reaction on oxide free surface of copper.

References:

- [1] J. Uribe-Godinez, R.H. Castellanos, E. Borja-Arco, A. Altamirano-Gutierrez, O. Jimenez-Sandoval, J. Power Sources 177 (2008) 286.
- [2] M. Vazquez, S.R. de Sanchez, E.J. Calvo, D.J. Schiffrin, J. Electroanal. Chem. 374 (1994) 189.
- [3] E.J. Calvo, D.J. Schiffrin, J. Electroanal. Chem. 243(1988)171.



Electrochemical conversion of carbon dioxide to valuable products

Ahmad Rouhollahi^{a*}, Fazel Ghahramanifard^a

^a Department of Chemistry, Faculty of Sciences, K.N. Toosi University of Technology, Tehran, Iran

Email: rouhollahi@kntu.ac.ir

Key word: Carbon dioxide, Electrocatalyst, Overpotential, Cyclic voltametry

Introduction:

Carbon dioxide is now known to be a major cause of global warming because it is the largest contributor to the green house effect. According to National Oceanic and Atmospheric Administration (NOAA), atmospheric concentrations of CO₂ increase each year by about 2 ppm [1]. Photosynthesis, photocatalytic and electrochemical reduction of CO₂ seem to be three of the most effective methods for the processing and recovery of the air carbon based sources. Since CO₂ is the most stable and the most oxidized state of carbon, the transformation of CO₂ to other compounds is fundamentally an energy requiring reduction process [2]. Direct electrochemical reduction of CO₂ on various bare metallic electrodes requires large overpotentials (more negative than -2 V vs saturated calomel electrode) [3]. It is therefore important to search for active electrocatalysts which can mediate electrochemical reduction of CO₂ at lower potentials. Numerous transition-metal (mainly Co and Ni) complexes, such as macrocyclic cobalt or nickel, cobalt phthalocyanine (CoPc), or porphyrin, have been reported to have such catalytic effects[3].

In this study, the electrochemical reduction of carbon dioxide by Cobalt-dimethylglyoxime complex [Co(DMG)₂ClPy] in acetonitrile solvent investigated.

Materials and methods:

All chemicals were analytical grade reagents and were purchased from Merck. Purity of nitrogen and carbon dioxide was % 99/999. The Co(DMG)₂ClPy solution was 1mM and 0.1M of tetrabutylammonium perchlorate used for electrolyte salt.

Apparatus:

Electrochemical studies were carried out using an Autolab potentiostat (PGSTAT30). A conventional three-electrode cell was used, comprising Ag⁺/AgCl wire as the reference electrode, a graphite rod as the counter electrode and glassy carbon (5mm in diameter) as the working electrode.

Result and discussion:

As shown in figure (1-B), CO₂ reduction was performed at a constant potential -1.6 V (vs Ag/AgCl) at Cobalt-dimethyleglyoxime complex in the CO₂-saturated solution. In non-aqueous medium, carbon monoxide, oxalic acid and formic acid were mainly produced from CO₂ reduction [4]. Valuable substance can produced by adding an proton source in solution by following equations (1-4):



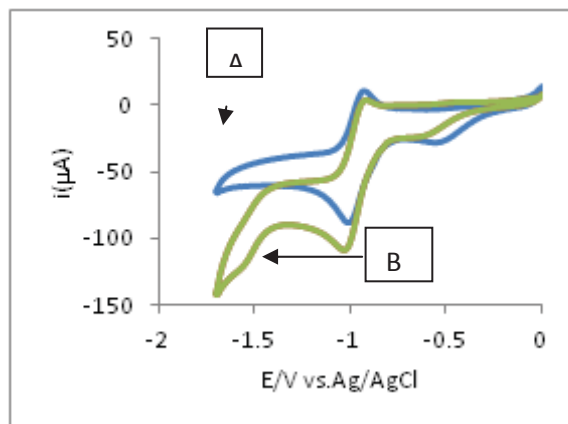


Figure 1. CVs of Co(DMG)₂ClPy (1mM) under N₂ (A) and CO₂ (B). Scan rate: 100mv/s. Supporting electrolyte: TBAP (0.1M) in acetonitrile

Conclusion:

The electrochemical reduction of CO₂ into useful substances can be achieved using an appropriate electrocatalyst which lower over potential of CO₂ reduction process. We have successfully used cobalt complex for the catalytic reduction of CO₂ in an ACN-based electrolyte in positive potential than standard potential reduction of CO₂.

Reference:

- [1] J. Edward and et al.; "What to Do with CO₂"; J. Phys. Chem. Lett; 1,3478-3479,2010.
- [2] Zh. Bian and et al. ; "Electrocatalytic reduction of carbon dioxide by a polymeric film of rhenium tricarbonyl dipyridylamine"; Polyhedron; 32,78-85, 2012.
- [3] A. Zhang and et al. ; "Electrocatalytic Reduction of Carbon Dioxide by Cobalt-Phthalocyanine-Incorporated Polypyrrole"; Electrochemical and Solid-State Letters; 12 (8), E17-E19,2009.
- [4] Maria Jitaru.; "Electrochemical carbon dioxide reduction-fundamental and applied topic", Journal of the University of Chemical Technology and Metallurgy; 42,4,2007.



Study of Platinum loading effect on performance of GDE for Glucose Oxidation

RasolAbdullahMirzaie^{1*}, Mohammad Safih Rahmanifar², Yekta Majidifard³

¹Fuel cell research laboratory, Dept. of chemistry ShahidRajaei teacher training university, Tehran,

Iranra.mirzaei@srttu.edu

²Dept. of chemistry, Faculty of science, shaheduniversity, Tehran, Iran

Email:ra.mirzaei@srttu.edu

Key words: GDE, Glucose fuel cell, Electro-Oxidation, Pt. Catalyst

Introduction:

Glucose is most abundantly found monosaccharide in nature and complete oxidation of glucose produces very high energy (-2.87×10^6 J/mole). To derive useful energy from glucose, direct conversion of chemical energy to electrical energy is the best option. In electrode preparation for glucose oxidation, different parameters such as catalyst loading [1-3], metal percentage [1], are influencing on electrode performance. In this paper effect of different loading of metal catalyst on glucose oxidation was studied.

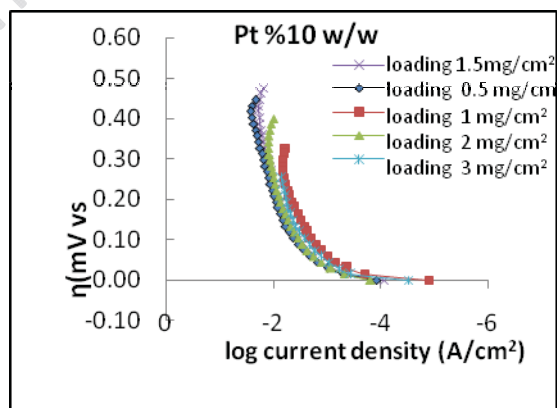
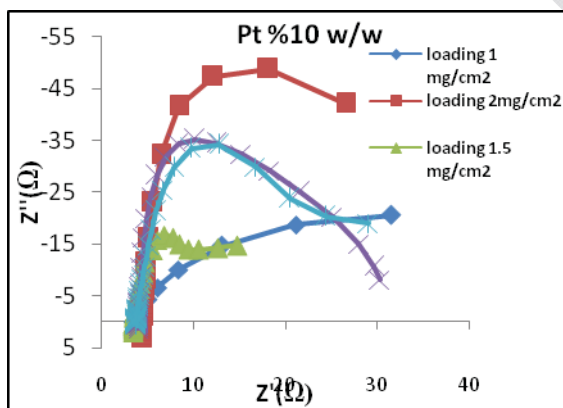
Experimental

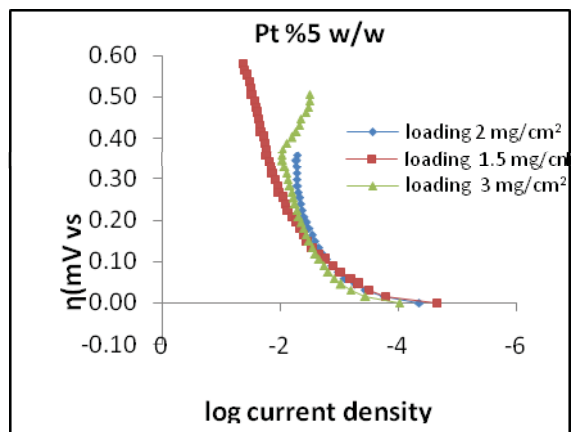
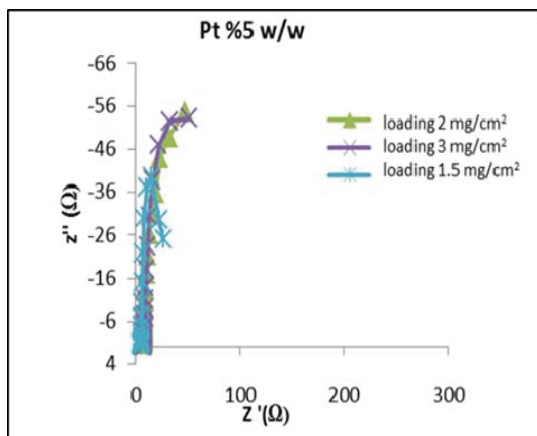
Two electrodes were prepared by immobilizing platinum on Vulcan with Pt/Vulcan ratio 5% and 10%. An aqueous solution of K_2PtCl_6 was prepared and glucose, as protecting agent, and Vulcan were added. A freshly prepared $NaBH_4$ solution was added drop wise under vigorous stirring condition and a black colloidal dispersion obtained. Then electro catalyst was

prepared by mixing catalyst, distilled water, Isopropyl alcohol and PTFE. After electrocatalyst preparation, it was coated on Carbon paper. The electrochemical experiments were performed in a three-electrode cell arrangement. A platinum sheet was used as counter electrode, while all potentials were measured with respect to Ag/AgCl electrode. Electrochemical experiments were carried out using Zahner Electrochemical systems.

Results:

The electro catalytic performance of the electrode was investigated by Cyclic Voltammetry (C.V) and electrochemical Impedance Spectroscopy (E.I.S), Linear Sweep Voltammetry (L.S.V) respectively. The result indicated that pt10%/Vulcan (loading 1.5 mg/cm²) a good electro catalytic activity toward the oxidation of glucose. Compared to the pt 5%/Vulcan (loading 0.5, 1 mg/ cm²), which displayed a low activity for glucose oxidation





Conclusion:

The Pt 10%/Vulcan (loading 1.5 mg/cm²) is the best electro catalytic activity toward the oxidation of glucose.

Reference:

- [1] Debika Basu, Suddhasatwa Basu, "Synthesis and characterization of Pt-Au/C catalyst for glucose electro-oxidation for the application in direct glucose fuel cell", *Int. J. hydrogen energy*, 36, 14923 -14929 (2011).
- [2] Popovic KD, Tripkovic AV, Adzic RR. "Oxidation of D-glucose in single-crystal platinum electrodes; a mechanistic study" *J. Electroanal Chem.*, 339:227-45 (1992)
- [3] Paul Wilde C, Zhang M, "Oxidation of glucose at electrodeposited platinum electrodes in alkaline solution" *J. Chem Soc Faraday Trans*, 89(2):385-9 (1993).



Effect of Activation Procedures on the Performance of H₂/ Air Proton Exchange Membrane Fuel Cell (PEMFC)

Somayeh Majidi^{a*}, Mohammad Zhiani^a

^aChemistry Faculty, Isfahan University of Technology, Iran

Email: s.majidi@ch.iut.ac.ir

Key words: Proton exchange membrane fuel cell, Activation procedure, Polarization curve, Electrochemical Impedance Spectroscopy.

Introduction:

A newly fabricated polymer electrolyte membrane (PEM) fuel cell usually needs a activation period to be activated and reach its best performance [1]. Activation procedures could be understood as all the actions that can bring the MEA to its highest and stabilized performance. Many different activation protocols developed base on continues, pulse and cycling of the potential or current. The US Fuel Cell Council (USFCC) has established cell activation protocols to standardize the process [2].

In this work two conditioning procedures to condition PEM cells, such as constant voltage 0.6V and USFCC protocol were applied to two PEM cells. The performances of activated cells were studied based on polarization curves and impedance spectroscopy. Results showed that selection of MEA activation procedure is important in H₂/air PEMFC and constant voltage procedure 0.6V produce better performance than another.

Material and methods:

In this study two similar MEAs were used. The MEAs were prepared with a Nafion membrane sandwiched between two electrodes. Both anode and cathode platinum load was 0.38 mg cm^{-2} . All tests were conducted on Scribner test station (model 850 C).

Two activation procedures, constant voltage 0.6 V and USFCC protocol were used. After activation process at 75°C , ambient pressure and H_2/air gas feed mode polarization curve, and EIS experiments were performed.

Results and discussion:

Fig. 1a show polarization curves of activated MEAs by constant voltage 0.6V and USFCC protocol.

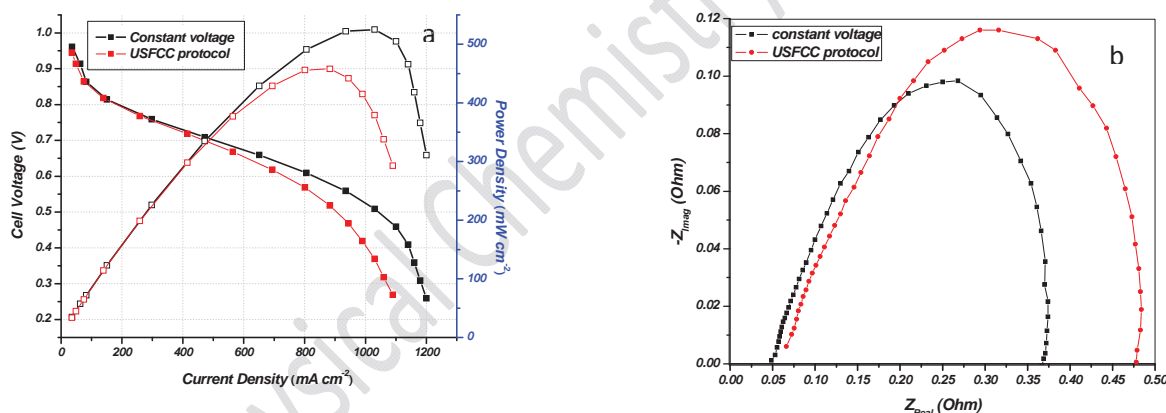


Fig 1: Polarization curve (a) and EIS spectra at 0.7V (b) of activated cells by constant voltage 0.6V and USFCC protocol at 75°C .

The results show MEAs activated by constant voltage 0.6V have the better performance than another. Fig. 1b depicts the impedance spectra for PEM fuel cells in Nyquist form at 0.7V.



In impedance spectra at 0.7V, there is only one semicircle at high frequency, reflecting the kinetics of oxygen reduction reaction [3]. The diameter of the arc for activated cell by constant voltage is lower than that of activated cell by USFCC procedure.

Fig. 1b also show the intersection of the imaginary impedance with the real impedance at high frequencies of the activated cell by constant voltage 0.6V toward another cell shifts to the right, so, it can be concluded that ohmic resistance of the MEA activated by USFCC protocol is higher than that of another MEA.

Conclusion:

In house MEAs were on-line activated using constant voltage at 0.6V and USFCC activation protocol. This process was studied by I-Vs polarization curves and impedance spectroscopy. Results showed that selection of MEA activation procedure is very important in H₂/air PEMFC. Indeed conditioning by constant voltage procedure at 0.6 V is an effective method compared to USFCC activation protocols.

References:

- [1] Z. Xu, Z. Qi, C. He, A. Kaufman, J. Power Sources 156 (2006) 315–320.
- [2] USFCC single cell test protocol. Available from: <http://www.fcchea.org/>
- [3] Jinfeng Wu, Xiao Zi Yuan, Haijiang Wang, Mauricio Blanco, Jonathan J. Martin, JiuJun Zhang, Int. J. Hydrogen energy 33 (2008) 1735 – 1746



Catalytic Decomposition of Natural Gas into the Carbon and Hydrogen

S. Hosein Mousavipour* , Maryam Shahamat, Samad Amini and peyman Khanipour

Department of Chemistry, College of Sciences, Shiraz University, Shiraz, Iran

*Corresponding Author: phone 0711-2284822, FAX 0711-6137443, mousavi@susc.ac.ir

Keywords: Natural Gas, Hydrogen Formation, Catalyst, Nickel

Introduction:

One of the major troubles caused by the activity of human beings in modern societies is the increasing rate of global warming that can be linked to increase in the concentration of greenhouse gases in the atmosphere. Many attempts have been made to reduce this rate. One of the optimistic options that being explored for reductions in anthropogenic greenhouse gases emissions is using hydrogen as fuel instead of gasoline or natural gas. Different methods are being explored and suggested for overcoming to this problem, while the economic issue is one of the major concerns. About 50 percent of the world's hydrogen is extracted from natural gas, with about 40 percent coming from steam methane reforming that its cost is relatively high.[1] The electrical spark or arc discharge methods or using catalyst to decompose natural gas into the heavier hydrocarbons, carbon, and molecular hydrogen is suggested, up to date. Here we are reporting the results of some experiments that different catalysts were used to decompose the natural gas components into the carbon and hydrogen.

Experimental:



All the experiments were carried out in flow system consists of a one meter tabular quartz reactor similar to those used previously in this laboratory.[2] The catalysts were placed in the tabular quartz reactor and a 43-cm-long section of the reactor was heated by a resistive furnace. The reactor temperature was controlled by a platinum/platinum-13%-rhodium thermocouple. The pressure in the reactor and also the flow rate of the reactants over the catalysts were controlled by BD/26.600G pressure transducer and two needle valves at the entrance and exit of the reactor. To analyze the products of the reactions, two GCs with flame ionization detector (Shimadzu GC-8A) and thermal conductivity detector (PYE Unicam 204) along with a 3 meter long silica gel column were used. A six-way gas sampling valve was used to take samples of a 3 cm³ sample loop into the gas chromatographs for analyzing.

Results:

Different experiments were carried out to determine the percentage of the reaction that takes place on the surfaces of different catalysts. At first, some experiments were carried out at the temperature range of 900K to 1000K and pressure range of 300 to 400 Torr, to determine the amount of the natural gas, pure methane, or pure ethylene that decomposes in the absence of the catalysts. Then the experiments were repeated at lower temperatures (800K to 900K) in the presence of the catalyst and the same range of pressure. The results show an increase in the decomposition rate of ethylene by ~50-65 percent in the presence of catalysts. The effect of different catalysts like Ni-SiO₂ and honeycomb form of metal nickel on the decomposition of the above mentioned reactants was investigated.[3,4] The results of one of the experiments in the presence of Ni-SiO₂ as catalyst and ethylene as reactant when the flow rate was 3.0 Torr/min are shown in Table 1. Our results indicate ~90% of ethylene decomposes into the methane, ethane, carbon, hydrogen and in some extend heavier hydrocarbons. In some other experiments, the results indicate 20% of methane is decomposed

into the carbon and hydrogen when methane is passed over the surface of catalysts. The detail of the experiments and obtained results will be discussed at the Conference.

Table 1. Concentration of the Products Produced when Ethylene Gas is Passed over Ni-SiO₂ Catalyst at 848 K and ~501 Torr.

Reactant	Blank concentration (mol/L)	Reaction mixture (mol/L)
[Methane]	0.0	9.48×10^{-6}
[Ethane]	0.0	2.79×10^{-6}
[ethylene]	1.7×10^{-4}	4.5×10^{-6}

Reference:

- [1] Boutot, T.; Liu, Z.; Whidden, T. K.; Yang, Y. *Procc. Hydrogen and Fuel Cells*, 2007.
- [2] Mousavipour, S. H.; Saheb, V.; Pirhadi, F. and Dehbozorgi M. R. *J. Iran. Chem. Soc.*, 4, 2007, 279.
- [3] Doroodmand, M. M.; Tahvildar, Z.; Sheikhi, M. H. *World Academy of Science, Engineering and Technology* 60, 2011, 779.
- [4] Ni catalyst supplied from Nano Pooshesh Felez Company, Tehran.



Rapid Photogeneration of Silver Nanoparticles in Ethanolic Solution Using a Triblock Copolymer: A Kinetic Study

Bahareh Yahyaei^a, Saeid Azizian^{*,a}

^a Department of Physical Chemistry, Faculty of Chemistry, Bu-Ali Sina University, Hamedan, Iran

E-mail address: saizizian@basu.ac.ir

Keywords: Ag nanoparticles, 2D maps, Kinetics, Nucleation, Growth, Photogeneration.

Introduction:

In recent years, synthesis and stabilization of metallic nanoparticles has been considered by many researchers, mainly due to their unique properties associated with the change from the macro- to the nanoscale [1]. Silver nanoparticles (Ag NPs) show exclusive optical, electrical, magnetic and chemical properties and strong biological activity because of their strong plasmonic absorption in the visible range and very large surface to volume ratio [2]. In the present study the synthesis of silver nanoparticles via low power UV irradiation of solution of AgNO₃ in ethanol, in presence F127 triblock copolymer (PEO_nPPO_mPEO_n) has been reported.

Experimental Section:

Silver nanoparticles were synthesized by an induced reduction under UV irradiation. A solution that was prepared by mixing the equal volume of solutions of AgNO₃ and F127 in ethanol with specified concentration was irradiated using a low power UV lamp (6W) in a quartz cuvette at different exposure time, t_e , and at 24°C.

Results and Discussion:

Kinetic of Ag NPs formation: The colour and the extent of silver nanoparticles depend on exposure time and the concentration of the ethanolic solutions of AgNO₃ and F127. To show the time dependency of silver nanoparticles formation, the solution of [AgNO₃] and [F127] with specified concentration was irradiated by UV lamp at different exposure time. The



results show that the extent of Ag NPs increases by increasing the exposure time. The dependency of the silver nanoparticles formation to the concentrations of reactants has been investigated by performing two sets of kinetic experiments. In the first set of experiments, the effect of [F127] on the Ag NPs formation was investigated at different F127 concentrations and the constant concentration of AgNO_3 . The second set of experiments was carried out at different AgNO_3 concentration but with constant concentration of F127 the results show that the extent of Ag NPs formation increases with increase in both AgNO_3 and f127 concentrations.

2D maps for probing the nucleation and growth of Ag NPs: In this study the 2D maps of the first derivative of the absorbance with respect to exposure time over the space of exposure time versus wavelength has been constructed. By using this method it has been shown that for the band at about 420 nm the switching was observed after 2 min of irradiation. The kinetic of nucleation process (up to 2 min of irradiation) have fitted with a first-order rate equation and the kinetic of growth process (after 3 min of irradiation) have been modelled with different kinetic models but the best fitting was obtained with second-order rate equation.

Conclusion:

UV irradiation of ethanolic solution of AgNO_3 in presence of F127 is a fast and facile method for high yield synthesis of silver nanoparticles. The UV-vis spectra of the formation of Ag NPs show that the extent of Ag NPs increases with increase in exposure time and also AgNO_3 and F127 concentrations. It has been shown that the 2D map technique can be used to find the switching time. The advantage of the present study in comparison with the previous works [3] is the formation of the higher extent of silver nanoparticles from the more dilute solution by using a lower power UV lamp (6W) in the short UV irradiation time.

References:

- [1] Y. Li, E. Boone, M. A. El-Sayed, Size effects of PVP-Pd nanoparticles on the catalytic Suzuki reactions in aqueous solution. *Langmuir* 18 (2002) 4921-4925.
- [2] D. Spadaro, E. Barlatta, F. Barreca, G. Currò, F. Neri, Synthesis of PMA stabilized silver nanoparticles by chemical reduction process under a two-step UV irradiation. *Appl. Surf. Sci.* 256 (2010) 3812-3816.



- [3]K. Shao, J. Yao, Preparation of silver nanoparticles via a non-template method. Mater. Lett. 60 (2006) 3826-3829.

15th Physical Chemistry Conference



The Aggregation Behavior of Dodecyl Betainate Gemini Surfactant using Viscosimetry and Dynamic Light Scattering

Hasti Aghdastinat^{a,*}, Soheila Javadian^a, Hossein Gharibi^a, Alireza Tehrani-Bagha^b

^aDepartment of Physical Chemistry, Tarbiat Modares University, Tehran, P.O. Box 14115-117, Iran

^bInstitute for Color Science and Technology, Tehran, Iran

Email: aghdastinat@gmail.com

Keywords: Cleavable Surfactant, Aggregation, Viscosity, Dynamic Light Scattering

Introduction:

Cleavable surfactants are amphiphiles in which a weak linkage has been deliberately inserted, normally, but not always, between the hydrophobic tail and the polar headgroup. The main objective behind the development of cleavable surfactants is to improve the rate of biodegradation and the rate of biodegradation has been studied for several of the surfactants [2]. pH labile linkages in surfactants result in special applications in industry and biological science such as targeting drug delivery, gene therapy and ... [3]. The viscosity of surfactant is greatly related to the size, shape and organization of micelles in solution [4]. In this article aggregation behavior of ester-containing gemini surfactant 'dodecyl betainate gemini (s=3)' which is new synthesized surfactant was investigated using viscosimetry and dynamic light scattering.

Methods:

Dynamic light scattering were performed with Malvern instrument (model ZEN3500, UK). All measurements were performed immediately after solution preparation. For each measurement, the refractive index and viscosity of the solutions were determined. The refractive index was determined using a Krüss digital refractometer model DR 201-95. Viscosity measurements were carried out using an Ubbelohde viscometer, suspended vertically in a thermostat. In order to check the reproducibility, the time of fall for every viscosity measurement was noted at least three times.



Results and Discussion:

For the first guess of shape and size of aggregations formed, different concentration of dodecyl betainate gemini ($s=3$) before and after critical micelle concentration (CMC) were prepared and viscosity was measured. It was found at concentrations higher than around 30 mM viscosity change dramatically with increasing the concentration. The effect of NaBr on viscosity was also investigated and it was found at concentration 0.5 mM the viscosity is similar to pure solutions, but at concentration NaBr=5 mM, viscosity increase dramatically. It is indicating that there is probably a phase transition from spherical micelles to cylindrical micelles. To confirm this guess, size and zeta potential of these solutions were determined with dynamic light scattering (DLS). The results of DLS show that dodecyl betainate gemini ($s=3$) form micelles around 2 nm and the addition of salt causes growing of micelles up to 12-18 nm.

Conclusions:

Addition of salt has considerable effect on aggregation behavior of dodecyl betainate gemini ($s=3$). The result of DLS confirm the result of viscosity. By tuning the concentration of surfactant and also the salt we can determined the conditions that a phase transition occur. This phenomenon makes this cleavable surfactant interesting for applications such as targeting drug delivery.

References:

- [1] C.A. Overkempe, A. Annerling, C.G. van Ginkel, P.C. Thomas, D. Boltersdorf, J. Speelman, Esterquats, in: K. Holmberg (Ed.), Novel Surfactants, vol. 114, Dekker, New York, 2003, chap. 11
- [2] Tehrani-Bagha AR, Holmberg H, "Cationic ester-containing gemini surfactants: Chemical hydrolysis and biodegradation", Current Opinion in Colloid & Interface Science 12 (2007) 81–91
- [3] Lundberg D, Holmberg K, "Nuclear magnetic resonance studies on hydrolysis kinetics and micellar growth in solutions of surface-active betaine esters", J surfactants. Deterg 7 (2004) 239–46.



- [4] Lijuan Han, Hong Chen , Pingya Luo, `` Viscosity behavior of cationic gemini surfactants with long alkyl chains``, *Surface Science*, 564 (2004) 141.

15th Physical Chemistry Conference



Ruthenium Nanoparticles Supported on the Periodic Mesoporous Organosilica as Highly Effective and Recyclable Catalyst for the Aerobic Oxidation of Alcohols

Babak Karimi*^a, Omolbanin Yari^a, Mojtaba Khorasani^a, Dawood Elhamifar^b

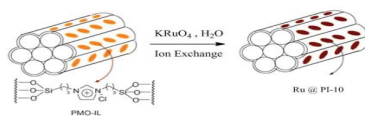
^aDepartment of Chemistry, Institute for Advanced Studies in Basic Sciences (IASBS), PO-Box 45195-1159,
Gavazang, Zanjan 45137-6731, Iran

^bDepartment of Chemistry, Yasouj University, Yasouj, 75918-74831, Iran

Keywords: Supported ionic liquids • mesoporous materials • periodic
mesoporous organosilicas (PMOs) • Functional PMOs

Abstract:

The periodic mesoporous organosilica is built from bridge organosilanes of type $(R'O)_3Si-R-Si(OR')_3$ wherein organic groups R, are homogeneously distributed throughout the stable inorganic framework [1-2]. Very recently, we have demonstrated for the first time that an ionic liquid based periodic mesoporous organosilica (PMO-IL, scheme 1) is an effective and powerful support for the immobilization and stabilization of Pd nanoparticles on the Suzuki-coupling reaction in water [3], and the aerobic oxidation of alcohols [4]. We have also investigated the use these materials in order to immobilize $Yb(OTf)_3$ -pypox catalyst system in the enantioselective Strecker reaction of imines with trimethylsilyl cyanide (TMSCN) to afford the corresponding chiral α -aminonitriles [5]. In continuation of this study, herein, we wish to disclose that a novel ruthenium-supported catalyst comprising PMO-IL material (Ru@PMO-IL) is a highly efficient catalyst for the selective oxidation of a wide variety of alcohols, including not only benzylic and allylic, but also alicyclic and aliphatic alcohols in the presence of molecular oxygen/ or air as the oxidant.



Referemces:

- [1] Asefa, T.; MacLachlan, M. J.; Coombs, N.; Ozin, G. A. *Nature* 1999, 402, 867.
- [2] Inagaki, S.; Guan, S.; Fukushima, Y.; Ohsuna, T.; Terasaki, O. *J. Am. Chem. Soc.* 1999, 121, 9611.
- [3] Karimi, B.; Elhamifar, D.; Clark, J. H.; Hunt, A.J. *Chem. Eur. J.* 2010, 16, 8047.
- [4] Karimi, B.; Elhamifar, D.; Clark, J. H.; Hunt, A. J. *Org. Biomol. Chem*, 2011, 9, 7420.
- [5] Karimi, B.; Maleki, A.; Elhamifar, D.; Clark, J. H.; Hunt, A. J. *Chem. Commun.* 2010, 46, 6947.



Scratch Resistant Sol-Gel based Nanocomposite Films on Polycarbonate:

DMTA, Small Angle X-ray Scattering and FTIR Studies

H. Yahyaei. ^{a*}, M.Mohseni^a, S.Bastani ^b

^a Department of Polymer Engineering and Color Technology, Amirkabir University of Technology,
Tehran, Iran, P.O.Box 15875-4413

^b Institute for Colorants, Paint and Coatings, Tehran, Iran

Email: yahyaei@aut.ac.ir

Key words: Sol-gel, Nanocomposite, Polycarbonate, Hybrids

Introduction:

Organic-inorganic hybrid materials are the most attractive compounds for coatings due to the combined properties of organic polymers such as processability, flexibility, low density and those of inorganic materials such as thermal stability and high hardness. The properties of nanocomposites are dependent on the size and shape of dispersed phase as well as interaction of two phases. Compatibility and interaction of two phases govern optical and mechanical properties. Inorganic nanoparticles can be dispersed in organic matrix physically. Alternatively they can be connected to the matrix with strong bonds. In the mean time connection of two phases with covalent bond is the most favorable method. In sol-gel process a network former such as tetraethyl orthosilicate (TEOS) take apart in the hydrolysis and condensation reactions and form inorganic network. An organoalkoxide can play the role of coupling agent and connect inorganic network to the organic one. Sol-gel type hybrid coatings provide several advantages such as : i) low temperature synthesis while yielding highly pure homogenous metal oxide materials., ii) low toxic solvent is used iii) desirable size and shapes can be obtained and iv) it is possible to have coating with high inorganic content.

Polycarbonate is a thermoplastic engineering polymer that has good properties such as high transparency, low density and high toughness. But low hardness causes PC to lose transparency when scratched. In plastic coating such as polycarbonate increasing of



temperature higher than T_g leads to curvature. Therefore, UV curable organic resins can be a good alternative. UV curable resins such as urethaneacrylate can create properties of organic coatings such as flexibility and barrier properties. The energy of UV irradiation can cure organic part and in the same time condense the sol-gel part.

The aim of this work is the study of the role of coupling agents on the structure and morphology of silica phase. The effect of this morphology on the mechanical properties of hybrid coatings used for PC has been discussed.

Materials and methods:

Tetraethyl orthosilicate (TEOS) from Wacker was used as the inorganic network former. 3-methacryloxy propyl trimethoxy silane (MEMO) supplied by Degussa was used as the network modifier. Both precursors were used as received without any purification. The organic part of the network contained urethane acrylate oligomer and acrylic monomers purchased from Cytec (Netherlands). An amine type co-photoinitiator and photoinitiator were supplied by Merck. Hydrochloric acid (37%) and ethanol were also provided by Merck.

Apparatus:

A Bruker FT-IR spectrophotometer with a resolution of 4 cm^{-1} was used to study the chemical structures of hybrid coatings. SAXS measurements were performed on a PW1700 x-ray scattering instrument using a copper radiation with $\lambda = 0.154\text{ nm}$ and pinhole collimation of the incident beam. Dynamic mechanical thermal analysis was carried out by means of a Tritec2000. Nano scratch test performed by using triboscopy apparatus.

Result and discussion:

Storage modulus is indication of the strength of materials against deformation in different temperature under oscillation forces [1]. Therefore, higher storage modulus means that coating can resist deformation. Increasing TEOS: MEMO ratio increases storage modulus. This can be attributed to a more compacted structure of silica phase in high TEOS:MEMO ratio that can create stronger structures. The Guinier and Porod plots of SAXS data for the hybrids showed a linear region, the R_g and D obtained from the slopes of the curves are listed in Table 1. Results show that by increasing in TEOS/MEMO mass fractal dimension increased that confirmed more compact structure of inorganic nanodomains[2]. Also, more

compact structures have smaller size. these facts, causes that these structures show higher mechanical and thermal properties such as elastic modulus and T_g . FTIR spectra confirmed SAXS data and a peak at 560 cm^{-1} that have been attributed to structural defect in silica network, appear when TEOS/MEMO decrease. Scratch test showed that increasing in elastic modulus increase scratch resistance of coatings.

Table 1. Gyration radius and fractal dimension of the hybrids coatings.

samples	Mass fractal dimension (D_m)	Gyration radius R_g (nm)
T ₂₀ I ₅₀	1.1	29
T ₅₀ I ₅₀	1.24	24.34
T ₈₀ I ₅₀	1.56	17.8

Conclusion:

Incorporation of nanosilica phase into organic phase can improve thermal and mechanical properties of coatings. Morphology of hybrid coating plays a crucial role in determination of nanocomposites. Coupling agent can compatibilize organic and inorganic phases but must be used in appropriate levels.

Reference:

- [1] M. Scandola. ;"Study of Organic Phase Mobility in Nanocomposite Organic-Inorganic Coatings" Macromol. Chem. Phys, 207, 864–869, 2006.
- [2] Limin Wu.; "Study on acrylic resin/titania organic–inorganic hybrid materials prepared by the sol–gel process";polymer;45,2967-2976,2004.



Nanoemulsion and Microemulsion Formulation for the Solubility Enhancement of valsartan

S. Najafabadyfarahani^a, A. Salabat^a

^aDepartment of Chemistry, University of Arak, Arak, Iran, P.O. Box 38156 – 879

E-mail: najafabadyfarahany@gmail.com

Key words: Nanoemulsion ,Solubility , Valsartan, Microemulsion

Introduction:

Valsartan drug used orally for the treatment of hypertension, exhibits a low bioavailability (23%), probably related to its poor water solubility. According to the Biopharmaceutical Classification Scheme, Valsartan is a water-insoluble, lipophilic and highly permeable compound. Therefore, it is possible to improve the Valsartan bioavailability by increasing its apparent solubility in water through Nanoemulsion and Microemulsion [1, 2]. The aim of this study is to design and develop Nanoemulsion and Microemulsion of Valsartan for enhancing its solubility, hence the oral bioavailability.

Materials and methods:

In this research work, first of all the In order to formulation of Nanoemulsion and Microemulsion system in water, the Ipm as oil phase, Tween 80 as surfactant, and Isobutanol as co-surfactant were selected. For this system Pseudo-ternary phase diagrams was constructed to identify the Nanoemulsion and Microemulsion existing zone (Fig1-b). Microemulsion was prepared by water titration method. Required quantity of Tween 80, Isobutanol, IPM by distilled water with continuous stirring until a transparent and homogenous Microemulsion is produced.

Nanoemulsions were prepared by a homogenization-sonication technique [3] by gradual addition of the aqueous phase to the oil phase. Rapidly using a magnetic stirrer and followed by bath sonication to yield the Nanoemulsion.

an excess amount of Valsartan was added to Microemulsion and Nanoemulsion formulation then shaken for 12h at 500 rpm and the supernatant layer was separated and subjected to centrifugation at 3,000 rpm for 15 min in order to remove the undissolved drug. Concentration of Valsartan in the samples was quantified spectrophotometrically in a UV-visible Spectrophotometer.

Result and discussion:

From the ternary phase diagrams shown in Figure 1, it was concluded that highest Microemulsion zone was achieved for the systems with 2.4:1 ratio of Tween 80: Isobutanol. The obtained data confirm enhanced solubility of Valsartan in optimized Nanoemulsion and Microemulsion as compared to its respective individual ingredients.

Conclusion:

Nanoemulsion and Microemulsion technique with proposed formulation led to improvement in Valsartan availability, suggesting the potential for technique's use as a topical vehicle for Valsartan delivery.

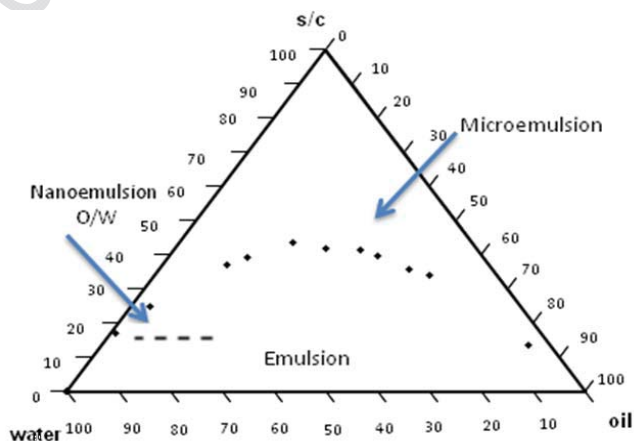


Fig. 1.a) Picture of a Nanoemulsion (left) and a Macroemulsion (right); **b)** Pseudo-ternary phase diagrams for IPM, Tween 80/ Isobutanol ratio of 2.4/1, Water



References:

- [1] Anton, N.; Vandamme, T. F. Nano-emulsions and micro-emulsions: clarifications of the critical differences. *Pharm. Res.* 2011, 28 (5), 978–985.
- [2] Gutiérrez, J. M., González, C., Maestro, A., Solè, I., Pey, C. M., & Nolla, J.. Nano-emulsions: New applications and optimization of their preparation. *Current Opinion in Colloid & Interface Science*, (2008), 13(4), 245–251.
- [3] Vyas, T. K.; Shahiwala, A.; Amiji, M. M. Improved oral bioavailability and brain transport of Saquinavir upon administration in novel nanoemulsion formulations. *Int. J. Pharm.* 2008, 347 (1_2), 93–101.



Nonequilibrium electronic transport properties of Diphenyl ethynylene:

Effect of anchoring groups

S. Jalili, M. Soleymani*

Department of Chemistry, Faculty of Science, K.N. Toosi University of Technology, Tehran, Iran

E-mail: Soleymani.maryam734@gmail.com

Keywords: Non-equilibrium Green's function, Rectifying effect, NDR behavior.

Introduction:

Over the past decade, molecular devices have received significant attention owing to their great potential applications in atomic-scale circuits. Many interesting physical properties have been predicted theoretically and verified experimentally, such as negative differential resistance (NDR), molecular rectification, and field-effect characteristics, etc [1]. One extensively employed method for theoretical study of molecular junction is based on density functional theory combined with non-equilibrium Green's Function technique (NEGF-DFT). Molecular junction is an open, semi-infinite, non-periodic, non-equilibrium system [2]. To get the molecular rectification, the electron donating groups and electron withdrawing groups (F, CF₃, Me, OMe, NMe₂) are placed on the different position of the Diphenyl ethynylene (DPE) molecular wire.

Computational method:

1. Geometry optimization:

In order to obtain a stable molecular structure, all models were optimized at the B3LYP level with LANL2DZ basic sets by using Gaussian03 program. Each of them was then sandwiched between two equilateral triangles of Au atoms. The geometries of the isolated molecules were extracted from the optimized extended molecules and then translated into the central region between the two Au (111)–(3×3) electrodes.

2. Electron transport calculation:

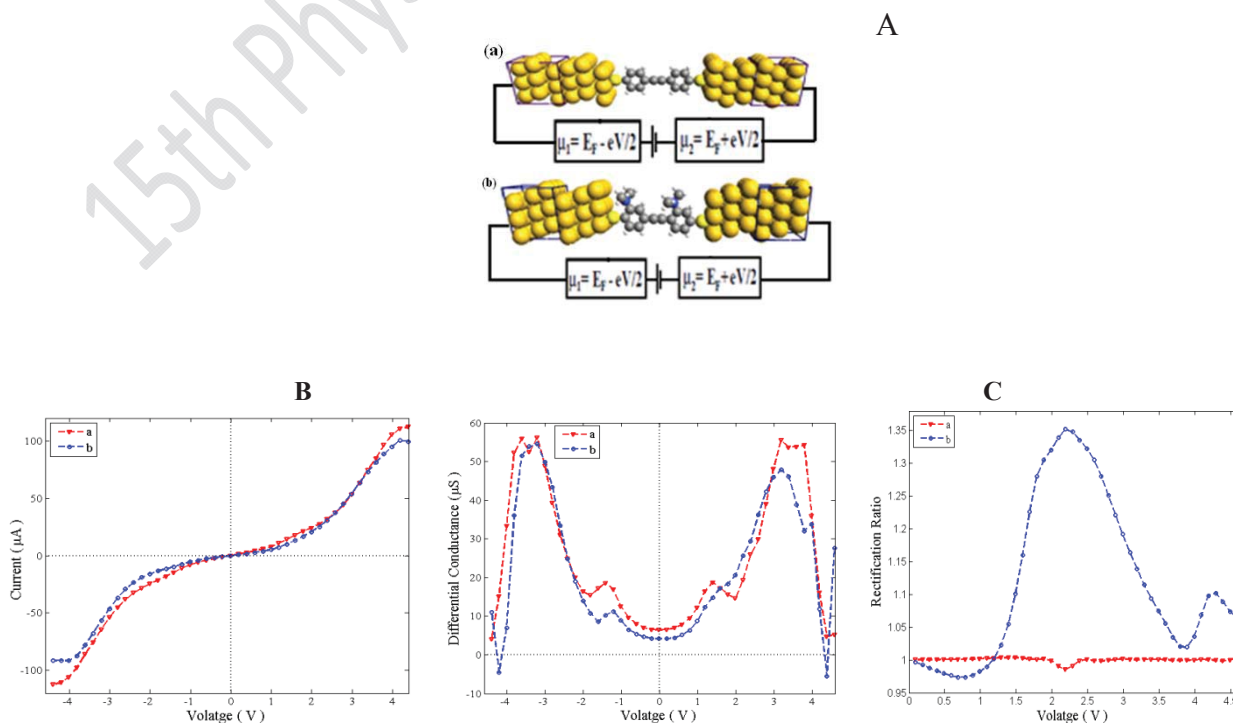
The electron transport properties of the Au/molecule/Au systems were investigated using the ATK 11.2.2 program which is based on density functional theory (DFT) combined with the first principle non-equilibrium Green's function (NEGF). The current–voltage (I – V) characteristics were obtained from the Landauer – Büttiker formula,

$$I(V_b) = \frac{2e^2}{h} \int_{\mu_L}^{\mu_R} [f(E - \mu_L) - f(E - \mu_R)] T(E, V_b) dE$$

Where $2e^2/h$ is the conductance quantum G_0 , and f is the Fermi function. μ_L , μ_R are the electrochemical potentials of the left and right electrodes, respectively: $\mu_L(V_b) = E_f - eV_b/2$ and $\mu_R(V_b) = E_f + eV_b/2$. E_f is the Fermi energy of the electrode. The energy range $[\mu_L(V_b), \mu_R(V_b)]$ contributing to the current integral was defined as the bias window. $T(E, V_b)$ is the total transmission coefficient [3].

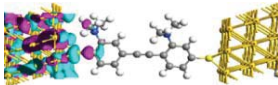
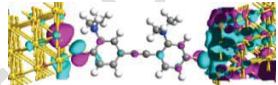


Result and discussions:

The computed electron transport properties of the two systems DPE (a) and DPE-2NMe₂ (b) are plotted in Figure 1. The results show that the anchoring group plays a crucial role in the conductivity of the molecular junctions. The current–Voltage (I – V) characteristics, conductance, rectification ratio and negative differential resistance (NDR) properties of these molecules were investigated systematically. The results were analyzed by the electronic structures of the isolated molecules, transmission coefficient, Molecular Projected Self-consistent Hamiltonian (MPSH), Partial Density Of State (PDOS) and Potential drop of the Au/molecule/Au systems.



E

Figure1. (A) illustration of junctions (a) and in the bias range V, (C) Differential (dI/dV) versus Rectification ratio applied bias defined as $R(V)$

	System (b)	
	Voltage:-4.2V	Voltage:+4.2V
MPSH	 363: -0.4973 eV	 363: -0.4775 eV
Voltage drop	Voltage:-2.2V	Voltage:-4.2V
		

Schematic molecular (b), (B) $I-V$ curves from -4.6 to $+4.6$ conductance voltage curves, (D) (R) as a function of voltage, $R(V)$ is $= |I(+V) / I(-V)|$,

(E) first row, Spatial distribution of MPSH states of molecule system (b) at ± 4.2 V bias, and second row, the change of the charge-density distribution, and potential drop across the molecule induced by applied voltages bias of -2.2 V and -4.2 V respectively. The chemical potential of the right electrode is negative and that of the left electrode is positive.

References:

- [1] S. Jalili ;H. Rafii-Tabar; "Electronic conductance through organic nanowires"; Phys. Rev. B; 71,165410, 2005.
- [2] M. Brandbyge; J-L. Mozos; P.Ordej'on; J.Taylor; K. Stokbro: "Density-functional method for non-equilibrium electron transport"; Phys. Rev. B; 65, 165401, 2002.
- [3] S. Datta; "Electronic transport in Mesoscopic Systems"; Cambridge University Press; New York; 1995.



15th Physical Chemistry Conference



Phosphonate monoesters as carboxylate-like linkers for metal organic frameworks

Simon S. Iremonger,^aJunmeiLiang,^aRamanathanVaidhyanathan,^a Isaac Martens, ^a George K. H. Shimizu,^aTomDaff,^b Mohammad ZeinAghaji,^bSaeidYeganegi,^{*b, c} and Tom K. Woob

^a Department of Chemistry, University of Calgary. Fax: (001) 403-289-9488; Tel: (001) 403-220-5347.

^b Centre for Catalysis Research and Innovation, Department of Chemistry, University of Ottawa, Fax: (001) 613-562-5170; Tel: (001) 613-562-5800 ext. 6145;

^c Department of Physical Chemistry, Faculty of Chemistry, University of Mazandaran, Babolsar, Iran.

KEYWORDS: Metal organic framework, carbon dioxide capture, enthalpy of adsorption, porous material.

Introduction

Metal-organic frameworks (MOFs) represent a new class of hybrid organic-inorganic supramolecular materials comprised of ordered networks formed from organic electron donor linkers such as carboxylates or amines and metal cations such as Zn^{+2} . [1] They can exhibit extremely high surface areas, as well as tunable pore size and functionality, and can act as hosts for a variety of guest molecules. Since their discovery, MOFs have enjoyed extensive exploring, with applications ranging from gas storage to drug delivery to sensing. [2] The topology of MOFs is intimately related to both the coordination environment favored by the metal ion and the geometry of the organic “linker” groups, which together form so-called secondary building units that establish the network symmetry. These characteristics further distinguish MOFs from other classes of porous materials, such as aerogels, which are amorphous, and ordered or partially ordered materials created from block copolymers.

Bidentate phosphonate monoesters are analogues of popular dicarboxylate linkers in MOFs, but with an alkoxy tether close to the coordinating site. Herein, we report 3-D MOF materials based upon phosphonate mono-ester linkers. Cu(1,4-benzenediphosphonate bis(monoalkylester)), CuBDPR, with an ethyl tether is nonporous; however, the methyl tether

generates an isomorphous framework that is porous and captures CO₂ with a high isosteric heat of adsorption of 45 kJ/mol.

Results

Herein, we report two new 3-D MOFs, Cu(1,4-benzenediphosphonate bis(monoalkyl ester)), CuBDPR, R = ethyl, 1; R = methyl, 2. Through a joint experimental and computational study, we demonstrate that the alkoxy tether can play a crucial role in mediating gas sorption. More generally, we show that phosphonate monoesters, like carboxylates, can strike a balance between robustness and crystallinity to form porous 3-D architectures. Compound 2 shows preferential adsorption of CO₂ over other gases and an exceptionally high ΔH_{ads} (45 kJ/mol) for CO₂.

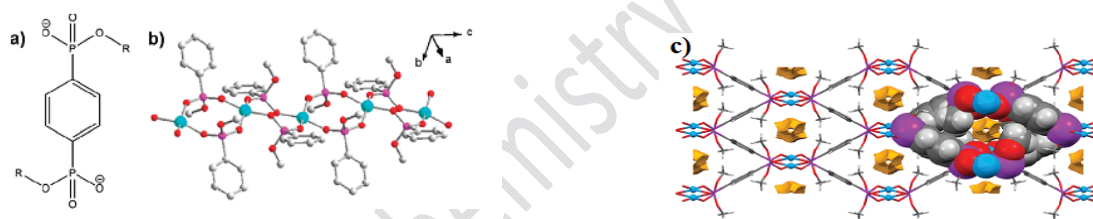


Figure 1. (a) The dianionic ligand, BDPR, where R = Et or Me. (b) Single crystal structure of one column of CuBDPMe, 2 (1 is similar), showing the bidentate coordination of the phosphonate mono-methyl ester and the 4-coordinate geometry of Cu. (c) 1-D pores in 2 with solvent accessible voids (1.2 Å probe in gold). In c, one channel is shown in a space filling representation.

Figure 1 shows the structures of both compounds 1 and 2. The crystal structure of 1 showed, formation of a 3-D network with channels. In 1, the ethyl groups of the phosphonate esters protrude into the pores restricting the aperture to ~4.5 Å. The channel walls are decorated with the ethyl groups of the ligand and the CuO₄ metal cores.

For compound 2, a modest uptake of CO₂ at ambient temperatures was observed (Figure 2), 30.9 cm³(STP)/g, 1.38 mmol/g, 6.06 wt% at 273 K and 1200 mbar. This equates to a loading of 0.45 CO₂ per Cu center. At zero loading, indicative of the highest energy sites, the ΔH_{ads} was calculated at 45 kJ/mol, a high value for a physisorptive process.

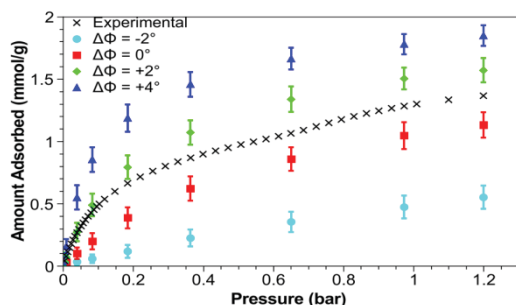
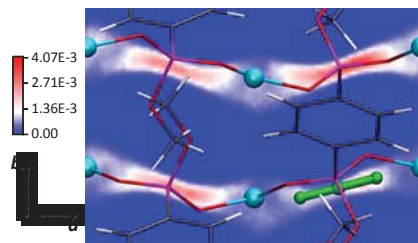


Figure 2. Comparison of experimental and simulated CO₂ adsorption isotherms at 273 K, where the geometry of the methoxy groups have been altered from the X-ray structure in silic

GCMC simulations were performed on **2** using the UFF parameters[3] and REPEAT[4] charges. The simulated isotherm using the X-ray structure of **2** is shown in Figure 2 (red) and was found to underestimate the CO₂ uptake by approximately 25% throughout the pressure range examined. Since the GCMC simulations used here to only allow for a fixed MOF framework, it was thought that this approximation may be responsible for the underestimated CO₂ uptake

All structures optimized to geometries in which the CO₂ molecules were oriented roughly perpendicular to the hypothesized end-on bridging mode. One key experimental observation supporting the lack of direct interaction of CO₂ with the Cu sites is that in the crystal structure, although the Cu centers are 4-coordinate, there is no ligated water. Figure 3 shows the CO₂ oxygen atom probability distribution resulting from a GCMC simulation at 1 atm CO₂ and 273 K. The plots show that there are four symmetrically equivalent binding sites in the unit cell. The guest molecules align along the channels with either the carbon or oxygen of the CO₂ at the midpoint between the methyl groups. The present study shows that phosphonate monoesters can balance crystallinity and permanent porosity giving a structure (**2**) accessible to CO₂ with a heat of adsorption measured as 45 kJ/mol. Moreover, the alkoxy group represents a mechanism for regulating porosity by both modifying the pore but also by potentially acting in a dynamic manner as a gate for guest diffusion. Further studies are ongoing.

a)



b)

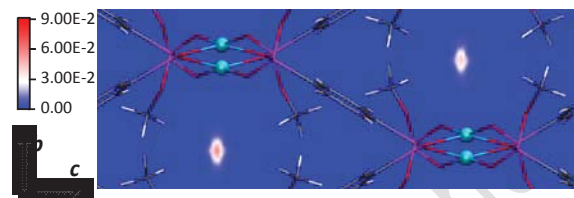


Figure 3. Probability density plots of the CO₂ oxygen atom in a unit cell of 2 at 1 bar, 273 K from simulation. In a) probabilities along the c-axis are projected onto the a-b plane while in b) probabilities along the b-axis are projected onto the b-c plane. A green CO₂ molecule is shown in a) for reference.

References

- [1] Kitagawa, S.; Matsuda, R. *Coord. Chem. Rev.* **2007** , 251, 2490.
- [2] Phan, A.; Doonan, C. J.; Uribe-Romo, F. J.; Knobler, C. B.; O'Keeffe, M.; Yaghi, O. M. *Acc. Chem. Res.* **2010** , 43 , 58.
- [3] Rappe, A. K.; Casewit, C. J.; Colwell, K. S.; Goddard, W. A., III; Skiff, W. M. *J. Am. Chem. Soc.* **1992** , 114, 10024.
- [4] Campana, C.; Mussard, B.; Woo, T. K. *J. Chem. Theory Comput.* **2009** , 5, 2866.



Local Depolarization in Hydrophobic and Hydrophilic Ionic Liquids/Water Mixtures: Car-Parrinello and Classical Molecular Dynamics Simulation

M. H. Ghatee*, A. R. Zolghadr

Department of Chemistry, Shiraz University, Shiraz 71454, Iran

(E-mail: ghatee@susc.ac.ir)

Keyword: CPMD; Hydrophobic and hydrophilic ionic liquids; Partial charges; Electrostatic screening

Introduction:

Room-temperature ionic liquids (RTILs) are salts in liquid phase [1]. The advent of the Car-Parrinello (CP) method in 1985 enabled one to use a quantum mechanical description of the electronic degrees of freedom combined with a classical phase space trajectory involving a fictitious electronic mass parameter [2]. Several *ab initio* molecular dynamics (AIMD) studies of pure IL can be found in the literature but the number of AIMD studies of IL/Water mixture is limited [3]. Seeking some details of mechanism and the extent of water miscibility of ILs with different nature we performed CPMD and Classical MD simulation calculations for pure bulk ILs and binary ILs/Water systems including hydrophobic [C₄mim][PF₆] and hydrophilic [C₄mim][BF₄] ILs.

Methods:

Car-Parrinello molecular dynamics simulations were performed with the CPMD code for neat water, pure bulk of each IL, and mixture of each with water. The general gradient-corrected density functional BP86, together with norm-conserving pseudopotentials. The electronic orbitals were expanded in a plane wave basis set with an energy cutoff of 100 Ry. All the CPMD simulations were performed using a fictitious electron mass of 800 au and at 298.15 K for 40 ps.

Results and Discussions :

CPMD approach was carried out for pure $[\text{C}_4\text{mim}]\text{PF}_6$ and $[\text{C}_4\text{mim}]\text{BF}_4$ ionic liquids and their mixtures with highly dipolar water solvent in order to study admixing mechanism as well as hydrophobic and hydrophilic interactions from an electronic point of view. First DFT results were analyzed on isolated ion pairs with various methods of assigning partial charges to the atomic centers. Next the trajectory of a 40 ps long Car-Parrinello MD were analyzed under bulk conditions. Water molecule influences the hydrophobic and hydrophilic ionic liquids to a different extent, which can be evidently probed by the atomic charges of partnering constituents (Figure 1). The reduction in simulated dipole moment of water upon admixing with hydrophilic ionic liquid is larger than with hydrophobic one, and roots from stronger electrostatic screening (Figure 2). Water molecules tend clustering when mixed with $[\text{C}_4\text{mim}]\text{PF}_6$, and upon admixing with $[\text{C}_4\text{mim}]\text{BF}_4$ they are essentially interact with anion while keeps residing on the imidazolium ring (Figures 3). The sketch of the density profiles of atoms and the spatial distribution of water and anion molecules around cation is also calculated (not shown here).

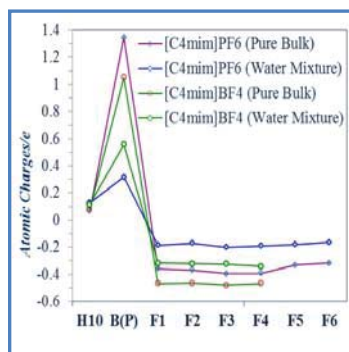


Figure 1: Comparison of ESP
(partial charges of anion)

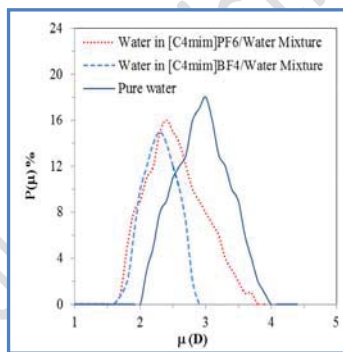


Figure 2: Simulated (CPMD)
dipole moment distribution

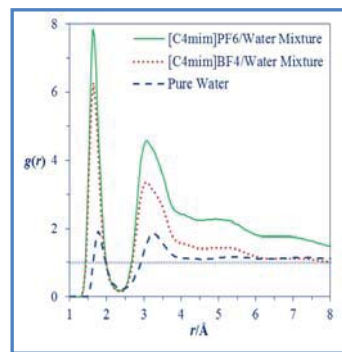


Figure 3: Comparison between
RDF of OW and HW

When mixed with water, the average charge on each F atom in BF_4^- (in PF_6^-) anion is $-0.3261e$ ($-0.1820e$). The simulated charge on each H atom of water ($0.3290e$) can be found evidently responsible for the effective $\text{H}\cdots\text{F}$ interaction in $[\text{C}_4\text{mim}]\text{BF}_4$ but ineffective in $[\text{C}_4\text{mim}]\text{PF}_6$. The fluctuation in molecular dipole moments in the CPMD ensemble of IL/Water mixture has been used to monitor the change in average dipole moment of water. These results and more detailed considerations provide insight into the hydrophilic and hydrophobic character from an electronic point of view.



References:

- [1] Earle, M. J.; Seddon, K. R. *Pure Appl. Chem.* 72, (2000)1391.
- [2] Car, R.; Parrinello, M. *Phys. Rev. Lett.* 55, (1985) 2471.
- [3] Zahn, S.; Wendler, K; Kirchner, B. *Phys. Chem. Chem. Phys.* 13, (2011) 15083.

15th Physical Chemistry Conference



Recovery of formic acid from an aqueous solution by 1- decanol at 323.15K

H. Ghanadzadeh Gilani^a; M. Azadian^{a*}; Sh. Asan^b.

^aDepartment of Chemical engineering, University of Guilan, Rasht, Iran

^bDepartment of Chemistry, Faculty of Science, University of Urmia, Urmia, Iran

E-mail address: soroosh_net12@yahoo.com

Abstract:

In this work, experimental solubility and tie-line data for the (water + formic acid + 1-decanol) system were obtained at $T = 323.15\text{ K}$ and atmospheric pressure. Data for the binodal curves were determined by cloud-point titration method. The concentration of each phase was determined by acidimetric titration, the Karl–Fischer technique, and refractive index measurements. A type-2 LLE phase diagram was obtained for this ternary system. The experimental tie-line data were compared with those correlated by the NRTL model and the binary interaction parameters were obtained.

Keywords: Liquid-liquid equilibrium; Tie-line data; Formic acid; 1-Decanol; NRTL model; Separation factor.

Introduction:

Formic acid is the simplest carboxylic acid which is an important intermediate in chemical synthesis. It is principally used as a preservative and antibacterial agent in livestock feed, but furthermore it is used to process organic latex into raw rubber, in the textile industry, for the



tanning of leather [1], This work presents the LLE data for (water + formic acid + 1-decanol) ternary system at 323.15 K, the phase compositions and tie-line data were measured for the first time. Distribution coefficients and separation factors were determined from the tie-line data, in order to evaluate the extracting ability of the solvent for the separation of (water + formic acid) mixture. The experimental LLE data were correlated with the non-random two-liquid (NRTL) model [2], and the values of the interaction parameter were obtained. This model has been successfully applied for the correlation of several ternary systems.

Methods:

1-Decanol with stated mass fraction purity higher than 0.99 was obtained from Merck. For the study of the equilibrium data, analytical grade Formic acid containing 98 wt% (Merck) was used. The purity of the acid was checked through acidimetric titration with 1 N NaOH.

A 250 cm³ glass cell connected to a thermostat was used to measure the LLE values at 323.15 K. The prepared mixtures were placed in the extraction cell and were vigorously agitated by a magnetic stirrer for 4h. The mixtures were then settled for 4 h at constant system temperature to separate completely into two liquid phases.

Results and discussion:

The system exhibited type- 2 phase behavior, having only two liquid pair of partially miscible (water + IDEC) and (FA + IDEC) one pairs of completely miscible (water + FA). The area of the two-phase region depends on the solubility of water in organic phase. IDEC with high boiling temperature has very low solubility in water, so it may be considered as a good candidate for liquid–liquid extraction process. To indicate the ability of the solvent in the recovery of formic acid, distribution coefficients for water ($D_1 = x_{13}/x_{11}$) and formic acid ($D_2 = x_{23}/x_{21}$) and separation factors (S) were calculated from experimental data. x_{13} and x_{23} are



the mole fractions of water and formic acid in organic rich phase, respectively. x_{11} and x_{21} are the mole fractions of water and formic acid in aqueous phase, respectively. The separation factor is defined as the ratio of distribution coefficients of formic acid (2) to water (1), $S = D_2/D_1$.

Conclusions:

Liquid-liquid equilibrium data for the (water + formic acid + 1-decanol) ternary system were determined at $T = 323.15$ K. The separation factor and distribution coefficient for the organic solvent used in this work were calculated. The experimental results indicate that 1DEC has high separation factors, indicating the ability of the solvent to extract formic acid from water. The consistency of tie-line data was verified by applying the Othmer-Tobias and Bachman equations. The NRTL model was used to correlate the experimental LLE data. The RMSD% values in the correlation by NRTL for the ternary system over the temperature range of 323.15 K were found to be 0.88%.

References:

- [1] E. Bartholome, E. Biekert, H. Hellmann, H. Ley, Ullmanns Encyklopadie der Technischen Chemie, 4. Auflage, Band 7, Verlag Chemie, Weinheim, 1974, pp. 362–373.
- [2] H. Renon, J.M. Prausnitz, AIChE J. 14 (1968) 35–144



Osmotic and activity coefficient of L –Serine in aqueous solutions of ionic liquid [cmmim][Cl] at T=298.15K

Mohammed Taghi Zafarani-Moattar^{*a}, Behnaz Asadazadeh^b

Physical Chemistry Department, University of Tabriz, Tabriz, Iran

E. mail: zafarani47@yahoo.com

Key word: [Cmmim][Cl] -L-Serine-water activity-Activity coefficient

Introduction:

Amino acids are the building blocks of other biomolecules such as peptides and proteins; therefore for their separation process it is important to study their behavior in aqueous systems containing electrolytes [1]. One of the thermodynamic properties of aqueous amino acid solutions is water activity which is an important thermodynamic property, because, it is closely related with the other thermodynamic properties such as vapor pressure, osmotic coefficient, activity coefficient, excess enthalpy, excess entropy, excess Gibbs energy and excess volume.

The aim of the present essay is to present experimental data on vapour-liquid equilibria using isopiestic method for binary aqueous solutions of L- serine, and the effect of ionic liquid on the activity coefficient of L-serine in aqueous solutions at 298.15 K. The results have been used to calculate the activity coefficients of all component in binary and ternary systems, using original pitzer equations [2] and modified pitzer for electrolyte+polar non-electrolyte mixtures [3].



Materials:

L- Serine (>0.99) and was obtained from Merck. The amino acid were used without further purification, and double distilled, deionized water was used. Ionic liquid [Cmmim][Cl] was prepared and purified using the procedure described in the literature.

Apparatus and Procedure :

In this study, the isopiestic method is used to obtain the activity of water in aqueous (serine +IL) solutions. It is based on the phenomenon that different solutions, when connected through the vapour space, approach equilibrium by transferring solvent mass by distillation. Equilibrium has been established once the temperature and pressure are uniform throughout the system, provided that no concentration gradients exist in the liquid phase. Equality of the solvent chemical potential implies the equality of the solvent activity. Since the solvent activity is known for one or more standard solutions, it will be known for each solution within the isopiestic system.

Results and Discussion:

From the calculated osmotic coefficient data, the activity of water solutions and the vapor pressure of this solution were determined at isopiestic equilibrium molalities. From the water activity data, activity coefficients of all component in binary and ternary systemes, using original pitzer and modified pitzer equations for (electrolyte + polar non-electrolyte) mixtures were obtained.

Conclusion:

The accurate water activity and osmotic coefficient of the ternary systems containing 1-carboxymethyl-3-methylimidazolium chloride [Cmmim][Cl]+L-serine and their



corresponding binary L-Serine aqueous solutions have been measured at 298.15 K. The experimental osmotic coefficient data were fitted satisfactorily to the Pitzer, modified Pitzer. The parameters obtained with the models were adopted to calculate the activity coefficients. The result shows that there is a salting-in effect between the molecules of [Cmmim][Cl] and L-Serine. The effects of electrolytes on the activity coefficient of an amino acid can be attributed to the formation of ion-pair complex between the ions in the solution and the charged amino and carboxyl group of the amino acid.

References:

- [1] Zhao, H.; Viscosity B-Coefficients and standard partial molar volumes of amino acids, and their roles in interpreting the protein (enzyme) stabilization; *Biophys. Chem.*; 122, 157-183, 2006
- [2] Pitzer, K. S. In *Activity Coefficients in Electrolyte Solutions*; CRC Press, Boca Raton, 1991; vol. 1.
- [3] Fernandez-Merida, L., Rodriguez-Raposo, R., and Estes, M.A. ; Modification of the Pitzer equation for application to electrolyte+polar non electrolyte mixtures; *J. Chem. Thermodynamics*; 26, 1121-1128, 1994.



Kinetic study of removal Tylosin from contaminated water by persulfate in the presence of immobilized silver nanoparticle

S.KamaliMoghaddam^a, M.H.Rasoulifard^a, M.Vahed pour^a

^aDepartment of Chemistry, Faculty of Sciences, University of Zanjan, Zanjan, Iran

Email: kamali8963@yahoo.com

Key words: Tylosin, Kinetic, Water and Wastewater, Antibiotics, Nano particle.

Introduction:

The major contaminants of livestock effluent are nitrogen and organic matters; however it may contain other contaminants such as potassium, phosphorus and growth factors (hormones and heavy metals) or acute contaminants such as pharmaceuticals. Much attention has been recently devoted to the fate of pharmaceutically active compounds such as antibiotics in soil and water. Among them, tetracycline (TC) and tylosin (TYL) antibiotics were shown to be poorly biodegradable and toxic for microorganisms. Application of Ag^{1+} -catalyzed peroxydisulfate, as an advanced oxidation process, introduces an effectual method for wastewater treatment. The advanced oxidation processes (AOPs) based on the in situ generation of reactive OH radical is applied. This radical species can quickly and nonselectively oxidize a broad range of organic pollutants. An accelerated reaction using $\text{S}_2\text{O}_8^{2-}$ to destroy antibiotics can be achieved via chemical activation with Ag^{1+} to generate sulfate radicals ($\text{SO}_4^{\cdot -}$). In this work, Silver ion (Ag^{1+})-catalyzed peroxydisulfate was studied for the degradation of Tylosin in an aqueous medium. The effect of different parameters, such as temperature, peroxydisulfate concentration, and Ag^{1+} concentrations,

were investigated. Degradation efficiency was not considerable when using peroxydisulfate alone. Studies revealed that increases in temperature and in the initial concentrations of peroxydisulfate and Ag^{1+} up to 100 mM and 0.4 mM, respectively, enhanced pollutant degradation.

Materials and methods:

Tylosintartrate (98% of purity) were obtained from Razi(Iran).Silvernitrate was obtained from AppliChem and ammonium peroxydisulfate from Merck. The solution was immediately prepared before the measurements to avoid a change in concentration due to self-decomposition. Added to the pollutant-and- Ag^{1+} solution in a glass bottle was 50 mL of synthetic solution containing the desired initial concentration of $\text{S}_2\text{O}_8^{-2}$; this was mixed using a magnetic stirrer. The pollutant solution samples were taken at the desired time intervals and were analyzed with a UV/Vis spectrophotometer (Shimadzu UV-160) at $\lambda_{\text{max}} = 305 \text{ nm}$ with a calibration curve based on the Beer-Lambert law. The efficiency of pollutant removal was expressed as the ratio of C_t to C_0 , as in Eq.(1), where C_0 is the initial concentration value of pollutant and C_t is the concentration value of pollutant at time t.

$$(1) \quad X = C/C_0$$

Result and discussion:

The degradation of Tylosin was investigated using $\text{S}_2\text{O}_8^{-2}$ alone, Ag^{1+} without peroxydisulfate, and both Ag^{1+} and $\text{S}_2\text{O}_8^{-2}$, (Figure 1). There was no observable loss of pollutant when $\text{S}_2\text{O}_8^{-2}$ was applied in the absence of Ag^{1+} , and the Tylosin removal was not considerable when using Ag^{1+} in the absence of $\text{S}_2\text{O}_8^{-2}$. The results reveal that a considerable

decrease in the concentration of the pollutant occurred when the sample was oxidized by $\text{S}_2\text{O}_8^{2-}$ in the presence of the Ag^{1+} catalyst because of sulfate radicals generated due to the chemical activation of peroxydisulfate with Ag^{1+} . In addition, increasing the reaction temperature may significantly accelerate the Tylosin degradation.

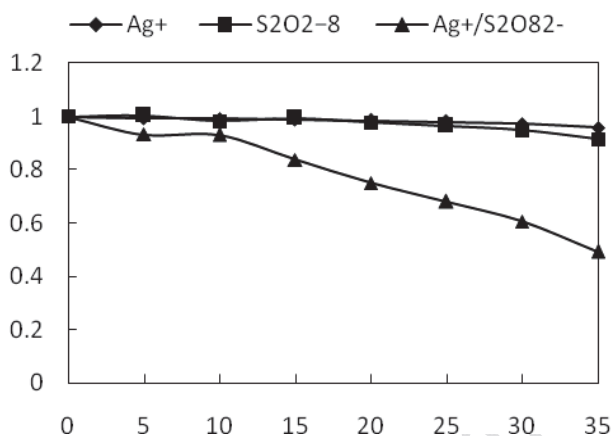


Figure 1. Effect of $\text{S}_2\text{O}_8^{2-}/\text{Ag}^+$ process in removal of Tylosin. $[\text{TYL}]_0=50\text{ppm}$, $[\text{S}_2\text{O}_8^{2-}]_0=100\text{mM}$, $[\text{Ag}^+]_0=0.4\text{mM}$, $\text{pH}_0=\text{natural}$, $T=25^\circ\text{C}$.

Conclusion:

Application of peroxydisulfate along with Ag^{1+} introduces an effectual and safe method for oxidative removal of Tylosin at the laboratory scale. The degradation rate of Tylosin was shown to be dependent on the temperature and the Ag^{1+} , Tylosin, and peroxydisulfate concentrations. An increase in peroxydisulfate concentration, meanwhile, enhanced the degree of degradation. The results indicate that degrees of degradation of Tylosin were obviously increased by increasing the initial concentration of Ag^{1+} .

Reference:



- [1] S.Yahiat.; "Removal of antibiotics by an integrated process coupling photocatalysis and biological treatment e Case of tetracycline and tylosin"; International Biodeterioration& Biodegradation 65 (2011) 997e1003.
- [2] M.h.Rasoulifard.; " Degradation of acid red 14 by silver ion-catalyzed peroxydisulfate oxidation in an aqueous solution "; Turkish J. Eng. Env. Sci.35 (2011), 1 – 8.
- [3] Kimberly A. Rickman.; " Kinetics and mechanisms of sulfate radical oxidation of b-lactam antibiotics in water "; Chemosphere 81 (2010) 359–365.



Calculation of Transport Properties of Fluids Using MET and Appropriate Equations of State

G. A. Parsafar*^a, P. Ansari^a

^aDepartment of Chemistry, Sharif University of Technology, Tehran, Iran

(Email: Parsafar@sharif.ir)

Keywords: Transport Properties, Modified Enskog Theory (MET), Equation of State III, LIR

Introduction

In this work, a method based on the modified Enskog theory [1] (MET) and some equations of state have been used for calculation of the transport properties of some fluids. This method has already been used for n-alkanes by using an empirical equation of state (EoS) and the MLIR introduced by Parsafar and Kalantar [2].

On the basis of the Enskog theory, the viscosity (η) of a dense hard sphere fluid is given as [1]:

$$\eta = \eta_0 \rho \left[\frac{1}{Y} + 0.800 + 0.761Y \right]$$

(1)

The quantity Y is related to the hard-sphere equation of state as:

$$Y = \frac{\rho}{\rho_{hs}} - 1$$

(2)

Enskog himself proposed and formulated its application to real dense fluids by suggesting that the internal pressure has to be added to p in Eq. (2), because of contribution of the intermolecular interactions in the pressure.

The main limitation of using the MET is lack of experimental data for co-volume, b_0 , that was substituted from hard sphere (HS) theory, and zero density transport properties was substituted from the kinetic theory of gases for the HS in the MET expression, because of the fact that dense fluids behave more and less like a HS fluid [2].

By substituting η_0 from the kinetic theory of gases and $2/3\pi\sigma^3$ for b_0 in Eq. (1), one finds that,

$$\frac{\eta Y}{\sqrt{T\rho}} = aY^2 + bY + c$$

(3)

Similarly, for the thermal conductivity (λ), one may show that:

$$\frac{\lambda Y}{\rho \sqrt{T}} (C_{V,m} + (9/4)R) = iY^2 + jY + k$$

(4)

Where a , b , c , i , j , and k are coefficients which may be temperature dependent. So a quadratic expression for both viscosity and thermal conductivity coefficients in terms of Y at high densities ($\rho > \rho_c$) for each isotherm is expected, where $Y = (T (\partial p / \partial T)) / \rho RT - 1$.

Methods:

To evaluate above mentioned expressions, we have used experimental values of densities and the transport properties to calculate Y from the differentiation of pressure given by the empirical equation of state, equation III [3] and LIR [4].

Results and discussion:

We have found that, the curves of $\eta Y / \sqrt{T} \rho$ and $\lambda Y / (p \sqrt{T}) (C_{V,m} + (9/4)R)$ versus Y , for different isotherms of a fluid fall onto a common curve at high densities and temperatures, but the curves depend on the nature of fluid.

The obtained coefficients of Eq. (3) are plotted versus temperature in Fig. 1, for oxygen. As shown in this figure, at high temperatures ($T \gg T_c$), the coefficients are constant for nonpolar molecules; however for polar molecules like water, they aren't constant even at high temperatures ($T \gg T_c$). Owing to the fact that simple fluids behave like the HS at very high temperatures, such observations are expected. Similar temperature dependencies for the coefficients of Eq. (4) has also been observed.

We have used this approach to predict the coefficients of Eqs. (3) and (4) for argon, oxygen, nitrogen and methane at different densities ($\rho \gg \rho_c$) and temperatures ($T \gg T_c$), using their empirical EoSs [5, 6, 7, 8, 9].

Conclusions:

By using experimental data of transport properties for one isotherm and equation III or LIR for calculation of Y for a dense fluid, we may calculate the transport property of that fluid at high temperatures ($T \gg T_c$) in this paper.

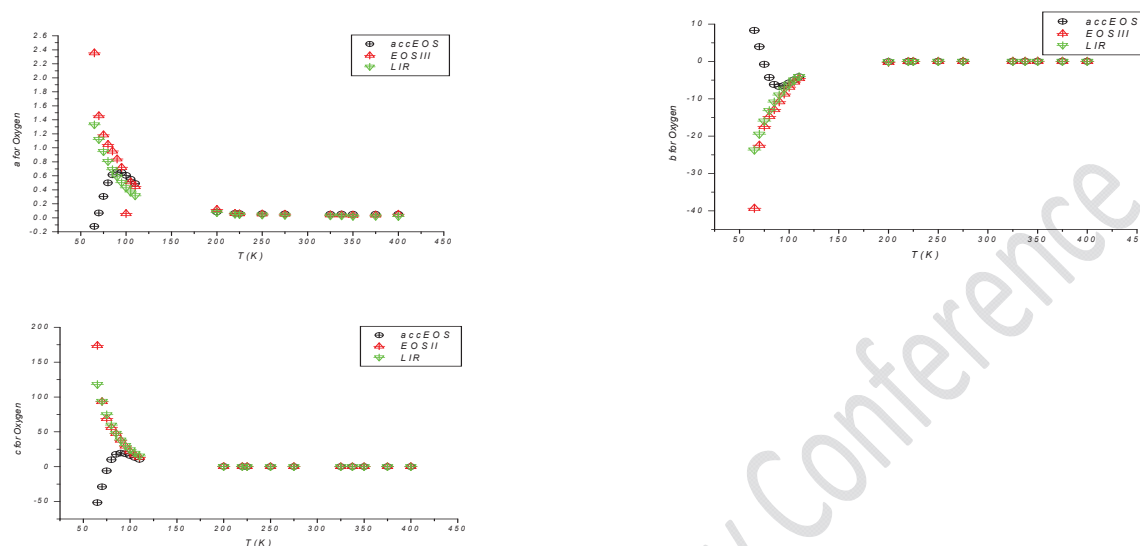


Fig. 1.a,b, and c in Eq. 3. versus T for Oxygen

References:

- [1] J.O. Hirschfelder, C.F. Curtiss, R.B. Bird, Molecular Theory of Gases and Liquids, John Wiley & Sons, New York, 1964.
- [2] G.A. Parsafar, Z. Kalantar, Calculation of the transport properties of dense fluids using modified Enskog theory and an appropriate equation of state, Fluid Phase Equilibria 253,108–117, 2007.
- [3] G. A. Parsafar, H. V. Spohr, G. N. Patey, An Accurate Equation of State for Fluids and Solids, J. Physical Chemistry B, 113, 11977, 2009.
- [4] G. A. Parsafar, E.A. Mason, Linear Isotherms for Dense Fluids: A New Regularity, J. Phys. Chem., 97, 9048, 1993.



- [5] Richard B. Stewart and Richard T. Jacobsen, Thermodynamic Properties of Argon from the Triple Point to 1200 K with pressure to 1000 MPa, J. Phys. Chem. Ref. Data, Vol.18, No.2, 1989.
- [6] Richard B. Stewart and Richard T. Jacobsen, W. Wagner, Thermodynamic Properties of Oxygen from the Triple Point to 300K with pressure to 80 MPa, J. Phys. Chem. Ref. Data, Vol.20, No.5, 1991.
- [7] R.Span, Erric. W. Lemmon, Richard.T .Jacobsen, W. Wagner, A. Yokozeki, A Reference Equation of State for the Thermodynamic Properties of Nitrogen for Temperatures from 63.151 to 1000 K and Pressures to 2200 MPa, J. Phys. Chem. Ref. Data, Vol. 29, No. 6, 2000.
- [8] U. Setzmann, W.Wagner, A New Equation of State and Tables of Thermodynamic Properties for Methane Covering the Range from the Melting Line to 625 K at pressures up to 1000 MPa , J. Phys. Chem. Ref. Data, Vol.20, No.6, 1991.
- [9] Daniel G. Friend, James F. Ely, and Hepburn Ingham, Thermophysical Properties of Methane, J.Phys. Chem. Ref. Data, Vol. 18, No. 2, 1989.

Kinetic study of uracil tautomerization in the gas phase

Sh. Ramazani*, Z. Deylami

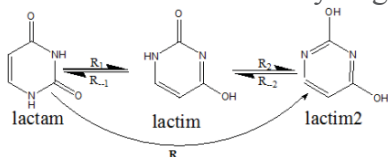
*Department of Chemistry, Yasouj University, Yasouj, Iran

Email: Z_deylami@yahoo.com

Key words: Kinetics, Potential Energy Surface, Rate Constant, Tautomerization.

Introduction:

In this research the kinetics and thermodynamic of reaction of uracil tautomers in gas phase have been studied. Hydrogen transfer from Lactam to produce lactim is carried out R1. In R2 reaction there is also a hydrogen abstraction. Reaction scheme is shown below:



Scheme 1

Uracil is one of the four nucleobases in the nucleic acid of RNA. It is a common and naturally occurring pyrimidine derivative. This tautomers is the hydrogen bond acceptor and can form two hydrogen bonds.

Materials and methods:

Ab initio calculations were carried out using the Gaussian 03 program. Molecular geometries and harmonic vibration frequencies of all stationary points along the reaction pathway were calculated with the mpwb95/6-31+G* level of theory.



The rate constant of the title reaction is calculated by RRKM theory. For an unimolecular reaction.

Where A^* is the energized reactant, A^\ddagger is the activated complex, and P represents product.

$$k(E) = \frac{\sigma}{h} \cdot \frac{W^\ddagger(E - E^\ddagger)}{\rho(E)}$$

This rate constant, $k(E)$, according to the RRKM theory can be expressed as:

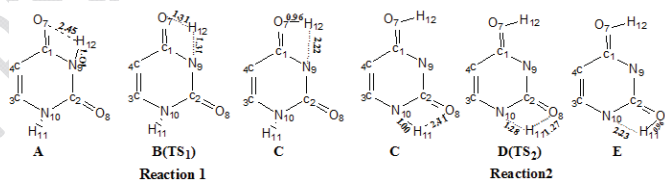
Where σ is the symmetry factor, $W^\ddagger(E - E^\ddagger)$ denotes the total number of states of the TS with activation energy E^\ddagger , and $\rho(E)$ represents the density of states of the energized reactant [1].

Result and discussion:

The potential energy surface (PES) along the minimum energy path and relative energies for reaction R1 and R2 are shown in Figure1 and 2. Two transition states are found tautomerism (TS1 and TS2). In this study we have consider lactim is an intermediate. Saddle point was verified to connect the proper reactant and product by performing an intrinsic reaction coordinate

(IRC) calculation [2]. Figure1 shows the intrinsic reaction coordinate (IRC) for reaction R at the mpwb1k/6-31+G(d,p) level. The calculated results showed this reaction is a hydrogen Abstraction process. The

optimized
stationary
scheme 2).



The geometries of all points obtained (see

Scheme 2. Optimized structures of lactam (A), TS₁ (B), lactim (C), TS₂ (D), and lactim2 (E) at the mpwb1k MPWB1K/6-31+G(d,p) level. Harmonic vibrational frequencies were calculated at the mpwb1k/6-31 +G (d,p) level of theory to determine zero point energies (ZPE) IN R1 reaction hydrogen atom number 12 abstracted with Oxygen atom number 7 to produce lactim. In R2 reaction hydrogen atom number 12 to is also abstracted with oxygen atom number 8 to produce lactim2 at this reaction. The potential energy surfaces (PES) for each pathway are plotted. Barrier height energy are 184.49 and 209.78 kJ/mol for R1 and R2 respectively.

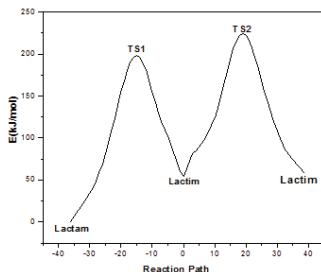


Figure1. Potential energy surface along the Plot for R,

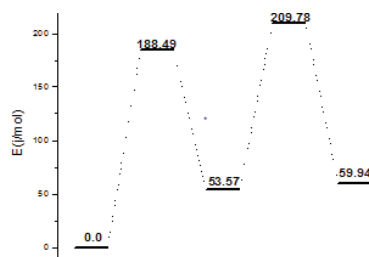


Figure 2. Relative energy (kJ/ mol)for all

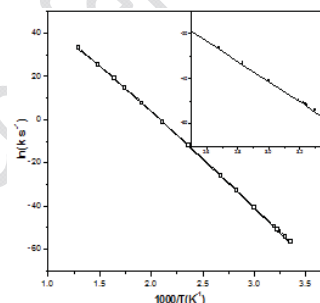


Figure 3: Arrhenius reaction at the mpwb1k/6-31+G(d,p) level.

Non-linear least-squares fit used to calculate rate constant expressions for rate constants

which are plotted in figure 3:

$$k_{\text{nonlin}} = (\exp 123.4) \left(\frac{T}{300} \right)^{-20} \exp \left[-\frac{463400(T-13.9)}{R(T^2 + 193.2)} \right]$$

$$k_{\text{lin}} = (\exp 122.8) \left(\frac{T}{300} \right)^{-19.7} \exp \left[-\frac{463400(T-11.9)}{R(T^2 + 129.1)} \right]$$

$$E_a = \frac{T^4 + 27.8T^3 - 193.2T^2}{(T^2 + 193.2)^2} - 20RT$$

$$E_a = \frac{T^4 + 23T^3 - 129.1T^2}{(T^2 + 129.1)^2} - 19.7RT$$

Conclusion:



ΔG and ΔH are 57.89, 56.40 kJ mol⁻¹ for the R reaction respectively. These results are shown that lactam is significant than lactim2.

Reference:

- [1] H. Eyring, S. H. Lin, and S. M. Lin, Basic Chemical Kinetics.
[2] S.H. Mousavipour, A. F. Ramos, R. M. Paeda, J. Phys. Chem. A, (2007)719-725.



High Solar Photocatalytic Degradation of Azo Dye Reactive Black 5 (RB5) by Bismuth Ferrite Synthesized via Ultrasound Method

M.H. Entezari^{a*}, T. Soltani^b

a Department of Chemistry, Ferdowsi University of Mashhad, 91775, Mashhad, Iran

b Department of Chemistry, Ferdowsi University of Mashhad, 91775, Mashhad, Iran

E-mail: moh-entezari@yahoo.com

Key words: Ultrasound, Sunlight, BiFeO₃, RB5, Photodegradation.

Introduction:

Sixty percent of dyes used in the textiles industries are azo dyes [1]. Lately, there has been considerable attention for the complete degradation of dyes through advanced oxidation processes (AOPs) that can oxidize types of organic pollutants to inorganic compound [2]. Recently, bismuth ferrite photocatalyst (BFO) has attracted considerable attention due to the narrow band-gap energy (2.1 eV) and high chemical stability [3].

Materials and methods:

In this work, pure bismuth ferrite (BFO) as a visible-light photocatalyst has been synthesized via ultrasonic-assisted method at mild conditions. The structure of BFO was examined. Then, the photocatalytic degradation of RB5 was investigated under sun light irradiation to get knowledge about the potential industrial applications.

Apparatus:



The ultrasonic irradiation with equipment operating at 20 kHz (W- 450 D), X-ray diffractometer (XRD, Philips PW1800), UV-vis spectrophotometer (Unico 2800), Fourier transform infrared (FT-IR) spectrometer (Avatar 370) were carried out.

Result and discussion:

The RB5 was completely degraded in 60 min under solar light irradiation via the sample synthesized via ultrasound with the average crystallite size of 40 nm. The BFO have higher photocatalytic activities in acidic and basic medium rather than natural medium. The isotherm of adsorption and the kinetic and mechanism of photocatalytic degradation of RB5, were investigated and compared using different concentrations of dyes. Also, the intermediates during photodegradation were specified.

Conclusions:

The characterization data show that high mineralization and complete degradation of RB5 were achieved under applied conditions. The photocatalytic degradation of dye fit well with the Langmuir-Hinshelwood model. The relation between equilibration constants in the dark and in the presence of sun light irradiation was discussed. The photocatalys was stable under visible light irradiation after various cycles. The result of using different scavengers shows that the cleavage of the cromophore structure, naphthalene and benzene rings was mainly related to the $h_{\nu b+}$ pathway.

Reference:

- [1] P. Borker, A.V. Salker, Mater. Sci. Eng. B 133 (2006) 55–60.
- [2] H. Zollinger (Ed.), 2nd revised Edition, VCH, 1991.



- [3] F. Gao, X. Chen, K. Yin, S. Dong, Z. Ren, F. Yuan, T. Yu, Z. Zou, J. M.Liu, Adv. Mater. 19 (2007) 2889-2892.

15th Physical Chemistry Conference



Twinkling star: A simple chemical oscillator

H. Sabzyan*, M. Seyedsharifi

Department of Chemistry, University of Isfahan, Isfahan 81746-73441, I. R. Iran

sabzyan@sci.ui.ac.ir, m.seyedsharifi@sci.ui.ac.ir

Keywords: Chemical oscillation, Reaction-diffusion, RGB Analysis

Introduction

Chemical oscillations occur in time and space when chemical reaction systems with non-linear kinetics are coupled to diffusion, sedimentation, dissolution, and/or adsorption processes. Having two or more sets of steady state conditions is the unique characterization of these non-linear kinetic systems. In the past three decades more than a thousand chemical oscillation systems have been observed either accidentally or after a clever design and systematic search. Larger number of steady states far from each other and with short stability periods may result in chaotic behavior which can be considered as superposition of two or more oscillations [1,2]

In this work, a new simple oscillator based on the dissolution rates of solid NaOH coupled to the diffusion of the dissolved species and displacement of the acid-base equilibrium of an indicator, affected also by the change in the ionic strength of the solution due to the dissolution of NaOH. This oscillation appears, thus, as a twinkling star around the NaOH pill.

Materials and Methods:

A solution of 0.0157 M phenolphthalein (phph) in 50/50 ethanol/water is prepared. 1ml of this phph solution is diluted with 3ml of water and then is poured into a 7×7 cm² flat

petri-dish to have a solution of about 2-4 mm depth. Next, one NaOH pill of known diameter is weighted and placed in the center of the petri-dish. The twinkling star starts oscillating appearing as the inward and outward travelling of the circular border between the colorless solution containing higher concentration of the NaOH(aq) and lower concentration of phph and the purple solution containing lower concentration of the NaOH(aq) and higher concentration of phph. This oscillation would continue until the entire pill is dissolved.

A Sony camcorder model HDR-J50E/BE36 is used to film and record the color evolution of the chemical oscillation system. A pair of 18 W visible light projectors is used as the full spectrum source of light which is necessary for the RGB analysis of the oscillating system. To prevent interference of the neutralization of phph by the CO₂ content of the air with the chemical oscillation, a 12M NaOH solution is placed in the reaction chamber as desiccant.

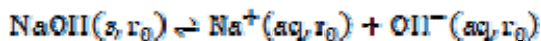


Figure 1. Snapshot of one cycle of the oscillation of the twinkling star with time. The purple and colorless phases contain lower and higher concentrations of the OH^- ion, respectively.

Results, discussion and conclusion:

When the NaOH is located in the phph solution, the produced OH^- ions migrate into the solution and react with phph and turn its color to purple. Concentration of OH^- around the NaOH pill increases so that the first solution phase around the NaOH pill turns to colorless.

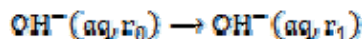
The chemical and physical processes involved in this oscillation are as follow:



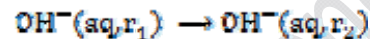
(1)



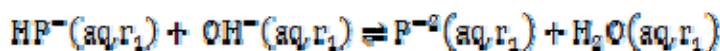
(4)



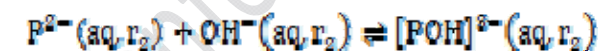
(2)



(5)



(3)



(6)

Colorless
Purple

Purple
Colorless



According to this reaction scheme, when concentrations of OH^- and $[\text{POH}]^{2-}$ are high, they diffuse circularly away from the NaOH pill. The diffusion rate of OH^- ions in the bulk of the phph phase is significantly lower than that in water. At very high phph concentration, no oscillation can be observed because all OH^- ions react with HP^- species and cannot form a different phase. The depth of solution should also be less than the height of the NaOH pill. After optimization of the conditions for obtaining longer oscillations, and the highest possible contrast, the twinkling star oscillations are recorded and converted into an RGB matrix data. A routine RGB analysis is carried out to locate and follow the exact position of the border,



instantaneously. The spatiotemporal oscillation is then modeled based on the chemical kinetics/dynamics given in Equations 1-6.

References:

- [1] Sagués, F.; Epstein, I. R., Dalton Trans. 2003, 1202.
- [2] Gray, P.; Scott, S. K. Chemical oscillations and instabilities, Claredon Press, Oxford, 1994



A novel method for prediction of thermal decomposition kinetics in different temperature profiles

F. Fathi* and A. Hassanzadeh

Department of Chemistry, Urmia University, Urmia, Iran

Email: f.fathi@live.com

Keywords: DSC, Thermal decomposition, Kinetics prediction, First order phase transition.

Introduction:

Prediction of the decomposition kinetics in different temperature profiles has applications in various fields such as military sciences or food science and technology. There are different approaches to predict degradation in different temperature profiles, one of which is using the DSC technique and theoretical calculations, then comparing theoretical results with experimental data. In this paper, a novel method was proposed for predicting the decomposition kinetics in different temperature profiles using DSC data.

Experimental:

The thermal degradation experiments of a typical sample (Vanadyl complex with Diamino propane – 3 – methoxy salicylaldehyde as its schiff base ligand) were performed within the temperature range of 50 – 550 °C at different heating rates on a LINSEIS STA PT-1000 DSC analyzer calibrated by Tin, Indium, Lead and Zinc and samples were held in Alumina crucibles. After data acquisition, data analyzing was done by MATLAB software.

Calculation:

After extracting baselines from raw data and determining the values of α (conversion), da/dt (reaction rate) at each heating rate [1], the variations of activation energy (E_a) and the multiplication of the reaction model and the frequency factor ($f \times A$) with regard to α were calculated using the isoconversional Friedman method [2]. In order to predict the reaction progress diagrams, it was assumed that the value of α can be obtained at any moment (or temperature) by the following equation:

$$\alpha = \sum_i \alpha(T(t + \Delta t), t + \Delta t) - \alpha(T(t + \Delta t), t)$$

where $\alpha(T(t + \Delta t), t + \Delta t)$ equals the value of α at the isothermal $T(t + \Delta t)$ and at the time $t + \Delta t$ and subsequently $\alpha(T(t + \Delta t), t)$ equals the value of α at the isothermal $T(t + \Delta t)$ and the time t . Fig. 1a depicts experimental diagrams and calculated theoretical diagrams according to above equation for three different heating rates (Fig. 1b).

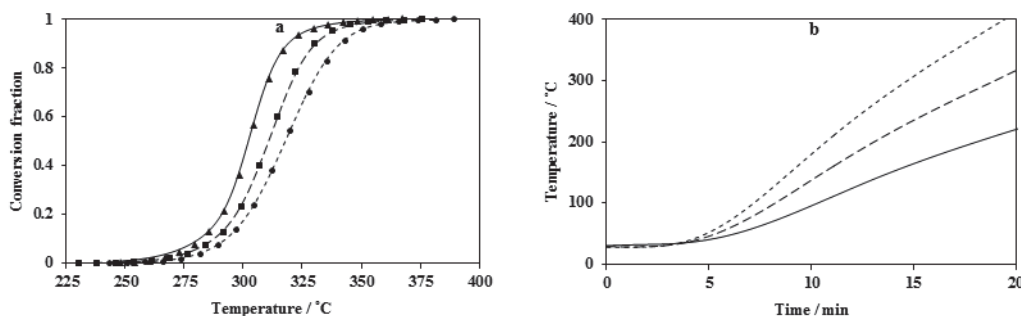


Figure 1. (a) Experimental (points) and theoretical (lines) diagrams of conversion fraction of X thermal decomposition and (b) Corresponding heating rates; Each line style in plot (a) is related to same line style in plot (b)

Fig. 2a illustrates the predicted conversion diagram (line) for the heating rate of Fig. 2b using above mentioned equation and as it can be observed in Fig. 2a, the predictive and experimental(points) data overlap very well and the accuracy of the work is validated.

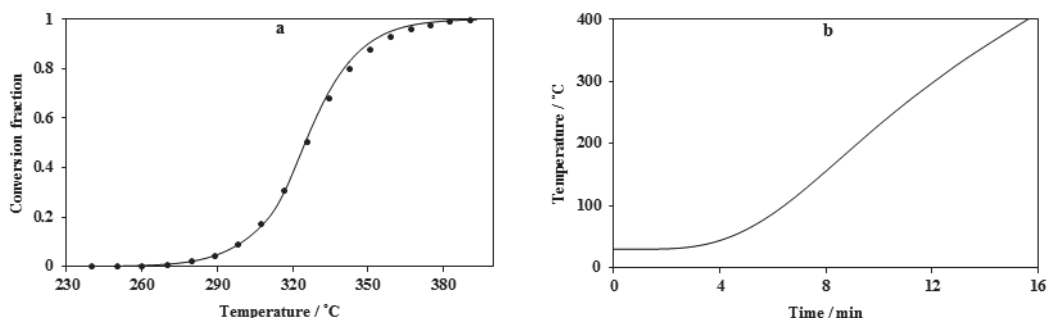


Figure 2.(a) Experimental (points) and predicted (line) diagrams of conversion fraction and (b) Corresponding heating rate

Conclusion:

As it was mentioned, the innovative method can be applied reliably for prediction of reaction progress in thermal analysis. But it must be considered that the method was examined for a first order phase transition and its validity for second order or lambda phase transitions may not be confirmed because the Friedman method which was used in our proposed method is applied particularly for first order phase transitions.

Reference:

- [1] Shah HV; Babb DA and Smith DW, Jr., Polymer 41: 4415-4422 (2000).
- [2] Friedman HL, J. Polym. Sci., Part C: Polym. Lett. 6: 183-195 (1964).



Kinetic study of reaction of ethane with radical of trichloromethane

Sh. Ramazani*, S. L. HashemiDashtaki

*Department of Chemistry, Yasouj University, Yasouj, Iran (Email:

L_hashemi23@yahoo.com)

Key words: Kinetics, Potential energy surface, Transition state theory, Rate constant.

Introduction:

In this investigation, reaction of ethane with radical of trichloromethane has been studied. This reaction is a hydrogen abstraction reaction.



In 1971 Hautecloque, s investigated it by IR absorption technique and reported its rate expression equal to $3.47 \times 10^{-10} e^{-75.74 [\text{kJ/mole}]/RT}$ ($\text{cm}^3 \text{ molecule}^{-1} \text{ s}^{-1}$), at 521-578 K [1]. In 1975 Hautecloque, s reported rate expression of this reaction $3.49 \times 10^{-10} e^{-75.74 [\text{kJ/mole}]/RT}$ and $1.9 (\text{cm}^3 \text{ molecule}^{-1} \text{ s}^{-1})$ at 511-573 K and 550 K, respectively [2]. In 1982 Matheson, I and Tedder, j used gas chromatography to investigate mentioned reaction at 377-523 K and reported its rate expression $1.66 \times 10^{-12} e^{-59.45 [\pm 2.38 \text{ kJ/mole}]/RT}$ ($\text{cm}^3 \text{ molecule}^{-1} \text{ s}^{-1}$) [3]. In this study we investigated it theoretically.

Materials and methods:

Geometries of all species have been obtained at the MP2 level with the 6-311++G (d,p) basis sets. All quantum chemical calculations have been carried out using Gaussian03

program. Transition state along the reaction path has been searched with scanning techniques. Frequency test shows that transition state has one imaginary frequency and it's reasonable. Rate constant of this reaction are calculated according to generalized transition-state theory (TST). TST explains the reaction rates of elementary chemical reactions. Original form of this theory was put forward in 1935, after that it was recognized that it provided a very valuable insight into how chemical reactions occur. The improved treatments usually have been referred as generalized transition-state theory. The general expression for transition state theory is as follows:

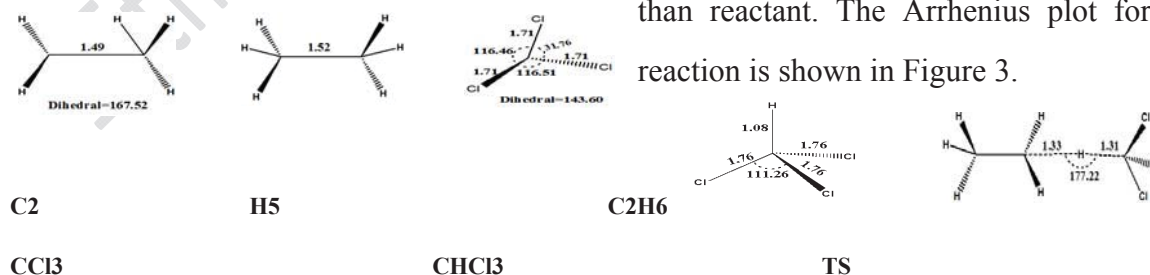
$$k(T) = \Gamma \frac{k_B T}{h} \sigma \frac{Q^\ddagger}{Q_A Q_B} \exp\left(-\frac{V_{MEP}^\ddagger}{k_B T}\right)$$

In this equation k_B and h are Boltzmann's and Planck's constants. σ is the degeneracy of reaction and Γ is the tunneling factor. The Q parameters are the sum of translational, vibrational, rotational and electronic partition functions for species.

Result and discussion:

Geometries of all species have been shown in scheme 1. Radical of trichloromethane abstracts hydrogen of ethane to produce product via transition state. In geometry of TS C...H bond is 1.32 Å, C...H bond is 1.30 Å and angle of C...H...C is 177.22°. Imaginary frequency is 1844.9i cm⁻¹. Potential energy surface and relative energies for reaction show in figure 1 and 2, respectively. As shown in figure 2, transition state 59.4(kJ mol⁻¹) is higher

than reactant. The Arrhenius plot for this reaction is shown in Figure 3.



Scheme1.Optimized structure at the MP2/6-311++G(d,p) level. Distance and angle are shown in angstrom and degree respectively.

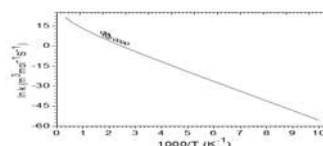
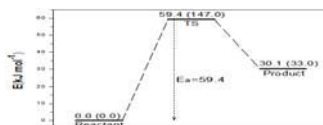
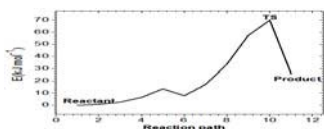


Figure 1.potential energy surface of

Figure 2. Relative energies of reaction

Figure 3. Arrhenius plot for reaction

reaction at theMP2/6-311++G(d,p).

at MP2/6-311++G(d,p) level. All values

that calculated

without Tunneling factor are corrected by zero point energies.

Symbols represent experimental data.

number in parentheses are at CCSD(T).

Non-linear least-squares fitty used to calculate rate constant expressions for rate constants which are plotted in figure 3:

$$k_{nonun} = (\exp 15.1) \left(\frac{T}{300} \right)^{3.7} \exp \left[- \frac{54094.5(T + 2.5)}{8.314(T^2 + 6.3)} \right]$$

$$E_a = \frac{T^4 + 5T^3 - 6.3T^2}{(T^2 + 6.3)^2} + 30.8T$$

Conclusion:

Reactant is 30.1 (kJ mol⁻¹) more stable than product. According to results, ΔG is 24.9, ΔH is 30.1 and TΔS is 5.5 (kJ mol⁻¹) and barrier energy for reaction is 59.4(kJ mol⁻¹).

Reference:

- [1] S. Hautecloque, C.R. Acad. Sc. Paris. 272 (1971).
- [2] S. Hautecloque. C.R. Acad. Sc. Paris. 280 (1975).
- [3] I. Matheson and J. Tedder, J. Chem. Kinet. 14 (1982) 1033.



Time-dependent charge reorganization of nonstationary π systems

S.M. Azami

Department of Chemistry, College of Sciences, Yasouj University, Yasouj, Iran.

(Email: azami@yu.ac.ir)

Keywords: Charge reorganization, Kekule structure, Charge density.

Introduction:

Charge reorganization in chemical species is a time-dependent phenomenon which takes place in several chemical processes such as electrochemical or photochemical reactions [1-3]. These reactions can be studied by either chemical kinetics or time-dependent quantum mechanics which provides a rigorous way for the corresponding wave function [4]. In the following, charge reorganization of a simple π system is studied using time-dependent techniques.

Methods:

The electronic wave function of π system of C_6H_6 is considered as a superposition of the corresponding ground and excited electronic states for which the σ electrons are excluded. The initial pre-constructed electronic wave function is then projected onto the superposition elements as wave packet at $t = 0$. To obtain propagation of this wave packet, which is not necessarily eigenfunction of the system's time-independent Hamiltonian, the time-dependent Schrödinger equation is numerically solved utilizing matrix representation of the Hamiltonian operator and wave packet.

Results and discussion:

The initial state of C_6H_6 π electronic structure is considered as one of its Kekule configurations as Fig. 1 at $t = 0$ shows it. This figure displays how the charge density is reorganized during the considered period of time and clearly shows that the electronic structure is transformed to the other Kekule structure after 0.04 femtoseconds.

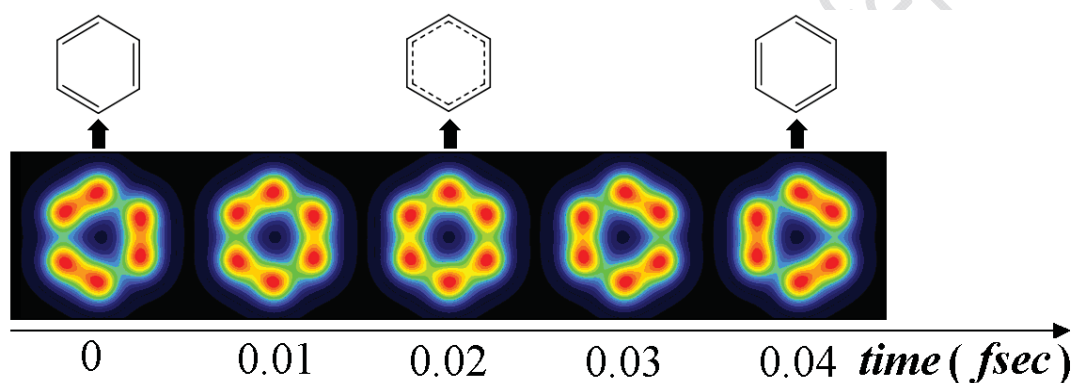


Fig. 1. Charge density reorganization of the π system.

Conclusions:

The π system of strongly delocalized electronic structures can be studied using time-dependent techniques and the results shows extremely fast charge reorganization in these systems. In the present work, it is shown that the π system of a hypothetical localized structure is transformed to some other localized structure.

References:

- [1] A. Burquel, et al.; Phys. Chem. A; 110, 3447-3453, 2006.
- [2] J.L. Bredas, et al; Chem. Rev.; 104, 4971-5003, 2004.
- [3] A.C. Morteani, et al; Phys. Rev. Lett.; 92, 247402, 2004.



- [4] J. Lindenberg, et al.; *Propagators in Quantum Chemistry*, John Wiley & Sons, Inc., Hoboken, New Jersey, Canada.

15th Physical Chemistry Conference



PARAMATICA: A MATHEMATICA Package for Biomolecular Force

Field Development

M. H. Karimi-Jafari*

^a Department of Bioinformatics, Institute of Biochemistry and Biophysics, University of Tehran, Tehran, Iran.

Email: mhkarimijafari@ut.ac.ir

Key words: Conformational analysis, CHARMM, Parameterization, Force Field

Introduction:

Popular biomolecular force fields (FF) such as AMBER, CHARMM, OPLS and GROMOS were designed, parameterized and continuously refined for main classes of biomolecules. Many research works deal with problems in which a novel residue, ligand or organic molecule is present in the system and thus researchers seek for new parameters that should be in agreement with the FF applied to other parts of the system. There are many alternative solutions for such problems but many of them provide general low quality parameters. A high quality receipt implies a high level of customization which is not a trivial task. In this work we review the current status of the PARAMATICA package that is designed for development of biomolecular FFs to new molecules.

Methodology:

The initial design of PARAMATICA obeys the general protocol proposed by CHARMM developers for CHARMM General FF (CGenFF) [1]. Extensions for other popular FFs will be in our future work. The potential energy $V(R)$ in the CHARMM FF is a function of the positions of all atoms and has the following general form:

$$V = \sum_{bonds} K_b (r - r_{0,b})^2 + \sum_{UB} K_{UB} (S - S_{0,UB})^2 + \sum_{angles} K_a (\theta - \theta_{0,a})^2 +$$

$$\sum_{dihedrals} K_{d,n} (1 + \cos(n\chi - \delta_{d,n})) + \sum_{improper} K_a (\theta - \theta_{0,a})^2 +$$

$$\sum_{\text{nonbonded}} \epsilon_{ij} \left[\left(\frac{R_{\text{min},ij}}{r_{ij}} \right)^{12} - 2 \left(\frac{R_{\text{min},ij}}{r_{ij}} \right)^6 \right] + \frac{q_i q_j}{4\pi \epsilon_0 r_{ij}}$$

where the sum covers all bond or angle vibrations, dihedral rotations, improper distortions, and non-bonded van der Waals or Coulomb interactions. Parameters in this equation must be optimized to reproduce a variety of target data such as molecular geometries, harmonic vibrational frequencies, rotational energy profiles and interaction strength and distance with TIP3P model of water. In addition to the routine procedure some tasks such as conformational search might also be necessary to identify the most important structures of molecules. All of these are implemented in a robust user-friendly fashion in PARAMATICA.

Results:

PARAMATICA acts as a control center for managing all tasks necessary for optimization and validation of the new set of parameters. Some of these tasks are actually performed in MOPAC2009, GAMESS, Firefly and NAMD program packages. An interface was provided for automatic input generation and output processing with any of these programs and all of them can be executed from inside of PARAMATICA. The PARAMATICA tool kit provides facilities for:

- 1) Extraction of available and missing parameters from CGennFF.
- 2) Random or grid-based conformational search.
- 3) Converting geometry specifications (Cartesian, Internal) to each other.
- 4) Unique definition and assignment of atom-names and atom-types.
- 5) Graph-based analysis of structures and numeration of bonds, angles and dihedrals (see Figure 1).
- 6) Providing initial guess for missing parameters by analogy or from QM calculations.
- 7) Normal mode analysis of force constant matrices.
- 8) Energy, gradient and hessian calculations from CHARMM FF.
- 9) Charge optimizations based on interaction with water molecules.
- 10) Optimization of dihedral parameters based on QM energy profiles.

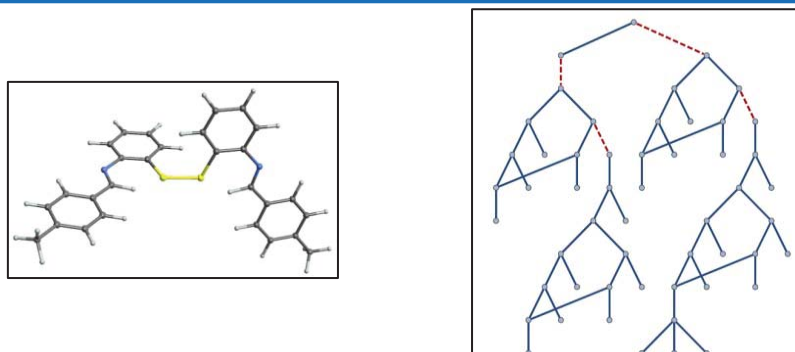


Figure 1. Graph based analysis of molecular structures. Red dashed lines represents missing bond parameters.

Conclusion:

Powerful functional programming and external communication abilities of MATHEMATICA were combined to an extensible package for analysis and parameterization of biomolecular force fields. The PARAMATICA tool box makes any related force field development tasks easy, fast and customizable.

References:

- [1] K. Vanommeslaeghe, *et al* , *J. Comput. Chem.*, **31** (2010) 671.



QTAIM 6-center Delocalization Effect of π Components of Electron Density on Local Aromaticity of Boron Nitride Sheets

S. Fakhraee^{a,*}, S. Sharifpour^b

^a Department of Chemistry, College of Sciences, Payame Noor university, Shiraz, 71365-944, Iran.

^b Department of Chemistry, College of Sciences, Payame Noor university, Ardakan, Yazd, 195, Iran.

*Email: fakhraee@pnu.ac.ir

Keywords: BN sheet, QTAIM, Aromaticity, Delocalization Index

Introduction:

The current formulation of quantum theory of atoms in molecules (QTAIM) is constructed so that only the σ -skeleton can be detected via the total charge density topology for bond paths (BPs) and bond critical points (BCPs). However, for planar molecules, the molecular π system can be detected as well by AIM theory and similar concepts can be generalized to π bonds too. This generalization is based on the fact that σ and π components of charge density do not mix for linear and planar molecule [1,2]. Aromaticity as a fundamental property plays a particular role in chemistry to measure the reactivity of molecules. There are different indices to evaluate the aromaticity, such as geometry based Harmonic Oscillator Model of Aromaticity (HOMA) [3] or magnetic based by π electron delocalization (DI)[4]. In the present work, planar boron nitride (BN) sheet is considered to investigate the change in π components of electron density by means of QTAIM. Also, the effect of substitutions on the aromaticity due to π components of electron density is evaluated by using 6-center DI within the framework of the AIM theory. The results are compared with HOMA indices.

Theoretical Method:

Geometry calculations and frequency tests were carried out at HF/6-31g* level of theory by Gaussian 03W program. Fig. 1(A) shows typical optimized structure of BN sheet where R refers to H, CCH, NCO, CNO, N₃ and OCN substituents, with the ability to conjugate with π electrons of BNsheet.

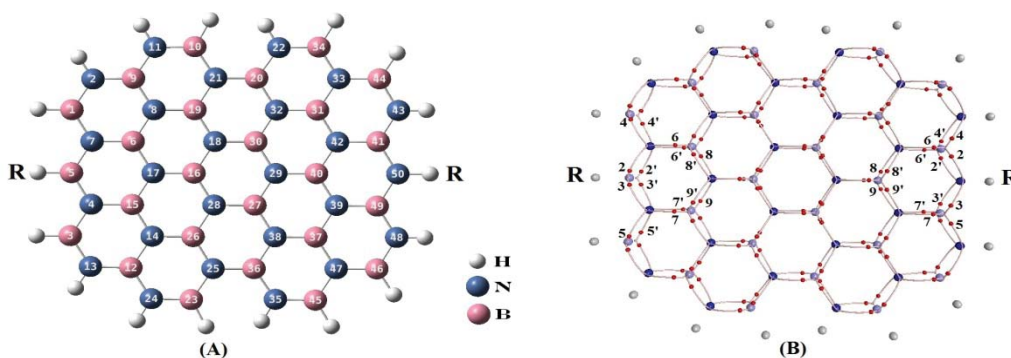


Figure 1: (A) Optimized structure of typical BN sheet substituted by R (R: H, CCH, NCO, CNO, N₃ and OCN). (B) The AIM molecular graphs correspond to π -BPs and BCPs. Six affected BCPs (2-6) are numbered for both substitutions in N₅₀ and B₅ side.

Substitution takes place on nitrogen 50 (N₅₀) and boron 5 (B₅), separately. AIM 2000 program was applied to represent the topological graphs of electron density corresponds to molecular π systems.

Results and Discussion:

The AIM graphs are represented for π system in Fig. 1(B). The results reveals that the most changes occurs in electronic properties corresponds to the CPs adjacent to substitution (2-7) and the other CPs remains almost unchanged. Table 1 summarizes the electron density ρ at these BCPs for both σ and π density, and the results of DI in comparison with HOMA indices. Generally, the local ring aromaticity decreases after substituting. When substitution takes place at N₅₀, the concentration of electron density in BCPs number 4 and 6 increases while it decreases for BCPs 2 and 8. This trend is reversed in cases in which the substitution is connected to B₅. The change in the value of ρ_{BCP} is reflected in the corresponding bond lengths. This phenomenon would change the local aromaticity of BN sheet. So, The calculated 6-center DI indices for π electron density of BN rings connected to substituents show a decrease in aromaticity after substituting. This trend is in a good agreement with HOMA indices.

Table 1: Electron density at CPs 2-7, DI and HOMA indices for BN rings connected to substituents N₅₀ and B₅ sides.

Substitution Connection	structure	σ electron density			π electron density			HOMA index	DI*10 ⁵
		2 & 3	4 & 5	6 & 7	2 & 3	4 & 5	6 & 7		
N ₅₀	BNsheet	0.2004	0.1984	0.1951	0.0213	0.0205	0.0194	0.894	5.128
	BNsheet-N ₃	0.1892	0.2070	0.2001	0.0206	0.0221	0.0205	0.876	4.656
	BNsheet-CCl	0.1871	0.2054	0.1988	0.0193	0.0217	0.0201	0.859	4.300
	BNsheet-OC	0.1876	0.2104	0.2019	0.0209	0.0226	0.0208	0.882	4.523
	BNsheet-NC	0.1895	0.2062	0.2001	0.0205	0.0220	0.0204	0.876	4.601
	BNsheet-CN	0.1810	0.2070	0.2024	0.0185	0.0222	0.0207	0.839	3.950
B ₅	BNsheet	0.1990	0.1962	0.1942	0.0186	0.0186	0.0186	0.880	6.140
	BNsheet-N ₃	0.2012	0.1934	0.1917	0.0202	0.0185	0.0186	0.859	5.086
	BNsheet-CCl	0.1990	0.1923	0.1916	0.0195	0.0181	0.0185	0.856	5.986
	BNsheet-OC	0.2103	0.1906	0.1894	0.0214	0.0181	0.0183	0.874	5.320
	BNsheet-NC	0.2026	0.1923	0.1908	0.0202	0.0183	0.0185	0.860	5.301
	BNsheet-CN	0.2062	0.1905	0.1888	0.0211	0.0179	0.0181	0.866	5.956

Conclusions:

The results of 6-center DI for π components of electron density of BNsheet show that the substitutions remove the uniformity of electron density and reduce local aromaticity of hexagonal BN ring connected to substituents.

References:

- [1] R.F.W.Bader, Atoms in Molecules, A Quantum Theory, Oxford University Press, (1990).
- [2] S. M. Azami, J. Phys. Chem. A., 114 (2010) 11794.
- [3] J. Kruszewski, T. M. Krygowski, Tetrahedron Lett. 36 (1972) 3839.
- [4] M. Mandado, M. J. Gonzalez-Moa, A. Mosguera, J. Comput. Chem. 28, (2007), 127.



Mapping electron dynamics in molecular H₂ using HHG time profiles

Behnaz Buzari^{a*}, Mohsen Vafaei^b, Hassan Sabzyan^a

^a Department of Chemistry, University of Isfahan, Isfahan 81746-73441, I. R. Iran

^b Department of Chemistry, Tarbiat Modares University, P. O. Box 14115-175, Tehran, I. R. Iran

Email: sabzyan@sci.ui.ac.ir, mohsenvafaei@gmail.com,

Keywords: HHG; H₂; TDSE; Homolytic; Ionic; Ultrashort intense laser; two-electron.

Introduction:

Prediction of the electron dynamics prior to the formation of an ion pair by an ultrashort laser field is the keystone to the control of chemical reactions. The hydrogen molecule is one of the most fundamental few-body, and the smallest quantum systems. Nevertheless, when exposed to strong laser fields, it exhibits a variety of specific ionization and dissociation phenomena in the nonperturbative electron dynamics regime [1,2].

Method:

The instantaneous electronic wavefunction (wave packet) of H₂ in a nonrelativistic intense laser field is obtained exactly by applying the time propagation technique for solving the one dimensional (1D) time-dependent Schrödinger equation (TDSE). Special attention is paid to the dynamics of the isolated *homolytic* and *ionic* doorways or transient species produced during the evolution of the two-electron wave packet of H₂ based on the three alternative forms of high-harmonic generation (HHG) spectra, including position, velocity, and acceleration moments.

Result and discussion:

The ultrafast electronic and nuclear dynamics of the preionization (doorway) *homolytic* and *ionic*

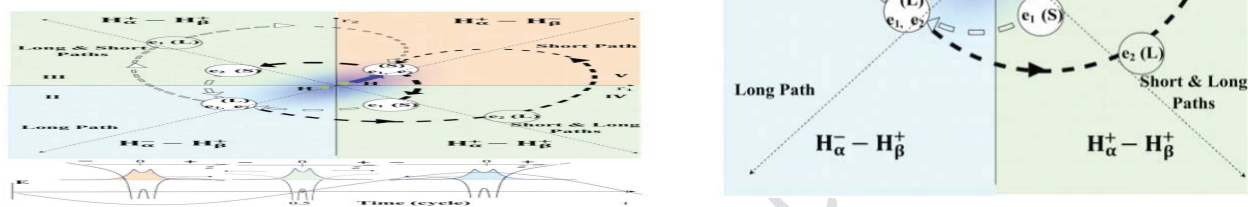
quasi-states of the two-electron molecular H_2 in the presence of ultrashort intense laser pulses of 532 nm wavelengths with $I = 1 \times 10^{14} \text{ Wcm}^{-2}$ intensity is studied beyond the Born-Oppenheimer (fixed nuclei) approximation.

Space of the electron density of the two-electron 1D H_2 system around the nuclei is partitioned into four physicochemically significant partitions, including *homolytic* $(e_1H_\alpha^+ - H_\beta^+e_2) \sim (e_2H^{+\alpha} - H^{+\beta}e_1)$ and *ionic* $(H_\alpha^+ - H_\beta^-) \sim (H_\alpha^- - H_\beta^+)$ transient species. The underlying mechanisms responsible for the formation and evolution of the *homolytic* and *ionic* transient species are explored based on probing variation of the two-electron norms of these states and their corresponding time-dependent HHG spectra.

Conclusion:

Analysis of the Gabor transform of the HHG spectra over the whole duration of the interaction shows that both electrons of the *ionic* $(H_\alpha^+ - H_\beta^-)$ transient species follow a short-path trajectory, while both electrons of the *ionic* $(H_\alpha^- - H_\beta^+)$ transient species follow a long-path trajectory. The role and sequence of the formation of these two complement ionic species switches with switching the starting phase of the laser field. At each evolution instance of the *homolytic* $(e_1H_\alpha^+ - H_\beta^+e_2) \sim (e_2H^{+\alpha} - H^{+\beta}e_1)$ species, the electronic wave packets of the two electrons are spread alternatively via both the SP and LP. These results are summarized in Figure 1.

FIG. 1. Simulation box, corresponding to the un-ionized central H_2 system introduced by Vafaei *et al.* [3], adopted in this study. The two (green) dots near the origin represent initial positions of the nuclei. SP and LP denote the short and long paths, respectively.



Reference:

- [1] Y.-J. Jin, X.-M. Tong, and N. Toshima, *Phys. Rev. A* **81**, 013408 (2010).
- [2] J. L. Sanz-Vicario, H. Bachau, and F. Martin, *Phys. Rev. A* **73**, 033410 (2006).
- [3] M. Vafaei, F. Sami, B. Shokri, B. Buzari, and H. Sabzyan, *J. Chem. Phys.* *in press*.



Computational investigation on the regioselective Sonogashira synthesis of 6-(4-nitrobenzyl)-2-phenylthiazolo[3,2-b]1,2,4 triazole

T. Hosseinnejad^{a*}, M. M. Heravi^a, R. Firouzi^b

^a Department of Chemistry, Faculty of Science, Alzahra University, Vanak, Tehran, Iran

^b Chemistry & Chemical Engineering Research Center of Iran (CCERCI) P. O. Box 14335-186, Tehran, Iran

Email: tayebeh.hosseinnejad@alzahra.ac.ir

Key words: Density functional theory, Polarized continuum model, Sonogashira reaction, Regioselectivity, 1,2,4 Triazoles.

Introduction:

Although many efforts have been devoted to the preparation of 1,2,4 - triazoles by palladium catalyzed annulations strategies [1], the recent work of Heravi et al.[2] have led to a regioisomeric substituted thiazolo [3,2-b]1,2,4 triazoles with high yield and good regioselectivity during Sonogashira coupling reaction. The main objective of this study is to computationally investigate the underlying reasons for the experimentally observed regioselectivity in Sonogashira synthesis of 6-(4-nitrobenzyl)-2-phenylthiazolo [3,2-b]1,2,4 triazole [2] (expressed as isomer **3**) in the gas and solution phases from the structural and thermodynamic viewpoints via density functional theory (DFT) calculations.

Computational details:

The calculation of energetics as well as geometry optimizations was performed at two levels of DFT methods to assess the performance of these methods in prediction of geometry and energy: i) 6-31G* using the popular B3LYP level of theory and ii) 6-311+G* basis set with modern M06 functional [3]. In the case of iodine, the relativistic effective core potential (RECP) determined by Hay-Wadt [4], LANL2DZ, with accompanying basis set was used. All DFT calculations have been performed using GAMESS suite of programs [5].

Result and discussion:

We have first determined the optimized structure of isomer **3** by performing geometry optimization procedure in the gas phase and also PCM method with DMF as solvent and then we have compared the optimized structure with the available crystallographical data. The average absolute deviation (AAD) of X-ray experimental data with M06/6-311+G* calculated values in the gas and solution phases are 0.54% and 0.42%, respectively. The M06/6-311+G* optimized structure of isomer **3** in the gas phase was presented in Fig. 1.

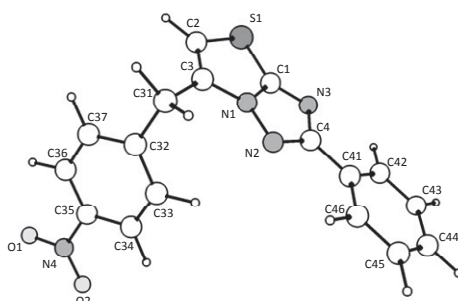


Fig.1

Table 1.

Regioselecti isomer	M06/6-311+G*				B3LYP/6-31G*			
	ΔE_c	ΔE_0	ΔH	ΔG	ΔE_c	ΔE_0	ΔH	ΔG
Isomer 3	34.65	41.24	42.67	50.37	28.47	35.46	41.45	49.79
Isomer 4	46.08	52.49	53.55	63.46	44.19	50.61	56.07	64.43



Thermochemical data, including reaction energies (with and without zero-point energy corrections), enthalpies and Gibbs free energies computed at B3LYP/6-31G* and M06/6-311+G* levels of theory in the gas and solution phases have been calculated and the gas phase calculated values have been presented in Table 1.

Conclusion:

In the first step, the validation of our calculated structural properties of the title compound was represented by comparison with the available X-ray crystallographical data that demonstrated a reliable agreement. Our calculated reaction enthalpies and free energies in the gas and solution phases indicate two important facts: i) the production of compound **3** is thermodynamically more favorable than its regioisomer **4** and ii) the employment of larger basis set and more modern functional leads to a decrease of about 4 kcal/mol in the difference between the reaction energies of regioisomer **3** and **4** while there is a close accuracy between these two levels of theory for the prediction of geometry.

References:

- [1] D.J. Dale et al.; "Gas-phase pyrolysis of 4-amino-3-allylthio-1,2,4-triazoles: a new route to [1,3]thiazolo[3,2-b][1,2,4] triazoles"; J. Chem. Soc. Perkin Trans.; 1, 424-428, 2001.
- [2] M.M.Heravi et al.; "Regioselective synthesis of 6-benzylthiazolo[3,2-b]1,2,4-triazoles during Sonogashira coupling"; Tetrahedron Lett. ; 46, 1607-1610, 2005.
- [3] D.G.Truhlar et al.; "The M06 suite of density functionals for main group thermochemistry, thermochemical kinetics, noncovalent interactions, excited states, and transition elements: two new functionals and systematic testing of four M06-class functionals and 12 other functional"; Theor Chem Account.; 120, 215-241, 2008.
- [4] W.R.Wadt et al.; "Ab initio effective core potentials for molecular calculations. Potentials for main group elements Na to Bi"; J. Chem. Phys.; 82, 284 -298,1985.
- [5] M. W. Schmidt et al.; "General atomic and molecular electronic structure system"; J. Comput. Chem.; 14, 1347-1363, 1993.



Interactions of Coinage Metal Clusters with Histidine and Their Effects on Histidine Acidity; Theoretical Investigation

Marjan Jebeli Javan^a, Zahra Jamshidi^{b*}, Zahra Aliakbar Tehrani^a & Alireza Fattahi^{a*}

^a Department of Chemistry, Sharif University of Technology, Tehran, Iran.

Email: fattahi@sharif.edu

^b Chemistry and Chemical Engineering Research Center of Iran, Tehran, Iran.

Email: jamshidi@ccerci.ac.ir

Key words: Coinage metal clusters, Histidine, Gas-phase acidity, QTAIM.

Introduction:

Nano cluster coinage metals and compounds have attracted lots of attention in medicine, catalysis fabrication of nano devices, and other applications according to their unique physical and chemical properties. The strength and reversibility of the inter-particle zwitterion-type electrostatic interactions between amino acid groups are evidenced by the slow disassembly upon increasing pH at ambient temperatures and its acceleration at elevated temperature. These findings provide new insight into the precise control of interfacial interactions and reactivities between amino acids anchored to nanoparticles and have broad implications in the development of colorimetric nanoprobes for amino acids. Histidine is one of the 20 naturally occurring α -amino acids that belongs to the group of aromatic and heterocyclic amino acids. It operates as a precursor of hormone histamine, and adjusts the amount of metal. It can bind a proton to the nonbonded electron pair of its ring nitrogen to become a weak acid at low pH. Histidine is the only amino acid that has a functional group that titrates in the physiological pH range. Histidine may be coordinated to metal atoms via amino groups, carboxyl groups, or the nitrogen atoms of the imidazole ring, thus acting as a mono-, bi-, or tridentate ligand. Gas-phase acidity (GPA) of organic compounds has been extensively investigated because it eliminates the effects of solvent and thus lets us study the intrinsic factors which influence the acidity of an organic compound. The reaction between metal clusters and organic molecules in the gas phase is an ideal environment in which the



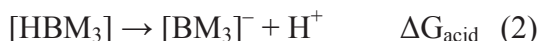
complexation mechanisms, the binding energies, the enthalpies, and the reactivity of the metal ions can be obtained in the absence of any complicating solvent effects.

Theoretical methods:

Geometries of the histidine complexes, in its neutral and anionic forms with M_3 clusters ($M = \text{Au, Ag and Cu}$) were fully optimized using the density functional theory (DFT) with B3LYP methods employing the Spartan 10 program. The 6-31+G** basis set was used for the atoms in histidine, while for M_3 clusters the Los Alamos effective-core potential (ECP) Lanl2DZ basis set was applied. The effect of solvation was taken into account using Polarized Continuum Model (PCM). The Natural bond orbital (NBO) was conducted for these complexes in order to obtain the natural charges. Quantum theory of atoms in molecules (QTAIM) analysis was performed with AIM2000 package to calculate the properties of bond critical points (BCPs).

Result and Discussion:

The interaction of histidine with M_3 clusters that serve as simple catalytic model of Au, Cu, and Ag nano particles was investigated. Theoretical calculation was performed with 6-31+G** LANL2DZ basis set. For this purpose, histidine amino acid was chosen in two different forms (anionic ($-$), and neutral (\cdot)). Interactions of M_3 clusters with these forms of histidine were explored and the corresponding thermodynamic properties were computed. Quantum theory of atoms in molecules (QTAIM) was used to determine the nature of bond between the amino acids and clusters. Natural bond orbital (NBO) analysis was also applied to investigate the charge transfer of complexes. Also, the acidity of His and His-OMe (denoted by HB in Eq (1)) was first calculated based on Eq (1). Then, using the same computational methods, the acidities of the metal-complexed species of these compounds (denoted by $[\text{HBM}_3]$, (where M_3 includes Au_3 , Ag_3 and Cu_3) were also calculated based on Eq (2).



Another goal of this work is to predict the pK_a values which are not experimentally available. In this paper, we predict the pK_a values in water for the same set of acids calculated in gas phase. Good agreement is found between our calculated pK_a values and GPAs of compounds.



Conclusion:

Interaction of histidine with Au₃, Ag₃ and Cu₃ clusters has been illustrated in the geometrical, spectroscopic, and energetic aspects. The bond lengths of A-X in histidine increase after complexation, and the stretching modes of these bonds undergo a red shift with respect to isolated ones. In the next step, the effects of Au₃, Ag₃ and Cu₃ clusters on the gas-phase acidity of histidine have been explored. The results of this study indicate that, upon metal complexation, the gas-phase acidity (GPA) of the studied weak organic acid drastically increases to the extent that it converts the weak acids of interest to a super acid. For instance, ΔG_{acid} of H₂SO₄ (known as a super acid in the gas phase) is 306.3 ± 3.1 kcal/mol. However, the acidities His and His-OMe examined herein are considerably enhanced (they become less endothermic, on average, by almost 40 kcal/mol) when the compound is complexed with Au₃, Ag₃ and Cu₃ clusters.

Reference:

- [1] A. H. Pakiari and Z. Jamshidi, *J. Phys. Chem. A.*, **2007**, *111*, 4391-4396.
- [2] Z. Zhong, S. Patskovskyy, P. Bouvrette, J. H. T. Luong and A. Gedanken, *J. Phys. Chem. B*, **2004**, *108*, 4046-4052.
- [3] A. Fattahi and E. Tavasoli, *J. Phys. Org. Chem*, **2008**, *21*, 112-118.



Protonated Phenol :Electronic Properties

Shirin Azizkarimim, Reza Omidyan* and Gholam Hasan Azimi

Department of Chemistry, University of Isfahan, Isfahan 81746-73441, I. R. Iran

E-mail: sh.karimi365@yahoo.com, r.omidyan@sci.ui.ac.ir

Keywords: aromatic molecules, Electronically transition, protonation, protonated molecules.

Introduction:

Aromatic molecules are important in the wide range of science. Particularly their biological role for constructing the molecular building blocks such as proteins and DNA is crucial. Phenol is one of the simplest aryl alcohols with several applications in the organic chemistry, biology and bio-chemistry. Hence, heavy experimental and theoretical studies were done on the electronic transitions and electronic structures of this molecule [1, 2].

Protonation is a fundamental chemical reaction. Recent advances in the laser spectroscopy and *ab initio* computational methods provide a good situation to study the isolated protonated aromatic molecules in the gas phase [3]. The protonation effect in the electronic properties of phenol and substituted phenol is the main subject of this study.

Computational methods:

The “*ab initio*” calculations, have been performed with the TURBOMOLE program, making use of (RI) approximation to evaluation of the electron-repulsion integrals. In all of calculations, the starting geometries were constructed with *C_s* molecular symmetry and the equilibrium geometry at the ground electronic states (*S*₀) has been determined at the

MP2/cc-pVDZ level. At the optimized excited state geometries, the energy of the ground state and two lowest excited states of A' and A'' symmetries were determined at the RI-CC2/cc-pVDZ and aug-cc-pVDZ levels.

Results and discussion:

Several isomers can be produced by protonation of phenol. Hence, our first goal was to find the most stable protonated isomer by optimization of the ground state geometry at the MP2/cc-pVDZ level. According to calculations, the most stable isomer of protonated phenol is Para-Isomer (C4), which is planar and has the Cs symmetry point group. The optimized S₁ excited state of C4 under the Cs symmetry is planar, although, without the symmetry restriction, the S₁ optimized geometry shows a drastic out of plan deformation in the benzene ring. The adiabatic electronic transition energy for S₁ (A'₁, ππ* state) at the CC2/aug-cc-pVDZ level has been determined the value of 4.34 eV for the C4 protonated isomer of phenol (see Table 1). The experimental value of 4.50 eV was reported by Pino et al for the 0-0 band of S₁ (ππ*) state in the neutral phenol [4]. This shows that the protonation has very small red shift effect on the S₁ state of phenol.

Protonated phenol (C4 isomer)		Neutral Phenol	
Excited State	Adiabatic Energy(eV)	Excited State	Adiabatic Energy(eV)
A' ₁ (ππ*)	4.34	A' ₁ (ππ*)	4.67
A'' ₁ (σπ*)	5.32	A'' ₁ (πσ*)	Notconverged



Table 1: Adiabatic transition energies of the lowest electronic excited states of the C4 protonated phenol and the neutral phenol, calculated at RI-CC2/aug-cc-pVDZ level of theory under the Cs symmetry point group.

Conclusion:

In comparison to neutral phenol, the main effect of protonation is a red shift of the first $\pi\pi^*$ electronic transition of protonated phenol. The full optimized geometry (without symmetry constraint) of the first $\pi\pi^*$ electronically excited state of protonated phenol showed a drastic geometry deformation. This behavior may lead to a short life time excited state of protonated phenol, which can be accompanied with a broad and structurless electronic spectrum.

References:

- [1] R. J. Lipert and S. D. Colson, J. Phys. Chem. **93**, 135 (1989).
- [2] C.-M. Tseng, Y. T. Lee, and C.-K. Ni, J. Chem. Phys. **121**, 2459 (2004).
- [3] F.O. Talbot, T. Tabarin, R. Antoine, M. Broyer , and P. Dugourd, J. Chem. Phys. **122**, 074310 (2005).
- [4] G. A. Pino, A. N. Oldani, E. Marceca, M. Fujii, S.-I. Ishiuchi, M. Miyazaki, M. Broquier, C. Dedonder, C. Jouvet, J. Chem Phys, **133**, 124313 (2010).



Physical chemistry: from theory to application, from laboratory to industry

A. H. Jalili^{a*}

^a Gas Science Department, Research Institute of Petroleum Industry, P.O. Box 14665-137, Tehran, Iran

(Email: jaliliah@ripi.ir)

Keywords: applied thermodynamics, phase equilibria, thermo-physical properties, natural gas sweetening, process simulation .

In the Iranian chemistry community, it has been judged that physical chemistry is a discipline studying chemical phenomena only from theoretical and physical points of view without any application in the society and industry. In this presentation, it will be demonstrated that physical chemistry, as one of the most active research areas of science, plays an important role to promote such industrial areas as oil and gas industries as well as many other practical disciplines. This way a demonstration will be presented to depict the road map from thermodynamics laboratory to simulation and design an industrial natural gas refinery plant. The presentation includes the following topics:

- An overview of natural gas sweetening industry and its national and economic importance.
- Measurement and modeling phase equilibria in systems comprised of acid gas + chemically reactive aqueous electrolyte solutions at low and high pressure regions.
- Measurement and modeling thermo-physical properties of complex aqueous solutions at low and high pressure regions.



- Measurement and modeling kinetics of absorption of acid gases in complex aqueous solutions.
- The importance and applications of the experimental data generated in the laboratory to process design and simulation.
- Development of a process simulation package to simulate and design a natural gas sweetening plant based on a specific newly formulated solution.
- Design and construction of a gas sweetening pilot plant to analyze long term process performance of newly formulated as well as conventional industrial solutions.

Acknowledgements:

The research council of the Research Institute of Petroleum Industry (RIPI) and the Research and Technology of National Iranian Gas Company (NIGC) for their support of this work are gratefully acknowledged.



Corrosion and scale inhibition of admiralty brass in cooling water system by aminotris-(methylenephosphonic) acid

K. Abutalebi^{a*}, N. Ghalebsaz Jeddi^a, S. Abutalebi

^aDepartment of Chemistry, Islamic Azad University Tabriz Branch, Tabriz, Iran

Email: kh.abotalebi@gmail.com

Key words: corrosion inhibitor, Antiscale efficiency, Admiralty brass, EIS, cooling water

Introduction:

Water is the most commonly used cooling fluid to remove unwanted heat from heat transfer surfaces [1,2]. Two of the main problems of cooling systems are corrosion and scale phenomena. Using phosphonates, $R_3C-P(O)(OH)_2$, as inhibitors is one method of preventing mineral scale and corrosion in these systems. Phosphonates are generally considered to be $CaCO_3$ and $CaSO_4$ scale inhibitors and react stoichiometrically with the calcium ions and form insoluble Ca-phosphonate precipitates which share some of the same harmful effects as the other forms of scale being inhibited [3]. In this work, the corrosion and scale inhibition property of the aminotris-(methylenephosphonic) acid (ATMP) have been studied by using potentiodynamic polarization and electrochemical impedance spectroscopy (EIS) techniques plus weighing.

Materials and methods:

The ATMP inhibitor was added to the cooling water system solution in different concentrations. Admiralty brass (AB) with chemical composition of 70% Cu, 29% Zn and

1% Sn were used as working electrode. At first, the working electrode was polished mechanically and then exposed to test solution. A Pt sheet and saturated calomel electrode (SCE) were used as a counter and reference electrode, respectively. All the measurements were conducted after 2 h. The potentiodynamic Tafel measurements were done by the scan rate of 2 mV/s. The EIS experiments were carried out in the frequency range of 10 kHz to 0.01 Hz. It could be understandable that the antiscaling efficiency is a function of the mass of scale on WE. If the mass of the scale deposited on WEs in blank and scale inhibitor added aqueous samples is defined as Δm_0 and Δm_1 , respectively, the antiscaling efficiency could be expressed as follows:

$$\eta = (\Delta m_0 - \Delta m_1) / \Delta m_0$$

Eq. (1)

Results and discussion:

The different concentrations of ATM scale inhibitor were added in the tested aqueous sample and the deposited scale mass on WE and the corresponding antiscaling efficiency calculated from Eq. (1) were listed in Table 1. It is seen that the best performance was observed with 60 ppm of ATMP. Polarization measurement has been done and polarization curves are shown in Fig. 2. The results indicate that all the cathodic polarization curves are parallel and suggest that the hydrogen evolution is activation controlled and the reduction mechanism is not affected by the presence of the inhibitor. By increasing the ATMP concentration up to 60 ppm, E_{corr} became constant and the I_{corr} was decrease from 9.2 to $1.5 \mu\text{A}/\text{cm}^2$. Based on the decrease of the cathodic and anodic currents, ATMP is considered as a mixed type inhibitor. By increasing the 80 and 100 ppm of ATMP, I_{corr} were increased because high concentration of ATMP can dissolve the Cu ions and causes the dezincification of alloy. Fig. 3 shows the obtained Nyquist diagrams of AB in water cooling system solution in presence of different concentrations of ATMP. The Nyquist plots show, at least, two “depressed” capacitive loops

with real impedances ranging from 3 to 12 $k\Omega cm^2$. The best anticorrosion performance was observed by only 60 ppm of ATMP and the corrosion resistance was found 20.6 $k\Omega cm^2$.

Table1. The scale mass on WE in various aqueous samples and the corresponding antiscle efficiency.

Aqueous samples	Blank	ATMP-20ppm	ATMP-40ppm	ATMP-60ppm	ATMP-80ppm	ATMP-100ppm
Δm	0.02	0.0114	0.0043	0.0028	0.0079	0.0138
Antiscale efficiency	-	43.2%	78.4%	85.7%	60.4%	30.6%

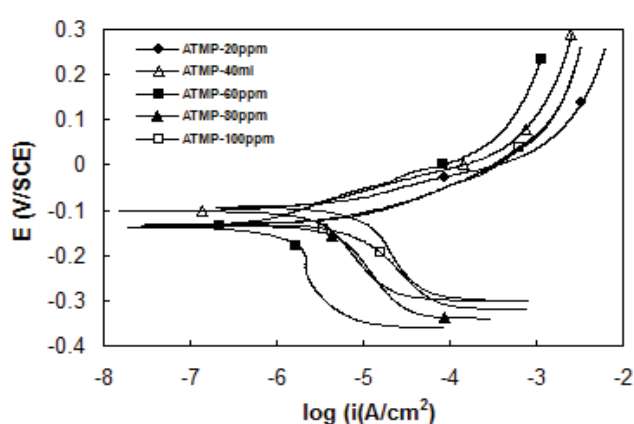


Fig 2. Polarization curves for AB in different concentration of ATMP

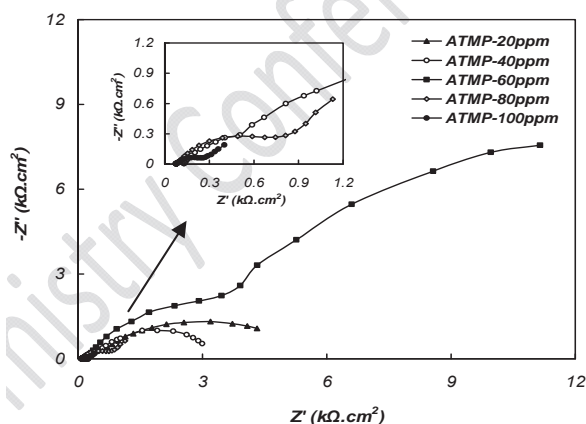


Fig 3. Nyquist plots of AB in different concentration of ATMP

Conclusion:

The corrosion and antiscale inhibition of ATMP have been evaluated. The results of weighting method show that the addition of 60 ppm of ATMP can inhibit scale formation and



the electrochemical methods suggest that the best anticorrosion performance can be observed by only 60 ppm of ATMP.

Reference:

- [1] R. Tourir, N. Dkhireche, M. Ebn Touhami, M. Lakhriss, B. Lakhrissi, *Desalination* 249 (2009) 922–928.
- [2] C. Wang, S. Li, T. Li, *Desalination* 249 (2009) 1–4.
- [3] B. Zhang, Y.N Chen, F.T. Li, *Colloids and Surfaces A*: 385 (2011) 11– 19.



Electrochemical Investigation to Evaluate the Inhibition Effect of Schiff Base (Salpr) Against Magnesium Corrosion in Acidic Media

Davood Seifzadeh*, Hadi Basharnavaz

Department of Applied Chemistry, Faculty of Sciences, University of Mohaghegh Ardabili, Ardabil, P. O. Box:
56199-11367, Iran

*Email: d_seifzadeh@uma.ac.ir

Keywords: inhibitor, corrosion, Mg, Acidic, EIS, EN.

Introduction:

Magnesium and its alloys are increasingly used in aerospace and automotive applications owing to their ultra lightness (Their density is thirds that of aluminum and one fourth that of iron) and high strength to weight ratio [1]. However, Mg is highly chemically reactive when exposed to air or water and forms oxide/hydroxide layer, which make it very susceptible to galvanic corrosion. The poor corrosion resistance of magnesium and its alloys restrict their wide application [2-3]. In this work, the inhibition effect of *N,N*-bis(salicylidene)-2-hydroxy-1,3-propandiamine (Salpr) Schiff base on magnesium corrosion was studied using different electrochemical methods including; potentiodynamic polarization, Electrochemical Impedance Spectroscopy (EIS) and Electrochemical Noise (EN) methods.



Materials and methods:

A three-electrode cell, consisting of magnesium working electrode (WE), a platinum sheet as counter electrode (CE), and a saturated Ag/AgCl electrode as a reference electrode, were used for electrochemical impedance spectroscopy (EIS) and polarization measurements. Electrochemical tests were carried out using a μ autolab3 potentiostat-galvanostat and Nova software (version 1.6) were used for data recording. Electrochemical noise data were also recorded using a μ autolab3 potentiostat-galvanostat and Nova (version 1.6) software.

Results and discussion:

Salpr inhibits both the anodic and cathodic reactions by blocking the local anodes and cathodes on the magnesium surface and acts as a mixed type inhibitor. Salpr is an effective inhibitor for corrosion of magnesium in 0.01 M concentration of hydrochloric acid, and the inhibition efficiency increases by raising the concentration of inhibitor. The inhibition efficiency increases from 27.64 % to 79.16% respectively, for the lowest and the highest concentrations of inhibitor. EIS results show that as the concentration of inhibitor increases, the charge transfer resistance is raised and the double layer capacity is decreased. The data obtained by analysis of electrochemical noise data in frequency domain, are in relatively good numerical and good trend agreement with the polarization and EIS results. Salpr acts through adsorption on the magnesium surface and its adsorption obeys the Langmuir adsorption isotherm. The values of ΔG_{ads} showed that Salpr adsorbs on the magnesium surface via physisorption. Surface morphologies of the magnesium samples were observed by Scanning Electron Microscopy (SEM) before and after the immersion of samples in inhibited and blank acid solutions. SEM images revealed that the magnesium surface damage is significantly decreased by the mentioned inhibitor.



Conclusion:

Salpr Schiff base behaves as efficient corrosion inhibitor and its inhibition efficiency increases by inhibitor concentration. Salpr acts through adsorption on the magnesium surface and its adsorption obeys the Langmuir adsorption isotherm. The data obtained by analysis of electrochemical noise data in frequency domain is relatively in good agreement with the polarization and EIS results.

Reference:

- [1] J. Hu, D. Huang, G. L. Song, X. Guo, *Corros. Sci.* **53** (2011) 4093-4101.
- [2] J. Zhang, Y. Chan, Q. Yu, *Prog. Org. Coat.* **61** (2008) 28-37.
- [3] H. Ashassi-Sorkhabi, D. Seifzadeh, M. G. Hosseini, *Corros. Sci.* **50** (2008) 3363-3370.



Non-isothermal degradation kinetics of Un-irradiated and High Energy Protons Irradiated Polyvinyl Butyral

Manoochehr Fathollahi¹, Hassan Behnjad^{1,*}, Muhammad Shadman²

¹Department of Chemistry, Faculty of Science, Tehran University, Tehran, Iran.

²Department of Chemistry, Faculty of Science, University of Zanjan, P.O.Box 313, Zanjan, Iran.

(*Corresponding author E-mail address: behnejad@gmail.com)

Key words: Thermal decomposition, Proton irradiation, polyvinyl butyral

Introduction:

One of the methods of modification, upgrading, stabilization and changing the properties of polymers is based on the irradiation with high energy accelerated radiation (gamma rays, X-rays, and accelerated ion beams). Irradiation of polymers with high energy radiations leads to the formation of very reactive intermediates in the forms of excited states, ions and free radicals. These intermediates are almost instantaneously used up in several reaction pathways which result in the arrangement or formation of new bonds structures. The ultimate effects of these reactions are the formations of oxidized products, grafts, cross-linking and scissoring of main or side chains which are also called degradation. The degree or dominance of these transformations depend on the nature of the polymer and the conditions of treatment before, during and after irradiation and close control of these factors make the modification of polymers possible by radiation processing.

In this study the thermal behavior and Kinetic models for decomposition of the irradiated and unirradiated polyvinyl butyral (PVB) were investigated based on DTA and DTG



thermograms, as well. Experimentally, solid-state kinetics is studied either isothermally or nonisothermally. Many mathematical methods have been developed to interpret experimental data for both heating protocols. These methods generally fall into one of two categories: model-fitting and model-free. Historically, model-fitting methods were widely used because of their ability to directly determine the kinetic triplet (frequency factor $[A]$, activation energy $[E_a]$ and model). There are many model fitting methods that extract the three kinetic parameters known as the kinetic triplet from nonisothermal data. These methods were used extensively earlier in solid-state kinetic analysis [1-7]. In the present work, we used nonisothermal model-fitting direct differential method.

Materials and methods:

The polyvinyl butyral (PVB) film with 20 μm of thickness made by RisØ Co., Denmark, were used in this experiment. Irradiation was carried out about 5 Secs with 30 MeV accelerated protons on the Cyclon-30 cyclotron made by IBA Company, Belgium. The thermograms of un-irradiated and irradiation samples (2 ± 0.1 mg) were recorded in a nitrogen atmosphere at a heating rate of 10 Kmin^{-1} from 30 to 700°C using a thermal analyzer (NETZSCH-Geratebau GmbH STA 409 PC).

Result and Discussions:

Thermal degradation is a very important process which helps in determining the influence of the polymer morphology on the thermal stability, the optimum temperature of operation and the activation energies related to the degradation processes. Thermogravimetric analysis (TGA) has been proved to be reasonably rapid and precise method for the determination of such kinetic parameters related to the degradation processes [8]. The kinetic analysis of thermal degradation of un-irradiated and irradiated PVB was carried out by using the

dynamic weight loss data from the thermogravimetry (TGA). The TGA/DTG thermograms of un-irradiated and irradiated PVB are shown in Fig.1. As shown in Fig.1.a the decomposition of un-irradiated PVB proceeds in two steps in the temperature range of 155.87-624.42 °C with the two peak temperature 321.48°C and 529.56 °C. But the decomposition of irradiated PVB as shown in Fig.1.b proceed in one major step in the temperature range of 269-509 °C with the peak temperature 388.5°C. The decomposition rate of a specimen can be represented by the rate expression [9] as Eq. (1), where α is the fraction of solid decomposed at time t , $f(\alpha)$ is a function of α depending on the reaction mechanism and k is the rate constant given by the Arrhenius equation, If Eq. (1) is combined with the Arrhenius equation and a constant heating rate $\beta = dT/dt$ (K/min) is employed, the decomposition rate equation can be written in differential form as (Eq. (2)), An empirical relation exists between frequency factors and activation energies. Where A is the pre-exponential factor (1/min), E is the activation energy (J/mol), R is the universal gas constant (8.314 J mol⁻¹K⁻¹), T is the temperature of reaction (K).

$$\frac{d\alpha}{dt} = kf(\alpha) \quad (1)$$

$$\frac{d\alpha}{dT} = \frac{A}{\beta} \exp\left(-\frac{E_a}{RT}\right) f(\alpha) \quad (2)$$

In this study, we adopted an approximation of the integrated form as (Eq. (3)), [9,10]. Where $F(\alpha)$ is the integral form of the empirical function $f(\alpha)$, $(E+2RT)$ is assumed to be constant for moderate temperature. In these data analysis, a homogeneous reaction Order-based (F) model, $F(\alpha) + (1-\alpha)^n$, is found to give the best fit of the data at the range of the major weight loss region whit different reaction order (n) for un-irradiated and irradiated samples as summarized in table 1.

$$\ln \left[\frac{F(\alpha)}{T^2} \right] = \ln \left[\frac{AR}{\beta(E_a + 2RT)} \right] - \frac{E_a}{RT} \quad (3)$$

As shown in Fig. 2, the plot of $\ln[F(\alpha)/T^2]$ vs. $1/T$ results in a straight line with a slope of $-E/R$ giving the activation energy $[E_a]$, and frequency factor $[A]$, can be calculated from the activation energy and the intercept on the Y axis. The values of activation energy, frequency factor and other thermal decomposition parameters for unirradiated and irradiated PVB are summarized in Table 1.

Conclusion:

The thermal properties of un-irradiated and irradiated PVB nitrogen were investigated by TGA/DTG, and compared. From the results obtained, the activation energies and frequency factor for thermal degradation of PVB film increase with the high energy protons irradiation. This study clearly indicates that the thermal stability of PVB as an effect of 30 MeV accelerated protons irradiation is increased significantly. The increasing in thermal stability is correlated with the morphological changes induced in the PVB polymeric sample as a consequence of irradiation leads to the formation of very reactive intermediates in the forms of excited states, ions and free radicals. These intermediates are instantaneously used up in several reaction pathways which result in the arrangement and formation of new strong bonds and stable structure of PVB.

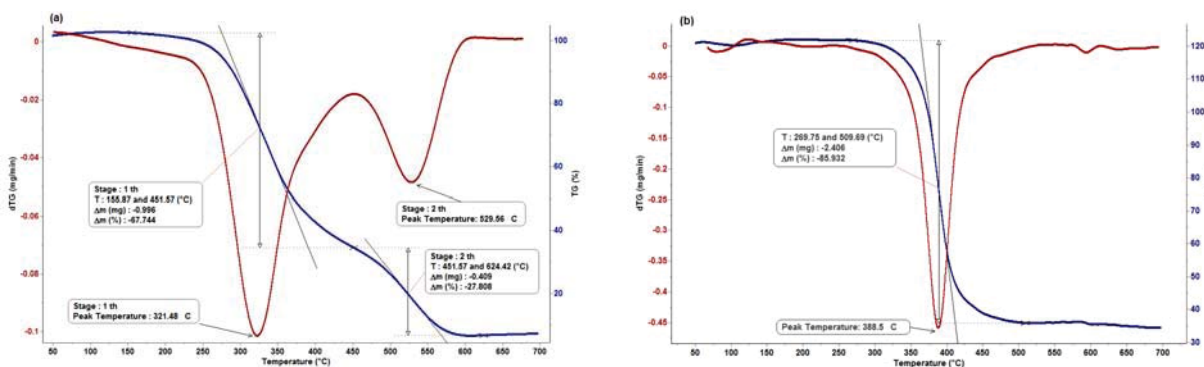


Fig.1. TGA/DTG curves of (a) Un-irradiated (b) Irradiated PVB in nitrogen

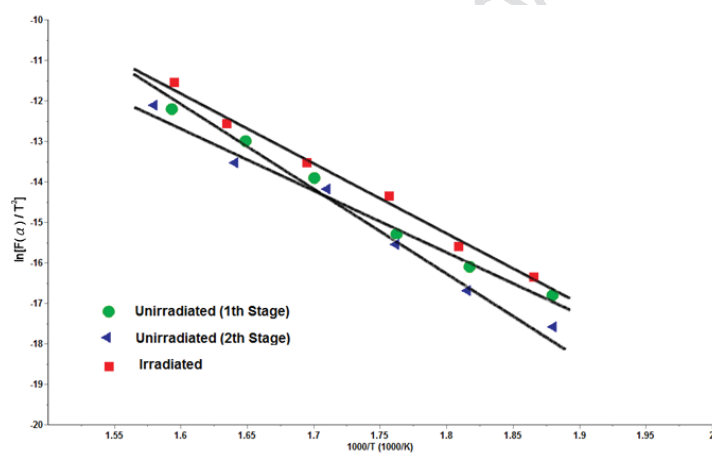


Fig. 2. Plot of $\ln[F(\alpha)/T^2]$ vs. $1/T$ for the determination of the activation energy

Table1. Results of thermal decomposition parameters for un-irradiated and irradiated PVB

Characteristics	Unirradiated		Irradiated
	1 st Stage	2 nd Stage	
T _{Onset} (°C)	155.87	451.08	269.75
Mass Changes (%)	-67.74	-27.81	-85.93
Peak Temperature (°C)	321.48	529.56	388.69
E _a (kJ/mol)	118.516	280.672	140.628
log A(-/s)	8.6164	20.67268	10.675
n	1.277	1.834	1.144
r	0.9862	0.9824	0.9969



Reference:

- [1] M. Shadman, F. Ziaie, S. Yeganegi, B. Niazi, F. Ziaee, A. Majdabadi, *e-Polymers*, No. 079, **2009**.
- [2] R. Gupta, V. Kumar, P.K. Goyal, Shyam Kumar, P. C. Kalsi, S. L. Goyal, *Advances in Applied Science Research*, 2 (2010) 248-254.
- [3] M. Fathollahi, S.M. Pourmotazavi, S.G. Hosseini, *Combust. Flame*, 138 (2004) 304-306]
- [4] M.Fathollahi, S.G.Hosseni, S.M.Pourmortazavi & F.Farahani; *J. of pyrotechnics*, Issue.18, Winter2003, p.p63-66
- [5] M. Shamsipur, S. M. Pourmortazavi, M. Fathollahi, *Journal of Energetic Materials*, (2011) 301-10.
- [6] S.M. Pourmotazavi, M. Fathollahi, S.S. Hajmirsadeghi, *Thermochimica Acta*, (2006) 443: 129-131.
- [7] S.M. Pourmotazavi, M. Fathollahi, S.S. Hajmirsadeghi, I. Kohsari, *Fuel*, (2008) 87, 244-251
- [8] Park JW, Oh SC, Lee HP, Kim HT, Yoo KO. *Polym Degrad Stab* (2000) ;67:535-40.
- [9] K.G.MALLIKARJUN, *E-Journal of Chemistry*, (2004) 1, 2, pp 105-109,
- [10] Yang TCK, Lin SSY, Chuang TH. *Polym Degrad Stab* 2002;78:525-32.



Cylindrical DBD Plasma Reactor: Cracking of Petroleum Fuel Oil into Light Olefins

^aSoulmaz Seyyed Shahabi, ^bMohammad Reza Khani, ^aMahtab Gharibi*, ^bAtieh Khosravi,

^aMohammad Reza Fadaie, ^bElham Dejban Guy, ^bBabak Shokri*

^aNational Petrochemical Company- Petrochemical Research & Technology Co. (NPC-RT),

Tehran Center, Iran, (m.gharibi@npc-rt.ir)

^bLaser and Plasma Research Institute and the Department of Physics, Shahid Beheshti University,

G.C., Tehran, Iran (b-shokri@suu.ac.ir)

Key words: Fuel Oil, Cracking, Non-thermal, Dielectric Barrier Discharge (DBD) plasma.

Introduction:

Petroleum fuel oil components such as light and heavy fuel oil (LFO and HFO) are various liquid or semi-solid materials from several industrial processes. Negligible quantities of fuel oil (C_{6+}) are produced by olefins plants using feedstocks of light paraffin such as ethane, whilst plants using naphtha or gas oil as feedstocks produce higher quantities of fuel oil.

Conversion (reforming, cracking, upgrading) of fuel oil to valuable hydrocarbon products is a very important technology for a variety of applications. In cracking process, it is necessary to get various useful hydrocarbon gases and oils. However, the chemistry of fuel oil upgrading is extremely complicated. Recently, a novel technology of plasma and catalytic process was studied by many researchers for hydrocarbon reforming [1-2]. In a plasma reactor there are many energetic electrons, ions and neutral particles being able to collide with hydrocarbons

and provide the energy required to crack the bands. Therefore, the produced radicals can join and introduce another hydrocarbon. These electrons could play the role of catalyst in FCC (Fluid Catalytic Cracking) process. Our approach in this work is to present briefly a new type of non-catalytic-non-thermal dielectric barrier discharge (DBD) plasma reactor [3] to convert C₁₁-C₁₈ heavy fuel oil (such as aromatic, naphthene and paraffin hydrocarbons) to lighter and marketable products at room temperature and under atmospheric pressure.

Materials and methods:

In the present work we have used a cylindrical DBD, 20 kHz ac power supply, cold trap and gas chromatography as shown in Fig. 1. This study consists of designing and developing the required DBD reactor, investigating the electrical behavior of the applied voltage and the gas flow rate on the plasma chemistry of the cracking quantitatively and qualitatively.

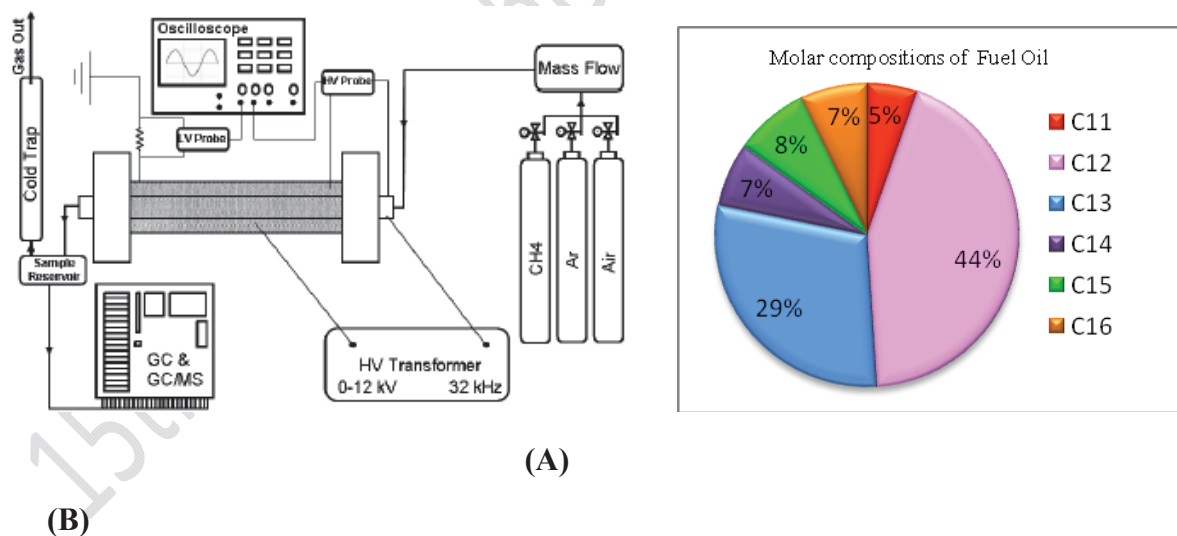


Figure 1. (A). Schematic representation of experimental setup used in this study.

(B). Molar compositions of Fuel Oil as a feed.



Result and discussion:

The results show that fuel oil can be cracked in the atmospheric pressure DBD and converted to relatively valuable (H_2 , CO, CO_2 , C_2 - C_5 valuable products) and partly heavier remaining hydrocarbons. Applied voltage and plasma-generating gas flow was 7.5 kV and 200 SCCM respectively. Qualitative analysis was done by GC-FID and verified by Gas Chromatography Mass Spectrometry (GC/MS).

Conclusion:

The valuable hydrocarbons have more percentage of the output products compared to the heavier hydrocarbons. Increasing the voltage and gas flow rate improve the cracking percentage that is assumed to happen due to increasing the stronger microdischarges in the DBD reactor.

References:

- [1]. Speight, J. G., *Fuel science and technology handbook*, Marcel Dekker: New York, **1990**.
- [2]. Chung, K. H., Xu, C., Hu, Y., Wang, R., *Oil Gas J.*, **1997**, 95, 66.
- [3]. M. R. Khani, S. H. Razavi Barzoki, M. Sahba Yaghmaee, S. I. Hosseini, M. Shariat, B. Shokri, A. R. Fakhari, S. Nojavan, H. Tabani, and M. Ghaedian. *IEEE Trans. Plasma Sci.*, **2011**, 39, 1807.



Methane conversion to Hydrogen and Higher Hydrocarbons by Kilohertz pulsed plasma

R. Lotfalipour, A. Mahdian and A. M. Ghorbanzadeh

Department of Physics, University of Tehran, Tehran 1439988961, Iran

Email: ata@khayam.ut.ac.ir

Keywords: Pulsed plasma, Methane conversion, Hydrogen, Hydrocarbons.

Introduction:

The production of hydrocarbons directly from methane requires high temperatures, which makes the process expensive and non-selective. One of the new approaches to activate reactants is the electric gas discharge. A series of plasma and chemical processes such as ionization, dissociation and excitation of molecules and atoms are initiated that make the ionized fluid far from thermodynamic equilibrium. In such non-equilibrium medium the temperature of electrons can reach several eV while the temperature of the reactants remains relatively low, near room temperature. Hence, the electron collisions are responsible for the dissociation of the molecules. There are various works demonstrating the possibility of methane conversion by non-thermal plasmas [1,2]. The main drawback of non-thermal plasmas is their low chemical energy efficiency, reaching 10% at most, which is far from the industrial demand that require high conversions at chemical efficiencies above 30%. The pulsed plasmas, however, demonstrated far better results [3-7]. The main advantage of the pulsed plasmas, relative to the continues ones, is due to its ability of rendering temporal non

equilibrium of population distribution among the molecular vibrational levels, through which the dissociation of the molecule take places more easily [8].

In this study we will examine the influence of electrode gap distance in the transformation of pure methane to produce hydrocarbons using short pulsed plasma reactor.

Methods:

Fig. 1 shows the experimental set-up. The reactor was made of a quartz tube consisting of two electrodes fabricated from aluminium. In order to produce uniform electric field, the upper electrode was shaped according to Ernest profile. The electric pulse is formed by discharging the bank capacitors through a high voltage thyatron switch. The repetition rate of pulsed discharge was controlled by a control-trigger from 3 to 20 kHz. The pulse voltage and current waveforms are sampled using current (Pearson 6585) and voltage (Tektronix P6015A) probes, which are connected to a four channel digital oscilloscope (Tektronix TDS3054C). The pulse energy is the area under the power waveform graph, calculated by the oscilloscope through the multiplication of current and voltage waveforms. The outlet products were analyzed using a three channel gas chromatograph (GC Varian CP-3800). The bulk gas temperature was estimated by the thermocouples attached to the outer wall of the reactor.

The conversion and selectivity are defined according to the following relations:

$$\text{Conversion} = \frac{m_{in}^{CH_4} - m_{out}^{CH_4}}{m_{in}^{CH_4}}$$

$$\text{Selectivity} = \frac{n_i \times m_{out}^i}{m_{in}^{CH_4} - m_{out}^{CH_4}}$$

Where $m_{in}^{CH_4}$, $m_{out}^{CH_4}$, m_{out}^i , and n_i are the moles of methane introduced, the moles of methane at the outlet, the moles of product i at the outlet and the carbon number of the product i , respectively.

Results and discussion:

Based on the oscillographs of voltage and current and the resulting power, the pulsed-power width was about 20 nanoseconds. At these short periods, nonequilibrium vibrational population distribution is built up. The different hydrocarbons up to C_6 were detected by FID detector, among which C_2 hydrocarbons and hydrogen were major products

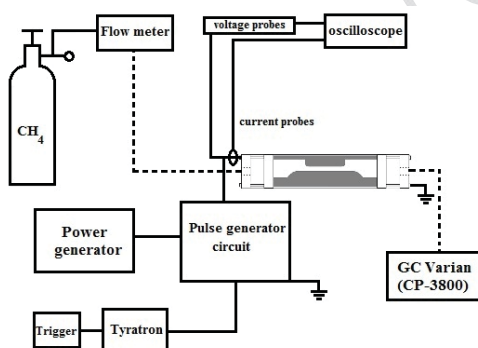


Fig. 1. A Schematic view of the experimental setup

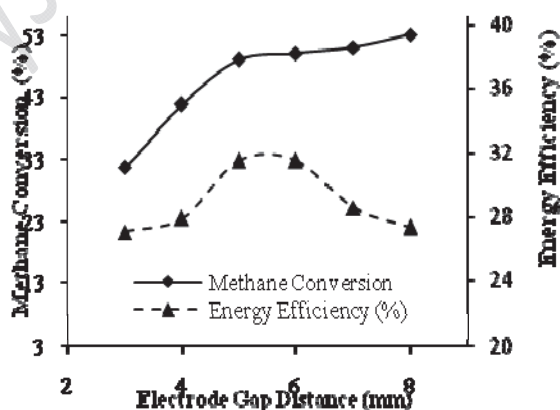




Fig. 2: Methane conversion and energy efficiency against electrode gap distance, applied voltage is 21 kV, frequency is 15.5 kHz and total feeding gas flow is 400 mL/min.

The methane conversion rate and energy efficiency versus the electrode gap distance is shown in Fig. 2. In general, there is an optimum value of gap distance at which the conversion performance is optimum. Hydrogen and acetylene were the main products of the conversion process, both having selectivities around 72%. The chemical energy efficiency reaches about 32% at conversion rate exceeding 50%, at the best point.

The optimum conversion parameters at gap distance of approximately 5 mm, is probably due to the optimum value of reduced field E/N , where E is electric field inside the plasma and N shows the total density of different molecules present in the medium. It should be noted that every parameter in a plasma, including the dissociation rate, is a function of reduced field.

Conclusions:

It was demonstrated that an optimum value of the electrode gap distance exists at which point the conversion performance of the plasma reactor was superior. The energy efficiency as high as 32% at conversion rates of more than 50% was obtained while the average temperature was around 100 °C. This achievement can be accounted for promising, regarding the low temperature processing of the methane.

References:

- [1] A. Marafee , C. Liu, G. Xu, R. Mallinson, and L. Lobban; Ind. Eng. Chem. Res.; 36 (3), 632- 637, 1997.
- [2] X. S. Li, A. M. Zhu, K. J. Wang, Y. Xu and Z. M. Song; Catalysis Today; 98, 617-624, 2004.
- [3] Y. Yun; Plasma Chemistry and Plasma Processing; 23, 283-296, 2003.



- [4] A. M. Ghorbanzadeh and N. S. Matin; *Plasma Chemistry and Plasma Processing*; 25, 57-72, 2005.
- [5] A. M. Ghorbanzadeh, H. Modarresi; *J. Appl. Phys.*; 101, 123303-123313, 2007.
- [6] X. S. Li, B. Zhu, C. Shi, Y. Xu , and A. M. Zhu; *AIChE Journal*; 55, 2854-2860, 2010.
- [7] Y. Sekine, N. Furukawa, M. Matsukata and E. Kikuchi; *J. Phys. D: Appl. Phys.*; 44, 274004-11, 2011.
- [8] A. M. Ghorbanzadeh, R. Lotfalipour, S. Rezaei; *International Journal of Hydrogen Energy*; 34, 293-298, 2009.



Conversion of Methanol to Light Olefins over Nanostructured Ce-MnSAPO-34 Catalyst Synthesized via Ultrasound Method

S. Aghamohammadi^{a,b}, M. Haghighi^{a,b*}, M. Charghand^{a,b}

^a Chemical Engineering Faculty, Sahand University of Technology, Tabriz, Iran

^b Reactor and Catalysis Research Center (RCRC), Sahand University of Technology, Tabriz, Iran

*Email: haghighi@sut.ac.ir

Keywords: Methanol, Olefins, MTO, Ce-MnSAPO-34, Hydrothermal, Ultrasound.

Introduction:

Nanostructured catalysts can be highly active for majority of reactions. In the present work, we report a research on the performance of bimetallic Ce-MnSAPO-34 catalyst in methanol to light olefins (MTO) process prepared by hybrid ultrasound-hydrothermal method.

Materials and methods:

Mn and Ce were introduced in to the SAPO-34 framework by isomorphous substitution and impregnation method respectively. Synthetic gel was transferred in to autoclave and heated at 200°C for 56 h. The catalyst was characterized with XRD and FESEM techniques. Catalytic conversion of methanol to olefins experiments were carried out in a U-shape Pyrex micro reactor (8mm i.d) at atmospheric pressure. Reaction gas, which was composed of 10 mol% methanol and 90 mol% H₂O, was allowed to flow with a gaseous space velocity of 4200 cm³/gr.hr⁻¹.

Result and discussion:

A detailed examination of diffraction pattern (as shown in Figure1) reveals the formation of SAPO-34 rhombohedral structure (JCPDS 01-087-1527) as indicated by diffraction peaks at $2\theta = 9.74$ and 12.85° . The average crystallite size was calculated 14.9 nm using Sherrer equation demonstrating the nanostructure framework of the synthesized catalyst. Implementing ultrasound method might be responsible for uniform particle size distribution achieved in this research [1]. Additionally, formation of some nano-scale particles over SAPO-34 crystals can be identified.

The effect of reaction temperature on the conversion of methanol over nanostructured Ce-MnSAPO-34 catalyst is shown in Figure 2. Specifically, as the temperature increases from 300 to 500°C , the methanol conversion changes from 85% to 100%. Temperature dependent selectivity variations over modified SAPO-34 are depicted in Figure 3. Both light olefins production and methanol conversion reach a maximum at 400°C .

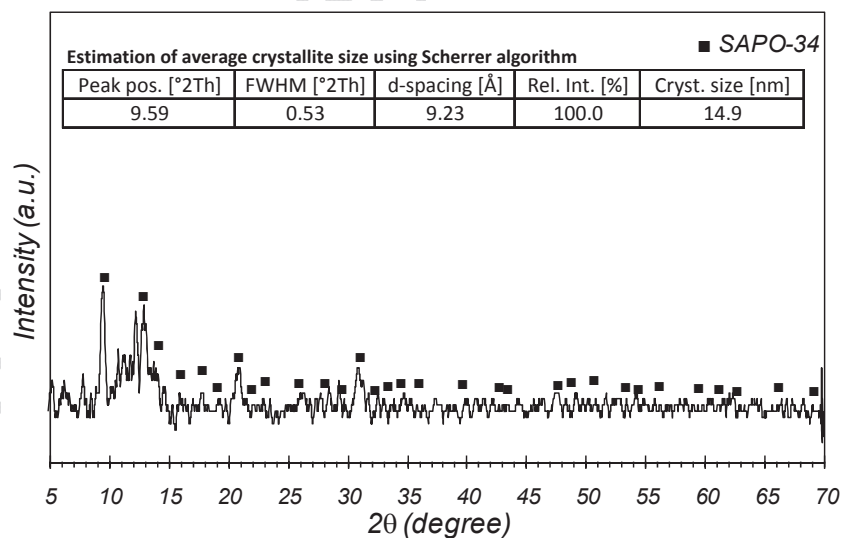


Figure 2: XRD pattern of Ce-MnSAPO-34.

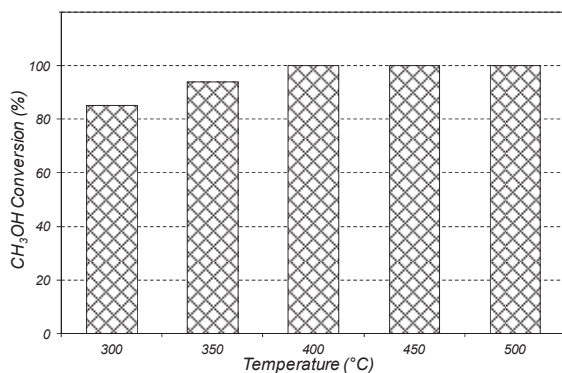


Figure 2: Methanol conversion over
Ce-MnSAPO-34 catalyst.

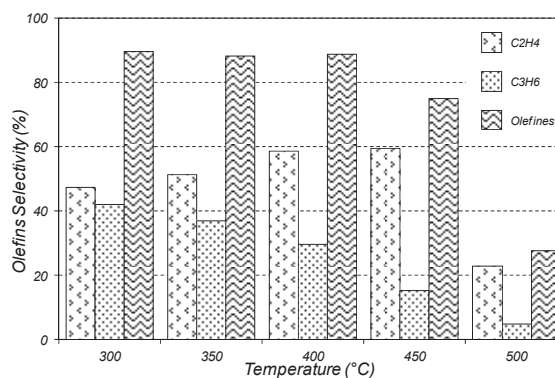


Figure 3: Olefins selectivities over
Ce-MnSAPO-34 catalyst.

Conclusion:

Introduction of Ce and Mn heteroatoms by the aid of ultrasound method lead to the excellent performance in MTO process. Light olefins selectivity reaches a maximum value of 90%.

References:

- [1] S. Askari and R. Halladj, "Ultrasonic pretreatment for hydrothermal synthesis of SAPO-34 nanocrystals", *Ultrasonics Sonochemistry*, 19, (3), 554-559, 2012.



Energetic of single-walled armchair, zigzag, and chiral silicon nanotube and investigate of the effect of stress on melting point with use molecular dynamic (MD) simulation

J. Davoodi^a, M. Soltani*^a

^aDepartment of Physic, University of Zanjan, zanzan, iran

Email: minasoltani85@gmail.com

Key Word: MD Simulation, Silicon Nanotube, Tersoff Potential, Stress, Melting Point

Introduction:

In this paper, are have performing simulations molecular dynamic (MD) simulation within an isobaric- isothermal ensemble. The tersoff potential many-body interatomic potential^[1] was used to model the energetic and dynamics of the stress on single wall silicon nanotubes (SWSiNTs), Our aim has been to calculate the melting temperature of SWSiNTs at the various radius size and investigate effect of stress on SWSiNTs too.

Simulation Details:

We considered three type of SWSiNTs, namely, armchair, zigzag, and chiral, of length 3.16, 4.8, 3.63nm respectively^[2]. The time for the simulation was set $\delta t = 1fs$. Each nanotube was equilibrated for 60000 time steps, during which the total energy remained content. The initial temperature was set at $T = 300K$, and was raised up to the melting point incrementally at 5K in each time step. The velocity Verlet algorithm was employed to integrate the equations of motion, and periodic boundary condition was applied along the axis of the nanotube in the z-direction

Result and Discussion:

The results are shown the transition a solid to liquid phase can be identified by a jump in the variation of cohesive energy with temperature (Figer 1.). An inspection of these variations

shows that the melting point of all type of nanotubes increase with the radii in a nonlinear manner. Such a behavior seems not to be radiuses dependent and more to be due to the symmetry property of the nanotubes themselves (Figer 2. left).. In other step, we supposed (8,0) zigzag nanotube for investigate the effect of stress on nanotubes (Figer2. right). We put it under various stress, and observed Stress on nanotube reducing stability of the nanotube and it's transition was down.

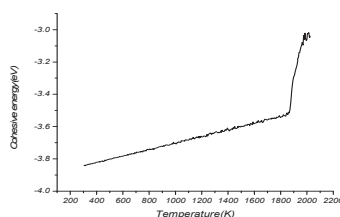


Fig. 1. Variation of the cohesive energy for the (14,14) armchair silicon nanotube during melting.



Fig. 2.left) The variation of the melting point (T_m) with the radius for set of armchair ($\theta = 30$ deg.) silicon nanotubes, right) The effect of stress on (8,0) zigzag nanotube

Conclusion:

The sum up, in this paper, we performed MD simulations based on tersoff potential, to investigate a solid-to-liquid phase transition involving three type of SWSiNTs. (zigzag, armchair, chiral). The results show that the melting temperatures of SWSiNTs depend on the nanotube radius as well a chiral angle and the stress on the nanotube makes coherent energy reduced and so, melting point reduced.

References:

- [1] J. Tersoff, Phys. Rev. Lett. 61, 2879 (1988).



[2] H. Raffi-Tabar, Computational Physics of Carbon Nanotube, Cambridge University Press, Cambridge (2008).

15th Physical Chemistry Conference



Experimental investigation on thermophysical properties of functionalized TiO₂-water nanofluids

M. M. Heyhat ^a, A.M. Rashidi ^b, F. Kowsary ^a

^a Mechanical Engineering Department, University College of Engineering, University of Tehran, Tehran, Iran

E-mail: mmheyhat@ut.ac.ir

^b Nanotechnology Research Center, Institute of Petroleum Industry (RIPI), Azadi Complex, Tehran, Iran

Keywords: Experimental study, Functionalization, Nanofluids, Thermophysical properties.

Introduction :

Nanofluids are a new class of nanotechnology-based heat transfer fluids produced by dispersing nanoparticles with sizes typically smaller than 100 nm into traditional heat transfer fluids such as water, ethylene glycol, and engine oil. Due to small sizes and very large specific surface areas of the nanoparticles, nanofluids have novel beneficial properties [1, 2]. In order to study the heat transfer performance of nanofluids and use them in practical applications, it is necessary first to study their thermophysical properties.

In this paper the four main thermophysical properties, i.e. density, specific heat capacity, thermal conductivity, and viscosity of TiO₂-water nanofluids at various particle volume concentrations and temperatures is measured experimentally. As the purchased nanoparticles had a hydrophobic surface, at first the TiO₂ nanoparticles are functionalized by a new chemical treatment and then dispersed in water. Furthermore, the measured data are used for comparison with the predicted values of the existing classical models.

Preparation of nanofluids:

The TiO₂ nanoparticles (Nanostructured&Amorphous Materials, Inc.) with a nominal average particle diameter of 15 nm and the density 3.9 g/cm³ were used. Distilled water was used as the base fluid. As the purchased nanoparticles had a hydrophobic surface, they agglomerated and precipitated when dispersed in water in the absence of a dispersant/surfactant. Thus, for better dispersion, TiO₂ nanoparticles were functionalized by a new chemical treatment as follows. The TiO₂ nanoparticles were mixed with 1,1,1,3,3,3, hexamethyldisilazane



(C₆H₁₉NSi₂) in a mass fraction ratio of 2:1. The resulting mixture was sonicated at 30 °C for 1 hour using ultrasonic vibration at sound frequency of 40 kHz. This process permitted to place the hydrophilic ammonium groups on TiO₂ nanoparticles surface. Then, the soaked nanoparticles were dried with a rotary evaporation apparatus. Finally, these dried functionalized nanoparticles were added to distilled water to produce the TiO₂-water nanofluids in different volume fractions (0.1, 0.5, 1, 1.5, and 2%). The nanofluids were sonicated continuously for 1 hour with an ultrasonic probe (400 W, 24 kHz).

Measurement of thermophysical properties:

The thermophysical properties of nanofluids are collected for temperatures ranging from 20 °C to 60 °C and for the nanoparticle volume fractions of 0.1, 0.5, 1, 1.5, and 2.0%. A SVM 3000 Stabinger Viscometer (Anton Paar GmbH) was used to measure the density according to ASTM D7042. The specific heat capacity was measured with a differential scanning calorimeter (DSC) (NETZSCH DSC 200F3-Maia) directly. The thermal conductivity was measured using a KD2 Pro thermal properties analyzer (Decagon devices, Inc., USA), which is based on the transient hot wire method. The U-tube (reverse-flow) capillary viscometer (Petrotest ® Instruments GmbH & Co. KG) was used to measure the kinematic viscosity of nanofluids and then the dynamic viscosity can be obtained by multiplying the measured kinematic viscosity by the density of the nanofluid.

Results and discussion:

Results show that the measured density and specific heat capacity are in good agreement with mixing theory and thermal equilibrium models, respectively [1]. Moreover, the measured viscosity and thermal conductivity of nanofluids are higher than the values of the base fluid. The thermal conductivity ratio of nanofluids increases with increasing particle volume concentration and slightly increases with increasing temperature and, conversely, the viscosity of nanofluids significantly decreases with increasing temperature and increases with increasing particle volume concentration. The existing correlations for calculating the thermal conductivity and dynamic viscosity of nanofluids failed to predict the experimental values correctly. Therefore, according to the experimental data two correlations are proposed for calculating these properties. Finally, obtained results show that the utilized functionalization



method can be an effective way to produce stable and suitable TiO_2 -water nanofluids with reasonable thermophysical properties.

References:

- [1] X.Q. Wang and A.S. Mujumdar “A review on nanofluids-part I: theoretical and numerical investigations” *Brazilian J. of Chemical Engineering*, Vol. 25, No. 04, pp. 613 - 630, 2008.
- [2] W. Yu and H. Xie, A review on nanofluids: preparation, stability mechanisms, and applications, *Journal of Nanomaterials*, Volume 2012, Article ID 435873, 17 pages.



Chemical Oxidative Cutting of Multiwalled Carbon Nanotubes Arrays with Electromagnetic Waves

R. Pelalak^{*a}, M. Maghrebi^b, M. Baniadam^c

^{a,b,c} Department of Chemical Engineering, University of Ferdowsi Mashhad, Mashhad, Iran

Email: Rasool6330@yahoo.com

Key words: Multiwalled Carbon Nanotubes, Cutting, Chemical Oxidative, Electromagnetic Waves

Introduction:

Shortened or end-opened carbon nanotubes (CNTs) showed various potential applications, such as dye-sensitized solar cells[1], DNA analysis[2], and so on[3]. Furthermore, good dispersion of short CNTs in a composite material is critical to minimize stress concentration at agglomerates and achieve optimal mechanical performance [4]. However; CNTs are long, entangled and insolubility which makes it difficult for such applications. Thus they must be cut or end-opened to operable lengths and so for dispersibility. To solve these issues, several methods of CNTs cutting have been reported. But, it is reported that methods are very complicated, energy-consuming and time-consuming [5]. In this study, we developed a facile, effective and controllable method to obtain shortened multi walled carbon nanotubes (S-MWCNT) in a shorter time. Electromagnetic Waves treatment with mainly chemically oxidation was used for shortening and efficiently dispersing of Arrays multi-walled carbon nanotubes (A-MWCNTs).

Materials and methods:

Aligned MWCNT prepared by chemical vapor deposition using a floating catalyst method (diameter > 100 nm, length of 100 μ m, and purity < 90%). Analytical graded potassium permanganate (KMnO₄) and sulfuric acid (H₂SO₄) were obtained from Merck, Inc.

A-MWCNTs (75 mg) were added to a mixture of 40 ml of KMnO₄ and 6 ml of H₂SO₄: 3/1 mol vessel (100 ml). The Teflon vessel is embedded under electromagnetic waves at

temperature of 90 °C. Digestion was performed for different times (5, 10, 20, 30, and 40 min) at a constant wave irradiation power of 700 W. Then, after the cutting treatment, each mixture was filtered using a hydrophilic PTFE membrane (0.22 μm).

Apparatus:

To harness the extent of cutting, shortened MWCNTs (S-MWCNTs) were fully characterized by UV–visible and Raman spectroscopes as well as scanning electron microscopies (SEM), transmission electron microscopies (TEM) and optical microscopy (OM).

Result and discussion:

TEM micrographs of A-MWCNTs and S-MWCNTs during 20 min are shown in Fig. 1. The A-MWCNTs are smooth (Fig. 6(a)), while there are some roughnesses after 20 min of treatment (Fig. 6(b)). Such roughnesses are frequently used to justify oxidation of the CNTs surface [6]. Also, open end of A-MWCNTs are shown in the Fig (2c). According to Fig. (6d), It seems that the cutting of CNTs mostly happened where the CNTs are bent. The bended parts of CNTs are related to the vulnerable pentagon and heptagon [7]. So, damages at these sites are harsh enough to eventually cut the CNTs (Fig. 6(d)).

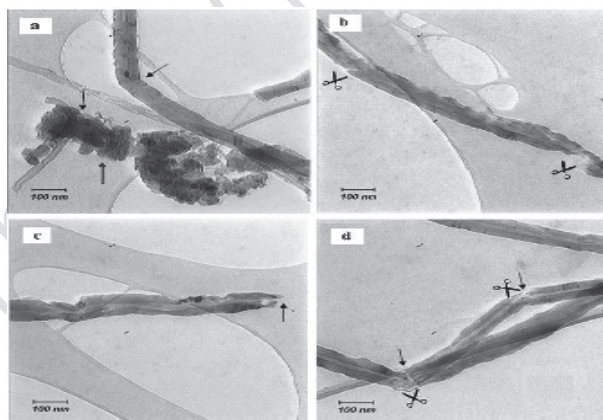


Fig. 1. TEM images of the MWCNTs samples: (a) A-MWCNTs (b),(c) and (d) S-MWCNTs at 20 min.



Conclusion:

The results show that with this treatment, the long tubes of A-MWCNTs ($>80\text{ }\mu\text{m}$) were efficiently and significantly shortened to below about $1\text{ }\mu\text{m}$ after 40 min the treatment. In the same time, the S-MWCNTs formed stable dispersion state in water without the help of surfactants that provided possibility for further functionalizations and applications. Also Decrease in the degree of S-MWCNT crystallinity was observed under 15 min reaction time that this Irregularity, improved after 20 min treatment. At the end, This method can be considered as an efficient route for the cutting of MWCNTs due to its fast and controllable procedure.

Reference:

- [1] Shengrui Sun, Lian Gao , Yangqiao Liu ,Optimization of the cutting process of multi-wall carbon nanotubes for enhanced, Thin Solid Films 519 (2011) 2273–2279.
- [2] Svetlana Kilina,¹ Dzmitry A. Yarotski,² A. Alec Talin,³ Sergei Tretiak , Unveiling Stability Criteria of DNA-Carbon Nanotubes Constructs by Scanning Tunneling Microscopy and Computational Modeling, Journal of Drug Delivery, 2011, 9 pages.
- [3] Changxin Chen and Yafei Zhang, Review on Optimization Methods of Carbon Nanotube Field Effect Transistors, The Open Nanoscience Journal, 2007, 1, 13-18.
- [4] B. Krause, T. Villmow, R. Boldt, M. Mende, G. Petzold, P. Pötschke, Influence of dry grinding in a ball mill on the length of multiwalled carbon nanotubes and their dispersion and percolation behaviour in melt mixed polycarbonate composites, Composites Science and Technology, 71 (2011) 1145–1153.
- [5] Y. Li, B. Wei, J. Liang, Q. Yu, D. Wu, Transformation of carbon nanotubes to nanoparticles by ball milling process, Carbon 37 (1999) 493.
- [6] G.-D. Lee, C.-Z. Wang, E. Yoon, N.-M. Hwang, K.-M. Ho, The role of pentagon-heptagon pair defect in carbon nanotube: The center of vacancy reconstruction, Appl. Phys. Lett., 97 (2010) 093106-093109.
- [7] H. K, S. A Reactivity of different kinds of carbon during oxidative purification of catalytically prepared carbon nanotubes, Solid State Ionics 141 (2001) 203-209.



Thermal conductivity investigation for CNT based polymer nanocomposites with effective structural parameters

A.Miranbaygi^a, A.Poorkamali^b, F.Kosari^c

^{a,b} Faculty of Mechanical Engineering, Shahid Rajaee

Teacher Training University, Tehran, Iran

^c Faculty of Mechanical Engineering, University of Tehran, Tehran, Iran

Email: amrnbgi@gmail.com

Keywords: Heat Transfer, Polymer Nanocomposite, Finite Element Method, Analytical Method, Carbon Nanotube

Introduction

Thermal conductivity of carbon nanotube polymer composites and its influences from MWNT volume fraction that are studied with element methods will be surveyed in this research. Nanopolymer in this research is made by epoxy that is reinforced with multiwall carbon nanotube. In next step the results of finite element method will compare with new runs based on effective medium theory and cylindrical inclusions in polymer composites. Also, the results will compare with the other model for more review[1,2]. Finally, behavior adaptation of volume fraction have been studied in Both analytical and finite element models, and accuracy of each method in expression the effect of volume fraction of fillers is measured to be used in future research with high reliability.

Method of Research:

In this project we check the influence of some of structural parameters on thermal conductivity of CNT-Epoxy composite. It is assumed that the nanotubes are distributed in axial direction in the composite structure. Mathematical solution for the effective thermal conductivity in axial direction is performed by using the effective medium theory [1-3]. A heterogeneous material with properties, be replaced with the homogeneous substance in the same conditions. In hypothetical homogeneous composites, filler materials are distributed uniformly in the matrix [2]. It is assumed that thermal conductivity is in steady state without heat generation. This structure has a similar response in both of analytical and finite element methods. It has a main role on simplification on related model [1,2]. In other words, molecular structure is unusable in analysis, therefore it must be replaced with similar structure. Therefore we replace this model with equivalent continuum model [4]. The fact that the outer layer of CNT has a greater thermal conductivity in Compared with inner layer, led to change the equivalent continuum model to effective solid fiber [5].

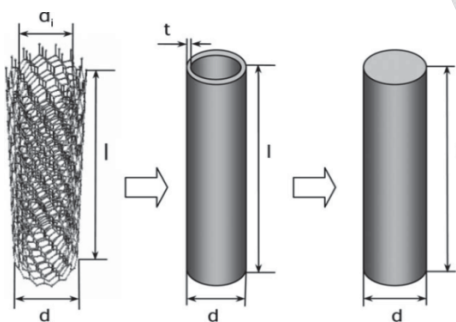


Fig.(1)-Models for MWNT: (a) graphene layers; (b) equivalent Continuum model; (c) effective solid fiber[5].

Also a finite element model of nanocomposite is used according to continuum mechanics. In finite element analysis different parameters such as length, diameter, volume fraction of



fillers and interfacial conductance or boundary thermal resistance as its inverse are studied by researchers [2]. In this paper For each parameter, the other parameters will be fixed. Then the quantity of volume fraction will be changed and its effect on thermal conductivity will be examined. Then the results will be checked with analytical results.

Result and discussion:

The research shows an increment of conductivity linearly with increase in volume fraction of the MWNT. Similar result will be found with theoretical model. This research also accredits finite element approach based on continuum mechanics in studying the.

Conclusion:

The influence of volume fraction of MWNT has been studied in this paper. thermal conductivity of carbon nanotube polymer composites and its influences from different parameters such as length, diameter, volume fraction of fillers and interfacial conductance or boundary thermal resistance as its inverse Could be checked with element methods and will be surveyed in future researches.

References:

- [1]. Golestanian, and M. Poorsina; "Thermal conductivity of SWNT nano composites determined using finite element methods"; material processing and design; 1597-1602,.
- [2]. Bagchi, and S.; "On the Effective Thermal Conductivity of Carbon Nanotube Reinforced Polymer Composites"; Composites Science and Technology; 66,1703-1712,2006.
- []. Spitalsky et al; " Carbon nanotube–polymer composites: Chemistry, processing, mechanical and electrical properties"; Progress in Polymer Science; 35,357–401,2010.



[4]C.Jianwei et al; "Thermal conductivity of carbon nanotubes"; Nanotechnology; 11, 65–69.2000.

[5].Endo etal; "Applications of carbon nanotubes in the twenty-first century"; Phil. Trans. R. Soc. Lond. A; 362, 2223–2238,2004.

15th Physical Chemistry Conference



Formation of Hydroxyapatite-Titania Nanostructured Bio-Ceramic Films by Plasma Electrolyte Oxidation

S. Abbasi^{a*}, F. Golestani-Fard^{a,b}, H.R. Rezaie^{a,b}

^a School of Metallurgy and Materials Engineering, Iran University of Science and Technology, P.O. Box:
16845-161, Tehran, Iran.

^b Center of Excellence for Advanced Materials, Iran University of Science and Technology, P.O. Box:
16845-195, Tehran, Iran.

Email: abbasi.iust.material@gmail.com

Keywords: Plasma electrolyte oxidation, Hydroxyapatite, Titania, Nanostructures.

Introduction:

Including a bioactive coating can improve the Ti-based implants and hard tissues bonding [1]. It has been demonstrated that the bonding of hard tissue and Ti-based implants can be improved by Hydroxyapatite ($\text{Ca}_{10}(\text{PO}_4)_6(\text{OH})_2$, HAp) which provides bioactivity and osteoconductivity. Co-existence of HAp and TiO_2 improves adhesion and corrosion resistance and creates a good combination of biochemical stability and mechanical properties of Ti-based implants [2]. Plasma electrolyte oxidation (PEO) is an advanced technique of HAp layer production that has raised a lot of attention in the past decade. PEO is an electrochemical process to deposit ceramic layers on light metal substrates. The main characteristic of this technique is producing electrical discharges along with plasma in the vicinity of metal surface [3].



In this research, Dependence of PEO processing parameters and physicochemical characteristics of synthesized HAp-TiO₂ nanostructured composite layers on Ti surface were investigated.

Materials and Methods:

A home-made rectifier with a maximum output of 600 V/30 A was used as the power source. Ti substrates served as anode and a cylindrical ASTM 316 stainless steel container was used as cathode. Details of the surface cleaning procedure can be found in our previous work [3]. Constant potential of 350 V in DC mode was applied to the samples for 3, 6 and 10 minutes. Coating electrolyte contained 1 g/l β -glycerophosphate (β -GP, C₃H₇Na₂O₆P, Merck) and 5, 10 and 15 g/l Calcium acetate (CA, Ca(CH₃COO)₂.xH₂O, Merck). Electrolyte temperature was kept constantly at 70 \pm 3°C during the process.

Results and Discussion:

HAp, anatase, α -tri calcium phosphate and calcium titanate were detected in fabricated layers. Fabricated coatings are fully crystalline even in samples coated in short periods of time. High current density passing through electrochemical cell in phosphate electrolytes has been reported before [4]. The rate of this addition increased especially when CA concentration changed from 10 to 15 g/l. This feature can be related to the raising of electrolyte conductivity by increasing in its concentration.

All layers are porous in accordance with the common feature of PEO fabricated layers. The effect of electrolyte concentration on morphology of layers is relatively independent of their growth time. By addition in electrolyte concentration 5 to 10 g/l more porous layers would form in the same period of time. This feature is a result of addition in the current density passed through samples as well as increasing in the rate of oxide layer formation.



The nanometric HAp crystals were produced as a consequence of the high cooling rate of the nucleated HAp crystals in electrolyte. This nanostructured HAp along with the porous top oxide layer resulted in better biocompatibility performance of samples.

Conclusion :

Porous TiO₂-HAp composite layers were fabricated by PEO technique. The increase in HAp phase fraction was ascending by addition in growing time and electrolyte concentration. As an important result the increase in HAp fraction in case of addition in electrolyte concentration from 10 to 15 g/l CA is much higher than in case of addition from 5 to 10 g/l CA. Nanometric crystals of TiO₂-HAp were observed.

References:

- [1] F. Samanipour, M.R. Bayati, F. Golestani-Fard, H.R. Zargar, A.R. Mirhabibi, S. Abbasi, *Mater. Lett.* 65 (2011) 926-928.
- [2] X. Zeng, J. Li, S. Yang, Q. Zheng, Z. Zou, *Appl. Surf. Sci.* 258, (2012) 4489-4496.
- [3] S. Abbasi, M.R. Bayati, F. Golestani-Fard, H.R. Rezaei, H.R. Zargar, *Appl. Surf. Sci.* 257 (2011) 5944-5949.
- [4] E.A. Abdel-Aal, D. Dietrich, S. Steinhäuser, B. Wielage, *Surf. Coat. Technol.* 202 (2008) 5895-5900.



Preparation and Characterization of Micro/Nanocapsules containing Tung Oil and its Use in Self-Healing Coatings

M. Kouhi^{a*}, M. Mohammadi^a

^a Department of Chemical Engineering, Faculty of Engineering, Shahid Bahonar University, Kerman, Iran

Email: masoume.kouhi@gmail.com

Keywords: micro/nanocapsule, urea-formaldehyde, in situ polymerization, tung oil

Introduction:

Many researchers are interested to find new ways for extending the useful life cycle of coatings that this lead to life growth of structures and equipment [1-3]. In this study, the encapsulation process of Tung oil, as an oxidative healing agent, in poly-urea formaldehyde was presented. These micro/nanocapsules were synthesized by in-situ polymerization. That it may improve and open new view in the field of capsule synthesis and coating science. Such coatings typically incorporate micro/nanocapsules that contain film-formers; which polymerize in the presence of air and heal the crack. Efficacy of these micro/nanocapsules in healing of cracks in an epoxy coating [4] and corrosion protection has been demonstrated. Also this method does not need to the catalyst that can solve the problem of the major discontinuity in coating matrix because the existence of the catalyst.

Materials and methods:

At room temperature, 130 ml of deionized water with 5 ml of 5 wt% dodecyl sulphate solution were mixed in 500 ml beaker. Under 200 rpm agitation 2.5 g urea, 0.25 g ammonium chloride and 0.25 g resorcinol were dissolved in solution. The pH was adjusted to approximately 3.0 by using 1 wt% solution of hydrochloric acid in deionized water. After 10 minutes of agitation 25 ml of Tung oil was added slowly and allowed to stabilize for 15 min under agitation before sonication. The tapered 18 mm tip sonication horn of a 1000 W ultrasonic homogenizer (Hielscher-UIP 1000) was placed in the solution, for 3 min at 30% intensity



(~3.0 kJ of input energy). After stabilization, 6.335 g of 37 wt% formalin was added. The emulsion slowly heated and maintained at 60°C under stirring at 600 rpm for 5 hours.

Apparatus:

For investigation of capsules characteristics, such as Shell wall integrity, aggregation phenomena, microcapsule size, micro/nanocapsule's core content and loss factor Scanning electron microscopy (SEM), Fourier transform infrared spectroscopy (FTIR) and Soxhlate apparatus were used. Also the self-healing ability and corrosion performance of the scratched epoxy coating, containing Tung oil capsules, were approved by EIS tests through two weeks and the results were compared with scratch and unscratched neat one.

Results and discussions:

SEM images showed that the capsules were spherical in shape, and had a rough, non-porous exterior shell wall. All of synthesized capsules were in the range of 500nm-10 μ m diameter. The spectrum obtained by FTIR confirmed that shell and core materials were made of urea-formaldehyde polymer and tung oil respectively. The mean core content of two synthesized capsule samples was around 90 wt% which gained by Soxhlet apparatus. Scratching of neat epoxy led to severe decline in corrosion resistance of coating and in last day of EIS study, the scratched one was degraded completely. But the capsule incorporated coating was stronger in preservation of its primary corrosion resistance, although there was a little depreciation in its corrosion behavior, along test period. In fact, this film was found to provide a very high level of protection to the underlying metal in the case of scratched neat coat.

Conclusion:

The used encapsulation process (in-situ polymerization, oil in water emulsion) was successful for incorporation of Tung oil in PUF shell. Synthesized micro/nanocapsules in paint films released healing material, which during cracking healed cracks efficiently with satisfactory anticorrosive properties. Incorporated Tung oil capsules through epoxy structure provided self-healing ability for coating without any catalyst requirement.

References:

[1] SR. White et al.; "Autonomic healing of polymer composites Nature"; 409, 794-797, 2001.



- [2] AC. Jackson et al.; *Macromolecular Rapid Communications*; 32(1),82-7,2011.
- [3] X. Liu et al.; "Characterization of diene monomers as healing agents for autonomic damage repair" *J Appl Polym Sci*; 101,1266–1272,2006.
- [4] M. Stern et al.; "Electrochemical Polarization: I. A Theoretical Analysis of the Shape of Polarization Curves"; *J. Electrochem. Soc.*; 104,56,1957.

15th Physical Chemistry Conference



Structural and magnetic properties of $\text{CoFe}_{2-x}\text{Al}_x\text{O}_4$ nanoparticles

H. Arabi*, E. Ansari, S.M. Zareii

Magnetism and Superconducting research lab, Department of Physics, Faculty of Sciences, University of Birjand, Iran

E-mail: arabi_h@yahoo.com

Keywords: $\text{CoFe}_{2-x}\text{Al}_x\text{O}_4$ nanoparticles, Spinel ferrites, Sol-gel method, X-ray diffraction, Magnetic properties

Introduction:

Cobalt ferrite due to its high coercivity, moderate saturation magnetization, high magneto crystalline anisotropy, high chemical and mechanical hardness is one of the good candidates for high-density recording media, sensors, transformer cores, and microwaves devices [1-2]. The substitution of non-magnetic Al^{3+} ions in cobalt ferrite can reduce the loss factor, and thus improve the efficiency of microwave devices and transformers applications. The present work reports the synthesis of $\text{CoFe}_{2-x}\text{Al}_x\text{O}_4$ nanoparticles and study of their structural and magnetic properties through X-ray diffraction and magnetization measurements.

Experimental:

The metal nitrates and citric acid dissolved in de-ionized water were used as the starting materials for sol-gel method. The ammonia solution was also used to adjust the pH value to 7. The solution was refluxed for 4 h at 100°C. The mixtures were evaporated at 80°C to form gels. The gels were dried at 220°C for more than 2 h. The powders were annealed at temperatures 800°C for 2 h.

Results and discussions:

The XRD patterns (Fig. 1) indicate the single-phase cubic spinel structure for all compounds. The size of crystallites calculated by Scherrer formula show the nano-size of crystallites (Table 1). For the complete series $\text{CoFe}_{2-x}\text{Al}_x\text{O}_4$ the crystallite sizes and lattice constants decrease with increasing x due to the fact that Al^{3+} ionic radius (0.51 Å) is smaller than that of Fe^{3+} ion (0.64 Å) [3]. It can be also seen that the X-ray density decreases with

Al^{3+} concentration for all compositions because the decrease in mass over takes the decrease in volume of the unit cell.

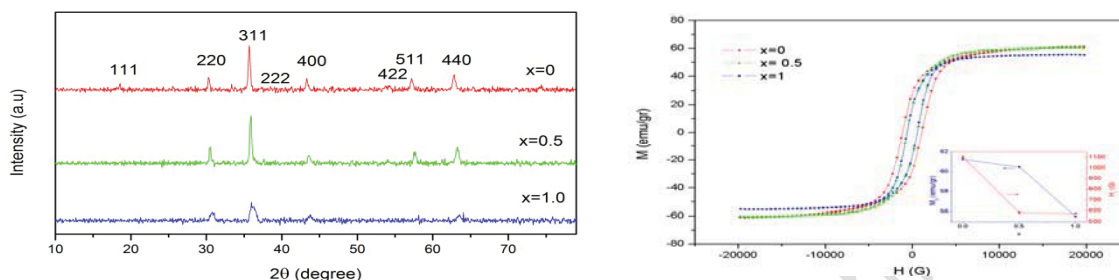


Figure 1. XRD patterns (Left panel) and M-H loops (Right panel) of $CoFe_{2-x}Al_xO_4$ nanopowders ($x=0, 0.5, 1$)

Magnetic measurements (Table 1) show that both the saturation magnetization (M_s) and coercivity (H_c) decreases with increasing of Al content due to the decreased superexchange interaction by the substitution of Al^{3+} ions in place of Fe^{3+} ions at octahedral site. For $x=0$, M_s is smaller than that of bulk value (74.08 emu/g) [2] which can be due to the spin disorder effects and formation of dead layer on the surface of nanoparticles.

Table 1. The crystallite size (D), lattice constant (a), X-ray density (d_x), saturation magnetization (M_s), remanent magnetization (M_r) and coercivity (H_c) of $CoFe_{2-x}Al_xO_4$ nanopowders.

x	$D(nm)$	$a(\text{\AA})$	$d_x(gm/Cm^3)$	$M_s(emu/g)$	$M_r(emu/g)$	$H_c(G)$
0.0	27.81	8.3379	5.377	61.253	28.005	1102.8
0.5	26.85	8.2930	5.128	60.476	17.384	583.41
1.0	8.95	8.2719	3.625	55.502	17.459	577.97

Conclusions:



The $\text{CoFe}_{2-x}\text{Al}_x\text{O}_4$ ($x = 0, 0.5, 1$) nanoparticles prepared by Sol-gel method possess cubic spinel structure. The nano-crystallite sizes and lattice constants decrease with increasing of Al content. The saturation magnetization and coercivity decrease on substitution for Fe by Al.

Reference:

- [1] M. Mozaffari et al.; "Investigation of magnetic properties of Al substituted nickel ferrite nanopowders, synthesized by the sol-gel method"; *Journal of Magnetism and Magnetic Materials*; 323, 2997–3000, 2011.
- [2] I.H. Gul et al.; "Optical, magnetic and electrical investigation of cobalt ferrite nanoparticles synthesized by co-precipitation route"; *Journal of Alloys and Compounds*; 507, 201–206, 2010.
- [3] P.S. Aghav et al.; "Effect of aluminum substitution on the structural and magnetic properties of cobalt ferrite synthesized by sol-gel auto combustion process"; *Physica B*; 406, 4350–4354, 2011.



Synthesis of NiMo Based Nanocatalysts over Al₂O₃ and ZrO₂ via Impregnation Method Used in Hydrodesulphurization Process

P. Jabbarnezhad^{a,b}, M. Haghighi^{a,b*}

^a Chemical Engineering Faculty, Sahand University of Technology, Tabriz, Iran

^b Reactor and Catalysis Research Center (RCRC), Sahand University of Technology, Tabriz, Iran

*Email: haghighi@sut.ac.ir

Keywords: NiMo/Al₂O₃, NiMo/ZrO₂, Impregnation, Nanocatalyst, Hydrodesulphurization.

Introduction:

Stringent regulations about diesel fuel quality in the near future require improvements in the catalytic performances of hydrodesulphurization (HDS) catalysts that are conventionally composed of alumina-supported sulfided NiMo or CoMo [1]. Recently, ZrO₂ supported catalysts have attracted more attention [2]. The purpose of the present paper is to compare the activity of NiMo sulfide supported over Al₂O₃ and ZrO₂ in the HDS of thiophene.

Materials and methods:

Al₂O₃ and ZrO₂ supported NiMo catalysts were obtained by the impregnation method using ammonium heptamolybdate and nickel nitrate. Prepared samples were characterized by XRD, FESEM and surface area analyzer BET. The HDS activity tests were performed in a stirred reactor at 160°C and atmospheric pressure (1 wt% thiophene in decane as a model fuel).

Result and discussion:

The XRD patterns of the samples are shown in Figure 1. As can be seen in the figure, sharp peaks related to gamma alumina (in NiMo/Al₂O₃) and tetragonal ZrO₂ (in NiMo/ZrO₂) are visible. The peaks related to active phases (NiO, MoO₃ and NiMoO₄) are not appeared at NiMo/ZrO₂ catalyst. This observation could be due to high dispersion of this species over the ZrO₂ support. Comparing FESEM images (Figure 2) showed that nanoscale particles of NiMo/ZrO₂ catalyst have uniform distribution. BET results (Figure 3) presented the surface area of the NiMo/ZrO₂ was lower than NiMo/Al₂O₃. Thiophene HDS activities of

nanocatalysts are illustrated in Figure 4. From the data, it could be observed that the ZrO_2 supported NiMo nanocatalyst exhibited much higher catalytic activities than that of Al_2O_3 -supported one.

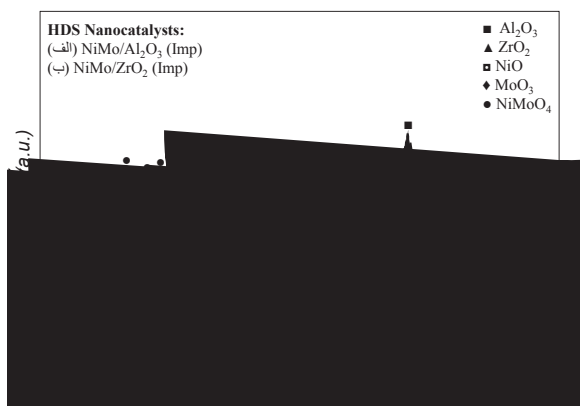


Figure 3: XRD patterns of NiMo/ Al_2O_3 and NiMo/ ZrO_2 nanocatalysts.

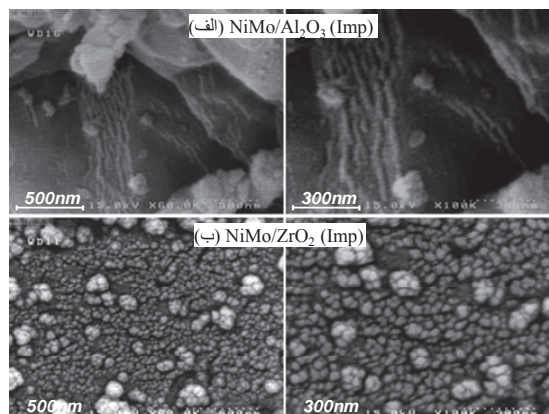


Figure 4: FESEM images of NiMo/ Al_2O_3 and NiMo/ ZrO_2 nanocatalysts.

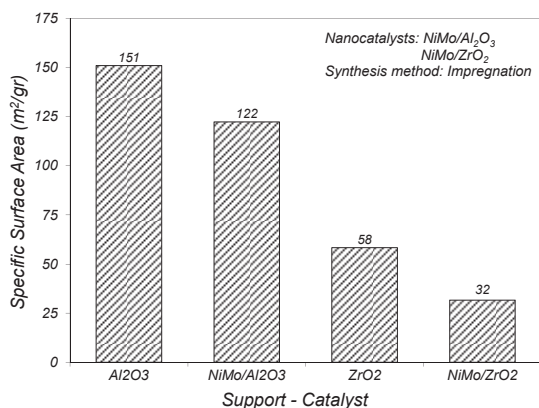


Figure 5: BET surface area of NiMo/ Al_2O_3 and NiMo/ ZrO_2 nanocatalysts.

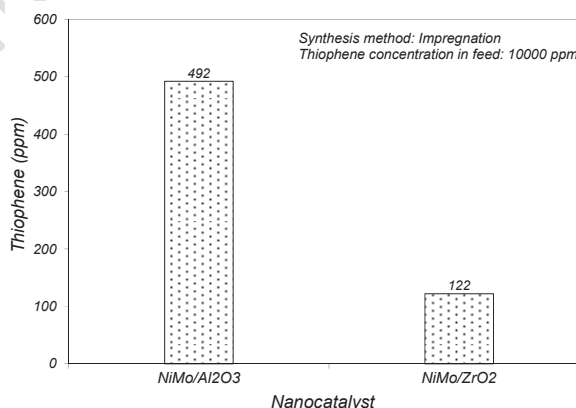


Figure 6: Hydrodesulphurization of thiophene over NiMo/ Al_2O_3 and NiMo/ ZrO_2 nanocatalysts.

Conclusion:

NiMo/ Al_2O_3 and NiMo/ ZrO_2 nanocatalysts were successfully synthesised by impregnation technique. Comparing XRD patterns of nanocatalysts showed high dispersion of active metal on support in NiMo/ ZrO_2 catalyst. Comparing FESEM images showed nanoscale particles of



NiMo/ZrO₂ have uniform distribution. The HDS activity results showed ZrO₂ supported NiMo catalyst exhibited much higher catalytic activities than that of Al₂O₃-supported one.

References:

- [1] G. Li et al., " Morphology and hydrodesulfurization activity of CoMo sulfide supported on amorphous ZrO₂ nanoparticles combined with Al₂O₃", Applied Catalysis A: General, 273, 233-238, 2004.
- [2] Y.Ji et al., "Promoting effects in hydrogenation and hydrodesulfurization reactions on the zirconia and titania supported catalysts", Applied Catalysis A: General, 257, 157-164, 2004.



Molecular Dynamics Simulation of Inhibition of Orotidine 5'-Monophosphate Decarboxylase Protein by 6-Hydroxy-UMP (BMP) Drug

Shirin Jamshidi^{a*}, Seifollah Jalili^b, Hashem Rafii-Tabar^a

^a Department of Medical Physics and Biomedical Engineering Shahid Beheshti University of Medical Sciences,
Tehran, Iran

^b Department of Chemistry, K.N.Toosi University of Technology, Tehran, Iran

Email: jamshidi@sbmu.ac.ir

Key words: Protein Inhibition, Molecular Dynamics Simulation, OMPDC, BMP

Introduction:

Orotidine 5'-monophosphate decarboxylase (OMPDC) is a protein and can act as a target for drugs that are directed against RNA viruses, such as poxviruses and flaviviruses. OMPDC's inhibitors, such as BMP, can also be effective against such biological agents as West Nile virus, Plasmodia, including the malaria causing *Plasmodium falciparum*, OMPDC is present in cancerous cells and hence BMP can also act as an anticancer drug. OMPDC produces a nucleotide called uridine 5'-monophosphate (UMP) from which BMP itself can be produced by substitution of one of its carbon atoms. Since the mechanism by which BMP inhibits OMPDC has been clarified, we intent to provide an insight into this mechanism by performing atomistic level computer-based simulations [1-4].

Materials and Methods:

Here, we have carried out molecular dynamics (MD) simulations for a 10 ns duration with the time-step set at 2 fs at the fixed temperature of $T = 300$ K. The binding free-energy calculations were performed via MM-PBSA (Molecular Mechanics Poisson-Boltzmann/surface area) method. The initial structure of OMPDC, obtained from x-Ray structures of OMPDC from *Saccharomyces cerevisiae* complexed with BMP, was extracted from PDB [1DQX code of Protein data Bank] site. Furthermore, two MD



simulations were performed separately to investigate the behavior BMP and OMPDC in water. MM-PBSA method does not provide the true free energy results, but could only be used to compare against similar systems, since the entropy contribution is not calculated with this method.

Apparatus:

The AMBER 10.0 was used to perform the MD simulations to provide the space-time trajectories of the OMPDC – BMP complex. Using these trajectories, AMBER tools package was employed to use the MM-PBSA method to calculate the free energy of binding. The calculations were performed at the Medical Nanotechnology Supercomputer Centre in the Department of Medical Physics & Biomedical engineering at the Shahid Beheshti University of Medical Sciences (Tehran, Iran).

Result and discussion:

The inhibitor of OMPDC displayed inhibition constant (K_i), the concentration of competing ligand in a competition assay which would occupy 50% of the receptors if no ligand were present, of 6.2×10^{-51} M. Interestingly, the K_i value for BMP was comparable with experimental results [1], and was seen to be better than K_m , the concentration of substrate at which enzyme activity is at half maximal, for the substrate OMP, which we have calculated to be 6.9×10^{-46} M. Binding of BMP and its structural features show that there are 12 hydrogen bonds and one Pi interaction with residues of the active site of OMPDC. With respect to K_i , the interaction of BMP with OMPDC has a higher affinity compared with OMP.

Conclusion:

Out MD simulations have provided some valuable data at atomic scales, which are unavailable from inspecting presently available crystal structures and experiments. The results of these simulations provide kinetic and thermodynamic properties concerning the inhibition of OMPDC enzyme, and the potential value of the knowledge gained for repressing its related diseases at atomic scales.



Reference:

- [1] Brian G. Miller and etal; Anatomy of a proficient enzyme: The structure of orotidine 5'-monophosphate decarboxylase in the presence and absence of a potential transition state analog; *PNAS*, 2000, vol. 97 no. 5, 2011–2016
- [2] Angelica M. and etal; Structure-Activity Relationships of Orotidine-5'-Monophosphate Decarboxylase Inhibitors as Anticancer Agents ; *J. Med. Chem.* 1648 2009, 52, 1648–1658
- [3] Angelica M. and etal; Structure–Activity Relationships of C6-Uridine Derivatives Targeting *Plasmodia* Orotidine Monophosphate Decarboxylase ; *J. Med. Chem.* 2008, 51, 439–448
- [4] Lakshmi P. Kotra and Emil F. Pai; Inhibition of Orotidine 5'-monophosphate decarboxylase discoveries and lessons ; *Nucleic Acids Symposium Series* 2008 No. 52 85–86



Partial molar entropy in nonextensive thermodynamics framework

Mohammad Kamalvand* and Esmat Mollakhalili

Department of Chemistry, Faculty of Science, Yazd University, Yazd, Iran

*Email: kamalvand@yazduni.ac.ir

Keywords: Partial molar entropy, Tsallis entropy, entropic index

Introduction:

The generalized entropy of Tsallis is [1]

$$S = k \frac{1 - \sum_i p_i^q}{q-1} \quad (1)$$

where k is a positive constant, usually the same as Boltzmann constant, p_i is the probability of the i 'th microstate and q is the entropic index and shows the degree of nonextensivity. In the limit of $q \rightarrow 1$, the Tsallis entropy converges to the Boltzmann-Shannon entropy

$$S = -k \sum_i p_i \ln p_i \quad (2)$$

The entropic index, q , may be any negative or positive constant, dependent on the nature of the system. Deviation of the entropic index from unity means deviation of the system behavior from Boltzmann-Gibbs statistics. This deviation can be due to different effects like long time memory, long range interactions or self-gravitation [2].

Partial molar entropy in Tsallis statistics:

For a complex system consists of two independent subsystems, named A and B , the probability of i 'th microstate of the complex system is $p_i^{A+B} = p_i^A \times p_i^B$. If this complex system obeys from Boltzmann-Gibbs statistics, the total entropy is $S_{A+B} = S_A + S_B$ where S_A

and S_B contain mixing entropy. For ideal mixtures, the average of interactions between A and B molecules is similar to the $A-A$ and $B-B$ interactions. For these mixtures,

$$S_{A+B} = S_{A,unmixed} - n_A R \ln x_A + S_{B,unmixed} - n_B R \ln x_B. \text{ However, if A-B interactions are}$$

different from A-A and B-B interactions, the total entropy of mixture deviates from ideal mixture. In Tsallis framework, for the complex system mentioned above, if we suppose

$$p_i^{A+B} = p_i^A \times p_i^B, \text{ the total entropy of the complex system will be}$$

$$S_{A+B} = S_A + S_B + (1-q) \frac{S_A \times S_B}{R}. \text{ Therefore, in this statistics, there is an additional term that}$$

is due to introducing entropic index, q , and power form of the Tsallis entropy. For a non-ideal mixture, if the entropic index relates to the intermolecular interactions, then

$$\Delta^{\text{ex}} S = (1-q) \frac{S_A \times S_B}{R}. \text{ The partial molar entropy of the } i\text{'th component, } \bar{S}_i, \text{ can be obtained by}$$

differentiation of the total entropy respect to the n_i , when T, P and $n_{j \neq i}$ are constant:

$$\bar{S}_i = \left(\frac{\partial S}{\partial n_i} \right)_{T, P, n_{j \neq i}} \quad (3)$$

This differentiation leads to the following equation for partial molar entropy of the component A in a non-ideal two component system:

$$\begin{aligned} \bar{S}_A = S_A - R \ln x_A + x_B (x_A S_A - R x_A \ln x_A) (1-q) + (x_B S_B - R x_B \ln x_B) (S_A - \\ R \ln x_A - R x_B) \frac{(1-q)}{R} - (x_B S_B - R x_B \ln x_B) (x_A S_A - R x_A \ln x_A) \frac{(1-q)}{R} \end{aligned} \quad (4)$$

Results and discussion:



The results of Eq. 4 for a number of liquid and solid alloys are collected in Table. 1. Comparison of the results with experimental data indicates that this equation has a great successfully to obtain partial molar entropy of the non-ideal mixtures.

Table. 1 Partial molar entropy (J/mol.K) of two non-ideal mixtures calculated from Eq. 4 in comparison with experimental data.

x_1		0.1	0.2	0.3	0.4	0.5	0.6	0.7	0.8	0.9
W-Ta [3]	\bar{S}_W (cal)	69.64	70.49	71.42	72.41	73.46	75.15	76.02	77.90	81.43
	\bar{S}_W (exp)	69.60	70.40	71.49	72.66	73.95	75.75	77.30	79.02	83.45
	\bar{S}_{Ta} (cal)	93.75	89.51	86.94	84.94	83.37	82.39	81.13	80.27	79.52
	\bar{S}_{Ta} (exp)	94.19	89.76	86.70	84.53	82.90	81.39	80.55	80.01	79.30
Zn-Pb[4]	\bar{S}_{Zn} (cal)	111.4	106.3	102.3	99.4	97.1	95.11	93.43	91.97	90.74
	\bar{S}_{Zn} (exp)	112.6	106.8	102.9	100.1	97.9	95.82	94.06	92.43	91.13
	\bar{S}_{Pb} (cal)	111.3	112.5	113.9	115.7	117.9	120.6	124.3	129.6	139.6
	\bar{S}_{Pb} (exp)	111.2	112.4	113.7	115.2	117.6	119.6	122.9	127.9	136.3

Conclusion

The obtained results in this research show that the Tsallis statistical mechanics can be used to obtain partial molar entropy of non-ideal mixtures. The maximum relative error in all obtained results (not reported here) is smaller than 5%.



References

- [1] Tsallis, C., Mendes, R. S., *Physica A*. **1998**, 261, 534.
- [2] Keshavarzi E, Helmi, A, Kamalvand, M., Entroy, in press.
- [3] Singhal, S. C., Worrell, W. L., *Metallur. Trans.* **1973**, 4, 893.
- [4] Hagiwara, H., Sugino, Sh., Fujiwara, H.; *Series A, Engineering and natural sciences*. **1974**, 23, 51.

15th Physical Chemistry Conference



Experimental Investigation on the Solubility of CO₂ and H₂S in Some imidazolium-based Ionic Liquids

Mohammad Shokouhi*, Amir Hossein Jalili, Masih Hosseini-Jenab, Ali Mehdizadeh

Gas Science Department, Gas Research Division, Research Institute of Petroleum Industry (RIPI), National Iranian Oil Company (NIOC), P.O. Box 14665-137, West Blvd., Azadi Sport Complex, Tehran, Iran. Tel.: +98

21 48252466. Fax: +98 21 44739716.

*E-Mail : shokouhi110@gmail.com ; shokouhim@ripi.ir;

Keywords: ionic liquids, Gas Solubility, Physical solvent. Modeling.

Introduction:

Room temperature ionic liquids (RTILs) are molten salts, which are liquid over a wide temperature range including ambient [1]. In this work, the solubility of CO₂ and H₂S in some ionic liquids, contain [hemim][PF₆], [hemim][BF₄], [hemim][OTf], [hemim][Tf₂N], [emim][EtSO₄], [emim][PF₃(C₂F₅)₂], [emim][BF₄], [emim][PF₆], [emim][Tf₂N], [hmim][BF₄], [hmim][PF₆], [hmim][OTf], [hmim][Tf₂N], [Omim][BF₄], [Omim][PF₆], [Omim][OTf], [Omim][Tf₂N] at temperature 303.15 K and pressures up to 1.5 MPa were experimentally measured. The solubility data were correlated using the Krichevsky–Kasarnovsky and also pitzer equations and Henry's law constants were obtained. Then the results interpreted by interaction parameters and free space in the solvent related to molecular structure of solvent, and compared with each other and other data in the literature.

Apparatus and procedure:

The volumetric method was used to measure the gas solubility [2]. *PVT* experimental data obtained using the NIST [3].

Using a Mettler model DL-37 Karl-Fischer volumetric titrator, the water content of ILs was found to be below 100 ± 10 ppm. The temperature of the double-wall equilibrium cell, which



was connected to a water recirculation bath (PMT Tamson model T 2500), was measured with a Lutron model TM-917 digital thermometer with a 0.01 K resolution using a Pt-100 sensor inserted into the cell. The equilibrium cell pressure was measured using a KELLER model PA-33X pressure transmitter sensor in the range of (0 to 2) MPa, which was accurate to within 0.01 % of full scale and that of the gas container was measured using a Druck model PTX 1400 pressure transmitter sensor in the range of (0 to 4) MPa, which was accurate to within 0.1 % of full scale. The calibration of pressure sensors was carried out against a dead-weight gauge.

Results and Conclusion:

The results of the solubility of CO₂ and H₂S in the some ionic liquids with different cations and anions are investigated at temperature 303.15 K and pressure up to 1.5 MPa. Henry's law constants and partial molar thermodynamic functions of solution were estimated from experimental data. The results were compared with previously reported experimental data [4,5] shows that the solubility of H₂S is higher than CO₂ in all ILs. Also for both CO₂ and H₂S, the solubility increase as the alkyl chain length/ or anion size increase which it is related to molar density of ILs and strength interaction between cations and anions. We obtain a relatively good linear correlation between Henry's law constants and the number of carbon in alkyl chain of cation for both CO₂ and H₂S.

References:

- [1] J.S. Wilkes, P. Wasserecheid, T. Welton (Eds.), *Ionic Liquids in Synthesis*; Wiley VCH Verlag, 2002.
- [2] A.H. Jalili, M. Rahmati-Rostami, C. Ghotbi, M. Hosseini-Jenab, A.N. Ahmadi. ; *J. Chem. Eng. Data* 54, 1844-1849, 2009.
- [3] NIST Scientific and Technical Databases; Thermophysical Properties of Fluid Systems: <http://webbook.nist.gov/chemistry/fluid/>
- [4] M. Shokouhi, M. Adibi, A.H. Jalili, M. Hosseini-Jenab, A. Mehdizadeh. ; *J. Chem. Eng. Data* ; 55, 1663, 2010.
- [5] A.H. Jalili, A. Mehdizadeh, M. Shokouhi, H. Sakhaeinia, V. Taghikhani, J.



Chem. Thermodynamics ; 42, 787–791, 2010.

15th Physical Chemistry Conference



Ionic association and solvation of the ionic liquid 1-hexyl-3-methylimidazolium chloride in molecular solvents revealed by volumetry and acoustic measurements

Rahmat Sadeghi*, Nosaiba Ebrahimi

Department of Chemistry, University of Kurdistan, Sanandaj, Iran

*E-mail: rsadeghi@uok.ac.ir

Keywords: Ionic liquid, Ionic association, Solvation, Volumetry, Acoustic measurements

Introduction:

Ionic liquids (ILs) are organic salts that are liquids at temperatures below 373.15 K. They have received considerable attention as alternatives to the traditional organic solvents. Due to the phenomenal growth of publications dealing with their interesting physical and chemical properties and possible applications they have been attracting intense interest in the scientific literature. In solution, the solvation and ionic association of ILs determine the unique properties of these systems and also most of the applications of ILs are closely related to these phenomena occurred in the IL solutions. In addition, a fundamental issue in the design of novel ionic liquids is the understanding of the nature/strength of cation-anion interactions and intermolecular forces in the bulk ionic fluid due to their intrinsic relation with most of their physicochemical properties, such as melting temperature, density, viscosity, surface tension, and vapor pressure [1-3].

The ILs based on 1-alkyl-3-methylimidazolium cation ($[C_n\text{mim}]^+$) are one of the most important and promising class of ILs since they can be used for synthesis of IL with different anions including organic ones [3]. Among all the imidazolium based ILs, 1-alkyl-3-methylimidazolium bromide ionic liquids are the most studied ILs and despite the potential utility of $[C_n\text{mim}]\text{Cl}$, few of its physical properties have been reported. In the present work,



in order to study of ionic association and solvation behavior of $[\text{C}_6\text{mim}][\text{Cl}]$ as well as their variation with the physicochemical properties of the molecular solvents, volumetry and acoustic measurements for different binary mixtures containing $[\text{C}_6\text{mim}][\text{Cl}]$ + solvent (methanol, ethanol, 1-propanol, 2-propanol, 1-butanol, acetonitrile, water) at different temperature were carried out.

Experimental Section:

Materials. $[\text{C}_6\text{mim}][\text{Cl}]$ and all of the solvents (methanol, ethanol, acetonitrile, 1-propanol, 2-propanol, and 1-butanol) were obtained from Merck. The solvents were used without further purification. $[\text{C}_6\text{mim}][\text{Cl}]$ was dried in high vacuum at 333.15 K using a rotary evaporator for at least 4 h in 0.7 kPa. Double distilled and deionized water was used.

Procedures. All the solutions were prepared by mass on a Sartorius CP124S balance precise to within ± 0.0001 g. The density and sound velocity of the mixtures were measured at different temperatures with a digital vibrating-tube analyzer (Anton Paar DSA 5000, Austria) with proportional temperature control that kept the samples at working temperature within $\pm 10^{-3}$ K.

Results and Discussion:

The experimental density and sound velocity data were obtained for the binary $[\text{C}_6\text{mim}][\text{Cl}]$ + water, methanol, ethanol, 1-propanol, 2-propanol, 1-butanol, and acetonitrile systems at the 288.15-313.15 K temperature range at 5 K intervals at atmospheric pressure. The standard partial molar volume and isentropic compressibilities of the free ions $[\text{C}_6\text{mim}]^+$ and Cl^- and ion pairs $[\text{C}_6\text{mim}]^+\text{Cl}^-$ in the investigated solvents were determined and their variations with temperature and type of solvents were also studied. Furthermore The infinite dilution solvation numbers of $[\text{C}_6\text{mim}][\text{Cl}]$ in the investigated solvents, n° , were calculated. The trend of all of the investigated volumetric and acoustic properties of $[\text{C}_6\text{mim}][\text{Cl}]$ in water with temperature is completely opposite to that for nonaqueous solvents. In nonaqueous solvents the sum of the molar volume of ions $[\text{C}_6\text{mim}]^+$ and Cl^- , $V^\circ(\text{IL})$, decrease by increasing temperature but the molar volume of the ion pair $[\text{C}_6\text{mim}]^+\text{Cl}^-$, V_{IP}° , increases



with temperature. However, both of $K^\circ(\text{IL})$ and K_{IP}° in nonaqueous solvents decrease with increasing temperature. The volume and isentropic compressibility changes occurring on ion pairing in nonaqueous solvents, $\Delta_{\text{IP}}V^\circ$ and $\Delta_{\text{IP}}K^\circ$, which are positive, increase by increasing the temperature. The obtained infinite dilution properties $V^\circ(\text{IL})$, $K^\circ(\text{IL})$ and n° which are a measure of the ion + solvent interaction, indicate that although the solvation of free ions $[\text{C}_6\text{mim}]^+$ and Cl^- in water is weaker than that in the investigated nonaqueous solvents, however, these infinite dilution properties do not show a similar trends for different nonaqueous solvents.

References:

- [1] Weingaertner, H. *Angew. Chem., Int. Ed.* 2008, 47, 654.
- [2] Parvulescu, V. I.; Hardacre, C. *Chem. Rev.* 2007, 107, 2615.
- [3] Wasserscheid, P.; Welton, T. *Ionic Liquids in Synthesis*; Wiley-VCH: Weinheim, Germany, 2003.



Calculation of radial distribution functions for methane by wavelets in different temperatures and comparison with computer simulation results

M. Katiraei

Department of Physics, Shiraz University, Shiraz, Iran

(Email: mm_katiraei@yahoo.com)

Keywords: Radial distribution function, Ornstein-Zernike equation, Wavelets

Introduction:

As we know, the wavelet transform, a family of orthonormal bases, is introduced as a technique for performing multiresolution analysis in statistical mechanics. The wavelet transform is a hierarchical technique designed to separate data sets into sets representing local averages and local differences. The advantage of the wavelet transform, is as an approximation scheme for the efficient calculation of thermodynamic properties[1]. In fact, wavelets analysis is a modern numerical tool that is an extension of the Fourier analysis [5]. In previous articles, we used this method for water[2] and methane[3] in 298K. In this article we have efforted to solve OZ equation for methane in different temperatures by using wavelets and their properties and compare the results with acquired results from the molecular dynamic (MD) simulations.

Methods:

In this article we calculate the radial distribution function (RDF) using the referenced interaction site model of molecular liquids. As we know, in this theory, it is purposed to calculate the RDFs by solving the set formed by the OZ equation and a closure relation. For a molecular liquid consisting of N-site molecules, the site-site Ornstein-Zernike (SSOZ) equation has the following form [4]:

$$nHn=nW*C*(nW+nHn)$$

(2-1)

Where H and C are the site-site intermolecular pair correlation functions and the direct correlation functions respectively, n is the diagonal matrix whose elements are number densities of each molecular species and W is the intramolecular correlation matrix. In order to solve OZ equation, for molecular liquids, a secondary relation as closure relation and knowing of intermolecular interactions is required. In this article the site-site interactions between molecules are represented by the Lennard-Jones (LJ) potential plus coulomb terms. Most of the numerical algorithms for solving relation (2-1) impose the Fourier representation of (2-1) written as:

$$\hat{G}(k)=\hat{H}(k)-\hat{C}(k)=\hat{W}(k)(I-n\hat{W}(k)\hat{C}(k))^{-1}\hat{C}(k)\hat{W}(k)-\hat{C}(k)\hat{W}(k)-\hat{C}(k)$$

(2-2)

Where $\hat{G}(k)$ is the Fourier transformed of indirect correlation functions, $\hat{W}(k)$ is the Fourier transformed of intramolecular correlation functions and I is the unity matrix. Tilde notation used above means 3D Fourier transform (FT) of the corresponding matrices. To solve equation (2-2) by wavelets, we expand matrices G and C in an arbitrary orthonormal basis set and by substituting in relation (2-1) we obtain the basis representation of the SSOZ equation and calculate the approximating coefficients[5].

Conclusion:

By using of the wavelet and the method of applying it in pervious relations, we can calculate pair correlation function in Fourier space and then by inverting it, we can obtain correlation function in real space and some thermodynamics properties. For this purpose, we have applied the hybrid scheme in which the coarse part of the solution is calculated by wavelets with the use of the Newton-Raphson procedure, while the fine part is evaluated by the direct iterations. The Coifman 2 basis set is employed for the wavelet treatment of the coarse solution. We have acquired a set of RDFs of methane in different temperatures. The calculated RDFs are in fairly agreement with those obtained by discontinues molecular dynamics(DMD) computer simulation. These agreements between the results show that the using of wavelets is useful and powerful method to study the fluids structure. For example, In figure (1), the results of solution of SSOZ equation for RDF of carbon-hydrogen interaction sites are compared with results from DMD computer simulation [6]. The methane

temperature is assumed 126.8 K and the L_J parameters are chosen: $\epsilon_{cc}=0.397\text{kJ/mol}$, $\epsilon_{ch}=0.168\text{kJ/mol}$, $\epsilon_{hh}=0.0711\text{kJ/mol}$, $\sigma_{cc}=3.357\text{\AA}$, $\sigma_{ch}=2.741\text{\AA}$, $\sigma_{hh}=2.134\text{\AA}$ [6].

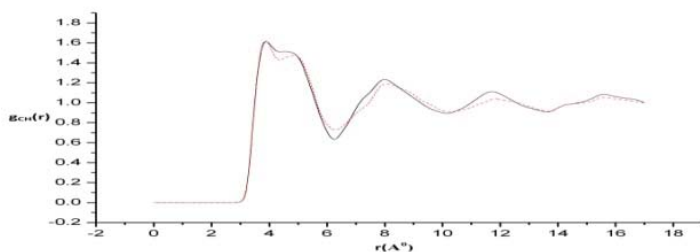


Figure (1). Carbon-hydrogen RDF in methane: the solid line represents DMD and the dashed line represents this work.

Reference:

- [1] Ahmed E. Ismail, Gregory C. Rutledge and George Stephanopoulos, J. Chem. Phys. 118 (2003) 4414.
- [2] M. Moradi and M. Katiraei, Physics Conference Of Iran, 1390, Urmia, Iran.
- [3] M. Moradi and M. Katiraei, 14th Iranian Physical Chemistry Conference, 1389, Kish, Iran.
- [4] D. Chandler and H. C. Andersen, J. Chem Phys. 57 (1972) 1930.
- [5] G. N. Chuev and M. V. Fedorov: J. Comput. Chem. 5 (11) (2004) 1369-1377.
- [6] Herna ´ndez de la Pen~a, Lisandro , van Zon, Rams es , Schofield, Je remy , Opps, Sheldon B, J Chem Phys 126, (2007).



Dyeing equilibrium parameters of polypropylene/Clay composite fibers with disperse dyes

N. Rabiei, M. Haghighat Kish, S. H. Amirshahi*, M. Radjabian

Department of Textile Engineering, Amirkabir University of Technology (Tehran Polytechnic), Tehran, Iran

Email: hamirsha@aut.ac.ir

Key words: Thermodynamic parameters, Dyeing, PP/Clay composite fibers, Disperse dye.

Introduction:

Polypropylene (PP) is a fiber-forming polymer which is greatly used in wide range of textile production. Despite bearing many great mechanical and chemical properties as well as low cost, the polymer has no acceptable dyeability using classical dyeing methods which are of importance in textile industry. To overcome the problem, many attempts have been made based on physical and chemical modification of polypropylene. The serious disadvantage of these approaches is to increase the cost of products.

Recently, incorporating clay nanoparticles into polypropylene matrix as a commercial and effective way to impart dyeability to polypropylene has been suggested. The proposed method could considerably improve dyeability of the polymer with classical dyeing methods. This improvement, however, was examined by several researchers using an unsuitable criterion, i.e. K/S value, which is unable to project what specifically happening in dyeing system [1].

In this study, therefore, we investigate the dyeing mechanism and dyeability of polypropylene fibers incorporated by clay nanoparticles with a disperse dye in terms of some



thermodynamic parameters such as standard affinity, enthalpy and entropy changes of dyeing bath as well as the equilibrium adsorption isotherm, which have not been reported by other researchers on PP/Clay composite fibers.

Materials:

The fiber grade polypropylene homopolymer, named Moplen HP552R, was purchased from Arak Petrochemical Co. (Arak, Iran), and used as received. 1 wt.% OMMT and 3 wt.% PP-g-MA as a compatibilizer for preparation of PP/Clay nanocomposite were employed. The selected disperse dye for this work was the commercial grade of C.I. Disperse Blue 56 named Serilene Blue RL without further purification that was purchased from Yorkshire Group, UK.

Apparatus and Methods:

0.1 g of PP and PP/Clay were individually dyed in the solutions containing 0.01, 0.02, 0.03, 0.04, 0.05 and 0.06 g/l of dye at three different temperatures, 80, 100 and 120 °C, until equilibrium sorption was obtained. The dye concentration in the bath was measured using Cary 100 UV-vis spectrophotometer.

Result and discussion:

For both types of fibers (PP and PP/Clay) the linear isotherms (Nernst Isotherm) describe the relationship between sorption extent of the dye on fiber and in solution. As expected, the standard affinity decreases with increasing of temperature for both fibers because the adsorption of dye on fibers is an exothermic process and releases heat energy. The standard affinities of dye to PP/Clay are considerably higher than those to virgin PP.



The enthalpy change of dyebath containing PP/Clay is lower than that of dyebath containing PP; i.e. the amount of heat energy released when dye molecules are absorbed into polymeric matrix in PP/Clay was lower than that in PP. It could be concluded, therefore, the dye molecules in PP are more strongly embedded within the polymer chains than PP/Clay.

The entropy change of the bath containing PP/Clay is lower negative value than PP's that means the dye molecules were embedded less compactly in the PP/Clay fiber than PP fiber. In fact, the negatively larger value of entropy change of PP indicates that after completion of dyeing, the mobility and freedom of dye molecules is appreciably reduced for the PP substrate. It can be attributed to the creation of suitable voids within the PP/Clay fiber because of incorporating of clay into the PP matrix.

Conclusion:

In respect of dyeing mechanism, while the dyeing sites are not available for both types of fibers, the clay particles provide a type voids that could keep the dye molecules. In addition, clay particles improve the accessibility of the fiber sites, which is very important for effective dyeing procedure. In other words, it seems that the created tortuous pathways can contribute to form the available spaces within PP/Clay fiber to hold and confine dye molecules.

Reference:

- [1] N. Rabiei et al.; "The kinetic and thermodynamic parameters of dyeing of polypropylene/Clay composite fibers using disperse dye"; *Dyes and Pigments*; 94,386-392, 2012.



Complexity of Density Dependencies of Thermal- and Internal- Pressure Compared to that of Total Pressure

SayyedHashemSajjadiandGholamabbasParsafar*

Department of Chemistry, Sharif University of Technology, Tehran, 11365-9516, Iran

Parsafar@sharif.edu

Introduction:

A simple equation of state (EoS) was recently been introduced [1] as

$$(Z - 1)v^2 = e + f/\rho + g\rho^2$$

or

$$(Z_{th} + Z_{in}) - 1 = f\rho + e\rho^2 + g\rho^4 \quad (1)$$

where $Z = pv/RT$ is the compressibility factor, Z_{th} and Z_{in} are thermal and internal contributions to compressibility factor, $v = 1/\rho$ is molar volume, and e , f , and g are temperature dependent parameters. This EoS has been found to be accurate for all types of nano- and bulk- solids, an ionic liquid model, confined water in the carbon nanotubes with different diameters [2], and bulk fluids, in the entire temperature and pressure ranges for which experimental data are reported, except for the isotherms within the critical region. The aim of this work is to investigate the validity of a 3-term expression similar to eq 1 for both thermal and internal contributions to the compressibility factor, separately.

Possibility of presenting thermal and internal pressures by a simple three-term expression in density

One may simply assume that in order to have EoS-III, both thermal and internal pressures have similar density dependencies, as

$$Z_{th} = \frac{P_{th}}{\rho RT} = 1 + a_{th}\rho^2 + f_{th}\rho + g_{th}\rho^4 \quad (2a)$$

$$Z_{in} = \frac{P_{in}}{\rho RT} = a_{in}\rho^2 + f_{in}\rho + g_{in}\rho^4 \quad (2b)$$

where P_{th} and P_{in} are the thermal and internal pressures respectively, and a_{th}/f_{th} and g_{th} are temperature dependent coefficients of the Z_{th} and a_{in}/f_{in} and g_{in} are those for the Z_{in} . Note that for $\rho \rightarrow 0$, a fluid behaves ideally, $Z_{th} = 1$ and $Z_{in} = 0$, because of the fact that there is no interaction among molecules in the ideal state. To examine such assumption, we have used empirical EoSs for some fluids to calculate their thermal pressure. Then eqs 2a and 2b have been fitted onto the calculated values for fluids. The results are shown in Figure 1a-c and Table 1 for some isotherms. From the results given in Table 1, we may conclude that EoS-III is accurate for all isotherms, except for those within the critical region, however, neither eq 2a nor eq 2b fit onto the thermal and internal contributions, respectively, if a wide density range is considered.

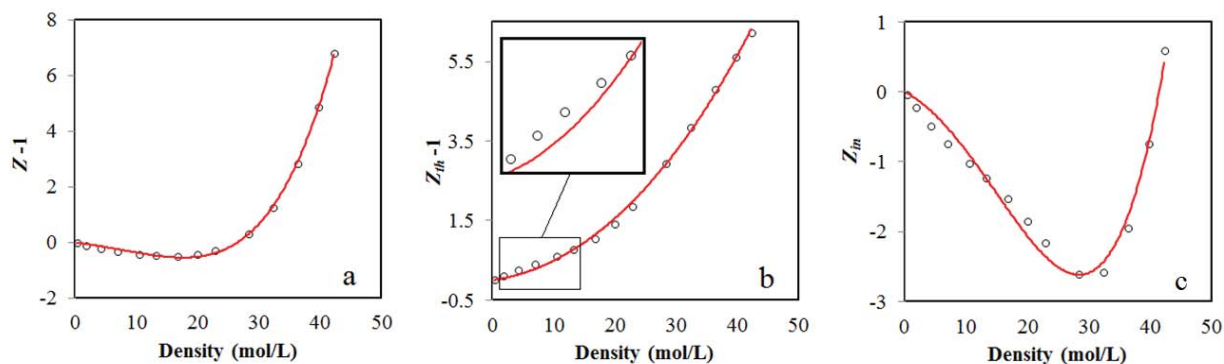


Figure 7. Calculated results obtained from the empirical EoS of Ar[3] at 180 K. Solid curves are the fit onto (a) eq1, (b) eq2a, and (c) eq 2b.

Table 1. Coefficient of determination (R^2) for fitting Z , Z_{fit} , and Z_{in} calculated from the empirical EoS, onto eqs1, 2a, and 2b, respectively, for given isotherms of Ar, N₂[4], and H₂O [5].

	T(K)	Δp (MPa)	Z	Z_{fit}	Z_{in}
Ar	160	0-375	0.99896	0.99795	0.96732
	180	0-495	0.99941	0.99845	0.97976
N ₂	130	0-480	0.99914	0.99497	0.96445
	150	0-530	0.99959	0.99791	0.98254
H ₂ O	630	20-1000	0.99999	0.99750	0.98789
	800	0-750	0.99858	0.99512	0.98571

Reference:

- [1] Parsafar, G. A.; Spohr, H. V.; Patey, G. N. *J. Phys. Chem. B* **2009**, *113*, 11977-11987



- [2] Sadeghi, M.; Parsafar, G. A. *J. Phys. Chem. B*, **2012**, *116* (16), 4943-4951.
- [3] Tegeler, Ch.; Span, R.; Wagner, W. *J. Phys. Chem. Ref. Data* **1999**, *28*, 3, 779-850.
- [4] Span, R.; Lemmon, E.W.; Jacobsen, R.T.; Wagner, W.; Yokozeki, A. *J. Phys. Chem. Ref. Data*, **2000**, *29*, 6, 1361-1433.
- [5] Wagner, W.; Pruss, A. *J. Phys. Chem. Ref. Data*, **2002**, *31*, 2, 387-535.

15th Physical Chemistry Conference



Modeling and experimental verification of the curing kinetics of an Epoxy/ Polyaminoamide/Nano-glassflake system by DSC

M.Ghaffari^{a,b,c,*}, M. Ehsani^a, H. A.Khonakdar^a, G. V.Assche^b, H.Terryn^c

^aIran Polymer and Petrochemical Institute, P.O. Box: 14965-115, Tehran, Iran

^bResearch Group Physical Chemistry and Polymer Science, Vrije Universiteit Brussel, Brussels, Belgium

^cResearch Group Electrochemical and Surface Engineering, Vrije Universiteit Brussel, Brussels, Belgium

Corresponding author: ghaffari.mehdi@gmail.com

Keywords: Epoxy, Nano-Glassflakes, Curing Kinetics, DSC.

Introduction:

Requirements of improved corrosion resistivity and mechanical properties of the epoxy coatings lead to the use of composite systems with the addition of glass flake in the epoxy coatings[1]. Curing is a determining step in coating process and properties as well. So, the understanding of the mechanism and kinetics of cure is the first essential step in the evaluation of processing-property relationship [2]. In this work, the curing kinetics of diglycidyl ether of bisphenol-A epoxy resin cured with a polyaminoamide in the absence and presence of nano-glassflakes (NGF) were studied by means of non-isothermal differential scanning calorimetry (DSC) experiments at four heating rates.



Experimental:

Calorimetric studies were carried out on a Mettler-Toledo DSC-821 thermal analyzer in covered high pressure stainless steel pans under nitrogen atmosphere at heating rates of 1, 2.5, 5 and 10 K min⁻¹.

Results and discussion:

The data were analyzed by Friedman, Ozawa and new method (modified Borchardt and Daniels-BD) approaches. Friedman method showed that E_a is roughly constant over the entire conversion range for both systems with and without NGF. The average values of E_a are 46.8 kJ.mol⁻¹ and 48.8 kJ.mol⁻¹ for the systems with and without NGF, respectively. According to Ozawa method, the calculated activation energy for the neat epoxy/polyaminoamide system is 53.8 kJ mol⁻¹, while these value decrease to 51.3 kJ mol⁻¹ in the presence of NGF. Also, in this method, the average $\ln(A/s^{-1})$ values are 10.89 ± 0.85 and 10.06 ± 0.73 for the neat resin and the system including NGF, respectively. According to the results of modified BD method, the calculated $\ln(A/s^{-1})$, E_a , and n are 9.52, 49.62 kJ mol⁻¹, 1.00 for the neat resin, while for the system including NGF the values are 8.98, 47.83 kJ mol⁻¹, and 0.97, respectively.

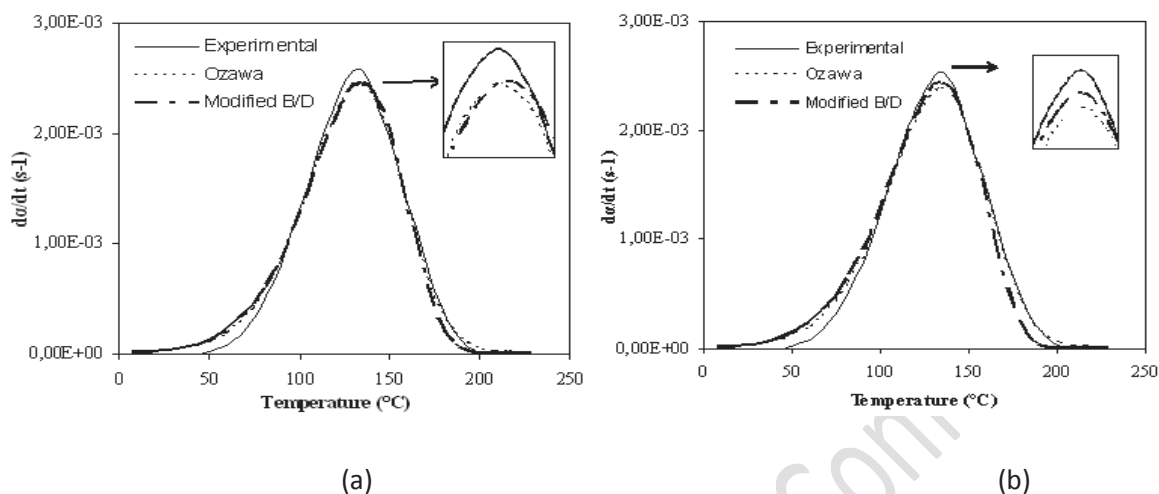


Fig.1. Curing rate versus temperature:

(a) epoxy/polyaminoamide at 10K min⁻¹, (b) epoxy/polyaminoamide/1%NGF at 10 K/min,

Conclusion:

In all analyses, the values of E_a for the nano-glassflake filled system are lower than those of the neat epoxy/polyaminoamide throughout the curing reaction, although these differences are low. Also, the experimental data obtained provided the evidence that the curing behavior showed an n^{th} -order characteristic for both neat and NGF-filled system.

Reference:

- [1] J. González-Guzmán, J.J. Santana, S. González, R.M. Souto: Title of Resistance of metallic substrates protected by an organic coating containing glass flakes. In Progress in Organic Coatings, Volume 68, Issue 3, July 2010, Pages 240-243.



- [2] G. Van Assche, A. Van Hemelrijck, H. Rahier, B. Van Mele, Modulated differential scanning calorimetry: Non-isothermal cure, vitrification and devitrification of thermosetting systems, *Thermochim. Acta* 286 (1996) 209-224.

15th Physical Chemistry Conference



First-principles study of Li adsorption in functionalized carbon nanotubes

M. Jamali*, S. Jalili

Department of Chemistry, K. N. Toosi University of Technology, Tehran, Iran

*E-mail: jamali@dena.kntu.ac.ir

Introduction

According to the increasing inquiry of better electrochemical materials for electrical energy device such as battery of high energy and power density, various types of lithium intercalation materials have been used to promote Li adsorption. To raise the Li adsorption capacity of the carbon-based electrode, the carbon nanotubes (CNTs) have been considered to be one of the promising candidates because of its outstanding electrical and mechanical properties. Therefore, many theoretical and experimental works have been assigned to study the intercalation of Li in single-walled carbon nanotubes (SWCNTs) [1]. In this study, we investigate the detailed energetic of lithium adsorption on the functionalized SWCNTs. Moreover, electronic properties of functionalized nanotubes before and after lithium doped were investigated.

Methods

All calculations were carried out using the Quantum-Espresso package in which the DFT methodology is implemented using plane wave expansions and pseudopotentials [2]. The structures considered here are $\text{NH}_2/(8,0)$, $\text{COOH}/(8,0)$ SWCNTs doped with lithium. The cutoff energies for plane waves were chosen to be 50 Ry. Calculations were performed in the supercell approximation. The lattice parameter along the axial direction of the nanotube is 3 times the unit length of the pristine nanotube. The Brillouin zones were sampled with $1 \times 1 \times 9$ Monkhorst–Pack meshes, which represent the convergence of our systems, along the Γ -Z direction [3].

Results and Discussion

After functionalization of (8,0) SWCNT with -NH_2 and -COOH groups, we doped Li in the inside and outside of these nanotubes. The adsorption of Li on different sites of $\text{NH}_2/(8,0)$, are presented in Figure 1. The binding energy, ($E_b = E(\text{CNT} + \text{Li}) - E(\text{CNT}) - E(\text{Li})$), of all Li-doped functionalized nanotubes was calculated and reported in Table 1. Considering the binding energy as a criterion for adsorption tendency, the internal adsorption of Li is more desirable than the external adsorption of Li. As indicated in Table 1, the binding energy of Li-doped $\text{NH}_2/(8,0)$ and $\text{COOH}/(8,0)$ for all sites is more than of Li-doped (8,0) SWCNT. Moreover, binding energy of site A for functionalized nanotubes is more than that of all other sites.

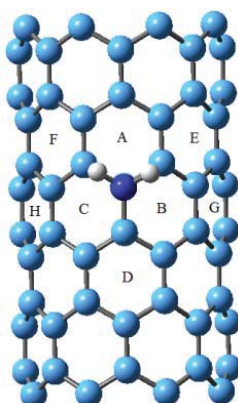


Figure 1. Model of Li adsorbed on $\text{NH}_2/(8,0)$ in different sites. Corresponding

system	site	binding energy
Li@(8,0)		-37.63
Li@NH₂/(8,0)	A	-47.76
Li@NH₂/(8,0)	B	-46.20
Li@NH₂/(8,0)	C	-46.19
Li@NH₂/(8,0)	D	-45.08
Li@NH₂/(8,0)	E	-46.05
Li@NH₂/(8,0)	F	-47.45
Li@NH₂/(8,0)	G	-45.40
Li@NH₂/(8,0)	H	-45.44
Li@COOH/(8,0)	A	-44.40
Li@COOH/(8,0)	B	-38.69
Li@COOH/(8,0)	C	-40.99
Li@COOH/(8,0)	D	-41.04

Table 1. Electronic binding energies (kcal/mol) determined for the Li doped into the inside of (8,0), $\text{NH}_2/(8,0)$ and $\text{COOH}/(8,0)$ SWCNTs of different sites

Also we have calculated band structure for $\text{NH}_2/(8,0)$, $\text{COOH}/(8,0)$, $\text{Li@NH}_2/(8,0)$ and $\text{Li@COOH}/(8,0)$ SWCNTs (Figure 2). According to band structures, conduction reduces with Li doping.

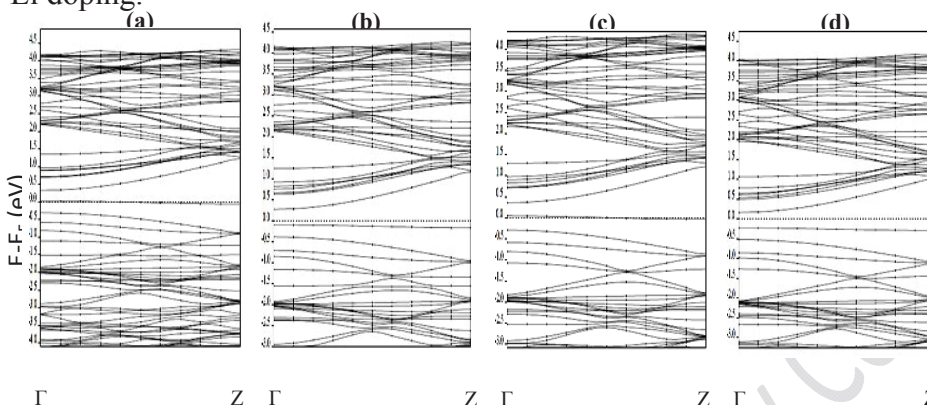


Figure 2. Electronic band structures for: (a) $\text{NH}_2/(8,0)$, (b) $\text{Li@NH}_2/(8,0)$, (c) $\text{COOH}/(8,0)$ and (d) $\text{Li@COOH}/(8,0)$ SWCNTs.

Conclusion

According to the first principles calculations, functionalization of (8,0) nanotube with $-\text{NH}_2$ and $-\text{COOH}$ groups increases the Li adsorption energies. After Li doping functionalized SWCNTs, conduction of functionalized SWCNTs is reduced.

Keywords: Density functional theory, functionalized SWCNT, Binding energy, band structure.

References

- [1] T. Kar, J. Pattanayak, S. Scheiner, J. Phys. Chem. A 105(45) (2001) 10397.
- [2] P. Giannozzi, S. Baroni, N. Bonini, J. Phys.: Condens. Matter 21 (2009) 395502.
- [3] J.P. Perdew, K. Burke, M. Ernzerhof, Phys. Rev. Lett. 77 (1996) 3865.



Viscometric study on the compatibility of poly(vinyl acetate)-poly(vinyl pyrrolidone) in solution

Abbas Mehrdad¹, Khadejeh Khezri^{2*}

¹Department of Physical Chemistry, Faculty of Chemistry, University of Tabriz, Tabriz, Iran

² Department of chemistry, Faculty of sciences, Payame Noor University, urmia, Iran

*Email: khezripnuchem@yahoo.com

Key words: polymer solution, compatibility, intrinsic viscosity

Introduction:

A simple method to analyze polymer-polymer miscibility in solution is the viscometric technique [1]. The viscosity study on ternary system of two different polymers and a solvent has been a subject of continuing interest, mainly due to its simplicity and importance in the characterization of the intermolecular interaction between the two different polymers in solution [2]. Compatibility of polymer can be explained in terms of the thermodynamic and hydrodynamic parameters [3].

Materials and methods:

The poly vinyl acetate (PVAc) used in this study had a reported nominal average molar mass of 140 kg.mol⁻¹. The poly vinyl pyrrolidone (PVP) used in this study had a reported nominal average molar mass of 58 kg.mol⁻¹. Acetonitrile used in this study was purchased from Merck Chemical Co. and had a reported mass fraction purity of 0.99. The polymer solutions were

filtered before use and their viscosities were measured using a jacketed Ubbelohde viscometer with 0.4 mm capillary.

Results and discussion:

The viscosities of PVAc solutions in pure acetonitrile and in pre-prepared PVP solution with constant concentration 2 kg.m^{-3} were measured at various temperatures. Also the viscosities of PVP solutions in pure acetonitrile and in pre-prepared PVAc solution with constant concentration 2 kg.m^{-3} were measured at various temperatures. According to the Huggins equation ($\eta_{red} = [\eta] + bC$), the intrinsic viscosity, $[\eta]$, of the polymer is obtained by extrapolation of reduced viscosity to zero polymer concentration. The obtained intrinsic viscosities and viscometric interaction parameter, b , are listed in Tables 1 and 2.

Table 1. Intrinsic viscosity, $[\eta]$ ($\text{m}^3.\text{kg}^{-1}$), of PVAc and PVP and $\Delta[\eta]$ ($\text{m}^3.\text{kg}^{-1}$)

T/K	$[\eta]_{\text{PVAc-0}}$	$[\eta]_{\text{PVAc-PVP}}$	$[\eta]_{\text{PVP-0}}$	$[\eta]_{\text{PVP-PVAc}}$	$\Delta[\eta]$
293.15	0.07396	0.06367	0.03866	0.03393	-0.01502
298.15	0.07101	0.05996	0.03706	0.03108	-0.01703
303.15	0.06851	0.05540	0.03578	0.02833	-0.02056
308.15	0.06667	0.04991	0.03399	0.02646	-0.02429
313.15	0.06473	0.04273	0.03263	0.02470	-0.02993

Table 2. Viscometric interaction parameter, b ($\text{m}^6.\text{kg}^{-2}$), of PVAc and PVP and Δb ($\text{m}^6.\text{kg}^{-2}$)

T/K	$10^3 b_{\text{PVAc-0}}$	$10^3 b_{\text{PVAc-PVP}}$	$10^3 b_{\text{PVP-0}}$	$10^3 b_{\text{PVP-PVAc}}$	$10^3 \Delta b$
293.15	2.227	3.282	1.074	1.288	1.269
298.15	2.262	2.977	1.011	1.317	1.021
303.15	2.272	2.869	0.972	1.258	0.883

308.15	2.187	2.779	0.945	1.134	0.781
313.15	2.167	2.979	0.918	1.077	0.971

The polymer solvent method and the classical dilution method were used studying the compatibility of polymers. In the polymer solvent method intrinsic viscosity and viscometric interaction parameter of a polymer in pure solvent were compared with intrinsic viscosity and viscometric interaction parameter of a polymer in solution of another polymer. The polymer blend is compatible if $\Delta[\eta] < 0$ and is incompatible if $\Delta[\eta] > 0$. Whereas $\Delta[\eta] = \Delta[\eta]_A + \Delta[\eta]_B$ and $\Delta[\eta]_A = [\eta]_{A-B} - [\eta]_{A-0}$. Where $[\eta]_{A-0}$ and $[\eta]_{A-B}$ are intrinsic viscosities of polymer A in pure solvent and in solution of polymer B, respectively. Another compatibility criterion is based on the difference between experimental and ideal values of viscometric interaction parameter. On the basis of this criterion, the polymer blend is compatible if $\Delta b > 0$ and is incompatible if $\Delta b < 0$. Whereas $\Delta b = \Delta b_A + \Delta b_B$ and $\Delta b_A = b_{A-B} - b_{A-0}$. Where b_{A-0} and b_{A-B} are viscometric interaction parameters A in pure solvent and in solution of polymer B, respectively. The results of Tables 1 and 2 indicate that the PVAc/PVP blends are compatible.

Conclusion:

In this work, the polymer solvent method was used to studying the compatibility of polymers. The obtained result reveals that PVAc/PVP blends are compatible.

Reference:

- [1] Garcia, R.; Melad, O.; Gomez, C. M.; Figueruelo, J. E.; Campos, A. *Euro. Polym. J.* 1999, 35, 47-55.



- [2] Zhang, Y.; Qian, J.; Ke, Z.; Zhu, X.; Bi, H.; Nie, K. *Euro. Polym. J.* 2002, 38, 333-337.
- [3] Mehrdad, A.; Talebi, I.; Rostami, M.R. *J. Chem. Eng. Data*, 2011, 56, 3029-3037.

15th Physical Chemistry Conference

Mass Calibration of Time of Flight Mass Spectrometer Using Alkali Salts

H.Azad, M.Tabrizchi, F.Abyar, H.Faroukhpour

Department of Chemistry, Isfahan University of Technology, Isfahan, Iran, 84156-83111

E-mail: h_azad_706@yahoo.com

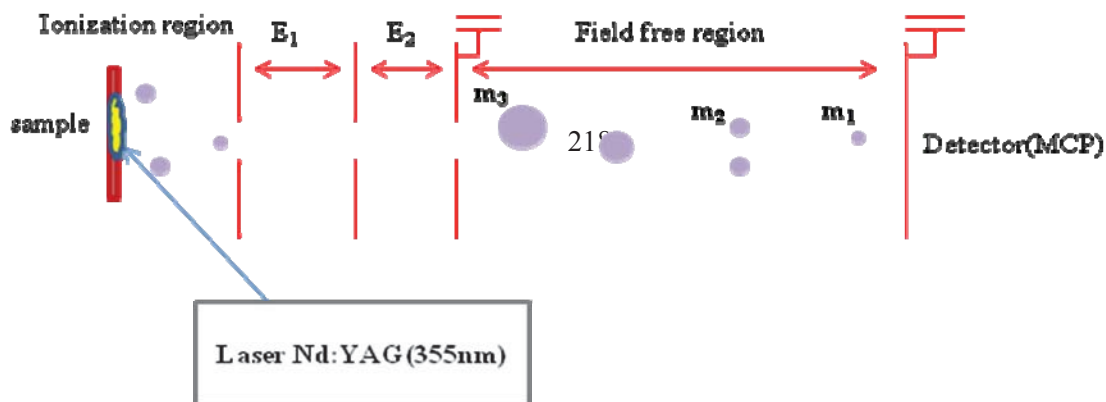
Keywords: Time of Flight, Calibration, Alkali halides, Clusters

Introduction:

Time of flight (TOF) mass spectrometry is one of the most important methods for quantitative and qualitative analysis of materials. The ionization source in TOF mass spectrometry can be electron impact, laser and synchrotron radiation. In this method the ions, produced by direct ionization or thermal desorption from an ionic salts, accelerated in a uniform electric field and then separated in a field free region based on their masses to charge ratio. In TOF mass spectrometry, the m/z ratio is proportional to the square of flight time. For accurate calibration known masses are required to obtain the parameters for converting the flight time to mass. In this work, the TOF mass spectra of alkali halides including LiCl, KCl, NaCl, CsCl and their mixtures were recorded and used for mass calibration.

Experiment:

Fig. 1 shows the set-up of the TOF mass spectrometer constructed in the Isfahan university of technology [1]. The ionization source of the set-up is laser radiation (355 nm) produced by a



Nd-YAG laser (Quantel model YAG980, France).

Fig.1 Set-up of the TOF mass spectrometer

During the experiment the TOF was under high vacuum (10^{-7} mbar). The TOF mass spectra of the samples were recorded at different laser intensities, detector and repeller plate voltages. The aqueous solution of alkali halides (0.1M) was prepared and coated on an aluminum surface, used as repeller. Sample was directly irradiation by the laser light to evaporate and ionize.

Result and discussion:

Fig.2 shows a typical mass spectrum obtained from a mixture of alkali salts. It is evident that the resolution is good enough to distinguish different isotopes. Also, we observed different clusters of the type of $M^+(NCl)$ [2] where M and N are alkali atoms. To calibrate the mass spectrum, the masses and flight times were fitted in a $m^{1/2} = at + b$. (Fig. 3).

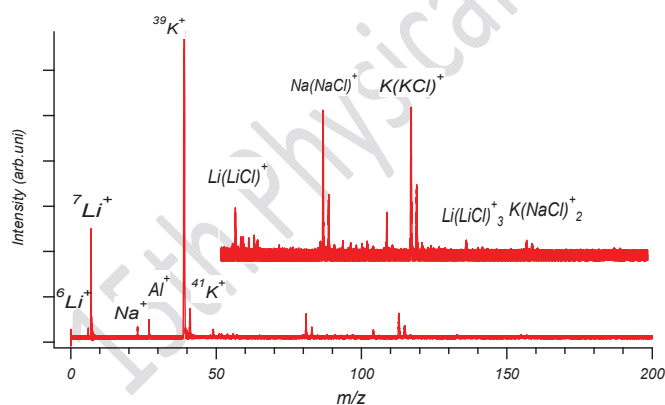


Fig.2 Typical TOF mass spectra of alkali salts.

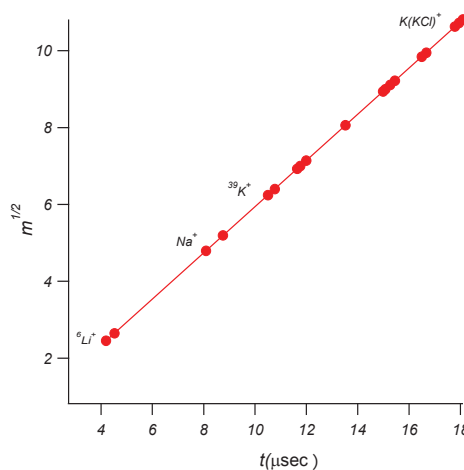


Fig. 3 Mass calibration curve



Conclusion:

We observed the presence of clusters such as M^+ as well as $M^+(NCl)$ such as $Li^+(LiCl)$, $Na^+(NaCl)$, $K^+(KCl)$, and $K^+(NaCl)_2$ produced by laser desorption ionization. Using the calibration method, a mass accuracy of ± 0.04 m/z was obtained.

References:

- [1] M. Tabrizchi, Construction of a Laser Ionization Time of Flight Mass Spectrometer, Iranian Patent No. 73361. 2012
- [2] C. R. Ponciano, R. Martinez and E. F. da Silveira, J. Mass Spectrom. 2007; 42: 1300–1309.



Electron (Spin & Charge) and Nanoelectronics

Hassan Sabzyan (sabzyan@sci.ui.ac.ir)

Department of Chemistry, University of Isfahan, Isfahan 81746-73441, I. R. Iran

Keywords: Nanoelectronics; Molecular electronics; Spintronics; Thermoelectric Effects.

Introduction

Further miniaturization of the electronic devices is not possible with traditional (macro/micro) methods of synthesis of transistor materials and production of integrated circuits. *Nanoelectronics* is a branch of nanoscience/nanotechnology that addresses the industrial quest and commercial thirst for this miniaturization down to nanometer scales. Design and study of the nanoelectronic circuits which fundamental components are molecules is referred to as *moletronics* or *moletronics*. Shrinking electronic devices to these scales increases capacity of data storage devices, increases speed of digital computing processes, and decreases power consumption of electronic instruments. Nanoelectronics(moletronics) provides also possibility of manufacturing nanometric actuators and sensors which will revolutionize sciences and technologies of motion control, measurement, and biological monitoring, diagnostic and interferences.

In order to design and properly apply effective nanoelectronic devices and circuits, behavior of electrons (their charge and spin) in static field-free molecular and intermolecular spaces, and in the electro-dynamical systems under static and time-dependent external electric and magnetic fields, and electron-nuclear interaction should be known exactly. spintronics is a version of electronics in which the spin of electrons contributes to the steady state response properties and characteristics of the transport phenomena in an electronic device. This contribution provides a variety of new features to the performance of electronic devices, such as more secure encoding/decoding of data, magnetic control of the device function, accurate production of local magnetic fields, and more reliable sensing and actuating. In spintronics, spin density can redistribute under local fields either with or without charge transfer.

Three critical problems are to be resolved prior to the use of nano-size and molecular devices in nanoelectronic circuits. These include: (i) limitations for packing moletronic devices in a three-dimensional space, (ii) possibility of tunneling between neighboring molecules, and (iii) energy dissipation in the nuclear motion of the molecules. The first two problems, which are well-defined in physicochemical contexts, are addressed so far by encapsulating the device with inert chemicals and/or capping with σ -bond insulating moieties, and spreading as far as possible the circuit components over a two-dimensional space. While, the interferences between electronic and nuclear motions which can result in thermoelectric effects and uncontrollable energy-dissipation in nanoelectronic devices and circuits [1], have not been investigated so far. These interferences are studied here based on QTAIM and normal mode analyses.

Results and Discussion

After presenting an introduction to nanoelectronics and thermoelectric effects, the nature of electron (charge & spin) is discussed [2] regarding its behavior in a molecular-size electronic device. Then, the evolutions of the molecular electronic and nuclear motions in a typical single-molecule device exposed to external electric field (EF) are studied. New molecular coefficients are introduced to describe and probe occurrence of Joule-like and Peltier-like effects in molecular nanoelectronic devices. A semiemirical intramolecular temperature scale is introduced to describe electronic and nuclear energy redistributions induced by EF over the molecular device space, which is used to introduce and plot intramolecular (or nanoscale) thermograph (Figure 1) based on which details of energy redistribution and electronic energy dissipation can be extracted and the performance of any prospective nanoelectronic device can be rated prior to synthesis and manufacturing of the device.

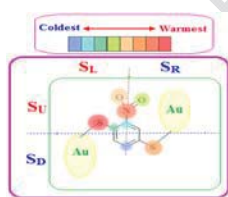


Figure 1: A typical Thermograph



References

- [1] H. Sabzyan and R. Safari, EPL, *in press* (2012).
- [2] H. Ebadi and H. Sabzyan, IJST 6 (2009) 486-509.

15th Physical Chemistry Conference



Quantum chemical studies on molecular structural conformations, energetic of methyl (methylene) silane

Fahimeh mollania^a, Fariba Mollania^b and Nasser L. Hadipour^{a,*}

^aDepartment of Chemistry, Tarbiat Modares University, Tehran, Iran

^bDepartment of Chemistry, Birjand University, Birjand, Iran

* E-mail: hadipour@modares.ac.ir

Abstract:

Recently, silicon based reactive diluents have been paid many attentions because silicon-containing compounds usually have outstanding chemical and thermal stability, and insulativity. These interesting investigations have proved the advantages of silicon based reactive diluents; meanwhile, they also suggest that the chemical structure of silicon-containing compounds should be carefully designed to guarantee the elaboration of these advantages [1,2].

We report our findings on relative energy, geometric properties of methyl (methylene) silane and its derivatives (see Fig.1). Geometry optimizations are carried out by B3LYP method. This is using 6-311++G** basis set of the Gaussian 98 system of programs [3]. The investigation in water solution was carried out by means of the self-consistent reaction field (SCRF) method [4] at the B3LYP/6-311++G** level of theory. To confirm the nature of the stationary species, frequency calculations are carried out. For minimum state structures, an only real frequency value is accepted. In order to find substituent effect on methyl (methylene) silane, theoretical study via DFT method is employed in the manuscript. The following substituents are taken into considerations: NO₂ and CH₃.

In this work, an AIM-analysis of the topology of the charge density were used to investigate the influence of the substituents at the methyl (methylene) silane on the structural, electronic and energetic properties of these constitutional isomers (see Fig. 2.). Changeability of the C–Si, C–N and C–C bond lengths was analyzed in terms of the natural bond orbital (NBO) method.

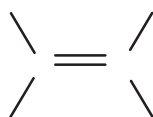
According to all of the theoretical calculations, the stability orders (ΔE in kcal/mol) for the methyl (methylene) silane in gas phase and solutions are as follows:



Geometrical parameters showed that the calculated geometric parameters for methyl (methylene) silane and its derivatives in gas phase, water, THF and DMSO solutions were very similar.

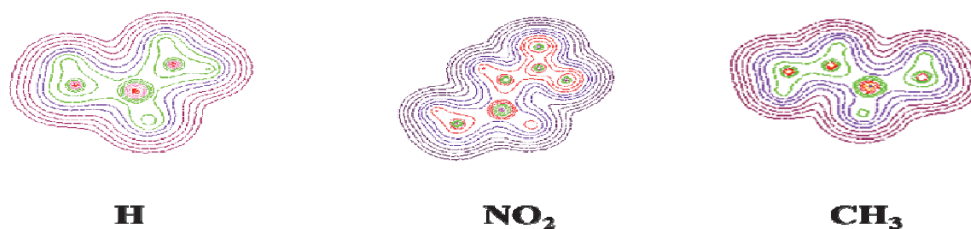
Keywords: methyl (methylene) silane; ab initio method; DFT method; solvent effect

Fig. 1. The structure of methyl (methylene) silane derivatives



R=H, CH₃ and NO₂

Fig. 2. The contour map of methyl (methylene) silane obtained from the B3LYP/6-311++G** wave function





Reference:

- [1] I. Fleming, A. Barbero, D. Walter, Stereochemical Control in Organic Synthesis Using Silicon-Containing Compounds, *Chem. Rev.* 97 (1997) 2063-2192.
- [2] Z. N. Parnes, G. I. Bolestova, Cleavage of silicon-carbon bonds in tetraorganosilanes and formation of new carbon-carbon bonds under the action of Lewis acids, *Synthesis*, 991 (1984)
- [3] M. J. Frisch et al, Gaussian 98, Revision A.6, Gaussian (Pittsburgh, PA, 1998).
- [4] L. Onsager, Electric Moments of Molecules in Liquids, *J. Am. Chem. Soc.* 58 (1936) 1486-1493.



A new method for exploring alien life

Homa Izadi and Afshin Shafiee

Department of Chemistry, Sharif University of Technology, Tehran, Iran

Email: homa_izady@yahoo.com

Key words: Alien life, Spectroscopy, Radio wave, Planet-shine

Introduction:

It's been nearly four decades since Carl Sagan first addressed the general public from a scientist's perspective, confronting the possibility of extraterrestrial life [1]. Different scientific hypothesis are proposed to answer this controversial question. The search for extrasolar terrestrial planets is in large part motivated by the hope of finding signs of life or habitability via spectroscopic biosignatures [2]. The main focus of these spectroscopic methods is the direct detection of extrasolar terrestrial planets. However, in some cases searching for spectroscopic signatures by a direct technique (i.e., a direct interaction of radiation and matter) is an impossible goal due to blind spots in the space. In this study, a new approach, based on indirect spectroscopy, for finding out extraterrestrial life on other planets is proposed and compared with another direct spectroscopy.

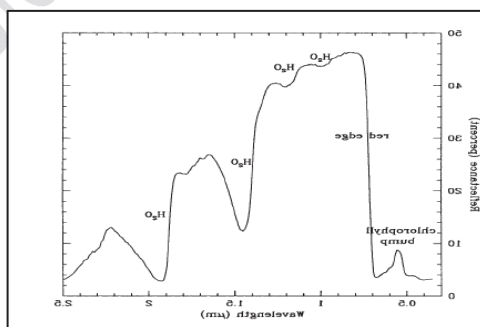
Method:

On the one hand, planet-shine spectrum is investigated, when reflected sunlight from a planet illuminates the night side of one of its moons. A low-resolution optical spectrum could be obtained which informs us from the vegetation of that planet. On the other hand, radio

astronomy is probed, a field that has become one of the most important tools of astronomical observations. Radio astronomy has been responsible for a great part of our understanding about the universe, its formation, composition, interactions, and even the predictions we can do about its future path.

Result and Discussion:

Earth's deciduous plants have a sharp order-of-magnitude increase in leaf reflectance between approximately 700 and 750 nm wavelength. This strong reflectance of Earth's vegetation suggests that surface biosignatures with sharp spectral features might be detectable in the spectrum of scattered light from a spatially unresolved extrasolar terrestrial planet. An ideal surface biosignature would be produced by a large and abrupt change in the reflectance at wavelengths that penetrate to the planetary surface (FIG. 1). There are some problems associated with not only this technique, but also with any optical-based technique. Since radio waves have a large wavelength, they experience less interference. As a result, they can travel across large distances. Moreover, the sunlight, cloudy conditions, and rain do not affect our observations.



Connection between life and volcanic activity is straightforward. Life is closely related to volcanic activity of planets and there is no possibility of existing life on any planet, unless volcanic activity could be existed on it [3]. Since these two issues are clearly connected, we



propose that using the volcanic activity via radio spectroscopy on far planets can lead us to put away planets which are without life. This helps us to search life on a limited subset of far planets.

Conclusion:

Spectroscopic methods are favourable approaches to investigate alien life. Among spectroscopic methods, radispectroscopy is a reasonable technique to study extraterrestrial life.

References:

- [1] David Grinspoon, *Lonely Planets: The Natural Philosophy of Alien Life*, (HorperCollins Publishers, New York, 2003).
- [2] S.Seager, *et al*, *Vegetation's Red Edge: A Possible Spectroscopic Biosignature of Extraterrestrial Plants*, (ASTROBIOLOGY, 2005).
- [3] A. Einarsson, *The connection between life and volcanic activity*, Iceland, 1996, <<http://www.ramsar.org/cda>>.



Evolution of the free electron wavepacket near a nucleus

H. Sabzyan*¹, S.F. Alavi¹, M. Vafae²

¹ Department of Chemistry, University of Isfahan, Isfahan 81746-73441, I. R. Iran

² Department of Chemistry, Tarbiat-Modares University, Tehran, I. R. Iran

sabzyan@sci.ui.ac.ir, fatemealavi77@gmail.com, mohsenvafae@gmail.com

Keywords: Free electron, Bound electron, TDSE, Evolution, Wavepacket

Introduction:

Electron scattering and photoionization (PI) of molecules have been investigated extensively over the past few decades, both theoretically and experimentally. These investigations provided numerous information in various applied fields such as plasma, radiation and astro-physics [1]. Although ionization of electron from atomic and diatomic species have been studied at femto and attosecond time scales so far, it is still impossible to follow evolution of a bound electron wave function into a free electron described ideally by a Dirac δ -function.

In this research, time-dependent Schrödinger equation (TDSE) is solved numerically to investigate the reverse phenomenon, i.e. evolution of the free electron wavepacket (WP) near a nucleus in terms of the transformation into bound electron wave functions. This evolution is quantified by evaluating the instantaneous contributions of the hydrogen-like s , p , d orbitals to the evolving WP. The departure from the initial WP has been quantified by calculating time-dependent autocorrelation coefficients of the WP. Effects of the

characteristics of the initial Gaussian WP, including its entrance direction, velocity, and initial widths, on the instantaneous contributions of the hydrogen-like orbitals and autocorrelation coefficients are also investigated.

Computational Method:

A two-dimensional Gaussian shape propagating WP of the form Eq. (1) is considered to represent the incoming free electron. In this WP, x_c and y_c are coordinates of the center of the WP, which is moved during the simulation with a classical speed of v along a defined direction. The σ_x and σ_y parameters denote the initial widths of the WP. This WP is initially set at the entrance point of $\vec{r}_0 = (x_0, y_0)$ and its evolution is followed by solving numerically the TDSE in a two dimensional space, which has the form (in atomic units) given in Eq. (2). In this equation, (x_N, y_N) and Z_N are the coordinates of the nucleus and its charge, and scp is the soft-core potential parameter that allow avoiding the singularity at the nucleus. Eq. (2) is solved numerically by a direct integration method using an appropriate split operator. A negative imaginary potential (NIP) acting as absorbing wall, operative only near the borders of the simulation box, is added to the Hamiltonian.

$$\Psi(x, y, t=0) = \frac{N}{2\pi\sigma_x\sigma_y} \exp\left[-\frac{(x-x_c)^2}{2\sigma_x^2} - \frac{(y-y_c)^2}{2\sigma_y^2}\right] \quad (1)$$

$$i\frac{\partial\Psi(x, y, t)}{\partial t} = \left[-\frac{1}{2}\left(\frac{\partial^2}{\partial x^2} + \frac{\partial^2}{\partial y^2}\right) - \frac{Z_N}{\sqrt{(x-x_N)^2 + (y-y_N)^2 + scp}}\right]\Psi(x, y, t) \quad (2)$$

Results, discussion and conclusion:

Examples snapshots of the evolving WP and variations of the hydrogen-like orbital

contributions to the WP are presented in Figs. 1 and 2. Results show that electronic WP spreads as it moves toward the nucleus, and scatter when comes close to nuclei. Part of WP is bounded to the nucleus temporarily. Increasing velocity of the WP, results in intensified peaks. Evolution of the asymmetric WP is accelerated in the direction it has a smaller σ value. Moreover, distancing the WP travel path from the nucleus decreases its scattering, and contributions of the hydrogen-like orbitals [3].

Fig. 1. Snapshots of the evolved WP near the H nucleus at different WP velocities 7.07 (a), 4.71 (b) and 3.53 au (c).

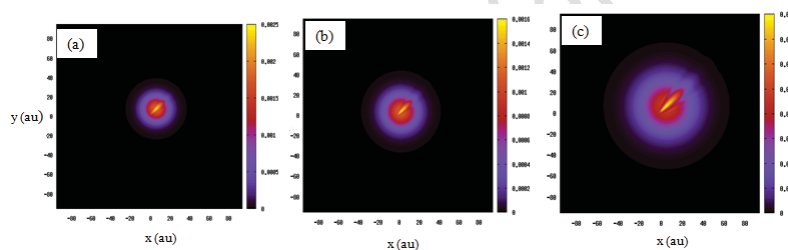
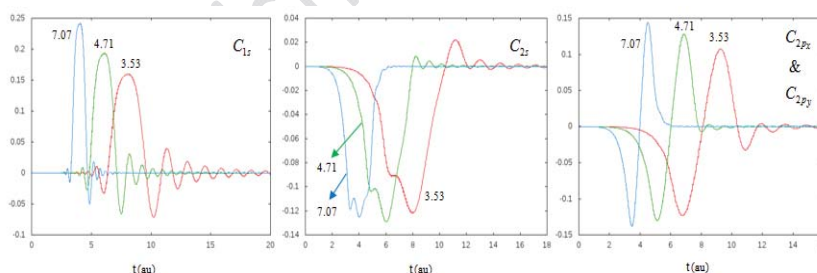


Fig. 2. Contributions of the s and p hydrogen-like orbitals, (C_{1s} , C_{2s} , C_{2px} and C_{2py}) to the evolved WP at different velocities (as labeled).



References:

- [1] H. Miyagi et al, Phys. Rev. A. **85**, 022708 (2012).
- [2] H. Ebadi and H. Sabzyan, *Journal of the Iranian Chemical Society (JICS)*, 6, 489 (2009).
- [3] S. F. Alavi, *Evolution dynamics of the free electron ...*, MSc Thesis; University of Isfahan (2011).

Electrostatic Properties of Halogen Bonds



H. Asadi and K. Eskandari

School of Chemistry, Damghan University, Damghan, 36716-41167, Iran.

Asadi1831@yahoo.com, eskandari@du.ac.ir

Key words: Halogen bond, Cooperativity, QTAIM, Atomic multipole

Introduction:

It is well known that a covalently bonded halogen atoms can act as electron acceptors and interact with electron donor species. This type of noncovalent interaction is usually called *halogen bond* [1]. Halogen bonds have attracted immense attentions in recent years, because of their importance in different fields of chemistry and biochemistry. In addition, the fact that halogens usually have negative partial charges (due to their high electronegativity), makes these negative-negative interactions more interesting for theoretical chemists. The nature of halogen bonds is still the objective of many researches [1,2]. Eskandari and Jalali studied halogen bonds by focusing on electrostatic properties of halogen atoms [3]. They showed that electric quadruples of halogen atoms are mainly responsible for their attractive interactions with negatively charged atoms. The main objective of this work is to investigate the cooperativity and anti-cooperativity effects on the electrostatic properties of the halogen atoms.

Methods:

Molecular geometries and electronic wavefunctions were fully optimized at MP2/6-311++G(d,p) 6d level using Gaussian 03 program. Bader's QTAIM was used to evaluate atomic electrostatic moments. Integration over atomic basins was carried out using standard mode of AIMAll program.

Results and Discussions:

The multipole expansion (ME) of electrostatic potential at a given point, S, in a vicinity of a molecule is given by:

$$V_s = \sum_i \frac{q_i}{r_{i,s}} + \sum_i \frac{(m_i \cdot r_{i,s})}{r_{i,s}^2} + \sum_i \frac{(r_{i,s} \cdot Q_i \cdot r_{i,s})}{2r_{i,s}^3}$$

In which, q_i , m_i and Q_i are, respectively, the atomic monopole moment, atomic dipole moment vector and the atomic traceless quadrupole moment of i -th atom. $r_{i,s}$ and $\mathbf{r}_{i,s}$ are the distance between atom i and the point \mathbf{s} and the unitary vector pointing from atom i to point \mathbf{s} , respectively. In this work, we used ME of electrostatic potential to study the halogen bonding interactions in $XY \cdots NH_3$ and $NH_3 \cdots XY \cdots NH_3$ systems. Here XY is Cl_2 , Br_2 , $ClBr$, FCl or FBr . To investigate the trends of halogen bonds in $XY \cdots NH_3$ and $NH_3 \cdots XY \cdots NH_3$ complexes, ME of electrostatic potential, V_s , at molecular surface, along the $X-Y$ bond of XY and $NH_3 \cdots XY$ systems has been calculated. Figure 1 displays the relation between V_s and electron density at the bond critical points, ρ_b , (as a measure of the intermolecular binding strength) of $Cl \cdots N$ and $Br \cdots N$ interactions. Clearly, there is no correlation between the values; however, a very good linear correlation is found when one excludes the FCl and FBr molecules (Figure 2). It seems the electrostatic terms are not the only terms which responsible for formation of halogen bonded complexes of FCl and FBr . NBO analysis also confirms that charge transfer is important in these complexes.

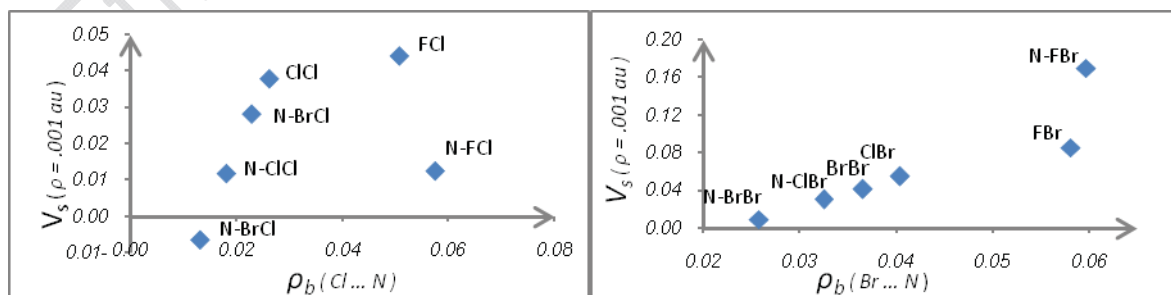


Fig. 1 Relation between V_s and ρ_b

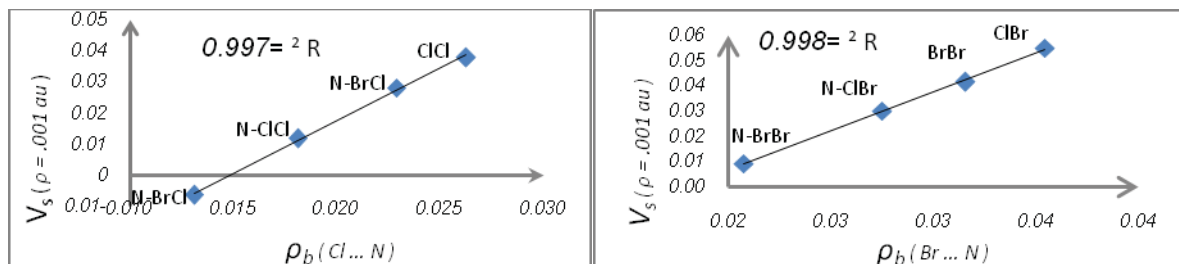


Fig. 2. Relation between V_s and ρ_b

Conclusion:

ME of electrostatic potential has been calculated in the vicinity of halogen atoms in XY and $NH_3 \cdots XY$ systems. In all of the cases, the zz component of atomic quadrupole moment of halogens is mainly responsible for formation of halogen bonds. Comparing XY and $NH_3 \cdots XY$ reveals that NH_3 reduces the quadrupole moments of halogens and hence destabilizes the second halogen bond in $NH_3 \cdots XY \cdots NH_3$.

References:

- [1] Halogen Bonding, Fundamentals and Applications; Metrangolo, P.; Resnati, G., Eds.; Springer, 2008.
- [2] K.Eskandari, H.Zarizy Chem.Phys.Let., 492 (2010) 9 (and references within it).
- [3] K.Eskandari, H. jalali, submitted.



Calculation of Rovibronic Transition Intensities for Diatomic Molecules

Ehsan Gharib Nezhad and Alireza Shayesteh

School of Chemistry, College of Science, University of Tehran, Tehran 14176, Iran

Email: shayesteh@khayam.ut.ac.ir

Key words: Line Intensities, Einstein A coefficient, MgH, Astrochemistry

Introduction:

Stars having remarkable emission lines in the optical spectra are called emission-line stars and widely distributed on the Hertzsprung-Russell diagram including various stellar types.¹ In addition to line positions, knowledge of Einstein A coefficients for rovibronic transitions has important applications in astrophysics.² Experimentally, Einstein A coefficients can be determined indirectly via lifetime measurement; however, this lifetime is related to the rate of radiative decay of an excited state to all lower energy levels.

Magnesium hydride is an important molecule in different astrophysical environments. Lines of the $A^2\Pi \rightarrow X^2\Sigma^+$ transition have been detected in different stellar regions such as the solar photosphere,³ the spectra of sunspot,⁴ nearby L dwarfs,⁵ and late-type stars.⁶ In addition, the $B'^2\Sigma^+ \rightarrow X^2\Sigma^+$ bands have been detected in sunspot umbral spectra.⁷

Theory:

Line intensities of rovibronic transitions are proportional to Einstein A coefficients which directly depend on transition wavenumber $\tilde{\nu}$ (in cm^{-1}), the Hönl-London factor $S_{J' \leftarrow J''}^H$, and the dipole moment operator $\mu(r)$ in Debye which is a function of internuclear distance r .

$$A_{J' \leftarrow J''} = 3.1361861 \times 10^{-7} \tilde{\nu}^3 \frac{S_{J' \leftarrow J''}^H}{2J' + 1} \left| \langle \psi_{v'J'}^e(r) | R(r) | \psi_{v''J''}^e(r) \rangle \right|^2 \quad (1)$$

$$[M_{v'J' \leftarrow v''J''}^e]^2 = \left| \langle \psi_{v'J'}^e(r) | R(r) | \psi_{v''J''}^e(r) \rangle \right|^2 \quad (2)$$

Where $R(r)$ is the electronic transition dipole moment in Debye and can be written as:

$$R(r) = \langle \psi_{v'J'}^e | \mu(r) | \psi_{v''J''}^e \rangle \quad (3)$$

Electronic dipole moments $R(r)$ can be computed theoretically from high level ab initio calculations.⁸ Using the matrix elements of dipole moment operator $\mu(r)$ in various internuclear distance, $[M_{v'J' \leftarrow v''J''}^e]^2$ were calculated numerically by program LEVEL.⁹ This program uses an effective Hamiltonian in which rovibrational levels can be calculated numerically. If one uses Condon's approximation, Einstein A coefficients would depend on Frank-Condon factors $q_{v' \leftarrow v''}$, defined by eq. 4.¹⁰ However, we do not make that approximation in program LEVEL, and use Eqs. (1) to (3) instead.

$$q_{v' \leftarrow v''} = |\langle v' | v'' \rangle|^2 \quad (4)$$



The $A^2\Pi$ and $B'^2\Sigma^+$ excited states of MgH are close to each other, and there are extensive perturbations between them. These include spin-orbit and rotational perturbations that mix their wavefunctions. The program PGOPHER¹¹ can simulate and fit rovibronic lines with the aid of spectroscopic constants including rotational and spin-orbit constants.

Result and discussion:

Because of spin-orbit coupling, we expect 12 branches for each vibronic transition of the $A^2\Pi \rightarrow X^2\Sigma^+$ system with various intensities. For example, Table 1 shows that Einstein A coefficients of the R_{22} branch of the (1-0) band depend significantly on the total angular momentum quantum number J .

Table 1. Einstein A coefficients of R_{22} electronic transition band of $A^2\Pi \rightarrow X^2\Sigma^+$

J'' energy $E(J'')$ $A(\text{calculated})$ $A(\text{PGopher})$									
R	0.5	1	5	353161.0000	0.121971000	-0.861079	16413.017	385553.230	397456.545
R	1.5	1	5	424416.0000	0.122034000	-0.861648	16413.998	429035.749	442267.975
R	2.5	1	5	454789.0000	0.121952000	-0.861980	16410.7425	450566.558	464440.244
R	3.5	1	5	471048.0000	0.121723000	-0.862064	16403.2785	462898.031	477118.363
R	4.5	1	5	480475.0000	0.121343000	-0.861877	16391.6151	470261.142	484665.203
R	5.5	1	5	485853.0000	0.120804000	-0.861390	16375.7781	474452.383	488934.105
R	6.5	1	5	488454.0000	0.120099000	-0.860561	16355.7986	476345.086	490825.702
R	7.5	1	5	488927.0000	0.119215000	-0.859340	16331.7236	476402.865	490817.641
R	8.5	1	5	487618.0000	0.118141000	-0.857662	16303.5965	474873.601	489166.955
R	9.5	1	5	484713.0000	0.116861000	-0.855450	16271.4773	471887.701	486010.635
R	10.5	1	5	480297.0000	0.115356000	-0.852609	16235.4418	467498.889	481405.439



R	11.5	1	5	474396.0000	0.113606000	-0.849030	16195.4646	461705.232	475350.441
R	12.5	1	5	466991.0000	0.111586000	-0.844581	16152.0176	454506.935	467849.043
R	13.5	1	5	458029.0000	0.109270000	-0.839106	16103.7042	445717.391	458711.969
R	14.5	1	5	447434.0000	0.106628000	-0.832426	16053.1082	435463.959	448071.637
R	15.5	1	5	435107.0000	0.103626000	-0.824325	15998.6709	423502.043	435681.780
R	16.5	1	5	420932.0000	0.100230000	-0.814554	15940.8175	409740.510	421450.019
R	17.5	1	5	404781.0000	0.096400400	-0.802820	15879.6988	394051.609	405248.216
R	18.5	1	5	386519.0000	0.092097200	-0.788776	15815.4635	376295.993	386940.567
R	19.5	1	5	366006.0000	0.087279600	-0.772019	15748.2602	356336.343	366385.678
R	20.5	1	5	343114.0000	0.081908600	-0.752071	15678.2533	334039.883	343454.630
R	21.5	1	5	317733.0000	0.075949100	-0.728371	15605.6235	309296.623	318036.809
R	22.5	1	5	289795.0000	0.069375400	-0.700257	15530.5658	282036.425	290063.636
R	23.5	1	5	259299.0000	0.062177300	-0.666944	15453.2956	252255.115	259533.756
R	24.5	1	5	226353.0000	0.054370400	-0.627505	15374.2721	220067.917	226564.712
R	25.5	1	5	191230.0000	0.046010200	-0.580836	15292.804	185704.470	191389.04
R	26.5	1	5	154455.0000	0.037213900	-0.525628	15210.3652	149734.680	154582.798
R	27.5	1	5	116917.0000	0.028190400	-0.460313	15126.7334	113021.386	117012.603
R	28.5	1	5	80047.1000	0.019285700	-0.383020	15042.2945	76994.154	80111.865
R	29.5	1	5	46064.1000	0.011047600	-0.291505	14957.4494	43870.705	46101.026
R	30.5	1	5	18329.8000	0.004321210	-0.183069	14872.6609	17018.765	18344.379

Conclusion:

Keeping the astrophysical importance of rovibronic intensities in mind, we have Einstein A coefficients of MgH for calculated the $A^2\Pi \rightarrow X^2\Sigma^+$ and $B'^2\Sigma^+ \rightarrow X^2\Sigma^+$ systems.



References:

- [1] Kogure, T.; Leung, K.-C., The Astrophysics of Emission-Line Stars. 1 edition ed.; Springer: 2007.
- [2] Bernath, P. F., Molecular astronomy of cool stars and sub-stellar objects. *International Reviews in Physical Chemistry* **2009**, 28 (4), 681-709.
- [3] Grevesse, N.; Sauval, A. J., A Study of Molecular Lines in the Solar Photospheric Spectrum. *Astronomy and Astrophysics* **1973**, 27, 29.
- [4] Sotirovski, P., Table of solar diatomic molecular lines spectral range 4900 - 6441 Å. *Astronomy and Astrophysics Supplement* **1972**, 6, 85.
- [5] Reid, I. N.; KIRKPATRICK, J. D.; GIZIS, J. E.; DAHN, C. C.; MONET, D. G.; WILLIAMS, R. J.; LIEBERT, J.; BURGASSER, A. J., FOUR NEARBY L DWARFS. *The Astrophysical Journal* **2000**, 119, 369-377.
- [6] Boesgaard, A. M., Isotopes of Magnesium in Stellar Atmospheres. *Astrophysical Journal* **1968**, 154 (185), 185.
- [7] Wallace, L.; Livingston, W. C.; Bernath, P. F.; Ram, R. S., An atlas of the sunspot umbral spectrum in the red and infrared from 8900 to 15,050 cm⁻¹ (6642 to 11,230 [angstroms]), revised. *Tucson: National Solar Observatory* **1999**, NSO Technical Report #99-001.
- [8] Saxon, R. P.; Kirby, K.; Liu, B., Ab initio configuration interaction study of the low-lying electronic states of MgH. *The Journal of Chemical Physics* **1978**, 69 (12), 5301-5309.
- [9] Le Roy, R. J. *LEVEL 8.0 Chemical Physics Research Report*: University of Waterloo, 2007.
- [10] Bernath, P. F., *Spectra of Atoms and Molecules*. Oxford University Press: 2005.
- [11] Western, C. M. *PGOPHER, a Program for Simulating Rotational Structure*, University of Bristol: 2010.



An accurate CHARMM compatible force field for bisphosphonate pharmaceuticals

M. Ashouri^{a*}, A. Maghari^a, M. H. Karimi-jafari^b

^a Department of chemistry, Faculty of sciences, Tehran university, Tehran, Iran

^b Institute of Biochemistry and Biophysics, University of Tehran, Tehran, Iran

Email: mashouri@khayam.ut.ac.ir

Key words: CHARMM, Force field, Bisphosphonates.

Introduction:

Bisphosphonates (BPs) are important pharmaceuticals, which are widely used in treating various bone disease and as carriers of radio nucleotides for therapeutic and imaging applications [1]. These compounds are characterized by a P-C-P backbone and two side groups (R1 and R2) that determine their activity. Modeling the interaction of BPs and their biological targets (FPPS enzyme and bone mineral) is of special interest for analysis of the mechanism of action of BPs and design of novel more potent derivatives. Such a modeling is initially performed at a molecular mechanical level of theory and availability of force field parameters is the prerequisite for it. In this work CHARMM additive force field is parameterized for some derivatives of bisphosphonates according to the CHARMM general force field (CGenFF) protocol [2].

Materials and methods:

The potential energy $V(R)$ in the CHARMM FF is a function of positions of all of atoms in the system and has the following general form:

$V =$

$$\begin{aligned} & \sum_{\text{bonds}} K_b (r - r_{0,b})^2 + \sum_{\text{VB}} K_{\text{VB}} (\phi - \phi_{0,\text{VB}})^2 + \\ & \sum_{\text{angles}} K_a (\theta - \theta_{0,a})^2 + \sum_{\text{dihedrals}} K_{d,n} (1 + \cos(n\chi - \phi_{d,n})) + \sum_{\text{impropers}} K_i (\psi - \\ & \psi_{0,i})^2 + \sum_{\text{nonbonded}} q_{ij} \left[\left(\frac{R_{\text{min},ij}}{r_{ij}} \right)^{12} - 2 \left(\frac{R_{\text{min},ij}}{r_{ij}} \right)^6 \right] + \frac{q_i q_j}{4\pi \epsilon_0 r_{ij}} \end{aligned} \quad (1)$$

where the sum covers all bond or angle vibrations, dihedral rotations, improper distortions, and non-bonded van der Waals or Coulomb interactions. To find missing parameters in BPs, all atom types are set according to CHARMM defined types and parameters that exist in CGenFF parameter set are used.

To determine the global minimum structure, all initial structures which are obtained from varying rotamers, are optimized by PM6 semi-empirical method with MOPAC and the most stable conformers are then used for further geometry optimization at the B3LYP/6-31G(d) and MP2/6-31G(d) levels of theory by GAMESS program. Structural properties of global minimum are used as initial guess for missing parameters. Force constants are determined from matrix of second derivatives with respect to internal coordinates. Initial guess for charges are obtained from electrostatic potential calculations at MP2/6-31G(d) and then all CGenFF protocol rules are applied for charges, also for all symmetric atoms in molecule the charges are symmetrized. Final charges are optimized to reproduce the interaction energies and distances with TIP3P model of water calculated at HF/6-31G(d) level.

Result and discussion:

The HEDP molecule and its different protonation states are used as model compound. Reasonable agreement between QM data and CGenFF available parameters provide the possibility of using them as initial guess for missing parameters (Fig.1). In Fig.2 water-compound model for some interaction sites and their relative distance and energy are shown. These results will be used as target data in charge optimization procedure. Reasonable

agreement are also found between MM energy profiles of flexible dihedrals and those obtained from MP2/6-31G(d) calculations.

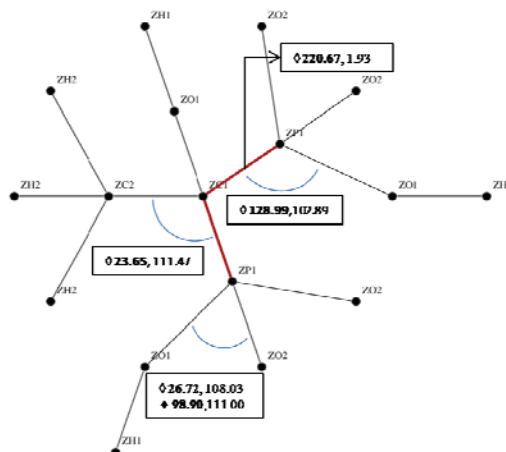


Figure1. Molecular graph of HEDP with atom-type labels and data from some force constants and related bond/angle \diamond calculated data from MP2/6-31G(d) \blacklozenge data from CGenFF reported parameters (Force constants [kcal mol⁻¹ A⁻², kcal mol⁻¹ rad⁻²])

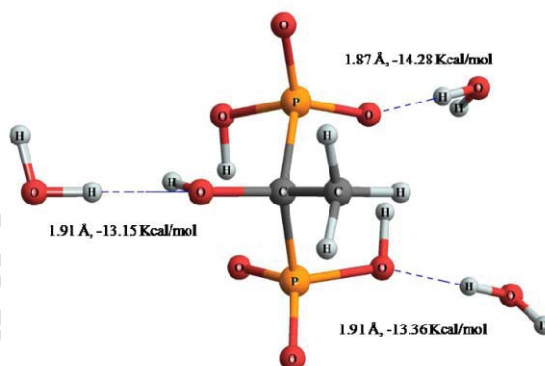


Figure2. Some interaction sites of HEDP with water molecules.

Conclusion:

CHARMM-compatible parameters are developed for bisphosphonates and the parameter set are used to generate a new force field that can be used in molecular mechanical simulations.

Reference:

- [1] R. Graham G. Russell; Bisphosphonates: The first 40 years; Bone, 49 :2–19(2011).
- [2] K. Vanommeslaeghe, *et al.*; CHARMM General Force Field (CGenFF): A force field for



drug-like molecules compatible with the CHARMM all-atom additive biological force fields”; J. Comput. Chem., 31(4): 671–690(2010).

15th Physical Chemistry Conference



Sum of Products Potential Energies Via Higher Order Singular Value Decomposition

N. Nahrjou*, R. Rajaie Khorasani

Department of Chemistry, Islamic Azad University North Tehran Branch, Tehran, Iran

(Email: nazaninnahrjou@yahoo.com)

Keywords: Sum of products, Potential energy, HOSVD, Tucker Decomposition.

Introduction:

One of the major obstacles in quantum molecular dynamics computations is the exponential growth of computational cost with increasing dimensionality. Devising new methods to lower computational complexity and cost is paramount for application to systems with higher dimensionality. In this regard, representing potential energies as sum of products can enable more efficient computations. Using the FHF and the ClHCl model systems, in this paper we investigate the feasibility of the Higher Order Singular Value decomposition (HOSVD) algorithm for representing potential energies as sum of products.

HOSVD:

Tensor decomposition involves representing a tensor as a sum of terms involving one dimensional arrays. In particular, Tucker decomposition represents an $I \times J \times K$ tensor X , as $\tilde{X} = G \times_1 \mathbf{A} \times_2 \mathbf{B} \times_3 \mathbf{C}$, where, G is an $(R_1 \times R_2 \times R_3)$ tensor known as the core tensor, the matrices \mathbf{A} , \mathbf{B} and \mathbf{C} , are called Tucker matrices, and integers R_1 , R_2 , R_3 are the Tucker ranks. The HOSVD algorithm computes the decomposition via matrix SVD computations [1, 2].

HOSVD algorithm:

Given an $I_1 \times I_2 \times \dots \times I_d$ tensor \mathbf{X} , and Tucker ranks R_1, R_2, \dots, R_d :

For $n=1$, to d

$\mathbf{X}_{(n)} \leftarrow$ Unfold \mathbf{X} in mode n

$\mathbf{A}^{(n)} \leftarrow R_n$ leading left singular vectors of $\mathbf{X}_{(n)}$

End

$\mathbf{G} \leftarrow \mathbf{X} \times_1 \mathbf{A}^{(1)\text{T}} \times_2 \mathbf{A}^{(2)\text{T}} \dots \mathbf{A}^{(d)}$

Output: $\mathbf{G}, \mathbf{A}^{(1)}, \mathbf{A}^{(2)}, \dots, \mathbf{A}^{(d)}$

Results and discussion:

We considered the ClHCl potential energy in terms of Jacobi coordinates with r as the ClH diatom bond length. The potential energy was discretized with 110 points for the radial coordinates and 60 points for θ , with (R, r) between 1.5 and 12 bohr, and θ in the range $[0, \pi]$. The resulting tensor was decomposed. Modes 1, 2 and 3 were chosen corresponding to R, r and θ respectively. We found that modes 1 and 2 do not allow rank truncation, however we can truncate the rank in mode 3 to 35 without practically any error (Table I).

Table 1. ClHCl with (R, r) between 1.5 and 12 bohr

Table 2. ClHCl with (R, r) between 0.2 and 12 bohr



Ranks	Relative Error	Compression Factor
(110,110,38)	4.73×10^{-15}	33%
(110,110,35)	8.35×10^{-13}	38%
(110,110,32)	1.15×10^{-10}	43%
(110,110,29)	1.12×10^{-8}	48%

Ranks	Relative Error	Compression Factor
(110,110,38)	4.94×10^{-6}	33%
(110,110,35)	6.37×10^{-6}	38%
(110,110,32)	8.23×10^{-6}	43%
(110,110,29)	1.10×10^{-5}	48%

This corresponds to a compression factor of 38%. We can even achieve a compression factor of 48%, with $R_3=29$ and an error of only 10^{-8} , this is chemically exact. We found that including grid points with very high potential energy, i.e. points for which the atoms are too close, can have adverse effects on the decomposition (table II). However these points do not have physical significance. Our investigations also indicated that a symmetric choice for the Jacobi coordinates (with r as the ClCl bond length) significantly increases the efficiency of the decomposition such that even the aforementioned adverse effect is more than compensated for (table III). It should be noted that our computations with FHF showed similar results.

Table 3. ClHCl with (R, r) between 0.2 and 12 bohr, symmetric model.

Ranks	Relative Error	Compression Factor
(110,110,38)	1.71×10^{-15}	33%
(110,110,35)	1.71×10^{-15}	38%
(110,110,32)	1.71×10^{-15}	43%
(110,110,29)	1.65×10^{-11}	48%

Conclusion:

Using HOSVD we were able to decompose potential energy functions for heavy-light-heavy model systems and obtain accurate some of product representations with significant data compression. Our investigations show this method to be very promising.

References:

- [1] L. R. Tucker, Psychometrika, **31**, 279 (1966).
- [2] L. De Lathauwer, B. De Moor and J. Vandewalle, SIAM J. Matrix Anal. Appl. **21**, 1324 (2000)



Theoretical studies of decomposition and reactivity of the $C_3F_7OCH_2O$ radical

A. Reisi-Vanani*, S. Hoseinpour

Department of Physical Chemistry, Faculty of Chemistry, University of Kashan, Kashan, Iran

Email: areisi@kashanu.ac.ir

Keywords: Decomposition, HFE-7000, IRC, Theoretical chemistry, PES

Introduction

Hydrofluoroethers (HFEs) are a kind of compounds which have been developed to replace CFCs in applications such as the cleaning of electronic equipment, heat transfer agents for semiconductor and electronics manufacture and fluid carriers for lubricant deposition [1]. The atmospheric oxidation of n- $C_3F_7OCH_3$ (HFE-7000) will be initiated by reaction with OH radicals that the initial attack of OH radical on HFE-7000 leads to the formation of haloalkyl radicals [2], which in turn reacts with atmospheric O_2 to give peroxy radicals ($C_3F_7OCH_2O_2\bullet$). The reaction of $C_3F_7OCH_2O_2$ radical with NO, NO_2 and HO_2 in the troposphere finally causes the formation of haloalkoxy radicals ($C_3F_7OCH_2O\bullet$).

Calculation method

Geometry optimization of the reactants, products and transition states have been obtained using B3LYP/6-311G(d,p) method. The vibration frequencies were attained in the same theory level for the optimized reactants, products and transition states. No virtual frequencies of all stationary points were identified (NIMAG=0). Transition states are defined by the presence of only one virtual frequency (NIMAG=1). To ascertain that the identified transition states connect reactants and products smoothly, intrinsic reaction coordinate (IRC) calculations were done at B3LYP/6-311G(d,p) level.

Results and discussion

Two possible pathways have been detected for reactivity and decomposition for $C_3F_7OCH_2O$ radical. (1) $C_3F_7OCH_2O$ radical react with O_2 atmospheric to perform O_2H and C_3F_7CHO . (2) is thermal decomposition of $C_3F_7OCH_2O$ radical to C_3F_7O and CH_2O . The C-H bond length of TS1 will change from 1.105 to 1.227Å (approx. 11%) the optimization structure of TS2, indicated that C-O bond increases from 1.344 to 1.981Å (approx. 47%). The energy barrier for path (1) and (2) obtained 4.3 and 16.8 kcal mol⁻¹, respectively. These results reveal that the reactants and products in a stable minimum potential energy surface (PES) are marked only with positive vibrational frequencies. Transition states of TS1 and TS2 are characterized by a negative frequency, which are -1023 and -376 cm⁻¹, respectively. The existence of transition state on the PES is obtained by IRC calculation performed at B3LYP/6-311G (d, p) level. The IRC plots (Figure. 1) clearly showed a smooth transition from reactants to products on the PES.

Rate constants for $C_3F_7OCH_2O$ radical were calculated using the following equation:

$$k_{TS1} = \frac{k_B T}{h} e^{-\Delta G^\ddagger / RT}$$

ΔG^\ddagger is the free energy of activation.

The final rate coefficients were corrected using transmission coefficient by Wigner's method [3].

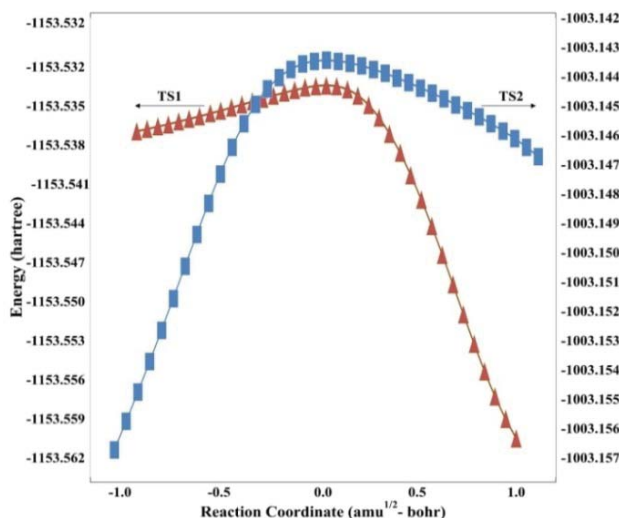


Fig. 1 IRC plots performed for transition states TS1 and TS2

The results showed that the rate constants for the C-H bond scission and C-O bond cleavage are 97.6 and 9.6 s^{-1} , respectively.

Conclusion

Two important channels (C-H bond scission and C-O bond cleavage) are considered in detail that the C-H bond scission is found to be favorable for the $\text{C}_3\text{F}_7\text{OCH}_2\text{O}$ radical reactivity. The energy barrier for C-H bond scission (TS1) and C-O bond cleavage (TS2) is 4.3 and $16.8 \text{ Kcal.mol}^{-1}$, respectively. The rate constants evaluated for the C-H bond scission and C-O bond cleavage are found to be 97.6 and 9.6 s^{-1} , respectively.

References

- [1] Molina, M. J.; Rowland, F. S., *Nature* (1974) 249, 810.
- [2] Bravo, I.; Díaz-de-Mera, Y.; et al., *Phys. Chem. Chem. Phys* (2010) 12(19), 5115.
- [3] Houston, P. L., McGraw-Hill New York (2001).



***Ab initio* study of the effect of the cluster size on the chemisorptions of NTCDA on the Ag(110) surface**

A. abbasi^{*a}, R. Scholz^b

^a Faculty of Science, Qom University, Qom, Iran,

^b Institut für Angewandte Photophysik, George-Bähr-Straße 1, 01069 Dresden

Email: afshin.abbasi@physik.tu-chemnitz.de

Key words: Organic semiconductors, NTCDA, *Ab initio*, Chemisorption

Introduction:

During the last decades, several studies have focused on the organic semiconductor due to their potentially interesting properties for electronic and optoelectronic applications [1, 2]. In such devices the transport properties of the organic material and the interaction between the metal contact and the molecules adsorbed at the metal-organic interface plays a key role [3, 4]. The net charge of the adsorbate multiplied by the distance between adsorbate and topmost metal layer may contribute to a substantial interface dipole, modifying the alignment between the frontier orbitals of the molecule and the Fermi energy of the metal in the contact. Therefore, a precise knowledge of the adsorbate geometry becomes mandatory for a quantitative understanding of the energetic defining injection or extraction of charges. In the present work, the adsorption of 1,4,5,8-naphthalene tetracarboxylic dianhydride (NTCDA) on a (110)-oriented silver substrate as a model of organic semiconductor contact is investigated with the second order Møller-Plesset perturbation theory (MP2) and density functional theory (DFT).

Theoretical model:

In the present study, we have applied MP2 using the resolution-of-identity approximation for the evaluation of two-electron integrals (RIMP2) as implemented in the TURBOMOLE 5.7 software package to optimize the adsorption geometry of NTCDA on the Ag(110) surface. For comparison with a method excluding dispersion interactions, we have applied DFT using



the hybrid functional B3LYP with an exchange-correlation energy calculated on an integration grid of medium density (m4). For this study, five different silver clusters were used to model the Ag(110) surface including Ag₁₆(9,4,3), Ag₂₂(9,4,9), Ag₃₂(15,16,1), Ag₃₄(9,16,9) and Ag₅₀(25,16,9). The notations represents for instance for the smallest cluster *i.e.* Ag₁₆(9,4,3), 9 atoms in the first layer, corresponding exactly to the unit cell required by chemisorbed NTCDA on Ag(110), and 4 and 3 atoms in the second and third layers, respectively, that are in total 16 silver atoms. For all these structures the geometry of the adsorbed organic molecule are fully optimized while the structure of metal clusters are kept fixed.

Results and discussions:

For several substrate clusters the heights of different atoms in NTCDA with respect to the topmost silver layer were obtained from the minimum of the BSSE-CP corrected PES, occurring typically at about 0.14 - 0.18 ° larger distance with respect to the optimized RIMP2 geometries without BSSE-CP correction. Irrespective of computational scheme and the cluster size, the two types of oxygen atoms of NTCDA occur at different heights, revealing distortions from planarity.

In sharp contrast to the adsorbate geometries which we consider to be reasonably converged for the largest substrate clusters, the MP2 adsorption energies do not follow any simple rule. This finding indicates that unavoidable boundary effects arising from the finite size of the metal clusters inhibit the definition of converged adsorption energy.

Conclusions:

In this work we used MP2 and DFT calculation to study the adsorption of NTCDA on the Ag(110) surface. Excluding the smallest cluster (Ag₁₆) which was not be able to model the adsorption geometry, other clusters represent mostly the same adsorption geometry. The next smallest cluster with 22 Ag atoms was used for the further investigations. The studies on the molecular orbitals reveal some efficient hybridization between the organic adsorbate π -orbitals and the orbitals of the metal substrate. These types of hybridizations are responsible for this chemisorption and may be the reason of charge transfer between the adsorbed molecule and the metal substrate. With the comparison of two *ab initio* methods which were used in this study we concluded that the lack of the dispersion terms at DFT



approaches have strong influence on the adsorption geometry. DFT gives the adsorption geometry which is strongly bended where the adsorption geometry at MP2 is nearly flat.

Reference:

- [1] L. S. Hung. etal . *Mater. Sci. Eng. R* **39**(5-6), 143–222 (2002).
- [2] A. Dodabalapur, *Solid State Commun.* **102**(2), 259–267 (1997).
- [3] X. Crispin etal. *J. Am. Chem. Soc.* **124**(27), 8131–8141 (2002).
- [4] D. Adams. etal. *J. Phys. Chem.B* **107**(28), 6668–6697 (2003).



15th Physical Chemistry Conference



15th Physical Chemistry Conference



15th Physical Chemistry Conference



15th Physical Chemistry Conference



Calculation the structural parameters and DOS of TaB₂ compound with p6/mmm space group using pseudopotential method

H. Salehi ^a, M. Masoudi ^{b*}

^a Deparetment of physics, Faculty of science, shahid Chamran University of Ahwaz, Ahwaz, Iran.

^b Group of physics, Payamenoor University of Ahwaz, Ahwaz, Iran.

* Corresponding author, E-mail address: masoudi_373ph@yahoo.com

Keywords: TaB₂, DFT, Structural parameters, DOS.

Introduction:

Transition metal diborides, attract for a long time much attention of physicists and material scientists due to their unique physical and chemical properties such as hardness, high melting point, etc [1]. Tantalum diboride (TaB₂) has the hexagonal AlB₂-like structure p6/mmm space group [2]. In 2008, phase pure TaB₂ powder was synthesized using reduction of Ta₂O₅ by B₄C and graphite at 1600C° in an alumina tube furnace under following Ar [3]. Tantalum diboride has high melting point, high hardness, good thermal and electrical conductivity, and resistance to most acids and bases [4]. This compound is an excellent candidate for ultra-high temperature propulsion systems due to specific mechanical properties. Besides, investigation of high temperature strength, thermal shock resistance and oxidation resistance are necessary to establish it as a competitive material for thermal protection systems [3].

Computational method:

The calculations have been performed with ultrasoft pseudopotential method in the framework of Density Functional Theory (DFT) by using the Plane Wave (PW) that implemented in Quantum Espresso software [5]. In this method, the Generalized Gradient Approximation has been used for exchange-correlation energy. The experimental lattice constants used in these calculations are $a=3.088 \text{ \AA}$, $c=3.241 \text{ \AA}$ [6].

Result and discussion:

In this research, the structural parameters a and c are calculated 3.096 \AA and 3.313 \AA respectively. Following this calculation, bulk modulus and its derivative, compressibility at zero pressure and etc calculated and compared with other results for this compound. Also, the influence of pressure on structural parameters is investigated. Increasing the pressure decreases the structural parameters. The plot of partial density of states of various orbitals in comparison to total density of states, in order to considering the quality of contribution distribution of different atoms orbital is brought in figure. 1.

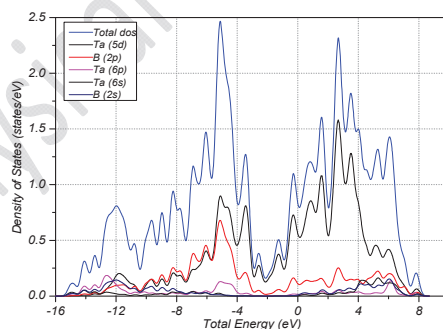


Fig. 1. Total density of states in comparison to partial density of states for TaB₂.

Conclusion:



Achieved results for structural parameters in present work are in good agreement with experimental results. Also for transformation in crystal planes in a -axis direction in compare of c -axis direction lower energy is needed. Figure of the density of states show that this compound is a kind of metal and figure of partial density of states indicate that B-2p orbital and Ta-5d orbital have the main contribution in the electronic conductivity of this compound.

References:

- [1] I.R. Shein, A. L. Ivanovskii, Condens. Matter, 20, P 415218, 2008.
- [2] W.J. Zhao, Y.X. Wang, Solid State Chemistry, 182, 2880-2886, 2009.
- [3] X. Zhang, G.E. Hilmas, W.G. Fahrenholtz, Material letters, 62, 425-4253, 2008.
- [4] J. D. Zhang, X.L. Cheng, D.H. Li, Computational Materials Science. 50: 474-478, 2010.
- [5] S. Baroni, et al, <<http://www.pwscf.org>>.
- [6] P. Villars, Crystallographic Data for Intermetallic Phases, Pearsons's Handbook, ASM International. Materials Park, 1997.



systems up to high temperature and high pressure conditions

Majid Moosavi*, Nima Soltani

Dept. of Chemistry, Faculty of Sciences, University of Isfahan, Isfahan 81746-73441, Iran

Email: m.mousavi@sci.ui.ac.ir

Keywords: Polymer, ANN, Group contribution method (GCM), Specific volume.

Introduction:

Thermodynamic and volumetric properties of polymeric systems play an important role in the polymer industry and are often a key factor in polymer production, processing, and material development, especially for the design of advanced polymeric materials [1]. Predicting the thermodynamic properties of polymers especially at high temperature-high pressure (HTHP) conditions is of great importance in industry. An artificial neural network (ANN) can be a suitable alternative to model the different thermodynamic properties of chemical systems. ANN is a simple method for modeling, which does not need explicit formulation of exact mathematical or physical relations between input and output data. In this study, the applicability of ANN in predicting the specific volume of polymeric systems up to high temperature and high pressure conditions is investigated.

The neural network used:

Many models of neural networks have been used to estimate of thermodynamic properties [2,3]. There are three main states in the operation of a neural network: learning, validation

and test. The learning or training is the process by which a neural network modifies the weights in answer to initial information. In this study, 2865 experimental data points of 25 polymers were used. A combined method that includes an artificial neural network and a simple group contribution method have been used to estimate the specific volumes of polymeric systems at different temperatures and pressures using the Matlab software. Temperature (T), pressure (P), molecular mass (M), and the structural groups that form the molecules were given as input variables.

Results and discussion:

Several network architectures were tested to select the most accurate scheme. The optimal number of neurons was determined by trial and error. The weights connection and biases were obtained using a feedforward backpropagation neural network for 2865 experimental data points. The best network topology was obtained as (18-20-1). The average absolute percent deviation (AAD%) is 0.06 for prediction of specific volume for all data. Fig. 1 shows a comparison between experimental and calculated values of specific volume of studied polymeric systems during training and during prediction. This study shows that the chosen artificial neural network and the group contribution method represent an excellent alternative for the estimation of specific volumes of polymeric systems with acceptable accuracy.

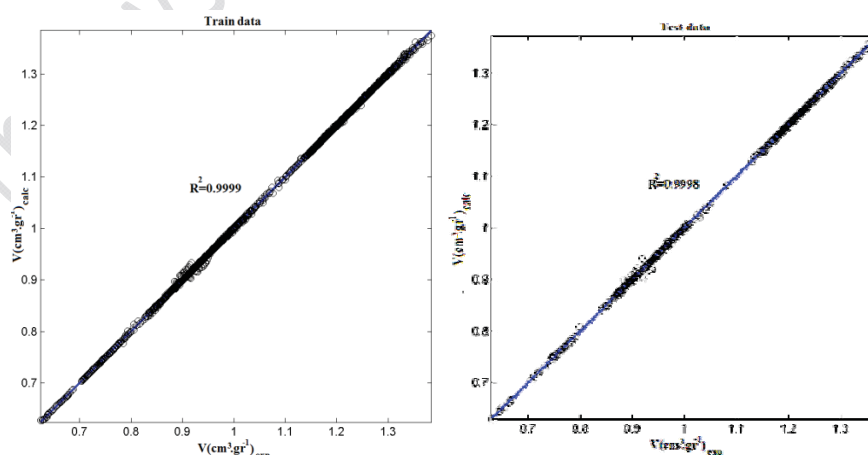


Fig. 1. Comparison between experimental and calculated values of specific volume of polymeric systems: (a) during training and (b) during prediction.

Conclusion:

A feedforward backpropagation neural network with (18-20-1) structure was designed to predict the specific volume of different polymeric systems. Total number of experimental data used to design the stated network is 2865, of which 75% were randomly chosen to train the network, 10% for validation, and 15% to test it. The average relative deviations for train, validation, and test sets are 0.05, 0.06, and 0.07, respectively.

References:

- [1] P.A. Rodgers, J. Appl. Polym. Sci. 48, 1061–80, 1993.
- [2] G. Espinosa, et al. Ind. Eng. Chem. Res., 40, 2757-2766, 2001.
- [3] D. Yaffe, Y. Cohen, J. Chem. Inf. Comput. Sci., 41, 463-477, 2001



An electrochemical investigation of the effect of nano sized TiO₂ particles on cathodic disbonding of epoxy-polyaniline coated mild steel

M.G. Hossieni*, P.Yardani Sefidi

Department of Physical Chemistry, Electrochemistry Research Laboratory, University of Tabriz, Tabriz, Iran.

Email: mg-hosseini@tabrizu.ac.ir

Key words: Cathodic disbanding, TiO₂ nanoparticles, Epoxy- polyaniline coating, EIS.

Introduction:

Corrosion of metals is an enormous problem throughout the world. Several techniques have been used to protect metals from corrosion. Among them, the use of organic coatings in conjunction with cathodic protection is considered efficient approach to combat corrosion. Although the combination offers various merits, the serious problem called cathodic disbondment could be raised in the presence of failures on the protective coatings[1]. The applied cathodic potential that activates cathodic reactions at the edge of the defects is the driving force for this phenomenon. In fact, cathodic disbanding as a consequence of cathodic protection occurs due to hydrogen evolution and accumulation of OH⁻ ions at the coating- substrate interface[2]. Attempts have been made to use corrosion pigments to improve the cathodic disbonding resistance of the organic coatings. In recent years, attempts have been done to use nano sized anticorrosion pigments to improve the coating resistance against cathodic disbanding[3]. Electrochemical Impedance Spectroscopy (EIS) has taken an undeniable position in corrosion studies. EIS is considered a powerful nondestructive test to evaluate performance of the protective coatings[4]. The scope of this work is to study the

effect of TiO₂ nanoparticles addition on the resistance of epoxy- polyaniline (EP-PANI) coating to cathodic disbanding via EIS. Further investigation was facilitated using surface analysis.

Experimental (materials, apparatus and methods):

Specimens of mild steel in the form of 1×1 cm² were mounted, so that only one side of the electrode was in direct contact with the electrolyte. The test mild steel panels were pre-treated by degreasing in ethanol for 10 min. For preparation of the coatings, 0.306 g of pure PANI and PANI-EP- TiO₂ nanocomposites powder were suspended in 3 ml TEPA, followed by proper mixing using a magnetic stirrer, with speed of 300 rpm for 12h. Then 1g of EP resin was mixed with 0.2 g suspension. The obtained liquid paints were coated on substrate by brushing and then samples were dried in 50°C for 24h. A 3.5% NaCl solution was prepared from laboratory grade NaCl and distilled water. An area of 1 cm² of samples (PANI-EP, PANI-EP-TiO₂) was exposed to the electrolyte without applying potential for 150h at 65°C. Then an area of 1 cm² of samples was exposed to the electrolyte with applying -1.5 V vs Ag/AgCl via Power Supply (ADAK, PS-405) for 150h at 65°C (according to ASTM G8). EIS measurements were performed on Potentiostat/Galvanostat (EG& G model Parstat 2263). EIS measurements were carried out over a frequency range of 100 kHz to 0.01 Hz, using ±5 mV amplitude of sinusoidal voltage as perturbing signal. Experimental data was fitted and analyzed by ZView(II) software. Corrosion cell equipped with graphite as counter electrode and Ag/AgCl as reference electrode. The coated mild steel panel was the working electrode.

Results and discussion:



The results showed two time constants for PANI-EP in the absence of voltage and for PANI-EP-TiO₂ in the presence of -1.5 V, and one relaxation time for PANI in the presence of -1.5 V and for PANI-EP-TiO₂ in the absence of voltage. The electrochemical elements such as corrosion resistance of coatings (R_{Coat}) was obtained. Results showed that the resistance of PANI-EP and PANI-EP-TiO₂ without applying potential after 150h immersion was 3675 $\Omega.cm^2$ and 9818 $\Omega.cm^2$, respectively. Also, at the end of immersion time disbanding phenomenon was observed for PANI-EP. Under the voltage of -1.5 V, the resistance of PANI-EP and PANI-EP-TiO₂ after 150h immersion was 29852 $\Omega.cm^2$ and $6.4393 \times 10^5 \Omega.cm^2$, respectively. Results confirm that in the presence of TiO₂ nanoparticles the corrosion resistance, adhesion and cathodic disbonding resistance increased. This enhancement is related to decreasing the diffusion of electrolyte and delayment in achieving of the corrosive ions on substrate[3].

Conclusion:

This study indicated that incorporation of TiO₂ nanoparticles in EP-PANI coating greatly increased adhesion and resistance to cathodic disbonding as well. The ability of TiO₂ nanoparticles incorporated organic coating to resist disbondment was related to the role of TiO₂ nanoparticles on delayment in diffusion and achievement of the corrosive ions on substrate.

References:

- [1] R.Naderi; M.M.Attar; "Cathodic disbondment of epoxy coating with zinc aluminum polyphosphate as a modified zinc phosphate anticorrosion pigment"; Progress in Organic Coatings; 69,392-395,2010.



- [2] M.Mahdavian; M.M.Attar; “The effect of benzimidazole and zinc acetylacetonate mixture on cathodic disbanding of epoxy coated mild steel”; Progress in Organic Coatings; 66, 137-140, 2009.
- [3] B.Ramazanzadeh; M.M.Attar; “ studying the effects of micro and nano sized zno particles on the corrosion resistance and deterioration behavior of an epoxy- polyamide coating on hot-dip galvanized steel”; Progress in Organic Coatings; 71, 314-328, 2011.
- [4] E.Barsoukov; J.Ross Macdonald (Eds.); “Impedance Spectroscopy Theory, Experiment And Applications; second ed.; John Wiley And Sons;2005.



Er³⁺-PVC Membrane Sensor Based on 3-hydroxy-N'-((pyridin-2-yl)methylene)naphthalene-2-carbohydrazide

B. Hatamluyi^{*}, H.A. Zamani

Department of Chemistry, Mashhad branch, Islamic Azad University, Mashhad, Iran

Email: behnazhatamluyi@yahoo.com

Key words: Sensor, Ion-Selective Electrode, Potentiometry, PVC Membrane.

Introduction:

Erbium has no biological role but is said to stimulate the metabolism. All erbium compounds should be regarded as highly toxic, although initial evidence would appear to suggest that the danger is limited [1]. Solvent polymeric membrane based ISEs, together with the incorporation of ion carriers, have shown to be a very useful tool for clinical, environmental, and chemical analyses as well as for process monitoring. Potentiometric detection based on ion-selective electrodes (ISEs) offer the advantages of speed and ease of preparation and procedures, relatively fast response, reasonable selectivity through judicious choice of the membrane active materials, wide linear dynamic range, and low cost [2,3]. In this research, we wish to report the preparation of an Er³⁺ PVC-based membrane electrode based on 3-hydroxy-N'-((pyridin-2-yl)methylene)naphthalene-2-carbohydrazide (L) as a neutral ion carrier.

Materials and methods:



The Merck and the Aldrich Chemical Co. were the providers of the following reagent grades: benzyl acetate (BA), nitrobenzene (NB), Dibutyl phthalate (DBP), acetophenone (AP), high relative molecular weight PVC, sodiumtetraphenyl borate (NaTPB), tetrahydrofuran (THF) and chloride and nitrate salts of the cations used. Triply distilled deionized water was used throughout.

Apparatus:

All electromotive force (emf) measurements were carried out with the following cell assembly; Ag/AgCl| internal solution, (1×10^{-3} M ErCl_3)|PVC membrane|test solution| Hg_2Cl_2 , KCL (saturated). A Corning ion analyzer 250 pH/mV meter was used for the potential measurements at 25.5 ± 0.1 °C. The activities were calculated according to the Debye-Huckel procedure.

Result and discussion:

In this study, a plasticizer/PVC ratio of about 2.2 was found to be the most suitable ratio. The obtained data revealed that, the membrane incorporating 67% DBP, 30% PVC, 2% ligand, in the presence of 1% sodium tetraphenyl borate (NaTPB) as a suitable lipophilic additive considerably improved the sensitivity of the erbium sensor and showed the best sensitivity, with a good Nernstian slope of 20.5 ± 0.4 mV/decade of Er^{3+} concentrations (1.0×10^{-6} – 1.0×10^{-2} M) and a detection limit 5.3×10^{-7} M. The pH dependence of the responses of the membrane was investigated by the sensor behavior in a 1.0×10^{-3} M Er^{3+} solution. The potential response of the sensor is independent of pH, in the pH range of 2.8–9.5. The dynamic response time of the membrane was measured at various concentrations (1.0×10^{-6} to 1.0×10^{-2} M) of the test solutions and the results exhibited that the sensor has a fast response time of ~5 s. To investigate the membrane electrode selectivity, its potential response was



monitored in the presence of various interfering foreign cations using the matched potential method (MPM) [2]. The electrode shows a very good selectivity towards Er^{3+} ions over a wide variety of cations, including alkali, alkaline earth, transition and heavy metal ions. The proposed sensor was successfully applied as an indicator electrode for the potentiometric titration of $1.0 \times 10^{-4} \text{ M}$ of Er^{3+} ions with a $1.0 \times 10^{-2} \text{ M}$ EDTA.

Conclusion:

The results obtained from the above mentioned study reveal that a potentiometric PVC-based membrane sensor based on

3-hydroxy-N'-((pyridin-2-yl)methylene)naphthalene-2-carbohydrazide (L) functions as an excellent Er^{3+} selective sensor and can be used for the determination of this ion in the presence of considerable concentrations of common interfering ions. The short response time, applicable pH range, lower detection limit, and potentiometric selectivity coefficients of the proposed sensor make it a superior device for the determination of this ion.

References:

- [1] R.E.Kirk, and etal; "Encyclopedia of Chemical Technology"; Wiley; Chichester; 1982.
- [2] E. Bakker etal. ; "Carrier-based ion-selective electrodes, bulk optodes. 1. General characteristics" ; Chemical Review ; 97,3083-3132,1997.
- [3] E. Pretsch etal. ; "Carrier-based ion-selective electrodes and bulk optodes. 2. Ionophores for potentiometric and optical sensors" ; Chemical Review ; 98,1593-1687,1998.



Modeling of Methane and Ethane mixture Gas Hydrate Formation kinetics based on Non-equilibrium Thermodynamics

P.Naeiji, F.Varaminian*

School of Chemical Engineering of Semnan University, Semnan, Iran

(Email: fvaraminian@semnan.ac.ir)

Keywords: Methane, Ethane, Formation Kinetics, Thermodynamic Natural Path, Gas Hydrate.

1. Introduction

In this study, formation kinetics of methane and ethane mixtures gas hydrate was predicted. The thermodynamic natural path in chemical reaction kinetics was used for the kinetics modeling of the hydrate formation in a volume constant process [1]. In this method, the system was considered as a classical thermodynamic or macroscopic view.

2. Methods

In this study, a conceptual model was proposed that defines a macroscopic driving force and uses only the initial conditions (temperature and pressure) and final conditions (equilibrium conditions). The basic idea is that there is only a unique path for each experiment that on this path decays the chemical affinity. Prigogine and Defay [2] defined the chemical affinity as a generalized force in terms of potential difference as:



$$A_i = -\sum [\nu_m \mu_{m_i}]_{T,V} \quad (1)$$

Where ν_m is the stoichiometric coefficient and μ_m is the chemical potential. Considering to the correlation of μ_m with its chemical potential in some arbitrary state and an activity ratio, Q_i :

$$A_i = -RT \sum \ln(\zeta_{Q_i}) \quad , \quad \zeta_{Q_i} = \frac{Q_i}{K} \quad (2)$$

Where K is thermodynamic equilibrium constant and ζ_Q is a dimensionless measure of the extent of reaction. Accordingly, the affinity decays towards zero for this chemical reaction so that:

$$\dot{A}_{T,V} < 0 \quad (3)$$

Where $\dot{A}_{T,V} = [\partial A / \partial t]_{T,V}$ is the affinity decay rate. The correlation of $\dot{A}_{T,V}$ with the elapsed time is:

$$\dot{A}_{T,V} = A_r [1/t_i - 1/t_k] \quad (4)$$

Where A_r is the affinity rate constant and t_k is the expected time to attain equilibrium. In order to directly correlate A_i with t_i , Eq. (4) must be integrated, which yields:

$$A_i = A_r \ln[\zeta_{t_i} \cdot \exp(1 - \zeta_{t_i})] \quad (5)$$

Where $\zeta_{t_i} = (t_i/t_k)$. By calculating ζ_Q , A_i can be calculated by Eq. (2) for the hydrate formation system. By plotting A_i versus $\ln[\zeta_{t_i} \cdot \exp(1 - \zeta_{t_i})]$, A_r and t_k can be obtained.

3. Results and discussion

The experimental data of the gas hydrate formation of methane-ethane mixtures of 0.199 and 0.603 mole fraction of methane at constant operating temperature of 277.15 K have been studied.

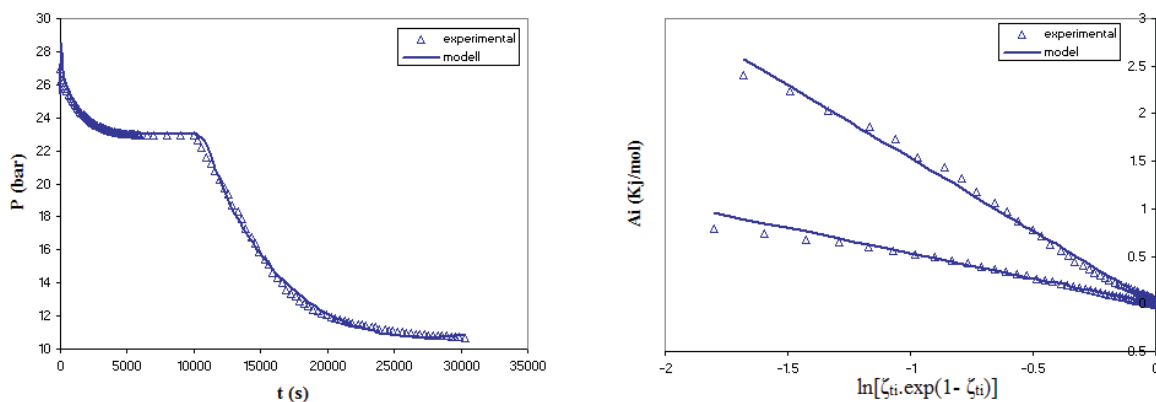


Fig 1. Chemical affinity versus $\ln[\zeta_{ti} \cdot \exp(1 - \zeta_{ti})]$ (on the right), experimental and modeling results (on the left) for 0.199 mole fraction of methane in the mixture (forms sI hydrate structure).

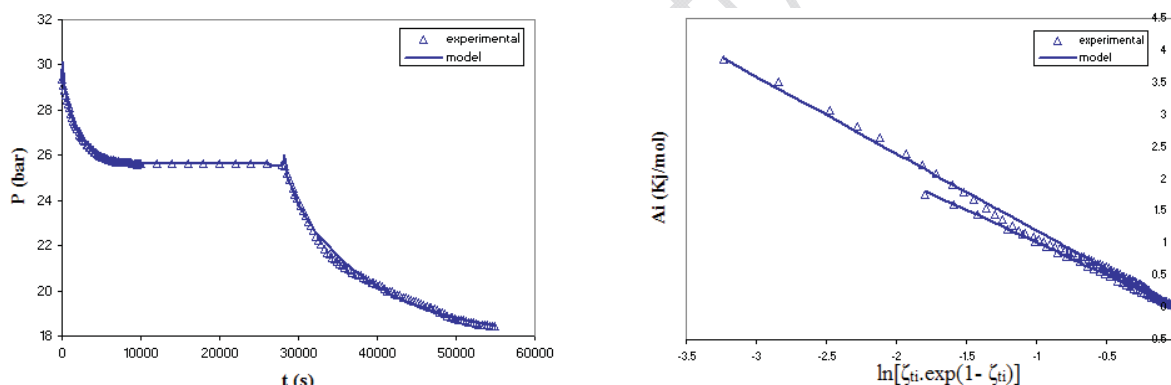


Fig 2. Chemical affinity versus $\ln[\zeta_{ti} \cdot \exp(1 - \zeta_{ti})]$ (on the right), experimental and modeling results (on the left) for 0.603 mole fraction of methane in the mixture (forms sII hydrate structure).

4. Conclusions

The results indicated that this model can well predict constant volume experimental data for both of crystals I and II hydrate former. The both of mixtures form hydrate at 2 steps.



References

- [1] Mottahedin, M., Varaminian, F., J. Non-Equilib. Thermodyn, 36, 3-22 (2011).
- [2] Garfinkle, Moishe., Discrete Dynamics in Nature and Society, Vol. 4, pp. 145-164 (1999).

15th Physical Chemistry Conference



Experimental Study of the Effect of Hydrophilic Silica Nanoparticles on Foam Performance in Alkaline-Surfactant-Gas flooding

A.Siosewardan^{a*}, S.A.Tabatabae Nejad^a, E.Khodapanah^a

^a Department of chemical engineering faculty, Sahand university of technology, Tabriz, Iran

Email: assmn65@yahoo.com

Abstract

Alkali-Surfactant-Gas (ASG) flooding is one of the novel chemical techniques in Enhanced Oil Recovery. In this technique, the co-injection of gas and chemical slug results in the formation of foam. Foam reduces the mobility of injected chemical solutions and improves the displacement efficiency of the process. Foams in practice are generally generated and stabilized with surfactants. However, surfactant stabilized foams have some weakness. If nanoparticles were utilized instead of or with surfactants, foams stabilized with such particles could have a number of important advantages. The main purpose of this research is creation of stable foam with nanoparticles and utilizing this nanoparticle stabilized foam for mobility control of injected fluids in enhanced oil recovery applications. Finally, the performance of the foam that is created and stabilized with mixture of surfactant and nanoparticles was compared with the foam that is created and stabilized with only surfactant in alkaline-surfactant-gas process in terms of oil recovery from core flood experiments. In this research, hydrophilic silica nanoparticles with an average size of 10 nm were used. The



mixture of surfactant and hydrophilic silica nanoparticles in various concentration were used to foam generation. The results of the experiments showed that the concentration of surfactant and nanoparticles should be selected optimize. In the experiments, most oil recovery was obtained when the concentration of both surfactant and hydrophilic silica nanoparticles in chemical solution was selected 0.5 weight percent.

Key words: Enhanced Oil Recovery, Chemical Flooding, Foam, Nanoparticles, Mobility Control

Introduction

One of the main criteria for the success of ASG process is the formation of stable foam with adequate mobility reduction characteristics [1]. Surfactant stabilized foams have some weakness. However, if nanoparticles were utilized instead of or with surfactants, foams stabilized with such particles could lead to removing restrictions on the use of surfactants [2]. Nanoparticles are finding their way into various branches of the petroleum engineering industry [3-7]. Certain small solid particles have been used in conjunction with surfactant molecules, which they adsorb at fluid/fluid interfaces, to stabilize drops in emulsions and bubbles in foams [8]. In contrast to surfactant molecules, adsorption of solid particles to fluid/fluid interfaces does not change the interfacial tension [9]. This research is based on utilizing hydrophilic silica nanoparticles with surfactant to make stable foam for enhanced oil recovery applications.

Materials and Methods

Sodium dodecyl sulfate (SDS) which is an anionic surfactant, Hydrophilic silica

nanoparticles with an average size of 10 nm and Sodium carbonate (Na_2CO_3) as alkaline were used in chemical coreflood experiments. One type of Synthetic formation brines, representing formation fluid of a reservoir, with total dissolved solids of 103000 mg/L was used in corefloods. Water flooding as secondary recovery technique was performed with Persian Gulf water. The crude oil used for corefloods has a viscosity and density of 3.46 cP and 30 °API. Nitrogen with 99.99% purity was used for mobility control of injected fluids. ASG coreflood experiments were conducted after the optimal chemical formulation was identified through aqueous stability, phase behavior, and foam stability tests. Coreflood experiments were performed at 100 bars and 60 °C.

Apparatus

Figure 1 shows the schematic of ASG coreflood setup.

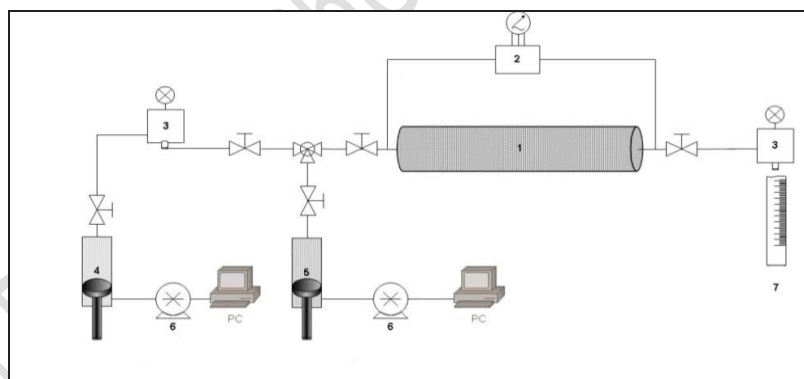


Figure 8: schematic of ASG coreflood setup

1) Sandpack, 2) Differential pressure difference, 3) Backpressure regulator, 4) Gas accumulator, 5) Liquid accumulator, 6) High performance liquid chromatography (HPLC) pump, 7) Sampler



Results and Discussion

It was observed that when the concentration of hydrophilic Silica nanoparticle was low, there were not enough particles to attach completely at the interface around the bubbles in foam and when particle concentration increased, more particles could be adsorbed at the bubble interface, which stabilized the produced foam. But, with further increased nanoparticle concentration, the particle aggregation occurred, which inhibited foam generation. When the surfactant concentration was selected enough, the attachment of surfactant to nanoparticle surface can change nanoparticles surface properties and show surface activity useful for foam generation. But, as the more surfactant molecules were adsorbed onto the particle surface, the particle surface charge decreased and the electrostatic repulsion between particles decreased that led to particle aggregation.

Conclusion

Silica nanoparticles can function in similar ways to surfactants and stabilize foams in the absence of any other surface-active agent, but certain differences in behavior are inevitable. When the concentration of nanoparticles and surfactant are selected optimize, strong and stable foams are created and displacement efficiency is increased that leads to more oil production.

References

- [1] Srivastava, M., Zhang, J., Nguyen, Q.P., and Pope, G. A., (2009), "A Systematic Study of Alkali Surfactant Gas Injection as an EOR Technique", Paper SPE 124752 presented at the 2009 SPE Improved Oil Recovery Symposium held in Tulsa, USA.
- [2] Zhang, T., Roberts, M.R., A, Bryant, S. L., and Huh, C., (2009), "Foams and Emulsions Stabilized with Nanoparticles for Potential Conformance Control Applications" SPE Paper 121744, presented at SPE Intern. Symp. Oilfield Chemistry



- [3] Huang, T. and Crews, J. B., (2008) "*Nanotechnology Applications in Viscoelastic Surfactant Stimulation Fluids*", SPE Production & Operations, 51 2 - 517, November 2008.
- [4] Sensoy, T., Chenevert, M. E., and Sharma, M. M., (2009), "*Minimizing Water Invasion in Shale Using Nanoparticles*", SPE 124429 presented at the 1009 SPE Annual Technical Conference and Exhibition, New Orleans.
- [5] Zhang, T., Davidson, A., Bryant, S. L., and Huh, C., (2010), "*Nanoparticle-Stabilized Emulsions for Applications in Enhanced Oil Recovery*", SPE 119885 presented at the 1010 SPE Improved Oil Recovery Symposium, Tulsa.
- [6] Espinosa, D. R., Caldelas, F. M., Johnston, K., Bryant, S. L., and Huh, C., (2010), "*Nanoparticle-Stabilized Supercritical CO₂ Foams for Potential Mobility Control Applications*", SPE 129925 presented at the 2010 SPE Improved Oil Recovery Symposium, Tulsa.
- [7] Pourafshary, P., Azimipour, S. S., Motamedi, P., Samet, M., Taheri, S. A., Bargozi, H., and Hendi, S. S., (2009), "*Priority Assessment of the Investment in Development of Nanotechnology in Upstream Petroleum Industry*", SPE 126101 presented at the 2009 SPE Saudi Arabia Section Technical Symposium and Exhibition, AlKhobar, Saudi Arabia.
- [8] Binks, B.P. and Horozov, I .S., (2005), "*Aqueous foams stabilized solely by silica nanoparticles*", Angewandte Chemie-International Edition.
- [9] Binks, B.P., (2002), "*Particles as surfactant -similarities and differences*", Current Opinion in Colloid & interface Science.



A Comparative Synthesis of Ni-Cu Oxides over Al₂O₃-ZrO₂ Nanocomposite via Impregnation and Sol-Gel Methods Used for CH₄/CO₂ Reforming

M. Sharifi^{a,b}, M. Haghighi^{a,b*}, F. Rahmani^{a,b}, S. Karimipour^{a,b}

^a Chemical Engineering Faculty, Sahand University of Technology, Tabriz, Iran

^b Reactor and Catalysis Research Center (RCRC), Sahand University of Technology, Tabriz, Iran

*Email: haghighi@sut.ac.ir

Keywords: Ni-Cu/Al₂O₃-ZrO₂, CH₄/CO₂ Reforming, Syngas, Nanocatalyst.

Introduction:

In dry reforming of methane, Ni/Al₂O₃ catalyst suffers from less activity and stability, due to the side reactions [1, 2]. Addition of zirconia and Cu as promoters to Ni/Al₂O₃ has increased stability and activity, respectively [1-3]. Zirconia decreased coking and sintering of active phases [2]. In this research, the properties of Ni/Al₂O₃ catalyst were improved by utilization of sol-gel method and ZrO₂ and Cu addition as suitable promoters.

Materials and methods:

Ni(10wt%)-Cu(3wt%)/Al₂O₃-ZrO₂(10wt%) catalysts were prepared by a direct sol-gel process utilizing citric acid as gelling agent and impregnation method. The structure, morphology, surface area and functional groups of the synthesized nanocatalysts were assessed using XRD, FESEM, BET and FTIR analysis, respectively. Catalytic performance was evaluated by the dry reforming of methane in a U-shape quartz micro reactor (8 mm i.d.), operated under atmospheric pressure, CH₄/CO₂=1 and GHSV=24 (l/gr.hr).

Result and discussion:

XRD patterns confirmed the formation of amorphous structure and non-existence of Cu spinel for the catalyst synthesized by sol-gel method. Extremely broad and weak diffraction peaks of Ni oxides suggested the high dispersion of these species on the surface of the support. FESEM images of nanocatalysts indicated that utilization of sol-gel method led to uniform, tuneable and smaller nanoparticles and homogenous dispersion. The quantitative analysis showed the high specific surface area for the sol-gel sample (148 m²/g).

The catalytic performance results showed that the synthesized nanocatalysts had high activity and stability. However, the sol-gel sample exhibited better catalytic performance. Moreover, production of syngas with H₂/CO ratio very close to unity at 850°C was achieved in the both nanocatalysts as a result of high activity of copper for methane decomposition, which is the rate limiting step of the overall reaction.

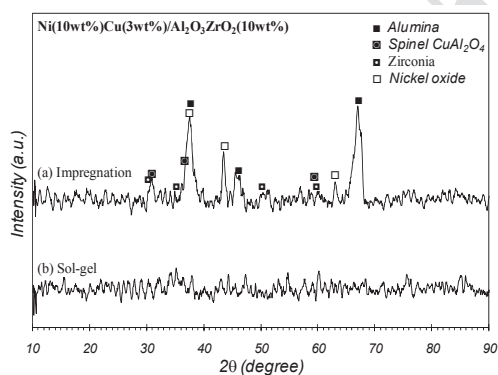


Figure 9: XRD patterns of Ni-Cu/ZrO₂-Al₂O₃.

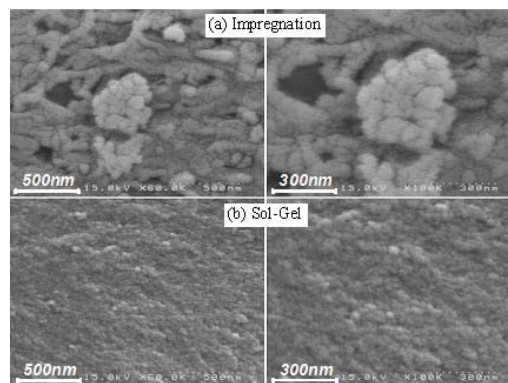


Figure 10: FESEM images of Ni-Cu/ZrO₂-Al₂O₃.

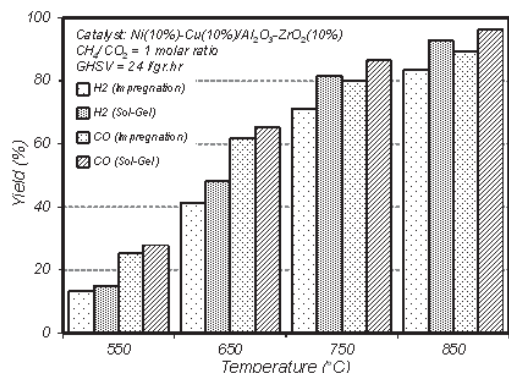


Figure 11: Product yield over Ni-Cu/ZrO₂-Al₂O₃.

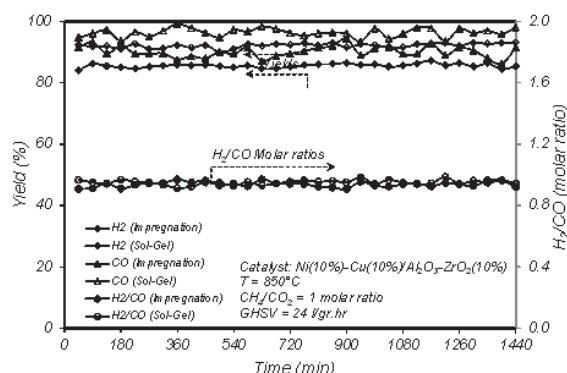


Figure 12: Stability test of Ni-Cu/ZrO₂-Al₂O₃.

Conclusion:

Ni-Cu/Al₂O₃-ZrO₂ nanocatalysts were synthesized by sol-gel and impregnation methods. Sol-gel method prevents Cu spinel formation due to high dispersion of ZrO₂ between Al₂O₃ and Cu species. As a result of the better characterization results, synthesized catalyst by sol-gel method exhibited higher catalytic performance and H₂/CO ratio very close to unity.

References:

- [1]H. Li and et al, "Study on CO₂ reforming of methane to syngas over Al₂O₃-ZrO₂ supported Ni catalysts prepared via a direct sol-gel process," Chemical Engineering Science, vol. 59, pp. 4861-4867, 2004.
- [2]S. Therdthianwong and et al, "Improvement of coke resistance of Ni/Al₂O₃ catalyst in CH₄/CO₂ reforming by ZrO₂ addition," Fuel Processing Technology, vol. 89, pp. 160-168, 2008.
- [3]P. Lopez and et al, "Hydrogen production from oxidative steam reforming of methanol: Effect of the Cu and Ni impregnation on ZrO₂ and their molecular simulation studies," International Journal of Hydrogen Energy, 2012.



Co and Cu Doped Ni/Al₂O₃-ZrO₂ Nanocatalysts Treated by Non-Thermal Plasma and Used for Dry Reforming of Methane

N. Rahemi^{a,b}, M. Haghighi^{a,b}, A. A. Babaluo^{a,c}, M. FallahJafari^d, P. Estifae^{a,b}

^aChemical Engineering Faculty, Sahand University of Technology, Tabriz, Iran

^bReactor and Catalysis Research Center (RCRC), Sahand University of Technology, Tabriz, Iran

^cNanostructure Material Research Center (NMRC), Sahand University of Technology, Tabriz, Iran

^dNational Iranian Oil Refining & Distribution Company (NIORDC), Tehran, Iran

*Email: haghighi@sut.ac.ir

Keywords: Ni-Co/Al₂O₃-ZrO₂, Ni-Cu/Al₂O₃-ZrO₂, Reforming, Nanocatalyst, Plasma.

Introduction:

Promoters like cobalt and copper beside carbon suppression, can improve Ni dispersion over the support via controlling the size of Ni ensembles [1,2]. To this aim in this work, the effect of mentioned promoters on activity and stability of plasma treated Ni/Al₂O₃ catalyst is investigated.

Materials and methods:

The Ni(10wt%)/Al₂O₃-ZrO₂(10wt%) nanocatalysts with two kinds of promoter (3wt% Co and 3wt% Cu) were prepared by non-thermal plasma method. The non-thermal plasma treatment time was 15 min and the treatment was repeated for three times in order to get a uniformly treated powder. XRD, FESEM, TEM, BET and FTIR techniques have been used to

investigate the effect of the non-thermal plasma on the structure of Ni/Al₂O₃-MgO nanocatalyst.

Result and discussion:

FESEM image of Ni-Co/Al₂O₃ in Figure 1 shows nano-size particles with uniform and agglomeration free morphology. TEM image of Ni-Co/Al₂O₃ in Figure 2 illustrates small active phase particles with high dispersion. Strong interaction between support and active sites that can be seen in TEM image is originated from plasma. Non thermal plasma via flattening the particles over the support intensifies interaction between particles.

Catalytic experiments were evaluated in the temperature range of 550–850°C in the quartz packed bed reactor. The effect of temperature, CH₄/CO₂ ratio, GHSV, yield, H₂/CO ratio and stability test has also been studied.

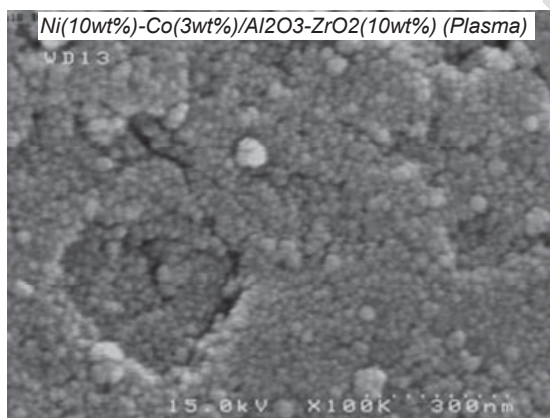


Figure 13: FESEM image of Ni-Co/Al₂O₃-ZrO₂.

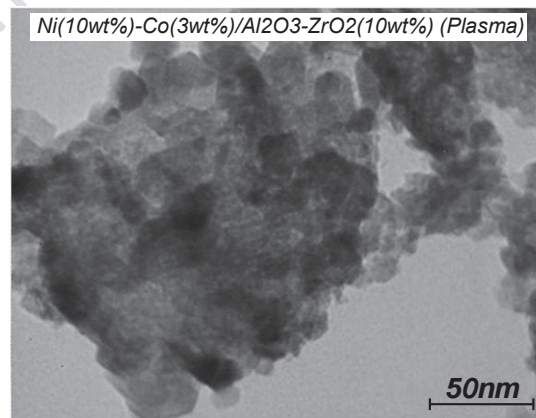


Figure 14: TEM image of Ni-Co/Al₂O₃-ZrO₂.

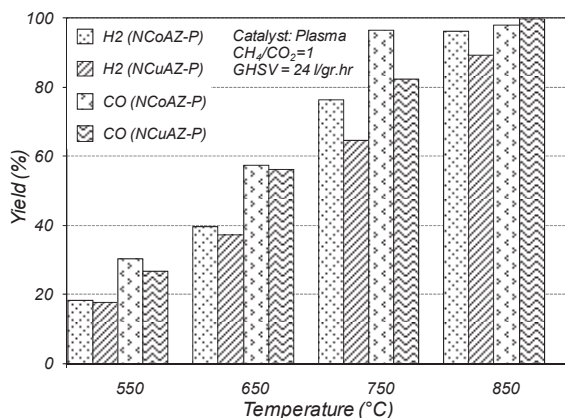


Figure 15: H₂ and CO yields over synthesized nanocatalysts at different temperatures.

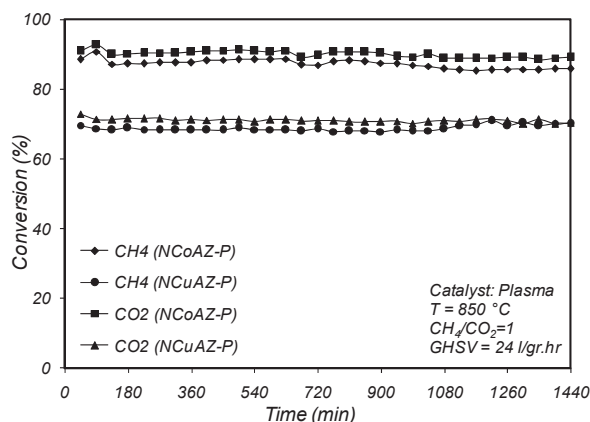


Figure 16: Time on stream performance of synthesized nanocatalysts.

Comparison of product yield in Figure 3 shows better catalytic activity of Ni-Co/Al₂O₃ rather than Ni-Cu/Al₂O₃ in dry reforming of methane. It seems Co can decompose methane better than Cu in dry reforming. Another role of promoters like Co and Cu is controlling the ensemble size of Ni. Due to sintering of copper in temperature range of dry reforming, big ensembles of Cu and consequently Ni, will not be able to decompose methane as well as small Ni particles in Ni-Co/Al₂O₃. Figure 4 shows good stability of both catalysts that confirms effect of plasma in synthesis of anti-coke and stable catalysts.

References:

- [1] J.-H. Lee et al., "Stabilization of Ni/Al₂O₃ catalyst by Cu addition for CO₂ reforming of methane", *Applied Catalysis A: General*, 269, (1-2), 1-6, 2004.
- [2] Y. H. Hu et al. (2004) Catalytic Conversion of Methane to Synthesis Gas by Partial Oxidation and CO₂ Reforming. In: *Advances in Catalysis*, vol Volume 48. Academic Press, pp 297-345



Surface tension prediction of binary mixtures by using scaled particle theory coupled with one fluid theory

M. JamaliNeiresi^{*a}, R. Tahery^b

^aScience Department, Islamic Azad University, Tehran central Branch, Tehran, Iran

^bChemical Engineering Department, Islamic Azad University, Tehran central Branch, Tehran, Iran

Email: mahtab_jamali_n@yahoo.com

Key words: Surface tension, Binary mixture, Scaled particle theory, One fluid theory, Hard sphere diameter

Introduction:

The surface of a liquid has interesting properties which appear as the surface tension. The surface tension play an important role in chemical industry, biological membranes operation, electrochemical reactions, mass transfer such as distillation, adsorption, extraction and several other processes [1].

There are a lot of methods to predict the surface tension of binary mixtures including Escobedo and Mansoori, Miller and Fainerman, Ramkrishna and..., but these methods required more information and data about structure, density, critical temperature and pressure, molar volume and some other properties. So, in this paper we present a very simple model to predict surface tension of binary mixtures. This model gives useful information such as hard sphere diameter.

Theory and Method:

The scaled particle theory (SPT) of fluids was presented by Reiss et al. and is concerned primarily with systems of hard spheres [2]. The resultant relation of the scaled particle theory for the surface tension calculation is presented by the following expression[3]:

$$\sigma = \frac{kT}{4\pi a^3} \left[\left(\frac{12y}{(1-y)} \right) + 18 \left(\frac{y}{(1-y)} \right)^2 \right] - \frac{Pa}{2} \quad (1)$$

Where σ , k , T , a and P are respectively the surface tension, Boltzmann constant, temperature, hard sphere diameter and pressure and y is the reduced density, which is given as $y = \frac{\pi N a^3 \rho}{6}$,

Where ρ is the density of pure fluid and N is Avogadro's number[3]. As it mention before SPT was developed for pure fluid but we extend this theory to binary mixture by using mixing rule. We assume that by mixing of pure fluids we have hypothetical fluid. Physical property of this hypothetical fluid can be obtained by using $a_M = a_1 x_1 + a_2 x_2$ and $\rho_m = \frac{MW_m}{V_m}$,

Where x_1 , x_2 , MW_m and V_m are mole fraction of component 1 and 2, molecular weight of mixture and molar volume of mixture respectively. Molar volume of mixture is calculated by $V_m = V_1 x_1 + V_2 x_2$. We can write Eq. (1) for hypothetical fluid as following:

$$\sigma = \frac{kT}{4\pi a_m^3} \left[\left(\frac{12y_m}{(1-y_m)} \right) + 18 \left(\frac{y_m}{(1-y_m)} \right)^2 \right] - \frac{Pa_m}{2} \quad (2)$$

Where σ_m and a_m are respectively surface tension and hard sphere diameter of hypothetical fluid and also the reduce density is given

$$\text{as } y_m = \frac{\pi N a_m^3 \rho_m}{6}.$$

Results and Discussion:



We apply SPT & OFT to 115 organic-organic compounds (including alkanes, alkanols, alcohols, cyclic ethers, amines, aromatic compounds, acids and...) binary mixtures at 318.7 K and at wide range of temperature. The average absolute deviations (%AAD) results for these binary mixtures obtained 3.48%. This work suggests that our model can be applied to calculate the surface tensions of a wide range of mixtures with good accuracy.

Conclusions:

SPT coupled with OFT can be used for prediction of surface tension of binary mixtures with satisfactory results. The results for binary organic solution is very good while the results for aqueous solutions and organic solution containing alcohols the results is poor.

Reference:

- [1] R. Tahery, H. Modarress, J. Satherley, Surface tension prediction and thermodynamic analysis of the surface for binary solutions, *Chem. Eng. Sci.*; 60, 4935-4952, 2005.
- [2] H. Reiss, H.L. Frisch, J.L. Lebowitz, Statistical mechanics of rigid spheres, *J. Chem. Phys.* ; 31, 369-380, 1959.
- [3] S.W. Mayer, Dependence of Surface Tension on Temperature, *J. Chem. Phys.* ; 38, 1803-1808, 1963.



**UV/Vis Spectral & Viscosity Investigation of Interaction Bis 5-Phenyl Azo Salicyl aldehyde
Ethylene di imin Cobalt (II) With Calf Thymus Deoxy Ribonucleic Acid .**

N.Sohrabi , N.Rassoli , M.Kamkar.d

Department of Chemistry P.N.U of Iran 19395-3697

E.MAIL : sohrabnas@pnu.ac.ir

KEYWORD: Salen , DNA , UV/Vis Spectroscopy , Viscosity , Thermal Denaturation

INTRODUCTION:

Schiff-base ligands have been reported to show a variety of biological action by virtue of the azomethine linkage, which is responsible for various anti-bacterial, anti-fungal, anti-cancer, anti-viral, herb cal, clinical and analytical activities and this activity tends to increase in metal(II) Schiff-base complex [1] . The chemistry of Schiff-base ligands and their metal complex has expanded enormously and encompasses a vast area of organometallic compounds and various aspect of bioinorganic chemistry [2]. The chemistry of metal complexes containing Schiff base ligands derived from condensation of aldehydes and amines is of enduring significance, since they have common features with metalloprophyrines with respect to their electronic structure and catalytic activities that mimic enzymatic oxidation [3].

Arturo Silvestre et al , reported on the interaction of calf thymus DNA with Fe(III) Salen, that results obtained have been interpreted in terms of an electrostatic binding of $[\text{Fe}(\text{salen})]^+$ cation and the phosphate group of DNA [3]. Design and synthesis of small synthetic systems that recognize specific sites of DNA is an important area of much current research these could be at least in part due to the formation of none covalently associated complexes by several such molecules with nucleic acids.

In this study the interaction of CoBBASE with CT-DNA was analyzed by using spectroscopic method in various conditions as concentration and temperature, and then binding constants, binding mode, and the binding thermodynamic parameters was determined. The results obtained by UV spectroscopy with changing in temperature, DNA thermal denaturation and viscositymetry.



Materials and Methods

In this study we use CoBBASE that is a red solid with $M_w = 532.24 \text{ g/mol}$ and CT-DNA that obtained from Sigma Aldrich and NaCl, HCl, H_2SO_4 , EDTA. Absorbance spectra were recorded using a lambda 25 double beam spectrophotometer. The absorbance measurements were performed by keeping the concentration of the CT-DNA constant while varying the CoBBASE added to the cell. The absorbance at 403 nm was recorded after each addition of CoBBASE and repeat this way in various temperatures such as, 30, 35, 40, 45 and 50°C. The intrinsic binding constant K_b was determined for interaction between CoBBASE and CT-DNA.

Also we studied the effects of addition of various concentration of metal complex with concentration of $9.4 \times 10^{-5} \text{ mM}$ to CT-DNA. And then the viscosities of solution contain CT-DNA and CoBBASE complex were studied by Ostwald viscometer.

Denaturation and changing in melting temperatures for DNA in the absence and in the presence of various CoBBASE complexes were measured by following the changes in the UV-vis absorption spectra at 260 nm as a function of temperature. The absorption intensities at 260 nm were plotted against individual temperatures in the presence of each concentration of CoBBASE complex, and the midpoints of the inflection regions in the temperature vs A_{260} curves were taken as the corresponding T_m values.

Result and discussion:

The UV-vis spectra of CoBBASE at 25°C between 200-700 nm showed two peaks at 275 and 403 nm, that peak on 403nm assigned to transfer charge in complex.

To study about thermal stability of CoBBASE, we repeat UV-vis spectroscopy in various concentration with increasing temperature in 30,35,40,45 and 50°C.

The UV-vis spectra of interaction between CoBBASE and CT-DNA were recorded in various temperatures. UV-vis spectra shows that by increasing concentration of CoBBASE vs CT-DNA absorbance increase and it has the same treat for all temperatures 25, 30,35,40,45 and 50°C.

Intercalating agents are expected to destack the base pairs causing elongation of the double helix resulting in an increase in the viscosity of CT-DNA. On the other hand viscosity of CT-DNA in the presence of Co^{2+} BBASE, which bind to CT-DNA by non-intercalative mode has been found to decrease



in the presence of small amount of complex and subsequently increase as the CoBBASE concentration increases. In the presence of CoBBASE complex viscosity of CT-DNA has been found to depend on complex concentration[4].

The viscometers data shows that there are two phase of binding between the Co (II) complex and CT-DNA. In principle, decrease in viscosity could be explained by the effects like change in conformation flexibility or salivation of the CT-DNA molecules. By increasing in CoBBASE concentration, viscosity of CT-DNA show increase, it would indicate that the binding of CoBBASE complex with CT-DNA could be surface binding or by forming bridged adduct.

Interaction of small molecules with double helix is known to increase the melting point temperature at which the double helix denatures into single stranded DNA. The melting temperature can be determined by monitoring the absorbance of the DNA at 260nm as a function of temperature.

Thermal denaturation profile of CT-DNA solution in the absence and presence of increasing amount of CoBBASE, were obtained by plotting the absorbance for each solution by mole ratio of CoBBASE to CT-DNA as 0, 0.013, 0.026, 0.052 and 0.104 as a function of temperature.

It is known that when the temperature in the solution increases, the double stranded DNA gradually dissociate into single strand; T_m is therefore defined as a temperature where half of total base pairs is unpaired. The DNA melting temperature T_m is strictly related to the stability of the double helix, and the interaction of chemical with DNA may alter T_m , by stabilizing or destabilizing the final complex. The presence of the positive charge on the intercalate should further increase the attractive interaction with the negatively charged phosphate groups and help the intercalative mechanism[5].

The melting temperature carried out for CT-DNA in the absence of any added complex revealed at T_m of $74.5 \pm 0.5^\circ\text{C}$ under our experimental condition, the melting temperature of CT-DNA 1.268×10^{-5} M increase about 1 to 8°C at mole ratio of CoBBASE to CT-DNA as 0, 0.013, 0.026, 0.052 and 0.104. These results are indicative of strong metal complex=DNA interaction, that stabilize the native DNA conformation.

Conclusion:

The binding of CoBBASE complex to CT-DNA, while the wavelength of maximum absorption, λ_{max} does not show considerable changes the amount of absorption increases, represents the outside-binding and



hydrophobic interaction modes. The increasing of viscosity of CT-DNA upon addition of CoBBASE represents the stable interaction by non-intercalative mode between CT-DNA and CoBBASE.

The CT-DNA-binding process is endothermic for CoBBASE and has the large positive entropy value. These can be represent the predominate role of electrostatic interactions and outside binding mode. The increasing of melting temperature (T_m) of CT-DNA upon addition of CoBBASE represents the stable interaction between CT-DNA and CoBBASE.

Refrence :

- (1) (a) Sigman, D. S., Bruice, T. W., Mazumder, A., and Sutton, C. L. (1993) *Acc. Chem. Res.* 26, 98. (b) Barton, J. K., and Pyle, A. M. (1990) *Prog. Inorg. Chem.* 38, 413. (c) Burkhoff, A. M., and Tullius, T. D. (1988) *Nature* 331, 455. (d) Riordan, C. G., and Wei, P. J. (1992) *J. Am. Chem. Soc.* 116, 2189.
- (2) (a) Tan, J. D., Hudson, S. E., Brown, S. J., Olmsted, M. M., and Mascharak, P. K. (1992) *J. Am. Chem. Soc.* 114, 3841. (b) Nagai, K., Carter, B. J., Xu, J., and Hecht, S. M. (1991) *J. Am. Chem. Soc.* 113, 5099. (c) Nicolau, K. C., Maligres, P., Shin, J., de Leon, E., and Rideout, D. (1992) *J. Am. Chem. Soc.* 114, 7825.
- (3) Sato, K., Chikira, M., Fujii, Y., and Komatsu, A. (1994) *J. Chem. Soc., Chem. Commun.*, 625.
- (4) (a) Gravert, D. J., and Griffin, J. H. (1993) *J. Org. Chem.* 58, 820. (b) Gravert, D. J., and Griffin, J. H. (1996) *Inorg. Chem.* 35, 4837.
- (5) (a) Mandal, S. S., Vinaykumar, N., Varshney, U., and Bhattacharya, S. (1996) *J. Inorg. Biochem.* 63, 265. (b) Bhattacharya, S., and Mandal, S. S. (1997) *Biochem. Biophys.*



Poster Session:

- Applied Chemistry
- Computational Chemistry
- Classical Thermodynamics
- Electrochemistry
- Chemical Kinetics
- Nanotechnology
- Quantum Mechanics & Spectroscopy
- Surface Chemistry
- Statistical
- Thermodynamics



Applied Chemistry



Prediction of thermodynamic properties of ethers and glycol ethers using a group contribution method

Maryam Abareshi^{a,*}, Majid Moosavi^b

^aDept. of Chemistry, Payame Noor University, 19395-3697 Tehran, I. R. of Iran

^bDept. of Chemistry, Faculty of Sciences, University of Isfahan, Isfahan 81746-73441, Iran

Email: maryamabareshi@yahoo.com

Keywords: Equation of state, Ether, Glycol ether, Molar density.

Introduction:

Ethers offer specific advantages as clean fuel or fuel additive and glycol ethers are widely used as detergents by means of forming stable homogeneous solutions. PVT data are needed for the simulation of the behavior of ethers and glycol ethers in real operation conditions for some applications. Despite these facts, literature density data for these compounds are scarce [1]. In this work, the group contribution method has been applied in combination with the GMA equation to calculate the molar density and other thermodynamic properties of some long chain organic compounds i.e. ethers and glycol ethers.

Theory:

The GMA equation is modified to [2,3]:

$$\left(\frac{2Z}{n} - 1\right) V_m^3 = A' + B' \rho \quad (1)$$

where $A' = A_m n^3$ and $B' = B_m n^4$. This new regularity was called GCM-GMA equation. The molar density at any temperature and pressure can be obtained via the following equation:

$$B_m n^5 \rho^5 + A_m n^4 \rho^4 + n \rho - \frac{2P}{RT} = 0 \quad (2)$$

To predict the GCM-GMA equation parameters for ethers and glycol ethers using group contribution method, we consider $-\text{CH}_2\text{O}$ as a new functional group. The contribution of this new group may be calculated via the following expressions, where diethyl ether has been chosen as a basic compound:

$$(A_m)_{\text{diethyl ether}} = \left(\frac{2}{4}\sqrt{A_{11}} + \frac{1}{4}\sqrt{A_{22}} + \frac{1}{4}\sqrt{A_{\text{CH}_2\text{O}}}\right)^2 \quad (3)$$

$$(B_m)_{diethyl\ ether} = \left(\frac{2}{4} \sqrt{B_{11}} + \frac{1}{4} \sqrt{B_{22}} + + \frac{1}{4} \sqrt{B_{CH_2O}} \right)^2 \quad (4)$$

Results and discussion:

The accuracy of the GCM-GMA equation for ethers and glycol ethers can be investigated using the experimental PVT data. Fig. 1(a) and (b) shows that the linearity of $((2Z/n)-1)V_m^3$ versus ρ holds very well for each isotherm of dibutyl ether and diethylene glycol butyl ether.

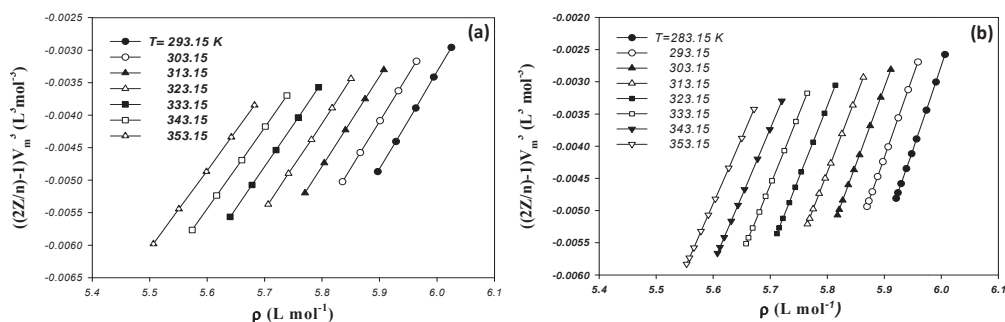


Fig. 1. Linearity of $((2Z/n)-1)V_m^3$ versus ρ for (a) dibutyl ether (b) diethylene glycol butyl ether.

The calculated values of A_m and B_m along with Eq. (2) are used to calculate the molar density of ethers and glycol ethers at different temperatures. As an example, Table 1 shows bias and AAD for different ethers and glycol ethers at 323.15 K for the given pressure range (ΔP). The values of AAD and bias show that the GCM-GMA equation can predict the experimental molar density of ethers and glycol ethers with a good accuracy at any temperature and pressure.

Table 1. Bias and AAD of the calculated molar density for different ethers and glycol ethers at 323.15 K for the given pressure (ΔP), using the calculated values of A_m and B_m parameters along with Eq. (2).

Fluids	ΔP (Mpa)	Bias	AAD	NP	Fluids	ΔP (Mpa)	Bias	AAD	NP
Diethyl ether	0.35-19.51	-0.00	0.02	5	DEGME	0.1-25	0.80	0.80	9
Dibutyl Ether	0.1-19.6	-0.86	0.86	5	DEGEE	0.1-25	-0.13	0.13	9
EGME	0.1-60	-1.27	1.27	13	DEGDME	0.1-100	1.84	1.84	11
EGEE	0.1-60	-1.08	1.08	13	DEGBE	0.1-25	0.033	0.033	9
MEGDME	0.1-100	1.48	1.48	11	PGPE	0.1-25	-2.33	2.33	9

Conclusions:



In this work, the GCM-GMA equation was successfully applied to the ethers and glycol ethers. In order to obtain the contribution of $-\text{CH}_2\text{O}$ group, diethyl ether has been used as basic compound.

The results show that this equation can predict the molar density and other thermodynamic properties of ethers and glycol ethers with a good accuracy at different temperatures and pressures.

References:

- [1] X. Meng, et al. *Fluid Phase Equilib.*, 271, 1-5, 2008.
- [2] M. Moosavi, *Ind. Eng. Chem. Res.*, 49, 6662-6669, 2010.
- [3] M. Moosavi, *Fluid Phase Equilib.*, 310, 63-73, 2011.



Investigation of thermodynamic properties of hydrocarbons using an extended LJ potential-based EoS at high temperature-high pressure conditions

Majid Moosavi^{a,*}, Maryam Abareshi^b

^aDept. of Chemistry, Faculty of Sciences, University of Isfahan, Isfahan 81746-73441, Iran

^bDept. of Chemistry, Payame Noor University, 19395-3697 Tehran, I. R. of Iran

Email: m.mousavi@sci.ui.ac.ir

Keywords: Equation of state, Hydrocarbon, Molar density, Derived properties, HTHP.

Introduction:

Density prediction of hydrocarbons at extreme temperature and pressure conditions are most relevant to petroleum engineering studies of ultra-deep reservoirs [1]. Many equations have been used to predict the density and other thermodynamic properties of hydrocarbons [1,2]. Recently, a general EoS has been introduced for a wide variety of fluids and solids by Parsafar et al. [3]. The purpose of this research is to predict the density and other thermodynamic properties of different hydrocarbons up to the extremely HTHP conditions using the ELJ-based EoS.

Theory:

LIR EoS was derived based on the LJ (12,6) potential as follows:

$$(Z-1)V_m^2 = a(T) + b(T)\rho^2 \quad (1)$$

where $a(T) = a_2 - a_1/RT$ and $b(T) = b_1/RT$. This EoS shows deviations for some systems. For these systems, Ghatee and Bahadori [26] proposed an effective potential of Mie(6,3) form as follow:

$$(Z-1)V_m^2 = c(T) + (d(T)/\rho) \quad (2)$$

where $c(T) = c_2 + c_1/RT$ and $d(T) = d_1/RT$. However, there remain some materials for which neither Eq. (1) nor Eq. (2) work well especially at HTHP conditions. For these systems the ELJ (12,6,3)-based EoS has been suggested as follows [3]:

$$(Z-1)V_m^2 = e(T) + \frac{f(T)}{\rho} + g(T)\rho^2 \quad (3)$$

Results and discussion:

The experimental PVT data of 38 compounds were used to investigate the validity of regularities presented in Eqs. (1), (2), and (3). As examples, Fig. 1 shows the isotherms of n-heptane for temperatures up to 573 K and pressures up to 500 MPa. The isotherms deviate significantly from both Eqs. (1) and (2) whereas Eq. (3) gives an excellent fit to the data.

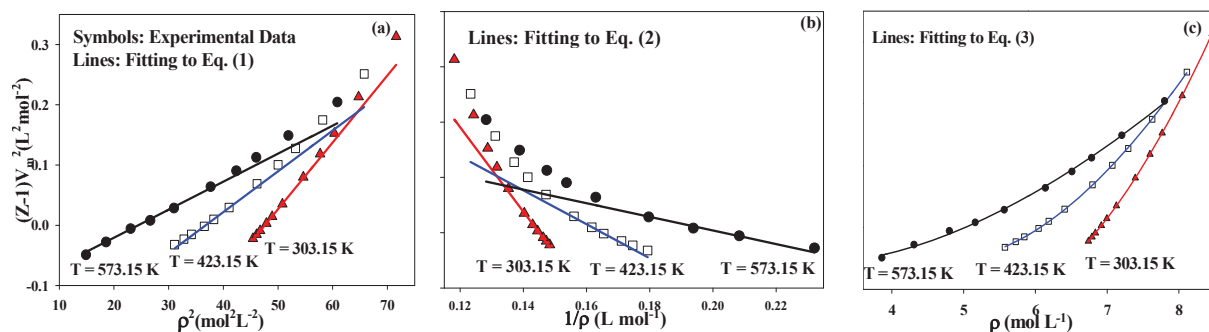


Fig. 1. The isotherms of n-heptane. The points are experimental results and solid lines are fits to (a) Eq. (1), (b) Eq. (2), and (c) Eq. (3).

Table 1 shows bias and AAD of the calculated density for different hydrocarbons and indicates that this EoS works well for predicting the density of hydrocarbons. The AAD values between experimental and calculated densities from this equation and those predicted by some other equations have been compared in Table 2. Much better results obtained by the ELJ-based EoS.

Table 1. bias and AAD of the calculated molar density for different hydrocarbons at different temperatures.

Hydrocarbon	T(K)	Bias(%)	AAD (%)
CH ₄	300.00	-0.16	0.33
C ₈ H ₁₈	298.15	0.05	0.05
C ₁₂ H ₂₆	323.19	-0.05	0.05
C ₂₀ H ₄₂	373.15	0.14	0.14
Benzene	348.15	-0.01	0.03
Tetralin	298.15	-0.13	0.13
Cyclohexane	377.59	0.41	0.41
Isooctane	197.93	-0.33	0.33

the density and other thermodynamic properties of some

Table 2. Comparison between this work and some other EoSs for density prediction of selected hydrocarbons.

Conclusions:

We have developed the ELJ-based EoS to predict

Hydrocarbon	AAD (%)		
	PC-SAFT	HTHP VT-SRK	This work
Methane	1.79	0.81	0.13
Propane	1.91	1.54	0.12
n-C30	2.59	1.98	0.11
Benzene	0.80	1.57	0.18
Toluene	0.94	0.70	0.21

hydrocarbons systems. The capability of this EoS to predict density has been demonstrated. This



EoS can predict density and other thermodynamic properties such as isobaric expansion coefficient, isothermal compressibility, and internal pressure of hydrocarbons. Our results are in a good agreement with the experimental and the previous literature data.

References:

- [1] K. Liu, et al. J. of Supercritical Fluids 55, 701–711, 2010.
- [2] E.C. Voutsas, et al. Fluid Phase Equilib., 240, 127-139, 2006.
- [3] G.A. Parsafar, et al. J. of Phys. Chem. B., 113, 11977–11987, 2009.

15th Physical Chemistry Conference



Extraction of aromatic compounds from hydrocarbon fuels by ionic liquids: a quantum chemical study

Amir H. Jalili^{a*}, S. Arezoo Mirghasemi^b, N. Farahani^b

^a Gas Science Department, Research Institute of Petroleum Industry, P.O. Box: 14665-137, Tehran, Iran

^b Department of Chemistry, Islamic Azad University- North Tehran Branch, Tehran, Iran

Key words: Ionic liquid, DFT, Selectivity, Separation, Aromatic, Aliphatic.

Introduction:

Ionic liquids (ILs) are liquid salts consisting of a large, mostly organic, cation and a great variety of anions. Their physical properties include wide liquid temperature range (~300 K), low vapor pressure and the ability of tailoring [1] for a specific application. Several (ILs) are suitable for extraction of aromatic/aliphatic mixtures [2]. In general, this means high solubility for aromatic hydrocarbons in the solvent combined with a high selectivity resulting from a low solubility of the aliphatic components. A growing number of experimental data for solubility and separation of aromatic and aliphatic hydrocarbons by ILs have been generated in the past few years [3-9]. In this work, the interaction of benzene and hexane with 1-ethyl-3-methylimidazolium-based ILs with anions thiocyanate ([SCN]⁻), tetrafluoroborate ([BF₄]⁻), hexafluorophosphate ([PF₆]⁻), ethylsulfate (EtSO₄]⁻), and bis(trifluoromethylsulfonyl) amide ([Tf₂N]⁻) as solvent in extraction process of benzene from hexane were investigated using extensive quantum chemical *ab initio* calculations. The results of theoretical *ab initio* calculations are compared with reliable experimental data and other theoretical studies.

Method of Calculation:

Quantum chemical calculations were performed using Gaussian version 03 suite of programs. Geometry optimizations and interaction energy of systems were calculated through density functional theory (DFT) using B3LYP/6-311g** and B3LYP/6-311G++(2d,2p) levels of theory. Atomic charges of ionic and neutral species were calculated by electrostatic surface potential fits, using the CHelpG procedure to electron densities obtained at B3LYP/6-311** level.



Results and Discussion:

Calculations indicate that the interaction energy of anion and cation in the pure IL changes according to following sequence:



It was found that the interaction energy of anion and cation of the IL with benzene and hexane correlates well with activity coefficients at infinite dilution of solutes in the ILs. Furthermore, results show that the solubility of benzene and hexane decrease with the increase in the interaction energy between anion and cation of the ILs, while the selectivity for dissolution of benzene and hexane increases as the interaction energy between anion and cation of the IL increases. Results of *ab initio* calculations for the benzene + IL and hexane + IL systems were analyzed and compared with those of sulfolane as an industrial solvent for separation of aromatics from aliphatics. It has been deduced that the interaction energy of ILs with benzene and hexane is stronger than those of sulfolane with them. The calculations showed that, ILs have more selectivity for purification and extraction of aromatic hydrocarbons from aliphatic hydrocarbons compared to sulfolane. The results of theoretical *ab initio* calculations were confirmed through comparison with reliable experimental data available in the literature.

References:

- [1] Antje R.Hansmeier, Mark Jongmans, G. Wytze Meindersma, Ander B. de Haan, *J. Chem. Thermodyn.* 42, 484-490, **2010**.
- [2] G. Wytze Meindersma, Anita (J.G.) Podt, Andre' B. de Haan. *Fuel Process. Technol.* 87, 59 – 70, **2005**.
- [3] Elena Gómez, Irene Domínguez, Noelia Calvar, Angeles Domínguez., *J. Chem. Thermodyn.* 42, 1234-1239, **2010**.
- [4] Julinan Garcia ,Adela Fernandez, José S. Torrecilla, Mercedes Oliet, Francisco Rodríguez, *J. Chem. Eng. Data* 55, 258-261, **2010**.
- [5] Andrzej Marciniak, *J. Chem. Eng. Data* 56, 368–374, **2011**.
- [6] Pei-Fang Yan, Miao Yang, Chang-Ping Li, Xiu-Mei Liu, Zhi-Cheng Tana, Urs Welz-Biermann, *Fluid Phase Equilib.* 298, 287-292, **2010**.



- [7]Julin Garca ,Adela FernJndez, José S. Torrecilla, Mercedes Oliet, Francisco Rodrguez, *Fluid Phase Equilib.* 282, 117–120, **2009**.
- [8]Urszula Doman'ska, *Pure Appl. Chem.* 77, 543–557, **2005**.
- [9]Urszula Doma'nska, Aneta Pobudkowska, Marek Kr'olikowski, *Fluid Phase Equilib.* 259, 173–179, **2007**.

15th Physical Chemistry Conference



Complexation of trioxide tungsten and p-sulfonatocalix[4]arene In aqueous solution

K.Zare^a, N. Shadmani^{b*}

^aDepartment of Chemistry, Islamic Azad University, science and research Branch, Tehran, Iran

^bDr. Student, Department of Chemistry, Islamic Azad University, science and research Branch, Tehran, Iran

Email: n.shadmani@gmail.com

Keywords: p-Sulfonatocalix[4]arene, Tungsten, Spectrophotometric techniques, Formation constant

Introduction:

Calix[n]arene characterized by their versatile molecular recognition properties towards neutral, cationic and anionic guests and by their propensity to act as molecular building blocks for the design of large supramolecular assemblies [1,2]. The water soluble calix[n]arene (n=4-8) derivatives have received considerable attention in recent years because of their selective metal ion binding properties in aqueous solution, the formation of basket-like bilayer structures in the solid state, and the observation of H₂O... π aromatic hydrogen bonding. Calixarenes have been studied in the context of electrochemical selective, sensor, stationary phases and solid phase extraction phases [3, 4]. Complex is known to be suitable starting material to the Calixarene supported organo tungsten complex.

Materials and method:

p-sulfonatocalix[4]arene (Fig1) was purchased from professor Z. Asfari and used with further purification. Sodium Tungstat (purity 99.9%), NaOH and HCl (1N) were purchased from Merk, respectively. 2.5 ml solution of ligand and ($5 \times 10^{-4} \text{ mol}^{-1} \text{ dm}^{-3}$) were titred with stepwise addition of the tungsten (VI) solution, $(1.5-3.5) \times 10^{-2} \text{ mol}^{-1} \text{ dm}^{-3}$. Absorption spectra, 280-310 nm, were measured on Scinco S-4100 UV-ViS Scanning spectrophotometer with a notebook using 3cm quartz cells. The system was thermostate (298.15K) by circulating water from an isothermal bath.

Result and discussion:

Assuming that the absorbance of the ligand would change upon complexation with the W (VI) metal ion, we performed spectrophotometric measurements. Treatment of the spectrophotometric data (280-310 nm) with an interval of with the computer program squad [5]. The storchimetric formation constants were computed from the data using the computer program. In all cases, the resulting average and shown in the text, table and plot.

Agent	$\Delta G^\circ / \text{KJmol}^{-1}$	$\Delta H^\circ / \text{KJmol}^{-1}$	$\Delta S^\circ / \text{KJk}^{-1}$	Log K
The complex at temperature 298.15 /k	-26.9452	-178.356	-0.508	4.72±0.005

Conclusion:

The interesting curves of the ligand and by Tungsten (VI) (Fig2) shows a sharp break point when the concentration ratio of metal ion to of a stable complex for the metal ion. In according to Want's Hoffe equation ,using slope and interception in graph Ln K versue 1/T, ΔH° and ΔS° can be calculated respectively. Reaction ΔG° , ΔH° and ΔS° is negative, means reaction is spontaneous, complex formation is exothermic and less disordering, respectively, this results in host-gust complex, it's great equilbirium constant ($K=10^{4.72}$) ,so it is states more stability.

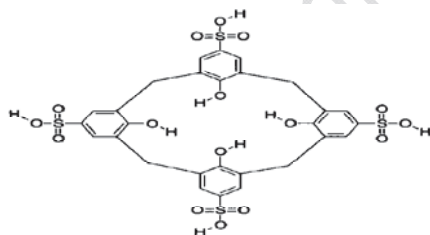


Fig.1. The Structure of 25,26,27,28 tetrahydroxy-Ligand SC₄ by ion metal at 298.15k and 280nm

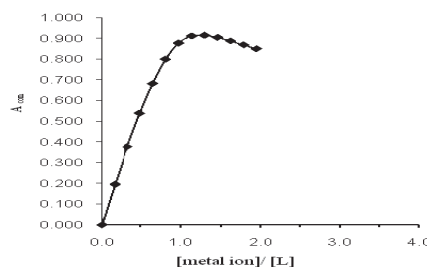


Fig.2. Spectrophotometric titration plots of the 5, 11, 17, 23 tetrasulfonic Calix[4]arene

Reference:

- [1] R. Ungaro, E. Dalcanale "Supramolecular Science: Where it is and Where It Is Going?" Kluwer Academic Publisher, Netherlands 1999.
- [2] P. Lhotak.; "Anion Receptors Based on Calixarenes"; J.Top Curr Chem; 255, 65–95,



2005.

[3] V. Stankovic, et al." Silver electrowinning from silver (I)–calixarene complexes by two-phase electrolysis" J Appl Electrochem; 37, 1279–1286, 2007.

[4] S. Abd Hamid, et al." Application of a Newly Synthesized Calixarene in Metal Ions Extraction" J Clean, 36, 498 – 503, 2008.

[5] D. J. Leggett," Computational methods for the determination of formation constants"; Plenum, New York, 1985.

15th Physical Chemistry Conference



A New Equation of State for Alcohols

L. Maftoon-Azad^a, Sh. Elyasi^b

^a Department of Chemistry, Persian Gulf University, Boushehr, Iran

^{a, b} Email: elyasi89@yahoo.com

Key words: Water, Liquid Alcohols, Equation of State

Introduction:

Of the various interrelations between state properties, one of the most important is the equation of state, defined as a relation between pressure, volume and temperature. It is common to assume that all pure substances (especially gases and liquids) obey an equation of state and this assumption is made in the subsequent thermodynamic developments. Among pure substances, we are interested in alcohols with desirable physical and chemical properties, that make these compounds very useful in industrial and scientific applications. In this work we have proposed an equation of state that can predict the PVT behavior of water and alcohols in different pressure and temperature ranges.

Methods:

The basic form of the equation of state is developed by Jeffery and Austin [1-2]

$$\frac{p}{\rho RT} = 1 + \left(\alpha - b^* - \frac{a_{vw}}{RT} \right) \rho + \alpha \rho \left[\frac{1}{1 - \lambda b \rho} - 1 \right] \quad (1)$$

Where p , ρ , and T are Pressure, density and temperature, respectively. λ is the only adjustable parameter of this equation. α and b are the repulsive contribution to the second virial coefficient and the van der Waals co-volume. α and b are temperature dependent parameters. They specified a functional form of $b(T)$ that increases rapidly with decreasing T .

$$\frac{b(T)}{V_B} = 0.25e^{1/(2.3T/T_B+0.5)} - b_1e^{2.3T/T_B} + b_2 \quad (2)$$

Where T_B and V_B are Boyle temperature and volume. In this work we have shown that critical temperature and volume can be used to predict the whole PVT surface for water and normal alcohols instead of Boyle temperature and volume. α , b^* , λ , b_1 and b_2 are fitted by the experimental data for water. Results are shown in table 1.



Table 1. Temperature dependant parameters for water.

b_2	b_1	λ	b^*	α
0.243	0.022	0.335	7.0×10^{-6}	7.1×10^{-5}

We obtained the densities for water with this new equation of state. The agreement with experiment is quite good within 1.27%. Then we have utilized this equation of state for predicting the PVT behavior of alcohols.

Results and Discussion:

We obtained the densities for alcohols applying Eqs 1, 2 and using α , b^* , b_1 and b_2 of table 1. λ is adjusted for each alcohol. Results are shown in table 2.

Table 2. Results for water and 14 alcohols. (AAD: Average Absolute Deviation)

λ	AAD (%)	Max dev (%)	ΔP (bar)	ΔT (K)	NP	Fluid
0.330	0.025	1.27	0.006-221	273-647	79	water
0.330	0.19	1.66	1-111	178-317	108	methanol
0.368	0.27	0.95	1-350	278-348	30	ethanol
0.363	0.26	0.60	0.02-1.12	298-373	9	1-propanol
0.511	0.32	2.65	4-96	280-392	150	2-propanol
0.557	0.51	1.07	10-245	323-362	125	1-butanol
0.521	0.34	2.22	10-250	313-362	150	2-butanol
0.499	0.26	1.05	5-250	312-362	120	1-pentanol
0.530	0.32	1.04	10-250	333-362	100	1-hexanol
0.509	0.27	1.26	10-220	313-352	132	2-hexanol
0.495	0.35	1.41	10-220	313-362	132	1-heptanol
0.499	0.30	1.44	10-220	313-362	132	2-heptanol
0.495	0.23	0.88	10-220	323-362	108	1-octanol
0.422	0.71	4.56	1-1000	293-318	66	1-nonanol
0.466	0.27	-1.03	10-220	313-362	110	1-decanol

Conclusion:

In the present work we have predicted the volumetric properties of water and different alcohols at vast ranges of temperature and pressure using just one adjustable parameter.



Critical parameters are used as scaling factors. The accuracy of the equation of state is very good.

References:

- [1] Jeffery, C. A.; Austin, P. H. *J. Chem. Phys.* **1998**, 110, 484.
- [2] Haynes, W. M.; CRC Hand book of chemistry and Physics, 91st edition. **2010**, Colorado, USA.

15th Physical Chemistry Conference



viscometric studies of binary mixtures of formamide with alkan-2-ols

k. mohamadian*^a and M.almasi^a

^a Department of Chemistry, Science and Research Branch, Islamic Azad University, Khuzestan, Iran

Email : kosarmohamadian@yahoo.com

m.almasi@khuzestan.srbiau.ac.ir

Abstract :

excess viscosities for binary liquid mixtures of formamide with (C₃-C₇) alkan-2-ols have been calculated from the viscosities measured at 298.15 K over the whole composition. The viscosity-mole fraction data of the five systems were used to test law proposed to describe the viscosity of mixtures : the model by Redlich-Kister were tested. Deviations with respect to ideal behaviour were interpreted in terms of specific interactions between unlike molecules.

Keywords : excess viscosities , Redlich-Kister , binary mixtures , formamide

Introduction:

Excess properties of mixtures provide information about the molecular interactions between the various components and can be used for the development of molecular models describing the thermodynamic behavior of mixtures [1– 2].

Although alcohol liquid mixtures have been extensively studied, little is known of binary mixtures of alcohols with amides.

Methods:

The viscosities were measured with an Ubbelohde viscometer and experimental data for the binary systems were fitted by the least-squares method to the Redlich–Kister equation.

Results and Discussion:

The excess viscosities, η^E , for the five binary systems were evaluated using the equation

$$\eta^E = X_1 X_2 \sum_{k=0}^p a_k (1 - 2X_1)^k \quad (1)$$

$$\Delta\eta = \eta - (x_1\eta_1 + x_2\eta_2) \quad (2)$$

In the above equations x , is the liquid mole fraction and p , stands for the number of components in the mixture, where the index k may be given the value p , the polynomial order and η , is viscosity of mixture. Experimental data and fitted equations for the five binary systems are depicted in Fig. 1.

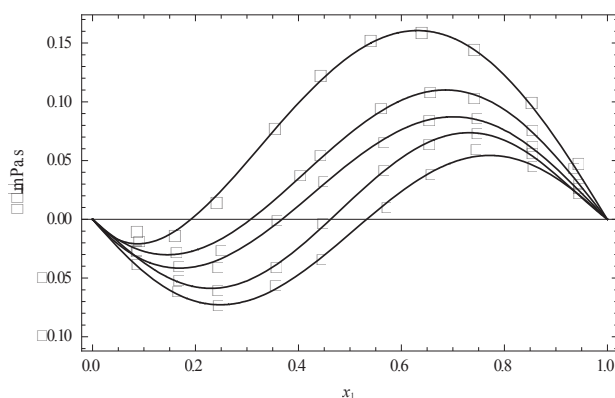


Fig. 1 viscosity, $\eta\Delta$ at 298.15 K for the binary systems: (\blacklozenge) 2-propanol+formamide, (Δ) formamide + 2-butanol, (\blacksquare) formamide+2-pentanol, (\bullet) formamide + 2-hexanol, (\square) formamide+2-heptanol

for Form Amide + (C₃-C₇) alkan-2-ols mixtures the η values exhibit sigmoid trend, wherein η changes sign from negative to positive as the concentration of FA in the mixture is increased. small negative/positive η values for Form Amide + (C₃-C₇) alkan-2-ols mixtures indicate the presence of significant interactions between unlike molecules in these mixtures.[3]

Conclusions :

excess viscosities for binary liquid mixtures of formamide with (C₃-C₇) alkan-2-ols have been calculated were measured at 298.15 K. It is observed that the order of interactions in these mixtures depends upon the number and position of hydroxyl groups in these alkanol molecules.

References:

- [1] Iloukhani, H., Almasi, M.: Densities, viscosities, excess molar volumes, and refractive indices of acetonitrile and 2-alkanols: Experimental results and application of the Prigogine-Flory-Patterson theory. *Thermochim Acta*. **495**, 139-148(2009)



- [2] Almasi, M.; Iloukhani, H. Densities, Viscosities, and Refractive Indices of Binary Mixtures of Acetophenone and 2-Alkanols. *J. Chem. Eng. Data* **2010**, 55, 1416–1420.
- [3] Kumar Nain, A.,: Molecular interactions in binary mixtures of formamide with 1-butanol, 2-butanol, 1,3-butanediol and 1,4-butanediol at different temperatures: An ultrasonic and viscometric study. *Fluid Phase Equilibria* 265 (2008) 46–56

15th Physical Chemistry Conference



Thermodynamic study of molecular interactions in binary systems

k. mohamadian*^a and M.almasi^a

^a Department of Chemistry, Science and Research Branch, Islamic Azad University, Khouzestan, Iran

Email : kosarmohamadian@yahoo.com

m.almasi@khuzestan.srbiau.ac.ir

Abstract :

Densities indices of mixing of Form Amide with(C₃ - C₇)-alkan-2-ols, have been measured as a function of composition range at (*T*) 298.15 K and ambient pressure. Excess molar volumes V_m^E was calculated and correlated by the Redlich-Kister type function to derive the coefficients and estimate the standard error. For mixtures of Form Amide with alkan-2-ols V_m^E , is positive,in binary systems in All reng of composition.

Keywords : Form Amide, (C₃ - C₇)-alkan-2-ols, Redlich-Kister, Excess molar volume

Introduction:

Excess properties of mixtures provide information about the molecular interactions between the various components and can be used for the development of molecular models describing the thermodynamic behavior of mixtures [1– 2].

Methods:

The mixtures were prepared by weighing known masses of pure liquids in airtight, narrow-mouth ground stoppered bottles taking due precautions to minimize evaporation losses. All of the mass measurements were performed on an electronic balance (Mettler AE 163, Switzerland) accurate to 0.01 mg.

Results and Discussion:

The excess molar volumes V_m^E for the five binary systems were evaluated using the equation

$$V_m^E = \sum_{i=1}^N x_i M_i (\rho^{-1} - \rho_i^{-1}) \quad (1)$$

where ρ is the density of the mixture, ρ_i is the density of pure component i , x_i is the mole

fraction, M_i is the molar mass of component i , and N stands for the number of components in the mixture. V_m^E for the binary systems were fitted by the least-squares method to the

Redlich–Kister [3] equation:

$$V_{ij}^E = x_i x_j \sum_{k=0}^n A_k (x_i - x_j)^k \quad (2)$$

Experimental data and fitted equations for the five binary systems are depicted in Fig. 1.

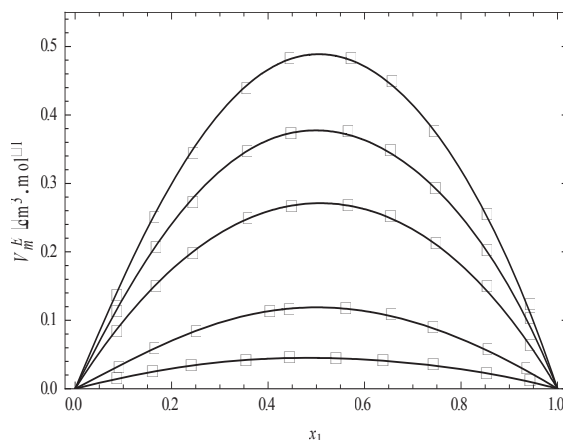


Fig. 1 Excess molar volumes at 298.15 K for the binary systems: (◆) 2-propanol+formamide, (Δ) formamide +2-butanol, (■) formamide+2-pentanol, (●) formamide + 2-hexanol, (□) formamide+2-heptanol

excess molar volumes are positive over the whole range of mole fractions. Positive values would indicate that molecular interactions between different molecules are weaker than interactions between molecules in the same pure liquid. In the mixtures attractive interactions between unlike species decrease and repulsive interactions predominate, leading to positive excess molar volumes.

Conclusions:

Densities and excess molar volumes V_m^E of binary mixtures of Formamide + ($C_3 - C_7$) alkan-2-ols were measured at 298.15 K. The measured data and calculated values of all systems are in good agreement.

References:



- [1] Iloukhani, H., Almasi, M.: Densities, viscosities, excess molar volumes, and refractive indices of acetonitrile and 2-alkanols: Experimental results and application of the Prigogine–Flory–Patterson theory. *Thermochim Acta.* **495**, 139–148(2009)
- [2] Almasi, M.; Iloukhani, H. Densities, Viscosities, and Refractive Indices of Binary Mixtures of Acetophenone and 2-Alkanols. *J. Chem. Eng.Data* **2010**, 55, 1416–1420.
- [3] Redlich, O., Kister, A.T.: Algebraic representation of thermodynamic properties and the classification of solutions. *Ind. Eng. Chem.* **40**, 345–348 (1948)

15th Physical Chemistry Conference



Kinetic Studies for Adsorption of Azure B Dye over Synthesized Fe-ZSM-5 and Co-ZSM-5 Nanozeolites

Mehdi Ghobakhlou^{a*}, Abdolraouf Samadi-Maybodi^a and Seyed Karim Hassani Nejad-Darzi^b

(a) Analytical Division, Faculty of Chemistry, University of Mazandaran, Babolsar, Iran, P.O.Box: 47416-95447. Tel/Fax: +98(112)5342350.

(b) Faculty of Basic Science, Babol University of Technology, Babol, Iran, P.O.Box: 47148-71167.

Keywords: Cu-ZSM-5, Fe-ZSM-5 nanozeolites, Azure B, Langmuir.

Introduction:

Many industries such as textile and printing use dyes and pigments and thus produce highly colored waste effluents. Disposal of these wastes into water causes environmental problems [1]. Various treatment processes such as physical separation, chemical oxidation and biological degradation have been widely investigated to remove dyes from wastewater [2]. Activated carbon has been the most widely used adsorbent; it suffers drawbacks of higher cost in production and regeneration [3]. Synthetic and natural zeolites are important alternatives as adsorbents due to their high ion-exchange and adsorption capacities as well as thermal and mechanical stabilities [4]. Modified nanozeolite with cobalt and iron has some ion exchangeable cations such as Cu^{2+} and Fe^{2+} in channels. Such cations give a high cation exchange capability to zeolite, hence it can be exchanged with organic and inorganic cations such as Azure B dye [5].

Materials and methods:

aluminumisopropoxide, TPAOH, NaOH, TetraethylorthoSilicat (TEOS), FeCl_3 , $\text{CuSO}_4 \cdot 5\text{H}_2\text{O}$ and double distilled water. The synthesized nanozeolites were calcinated in an electrical furnace at 550 °C for 5 h to remove of organic template. For investigation of adsorption experiments, 0.01 g of nanozeolite was mixed with 25 mL of the aqueous solutions of various initial concentrations of Azure B (AB). The flasks with their contents were shaken for the different adsorption times at the various temperatures and neutral pH. Also, the effect of



mixing rate and pH was studied. At the end of adsorption interval, the supernatant was centrifuged for 12 min at 15000 rpm.

Apparatus:

The Casagrande tool has been applied for determining the concentration of AB in the supernatant solution before and after the adsorption was determined with a 1.0 cm light path quartz cells using a Uv-Vis spectrophotometer (PG instrument Ltd-Model T90+) at a maximum wavelength (λ_{max}) of 548 nm.

Results and Discussion:

The pseudo-first order kinetic model has been widely used to predict the kinetics of dye adsorption. A linear form of pseudo-first order model was described by Lagergren [6]. where q_e and q_t are the adsorption capacities at equilibrium and at time t , respectively (mg g^{-1}); k_1 is the rate constant of pseudo-first order adsorption (L min^{-1}). Also, the pseudo-second order rate equation can be represented in the following form [7]. where the equilibrium adsorption capacity q_e , and the pseudo-second order constants k_2 (g(mg.min)^{-1}) can be determined experimentally from the slope and intercept of the plot t/q_t versus t . The pseudo-first order and pseudo-second order models were used for adsorption of AB onto Fe-ZSM-5 nanozeolite. Results specified that the kinetic data could not be matched with the pseudo-first order kinetic model.

Conclusion:

In this work, we introduce a method for synthesis of Fe-ZSM-5 and Cu-ZSM-5 nanozeolite. The synthesized nanozeolites were characterized by XRD, FT-IR, and SEM techniques. The efficiency adsorption of the modified nanozeolites were studied by investigation removal of Azure B from wastewaters using Uv-vis spectrophotometry method. Results indicated that the modified Fe-ZSM-5 and Cu-ZSM-5 nanozeolite can be utilized as a good adsorbent for Azure B. Application of modified ZSM-5 nanozeolite as an adsorbent was found to increase efficiency of Azure B adsorption as compared to the unmodified ZSM-5 nanozeolite. The Langmuir and Freundlich and adsorption isotherms models were applied to the adsorption data of AB onto Fe-ZSM-5 nanozeolite and modified Fe-ZSM-5 nanozeolite at 298. The



Langmuir isotherm was the best model to explain the experimental data. Temperature affected the adsorption capacity and kinetics as well as the equilibrium of the adsorption process. The adsorption kinetics of AB onto Fe-ZSM-5 nanozeolite is well described by a pseudosecond-order kinetic model.

Reference:

- [1] O. Ozdemir, B. Armagan, M. Turan, M. S. Celik, Dyes Pigm. 49-62,2004.
- [2] S. Wang, H. Li, S. Xie, S. Liu, L. Xu, Physical and chemical regeneration of zeolitic adsorbents for dye removal in wastewater treatment, Chemosphere. 65,82-87,2006.
- [3] S. B. Wang, Y. Boyjoo, A. Choueib, Z. H. Zhu, Removal of dyes from aqueous solution using fly ash and red mud Water Res. 39,129-138,2005.
- [4] S. M. Dal Bosco, R. S. Jimenez, W. A. Carvalho, Removal of toxic metals from wastewater by Brazilian natural J. Colloid Interface Sci. 281,424-431, 2005.
- [5] R. Han, Y. Wang, W. Zou, Y. Wang, J. Shi, Comparison of linear and nonlinear analysis in estimating the Thomas model parameters for methylene blue adsorption onto natural zeolite in fixed-bed column J. Hazard. Mater. 145,331-335,2007.
- [6] S. Lagergren, Handlingar. 24,1,1898.
- [7] F. Haghseresht, G. Lu, Energy Fuels. 12,1100,1998.



Mixed ionic surfactant system for stable suspension of multiwalled carbon nanotubes

S.javadian* and M.Sharifi.

Department of physical chemistry, tarbiat modares university.

Email: javadian_s@modares.ac.ir

Keywords: dispersion, carbon nanotube, surfactant.

Introduction:

Carbon nanotubes (CNT) and CNT materials have attracted widespread interest in research and increasing industrial attention. These materials have extraordinary conductivity that varies with length change¹. Carbon nanotubes have many applications in polymer industry² and water treatment³. Carbon nanotubes have high VanderWaals interaction energy that causes a strong bundling of carbon nanotubes. This high interaction force makes the dispersion stability a challenging task. Different ways have been examined to solve this problem. But using the surfactant is one of the chemical methods that does not impact on the nanotube properties. Herein, we investigated the dispersive effects achieved by surface-active agents on MWNTs. Dodecyl trimethyl ammonium bromide (DTAB) is a weak dispersive agent in below its critical micelle concentration (cmc). But when DTAB is mixed with sodium dodecyl sulfate (SDS), in high percent of DTAB, shows little dispersion and when the percent of SDS is higher than DTAB, due to synergism effect, shows good dispersion. We should note that there is limitation in choosing the percent of surfactants in mixture. Ionic surfactants make ion pairs in some percent and sediment.

Materials and methods:

Multiwalled carbon nanotubes were produced by Neutrino CO. the purity is >95Wt%. DTAB and SDS were purchased from MERK. To investigate the interaction of carbon nanotubes with mixture of surfactants, the following preparation steps were used. First, the aqueous solutions of mixed surfactants were prepared in distilled water at reach anionic and reach cationic area. Each area was prepared at concentrations from 5 to 35mM. 0.01mg powder of



carbon nanomaterial was added to the surfactant solutions. The resultant dispersions were mixed by continuous stirring with magnetic stirrer for approximately 6 h and each sample was sonicated for 100 min. Then all samples were centrifuged for 20 min at 10000rpm. To remove the big clusters and the supernatant was used for further studies. The final concentrations of CNTs in supernatant were determined from UV–VIS absorption spectra.

Apparatus:

Magnetic stirrer (ms-mp8) and ultrasonic cleaner set (WUC-D10H) were purchased from wised Co. balance (adventurer pro. AV264C) were purchased from OHAUS Co.

Result and discussion:

The UV_Vis spectrum of centrifuged solutions shows, by increasing the concentration of mixed surfactants, the dispersion of nanotube increases and we see the best synergism effect occur in 10% (DTAB/SDS). But beyond 15mM concentrations, we see Partial reduction in absorbance. According to former research, it seems we have phase transition in this region. Surfactants preferred to aggregate with each other, in cylinder like micelles. Then surfactants leave the nanotubes and dispersion decreases. As a result there is an optimum concentration for synergism effect.

Conclusion:

We have demonstrated that mixture of ionic surfactant in low concentrations, can disperse more carbon nanotubes, compared with pure surfactants at same concentration. Due to this research we can use surfactants in low concentrations to achieve acceptable dispersion of nanotubes.

Reference:

- [1] Naeemi, A.; Sarvari, R.; Meindl, J. D. *IEEE*. **2005**, 26, 2.
- [2] Jin, Zh.; Huang, L.; Goh, S. H.; Xu, G.; Ji, W. *Chem. Phys. Lett.* **2000**, 332, 461-466.
- [3] Bai, Y.; Park, I.S.; Lee, S. J.; Bae, T.S, Watari, F.; Uo, M.; Lee, M.H. *Carbon*. **2011**, 49, 3663–3671.

Determination of the optical constants Co(II) complex of Schiff base



N,N'-bis(2-hydroxy-4-methoxysalicylidene)- ethylenediamin by reflectance and transmittance spectra.

Maryamnegari Moradi, Simin

Department Of chemistry, ISLAMIC AZAD UNIVERSITY Yazd Branch

Email: maryamnegari@yahoo.com

Keywords: complex; Refractive index dispersion; Complex dielectric constant

Introduction:

Schiff bases are an important class of ligands in coordination chemistry and find extensive application in different fields. Schiff bases based on N,N'-bis(2-hydroxy-methoxysalicylidene)-ethylenediamin can be used to obtain optical materials and conducting polymers. Thus, new optical and organic conducting materials can be produced by these compounds.

Materials and methods:

1 mmole N,N'-bis(2-hydroxy-4-methoxysalicylidene)-ethylenediamin 0.384 gr and 1 mmole Co(NO)₃·6H₂O 0.2920 gr was added to MeOH in 20 ml. reaction was refluxed for 8 h and a precipitate was observed. The solid complex was washed with methanol and dried at room temperature. refluxed for 8 h and a precipitate was observed. The solid complex was washed with methanol and dried at room temperature. Complex was calculated from the transmittance and reflectance spectrum.

Result and discussion:

The refractive index is one of the major parameters in optical constants

The complex refractive index of the film can be expressed as

$$n = n + ik$$

where n and k are the real and imaginary parts of the refractive index. k is the extinction coefficient given by

$$k = \frac{\alpha \lambda}{4\pi}$$

The refractive index of the film can be obtained from the following relation

Using data obtained from the transmittance spectra

Refraction index of the complex can be analyzed by Cauchy equation. Cauchy equation is an empirical relationship between the index of refraction and wave length. We place the index and wave length data gained from complexes in Cauchy equation and calculate Cauchy coefficients including a, b, through fitting by Statistica software. The parameter A in the Cauchy equation has the physical meaning of the electronic refractive index at infinite wavelength [1].

$$n = a + \frac{b}{\lambda^2} + \frac{c}{\lambda^4}$$

The complex dielectric constant of

where ϵ_r is the real part and ϵ_i is the imaginary part of the dielectric constant. The real part and imaginary parts are described by [2]

$$\epsilon_r = n^2 - k^2 = \epsilon_r - \left[\frac{\omega_p^2 T^2}{(1 + \omega^2 T^2)} \right]$$

$$\epsilon_i = 2nk = \epsilon_i + \left[\frac{\omega_p^2 T^2}{\omega T (1 + \omega^2 T^2)} \right]$$

Conclusions:

Optical properties of metal complex thin film have been investigated by reflectance and transmittance spectra between 4000 and 400 cm⁻¹ at temperature room. The optical constants (refractive index n, extinction coefficient k, and dielectric Constant ϵ) of the thin film were calculated. The refractive index dispersion obeyed the Cauchy model and Cauchy parameters were determined from fitting data as $A=0.71$, $B=3 \times 10^{-7} \text{ cm}^{-2}$ at the spectra range of 1700–4000 cm⁻¹. The dielectric spectrum shows a Cole–Cole plot.

Reference:

- [1] F.A. Jenkins, H.E. White, Fundamentals of Optics, McGraw-Hill, New York, 1957.
- [2] A.K. Wolaton, T.S. Moss, Proc. R. Soc. 81 (1963) 5091.



15th Iranian Physical Chemistry Conference



Determination of the optical constants Pd(II) complex of Schiff base 6,6'-dimethoxy-2,2'-[hexane-1,6-diylbis(nitrilodimethylidyne)]diphenol by reflectance and transmittance spectra.

Maryamnegari Moradi, Simin

Department Of chemistry, ISLAMIC AZAD UNIVERSITY Yazd Branch

Email: maryamnegari@yahoo.com

Keywords: complex; Refractive index dispersion; Complex dielectric constant

introduction:

Schiff bases are an important class of ligands in coordination chemistry and find extensive application in different fields. Schiff bases based on 6,6'-dimethoxy-2,2'-[hexane-1,6-diylbis(nitrilodimethylidyne)]diphenol can be used to obtain optical materials and conducting polymers. Thus, new optical and organic conducting materials can be produced by these compounds.

Materials and methods:

1 mmole 6,6'-dimethoxy-2,2'-[hexane-1,6-diylbis(nitrilodimethylidyne)]diphenol 0.328 gr and 1 mmole PdCl₂ 0.0177 gr was added to MeOH in 20 ml. reaction was refluxed for 8 h and a precipitate was observed. The solid complex was washed with methanol and dried at room temperature. Complex was calculated from the transmittance and reflectance spectrum.

Result and discussion:

The refractive index is one of the major parameters in optical constants

The complex refractive index of the film can be expressed as

$$n = n + ik$$

where n and k are the real and imaginary parts of the refractive index. k is the extinction coefficient given by

$$k = \frac{\alpha \lambda}{4\pi}$$

The refractive index of the film can be obtained from the following relation

Using data obtained from the transmittance spectra

Refraction index of the complex can be $n = \left(\frac{1 + \sqrt{R}}{1 - \sqrt{R}} \right)$ analyzed by Cauchy equation. Cauchy equation is an empirical relationship between the index of refraction and wave length. We place the index and wave length data gained from complexes in Cauchy equation and calculate Cauchy coefficients including a, b, through fitting by Statistica software. The parameter A in the Cauchy equation has the physical meaning of the electronic refractive index at infinite wavelength[1].

$$n = a + \frac{b}{\lambda^2} + \frac{c}{\lambda^4}$$

The complex dielectric constant of

where ϵ_r is the real part and ϵ_i is $\hat{\epsilon} = \epsilon_r + \epsilon_i$ the imaginary part of the dielectric constant. The real part and imaginary parts are described by[2]

$$\epsilon_r = n^2 - k^2 = \epsilon_r - \left[\frac{\omega_p^2 T^2}{(1 + \omega^2 T^2)} \right]$$
$$\epsilon_i = 2nk = \epsilon_i + \left[\frac{\omega_p^2 T^2}{\omega T (1 + \omega^2 T^2)} \right]$$

Conclusions:

Optical properties of metal complex thin film have been investigated by reflectance and transmittance spectra between 4000 and 400 cm⁻¹ at temperature room. The optical constants (refractive index n, extinction coefficient k, and dielectric Constant ϵ) of the thin film were calculated. The refractive index dispersion obeyed the Cauchy model and Cauchy parameters were determined from fitting data as $A=0.33$, $B=0.88 \times 10^{-7} \text{ cm}^{-2}$ at the spectra range of 1700–4000 cm⁻¹. The dielectric spectrum shows a Cole–Cole plot.

Reference:

- [1] F.A. Jenkins, H.E. White, Fundamentals of Optics, McGraw-Hill, New York, 1957.
- [2] A.K. Wolaton, T.S. Moss, Proc. R. Soc. 81 (1963) 5091.



Viscometry and Spectral Investigation on Interaction of Cu(II)Salen Complex and Bovine Serum Albumin: A Thermodynamic approach

E. Babaei-Tari^{*a}, N. Rasouli^b, N. Sohrabi^a

^{*a} Exir Pharmaceutical Company, Boroujerd, IRAN

^{b,a} Assistant Professor, Department of Chemistry, Payame Noor University, PO BOX 13395-3697, Tehran, IRAN

Email: babaei@exir.co.ir

Keyword: Metallosalen, Cu(II)Salen, Bovine serum albumin(BSA), Binding isotherm.

Introduction:

In recent years, metal complexes with salen ligands derived from the condensation of salicylaldehyde with a diamine, have been widely studied [1]. Many compounds expose their antitumor activity through binding to DNA and can cause DNA damage in cancer cells by blocking the division of cancer cells and resulting in cell death [2]. Serum albumin is the most abundant protein in the circulatory system of a wide variety of organisms and plays an important role in the transport and deposition of many drugs. Thus, an understanding of the features of drug interactions with albumin can provide insights into chemo therapy and drug design. Bovine serum albumin (BSA) is usually employed as a model protein because of its low cost and availability and because it is structurally homologous with human serum albumin[3]. In this work the interaction of Cu(II)Salen with BSA was studied using UV/Vis spectroscopic method.

Materials and methods:

BSA was obtained from Sigma Chemical Co. Cu(II)Salen synthesized in laboratory and all of the other materials used were of analytical grade from Merck Co. Differential absorption titration experiments were carried out in different Cu(II)Salen concentrations and BSA constant concentration in ethanol and 5 mM phosphate buffer, pH=7.

Apparatus:

Experiments were carried out by a Perkin Elmer Lambda 25 UV/Vis spectrophotometer equipped with thermal bath. Viscosity of solution measured by Viscometer DV-II+Pro Model Brookfield.

Result and discussion:

At first the physicochemical properties of Cu(salen) was studied in various temperatures and concentrations. Then interaction of Cu(II)Salen complex with bovine serum albumin (BSA) in 5 mM phosphate buffer, pH=7 was studied by differential UV/Vis spectroscopy method at different temperature and then the binding isotherm, binding capacity and scatchard graphs were plotted. To obtain approximated values of binding parameters, it might be possible to fit the binding data to Hill equation (1) [4].

$$\log \left(\frac{v}{n-v} \right) = \log K_b + n_H \log [L] \quad (1)$$

Where v as a average number of bound ligands to one macromolecule of BSA, $[L]_f$ is the free ligand concentration, n , K_b and n_H are the number of binding sites, binding constant and Hill coefficient. The thermodynamic parameters such as ΔG_b , ΔH_b , ΔS_b was calculated by analyzing the UV/Vis data with a simple binding model (Table 1). The viscosity of BSA in the absence and presence of Cu(II)Salen was measured.

Table 1: Thermodynamic parameters of binding at different temperature in 5 mM phosphate buffer, pH 7.0

T(°K)	n_H	$\ln K_b$	ΔH_b° (KJ/mol)	ΔG_b° (KJ/mol)	ΔS_b° (J/mol)
298	2.96	9.81	178.58±6.61	-24.32±0.9	680.53±25.18
303	2.90	11.12	178.58±6.61	-28.03±1.04	681.54±25.22
308	2.89	12.27	178.58±6.61	-31.43±1.16	681.52±25.22
313	2.84	13.42	178.58±6.61	-34.94±1.29	681.85±25.23
318	2.64	14.32	178.58±6.61	-37.88±1.40	680.37±25.17

Conclusion:

The positive values of n_H indicates that BSA has one set binding site and positive cooperative. The degree of binding of between Cu(II)Salen and BSA raises with increasing temperature. Because of Positive enthalpy of binding and regard to positive changes of entropy the interaction between Cu(II)Salen and BSA is hydrophobic and prevailing force



will be entropy. The increasing of viscosity of BSA upon addition of Cu(II)Salen concentration represents the stable interaction between BSA and Cu(II)Salen .

References:

- [1] Abdul hakim. A. Ahmed., Salima. A. BenGuzzi, Synthesis And Characterization of Some Transition Metals Complexes of Schiff Base Derived From Benzidine and Acetylacetone, J. Sci. appl. 2, 1, 83-90, 2008.
- [2] N.Raman, S.Sobha, M.Selvaganapathy, Probing the DNA Binding Mode of Transition Metal Based Biologically Active Compounds: Validation by Spectroscopic Methods., Int. J. Pharma. Bio Sci., 3, 1, 251-268, 2012.
- [3] N. Wang, L. Ye, B.Q. Zhao, J.X. Yu, Spectroscopic studies on the interaction of efonidipine with bovine serum albumin, Braz. J. Med. Biol. Res. 41,7, 589-595, 2008.
- [4] M. R. Housaindokht, A. A. Moosavi-Movahedi, Determination of binding affinities of glucose oxidase for sodium n-dodecyl sulfate, Int. J. Biol. Macromol., 16(2), 77-80, (1994).



The study of electronic structure of some organic nanoconductors

NargesBagheri^{a*}, ParisaKoukabi^a and Mehdi Kheirmand^b

^aDepartment of Chemistry, Islamic Azad University, Firoozabad Branch, Firoozabad, Fars, Iran

^b Assistant Prof. of chemistry, Yasouj University

E-mail: parisakoukabi@yahoo.com

Keywords: conductive polymer, electronic structure, Natural band orbital

Introduction:

Many researchers are investigate about the nano conductive polymers. In this research, we were optimized structure of some conductive polymer and then influence of the molecular size and any physical properties effect on conductivity of them were evaluated.

The nano polymer molecules that have duplex or triplet conjugated band are conductive. Whatever the polymers chain when get highest the conductivity of a polymer is major. In this work ,after optimize the structure of the polymer we were calculate the distance between HOMO and LUMO or computation the HOMO-LUMO gap, then compare the out come with each other to know which polymer are conductive than the other.

In this article we were assist to the correlation between molecular structure and tendency of decreasing the HLg, but not to the numerus of the calculation.[1,2]

Materials and methods:

We were use C₂ to C₁₀ conjugated polyethylene, poly benzene, poly vinyl benzene and poly phoran. In this work we were optimized at HF/6-31+G* level of theory using Gussian 03 software package. The Electronic Structure, HOMO-LUMO Energies, Occupancy and Charge Transfer wereevaluated.

Apparatus:

The basic tool has been applied for consequent better Gussian2003 software to get the better out put. At first we were draw the molecule with Portable-Hyper Chem ,then optimize it after

that get it to the Gauss View software for prepare it for out put and Gaussian 03 get us the result.

Result and discussion:

1. when the length of the nano conductive polymer are increasing the HLG decrease.
2. By increasing the length of the nano conductive polymer the Occupancy are decrease.
3. With increasing the duple band of the nano conductive polymer the Charge Transfer are increasing too.

Conclusion:

Results showed that by increasing the polymer chain, electronic conductivity increased and HOMO-LUMO gap decreased. The natural bond orbitals are also adopted as building blocks of the conductive polymers whose intramolecular charge transfers are studied. (figure1)

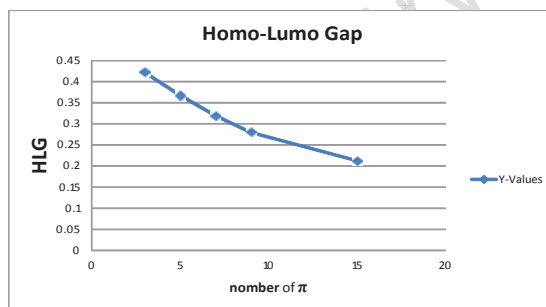


Figure 1: survey of HLG respect to increasing the double band in nano conductive polymer that branch of benzene monomer.

Refrence:

- [1]. H. Tran, N. Ian, M. Julio, D. Arcy, H. Tsang, Y. Wang, R. Benjamin, Mattes and Richard B, *Macromolecules*, 2008, 41, 7405.
- [2]. M. Ginic-Markovic, G. Janis, Matisons., R. Cervini, P. George, Simon and Peter M, *Chem. Mater*, 2006, 18, 6258.



Activity coefficients of major ions in Lake Urmia brine at different temperatures

Dr.N.Heidari^a, S.Panahi^{a*}, S.Faridvand^b, L.Golshani^b

^a Department of chemistry, Faculty of sciences, Urmia university, Urmia, Iran

^b Department of chemistry, Faculty of science, Payam nour university, Urmia, Iran

Email: sepidehpanahi64@yahoo.com

Key words: Activity coefficients, Pitzer equations, Electrolyte, Lake Urmia brine.

Introduction:

Lake Urmia in the northwestern corner of Iran is one of the largest permanent hypersaline lakes in the world and is a terminal lake meaning that water leaves the lake only by evaporation. As is generally the case, this leads to a saltwater body and in the case of Lake Urmia, salinity is quite high. The lake has dramatically decreased in volume over the past decade-and-a-half, further concentrating salts in the lake, raising salinity to more than 300 g/L. The main cations in the lake water include Na^+ , K^+ , Ca^{2+} , Li^+ and Mg^{2+} , while Cl^- , SO_4^{2-} , HCO_3^- are the main anions. The Na^+ and Cl^- concentration is roughly 4 times the concentration of natural seawater. Sodium ions are at slightly higher concentration in the south compared to the north of the lake, which could result from the shallower depth in the south, and a higher net evaporation rate. Conventional single ion activity coefficients of major ions in Lake Urmia brine have been estimated using Pitzer's thermodynamic treatment of mixed electrolyte solutions. It has been shown that Pitzer's equations are applicable to such natural concentrated brines. The system of equations developed by Pitzer for conventional single ion activity coefficients makes it possible to extend the specific ionic interaction model over a range of solution compositions, temperatures and pressures. It is known that one of the principal thermodynamic properties for the prediction of mineral solubilities in brines is activity coefficients. The number of possible neutral species in natural brines is much larger than the number of single ions. Therefore it is convenient for such complex mixtures to calculate the conventional single ion activity coefficients, because these values can then be combined to obtain the activity coefficient for any neutral species represented in brines. The



purpose of this paper is to study the conventional single ion activity coefficients of major ions in the Lake Urmia brine body under different temperatures.

Materials and methods:

The system of equations developed by Pitzer was used in calculating the ionic activity coefficients in solutions of high concentrations and different temperatures. The use of Pitzer model in much more concentrated solutions than seawater has been illustrated by Pitzer and Kim (1974), Downes and Pitzer (1976) and Harvie and Weare (1980). Therefore, we decided to use the Pitzer model for the estimation of conventional single ion activity coefficients of major ions in Lake Urmia brine, with total salt content more than 10 times that of ordinary seawater.

Result and discussion:

Pitzer equations give a good account of the properties of the major brine components. The knowledge of single ion activity coefficients in natural brines at different temperatures enables us to examine some aspects of mineral solubility at different temperatures like gypsum solubility.

The results of the calculations of the activity coefficients of Lake Urmia brine show that Lake Urmia brine is oversaturated with respect to salts and the degree of oversaturation has been increasing very significantly during the last years.

Reference:

- [1] Pitzer, K.S. and Kim, J.J., 1974. Thermodynamics of electrolytes. IV. Activity and osmotic coefficients for mixed electrolytes. *J. Am. Chem. Soc.* 96: 5701-5707.
- [2] Downes, C.J. and Pitzer, K.S., 1976. Thermodynamics of electrolytes. Binary mixtures formed from aqueous NaCl, Na₂SO₄, CuCl₂ and CuSO₄ at 25 °C. *J. Solut. Chem.*, 5: 389-398
- [3] Harvie, C.E. and Weare, J.H., 1980. The prediction of mineral solubilities in natural waters: the Na-K-Mg-Ca--Cl-SO₄ -H₂O system from zero to high concentration at 25°C. *Geochim. Cosmochim. Acta*, 44: 981-997.



The apparent heat capacity and enthalpy of lake Urmia brine in different temperatures by using Pitzer equations

S.Faridvand^{b*}, Dr.N.Heidari^a, L.Golshani^b, S.Panahi^a

^a Department of chemistry, Faculty of sciences, Urmia university, Urmia, Iran

^b Department of chemistry, Faculty of science, Payam nour university, Urmia, Iran

Email: sfaridvand@yahoo.com

Key words: Enthalpy, Heat capacity, Pitzer equations, Urmia brine.

Introduction:

Lake Urmia (or Ormiyeh) is one of the largest hypersaline lakes in the world. Urmia Lake, located in northwestern Iran, with a total surface area between 4750 and 6100 km² and a maximum depth of 16 m at an altitude of 1250 m. The main cations in the lake water include Na⁺, K⁺, Ca⁺², Li⁺ and Mg⁺², while Cl⁻, SO₄⁻², HCO₃⁻ are the main anions. The Na⁺ and Cl⁻ concentration is roughly 4 times the concentration of natural seawater. Sodium ions are at slightly higher concentration in the south compared to the north of the lake, which could result from the shallower depth in the south, and a higher net evaporation rate.

The thermochemical properties (osmotic coefficient, enthalpy and heat capacity) of saline water from 5 to 35°C have been calculated by Pitzer equations. In earlier studies, the thermochemical properties of saline water have been examined using an extended Debye–Huckel equation, which was an extension of the equation as formulated by Lewis and Randall. More recently, the PVT properties have been calculated by Pitzer equations. In this paper, we have calculated the thermochemical properties of Urmia lake (heat capacity, enthalpy) to these equations.

Materials and methods:

Apparent heat capacity (ϕC_p) and relative enthalpy (ϕL) have been calculated by using these equations of the form

$${}^{\circ}C_p - \bar{C}_p^0 = A_j \{ I / (1.2m) \} \ln(1 + 1.2I^{0.5}) + 2RTm(B^J + mC^J)$$



$${}^{\phi}L = (A_H I / 1.2m) \ln(1 + 1.2I^{0.5}) - 2RTm(B^L + mC^L)$$

Where I is the ionic strength, m is the molality of brine ($m = \sum m_i$, i is an ion); A_X ($X = \phi, J$ and H) is the Debye–Huckel slope, and \bar{C}_p^0 is the apparent molal heat capacity of brine and B^X and C^X are Pitzer parameters.

Result and discussion:

The results of this study will give reliable estimates of the thermodynamic properties of saline waters, rivers, lakes and seawater brines. The results at high temperatures may also be useful in studies of hydrothermal waters in the ocean. These calculations used in establishing the thermodynamic equilibrium of the Urmia Lake and we can consider that the degree of oversaturation has been increasing very significantly during the last years so we can present some procedures to prevent these problems.

Reference:

- [1] Ananthaswamy, J., Atkinson, G., 1984. Thermodynamics of concentrated electrolyte mixtures: 4. Pitzer–Debye–Huckel limiting slopes for water from 0 to 100 °C and from 1 atm to 1 k bar. *Journal of Chemical and Engineering Data* 29, 81–87.
- [2] Bromley, L.A., 1968a. Heat capacities of sea water solutions: partial and apparent values for salts and water. *Journal of Chemical and Engineering Data* 13, 60–62.
- [3] Bromley, L.A., 1968b. Relative enthalpies of sea salt solutions at 25 °C. *Journal of Chemical and Engineering Data* 13, 399–402.



Decolorization and degradation of Reactive Orange7 pollutant by using ozonation method

Jalal Basiriparsa^{*}, Zohreh Meratifashi

Department of applied chemistry, Bu-Ali sina university, Hamedan, Iran

Key words: Ozone, Degradation, Reactive Orange7, pollutant, RSM

Introduction:

Large amounts of chemically various dyes are used for several industrial application. Due to environmental implications, new technologies have been evaluated for degradation of these compounds in textile effluents. Some studies suggest employing advanced oxidative processes (AOPs) in isolation or combined for preliminary assessment.

AOPs have been defined as the aqueous phase chemical oxidation of target organic or inorganic pollutants by a process involving hydroxyl free radicals.

Ozone (O₃) is one of the strongest oxidants used for disinfection, sterilization, green oxidation of pollutants, water and waste treatment, wood pulp bleaching, and chemical synthesis. The extending of application is attributed to oxidizing properties of O₃. Ozone provides green oxidation since decomposition of ozone leads to environmentally friendly products (O₂).

In general ozone oxidation path ways include direct oxidation by ozone or indirect oxidation by hydroxyl radical (OH).

Using ozonation for decolorizing wastewater has the following advantages: 1) ozone is readily available, soluble in water and easily monitored; 2) it dose not increase the volume of wastewater and sludge; 3) leaving no by product that need to be retreated.

Experimental (material and method):

An azo dye RO7, was selected as model solution, which was commercial dye and used without further purification. This azo dye was provided by alavan sabet company (Hamedan). Other chemicals, purchased from Merck, were of analytical grade. All solutions were prepared by using deionized water.



Ozone gas produced from air by ozone generator (Onnic.ES215A). In all experiments, the samples of RO7 was taken periodically from the reactor and analyzed by the UV-visible spectrophotometer (JASCO. v- 630) via the decrease in absorbance at 480 (nm). COD measurements were also carried out to investigate the mineralization of the solution, according to a close reflux, colorimetric method using a HACH DR 2800 spectrophotometer.

Results and discussion:

Response surface methodology (RSM) was employed for experimental design, modeling and parameter optimization. Accordingly reduced quadratic model was developed to give the substrate color removal efficiency percentage, (CE%) as function of effective parameters such as: initial pollutant concentration and initial pH of the solution.

Maximum color removal efficiency was achieved at the obtained conditions of: initial dye concentration 60 ppm and pH=7.75. Under these conditions, process achieved about 94.97% color removal after 20 minute.

In optimum conditions, chemical oxygen demand (COD) was investigated and COD reduced to 32% after 90 minute.

Maximum efficiency in the process was obtained approximately in natural pH, due to in such condition better ozone solubility can be occurred in solution. In addition presence of hydroxyl radical in solution can facility oxidation of organic pollutant effectively.

Conclusions:

Ozonation method was used to remove color from dye solutions containing C.I Reactive Orange7. The effect of operation parameters on color removal efficiency was investigated and optimized by using RSM. The removal of efficiency of RO7 and COD of the aqueous solution in pH=7.75 and initial dye concentration 60ppm, were 94.97 and 32 respectively.

Reference:

[1] E. J. Rosen feldt and etal. Comparision of the efficiency of OH radical formation during ozonation and the advanced oxidation processes O_3/H_2O_2 and UV/H_2O_2 , water research, 40, 3695-3704, (2006).



- [2] H. Kusic and etal. Mineralization of organic pollutant content in aqueous solution by means of AOPs: UV and ozone-based technologies, *Chemical Engineering Journal*, 123, 127-137 (2006).
- [3] A. R. Tehrani Bagha and etal. Degradation of persistent organic dye from colored textile wastewater by ozonation, *desalination*, 260, 34-38, (2010)

15th Physical Chemistry Conference



(Liquid + Liquid) Equilibria for (Water + Acetic acid + Xylene or M-xylene or O- xylene or P- xylene): Experimental Data and Prediction

Kh. Bahrpaima ^{*a}, S. H. Sajjadi ^a

^a Department of Chemistry, Firoozabad Branch, Islamic Azad University, Firoozabad, Iran

E-mail: hadi_sajjadi64@yahoo.com

Key words: Liquid extraction; Phase equilibria; Ternary system; UNIQUAC model

Introduction:

Phase equilibrium data of ternary systems are very important for simulation, design and optimize of separation operations. A large amount of investigation has been carried out in recent years on the LLE measurements of ternary systems, in order to understand and provide further information about the phase behavior of such systems [1–4]. Since, the liquid extraction of acetic acid from aqueous solution is industrially and scientifically important, the precise LLE data of a liquid mixture composed of (water + acetic acid + organic solvent) are required. In this work, we extend our studies by using isomers of xylene (m- xylene , o- xylene and p- xylene) to extract of acetic acid for the ternary mixtures of {water + acetic acid + xylene, m- xylene, o- xylene or p- xylene) were obtained at 298.15 K and ambient pressure.

Materials:

The chemicals acetic acid (99.9%) xylene, m- xylene, o- xylene and p-xylene (99.5%) were obtained from Merck and were used without further purification. Deionized and redistilled water was used throughout all experiments.

Methods and Apparatus:

The equilibrium data were determined using an experimental apparatus of a 250 ml glass cell where the temperature of the apparatus controlled by a water jacket and maintained with an uncertainty of within ± 0.1 K.

The mixture was vigorously agitated by a magnetic stirrer for 4 h. The prepared mixtures were then left to settle for 4 h for phase separation.



The samples of both phases were collected and the tie line values were obtained by titration of the samples with a known concentration NaOH aqueous solution.

The binodal curve values were determined by means of the cloud point method. A known composition, homogeneous and transparent (acetic acid + water) was prepared in a glass equilibrium cell at constant temperature. Then solvent (isomer of xylene) was progressively added to the mixture using a micro-burette. The cloud point was determined by observing the transition from a homogeneous to a heterogeneous mixture as indicated by the mixture turbidity.

Result and discussion:

The experimental LLE data for (water + acetic acid + isomer of xylene) at temperature of (298.2) K, are presented. Experimental LLE data of this work were analyzed and predicted using UNIQUAC model. In general, the LLE data of these ternary systems predicted well with this equilibrium model. The average RMSD value between the observed and calculated mass percent obtained.

Conclusion:

LLE data of the ternary system {water + acetic acid + isomer of xylene} were presented at 298.15 K. It can be concluded that xylene, m- xylene, o- xylene and p- xylene with high separation factor, very low solubility in water, low cost, high boiling point may be adequate solvents to extract acetic acid from its dilute aqueous solutions.

References:

- [1] A. Arce et al; J. Chem. Thermodyn.; 33 139–146, 2001.
- [2] H. Higashiuchi et al; Fluid Phase Equilibr.; 110, 197–204, 1995.
- [3] E. Ince et al; J. Chem. Thermodyn.; 35, 1671–1679, 2003.
- [4] J. M. Correa et al; J. Chem. Eng. Data; 34, 415, 1989.



Using artificial neural network to predict the specific volume of polymeric High temperature and high pressure density prediction of hydrocarbons using artificial neural network method

Majid Moosavi*, Nima Soltani

Dept. of Chemistry, Faculty of Sciences, University of Isfahan, Isfahan 81746-73441, Iran

Email: m.mousavi@sci.ui.ac.ir

Keywords: Hydrocarbon, ANN, Group contribution method (GCM), Molar density.

Introduction:

The volumetric properties of hydrocarbons are of particular interest in connection with the production and refining of petroleum. Density prediction of hydrocarbons at extreme temperature and pressure conditions are most relevant to petroleum engineering studies of ultra-deep reservoirs [1]. An artificial neural network (ANN) can be a suitable alternative to model the different thermodynamic properties. ANN is an especially efficient algorithm to approximate any function with a finite number of discontinuities by learning the relationships between the input and output vectors [2]. Thus, an ANN is an appropriate technique to model the nonlinear behavior of chemical properties.

The neural network used:

Many models of neural networks have been used to estimate of thermodynamic properties [3,4]. In this work a feedforward backpropagation neural network was used, which is one that is very effective in representing nonlinear relationships among variables. In this study, Densities of hydrocarbon systems have been estimated using a combined method that includes an artificial neural network and a simple group contribution method. A total of 2891 data points of density at several temperatures and pressures, corresponding to 40 different hydrocarbons including short- and long-chain alkanes ranging from CH₄ to n-C₄₀H₈₂, and also several cycloalkanes, highly branched alkanes and aromatic hydrocarbons have been used to train, validate and test the ANN model using the Matlab software. Temperature (T),

pressure (P), molecular mass (M), and the structural groups that form the molecules were given as input variables. The output parameter is ρ .

Results and discussion:

Table 1 shows the overall minimum, maximum, and the average deviations for the calculated liquid density for the hydrocarbon systems using the proposed network 12-21-1. Fig. 1 shows a comparison between experimental and calculated values of liquid density of hydrocarbons during training and during prediction. The study shows that the chosen artificial neural network and the group contribution method represent an excellent alternative for the estimation of densities of hydrocarbon systems with acceptable accuracy.

Table 1. Overall minimum, maximum, and average deviations for the calculated liquid density for the hydrocarbon systems using Artificial Neural Network model.

ANN model	Training set	Prediction set	Validation set	Total set
Experimental data				
No. of data point	2168	434	289	2891
Deviations				
AAD _{min} %	0.0005	0.0011	0.0006	0.0005
AAD _{max} %	9.8326	10.0877	4.4433	10.877
Bias	-0.0149	0.0779	0.0420	0.0047
AAD	0.3005	0.3902	0.3376	0.3177
RMSD	0.6182	0.8885	0.6106	0.6651
No.AAD<5%	2163	431	289	2883
No.AAD>10%	0	1	0	1

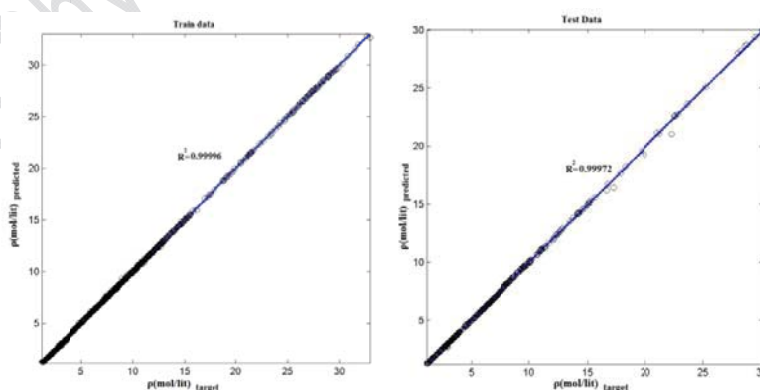


Fig. 1. Comparison between experimental and calculated values of liquid density of hydrocarbons: (a) during training and (b) during prediction.



Conclusion:

An ANN with (12-21-1) structure was designed to predict the density of different kinds of hydrocarbon systems. Total number of experimental data used to design the stated network is 2891, of which 75% were randomly chosen to train the network, 10% for validation, and 15% to test it. The average relative deviations for train, validation, and test sets are 0.30, 0.34, and 0.39, respectively.

References:

- [1] M.T. Hagan, H.B. Demuth, M. Beal, Neural Network Design, PWS Co. Boston, U.S.A., 1996.
- [2] K. Liu, et al. J. of Supercritical Fluids 55, 701–711, 2010.
- [3] G. Espinosa, et al. Ind. Eng. Chem. Res., 40, 2757-2766, 2001.
- [4] D. Yaffe, Y. Cohen, J. Chem. Inf. Comput. Sci., 41, 463-477, 2001.



Physicochemical evaluation of Microemulsion formulations for Water+Ipm+Tween 80+Isobutanol Pseudo-ternary System

S. Najafabadifarahani^{a*}, A. Salabat^a

^aDepartment of Chemistry, University of Arak, Arak, Iran, P. O. Box 38156 – 879

E-mail: najafabadyfarahany@gmail.com

Key words: Microemulsion, Pseudo-ternary ,phase diagram, Physicochemical properties.

Introduction:

Microemulsions are clear, thermodynamically stable solution mixtures of at least three components, namely, two immiscible solvents and a surfactant. The three basic types of Microemulsions are direct (oil dispersed in water, o/w), reversed (water dispersed in oil, w/o) and bicontinuous structure [1]. The Microemulsion region is usually characterized by constructing ternary-phase diagrams. To construct a pharmaceutically accepted Microemulsion system it is important to know its physicochemical properties. For the selection of components of a biocompatible Microemulsion system, The changes in the internal structure of a Microemulsion can be monitored by analyzing some physicochemical properties such as conductivity, viscosity, density, PH, Refractive Index [2]. The aim of this study is Physicochemical evaluation of Microemulsion formulations.

Experimental Section:

A Microemulsion system comprising Ipm as an oil, a non ionic surfactant Tween 80, alkanol cosurfactant (Isobutanol) and water was selected. The pseudo-ternary phase diagram has been delineated for the chosen system at a constant surfactant: cosurfactant mass ratio of 2.4:1 (Fig.1.a). The gradual compositions A–F were selected for further investigations. Ipm and water were first mixed with Tween 80 and then Isobutanol was added to the mixture at 298.15 K to obtain the desired Microemulsion compositions. The changes in the samples were observed visually everyday for 1 month. Transparent, single phase mixtures were designated as Microemulsions. pH of all the six selected Microemulsions (A-F) determined at constant temperature. The electric conductivity (σ) was measured by means of digital conductivity meter with precision of $\pm 10^{-3}$ μ S. Densities (model DE51) and refractive index

(model RE50) were measured with precision of $\pm 2 \times 10^{-5} \text{ g.cm}^{-3}$ and $\pm 10^{-5}$, respectively. Viscosity was measured by Brookfield DV viscometer (model LVDV-II+).

Result and discussion:

The variation of dynamic viscosity, conductivity, refractive index and density with water content of oil-surfactant/co-surfactant mixture has been shown in (Fig.1.b). The rapid change in the physicochemical properties such as viscosity, conductivity, refractive index and density is probably due to the change in the microstructure of the Microemulsion system. The change in the internal structure could be due to either the change in the shape of droplets or may be due to the transition from w/o to bicontinuous Microemulsion. The transition point of viscosity, conductivity and density plots occurs at 25-30 % weight percent of aqueous phase and confirms the presence of percolative behavior.

Conclusion:

Physico-chemical analyses of the Microemulsion system show the structural transition from w/o to o/w via bicontinuous phase at 25-30 water weight percent (Fig1-b).

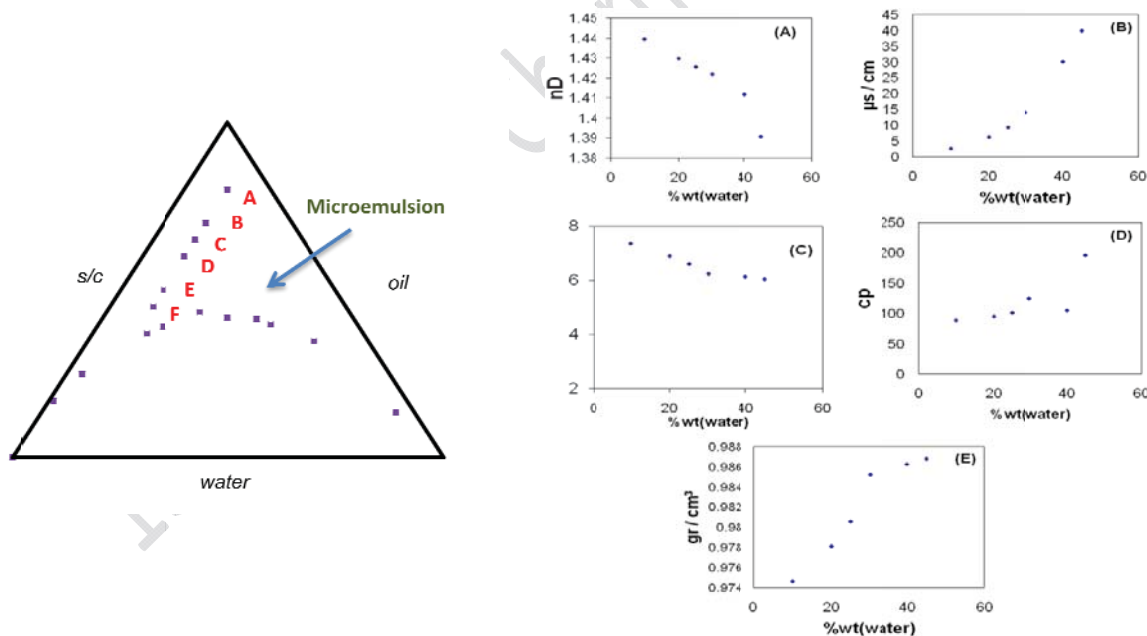


Fig.1. a) pseudo-ternary phase diagram for IPM ,Tween 80/Isobutanol ratio of 2.4:1,water; b) variation of dynamic refractive index (A),conductivity(B), PH(C)viscosity(D) and density (E)

Reference:



- [1] P. Kumar and K. L. Mital. Handbook of Microemulsion: science and technology, Marcel Dekker, New York, 1999.
- [2] K. E. Bennett, J. C. Hatfield, H. T. Davis, C. W. Macosko, and L. E. Seriven. Viscosity and conductivity of Microemulsions. In: Robb, I. D. (ed.), Microemulsions, Plenum, New York, pp 65–84(19)

15th Physical Chemistry Conference



Investigation of Protein Albumin Partitioning in Aqueous Two-Phase Systems Containing Polyethylene Glycol and Inorganic Salts

A. Salabat^b, F. Sobbuhi^{a*}

^{a,b} Chemistry Department, Arak University, P.O. Box 38156-879, Arak, Iran

Email: F_Sobbuhi@yahoo.com

Key words : Aqueous two-phase system; Liquid-Liquid equilibria; Sodium sulfate.

Introduction:

Aqueous two-phase systems (ATPS) have been utilized very extensively in many different industries such as biotechnology, petroleum, paint, adhesives and pharmaceuticals ones. In particular, ATPS have attracted considerable attention in relation to the large-scale recovery and purification of bioproducts. ATPS usually can be made from aqueous solutions of two water-soluble polymers or a polymer and a salt. The most common ATPS used for the separation of biomolecules are polyethylene glycol (PEG)/ dextran or PEG/salt systems. The salt-polymer-water systems have some advantages such as low viscosity and low cost compared to polymer-polymer-water systems[1-2]. In continuation of our previous works, in this research, the partitioning behavior of Albumin protein in the aqueous two-phase system of PEG 6000 and $MgSO_4$, Na_2SO_4 , $(NH_4)_2SO_4$ at 298.15 K has been studied. The effect of the salts on the partitioning coefficient determined of the protein was determined.

Experimental Section:

Polyethylene glycol, of molecular weight 6000 $g \cdot mol^{-1}$, magnesium sulfate heptahydrate (GR, min 99.5%), ammonium sulfate (GR, min 99.5%) and sodium sulfate (GR, min 99%) were obtained from Merck. Albumin bovin serum were obtained from Acros. All chemicals were used without further purification.

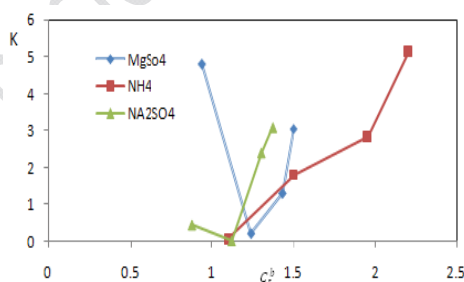
Aqueous two-phase systems were prepared from solid PEG and different salts containing magnesium sulfate, sodium sulfate, or ammonium sulfate and albumin protein in pure water. The total weight of these components for each sample was about 10 g. The initial amounts of the protein were 0.01 g. The mixtures were shaken for about 2 h and then placed in a

thermostatic water bath at 298.15 K for at least 24 h to ensure complete equilibration, as indicated by the absence of turbidity in each phase. After equilibrium of the systems, the samples of the upper and lower phase were taken out carefully for analysis using syringes. The liquid-liquid equilibrium data from our previous work[3]. was used for the preparation of the samples. Therefore, the concentration of the PEG and salts are known for any selected tie lines. The protein concentration were determined by a single beam UV visible spectrophotometer at 278.5 nm for lower phase and at 311 nm for upper phase.

Result and discussion:

The results showed that, when concentration of the salts in lower phase is about 1.1 M, The hydrophilic sites of protein were quite available. This result caused that protein retention be more in aqueous phase. At lower concentration of this value, for both magnesium sulfate, sodium sulfate, and more than this value for all salts, helix of protein are formed in such away that rotation of hydrophilic chain to the inner helix structure and hydrophobic parts to the outer of structure. So at concentration of about 1.1 M salts, salt effect caused protein removed from aqueous phase to organic phase (Salting- out effect). The experimental partition coefficient data were correlated to the modified virial- type model :

$$\frac{1000}{n_w M_w} \frac{G^E}{RT} = \sum_i \sum_j A_{ij} m_i m_j - \frac{4A_{yI}}{b} \ln(1 + b\sqrt{I})$$



Reference:

- [1] Zaslavsky, A.; Gulyaeva, N.; Zaslavsky, B. Partitioning behavior of amino acids in aqueous two-phase systems containing polyethylene glycol and phosphate buffer. J. Chromatogr. B 2000, 743, 271-279.
- [2] Eiteman, M.A.; Gainer, J. L. A correlation for predicting partition coefficients in aqueous two phase systems. Sep. Sci. Technol. 1992, 27, 313-324.



- [3] Salabat, A. Influence of salt on phase composition in aqueous two-phase systems: Experiment and Prediction. *Fluid Phase Equilib.* 2001, 187, 489-498.

15th Physical Chemistry Conference



Solubility product of salts in Lake Urmia brine at different temperatures

Dr.N.Heidari^a, L.Golshani^{b*}, S.Faridvand^b, S.Panahi^a

^a Department of chemistry, Faculty of sciences, Urmia university, Urmia, Iran

^b Department of chemistry, Faculty of science, Payam nour university, Urmia, Iran

Email: leylagolshani@yahoo.com

Key words: Solubility product, Osmotic coefficients, Pitzer equations, Urmia brine.

Introduction:

Lake Urmia is a salt lake in northwestern Iran, near Iran's border with Turkey. The lake is between the Iranian provinces of East Azerbaijan and West Azerbaijan. It is the largest lake in the Middle East, and the third largest salt water lake on earth. The main cations in the lake water include Na^+ , K^+ , Ca^{2+} , Li^+ and Mg^{2+} , while Cl^- , SO_4^{2-} , HCO_3^- are the main anions. The Na^+ and Cl^- concentration is roughly 4 times the concentration of natural seawater. Sodium ions are at slightly higher concentration in the south compared to the north of the lake, which could result from the shallower depth in the south, and a higher net evaporation rate.

The future hydrological and geochemical evolution of closed basins depends very strongly on water evaporation and mineral precipitation from these basins. One of the problems of the development of closed natural basins is to what degree they can be evaporated under existing natural conditions. The progress in branches of physical chemistry dealing with concentrated electrolyte solutions allows the application of the newest, up-to-date approaches to understanding the geochemical aspects of natural phenomena. The ion interaction approach developed by Pitzer presents a very valuable tool for the theoretical prediction for various aspects of geochemical development of natural hypersaline brines. The great advantage of Pitzer's model is that it allows avoiding some of the restrictions or assumptions such as the intrinsic limitation to low or moderate concentrations or the extrapolation of solution properties beyond the solubility limit of electrolytes in pure water. Therefore, the progress in physical chemistry of electrolyte solutions allows the application of new physico-chemical approaches either to the explanation or to the prediction of geochemical development of natural basins under various climatic conditions.



Materials and methods:

The dissolution-precipitation equilibrium of an ionic mineral can be described by the formula:



where ν_M , ν_X , z_m and z_X are the amounts of cations and anions in a solute molecule and cation and anion charges, respectively. If the activity of the solid phase is considered to be equal to 1, then this constant is defined as:

$$K_{sp, M_{\nu_M} . nH_2O} = a_M^{\nu_M} . a_X^{\nu_X} . a_{H_2O}^n = (m_{M, sat} . \gamma_M)^{\nu_M} . (m_{X, sat} . \gamma_X)^{\nu_X} . a_{H_2O}^n$$

where $m_{M, sat}$ and $m_{X, sat}$ are the molal concentrations of the cation and anion, respectively, in the liquid phase saturated with respect to the solid phase; and γ_M and γ_X are the conventional single-ion activity coefficients of cation and anion at proper concentrations, respectively; a_{H_2O} is the water activity of the liquid phase.

Result and discussion:

Pitzer equations give a good account of the properties of the major saline water components. The result of the calculations of the osmotic coefficients of lake Urmia brine show that: I) Lake Urmia brine is oversaturated with respect to salts II) the degree of oversaturation has been increasing very significantly during the last years.

Reference:

- [1] Boris S .Krumgalz ,2001, Application of the Pitzer ion interaction model to natural hypersaline brines, Journal of Molecular Liquids.91.3-19
- [2]GuoxiangZhang.NicolasSpycher,EricSonnenthal, and, Carl Steefel,2006,Implementation of a Pitzer Activity model in to toughreact for modeling concentrated solution, Proceedings, tough symposium 2006
- [3].Jerry P.Greenberg and Nancy Moller,1989,The Prediction of mineral solubilities in natural waters:A chemical equilibrium model for the Na-K-Ca-Cl-SO₄-H₂O system to high concentration from 0 to 250 °C, Geochimica et Cosmochimica Acta Vol.53.PP.2503-2518



Synergism/antagonism studies between antifoam-antihydrate using surface tension technique

A.A. Nazari Moghaddam^{a*}, S.A. Alavi^a, A. Bagheri^b, F. Varaminian^c, A. Heidarinasab^a, A. Abolhasani^d

^a Department of Chemical Engineering, Science and Research branch, Islamic Azad University, Tehran, Iran

^b Department of Physical Chemistry, Faculty of Chemistry, Semnan University, Semnan, Iran

^c School of Chemical, Petroleum and Gas Engineering, Semnan University, Semnan, Iran

^d Department of Chemical Engineering, Faculty of Engineering, Arak University, Arak, Iran

Email: a.nmoghadam@yahoo.com

Key words: Surface Tension, Antifoam, Antihydrate, CMC, CAC.

Introduction:

Antifoams and Antihydrates are chemical compounds designed to prevent the formation of foam and hydrate, respectively. Antifoam efficiency is depend upon the bulk solution chemistry, operating conditions and surface active agents (surfactant base of them) creating the foam. Kinetic Antihydrates are polymers or co-polymers. They prevent gas molecules to imprison in water hydrogen-bond cages [1].

Antifoams and antihydrates use in many industrial plants together to prevent decreasing operational efficiency. When they are mixed together, several properties of the mixed system change compare to those of single systems, as a result of synergism/antagonism(negative synergism)[2].

Material and Methods:

Equilibrium surface tensions were investigated on pure non-ionic surfactant(Brij-35) as an antifoam, polyvinylpirolidone($M_w \approx 10000$ g/mole)(PVP-10) as a kinetic antihydrate and mixtures of them at various mole fractions. The CAC(critical aggregation concentration) and CMC(critical micelle concentration) points were measured by tensiometer(model Sigma 701, KSV). The synergism behavior of antifoam-antihydrate mixture was studied between Brij-35

and PVP-10. Synergistic effects in mixtures have been extensively studied and different theoretical approaches have been proposed.

Result and discussion:

Rubingh [3] introduced the concept of the interaction parameter, β , based on regular solution theory, which describes the synergism between two surfactants. The value of the β -parameter gives an indication of the strength of the interaction between the surfactants. Where β is the molecular interaction parameter:

$$\beta = \frac{\ln\left(\frac{y_1 C_{12}}{C_1^0 X_1}\right)}{(1 - X_1)^2} \quad (1)$$

The surface tension of pure Brij-35 and PVP-10 were studied at various temperatures (Fig. 1)

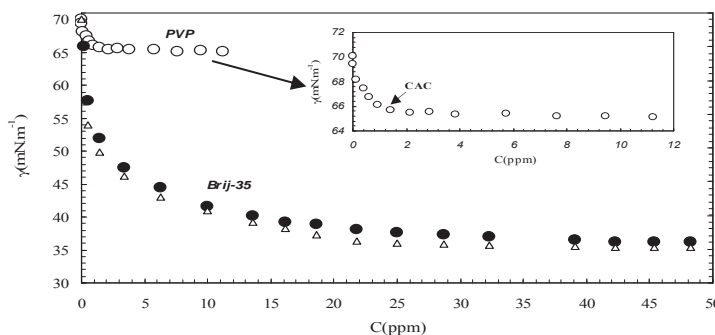


Fig. 1. Plot of the surface tension vs. concentration

Conclusions

The surface tension of pure an antifoam, a kinetic antihydrate and mixture of them at various mole fraction were investigated. The CAC and CMC points of them and the synergism behavior of antifoam-antihydrate mixture was studied by this method.

Reference:

- [1] M.A. Kelland and etal; "Studies on some alkylamide surfactant gas hydrate anti-agglomerants" ; 61,4290-4298,2006.
- [2] M.J. Rosen; "Surfactants and interfacial phenomena"; Wiley, New York,1989.
- [3] D.N. Rubingh and etal; "Mixed Micelle Solutions"; Plenum, New York, 1979.



Investigation of surface properties of ionic liquid/alcohol binary systems at various temperature

A.A. Nazari Moghaddam^{a*}, A. Bagheri^b, S.A. Alavi^a, A. Heidarinasab^a, F.B. Moadabdoost^d

^a Department of Chemical Engineering, Science and Research branch, Islamic Azad University, Tehran, Iran

^b Department of Physical Chemistry, Faculty of Chemistry, Semnan University, Semnan, Iran

^c Department of Pure Mathematics, Sari branch, Islamic Azad University, Sari, Iran

Email: a.nmoghadam@yahoo.com

Key words: binary system, ionic liquid, UNIFAC, Gibbs adsorption, extended Langmuir

Introduction:

Knowledge about the physico-chemical properties, such as surface thermodynamics is necessary in any process designing. Ionic liquids employed in new chemical processes so it is important to know about their properties [1]. The surface tension of a liquid mixture is not a simple function of the surface tension of the pure components, because in a mixture the composition of the surface is not the same as that of the bulk [2].

Methods:

Domańska and et al [1] studied on surface properties of non-ideal binary systems of an ionic liquid (1-butyl-3-methylimidazolium) and long chain alcohols (1-butanol, 1-pentanol and 1-hexanol) in temperature range of 298.15K to 338.15K. In this work, the activity coefficients in surface and bulk were evaluated using the UNIFAC group contribution model and then this coefficients is used to estimate the relative Gibbs adsorption and the thickness of surface layer. The thickness of surface layer (t) has been calculated from the Panayiotou equation modified for liquid surfaces [2]:

$$t = -\frac{1}{RT} \left(\frac{\partial \sigma}{\partial \ln a_2} \right) \left(\frac{\phi_2^s}{v_2} - \frac{\phi_1^s x_2^b}{v_1 x_1^b} \right)^{-1} \quad (1)$$

where ϕ_1^s and ϕ_2^s are the volume fraction of components 1 and 2 in the surface phase. Values of surface tension of binary systems were predicted by Sprow and Prausnitz equation:

$$\sigma = \sigma_i + \frac{RT}{A_i} \ln \frac{x_i^s \gamma_i^s}{x_i^b \gamma_i^b} \quad (2)$$

Result and discussion:

The surface tension decreases by increasing temperature and increases by increasing the Ionic liquid mole fraction, the variations of the surface tensions for three mixtures with temperature are linear in the temperature range of 298.15–338.15K. The relative adsorption $\Gamma_{2,1}$, and thickness of surface layer, t , for alcohol/ionic liquid systems calculated based on Eqs. (1, 2). In these mixtures, the variation of the thickness and relative adsorptions with composition follows distinctively same patterns. In these systems, the relative adsorptions are positive with a pronounced maximum in the ionic liquid-rich region and a shallow minimum for thickness of surface layer in the alcohol-rich region. In addition, to find more information about the surface structure of binary mixtures, surface mole fraction was calculated using an extended Langmuir model. In all temperatures, $\Gamma_{2,1}$, increased by increasing the length of the alcohol chains. This trend is nonlinear and surface tension decreased rapidly with increasing alcohol concentration. From the molecular point of view, the thickness of surface layer and relative Gibbs adsorption are strongly dependent on the molecular interactions, molecular size, surface tension and temperature.

Conclusions:

The UNIFAC models are used for calculation of the activity coefficients of species in the surface and bulk phases. The Sprow and Prausnitz equation as well as UNIFAC model has been used to predict the mixture's surface tension and relative Gibbs adsorption. The surface tension predictions are found to be extremely sensitive to the values of the molar surface areas used in the computation. The thickness of three miscible liquid–air surfaces has been calculated by combining relative Gibbs adsorption and UNIFAC model. Our calculations indicate that the thickness of surface layer is generally of the order of Angstrom and is affected by varying of composition.

Reference:



- [1] U. Domańska and etal; "Effect of temperature and composition on the surface tension and thermodynamic properties of binary mixtures of 1-butyl-3-methylimidazolium thiocyanate with alcohols" ; J. Colloid and Interface Sci.; 348,661-667,2010.
- [2] A.A. Rafati and etal; "Application of the UNIFAC model for prediction of surface tension and thickness of the surface layer in the binary mixtures" ; J. Colloid and Interface Sci.; 355,252–258,2011.

15th Physical Chemistry Conference



Non-isothermal Crystallization Kinetics Study of Biodegradable Polyethylene Azelate/SiO₂ Nanocomposite

M.R. Memarzadeh^a, M. Mohsen-Nia^{a, b*}

^aDepartment of Chemistry, University of Kashan, Kashan, Iran

^bDivision of Chemistry and Chemical Engineering, Caltech, Pasadena, California, USA

E-mail: moh.moh@cheme.caltech.edu

Key word: Nanocomposite, Crystallization Kinetics, Avrami, PEA

Introduction:

The rapid development of polymers, polymer-based nanocomposites and their wide applications are obviously one of the characteristics of the last century. However, the wide applications of these materials also result in an irreversible buildup of polymer waste in the environment. Therefore, synthesis and modification of the biodegradable polymers and polymer-based nanocomposites through innovative technology is an impressive task from the view point of materials science [1]. A renewed interest in aliphatic polyesters has resulted in developing materials important in different industrial applications, e.g. the biomedical and ecological fields. Mechanical properties and degradation rates of biodegradable aliphatic polyesters depend strongly on their chemical structures, but they also depend on their morphology and crystalline structures which in turn are determined directly by the thermal treatment imposed on the polymers during solidification process [2]. Therefore, it is very important to investigate the crystallization kinetics and morphology of these biodegradable aliphatic polyesters, to understand the relationship between structural features and crystallization conditions. However, over the last few years, the studies show that biodegradability of polymer-based nanocomposites is faster than pure polymers.

In this work, polyethylene azelate/silica (PEA/SiO₂) nanocomposites containing 3 wt.% SiO₂ were prepared via in situ polymerization method. The non-isothermal crystallization behavior of PEA/SiO₂ nanocomposites has been studied by the Avrami equation.

Materials and methods:

All the materials for preparation of polymer matrix such as azelaic acid, ethylene glycol, Para toluensulphonic acid (PTSA) and zinc acetate dehydrate were purchased Merck chemical



Co., Germany. Fumed silica nanoparticles (SiO_2) used for nanocomposite preparation were supplied by Degussa AG (Hanau, Germany) under the trade name AEROSIL® 200, having a specific surface area $200 \text{ m}^2/\text{g}$ ($>99.8\% \text{ SiO}_2$) and average primary particle size 12 nm.

Apparatus:

In this work, the crystallization behavior of the prepared nanocomposite was studied by using differential scanning calorimetry (DSC) analysis. The effects of SiO_2 nanoparticles on the crystallization temperatures and cooling rates were also investigated.

Result and discussion:

Non-isothermal crystallization exotherms were measured over the cooling rate of 5, 10, 15 K/min by calorimetry. The crystallization kinetics data were correlated by Avrami equation. According to the obtained results, the Avrami equation can successfully describe the crystallization behavior under the non-isothermal crystallization. The Avrami exponents n were found to range from 2.7 to 3.0 for pure PEA and 3.1 to 5.0 for PEA/ SiO_2 nanocomposite, suggesting that the nanocomposite crystallizes via a heterogeneous nucleation and spherulitic growth mechanism.

Conclusion:

The non-isothermal crystallization behavior of pure PEA and PEA/ SiO_2 nanocomposites has been studied by using Avrami equation. It is found that the addition of nanoparticles of SiO_2 influenced the mechanism of nucleation and the growth of polyethylene azelate crystallites. Also, the nanocomposites show a higher Avrami value than of the neat PEA, implying a more complex crystallization configuration.

References:

- [1] K. Chrissafis et al; "Thermal decomposition of poly(propylene sebacate) and poly(propylene azelate) biodegradable polyesters: Evaluation of mechanisms using TGA, FTIR and GC/MS" ; Journal of Analytical and Applied Pyrolysis; 92, 123-130, 2011.
- [2] Y. Peneva, L. Minkova; "Non-isothermal and isothermal crystallization of nanocomposites based on functionalized polyethylenes; Polymer Testing; 25, 366-376, 2006.



15th Physical Chemistry Conference

Comparison of H₂, CH₄ and CO₂ gas adsorption on Boron Nitride Nanoscrolls

Haniyehsadat Vizhegan^{*a}, Sayed Mortaza Mousavi Khoshdel^b

^a shahrerey Brunch, Islamic Azad University, Tehran, Iran

Corresponding Author E-mail: Vijegan@hotmail.com

^b Molecular Simulation Research Laboratory, Faculty of Chemistry, Iran University of Science & Technology, Tehran, Iran

Key words: DFT, BN nanoscroll, Gas storage, MPW1P91

Introduction:

Nanometric structures have been intensively studied during the last years. Carbon-based materials are among the most investigated in literature, but since 1960s there are very few works on Carbon Nanoscroll (CNSs).

In principle, CNSs and boron nitride nanoscroll (BNSs) can be formed by rolling up graphite and boron nitride layers. Nanoscrolls can be formed tubular and conical, also depend on wrapping angle of sheet around the axis, we can have three forms: (armchair, chiral and zigzag).

As we know, one important characteristic is that nanoscrolls occupy considerable high and fully accessible surface area. These features are potentially advantage to adsorption storage of gases. Because of the novel scroll topology, their properties differ from single wall or multi wall nanotubes. On the basis of the previous works, it seems that nanoscrolls with an expansion of interlayer spacing could be very promising materials for gas storage, for hydrogen storage the highest binding energy was found for the 7 Å distance.

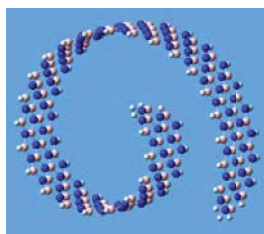


Fig.1-optimized structure of BNSs

Methods:

Since a program to draw the nanoscroll structures was not available, we were programming. This program has the capability of produce nanoscrolls with desired length, width and distance between layers. Various nanoscrolls with different inter layer spacing were formed and optimized using of theory (DFT) to calculate the MPW1PW91 method and 6-311++G** basis set.

Results and Discussion:

To prevent the opening of the spiral structure in the optimization process, this structure was freezed and all other structural parameters including length and bond angle were optimized.

Then:

1. Molecular hydrogen, carbon dioxide and methane gases were optimized.
2. Molecular hydrogen, carbon dioxide and methane was placed between layers and perpendicular sheets in two position a) between nitrogen atoms b) between boron atoms
3. The resulting structure was optimized.

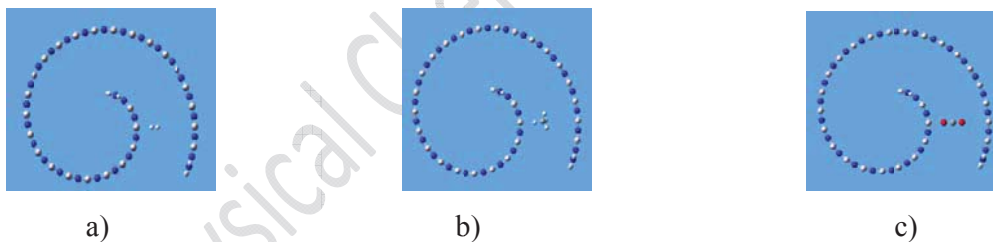


Fig.2 optimize structure of BNSs with a) H₂ b) CH₄ c) CO₂

To obtain the potential curve, nitrogen and boron gases in between layers, according to the top structure were scans. We use MPW1PW91 method and 6-31G basis set in all the calculations and 6-311++G** extra basis was used for H₂, CH₄ and CO₂ gases and six atoms around of boron and nitrogen.

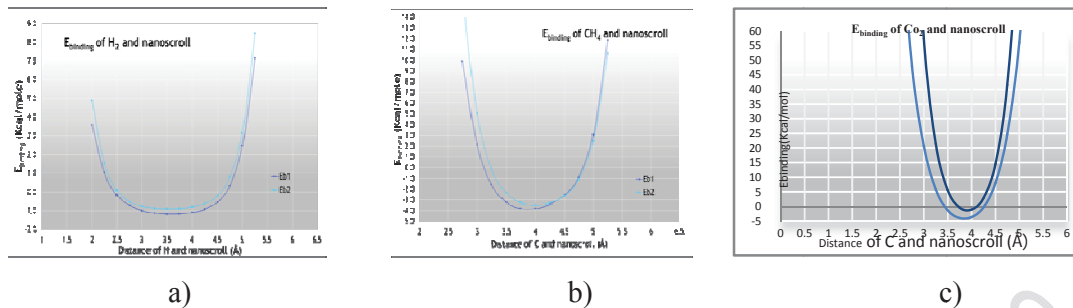


Figure 3: a) potential energy curve (Eb1: scan of H_2 between two boron atoms), (Eb2: scan of H_2 between two nitrogen atoms), b) potential energy curve (Eb1: scan of CH_4 between two boron atoms), (Eb2: scan of CH_4 between two nitrogen atoms), c) potential energy curve (Eb1: scan of CO_2 between two boron atoms), (Eb2: scan of CO_2 between two nitrogen atoms)

Conclusions :

According to the result of the calculations which can be seen in the graphs, hydrogen bond energy on the boron atom is -1.174 kcal/mol and on the nitrogen atom is -0.92 kcal/mol. These energies are more than energy of nanotubes (maximum -0.7) and make acceptable physical adsorption. Energy of methane adsorption on the boron atom is -3.8 kcal/mol and on the nitrogen atom is -3.5 al/mol that shows strong physical adsorption. Energy of carbon dioxide adsorption on the boron atom is -3.8 kcal/mol and on the nitrogen atom is -1.04 Kcal/mol. Because of large size methane and carbon dioxide curve surfaces potential is thinner and repulsion energy near the wall of nanoscroll is stronger. The minimum points of the curve at fig3-a do not reach to area flat but could be obtained big binding energy with increase distance between the layers. The result of calculation show the binding energy is positive in distance 6Å between the layers and in this distance hydrogen molecule cannot be perpendicular sheet. Different between bonding energy of boron atoms and different between bonding energy of nitrogen atoms in carbon dioxide are due to the electronegativity of nitrogen and oxygen atoms and repulsion partial charges on them.

References

- [1]F. S. Berga, V. R. Coluci, S. B. Legoas, R. Giro, D. S. Galavao, R. H. Baughman, *nano letters*, 2004, 45, 801
- [2]T. T. Xu, J. Zheng, N. Wu, A. W. Nicholls, J. R. Roth, *Nano letters*, 2004 , 45, 963
- [3]G. Mpourmpakis, E. Tylianakis, G. E. Froudakis, *Nano letters*, 2007, 77, 1893



- [4] X. Peng, J Zhou, W. Wang, D. Cao, *Carbon*, 2010, 48, 3760

15th Physical Chemistry Conference



Effect of surfactant solutions on methanol synthesis catalyst preparation

N. Mirhosseini^a, M. Bahmani^b, F. Yaripour^b, R. Miremaddedin^b, A. Taeb^{a*}

^aChemical engineering Department, Iran University of Science and Technology, Tehran, Iran

Email: n.mir89@yahoo.com

^bCatalyst Research Group, Petrochemical Research & Technology Company NPC-RT, Tehran, Iran

Keywords: Methanol, Cu catalyst, Co-precipitation, Non-ionic surfactant

Introduction:

Methanol is mainly synthesized from syngas using ternary copper based catalyst Cu/ZnO/Al₂O₃ were prepared by co-precipitation method [1]. The performances of Cu-based catalysts may be improved by modifying of the preparation methods. The catalyst composition and preparation conditions may directly affect the structure and interaction between different components and related catalyst performance [2]. In the present study, The effect of washing by various surfactant solutions on physico-chemical properties of copper oxide prepared via precipitation method was investigated. In order tot, Increasing the number of washing has successfully removed undesired nitrate. The used surfactants was a non-ionic type, which reduce surface tension of water from 72 to 31 dyne/cm³, used the Du Noüy ring method (KSV sigma 700).

Experimental:

the preparation of catalysts were similar to that reported by Baltes et al [3]. After aging, the precipitates were filterated and washed first with demineralized water and then with various non-ionic surfactants solutions sequentially. Finally, the filter cake was dried overnight at 100 °C and was calcined at 320 °C for 3 h under air flow. The catalyst activity was studied in a tabular micro reactor under industrial conditions (230°C, 50bar) for 120 h. feed and product gas analysis was performed using online gas chromatograph equipped with a Thermal Conductivity (TCD) and Flame Ionization (FID) Detectors. The physicochemical properties of the catalyst and precursors were characterized by of nitrogen physisorption, X-ray Diffraction (XRD), Temperature Programmed Reduction (TPR) and nitrous oxide titration.

Result and discussion:

Conversion, activity and selectivity of various prepared catalysts are reported in the Table. This Table shows that the CO conversion and space time yield (STY) of prepared catalysts are much larger than Commercial catalyst.

Table 1: results of CO hydrogenation tested in micro-reactor resulting of reactor test

Catalyst name	Final washing solution	STY (g _{CO} /kg _{cat} ·h)	CO conversion (%)	Selectivity (mol %)				
				MeOH	EtOH	2-Prop	DM	othe
P _{wtr} Cat.	Water	668.041	46.4900	97.366	0.130	0.0005	0	2.50
P _{Tx-100} Cat.	Triton-X100	681.349	46.800	98.157	0.412	0.293	0	1.13
P _{LAE} Cat.	Lauryl alcohol Ethoxilate	640.302	46.284	99.274	0.188	0.0062	0	0.53
P _{Eth} Cat.	Ethanol	579.147	47.233	98.422	0.295	0.0649	0	1.21
Commercial Cat.	—	348.291	39.953	98.074	0.078	0.0795	0	1.7685

The XRD patterns of the precursors at the different temperature show similarity as presented in Fig 1. Observed phases are Tenorite, Zincite, Rosasite and Copper Aluminum Carbonate Hydroxide Hydrate.

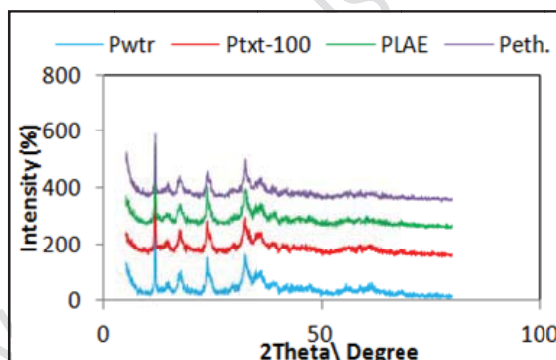


Fig 1: The XRD pattern of the precursors.

Conclusions:

The present catalysts exhibit the quite activity, STY and satisfactory methanol selectivity, the STY experiences a serious drop near 60 % after approximately 24 h reaction. As shown in fig 2. One can see that the washing with ethanol does not regenerate satisfactory STY, so the change of washing solution is responsible for the increase of STY. CO conversion is recovered to 70% of initial activity with addition of water and triton X-100 in final washing.

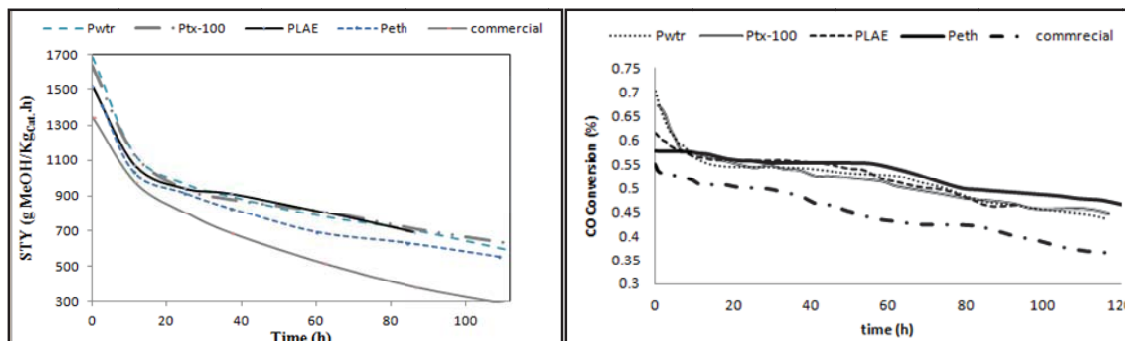


Fig 2: STY and CO conversion of catalysts versus time on stream.

References:

- [1] G. Xian-ji, L. Li-min, L. Shu-min, B. Gai-ling, H. Wen-hua, (2007) , 35(3), 329.
- [2] Z. Hui-dong, B. Shao-fen, L. Xin-mei, Y. Zi-feng, J Fuel Chem Technol, (2010), 38(4), 462.
- [3] C. Baltes, S. Vukojevi, F. Schüth, Journal of Catalysis, 258 (2008) 334–344.



Surface protection of copper using organic compounds in acidic media

F.soltani¹, H.Hamidian¹, S.M.A.Hosseini^{2*}, and S.Daneshmoghdam¹

¹Dept.of Chemistry, Payame Noor University, Kerman

²Dept.of Chemistry, Shahid Bahonar University, Kerman

*Email:s.m.a.hosseini@uk.ac.ir

Abstract:

The inhibiting efficiency of the different additives (1-{4-[2-(5-methyl-1,3,4-thiadiazol-2-yl)-1-diazenyl]phenyl}-1H-1,2,3,4-tetraazole-5-thiol, B1 and 1-{4-[2-(1,3-benzothiazol-2-yl)-1-diazenyl]phenyl}-1H-1,2,3,4-tetraazole-5-thiol, B2) evaluated by means of electrochemical techniques such as polarization curves and ac impedance measurements. Results obtained showed that the inhibition efficiency (IE%) increases with increasing the inhibitors concentration. The results indicate that the surface layer is of dielectric nature, and the film formed on the copper is uniform and protective.

Introduction:

One of the most important methods in the corrosion protection of copper is the use of organic inhibitors. Most of the inhibitors are organic compounds and their derivatives such as azoles [1,2,3], amino acids [4]. Corrosion inhibitors change the corrosion potential, impede the cathodic and anodic corrosion reaction via polarization on the metal surface and thus create passivity on the metal and alloy. The present investigation deals with corrosion inhibition of copper using two newly synthesized B1 and B2 inhibitors in acid solution at different temperatures.

Experimental:

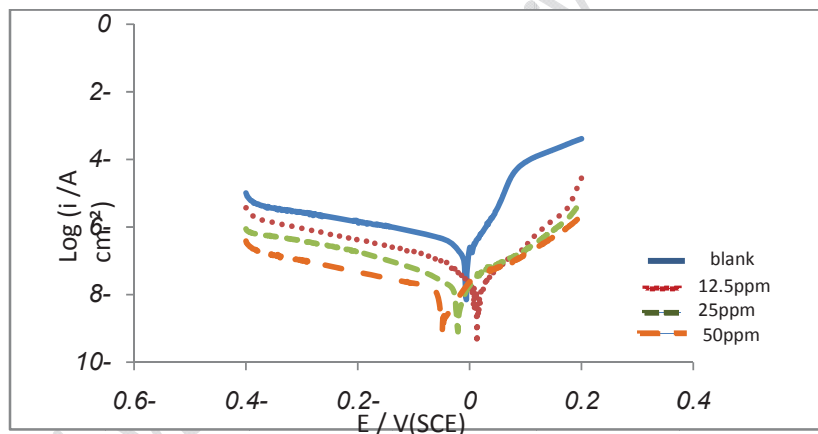
All of the corrosion tests were performed on a copper bar. For the electrochemical measurements, pre-treatment of the surface of specimens was carried out by grinding with emery paper of 400 up to 3000 grit, rinsing with bidistilled water, acetone and dried at room temperature before use.

Electrochemical studies:

Impedance measurements were carried-out in the frequency range of 50 m Hz to 100K Hz, by applying 10 mV ac voltage peak- to- peak. The working electrode was prepared from a copper rod. A saturated calomel electrode (SCE) was used as the reference; a platinum electrode was used as the counter-electrode. The potentiodynamic Tafel measurements were started from the cathodic to the anodic direction(-0.5 V to 0.3 V) with a scan rate of 1mVS^{-1} .

Results and discussion:

The EIS results indicates that the impedance of inhibited copper increase with increasing inhibitor concentration and consequently the inhibition efficiency increases. The polarization curves (Fig. 1) confirms the conclusion of impedance technique, giving some additional information about the type of inhibition.



Polarization curves recorded for copper electrode in 0.5 M HCOOH solutions without and with various concentration of the B1

Conclusions:

The inhibitors affect polarization curves via physicochemical adsorption. The inhibitor B1 decrease corrosion current densities and increase inhibition efficiency more than inhibitor B2

References:

- [1] E.M. Sherif, S.M. Park, *Electrochim. Acta* 51 (2006) 6556–6562.
- [2] E.M. Sherif, S.M. Park, *Corros. Sci.* 48 (2006) 4065–4079.
- [3] M.M. Antonijevic, S.M. Milic, M.D. Dimitrijevic, M.B. Petrovic, M.B.



Radovanovic, A.T. Stamenkovic, *Int. J. Electrochem. Sci.* 4 (2009) 962–979

[4] J.B. Matos, L.P. Pereira, S.M.L. Agostinho, O.E. Barcia, G.G.O. Cordeiro, E.D. Elia, J. *Electroanal. Chem.* 570 (2004) 91–94.

15th Physical Chemistry Conference



Corrosion inhibition of brass by two synthesized compounds in Formic acid

F.soltani¹, S.M.A.Hosseini^{2*}, H.Hamidian¹ and A.R.Mohadesi¹

¹Dept.of Chemistry, Payame Noor University, Kerman

²Dept.of Chemistry, Shahid Bahonar University, Kerman

*Email: s.m.a.hosseini@uk.ac.ir

Abstract:

The corrosion behavior of brass are investigated by two newly synthesized organic compounds 1-{4-[2-(5-methyl-1,3,4-thiadiazol-2-yl)-1-diazenyl]phenyl}-1H-1,2,3,4-tetraazole-5-thiol and 1-{4-[2-(1,3-benzothiazol-2-yl)-1-diazenyl]phenyl}-1H-1,2,3,4-tetraazole-5-thiol in Formic acid. using electrochemical impedance spectroscopy(EIS) and potentiodynamic polarization measurements. The results obtained at different concentrations of inhibitors and at different temperatures were used to evaluate various thermodynamic parameters. It is found that the inhibition efficiency increases with increasing inhibitors concentrations. SEM micrographs indicates formation of uniform film on the surface.

Key words: brass, EIS measurement, organic inhibitors

Introduction:

Industrial establishments face heavy financial losses due to the corrosion of copper alloys. The organic materials which act as inhibitors are able to form a protective film on the surface of metal and alloy either physically or chemically[1]. As far as brass alloy is concerned it is noticed that presence of heteroatom such as nitrogen, oxygen, sulphur and phosphorous in the organic compound improves its action as corrosion inhibitor [2,3]. In this study, the inhibiting effect of two newly synthesized compounds on the corrosion behavior of brass in Formic acid solution has been carried out by different techniques.

Experimental:

The inhibitors were synthesized according to laboratory procedures. All the corrosion tests were performed on brass bars. Before each polarization measurement. A saturated calomel

electrode(SCE) and platinum wire were used as a reference and counter electrode respectively, in a three electrode electrochemical cell.

Electrochemical studies:

Polarization measurements carried out after immersing the brass electrode in 0.5 M HCOOH solution without and with different concentrations of the two synthesized inhibitors, in the potential range -0.9 to 0.3 V at a scan rate of 1.0 mV S⁻¹.

Impedance measurements of the brass electrode at its open circuit potential after immersion in 0.5 M HCOOH solution and in the presence of various inhibitors concentrations were performed over the frequency range from 10m Hz to 100 kHz.

Results and discussion:

The EIS and polarization curves results indicates that the inhibition efficiency increases with increasing inhibitor concentration . the corrosion of the polarization curves are presented in table 1

	Conce/ppm	I_{corr} ($\mu A\ cm^{-2}$)	-E mV/ SCE	β_c (mV dec ⁻¹)	β_a (mV dec ⁻¹)	E_p (%)
Blank		1.30	476	100	100	
B1	10	0.40	396	50	50	68%
B1	20	0.16	385	40	133	87%
B1	40	0.05	371	50	50	96%
B2	2	0.16	369	64	50	87%
B2	4	0.13	346	43	50	90%
B2	8	0.06	318	36	33	95%

The result of table 1 indicat that E_{corr} remain almost unchanged while i_{corr} reduced remarkably with increasing inhibitors concentration which result in increase of inhibition efficiency.

Conclusions:

Both of the inhibitors decrease corrosion current densities . The investigated inhibitors affect cathodic and anodic polarization curves via physical-chemical adsorption, the inhibitor B1 increases inhibition efficiency more than B2.

References:



- [1]R. Subramanian, V. Lakshminarayanan, *corros .Sci.*44 (2002) 535-554
[2]M.M.Antonijevic,M.B . Petrovic,*Int J. Electrochem.Sci.*3(2008) 1-28
[3]F.Altaf, R. Qureshi, S. Ahmed, A.Y. Khan, A. Naseer , *J. Electroanal. Chem.* 642 (2010) 98-101

15th Physical Chemistry Conference



**The investigation of 3-methyl 4-[1- (4- methoxy phenyl) methylidene] -5-
iso oxazolone and 3- acidic media.methyl 4-[1- (4- dimethyl. amino) phenyl]
-5- iso oxazolone as inhibitors on Mild steel in acidic media.**

S.M.A.Hossein^{a*}, J. Javdani^b

^aDepartment of Chemistry, faculty of Science, Shahid Bahonar University of Kerman,

^bDepartment of Chemistry, faculty of Science, Payame Noor University of Kerman, Kerman

E-mail: s.m.a.hosseini@uk.ac.ir

Abstract:

The corrosion behavior of mild steel (st 60) in 0.5 M sulfuric acid containing different amounts of 3-methyl 4-[1- (4- methoxy phenyl) methylidene] -5- iso oxazolone and 3-methyl 4-[1- (4- dimethyl. amino) phenyl] -5- iso oxazolone as an inhibitor at a temperature range 25-55⁰C were investigated by potentiostatic and EIS techniques. Corrosion parameters (corrosion Potential, corrosion current density, inhibition efficiency, cathodic Tafel slops and degree of surface coverage) were obtained by plotting potentiostatic polarization curves, then using the obtained parameters, the thermodynamic parameters (ΔG_{ads} , ΔH_{ads} , ΔS_{ads} , and E_a) were calculated.

Temperature showed negative effects on the performance of inhibitors and causes increase in the corrosion current density in the presence and absence of the inhibitor. The results indicate that increasing the concentration of the inhibitor increases the efficiency of the inhibitor.

The results also reveal that inhibitors are of mixed type, and their performance in controlling the corrosion of steel is attributed to the chemical/ physical adsorption.

(EIS) graphs leading to calculated parameters such as polarization resistance via simulated equivalent circuits and showed the improve in inhibition capability of the alloy with the inhibitors, and finally, SEM and infrared spectra are used for surface analysis.

Keywords:, mild steel, , MIN, MIO (as an inhibitor)

Introduction:

The inhibition of metal and alloys in acid solutions can be related to the addition of a variety of organic compounds, which has been explored by several investigators. The selection of



appropriate inhibitor mainly depends on the type of acid, its concentration, temperature, the presence of dissolved inorganic and / or organic substances, even in minor amounts, and, of course, on the types of metallic material that exposed to acidic solutions. It has been proved that organic compounds containing heteroatoms with high electronic density, such as nitrogen, sulfur, and oxygen, or those containing multiple bonds, which are considered as adsorption centers, are effective corrosion inhibitor [1].

Results and discussion:

Open-circuit potential, Potentiodynamic polarization and EIS measurements.

The exposing time before open- circuit potential (OCP) of the specimens get stabled was 15 min. These values were recorded and plotted to ascertain the effect of inhibitor on the nature and incipient tendencies of the surface to corrode. Potentiodynamic polarization curves for type st60 mild steel in 0.5 M H₂SO₄ solution containing 10 -40 ppm of inhibitors separately along with the blank acid solution containing no inhibitor are similar to those reported earlier [2-3]. Corrosion current density decreased and inhibition efficiency increased with increasing inhibitor concentration . EIS graphs showed appreciable increase in corrosion resistancen of the sample .

Effect of temperature

The effect of temperature(25-55⁰C) on the various corrosion parameters, E_{corr} , i_{corr} , Θ , and IE, for mild steel in 0.5 M H₂SO₄ solution in the absent and presence of 40ppm of MIN and MIO was investigated . It was observed that the inhibition efficiencies are found to decrease by increasing the solution temperature from 25⁰Cto 55⁰C.

Conclusion:

- *The investigated organic compounds exhibit good inhibiting properties, which are of the mixed type, but dominantly act as anodic inhibitors for mild steel in 0.5 M H₂SO₄.
- *The IE increases with the increase of the inhibitor concentration and inhibition efficiencies are in the order MIN> MIO.
- *Adsorption of the inhibitors on the surface obeys the langmuir adsorption isotherm.
- *The increase in activation energy after the addition of inhibitors to acid solution and the value of standard free energy of the adsorption indicate that the adsorption is more physical



than the chemical. The negative sign of the ΔG_{ads}^0 and ΔH_{ads}^0 indicate that the adsorption process is spontaneous and exothermic.

*The SEM and FTIR results reveal the formation of a protective film on the surface of the alloy .

Reference:

- [1]S. M. A. Hosseini, A. Azimi, Materials And Corrosion59 (2008) 41-45.
- [2]R. L. Every, O. L. Riggs, Mater. Prot. 3 (1964) 46-58.
- [3]M. Schorr, J. yahalom,Corros. Sci12 (1972) 867-868.



The investigation of 3-methyl 4-[1- (4- methoxy phenyl) methylidene] -5- iso oxazolone and 3-methyl 4-[1- (4- dimethyl amino) phenyl] -5- iso oxazolone as inhibitors on Mild steel in acidic media.

S.M.A.Hossein^{a*}, J. Javdani^b

^aDepartment of Chemistry, faculty of Science, Shahid Bahonar University of Kerman,

^bDepartment of Chemistry, faculty of Science, Payame Noor University of Kerman, Kerman

E-mail: s.m.a.hosseini@uk.ac.ir

Abstract:

The corrosion behavior of mild steel (st 60) in 0.5 M sulfuric acid containing different amounts of 3-methyl 4-[1- (4- methoxy phenyl) methylidene] -5- iso oxazolone and 3-methyl 4-[1- (4- dimethyl. amino) phenyl] -5- iso oxazolone as an inhibitor at a temperature range 25-55⁰C were investigated by potentiostatic and EIS techniques. Corrosion parameters (corrosion Potential, corrosion current density, inhibition efficiency, cathodic Tafel slopes and degree of surface coverage) were obtained by plotting potentiostatic polarization curves, then using the obtained parameters, the thermodynamic parameters (ΔG_{ads} , ΔH_{ads} , ΔS_{ads} , and E_a) were calculated.

Temperature showed negative effects on the performance of inhibitors and causes increase in the corrosion current density in the presence and absence of the inhibitor. The results indicate that increasing the concentration of the inhibitor increases the efficiency of the inhibitor.

The results also reveal that inhibitors are of mixed type, and their performance in controlling the corrosion of steel is attributed to the chemical/ physical adsorption.

(EIS) graphs leading to calculated parameters such as polarization resistance via simulated equivalent circuits and showed the improve in inhibition capability of the alloy with the inhibitors, and finally, SEM and infrared spectra are used for surface analysis.

Keywords: mild steel, MIN, MIO (as an inhibitor)

Introduction:

The inhibition of metal and alloys in acid solutions can be related to the addition of a variety of organic compounds, which has been explored by several investigators. The selection of appropriate inhibitor mainly depends on the type of acid, its concentration, temperature, the



presence of dissolved inorganic and / or organic substances, even in minor amounts, and, of course, on the types of metallic material that exposed to acidic solutions. It has been proved that organic compounds containing heteroatoms with high electronic density, such as nitrogen, sulfur, and oxygen, or those containing multiple bonds, which are considered as adsorption centers, are effective corrosion inhibitor [1].

Results and discussion:

Open-circuit potential, Potentiodynamic polarization and EIS measurements.

The exposing time before open- circuit potential (OCP) of the specimens get stabled was 15 min. These values were recorded and plotted to ascertain the effect of inhibitor on the nature and incipient tendencies of the surface to corrode. Potentiodynamic polarization curves for type st60 mild steel in 0.5 M H₂SO₄ solution containing 10 -40 ppm of inhibitors separately along with the blank acid solution containing no inhibitor are similar to those reported earlier [2-3]. Corrosion current density decreased and inhibition efficiency increased with increasing inhibitor concentration . EIS graphs showed appreciable increase in corrosion resistancen of the sample .

Effect of temperature

The effect of temperature(25-55⁰C) on the various corrosion parameters, E_{corr} , i_{corr} , Θ , and IE, for mild steel in 0.5 M H₂SO₄ solution in the absent and presence of 40ppm of MIN and MIO was investigated . It was obsorved that the inhibition efficiencies are found to decrease by increasing the solution temperature from 25⁰Cto 55⁰C.

Conclusion:

- *The investigated organic compounds exhibit good inhibiting properties, which are of the mixed type, but dominantly act as anodic inhibitors for mild steel in 0.5 M H₂SO₄.
- *The IE increases with the increase of the inhibitor concentration and inhibition efficiencies are in the order MIN> MIO.
- *Adsorption of the inhibitors on the surface obeys the langmuir adsorption isotherm.
- *The increase in activation energy after the addition of inhibitors to acid solution and the value of standard free energy of the adsorption indicate that the adsorption is more physical



than the chemical. The negative sign of the ΔG_{ads}^0 and ΔH_{ads}^0 indicate that the adsorption process is spontaneous and exothermic.

*The SEM and FTIR results reveal the formation of a protective film on the surface of the alloy .

Reference:

- [1]S. M. A. Hosseini, A. Azimi, Materials And Corrosion59 (2008) 41-45.
- [2]R. L. Every, O. L. Riggs, Mater. Prot. 3 (1964) 46-58.
- [3]M. Schorr, J. yahalom,Corros. Sci12 (1972) 867-868.

15th Physical Chemistry Conference

DFT and Experimental vibrational analysis of Ofloxacin by Quantum liquid DFT calculation

Afsaneh Amiri^{1*}, Milad Nouralie^{1,2}, Alla Aslanzadeh^{1,2}, Atena Tavasoli^{1,2}, Simin Tadayon¹

¹Department of Chemistry, Islamic Azad University, Central Tehran Branch, Tehran, Iran.

²Young Researchers Club, Central Tehran Branch, Islamic Azad University, Tehran, Iran.

Email: afsaamiri@gmail.com

Keywords: Ofloxacin, Vibrational analysis, B3LYP, DFT, FT-IR, UV-VIS, ¹H-NMR.

Introduction:

Ofloxacin ((*RS*)-7-fluoro-2-methyl-6-(4-methylpiperazin-1-yl)-10-oxo-4-oxa-1-azatricyclo[7.3.1.0^{5,13}]trideca-5(13),6,8,11-tetraene-11-carboxylic acid) (Fig.1) is a synthetic chemotherapeutic antibiotic of the fluoroquinolone drug class considered to be a second-generation fluoroquinolone [1, 2]. Ofloxacin is a broad-spectrum antibiotic that is active against both Gram-positive and Gram-negative bacteria. It functions by inhibiting DNA gyrase, a type II topoisomerase, and topoisomerase IV, [3] which is an enzyme necessary to separate (mostly in prokaryotes, in bacteria in particular) replicated DNA, thereby inhibiting bacterial cell division. In this research study, the formation potential Molecular structure, Vibrational analysis of Ofloxacin have been investigated by DFT calculation.

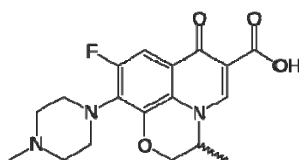


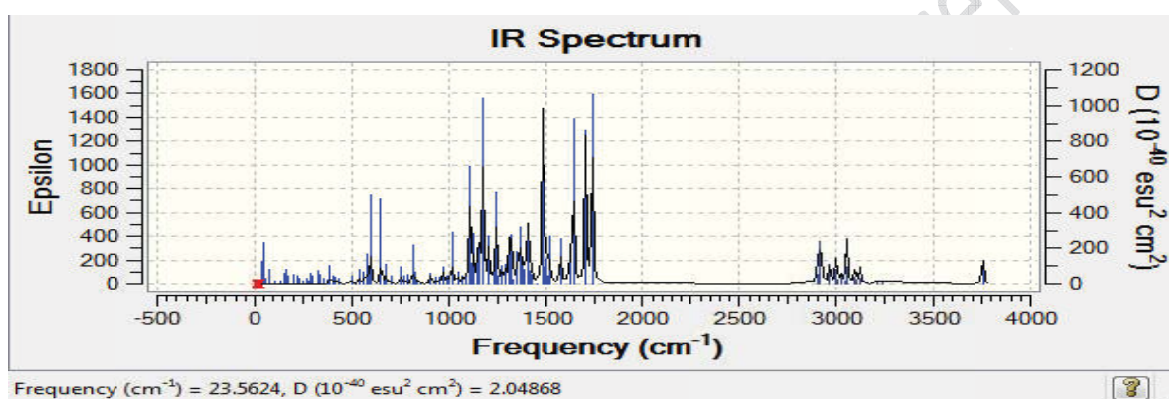
Fig. 1. Ofloxacin molecular structure

Material and Methods:

The geometry of the system has been fully optimized with the hybrid DFT and HF. DFT and HF calculations were performed with the GAUSSIAN 03W programs on a Pentium-PC computer with 3600 MHz processor [4]. To verify that the concluding structure wasn't in the local minimum point, the normal mode frequency calculation was carried out for the optimized molecules. The Vibrational analysis (FT-IR, UV-VIS, NMR) of the molecule in the liquid phase, were carried by using the Onsager SCRF method at the B3LYP/6-311+G**.

Result and Discussion:

Computational calculations of Ofloxacin have been carried out using the Becke-3-Lee-Yang-Parr density (B3LYP) functional methods with 6-311+G (d, p) basis set. The geometry optimization and fundamental frequencies of the most stable configuration have been calculated. The FTIR spectra of the compound have been recorded and compared to the calculated frequency values. The ¹H NMR chemical shifts have been calculated using the gauge-independent atomic orbital approach. (Fig.2).



Conclusion:

The calculated parameters were compared to experimental characteristic of Ofloxacin. Respectively good correlation in the range is 0.9005- 0.9878 between experimental and theoretical spectra was noted.

References:

- [1] Nelson, JM.; Chiller, TM.; Powers, JH.; Angulo, FJ. (Apr 2007). "Fluoroquinolone-resistant *Campylobacter* species and the withdrawal of fluoroquinolones from use in poultry: a public health success story". *Clin Infect Dis* **44** (7): 977–980.
- [2] Kawahara, S. (December 1998). "[Chemotherapeutic agents under study]". *Nippon Rinsho* **56** (12): 3096–3099.
- [3] Drlica K, Zhao X (1 September 1997). "DNA gyrase, topoisomerase IV, and the 4-quinolones". *Microbiol Mol Biol Rev*. **61** (3): 377–392.
- [4] M. j. Frisch et al. *GAUSSIAN 03*, Revision C. 01, Gaussian Inc., Wallingford. CT, 2004.



15th Physical Chemistry Conference



An investigation of Langmuir, Freundlich, and Temkin isotherms for neodymium removal by modification of polyethylene terephthalate (PET) fibers from environmental samples

Zahra Azizi,^{*a} Mina Khoshnudi,^b Homayon Ahmad Panahi,^c Neda Bisadi^a

^aDepartment of chemistry, Karaj Branch, Islamic Azad University, Karaj, Iran.

^bDepartment of chemistry, Shahre-ray Branch, Islamic Azad University, Tehran, Iran.

^cDepartment of chemistry, Tehran Markaz Branch, Islamic Azad University, Tehran, Iran.

Corresponding Author E-mail: zahra.azizi@kiauo.ac.ir, zahraazizi@yahoo.com

Key words: Polyethylene Terephthalate, Adsorption, Isotherm, Waste Water, Neodymium

Introduction:

In particular, polyethylene terephthalate (PET), member of the polyester family of polymers, has many applications in synthetic fibers, drink, food, liquid containers, and the other utility in chemistry and technology, which have attracted great attention due to large specific surface areas and high adsorption rates. Since the presence of heavy metal ions in wastewater may be harmful to human beings and all living bodies, therefore metal removal from water contaminations is an important environmental concern in waste management. Consequently, commercial polyethylene terephthalate are mainly used as a separation processes due to functionalizing groups. Polyethylene terephthalate can easily transformed to fibrous adsorbent by grafting acrylic acid/acryl amide (AA/AAm) comonomers onto poly PET. In this work, the ability to remove neodymium ion from aqueous solutions has studied using modified polyethylene terephthalate by acrylic acid (PET-AA) and acrylamide (AAm), as adsorbent [1, 2].

Materials and methods:

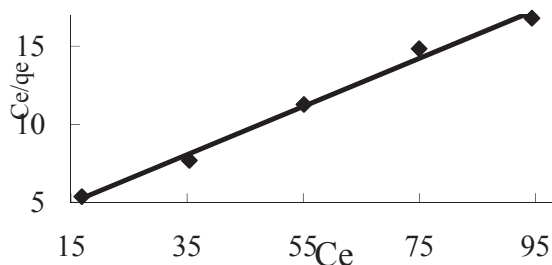
Acrylic acid, acryl amid, benzoyl peroxide, acetone, $\text{Nd}(\text{NO}_3)_3$, NaH_2PO_4 , Na_2HPO_4 , CH_3COONa and CH_3COOH were products of Merck (Darmstadt, Germany). The stock solution (1000 mg L^{-1}) of $\text{Nd}(\text{III})$ was prepared by dissolving appropriate amounts of $\text{Nd}(\text{NO}_3)_3$, in deionized water. The 0.01M acetic acid–acetate buffer (pH 3– 6.5), 0.01M

phosphate buffer (pH 6.5–9) were used to adjust the pH of the solutions, when needed. An inductive couple plasma-atomic emission spectroscopy (ICP-AES), Varian Australia, model Vista was used for concentration measurement of metal ions. The modified fiber (PET-AA:AAM) was investigated by different experimental techniques of characterization such as fourier transform infrared spectroscopy (FT-IR), thermogravimetric analysis (TGA), scanning electron microscopy (SEM) and elemental analysis (CHN).

Results and discussion:

The PET-AA:AAM was examined in a series of batch adsorption experiments for removal neodymium ion from wastewater sample. The ion adsorption of PET-AA:AAM was determined by the inductively coupled plasma-atomic emission spectroscopy (ICP-AES) method. Effects of pH, concentration of the metal and temperature have also studied. The equilibrium adsorption data of Nd(III) on modified fiber were analyzed by Langmuir, Freundlich, and Temkin models [3]. Based on equilibrium adsorption data, the Langmuir, Freundlich, and Temkin constants were determined as 6.493, 1.37, and 0.734 at pH 6 and 25°C, respectively.

Langmuir isotherm model			
$q_{max}(\text{mg/g})$	$K_L(\text{L/mg})$	R_L	R^2
6.493	0.0584	0.047	0.991
Freundlich isotherm model			
$K_F(\text{mg g}^{-1})(\text{L mg}^{-1})^{1/n}$	n		R^2
1.37	3.215		0.925
Temkin isotherm model			
$A(\text{L g}^{-1})$	$B(\text{J mol}^{-1})$	$b(\text{J mol}^{-1})$	R^2
0.734	1.316	1882.65	0.946



Conclusion:

A fibrous adsorbent was applied by grafting acrylic acid/acryl amide comonomers onto PET. The resin has a good potential for enrichment of trace amount of Nd(III) from large sample volumes. Based on the Langmuir isotherm analysis, the monolayer adsorption capacity was determined to be 6.49 (mg g^{-1}) at 25°C. The R_L values showed that the PET-AA/AAM fiber was favorable for the adsorption of Nd(III).

Reference:



- [1] Z. G. Liu; J. H. Ouyang; Y. Zhou; *Journal of Alloys and Compounds*; 475, 21, 2009.
- [2] L. E. Nielsen; R. F. Landel; *Properties of Polymers and Composites*; Dekker, New York; 1994.
- [3] J. R. E. Marie; D. N. Ronald; M. C. Per, *Langmuir*; 18, 1604, 2002.

15th Physical Chemistry Conference



Viscosity deviation of binary mixtures of Dimethyl Carbonate and a homologous series of 2-Alkanols at different temperatures

N. Namakishooshtari^{a*}

^aDepartment of Chemistry, Science and Research Branch, Islamic Azad University, Khouzestan, Iran

Email: navid29ab@yahoo.com

Key words: Viscosity deviation, Binary mixture, Dimethyl Carbonate, 2-Alkanols

Introduction:

Viscosity deviation properties of mixtures provide information about molecular interactions between the various components and can be used for the development of molecular models describing the thermodynamic behavior of mixtures [1– 2]. The dynamic viscosity deviations of mixtures are of great industrial interest, as it provides direct information about the energetic effects arising between the molecules present in the mixture, so it can help explaining the rearranging of the bondings that occurs during the mixing process, which is essential when studying new theoretical approaches to the liquid state, either pure or mixture.

Materials and methods:

Dimethyl carbonate, 2-propanol, 2-butanol, 2-pentanol, 2-hexanol and 2-heptanol were purchased from Merck company with purity higher than 99% , then used without further purification. Kinematic Viscosities were measured with an Ubbelohde viscometer. then dynamic viscosities (η) calculated by multiplying the kinematics viscosity in density . The temperature in the cell was regulated to ± 0.01 K. The mixtures were prepared by weighing known masses of pure liquids in airtight, narrow-mouth ground stoppered bottles taking due precautions to minimize evaporation losses.

Apparatus:

Densities of the pure liquids and binary mixtures at various temperatures were measured by means of an Anton Parr densimeter and a digital balance made by Mettler Toledo company. temperature was regulated with laboratory bath made by Petrotest company. Kinematic

Viscosities were measured with an Ubbelohde viscometer made by Townson & Mercer company with an uncertainty of $\pm 1 \times 10^{-2} \text{ mPa} \cdot \text{s}$.

Result and discussion:

The viscosity deviation $\Delta\eta$ in all studied mixtures were evaluated using the equation:

$\Delta\eta = \eta - x_1\eta_1 - x_2\eta_2$ (1) Where η is the dynamic viscosity of the mixture, η_1 and η_2 are viscosities of pure components, x_1 and x_2 are the mole fractions. $\Delta\eta$ for the binary systems were fitted by the least-squares method to the Redlich–Kister equation [3].

$$\eta_{ij} = x_i x_j \left(A_0 + \sum_{k=1}^n A_k (1 - 2x_i)^k \right) \quad (2)$$

viscosity deviation of all mixtures are negative and get more negative with increasing of chain length of 2-Alkanols and temperature decreasing.

Experimental data and fitted equations for all of binary systems are depicted in Fig. 1

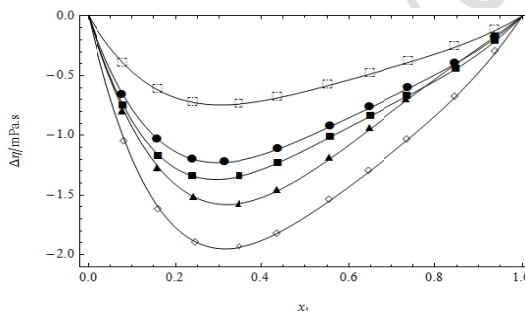


Fig. 1 dynamic Viscosity deviations $\Delta\eta$ for binary mixtures of Dimethyl carbonate with (◻) 2-propanol, (●) 2-butanol, (■) 2-pentanol, (▲) 2-hexanol, (◇) 2-heptanol at $T = 298.15 \text{ K}$. The solid curves were calculated from coefficients of equation (2)

Conclusion:

Negative quantities of viscosity deviations of Dimethyl carbonate and 2-alkanols mixtures show that dominant factors are physical interactions that are less strong than pure components.

Reference:

[1] Iloukhani, H., Almasi, M.; "Densities, viscosities, excess molar volumes, and refractive indices of acetonitrile and 2-alkanols"; J. Thermochim Acta. 495, 139–148 (2009)



- [2] Almasi, M.; Sarkoohaki, B. "Densities, Viscosities, of Binary Mixtures of Cyclohexanon and 2-Alkanols"; *J. Chem. Eng. Data* 2012, 57, 309–316.
- [3] Redlich, O., Kister, A.T.; "Algebraic representation of thermodynamic properties and the classification of solutions". *Ind. Eng. Chem.* 40, 345–348 (1948)

15th Physical Chemistry Conference



Investigating the impact of the onion change on the interaction potential of 1-butyl-3-methylimidazolium ionic liquids by using the experimental pVT data

M. ShekarKhand*, M. Bahadori

Islamic Azad University Marvdasht Branch, Marvdasht,

Iran Fax: +98 728 3311156

E-mail: honey.sh_66@yahoo.com

Key words: Ionic Liquids, Internal Pressure, Potential, Imidazolium

Introduction:

A broad range of applications of ionic liquids, including green solvent for synthesis and separation and electrolyte, are expected due to their low melting point, low-flammability, negligible vapour pressure, high conductivity and electrochemical stability [1,2]. Structures and properties of ionic liquids are controlled by interactions between ions. The size, shape, and composition of the ions affect the thermodynamic properties of ionic liquids by influencing the crystal packing ability and lattice energy of the ionic liquid [3]. In general, the internal interactions of ionic liquids will decrease with an increase in the size and complexity of the anionic and cationic components. This is due to a greater charge delocalization and charge isolation. Interestingly, this trend is not straightforwardly predictable.

Materials and methods:

The physical base of the internal pressure as $-(\partial U/\partial V)$ is a force tending to close together the molecules that is intermolecular interaction. The experimental pVT data can be used to calculate the internal pressure, as well. Therefore, this thermodynamic quantity is a fine measure to investigate the effect of the onion change on the ionic liquids internal interactions.

Result and discussion:

In this work to explore the behaviour of the internal interactions, the internal pressure of four ionic liquids was calculated from the experimental pVT data [4]. These ionic liquids consisted of a 1-butyl-3-methylimidazolium cation, and Bf_4 , PF_6 , Ntf_2 and OcSO_4 anion. For small



anions the variation of the internal pressure is similar. As the anion size increased the behavior of the internal pressure changes, because the interaction energy does lower due to the delocalization of Coulombic packing. Finally to estimate the appropriate potential model for the investigated polar fluids, three different reported potential models have been applied to the experimental internal pressure.

References:

- [1] Wasserscheid, P., R. Van Hal, A. Boesmann, *Green Chem.* **2002**, 4, 400
- [2] Mihkel K. Ionic Liquids in Chemical Analysis Edition: illustrated. CRC Press, **2008**.
- [3] Wasserscheid P., Welton T., Ionic Liquids in Synthesis, 2e. Wiley-VCH Verlag GmbH & Co. KGaA, Weinheim. **2008**.
- [4] <http://www.ilthermo.com>



Studies on corrosion of copper-aluminum alloys in artificial sea water

S.A. Nabavi-Amri* ¹; M. MirAhmadi¹

Thermodynamic research lab, School of Chemistry, Damghan University, Damghan, Iran

* E-mail: nabavi@du.ac.ir

Keywords: Corrosion, Copper-aluminum alloys, Sea water, Chart tafel

Introduction:

The corrosion of metals can be discussed in terms of terrestrial environments with temperate, tropical, and desert subdivisions, as well as aquatic environments, with salt and fresh water subdivisions [1]. Copper-aluminum alloys are frequently used in marine water systems. They have indeed an attractive price and offer interesting mechanical characteristics associated to a relatively good resistance to corrosion in sea water [1, 2]. With respect to increase the use of copper - aluminum alloys in these Aquatic environment the importance of examining these alloys corrosion in seawater has granted [3].

Materials and methods:

We used here artificial environment like the sea environment, to produce the copper-aluminum alloy we melted aluminum, and then gradually added copper to this molten. After each addition to prevent casualties reduce the temperature. Will be cutting and preparation of samples, all mechanical operations on the samples, such as cutting, grinding and pressing polishing were performed under water to prevent global warming and change their nature. The exact composition of the samples was determined with ICP method. Copper – aluminum alloys Chart tafel was measured in the range between 1 and -1.7 by autolab device.

Result and discussion:

Figure 1.a. shows variation of copper corrosion lower 60% wt Cu. Figure 1.b. and 2 showed the microstructure and XRD spectrum of Al and 11.58, 86.54% wt Cu respectively.

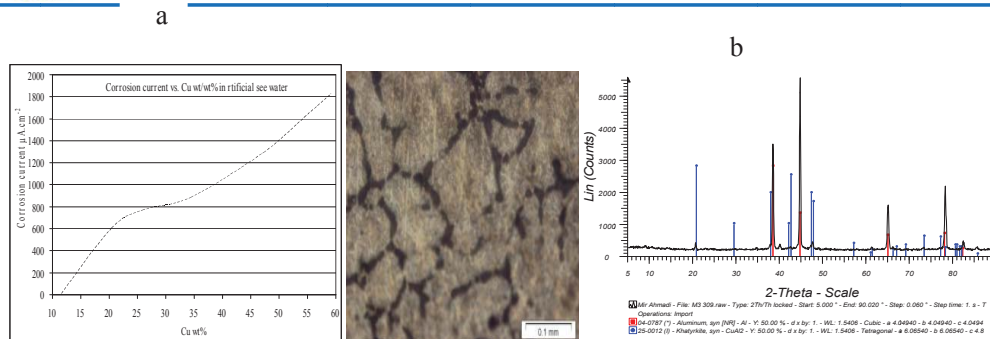


Fig. 1a. The variation between corrosion current %60wt Cu. **1b.** Microstructure and XRD Spectrum of Al and 11.58% wt Cu

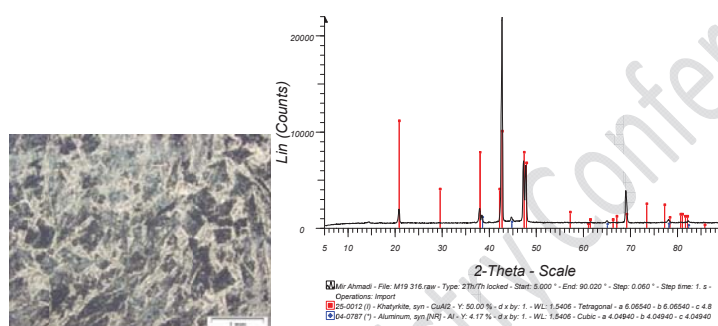


Fig.2. Microstructure and XRD Spectrum of Al and 54.45% wt Cu.

Conclusion:

The above figures show that corrosion increases with increasing %wt Cu that is certifiable by impedance and Tafel graphs.

References:

- [1] BC SYRETT, Sulfide attack in steam surface condensers, Conf on environmental Degradation of engineering materials in an aggressive environment, Virginia Polytechnic Institute, 1981.
- [2] AM BECCARIA, G POGGI, P TRAVERSO, A study of 70Cu30Ni commercial alloy in sulphide polluted and unpolluted sea water, Corrosion Science vol 32, N. 11, 1991, pp. 1263.
- [3] JN AL-HAJJI and MR REDA, The corrosion of copper alloys in sulfide polluted Sea water: the effect of sulfide concentration, Corrosion science Vol 34 n.1, 1993, pp. 163.



Characterization of α -amylase in Ardabil honey

S.S Seyedhatami^{a*}, H.Yaghobi^b, A.Shamel^a

^a Department of chemistry, Ardabil Baranch, Islamic Azad University, Ardabil, Iran

^b Department of biology, Ardabil Baranch, Islamic Azad university, Ardabil, Iran

Email: somayeh.seyedhatami@gmail.com

Key word: Activity, Enzyme amylase, Effect, Temperature, Honey

Introduction:

In honey there are many component α - glucosidase (invertase), α - and β - amylase (diastase), glucose oxidase, catalase and acid phosphatase. Over the years, the amylase component of honey has received attention as a freshness indicator [2]. The enzyme activity in honey has been widely studied for many years [1-2-3]. The aim of this study was to optimization method assay starch-iodine for determining activity sample of honey from beekeeper and consider effect temperature stability of amylase honey.

Materials and methods:

In the starch-iodine assay, 2 tubes were prepared with 420 μ L 0.2 M sodium acetate buffer (pH 5.3), 340 μ L 2% soluble starch and 40 μ L 0.5 M NaCl. After incubation at 40 °C for 10 min, 200 μ L of solution honey 30g/10 mL (assay tube) or 0.01 M Tris-chloride buffer (blank tube) were added. At time intervals, 20 μ L aliquots were taken out of each tube and added to iodine solution, which was prepared fresh everyday from iodine stock solution (1.1 g KI and 0.44 g resublimed I in 50 mL deionized water). The fresh iodine solution was prepared by dissolving 0.4 g KI in 100 μ L stock iodine solution and making it to 10 mL with deionized water. The amount of dilution for the fresh iodine solution that could be mixed with the 20 μ L of starch/enzyme solution to give an absorbance reading of 0.65 at 610 nm was predetermined for better reproducibility and averaged approximately 1 mL. The blank readings for absorbance at 610 nm were subtracted from the assay readings and recorded. One unit of activity with starch-iodine assay was calculated from the slope of the curve, which determined $\Delta 610\text{nm}/\text{min}$ because of the degradation of soluble starch and thus loss of iodine



binding ability. the thermal stability of the honey amylase was determined 40,50,60,70 and 80 °C in water bath.

Apparatus:

The spectrophotometry UV/Visible, Jenway model 6305 made in England has been Applied for measure the optical absorption.

Result and discussion:

Sample of honey was spring honey from one beekeeper of city Meshkin whit amount of enzyme 0.46 unit IU. Usually honeys of early spring and the lower contents of the enzyme is caused by lower concentration of nectar with a higher participation of saccharide and a reduced activity of bee colonies during their growing [2]. The honey amylase showed Michaelis–Menten type kinetics. the Lineweaver-Burk plot gave apparent K_m and V_{max} values at 40 °C and pH 5.3 of 0.34mg/mL and 0.007units/mL, respectively. The storage stability of the enzyme amylase from honey in Tris-chloride buffer pH 7 was tested at time intervals at 4 °C the enzyme was stable for over 8 week without losing any activity under these conditions. The temperature stability of the amylase from honey was tested at 40, 50, 60,70 and 80 °C in buffer at pH 7 After 1h incubation the enzyme lost 32%, 55%,62%,63% and 67% of its activity at temperature values of 40, 50, 60,70and 80 respectively.

Conclusion:

In this study ,we applied kinetics Michaelis–Menten for enzyme amylase of one sample from Ardabil established a number of stability and activity characteristics for α -amylase from honey.

Reference:

- [1]. S.Babacan,A.G.Rand; "Characterization of honey amylase; Food Science;72 ,50-55,2007
- [2]. L.Vorlová, A.Piidal; "Invertase and diastase activity in honey Czech provenience act; Univ. et silvic.Mendel.Brun; 5,57-66,2002.



- [3]. JW. White, I. Kushnir;" Effect of storage and processing temperatures on honey quality ;Food Technol;18 ,555-558,1964.

15th Physical Chemistry Conference



Kinetic and Isothermal Studies of Cadmium Sorption onto Poly (Ethylene Terephthalate) Fibers Grafted with 2-Hydroxy Propyl Methacrylate

A. Borzou^{*a}, M. Kalbasi^b, M. Hoodaji^b, M. Abdouss^c, A. Mohammadi^b

^a Department of Agriculture, Varamin-Pishva Branch, Islamic Azad University, Varamin, Iran

^b Department of soil science, Faculty of Agriculture, Islamic Azad University, Branch Khorasgan, Isfahan, Iran

^c Department of chemistry, Faculty of sciences, Amir Kabir University, Tehran, Iran

Email: arash_borzou@iauvaramin.ac.ir

Key words: Copolymer, Cadmium, Isotherm, Kinetic study.

Introduction:

This study deals with the use of poly (ethylene terephthalate) fibers (PET) grafted with 2-hydroxy propyl methacrylate for removal of the Cd(II) ions from aqueous solutions. Batch procedures were carried out to investigate the sorption of Cd(II) to the sorbents with particular focus on sorption kinetics and isotherms.

Materials and methods:

PET is used as the base and has grafted with 2-hydroxy propyl methacrylate as monomer with methods was recommended by Azizinejad, 2011;. The specific surface area and cation Exchange capacities of the samples were measured using BET-N₂ sorption analysis and Na-acetate method described by Chaari et al, 2009, respectively. All sorption experiments were conducted in batch experiments in 0.01M calcium chloride Ca (Cl₂), with the highest grafted copolymer yields at 298±2K, adsorbents concentration of 0.25%, pH 5.95, Shaking rate 150 rpm, Contact time for equilibrium 60 minutes, Volume solution 20 mL.

Isotherms studies condition were at different concentrations of Cd(II) from 5 to 60 mg/L. Kinetics studies were done at 5 mg per liter Cd concentration, shaking rate 0 rpm.

Result and discussion:

Experiments results were investigated by two isotherm models, Langmuir and Freundlich.

The best model was Langmuir based on the equation of: $\frac{1}{q_e} = \frac{1}{K_a q_m} \frac{1}{C_e} + \frac{1}{q_m}$ (Fig 1). This fact identifies the adsorption process is monolayer.

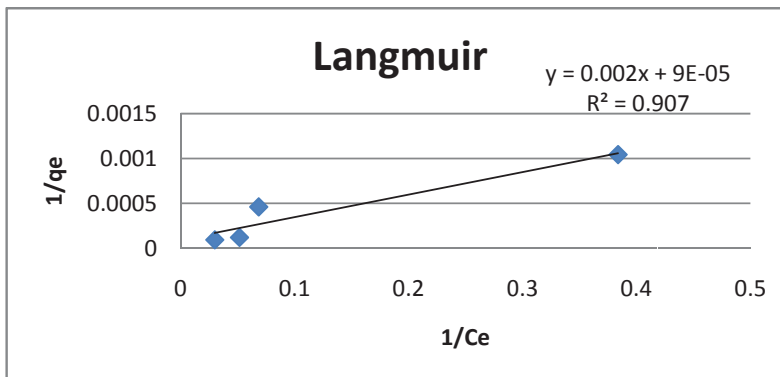


Fig 1: Longmuir isotherm model at fixed conditions.

Kinetics data were investigated by Pseudo-first-order and Pseudo-second-order models. The best results observed in Pseudo-first-order (Fig 2).

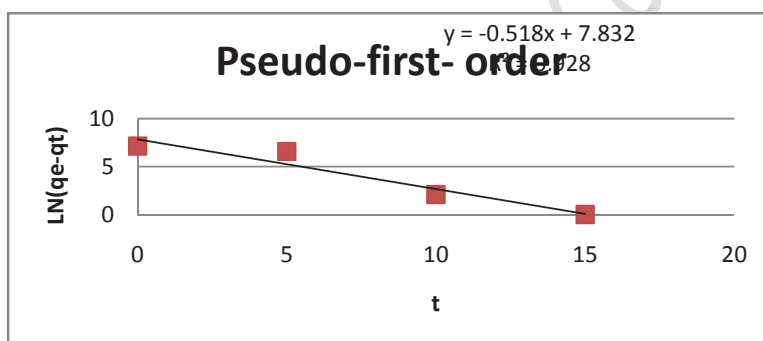


Fig 2: Pseudo-first-order kinetic model at fixed conditions.

Conclusion:

Our works showed that, adsorption of Cd(II) ions by modified PET was monolayer and it may be attributed to physisorption onto PET.

Reference:

- [1] Arslan, M. 2010. Preparation and use of amine-functionalized glycidyl methacrylate-g-poly (ethylene terephthalate) fibers for removal of chromium (VI) from aqueous solution. J fibers and Polymers; 11:3:325-330.
- [2] Azizinezhad, F., (2011). Grafting of 2-hydroxypropyl methacrylate onto poly (ethylene terephthalate) fibers and dye ability. Asian J. Chemistry; 23; 2: 839-842.



- [3] Chaari, M., M, Feki., and M, Medhube. ., 2009.. Adsorption of textile dye "Indaynthrene blue RS (C.V.a. vat blue 4)" from aqueous solutions onto smectite-rich clayey rock. J. Haz. Mat; 172:1623-1628.

15th Physical Chemistry Conference



Adsorption properties of 2-hydroxy propyl methacrylate grafted onto poly ethyleneterephthalate fibers for removal of Cd (II) ions.

A. Borzou*^a, M. Abdouss^b, M. Kalbasi^c, M. Hoodaji^c, A. Mohammadi^c

^a Department of Agriculture, Varamin-Pishva Branch, Islamic Azad University, Varamin, Iran

^b Department of chemistry, Faculty of sciences, Amir Kabir university, Tehran, Iran

^c Department of soil science, Faculty of Agriculture, Islamic Azad University, Branch Khorasgan, Isfahan, Iran

Email: arash_borzou@iauvaramin.ac.ir

Key words: Copolymer, Cadmium, Adsorption properties, poly (ethylene terephthalate)

Introduction:

Different methods for removing of heavy metals from industrial wastewater were applied such as, chemical precipitation, ion exchange, reverse osmosis and ion adsorption cited. Adsorption method with respect to high efficiency and ease of use is one of the most widely used methods introduced.

This research involves the use of the same polymer called poly (ethylene terephthalate) (PET) that is used as adsorbent. The polyester polymers have high crystalline properties and low hydrophilic and can resist biodegradation and high stability at acidic and basic pH conditions.

Materials and methods:

PET is used as the base and has grafted with 2-hydroxy propyl methacrylate as monomer with methods was recommended by Azizinejad, 2011;. The structure of the monomer has – OH alcohol as the active group. Various percentage of grafted copolymer was provided into 3 levels (0-20, 20-40 and upper than 40%).

Copolymer properties:

Cation exchange capacity (CEC) obtained using sodium acetate solution and calculated equal 177 meq per 100 g sorbent.

The point of zero charge (pH_{ZPC}) by the use of potentiometer, according to Chaari et al, 2009 method; was 5.86.



Specific surface area of the adsorbent with BET (Branuer – Emmet - Teller) method was determined 0.42 square meters per gram.

All sorption experiments were conducted in batch experiments in 0.01M calcium chloride Ca (Cl₂). Experiments were started with the highest grafted copolymer at adsorbents concentrations of 0.25%, cadmium concentration 5 mg per liter, Shaker speed 150 rpm, Volume solution 20 mL and at temperature (25±2°C).

Result and discussion:

In order to achieve the best conditions for cadmium following characteristics were studied. In each case, using the graph drawn between the desired properties and metal uptake was selected as the best conditions. The first characteristic (pH) was changed between 3.72 to 8.28. Appropriate pH was 5.95. Dimensional properties of contact time between adsorbent and the adsorbate. It was changed from 5 to 75 minutes. The most appropriate time was 60 minutes. Other properties include the concentration of cadmium, the percentage of graft copolymer was produced and the concentration of adsorbent. It has been changed the order of 5 to 60 mg per liter, 0 to above 40%, and 0.25 to 1% was considered. The most suitable adsorbate concentration was 5 mg per liter. Highest percentage of grafts was selected as the most appropriate option. Optimal adsorbent concentration was 0.25%.

Conclusion:

Appropriate conditions for the uptake of cadmium were obtained as follows. The optimum pH was 5.95, and the most suitable time was 60 min, the highest percentage of grafting copolymer was recommended, the most appropriate sorbent concentration equal to 0.25% and the adsorbate was (Cd) 5 mg liter. The results showed that the produced copolymer is suitable for cadmium absorption.

Reference:

[1] Azizinezhad, F., (2011). Grafting of 2-hydroxypropyl methacrylate onto poly (ethylene terephthalate) fibers and dye ability. Asian J. Chemistry; 23; 2: 839-842.



- [2] Chaari, M., M, Feki., and M, Medhube. ., 2009.. Adsorption of textile dye "Indaynthrene blue RS (C.V.a. vat blue 4)" from aqueous solutions onto smectite-rich clayey rock. J. Haz. Mat; 172:1623-1628.

15th Physical Chemistry Conference



Degradation of Acid Blue 113 as organic pollutants in aqueous media by ozonation.

J. BasiriParsa, S. mohamadi*

Department of Chemistry, Faculty of Chemistry, Bu-Ali Sina University, Hamedan, Iran

Email: saman.mohammadi2012@gmail.com

Keywords: ozone, organic pollutant, wastewater

Introduction:

Large amount of chemically various dyes are used for several industrial applications. Due to environmental implications, new technologies have been evaluated for degradation of these compounds in textile effluents. Some studies suggest employing advanced oxidative processes (AOPs) in isolation or combined for preliminary assessment [1]. AOPs have been defined as the aqueous phase chemical oxidation of target organic or inorganic pollutants by a process involving hydroxyl free radicals [2]. In general, ozone oxidation pathways include direct oxidation by ozone or indirect oxidation by hydroxyl radicals (OH^\bullet). Direct oxidation involves degradation of organics by ozone molecules under acidic conditions, in which an ozone molecule reacts with an unsaturated bond due to its dipolar structure, leading to a splitting of the bond. While the term indirect oxidation considers degradation mechanism of organic throughout hydroxyl radicals and it occurs under basic conditions [3].

Using ozonation for decolorizing wastewater has the following advantages: 1) Ozone is readily available, soluble in water and easily monitored. 2) It does not increase the volume of wastewater and sludge. 3) It removes color and reduces the organic matter in one step. The aim of this study is the degradation of the Acid Blue 113 (AB113) as organic pollutant by ozonation and optimization of effective parameters including initial pH and initial dye concentration by response surface methodology (RSM).

Materials and methods:

AB113 is a secondary diazo dye having the molecular ($\text{C}_{32}\text{H}_{21}\text{N}_5\text{Na}_2\text{O}_6\text{S}_2$) and molecular weight of 681.65, was selected as model solution, which was commercial dye and used without further purification. This diazo dye was provided by Alavansabet company (Iran).



Other chemicals, purchased from Merck, were of analytical grade. Initial pH of the model solution was adjusted using diluted sodium hydroxide or sulfuric acid solutions. All solutions were prepared by using deionized water.

Apparatus:

All experiments were carried out in a mixed reactor made of Pyrex glass with a total volume 600mL. A magnetic stirrer (Alfa, HS – 860) was used for mixing the solutions. The pH of the solutions was checked using a pH meter (AZ - 86502). Ozone gas produced from air by ozone generator (Onnic. ES215A). In all experiments, the samples of AB113 was taken periodically from the reactor and analyzed by the UV-visible spectrophotometer (JASCO. v-630) via the decrease in absorbance at 566 (nm).

Results and discussion:

Experiments were carried out at room temperature by varying the initial dye concentration from 30 to 100 (mg/L) and pH from 5 to 10. In optimization, the desired aim in terms of AB113 removal efficiency was defined as target to achieve 95.96% removal efficiency at 15 min. The optimum amounts for variables obtained with consideration of 8.24 and 30 mg/l, as starting values for initial pH, initial dye concentration. By increasing the dye concentration, the decolorization rate is decreased and the complete decolorization is attained more slowly. The reason could be that under the applied conditions, with the increase of the dye concentration, the ratio of ozone molecules to dye molecules in the solution decreases. The highest decolorization rate for AB113 occurred at the most basic conditions. In high pH the amount of the hydroxyl radical increased and the oxidation ability of hydroxyl radical because of its higher oxidation potential, significantly exceeded that of ozone molecule, Then removal efficiency will be higher.

Conclusion:

In optimization, the desired aim in terms of AB113 removal efficiency was defined as target to achieve 95.96% removal efficiency at 15 min. The optimum amounts for variables obtained with consideration of 8.24 and 30 mg/l, as starting values for initial pH, initial dye concentration.



References:

- [1] S.M.d.A.G.U.d. Souza, K.A.S. Bonilla, *Journal of Hazardous Materials*, 179 (2010) 35–42.
- [2] E.J. Rosenfeldt, K.G. Linden, S. Canonica, *Water Research*, 40 (2006) 3695 – 3704.
- [3] N. Kishimoto, Y. Morita, H. Tsuno, T. Oomura, *Water Research*, 39 (2005) 4661–4672.

15th Physical Chemistry Conference

Harmonic balance method and the nonlinear ion trap

AlirezaDoroudi¹, NaghmehSajadi², AminehRezaeianAsl²

¹Physics Department, Nuclear Science research School, Nuclear Science and Technology Research Institute,
Tehran, Iran

²Department of Physics, Center of Tehran Branch, Islamic Azad University, Tehran, Iran

Email: na.sajadi@gmail.com

Abstract:

Ion trap mass spectrometer is a device that can separate ions, according to their mass to charge ratio. One of the most common type of this spectrometer is quadrupole field ion trap. In this article we review the equations of motion of ions in a nonlinear ion trap and calculate the secular axial frequencies of ion motion by using harmonic balance method. The results obtained by the harmonic balance method are close to the results of iteration method.

Keywords: quadrupole field, ion trap, secular frequencies, harmonic balance method.

Introduction:

Recognition of exact behavior of ions in ion trap is very important. In the ideal ion trap, the equation of ion motion has the simple form and the main properties of motion can be obtained by solving the linear Mathieu differential equation. But in a real ion trap, the field distribution is no longer linear [1,2]. Nonlinear behavior causes by superposition of multipolar fields higher than quadrupole field inside the trap and the resulting equation of ion motion is the nonlinear Mathieu differential equation [3]. Application of the iteration method gives the following equation [4]:

$$\ddot{x} + \omega_A^2 x = \omega_A^2 x - g(x) = G(x), \quad x(0) = A, \dot{x}(0) = 0 \quad (1)$$

$$\ddot{x}_{k+1} + \omega_A^2 x_{k+1} = G(x_k), \quad x_k(0) = A, \dot{x}_k(0) = 0, k = 0, 1, 2, \dots \quad (2)$$

that:

$$G(x) = \omega_A^2 x - \omega_0^2 x - \alpha_2 x^2 \operatorname{sgn}(x) - \alpha_3 x^3 \quad (3)$$

$$\ddot{x}_1 + \omega_A^2 x_1 = G(x_0), \quad x_1(0) = A, \dot{x}_1(0) = 0, \quad x_0 = A \cos \omega_A t \quad (4)$$

$$\text{for } x \succ 0 \quad \omega_A = \omega_{A1} = \sqrt{\omega_0^2 + \frac{8}{3\pi} \alpha_2 A + \frac{3}{4} \alpha_3 A^2} \quad , \quad \frac{\omega_A}{\omega_0} = \frac{\omega_{A1}}{\omega_0} = \sqrt{1 + 6A^2 f_2 + \frac{12Af_1}{\pi}} \quad (5)$$

With this method, for the B domain:

$$\text{for } x \prec 0 \quad \omega_A = \omega_{B1} = \sqrt{\omega_0^2 - \frac{8}{3\pi} \alpha_2 B + \frac{3}{4} \alpha_3 B^2} \quad , \quad \frac{\omega_A}{\omega_0} = \frac{\omega_{B1}}{\omega_0} = \sqrt{1 + 6B^2 f_2 - \frac{12Bf_1}{\pi}} \quad (6)$$

Harmonic balance method:

One powerful method for solving the equations of nonlinear motions is harmonic balance method. In general, the nonlinear equation with hexupole superposition is :

$$\ddot{x} + x + \varepsilon x^2 = 0, x(0) = A \succ 0, \dot{x}(0) = 0 \quad (7)$$

The method of harmonic balance is capable of producing analytical approximation to the nonlinear system, but this method cannot be directly applied to equation 7 because $f(x) = x + \varepsilon x^2$ is not odd function of x . so we use the $\text{sgn}(x)$ function.

$$\ddot{x} + \omega_0^2 x + \alpha_2 x^2 \text{sgn}(x) + \alpha_3 x^3 = 0, \quad x \geq 0 \quad (8)$$

$$\ddot{x} + \omega_0^2 x - \alpha_2 x^2 \text{sgn}(x) + \alpha_3 x^3 = 0, \quad x \leq 0 \quad (9)$$

Using the harmonic balance method[1]:

$$x = \sum_{m=0}^M A_m \cos(m\omega t + m\beta_0) \quad (10)$$

Assuming $m=1$:

$$x = A_1 \cos(\omega t + \beta_0) = A_1 \cos\phi = A_1 \cos\omega t \quad (11)$$

By putting (11) in (8):

$$-(\omega^2 - \omega_0^2) A_1 \cos\omega t + \alpha_2 A_1^2 \cos^2\omega t \text{sgn}(A_1 \cos\omega t) + \alpha_3 A_1^3 \cos^3\omega t = 0 \quad (12)$$

By using Fourier transform:

$$-(\omega^2 - \omega_0^2) A_1 \cos\omega t + \alpha_2 A_1^2 \left(\frac{8}{3\pi} \cos\omega t + \frac{8}{15\pi} \cos 3\omega t - \frac{8}{105\pi} \cos 5\omega t \right) + \alpha_3 A_1^3 \left(\frac{3}{4} \cos\omega t + \frac{1}{4} \cos 3\omega t \right) = 0 \quad (13)$$

Eliminating the secular terms:

$$\omega_0^2 - \omega^2 + \frac{8A_1\alpha_2}{3\pi} + \frac{3A_1^2\alpha_3}{4} = 0 \quad (14)$$

and assuming $\alpha_2 = \frac{9}{2}f_1\omega_0^2$, $\alpha_3 = 8f_2\omega_0^2$ and A_1 domain, the first approximation frequency is:

$$\text{for } x > 0 \quad \omega_{A_1} = \sqrt{\omega_0^2 + \frac{8}{3\pi}\alpha_2 A_1 + \frac{3}{4}\alpha_3 A_1^2} \quad , \quad \frac{\omega_{A_1}}{\omega_0} = \sqrt{1 + 6A_1^2 f_2 + \frac{12A_1 f_1}{\pi}} \quad (15)$$

And with assuming B_1 domain in equation 9:

$$\text{for } x < 0 \quad \omega_{B_1} = \sqrt{\omega_0^2 + \frac{8}{3\pi}\alpha_2 B_1 + \frac{3}{4}\alpha_3 B_1^2} \quad , \quad \frac{\omega_{B_1}}{\omega_0} = \sqrt{1 + 6B_1^2 f_2 + \frac{12B_1 f_1}{\pi}} \quad (16)$$

Results:

Table 1 shows the calculated values of $\frac{\omega}{\omega_0}$ with assuming superposition of hexupole field (f_1) and octupole field (f_2). The amounts of domain B is used for $x < 0$. In this table values of $\frac{\omega}{\omega_0}$ are compared with $\frac{\omega_{exact}}{\omega_0}$, which[5]:

$$\frac{\omega_{exact}}{\omega_0} = 2\pi \left(\int_0^A \frac{4dx}{\sqrt{(A^2 - x^2) + 4f_2(A^4 - x^4)}} \right)^{-1} \quad (17)$$

Table1. Comparison of the calculated values of $\frac{\omega}{\omega_0}$ for different values of f_1 and f_2 with the exact results

f_1	f_2	B	$\frac{\omega_{exact}}{\omega_0}$	$\frac{\omega_1}{\omega_0}$ (error)
0.01	0.01	0.721825	1.01478	1.01481(0.0029563)
0.05	0.05	0.775049	1.07113	1.07156(0.0515804)
0.10	0.10	0.829421	1.13922	1.14072(0.131669)
0.15	0.15	0.872078	1.20689	1.20999(0.256859)
0.20	0.20	0.905442	1.27412	1.27935(0.410479)
0.25	0.25	0.931747	1.3404	1.34812(0.575947)
0.12	0.30	0.794033	1.39888	1.40648(0.543292)
0.05	-0.05	0.824202	0.883223	0.88545(0.252145)
0.01	-0.10	0.733768	0.824691	0.828434(0.453867)

Conclusion:

In this paper the nonlinear equation of ion motion in a nonlinear ion trap in the presence of the quadratic and cubic nonlinearity is solved by harmonic balance method. The secular frequencies of the ion motion are calculated as a function of the nonlinear field parameters.



The results of this paper which have been calculated in the framework of the harmonic balance method is close to the results of the iteration method and comparable with the exact results. Calculation shows that the difference between $\frac{\omega_1}{\omega_0}$ of this paper and the exact values of

$\frac{\omega_e}{\omega_0}$ is too small.

References:

- [1] P.R. Hunan, Solution of a quadratic nonlinear oscillator by the method of harmonic balance, *Journal of Sound and Vibration*, 2005
- [2] R.E. Mickens, Quadratic non-linear oscillators, *Journal of Sound and Vibration* 270(2004) 427-432
- [3] B.S. Wu, C.W. Lim, Large amplitude non-linear oscillations of a general of a general conservative system, *International Journal of Non-linear Mechanics* 39(2004)859-870
- [4] R.E. Mickens, Iteration method solutions for conservative and limit-cycle $x^{\frac{1}{3}}$ force oscillators, *Journal of sound and Vibration* 292 (2006) 964-968
- [5] A. Dorudi, A. Rezaeian Asl, Calculation of secular axial frequencies in a nonlinear ion trap with hexapole, octopole and decapole superpositions by a modified Lindstedt-Poincare method *International Journal of Mass Spectrometry*, Volume 309, 1 January 2012, Pages 104-108



Investigation of the removal of Basic Violet 2 by the walnut shell from aqueous solutions: study of the experimental parameters

N. Attari*

Department of Chemistry, Islamic Azad University, Tabriz Branch, Tabriz. Iran.

Email: Naime_attari@yahoo.com

Key words: Adsorption, Walnut shell, Basic Violet 2, Dye removal.

Introduction:

Dyes are an important class of pollutants which could be used in many industrial activities such as textile, dyestuffs, printing and some other industries as important materials. These materials may be harmful to aquatic creatures and humans because many dyes are non-bio degradable, toxic, and stable to light and heat[1,2]. Therefore, the effective removal of dyes from aqueous systems becomes environmentally important. To date, a number of chemical, physical, and biological methods have been developed for removing dyes from wastewater. Among them, adsorption technique is believed to be one of the most effective and simplest processes, and various adsorbents have been tested to remove dyes from water. This has led to the search for more efficient and cheaper alternate adsorbents[3]. Researches showed that the walnut shell was effective and low-cost adsorbent for removing of aqueous dyes. In this research, the walnut shell was used as adsorbent for removing Basic Violet 2 from aqueous solutions. The effect of different experimental parameters such as initial dye concentration, amount of adsorbent, temperature and pH on the efficiency of adsorption process has been investigated.

Experimental (materials, apparatus and methods):

C.I. Basic Violet 2 (BV2) was obtained from ACROS company (Belgium). The natural walnut shell was used as adsorbent. NaOH and HCl which were used for pH adjustment were purchased from Merck (Germany). In order to determining the optimum amount of adsorbent, 0.05-0.6 g of walnut shell with the grain size of 100 were added into 50 mL of BV2 solution (11 mg.L^{-1}), followed by stirring for 30 min inside shaker (Julabo, SW-20C) with 140 rpm.



The adsorbents were then separated from the suspension via centrifugation (Hettich Eba 8S) and the concentration of dye was determined using a UV-Vis spectrophotometer (Ultrospec 2000, England). For studying the effect of initial dye concentration, different concentrations of BV2 in the range of 2-12 mg.L⁻¹ were prepared. Then 0.05 g of the adsorbent with the grain size of 60 was added into 50 mL of BV2 solution with desired concentration, followed by stirring for 2-60 min inside shaker with 140 rpm. At a given time intervals, the adsorbent was separated from the suspension and the concentration of residual dye was detected. For investigating of the influence of temperature on the dye removal process, 0.05 g of the adsorbent was added into 50 mL of BV2 solution with the initial concentration of 12 mg.L⁻¹, followed by stirring for 1 h at various temperatures (318-348 K). Then the adsorbent was centrifuged and the concentration of dye was determined. Finally, in order to studying of the pH effects on the efficiency of dye removal process, first pH of 50 mL BV2 solution with the initial concentration of 12 mg.L⁻¹ was adjusted at 3,5,7,8,9,11 respectively with NaOH 0.1 N, HCl 0.01 N. After 2 h the absorbance of solutions was determined. Then pH of 50 mL BV2 solution with the initial concentration of 12 mg.L⁻¹ was adjusted at above mentioned pHs. After 1 h, 0.05 g of adsorbent with the grain size of 60 was added into solutions, followed by stirring for 1h with 140 rpm. At the final step, the adsorbent was separated and the concentration of residual dye was measured.

Results and discussion:

Investigating of the effect of the amount of adsorbent showed that adsorption capacity decreased from 10.08 to 0.85 mg.g⁻¹ with increasing of the amount of adsorbent from 0.05 to 0.6. Results confirmed that efficiency of dye removal process decreased with increasing the initial concentration of the dye solution. An explanation to this behavior is that as initial concentration increases, more and more organic dye substances are adsorbed on the surface of

the adsorbent and so the number of active surface sites decreased. Also, decreasing vacant surface sites become difficult to be occupied due to the repulsive forces between the dye molecules[4]. Results showed that the percentage of dye removal increased from 84% to 89% with increasing of temperature from 318K to 348K. As the temperature increased, number of active sites and the motions of dye molecules increased too. BV2 is a cationic dye and the



alkaline pH degraded the dye structure. So, the optimum amount of pH for studying the dye removal process via adsorption was obtained 5.

Conclusion:

The optimum amount of adsorbent was obtained 0.05g. The results confirmed that efficiency of dye removal process decreased with increasing initial concentration of the dye solution and increased with increasing of temperature. The optimum amount of pH was 5. The amount of dye removal under optimum conditions was 90%. Over all, walnut shell showed excellent adsorptive characterization for the removal of dye from wastewater and could be employed as a low-cost alternative adsorbent.

References:

- [1] S. Rehman khan, A. Inert, A. am ad rana, *J. sci. ind. Res.*, Sorption of reactive and acide dyes from aqueous solutions onto sawdust , 45, 35-38. 2010
- [2] S. Hashemian, *Main Group Chem.*, Study of the adsorption of acid dye from aqueous solutions using bentonite , 6, 97-107. 2007
- [3] Gupta, V.K., Suhas, Application of low- cost adsorbents for dye removal:A review, *Envir.Manag.*,90, 2313-2342. 2009.
- [4] V., Dulman, S.M., Cucu-Man, *J. Hazard. Mater.*, Sorption of some textile dyes by beach wood sawdust, 162, 1457-1464, 2009.

ab initio Study of the Intramolecular Proton Transfer Reaction in Imine - Enamine Equilibrium: Effect of the electron donors and acceptors Substitutions on their Kinetics

A. Akbari¹ and H. R. Shamlouei^{*2}

^{1,2} Islamic Azad University, Gachsaran Branch, Gachsaran, Iran

*shamlouei@gmail.com

Key Word: ab initio, Imine –Enamine, Substitution effect

Introduction:

Proton transfer reactions between proton donors and acceptors in the biological energy conversion process are not hidden to anyone. These proton transfer reaction occur in coupled to electron transfer reactions occur which is taken place in mitochondria [1,2]. Additionally hydrogen bonded systems have highest importance in biology, solution chemistry and acid-base systems. For instance the presences of hydrogen bonds in amino acids are necessary for the final three dimensional structures of proteins such as Tertiary and Quaternary structure. This significance of proton transfer reaction and hydrogen bonded systems create a center of attention for scientists and many research were done to understand the chemistry of proton transfer reaction [3] and nature of hydrogen bonding [4]. It is considerable that the amino acids have the amino and carboxylic group. The proton transfer reaction which occurs in Imine-Enamine equilibrium, is one of the simplest reactions can be assumed as model of reaction taken place in biosystems, so studying its chemistry and recognizing all effective factors on it helps us to understanding the processes in many biological systems. The goal of this research is to study the effect of substitutions on kinetic and thermodynamics of proton transfer reaction in imine-enamine equilibrium as the model of proton transfer reaction in biosystems.

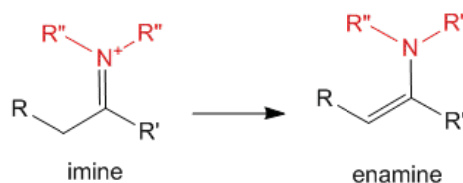


Fig1. Typical formula of Imine -Enamine reaction

By changing the R' the properties of imine and enamine alter. In this research the substitutions of R' were changed to produce new imine enamine systems with different properties and the kinetics of proton transfer reaction in those was studied.

Methods:

The energy surfaces for intramolecular proton transfer reaction between imine and enamine were calculated by MP2 method, 6-311++G(d,p) and the Gaussian03w package. For understanding the effect of substitutions on reaction kinetics, different substitutions were used instead of R. Selections of various substitutions were done in the manner that the constructed Enamine molecules have different properties.

Results:

In the first part of research, the energy surfaces of proton transfer between Imine and Enamine groups of the selected materials were calculated in gas phase. In Fig2 calculated energy surfaces for proton transfer reaction versus reaction coordinate (N-O distance) in Imine and Enamine with H substitution is shown. For understanding the effect of substitutions on reaction kinetics, the energy surface of proton transfer reaction of imine-enamine which have different substitutions mentioned in table1 were plotted and compared to others. In this part the energy surfaces for reactions taken place in electron donors and electron acceptors substitutions were compared.

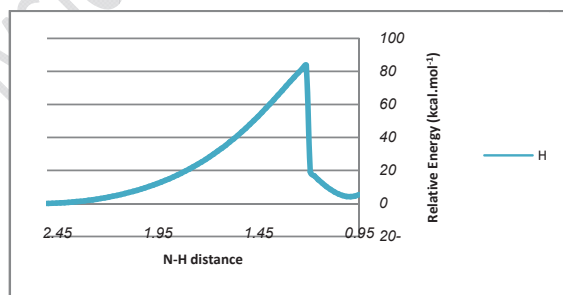
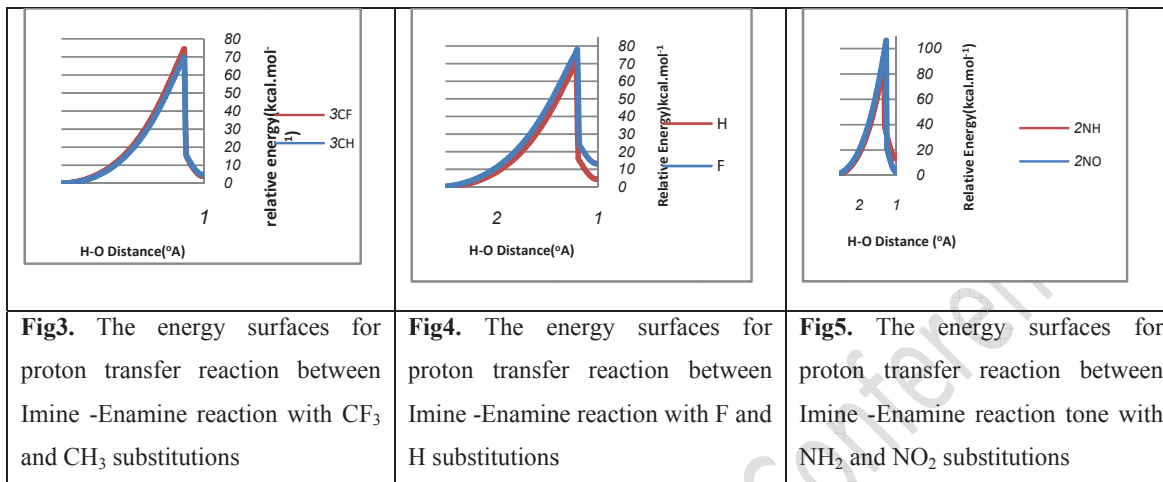


Fig.2 the energy surfaces versus reaction coordinates for Imine -Enamine reaction with H substitutions

In Fig3 comparison between energy surfaces of the proton transfer reactions in imine-enamine system with CH₃ and CF₃ substituent is illustrated. In Fig4 the comparison between the energy surface in proton transfer reaction in imine- enamine with -F and -H substitution

were shown. In Fig5 the energy surface of reaction in which two substitutions are equal to NH_2 and NO_2 were compare



The Figs 3 to 5 show that the energy surface, activation energy and enthalpy of proton transfer reaction is considerably affected by the nature of substitutions (electronegativity of substitutions). The activation energies of the reactions were determined by their corresponding energy surfaces. It was considerably from these results that the activation energies depend on the nature of substitutions. It is obvious from table2 that the activation energy for each substitution extensively depends on chemical nature (electronegativity) of substitutions.

Conclusion:

In this research the kinetics and thermodynamics of proton transfer reaction in Imine-Enamine system was studied. Then the effect of different substitutions on kinetics and thermodynamics was investigated. As the result of this research the electronegative substitutions that withdraw electrons from molecules and decrease the electron density from molecules will increase the activation energy of proton transfer reaction. Additionally the proton transfer thermodynamics (enthalpy) of proton transfer reaction are affected by nature of substitution and enthalpy of reaction increases as the substitutions draw the electron from molecule.

References :



- [1] P. J. Elving, W. T. Bresnahan, J. Moiroux, and Z. Samec, "524-NAD/NADH AS A MODEL REDOX SYSTEM: MECHANISM, MEDIATION, MODIFICATION BY THE ENVIRONMENT", *Bioelectrochemistry and Bioenergetics*, Vol.9 (1982) P:365
- [2] Pohl T, Spatzal T, Aksoyoglu M, Schleicher E, Rostas AM, Lay H, Glessner U, Boudon C, Hellwig P, Weber S, Friedrich T., "Electron and proton transfer in NADH:ubiquinone oxidoreductase (Complex I) from Escherichia coli", *Biochim Biophys Acta*, Vol.1797(2010) P:1894.
- [3] M.L. Paddock, G. Feher, M.Y. Okamura, "Proton transfer pathways and mechanism in bacterial reaction centers", *FEBS Letters*, VOL.555, (2003), P:45-50.
- [4] George A. Jeffrey, "An introduction to hydrogen bonding", (1997), Oxford University Press.



Intramolecular proton transfer reaction in Enol- Ketone equilibrium: ab initio Study of the electron donors and acceptors substitution effect on their kinetics and thermodynamics

F. Afshinpour¹ and H. R. Shamlouei^{*2}

^{1,2} Islamic Azad University of Gachsaran, Gachsaran, Iran

^{*}shamluei@iaug.ac.ir

Keywords: Intramolecular Proton Transfer Reaction, ab initio, Enol-Ketone

Introduction :

The crucial importance of proton transfer reactions between proton donors and acceptors in the biological energy conversion process not obscure to anyone. Some of the proton transfer reactions occurred in the presence of other procedures such as electron transfer. The processes of oxygen evolution in photosynthesis and oxidation processes in mitochondria are the examples in which the proton coupled electron transfer reactions occur [1,2]. Additionally hydrogen bonded systems have highest importance in biology, solution chemistry and acid-base systems. For notable example, the presences of hydrogen bonds in amino acids are important for the final three dimensional structures of proteins such as Tertiary and Quaternary structure. This significance of proton transfer reaction and hydrogen bonded systems create a center of attention for scientists and many research were done to understand the chemistry of proton transfer reaction [3] and nature of hydrogen bonding [4]. Intramolecular proton transfer in the enol-ketone equilibrium is one of the simplest reactions can be assumed as model of reaction taken place in biosystems, so studying its chemistry and recognizing all effective factors on it helps us to understanding the processes in many biological systems. In this research the substitutions of enole-ketone was changed to produce new enol and ketones with different properties and the kinetics of proton transfer reaction in those were studied.

Methods:

The energy surfaces for intramolecular proton transfer reaction were calculated by MP2 method, 6-311++G(d,p) and the Gaussian03w package. For understanding the effect of substitutions on reaction kinetics, different groups were used as substitutions. Selections of various substitutions were done in the manner that the constructed ketone molecules have different properties.

Results:

In the first part of research, the energy surfaces of proton transfer between enol and ketone groups of the selected materials were calculated in gas phase. In Fig.1 calculated energy surfaces for proton transfer reaction versus reaction coordinate (H-O distance) in enol and ketone with H substitution is shown.

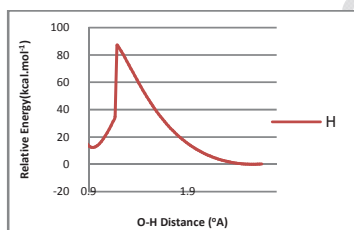
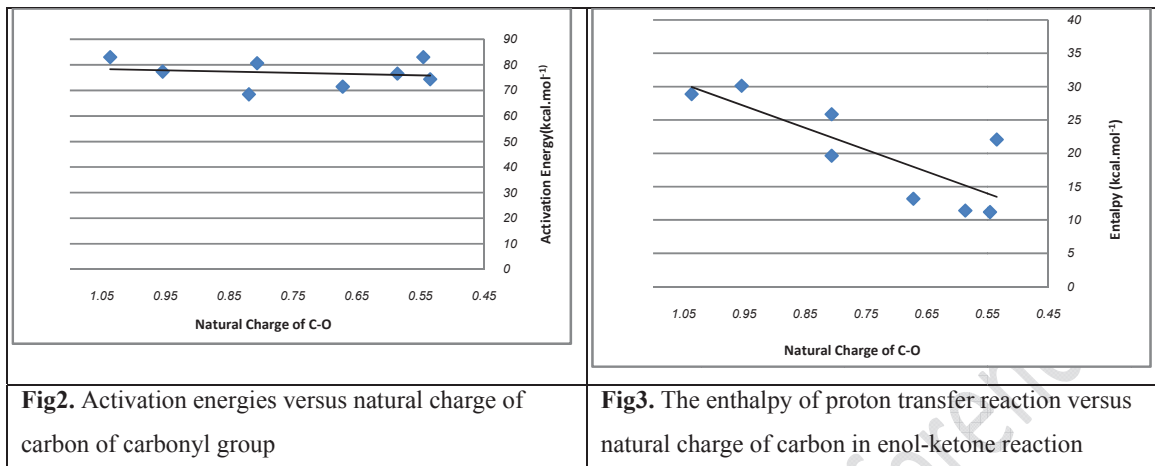


Fig1. The energy surfaces versus reaction coordinates for enol and ketone with H substitutions

For understanding the effect of substitutions on reaction kinetics, the energy surface of proton transfer reaction in enol-ketones which have different substitutions were plotted and compared to others. The activation energies of the reactions were determined by their corresponding energy surfaces. It was considerably from these results that the activation energies depend on the nature of substitutions.

As the result the activation energy for each substitution extensively depends on chemical nature of substitutions. In continuation the way of considering the substitution effect is represent. It is desirable to relate the activation energy of reaction to the type of substitutions. The effect of substitution can be taking into account by natural charge of central carbon atom. the consequence show that each substitution which has higher electronegativity attracts the electrons from carbon and makes its charge more positive. In this part of research the activation energy were plotted versus the natural charge of carbon in carbonyl group to illustrate the effect of substitution on activation energy (kinetics) of reaction. In Fig2 the result of activation energy versus natural charge of enol-ketone reaction is illustrated.



The Fig2 shows that the activation energies of reactions are considerably affected by the nature of substitution. On the other hand if substitutions connected to carbonyl groups are more electronegative and withdraw the electron from central carbon atom increases the activation energy of proton transfer reaction in enol-ketone reaction. Then the effect of substituent on enthalpy of reaction (thermodynamics) were determined by plotting the enthalpy of proton transfer reaction between enol-ketones versus their natural charge of carbon. In Fig3 the result of enthalpy of reaction versus natural charge of carbon is illustrated. This is obviously that each substituent which attracts the electron from molecule makes the ketone form of it more stable and increases the enthalpy of reaction.

Conclusion:

In this research the kinetics of proton transfer reaction in enol-keton system and effect of substitution on it was studied. As the result of this research each electronegative substitution which attracts the electron and decreases the electron density from molecules increases the activation energy of proton transfer reaction. This fact can be explained by the nature of TS in which the charge of carbonyl groups increases and each factor which increases the electron density helps to develop the reaction. Additionally the proton transfer thermodynamics (enthalpy) of proton transfer reaction are affected by nature of substitution and enthalpy of reaction increases as the substitutions attract the electron from molecule.

References:



- [1] P. J. Elving, W. T. Bresnahan, J. Moiroux, and Z. Samec, "524-NAD/NADH AS A MODEL REDOX SYSTEM: MECHANISM, MEDIATION, MODIFICATION BY THE ENVIRONMENT", *Bioelectrochemistry and Bioenergetics*, Vol.9 (1982) P:365
- [2] Pohl T, Spatzal T, Aksoyoglu M, Schleicher E, Rostas AM, Lay H, Glessner U, Boudon C, Hellwig P, Weber S, Friedrich T., "Electron and proton transfer in NADH:ubiquinone oxidoreductase (Complex I) from Escherichia coli", *Biochim Biophys Acta*, Vol.1797(2010) P:1894.
- [3] M.L. Paddock, G. Feher, M.Y. Okamura, "Proton transfer pathways and mechanism in bacterial reaction centers", *FEBS Letters*, VOL.555, (2003), P:45-50.
- [4] George A. Jeffrey, "An introduction to hydrogen bonding", (1997), Oxford University Press.



Fluorescence spectroscopic investigation of interaction between DNP and hemoglobin

Sh. Rashidipour^{a*}, M. Pirouzi^a, J. Chamani^a, M. Saberi^b

^a Department of Biology, Faculty of Sciences, Mashhad Branch, Islamic Azad University, Mashhad, Iran

^b Department of Medical Chemistry, School of Pharmacy, Mashhad University of Medical Sciences, Mashhad, Iran

Email: sh_r09@yahoo.com

Key words: Fluorescence spectroscopy, Hemoglobin, DNP

Introduction:

Proteins are important chemical substances in our lives and the main target of all medicines in the organism[1]. The interaction between proteins and drugs has attracted great interest among researchers for several decade. Hemoglobin (Hb) is an important protein in the vascular system of animals, consisting of two α -chains with 141 amino acids and two β -chains with 146 amino acids. Hb is a carrier of oxygen and removes hydrogen ions in the capillaries and carries them to the lungs.

DNP (2,4-Dinitrophenol) is an inhibitor of efficient energy(ATP) production in cells with mitochondria. It uncouples oxidative phosphorylation by carrying protons across the mitochondrial membrane, leading to a rapid consumption of energy without generation of ATP.

In this paper, the interaction between DNP and Hb was investigated by fluorescence spectroscopy.

Materials and methods:

All reagents used were of analytical grade and purchased from Sigma-Aldrich Co. (St. Louis, MO, USA). The solution of Hb were prepared with the following concentration: $[Hb] = 4.6 \times 10^{-3}$ Mm under physiological conditions. A phosphate buffer solution with a concentration of 50 Mm was employed. The DNP solution(10^{-5} Mm) was prepared by dissolution in a phosphate buffer.

Apparatus:

Fluorescence measurements were performed with a fluorescence spectrophotometer (Hitachi 2500, Japan) equipped with a Xenon pulse lamp and a thermostat bath. An appropriate buffer was taken as the blank and subtracted from the experimental spectrum to correct the background of the fluorescence. All the experiments were repeated at least three times and performed at room temperature.

Result and discussion:

Fig. (1) shows the fluorescence spectrum of Hb at pH=7.4. It was obvious that Hb had a strong fluorescence emission at 349 nm after being excited with a wavelength of 280 nm. The addition of varying concentrations of DNP caused a decrease in the fluorescence intensity of Hb. The maximum emission wavelength produced a blue shift. It was moreover an indication of the chromophore of protein being transferred to a more hydrophobic environment and the conformation of the protein becoming altered [2-4].

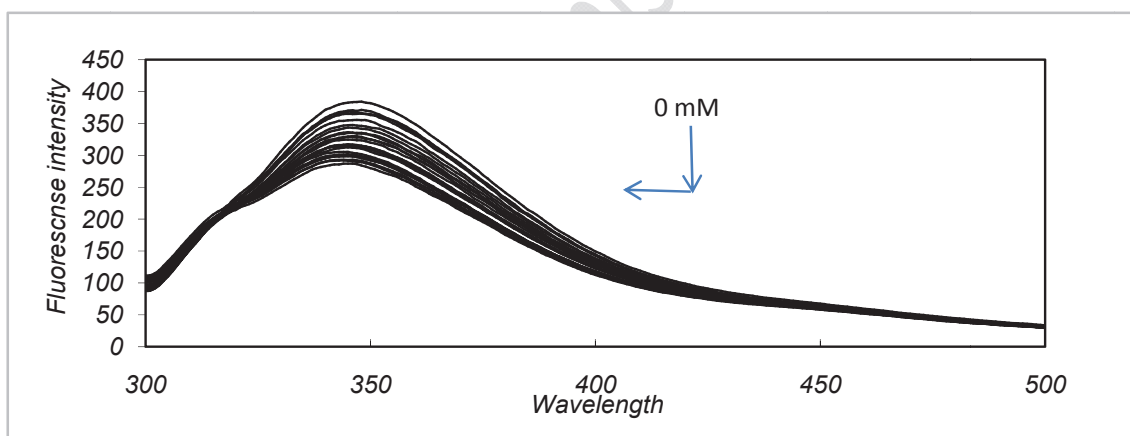


Figure 1. Fluorescence emission spectra of the Hb-DNP system. The concentration of Hb was 4.6×10^{-3} mM and the DNP concentration was increased from (0 to 10^{-5} mM); pH=7.4, 298 K.

Conclusion:

The results suggested that the structure of the environments of the tryptophan and tyrosine residues was altered and the physiological function of Hb was affected by DNP. Fluorescence data revealed that the fluorescence quenching of Hb by DNP was the result of the formed complex of Hb-DNP



It determined that usage DNP doses is a key parameters for drug delivery in pharmaceutical sciences

Reference:

- [1] F. Cui, Q. Zhang, X. Yao, H. Luo, Y. Yang, L. Qin, G. Qu, and Y. Lu. 4. *J Pestic Biochem Physiol* 90, 126-134 (2008).
- [2] Peters, T. *All about albumin*, Academic Press, San Diego (CA), **1996**
- [3] He, X.M.; Carter, D.C. Atomic structure and chemistry of human serum albumin. *Nature*, 1992, 358, 209-215
- [4] Chen, G.Z.; Huang, X.Z.; Xu, J.G.; Zheng, Z.Z.; Wang, Z.B. *The Methods of Fluorescence Analysis*, 2nd ed, Beijing Science Press **1990**, pp 2-12



Iran Hydrogen Economy: Problems and Challenges

Tahereh Kalateh¹, Muhammad Shadman^{1,*}

¹Department of Chemistry, Faculty of Science, University of Zanjan, P.O.Box 313, Zanjan, Iran.

(*Corresponding author E-mail address: Shadman@znu.ac.ir)

Key words:Hydrogen storage, Hydrogen civilization, Fuel cells,Nanostructures.

Introduction:

Fossil fuels including oil, natural gas and coal are the main sources of human energy that due to population and economic growth, the global demand for energy is expected to increase by 50% over the next 20 years. Therefore, the excessive use of fossil fuels due to increasing energy utilities are presented with the challenges of increased energy demand that this causes immediately address environmental concerns such as climate change. For example, in Tehran, because of emissions from the transportation sector, many health and environmental problems have caused. This significant increase in demand coupled with dwindling supplies of fossil fuels has raised concerns about the security of energy supply [1]. It is clear that the world oil production cannot be sustained indefinitely at its current rate. So an interest is growing to find alternative fuels in recent years. One of the best alternative fuels is hydrogen. Nowadays, hydrogen fuel has received significant attention as future transportation fuels. Hydrogen can be played important roles on economy of countries in futures. On the other hands, there are considerable research efforts in many countries to develop the hydrogen economy that was initiated about 37 years ago and it is based on the fact that hydrogen is a unique, ecologically clean energy carrier and would be expected to replace oil and natural gas for most uses, including transportation fuel [2, 3]. The Australian chemist *John Bockris* first used the phrase “hydrogen economy” in the early 1970s and the first World Hydrogen Conference was held in 1976[4]. In the meantime, our country Iran that has large reservoirs of natural gas, the second largest natural gas reservoir in the world, and other sources of energy such as hydro, solar, and biomass. So Iran should get rid of fossil fuel dependent economy and move to produce clean energy carriers like hydrogen to substitute gasoline and gas oil in the transportation sector. The rest of the paper is structured as follows: the next section is related



to status of the hydrogen economy in terms of hydrogen production, storage and how use of hydrogen in vehicles. Also, the last section investigates the using of the fuel economy of hydrogen and hydrogen preferred on gasoline.

Current status of the hydrogen economy:

Correspondingly, 95% of hydrogen production uses steam methane reforming (SMR) technology [4]. Liquid hydrogen must be stored in cryogenic systems with considerable energy losses [5]. Hydrogen is stored on-board vehicles primarily as compressed gas. Hydrogen can also be stored as a metal hydride. Solid hydrogen can store up to 3% by weight of hydrogen at 20°C [6]. Covalent and ionic hydrides can contain 7–12% by weight [4]. Although metal hydrides occupy less volume, they are heavier, more costly, and still in the early stages of research for on-board storage in vehicles. In many countries such as Iran, the extensive programs are designed to synthesis some nanostructures because these materials are very important to hydrogen storage and will use hydrogen in liquid and gas forms in transportation as soon as possible.

The Pathway Forward:

Hydrogen gaining is increased considerable both politically and scientifically and it is regarded one of the most promising energy carriers. Some uses of hydrogen are: (a) Fuel in internal combustion engines (ICE) (b) Energy carrier in fuel cell vehicles (FCV) (c) Electrical energy storage for stationary applications (EES) [7]. Applying hydrogen in ICE, FCV and EES can be the major goal to achieve clean renewable and sustainable energy in the world especially, in Iran. In order to best use of hydrogen, Iran should be solved to build low-cost stations and produce low-cost hydrogen. The investigations show that typical fuel economy for hydrogen and gasoline are \$3/100 km and \$5/100 km, respectively. Hydrogen can be produced at lower cost by switching hydrogen stations to hydrogen–gasoline stations in Iran. The next step for Iran is the build of hybrid engines that can work with hydrogen and gasoline. It should be noted to our researches are continued to complete the issue.

References:

- [1] A. Hajimiragha, M. W. Fowler, C. A. Cañizares, *Int. J. Hydrogen Energy* 34 (2009) 5275.



- [2] V. A. Goltsov, T. N. Veziroglu, *Int. J. Hydrogen Energy* 27 (2002) 719.
- [3] R. Shinnar, *Technology in Society* 25 (2003) 455.
- [4] W. C. Lattin, V. P. Utgikar, *Int. J. Hydrogen Energy* 32 (2007) 3230.
- [5] http://www.altenergyaction.org/mambo/index2.php?option=com_content&task=view&id=13&itemid=2
- [6] R. Uhrig, Engineering challenges of the hydrogen economy. The Bent of Tau Beta Pi Spring, 2004.
- [7] R. G. Reddy, *JMEPEG* 15 (2006) 474.

15th Physical Chemistry Conference



Investigation of Bio–Nano Interaction between Single-Walled Carbon Nanotube and some of amino acids

H. Yamola^{1*}, Ma.Boostan², M.boostan³,

¹Ph.D Student, Science and Research Branch, Islamic Azad University, Tehran,Iran.

²Department of Chemistry, Kash, Iran

³Department of Chemistry, Shahrerey Branch, Islamic Azad University, Tehran, Iran

*Corresponding Author: hamideh_yamola@yahoo.com

Key words: biological molecules, drug design, carbon nanotube

Introduction:

The rich potential of carbon nanotube in biosensors [1] and bioelectronics [2] lead to increasing research recently. As many of scientists have focused on biological applications of inorganic systems. Nanosensors based on biology in biomedical devices and bioreactors have considerable applied in the last years. Different fictionalization methods have been suggested for the biological applications of carbon nanotubes, and thus scrutiny of the interaction between biological molecules and carbon nanotubes became remarkably important [3]. Nanotube can be exist as a sheet formed of hexagons of carbon atoms meaning rolled-up sheet of graphite. Nanotube can be biocompatible of recognizing proteins after functionalization [4]. Amino acids the building blocks of protein are one of the big biological groups that can be attached to nanotubes. Study of the interaction strength between different amino acids and SWCNTs are very important. In the present work, we have considered the UV Vis spectrum of histidin, tryptophane and tyrosine before and after interaction between them and single wall carbon nanotube.

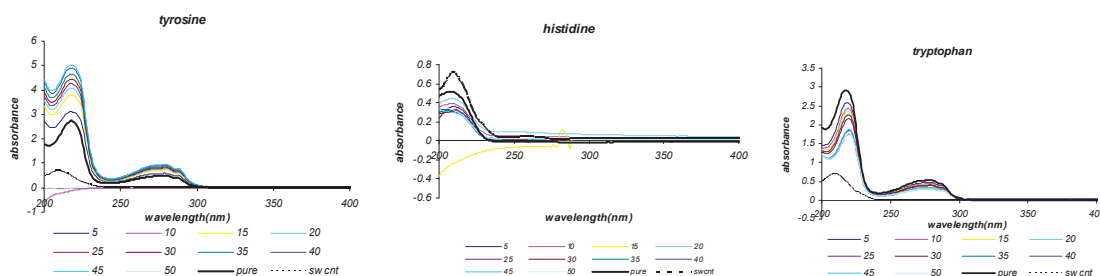
Experimental:

The powder samples of SWCNTs were prepared from petroleum industrial research home. The purified SWCNTs contained over 95 wt% carbon nanotube reported by .The amino acids were purchased from Sigma–Aldrich Chemical Co and used as received. SWCNT colloid solution was prepared by dissolving 10^{-3} (gr) of these powder samples in 500 ml ethanol. Also the 10^{-4} Molar solutions of each amino acid were provided and then several solutions of

amino acids in nanotube with different voluminal percent prepared and were studied. The investigations were followed by UV-VIS spectroscopy. All spectra were recorded at room temperature with a carry 5000 system.

Result and Discussion:

We have used UV-Vis spectroscopy's study to recognize the interaction between SWCNT and amino acids because of this spectroscopy has wide varied applications such as detection of Impurities. All of the spectrums have been recorded after preparing the solution with different voluminal percent and the results were studied. At first the spectrum of each of the pure amino acids were recorded, the spectrum of pure carbon nanotube was recorded too for doing these tests once we choose Tyrosine, One of the non-essential amino acids (Tyr) the results with different voluminal percent of carbon nanotube with this amino acid shown reasonable behavior to mean except two voluminal percent (10/50 and 50/50) other solutions have higher adsorption than pure amino acid and pure nanotube too. Adding Histidin (His), another amino acid as a basic amino acid to carbon nanotube gives the results like Glu but in 210 nm. Tryptophan showed the differ behavior and after adding nanotube to this amino acid adsorption decreased. These results could be helped to study SWCNTs as a drug deliver in drug design.



Conclusion:

- 1- Tyrosine had a notable interaction with carbon nanotube as a molecule deliver and this process is rather regular with concentration increasing. these results obtained via UV spectroscopy.
- 2-mixture of histidine and carbon nanotube showed lower absorption rather both nanotube and pure amino acid.



3-tryptophan, one of the amino acids had the interaction differ of others with nanotube that could be mentioned.

References:

- [1] Robers M, Rensink IJAM, Hack CE, Aarden LA, Reutelingsperger CP, Glatz JF, Hermens WT (1999) A new principle for rapid immunoassay of proteins based on in situ precipitate enhanced Ellipsometry. *Biophys J* 76(5):2769-2776
- [2] Goldsmith BR, Coroneus JG, Khalap VR, Kane AA, Weiss GA, Collins PG. Conductance-controlled point functionalization of single-walled carbon nanotubes. *Science* 2007; 315:77–81.
- [3] Fritz J, Cooper EB, Gaudet S, Sorger PK, Manalis SR (2002) Electronic detection of DNA by its intrinsic molecular charge. *Proc Natl Acad Sci USA* 99(22)14142-14146.
- [4] Chen RJ, Zhang Y, Wang D, Dai H (2001) Noncovalent sidewall functionalization of single-walled carbon nanotubes for protein immobilization. *J Am Chem. Soc* 123(16), 3838-3839.



Liquid-Liquid Equilibria for Ternary Mixture of (Water + Acetic Acid + Methyl Isobuthyl Ketone) at Different Temperature

J.Saien^{*}, S.Daliri, H.Bamdadi

Department of Applied Chemistry, Bu-Ali Sina University, Hamedan, Iran

Email: saien@basu.ac.ir

Key words: LLE, Temperature, Recommended system

Introduction:

LLE measurements and phase behavior of ternary systems including carboxylic acids has been the subject of much research in recent years in that LLE data are required for design of liquid-liquid extraction units.¹ In this work, LLE data for water + acetic acid + Methyl Isobuthyl Ketone ternary system are to be achieved at temperatures of 288.15, 313.15 and 333.15 K.

Materials and methods:

Acetic acid and methyl isobuthyl ketone were purchased with purities of 100% and more than 99.5% from Merck and Aldrich, respectively and were used without further purification. Standard 0.1 N sodium hydroxide solutions, Merck product, were used for titration. Water was bi-distilled before utilization. Ternary mixtures with known overall compositions were prepared by weighting in the special glass cells for measuring the tie line data and these cells were then shaking for 5 h at desired temperature and were allowed to rest for 12 h to achieve equilibrium. Taken Samples from each phase were titrated with 0.1 N sodium hydroxide solutions. The sample taken from organic phase was also analyzed using a gas chromatography (GC).

Apparatus:

The LLE data measurements were made in special glass cells located inside a shaker (N-BIOTEK-304) with adjustable shaking speed and temperature adjusting with an uncertainty of ± 0.1 °C. To weighting in all experiments, an electronic Ohaus (Adventurer Pro AV264, Switzerland) balance with the uncertainty of (0.1) mg was used. All experiments were made

under ambient pressure. The sample taken from organic phase was also analyzed using a gas chromatography (GC) (Shimadzu 14B), equipped with flame ionization detector (FID).

Result and discussion:

The experimental tie lines data for used system at different temperatures are presented in Figure 1. The distribution coefficient of acetic acid between phases (D), is according to equation:

$$D = \frac{(w_2)_{org}}{(w_2)_{aq}} \quad (1)$$

where $(w_2)_{org}$ and $(w_2)_{aq}$ are weight fractions of acetic acid in and organic in aqueous phases, respectively. The results of LLE show that the use of Methyl isobutyl ketone for extraction of acetic acid from its aqueous solution provides a distribution coefficient ranging from 0.8269 to 1.1788 within temperature ranges of this study (Figure 2). As shown in this figure with increasing temperature, a moderate increase can be seen in distribution coefficient.

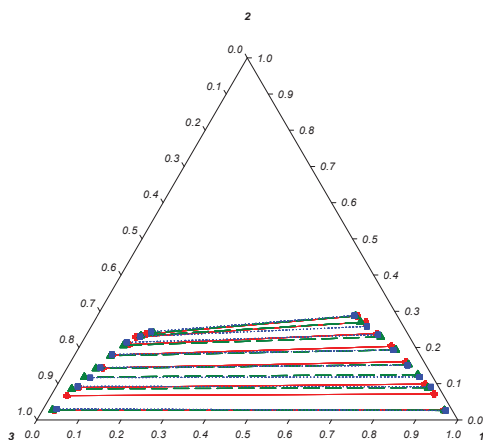


Fig 1. tie lines data for water (1) + acetic acid (2) + methyl isobutyl ketone (3) ternary system at 288.2 K. (●) and solid line, 313.2 K (■) and dot line, 333.2 K (▲) and dash line,

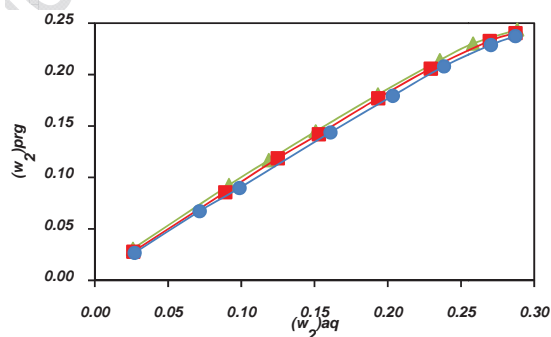


Fig 2. Distribution of acetic acid between phases at different temperatures: 288.2 K (●), 313.2 K (■), 333.2 K (▲).

Conclusion:

The LLE values for this ternary system were studied at temperatures of (288.2, 313.2, and 333.2) K and under ambient pressure. The effect of temperature on distribution coefficient of acetic acid between phases was moderate. The range of distribution coefficient was from 0.8269 to 1.1788 at different temperature.



References:

- [1] Ghanadzadeh, H.; Ghanadzadeh Gilani, A.; Bahrpaima, K.; Sariri, R., (2010). "Liquid+ liquid equilibria for ternary mixtures of (water+ propionic acid+ organic solvent) at T= 303.2 K. " *The Journal of Chemical Thermodynamics*, **42** (2): 267-273.

15th Physical Chemistry Conference

A Mining Waste as a Catalyst for the Upgrading of a Hardwood Chip Derived Pyrolysis Bio-Oil

Elham Karimi^{a,b}

^a University of Guelph, Guelph, Ontario, Canada

^b National Petrochemical Company of Iran. Research and Technology, Iran

E-mail: ekarimi@uoguelph.ca, e.karimi@npc-rt.ir

Key words: Diesel fuel, Bio-Fuel, Biomass Conversion, Pyrolysis Bio-Oil, Catalytic Upgrading, Bauxite Mining Waste, Red Mud

Introduction:

The fast pyrolysis of ligno-cellulosic biomass to fuel bio-oil holds substantial promise for the development of a large scale renewable fuel supply. [1] But the advantages of the pyrolysis route for this conversion lie in its conceptual simplicity, universal applicability and the fact that a pumpable and storable liquid product is obtained. Challenges arise from the fact that the process generates bio-oil with high oxygen (~ 40 %), water (20-25 %) and acid content (up to 10 %) and consequently low *pH* (~ 2) of the oil make the oil unstable and limit its direct use as a fuel. The two main approaches to a catalytic upgrading are hydrodeoxygenation using a supported hydrogenating metal or cracking using a zeolite. A very inexpensive and therefore potentially *sacrificial* catalyst system is Red Mud bauxite mining waste which is a highly complex mixture of iron, aluminum, silicon and titanium oxides. [2] Here, following to our previous researches, [3] a highly acidic bio-oil (*pH* < 3) produced by the fast pyrolysis of sawmill residue hardwood chips was successfully upgraded using Red Mud bauxite mining waste as the catalyst.



Materials and methods:



All reactions were carried out in a 300 mL Parr reactor (316 SS). Bio-oil, Red Mud and (where applicable) additional water were mixed and brought to the reaction temperature at a heating rate of 3 °C/min. Then the reactor was cooled down and the gas, liquid and solid phases were analyzed.

Apparatus:

GC analysis was performed on a Varian 3800 GC. Gas samples from the headspace of the reactor were qualitatively analyzed using an SRI 8610 micro-GC fitted with a TCD with the retention times calibrated against the linear C1 – C6 alkanes and C2 –C6 terminal as well as CO₂. Water contents were determined by Karl-Fischer titration. A Nicolet 380 FT-IR was used for IR analysis (neat, CaF₂ cells/plates). Heating values were determined using a IKA C 200 calorimeter. Elemental analysis was carried out using a Thermo Fisher FLASH analyzer.

Result and discussion:

The observed deoxygenation of the bio-oil can in principle occur through loss of CO₂ or dehydration. The latter can either take place directly or through iterative reaction cascades of initial hydrogenation of carbonyl groups to alcohols followed by renewed dehydration yielding alkenes, which in turn can then be hydrogenated to alkanes. [3a] As the pyrolysis bio-oil upgrading reactions described here proceed without the addition of an external reductant, the hydrogen required for the reductions steps must be derived from internal sources. The main source of hydrogen as a reductant is probably the reforming of some of the bio-oil into CO₂ and hydrogen, which has also been observed with Pt-based catalysts.

Conclusion:

Red Mud can act as Fischer-Tropsch (FT) and Water-Gas-Shift-Reaction (WGS) catalyst under reducing conditions at elevated temperature. The upgrading process proceeds without the addition of external hydrogen and yields a stabilized bio-oil with almost no oxygen content and much higher heating compared to the crude oil. Simultaneously, the Red Mud employed as the catalyst is converted from an alkaline ($pH > 12$) hazardous waste to a partially reduced magnetic neutral material. The co-processing of the two waste streams may thus offer attractive economic and ecologic synergies that suggests a co-processing of



waste streams may offer ecologically and economically attractive synergies.

References:

- [1] S. Czernik, A. V. Bridgwater, *Energy & Fuels* 18, 590-598, 2004.
- [2] G. Power, M. Grafe, C. Klauber, *Hydrometallurgy* 108, 33-45, 2011.
- [3] a) E. Karimi, C. Briens, F. Berruti, S. Moloodi, T. Tzanetakis, M. J. Thomson, M. Schlaf, *Energy & Fuels* 24, 6586-6600, 2010; b) E. Karimi, A. Gomez, S. W. Kycia, M. Schlaf, *Energy & Fuels* 24, 2747-2757, 2010; c) E. Karimi, I. F. Teixeira, L. P. Ribeiro, A. Gomez, R. M. Lago, G. Penner, S. W. Kycia, M. Schlaf, *Catal. Today* 2011, in press.



Experimental Study of the Effect of Hydrophilic Silica Nanoparticles on Foam Performance in Alkaline-Surfactant-Gas flooding

A.Siosewardan^{a*}, S.A.Tabatabae Nejad^a, E.Khodapanah^a

^a Department of chemical engineering faculty, Sahand university of technology, Tabriz, Iran

Email: assmn65@yahoo.com

Abstract:

Alkali-Surfactant-Gas (ASG) flooding is one of the novel chemical techniques in Enhanced Oil Recovery. In this technique, the co-injection of gas and chemical slug results in the formation of foam. Foam reduces the mobility of injected chemical solutions and improves the displacement efficiency of the process. Foams in practice are generally generated and stabilized with surfactants. However, surfactant stabilized foams have some weakness. If nanoparticles were utilized instead of or with surfactants, foams stabilized with such particles could have a number of important advantages. The main purpose of this research is creation of stable foam with nanoparticles and utilizing this nanoparticle stabilized foam for mobility control of injected fluids in enhanced oil recovery applications. Finally, the performance of the foam that is created and stabilized with mixture of surfactant and nanoparticles was compared with the foam that is created and stabilized with only surfactant in alkaline-surfactant-gas process in terms of oil recovery from core flood experiments. In this research, hydrophilic silica nanoparticles with an average size of 10 nm were used. The mixture of surfactant and hydrophilic silica nanoparticles in various concentration were used to foam generation. The results of the experiments showed that the concentration of surfactant and nanoparticles should be selected optimize. In the experiments, most oil recovery was obtained when the concentration of both surfactant and hydrophilic silica nanoparticles in chemical solution was selected 0.5 weight percent.

Key words: Enhanced Oil Recovery, Chemical Flooding, Foam, Nanoparticles, Mobility Control

Introduction:



One of the main criteria for the success of ASG process is the formation of stable foam with adequate mobility reduction characteristics [1]. Surfactant stabilized foams have some weakness. However, if nanoparticles were utilized instead of or with surfactants, foams stabilized with such particles could lead to removing restrictions on the use of surfactants [2]. Nanoparticles are finding their way into various branches of the petroleum engineering industry [3-7]. Certain small solid particles have been used in conjunction with surfactant molecules, which they adsorb at fluid/fluid interfaces, to stabilize drops in emulsions and bubbles in foams [8]. In contrast to surfactant molecules, adsorption of solid particles to fluid/fluid interfaces does not change the interfacial tension [9]. This research is based on utilizing hydrophilic silica nanoparticles with surfactant to make stable foam for enhanced oil recovery applications.

Materials and Methods:

Sodium dodecyl sulfate (SDS) which is an anionic surfactant, Hydrophilic silica nanoparticles with an average size of 10 nm and Sodium carbonate (Na_2CO_3) as alkaline were used in chemical coreflood experiments. One type of Synthetic formation brines, representing formation fluid of a reservoir, with total dissolved solids of 103000 mg/L was used in corefloods. Water flooding as secondary recovery technique was performed with Persian Gulf water. The crude oil used for corefloods has a viscosity and density of 3.46 cP and 30 °API. Nitrogen with 99.99% purity was used for mobility control of injected fluids. ASG coreflood experiments were conducted after the optimal chemical formulation was identified through aqueous stability, phase behavior, and foam stability tests. Coreflood experiments were performed at 100 bars and 60 °C.

Apparatus :

Figure 1 shows the schematic of ASG coreflood setup.

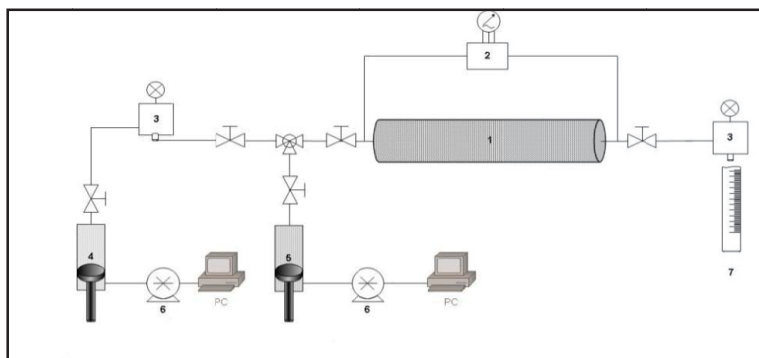


Figure 2: schematic of ASG coreflood setup

1) Sandpack, 2) Differential pressure difference, 3) Backpressure regulator, 4) Gas accumulator, 5) Liquid accumulator, 6) High performance liquid chromatography (HPLC) pump, 7) Sampler

Results and Discussion:

It was observed that when the concentration of hydrophilic Silica nanoparticle was low, there were not enough particles to attach completely at the interface around the bubbles in foam and when particle concentration increased, more particles could be adsorbed at the bubble interface, which stabilized the produced foam. But, with further increased nanoparticle concentration, the particle aggregation occurred, which inhibited foam generation. When the surfactant concentration was selected enough, the attachment of surfactant to nanoparticle surface can change nanoparticles surface properties and show surface activity useful for foam generation. But, as the more surfactant molecules were adsorbed onto the particle surface, the particle surface charge decreased and the electrostatic repulsion between particles decreased that led to particle aggregation.

Conclusion:

Silica nanoparticles can function in similar ways to surfactants and stabilize foams in the absence of any other surface-active agent, but certain differences in behavior are inevitable. When the concentration of nanoparticles and surfactant are selected optimize, strong and stable foams are created and displacement efficiency is increased that leads to more oil production.

References:

[1] Srivastava, M., Zhang, J., Nguyen, Q.P., and Pope, G. A., (2009), "A Systematic Study of



Alkali Surfactant Gas Injection as an EOR Technique”, Paper SPE 124752 presented at the 2009 SPE Improved Oil Recovery Symposium held in Tulsa, USA.

[2] Zhang, T., Roberts, M.R., A, Bryant, S. L., and Huh, C., (2009), “*Foams and Emulsions Stabilized with Nanoparticles for Potential Conformance Control Applications*” SPE Paper 121744, presented at SPE Intern. Symp. Oilfield Chemistry

[3] Huang, T. and Crews, J. B., (2008) “*Nanotechnology Applications in Viscoelastic Surfactant Stimulation Fluids*”, SPE Production & Operations, 51 2 - 517, November 2008.

[4] Sensoy, T., Chenevert, M. E., and Sharma, M. M., (2009), “*Minimizing Water Invasion in Shale Using Nanoparticles*”, SPE 124429 presented at the 1009 SPE Annual Technical Conference and Exhibition, New Orleans.

[5] Zhang, T., Davidson, A, Bryant, S. L., and Huh, C., (2010), “*Nanoparticle-Stabilized Emulsions for Applications in Enhanced Oil Recovery*”, SPE 119885 presented at the 1010 SPE Improved Oil Recovery Symposium, Tulsa.

[6] Espinosa, D. R., Caldelas, F. M., Johnston, K., Bryant, S. L., and Huh, C., (2010), “*Nanoparticle-Stabilized Supercritical CO₂ Foams for Potential Mobility Control Applications*”, SPE 129925 presented at the 2010 SPE Improved Oil Recovery Symposium, Tulsa.

[7] Pourafshary, P., Azimipour, S. S., Motamedi, P., Samet, M., Taheri, S. A., Bargozin, H., and Hendi, S. S., (2009), “*Priority Assessment of the Investment in Development of Nanotechnology in Upstream Petroleum Industry*”, SPE 126101 presented at the 2009 SPE Saudi Arabia Section Technical Symposium and Exhibition, AlKhobar, Saudi Arabia.

[8] Binks, B.P. and Horozov, I .S., (2005), “*Aqueous foams stabilized solely by silica nanoparticles*”, Angewandte Chemie-International Edition.

[9] Binks, B.P., (2002), “*Particles as surfactant -similarities and differences*”, Current Opinion in Colloid & interface Science.



Conversion of CH₄ and CO₂ Mixture to Syngas over Ni/Al₂O₃-CeO₂ Nanocatalyst Synthesized via Impregnation and Sol-Gel Methods

S. Aghamohammadi^{a, b}, M. Haghighi^{a, b*}, S. Karimipour^{a, b}

^a Chemical Engineering Faculty, Sahand University of Technology, Tabriz, Iran

^b Reactor and Catalysis Research Center (RCRC), Sahand University of Technology, Tabriz, Iran

*Email: haghighi@sut.ac.ir

Keywords: Ni/Al₂O₃-CeO₂, Dry reforming, Syngas, Nanocatalyst, Impregnation, Sol-Gel.

Introduction:

Nanocatalyst technology provides a method to control the structure of catalyst particles, thereby controlling their catalytic function [1]. In the present work, we report research on the performance of Ni/Al₂O₃-CeO₂ nanocatalyst, prepared by sol-gel and impregnation methods, in carbon dioxide reforming of methane to identify the effect of preparation method.

Materials and methods:

In order to synthesize Ni (10%)/Al₂O₃-CeO₂ catalysts, respective metal nitrates and citric acid as gelling agent were applied. Sol-gel synthesis method was followed by drop wise adding of citric acid into solution as gelling agent, and then concentrated in a water bath at 65°C to form wet gel. Physiochemical properties were identified by XRD, FESEM, FT-IR and BET techniques. Performance tests were carried out to investigate the influence of temperature, feed ratio and gas hourly space velocity (GHSV) on the catalysts activity. The stability test was conducted for 600 min. The catalysts were reduced in situ at 700°C for 120 min.

Result and discussion:

Reaction tests were carried out to obtain the best operational conditions over Ni(10%)/Al₂O₃-CeO₂ synthesized nanocatalysts. It indicated that higher temperature is favor to produce H₂ and CO as shown in Figure 1. Feed ratio equals to one and relative lower GHSVs exhibit higher activities as shown in Figures 2 and 3, respectively. For all examined tests, the value

of CO and H₂ yield for the sol-gel made catalyst is higher than that of impregnated one. Lower activity of the catalyst synthesized with impregnation method can be ascribed to the existence of spinel phases (evidenced by XRD analysis) in this sample which makes it more difficult to obtain metallic phase of Ni [2]. Stability test was conducted at the best operational conditions obtained from the previous tests. Catalyst prepared by sol-gel method exhibits higher activity sustaining CO and H₂ yield at higher values.

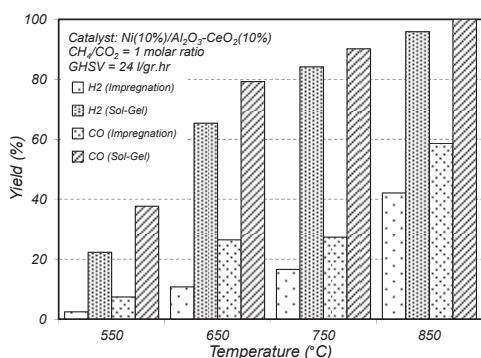


Figure 3: Product yields vs. temperature over Ni/Al₂O₃-CeO₂ nanocatalyst synthesized via impregnation and sol-gel methods.

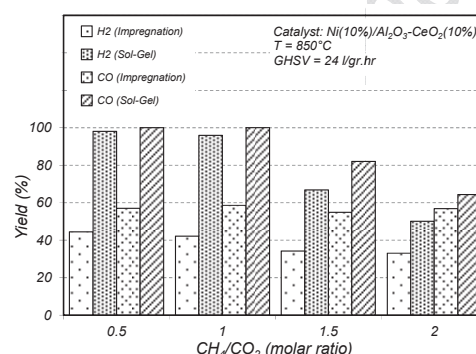


Figure 4: Product yields vs. CH₄/CO₂ molar ratio over Ni/Al₂O₃-CeO₂ nanocatalyst synthesized via impregnation and sol-gel methods.

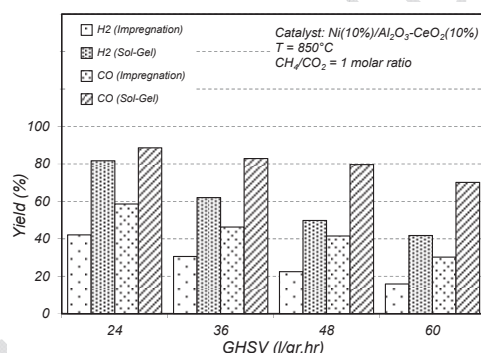


Figure 5: Product yields vs. GHSV over Ni/Al₂O₃-CeO₂ nanocatalyst synthesized via impregnation and sol-gel methods.

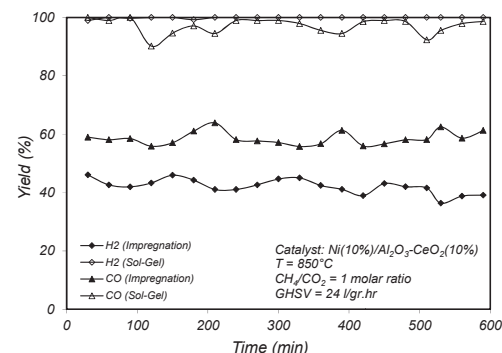


Figure 6: Time on stream performance of Ni/Al₂O₃-CeO₂ nanocatalyst synthesized via impregnation and sol-gel methods.

Conclusion:

Dependence of catalytic performance during CO₂ reforming of methane on synthesis method was investigated. Sol-gel made catalysts demonstrates superior activity owing to exhibiting better properties.



References:

- [1] S. Y. Foo et al., "Kinetic study of methane CO₂ reforming on Co-Ni/Al₂O₃ and Ce-Co-Ni/Al₂O₃ catalysts", *Catalysis Today*, 164, (1), 221-226, 2011.
- [2] N. Rahemi, M. Haghighi and S. Karimipour, "A comparative synthesis and characterization of Ni/Al₂O₃-CeO₂ nanostructured catalyst from Al/Ce/Ni nitrates via impregnation and sol-gel methods ", 13th Iranian national chemical engineering congress & 1st international regional chemical and petroleum engineering Kermanshah, Iran, 2010.



Utilization of greenhouse gases through methane dry reforming over Fe-V₂O₅/ZrO₂ catalysts

P. Karimi^{a*}, M.A. Takassi^b, A. Gharibi Kharaji^b, M. Almasi^a

^aDepartment of Chemistry, Science and Research Branch, Islamic Azad University, Khozestan, Iran

^bDepartment of Chemical Engineering, Petroleum University of Technology, Ahwaz, Iran

Email: parikarimi2010@yahoo.com

Key words: Global warming, Dry reforming, Fe-V₂O₅ catalyst, Syngas, ZrO₂ support

Introduction:

The most energy utilization in the modern societies today is based on combustion of fossil fuels such as coal and natural gas. CO₂ is the product of complete oxidation or combustion of any material that contains carbon. Utilization of CO₂ and other greenhouse gases to produce useful chemicals could be a suitable solution to this problem. Catalytic dry reforming which converts two gases, CH₄ and CO₂, with high global warming potential to valuable syngas, a mixture of CO and H₂, has received considerable attention in recent years [1-2].

Materials and methods:

Nano ZrO₂ powder was purchased from East Nano Material Co. Inc. and used as a catalyst support. Fe-V₂O₅ supported nano ZrO₂ catalyst were prepared using coprecipitation method. After coprecipitation, the product was dried at room temperature and subsequently calcined at 923 K for 4 h in air. The dry reforming reaction was carried out at a temperature range of 673-973 K, 1.3 bar and CO₂: CH₄ = 1:1 in a fixed-bed reactor when the entrance of mass flow rate was 400 ml/min using ZrO₂ and Fe-V₂O₅/ZrO₂ catalyst, and 5g of the catalysts was used. The stability test of catalysts was measured at 973 K when the entrance of mass flow rate was 600 ml/min, and 3g of the catalysts was used.

Apparatus:

The prepared catalyst was calcined in furnace (Griffin). The catalyst structure was studied using techniques XRD (Seifret ID3003), XRF (ARF). The catalytic activities were studied in a fixed-bed reactor (20mm ID and 150mm length). The temperature of the reactor was

measured using a Type- K sensor. A thermocouple, connected to a PID temperature controller was used for adjusting the temperature of the reaction. The mass flow rate was controlled and measured using mass flow controllers (Hitachi). At the entrance and exit reactor's was installed a pressure gage. A cold trap at the outlet of the reactor was used to condense out any water from the gas product stream. All products were analyzed by gas chromatography (Young Lin) equipped by Q and MS capillary columns and a HID detector.

Result and discussion:

The results of the XRD for the Fe-V₂O₅/ZrO₂ catalyst showed that there was V₂O₅ at this catalyst. The Iron, has good distribution at the surface of the catalyst. The results of the XRF showed that 60% Zr wt., with 4% V wt. and 3%Fe wt. there were at the structure of the catalyst. The results of this reaction showed that in all of temprature at constant presure the yeild of synthesis of methane with Fe-V₂O₅/ZrO₂ catalyst is higher than ZrO₂ catalyst. However, it showed that this catalyst had better catalytic activity for reforming reaction. Efficiency of hydrogen production for both catalysts at different temprature were increased and had reverse relationship with time. Also Efficiency of hydrogen production for ZrO₂ catalyst was always greater than Fe-V₂O₅/ZrO₂. Study of Kinetics of these catalysts in this reaction showed the Fe-V₂O₅/ZrO₂ catalyst had lower activation energy than ZrO₂ catalyst. (Figures 1, 2 and 3)

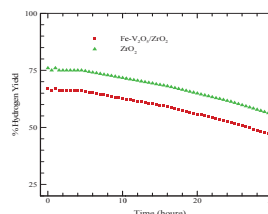
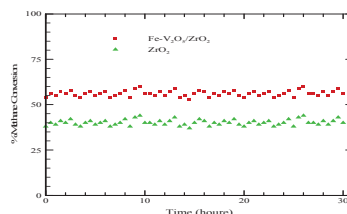
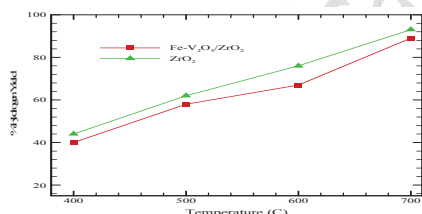


Fig.1.Changes of % methane conversion vs temperature Fig.2.Changes of %methane conversion vs.time Fig. 3. Hydrogen Yield vs.time

Conclusion:

According to higher catalytic activity of the Fe-V₂O₅/ZrO₂ catalyst, it can introduce to methane reforming by follow reaction rate : $r_{CO} = 120.9 \cdot \text{EXP}(-44.71/RT) P_{CH_4}^{0.17} P_{CO_2}^{0.43}$

References:



- [1] A. Gharibi Kharaji et al; "Selectivity and Performance of Fe-V₂O₅/γ-Al₂O₃ Nano Catalyst for Methanol Production with RWGS Reaction"; *Journal of American Science*; 7(12), 2011
- [2] M.-S. Fan et al; "Utilization of greenhouse gases through carbon dioxide reforming of methane over Ni-Co/MgO-ZrO₂: Preparation, characterization and activity studies"; *Applied Catalysis B: Environmental*; 100,365-377, 2010.

15th Physical Chemistry Conference



Sol-Gel vs. Impregnation Synthesis of Ni-Cu/Al₂O₃ Nanocatalyst Used in Reforming of Methane

A. A. Eslami^{a,b}, M. Haghighi^{a,b*}, S. M. Sajjadi^{a,b}, F. Rahmani^{a,b}

^a Chemical Engineering Faculty, Sahand University of Technology, Tabriz, Iran

^b Reactor and Catalysis Research Center (RCRC), Sahand University of Technology, Tabriz, Iran

*Email: haghighi@sut.ac.ir

Keywords: Sol-Gel, Impregnation, Ni-Cu/Al₂O₃, Reforming, Syngas, Nanocatalyst.

Introduction:

The production of syngas via dry reforming of methane is a crucial process to utilize CO₂ as a greenhouse gas. Ni-based catalysts are extensively used for this process because of being easy accessible and inexpensive rather than noble metals [1,2]. Using Cu as a promising promoter with an effective preparation method like sol-gel can suppress the coke formation on Ni, and as a result, the activity will be enhanced.

Materials and methods:

In this work, the Ni-Cu/Al₂O₃ were synthesized via sol-gel (NCA-SG) and impregnation (NCA-I) methods to obtain Ni(10%)Cu(3%)/Al₂O₃. The synthesized catalysts were characterized by XRD, EDAX, BET, FTIR, and TG-DTG analysis, and their catalytic performances were evaluated by dry reforming of methane in a U-shape quartz micro reactor (6 mm i.d.), operated under atmosphere pressure, CH₄/CO₂=1, and GHSV=24 l/gr.hr.

Result and discussion:

XRD data confirmed the formation of amorphous structure for the NCA-SG catalyst. Broad and weak diffraction peaks of NiO suggested the high distribution of the NiO species on the support surface of NCA-SG catalyst. FESEM micrographs indicated significantly small nanoparticles with uniform distribution for sol-gel method (20-50 nm). Moreover, EDAX analysis revealed agreeable composition of species on the catalysts surface. Specific surface analysis revealed that the nanocatalysts had large enough surface area, in particular, NCA-SG

(196 m²/g). According to the results of the catalytic performance tests, NCA-SG nanocatalyst exhibited better catalytic activity and stability for methane dry reforming. Higher conversion and superior selectivity of H₂/CO close to 1 is related to improved physicochemical properties. The characterization results confirmed remarkable effect of the sol-gel method on the sample morphology, structure and catalytic activity and stability.

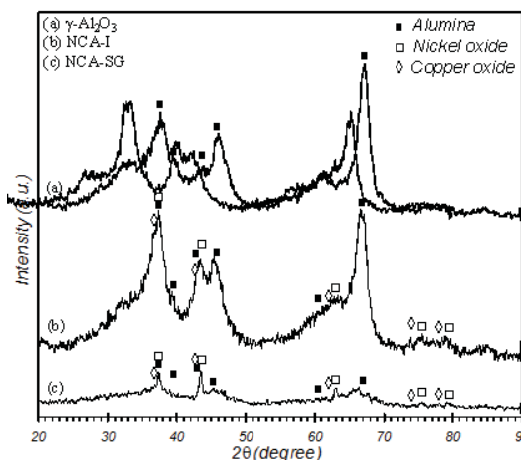


Figure 7: XRD patterns of Ni-Cu/Al₂O₃ nanocatalyst.

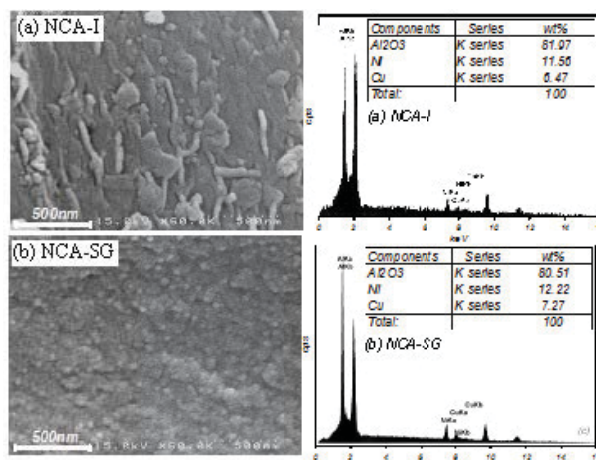


Figure 8: FESEM-EDAX analysis of Ni-Cu/Al₂O₃ nanocatalyst.

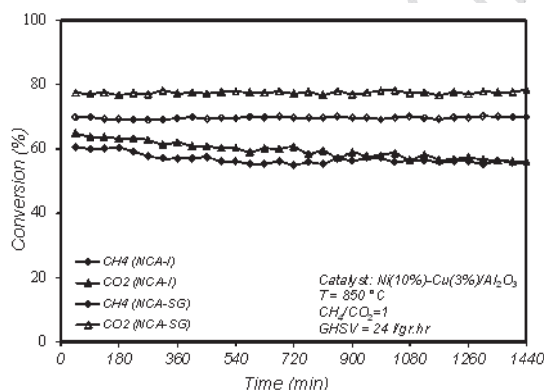


Figure 9: CH₄ and CO₂ conversion over Ni-Cu/Al₂O₃ nanocatalyst.

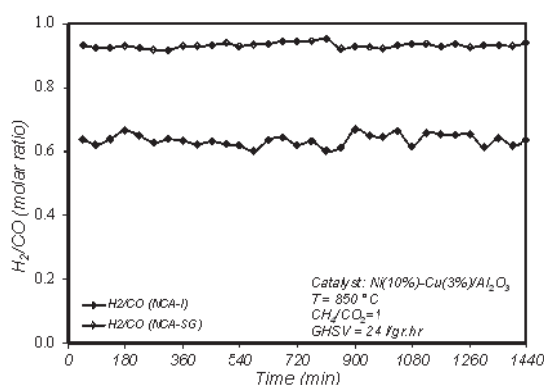


Figure 10: H₂/CO ratio in product over Ni-Cu/Al₂O₃ nanocatalyst.

Conclusion:

In order to investigate the effect of preparation method on the properties and catalytic performance, Ni-Cu/Al₂O₃ nanocatalysts were synthesized via sol-gel and impregnation



methods. Based on the characterization results, sol-gel method endowed the sample with small nanoparticle size, uniform distribution and higher surface area. As a result, higher catalytic activity and stability was achieved. Therefore, the sol-gel method leads to an excellent preparation of Ni-Cu/Al₂O₃ nanocatalysts for dry reforming of methane.

References:

- [1] J. Newnham et al., "Highly stable and active Ni-mesoporous alumina catalysts for dry reforming of methane", *International Journal of Hydrogen Energy*, 37, (2), 1454-1464, 2012.
- [2] S. Barama et al., "Catalytic properties of Rh, Ni, Pd and Ce supported on Al-pillared montmorillonites in dry reforming of methane", *Catalysis Today*, 141, (3-4), 385-392, 2009.



Computational Chemistry



Molecular Dynamics study of diffusion of Halocarbons in FAU zeolite

R. Rabiei^{*a}, B. Najafi^a and S. Alavi^b

^aDepartment of chemistry, Isfahan University of Technology, Isfahan, Iran
(e-mail: rzh.rabiei@gmail.com)

^bDepartment of chemistry, University of Ottawa, Ottawa, Canada

Keywords: Halocarbon, FAU zeolite, Diffusion coefficient, Simulation

Introduction:

The diffusion of Halocarbons in zeolites is attracting at present due to its relevance to environmental issues concerning ozone-depleting chlorofluorocarbons (CFCs) [1] and the removal of chlorinated solvent residues from contaminated groundwater and soils [2].

This paper deals with diffusion of different Halocarbons in FAU zeolite. Diffusion plays an important role in the use of zeolites in catalysis and separation processes based on adsorption and zeolites membranes. Zeolites have been commonly used as catalysts and adsorbents for a long time [3],[4].

Methods:

The adsorbate-adsorbent and adsorbate-adsorbate interactions were modeled by an interatomic potential consisting of Lennard-Jones (LJ). The zeolite was modeled as follows: Si₁₉₂O₃₈₄ with $q(\text{Si})=+2.4$ and $q(\text{O})=-1.2$. Potential charges of guest molecules are reported in Table 1.

Table 1. Potential charges of Halocarbons

molecules	C	F	Cl
CF ₄	0.800	-0.200	
CFCl ₃	0.616	-0.176	-0.086
CF ₂ Cl ₂	0.210	-0.086	-0.019
CF ₃ Cl	-0.039	-0.033	0.024

Molecular dynamic simulations were performed in DL_POLY program in the NVT (3×10^6 steps) and then NVE (5×10^6 steps) ensemble in range of temperatures between 200 K and 700 K. The mean square displacements (MSDs) of guest molecules at different temperatures were evaluated by means of the following classical education:

$$MSD(t) = \langle \Delta r_j^2(t) \rangle = \frac{1}{2} \sum_{j=1}^N [r_j(t) - r_j(0)]^2$$

The diffusion coefficients were obtained by fitting the MSD plots as a function of the time, assuming the following Einstein relation:

$$MSD(t) = A + 6Dt$$

Results and Discussion:

The diffusion coefficients of different Halocarbons in FAU zeolite is shown in figure 1.

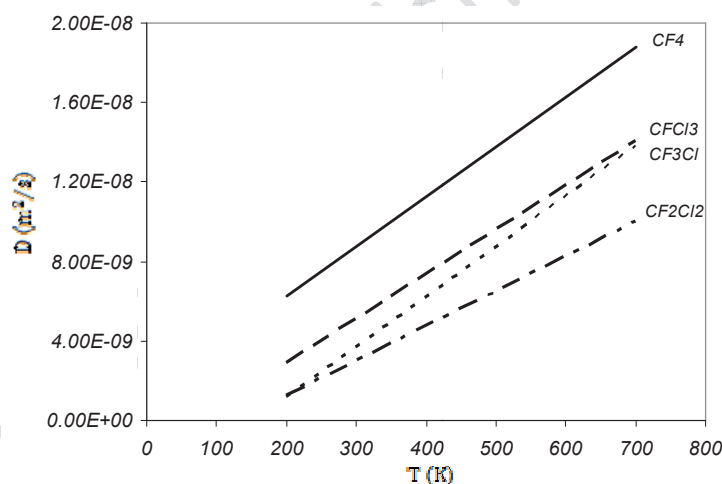


Figure 1. Diffusion coefficients of Halocarbons

For comparison diffusion coefficients of Halocarbons we calculated dipole moments of these molecules by Gaussian software. These dipole moments are reported in Table 2.



Table 2. Molecular masses and dipole moments of Halocarbons

molecules	molecular mass	dipole moment
CF ₄	88.004	0.0000
CF ₃ Cl	104.459	0.8053
CF ₂ Cl ₂	120.913	0.9335
CFCl ₃	137.368	0.8585

Conclusions:

Diffusion coefficient increase with both molecular mass and dipole moment. CF₂Cl₂ with max_of dipole moment, has min of Diffusion coefficient.

Reference:

- [1] Manzer. L. E. Science. 24 (1990) 931.
- [2] Hutchings, G. J., Heneghan, C. S., Ian, D. H. Nature. 384 (1996) 341.
- [3] Coppens, M. O., Keil, F. J., Krishna, R. Rev. chem.. Eng. 2000, 16, 71.
- [4] Bergh, J. V. D., Ban, S., Vlugt, T. J. h., Kapteijn, F. J. Phys. Chem. C 2009, 113, 17840-17850



A Computational Analysis of Interaction of Different isomers of Curcumin with Protein Kinase C δ (PKC δ)

M. Ighaei¹, J. Jahanbin Sardroodi¹, F. Mehrnejad², A. Rastkar Ebrahimzadeh³, B. Shirforoush Sattari¹

¹Department of Chemistry, Faculty of Science, Azarbaijan University of Shahid Madani, Tabriz, Iran

²Department of Cellular and Molecular Biology, Faculty of Science, Azarbaijan University of Shahid Madani, Tabriz, Iran

³Department of Physics, Faculty of Science, Azarbaijan University of Shahid Madani, Tabriz, Iran

Email: jsardroodi@azaruniv.edu

Key words: Curcumin , protein kinase C , DFT, Autodock

Introduction:

Protein kinase C (PKC) is a family of serine /threonine protein kinase . PKC isoforms play important role in the pathology of several diseases such as cancer, diabetes, stroke, heart failure, and Alzheimer's disease. Therefore, PKC has been a subject of intensive research and drug development, particularly in cancer research. The C1 domains of PKC have become an attractive target in designing the its based drugs. Several classes of high-affinity ligands that target the C1 domain have been previously described. Recently it was found that curcumin bind to the C1 domain and modulate PKC. [1]

Curcumin is the active ingredient of the dietary spice turmeric and has been consumed for medicinal purposes for thousands of years. Modern science has shown that curcumin modulates various signaling molecules, including inflammatory molecules, transcription factors, enzymes, protein kinases, protein reductases, carrier proteins, cell survival proteins, drug resistance proteins [2]

There are some studies about recognizing how PKC is modulated by curcumin in vito and vivo [3] but there isn't any theoretical study about it, so in the present study, we investigate interaction of different isomers of curcumin with PKC δ by computational methods.

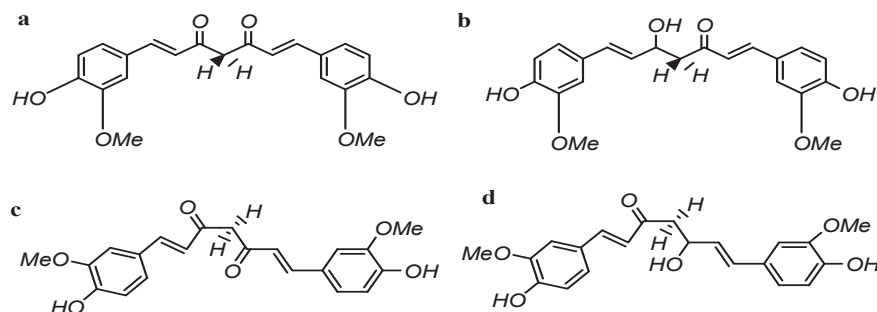


Figure1. Different isomers of curcumin

Computational Methods:

Equilibrium geometries were optimized using the DFT/ B3LYP with 6-311G (2d, 2p) basis set.

All calculations were performed with Gamess- us package. Then the optimized curcumin structures and C1B subdomain of protein kinase C δ (PDB code: 1PTQ) were subjected for docking analysis using Autodock 4.2. 100 docking runs were performed. After the simulation were complete, the docked structures were analyzed and the interaction were seen. Hydrogen bond interactions and the binding distance between the donors and acceptors were measured for the best conformers.

Results of Docking Simulations:

Table 1 shows results of docking simulation including the number of produced clusters of conformers using RMSD-tolerance of 2.0 Å out of 100 docking runs (A), the number of conformation in first cluster (B), binding energy of lowest energy conformation in this cluster (C), ligand efficiency (D), internal energy (E), electrostatic energy (F), torsional energy (G), unnbond energy (H) which residue that participate in hydrogen bonding interactions (I).

Table1. Some results of Docking Simulation

isomers	A	B	C	D	E	F	G	H	I
a	54	5	-7.91	-0.29	-10.9	-0.22	2.98	-1.82	LEU29, HIS40
b	16	12	-8.74	-0.32	-11.72	-0.41	2.98	-1.44	TYR8, GLY28, LYS30
c	29	1	-7.73	-0.29	-10.71	0.14	2.98	-1.85	THR12, TYR8, LYS30



d	20	37	-8.52	-0.32	-11.51	-0.22	2.98	-1.2	TYR8, GLY28
---	----	----	-------	-------	--------	-------	------	------	-------------

Conclusion:

According to the results of table 1 which show large values of efficiency and binding energy for binding of isomer **e** (enol – ceto form) to pkc δ , selecting this isomer between other is the best. So increasing the amount of isomer (**e**) in bulk curcumin leads to increase modulation of pkc δ and improve medicinal properties of curcumin.

Refrence:

- [1] A .Majhi, G. M, Rahman, SH, panchal, Bioorg & Med Chemistry 18 (4), 2010, 1591 -1598
- [2] S. C, Gupta, S.Patchva, W. Koh, B. B, Aggarwal, Clinical and Experimental Pharmacology and Physiology, 39 (3), 2012, 283-299
- [3] R. Garg, A.G. Panchandani, G.B. Maru, Carcinogenesis 29 (6), 2008, 1249-1257



DFT study of the electronic structures and energetics of different isomers of curcumin

Masoumeh Ighaei¹, Jaber Jahanbin Sardroodi¹, Faramarz Mehrnejad², Ali Reza Rastkar Ebrahimzadeh³

¹Department of Chemistry, Faculty of Science, Azarbaijan University of Shahid Madani, Tabriz, Iran

²Department of Cellular and Molecular Biology, Faculty of Science, Azarbaijan University of Shahid Madani, Tabriz, Iran

³Department of Physics, Faculty of Science, Azarbaijan University of Shahid Madani, Tabriz, Iran

Email: jsardroodi@azaruniv.edu

Key words: Curcumin, isomer, DFT, GAMESS-US

Introduction:

Curcumin is the mainly yellow phenolic material of tumeric and widely used as feed coloring additive. Numeric experimental studies have demonstrated that curcumin has various biological activities, including antioxidant activity, cancer prevention activity, antiangiogenesis activity, AD disease prevention activity.

In this paper accurate quantum chemical studies employing DFT study on different isomers of curcumin in the gas phase and aqueous solution has been carried out with the objective of finding the equilibrium structure, charge, bonding characteristic and nature of molecular orbitals particularly the highest occupied and lowest unoccupied that are important for binding.

Computational details:

Equilibrium geometries in the gaseous phase were optimized using the DFT method. The DFT approach utilized B3LYP functional and 6311-G (2p, 2d) basis set was used. Then the optimized curcumin structure was placed in water to study changes to the geometry and charges in water at the DFT/B3LYP by using the self-consistent reaction field models in which

the solvent was treated to be a dielectric continuum. We use GAMESS-US package for all computations. Four possible isomeric structures of curcumin have primarily been considered. These isomers were shown in figure 1.

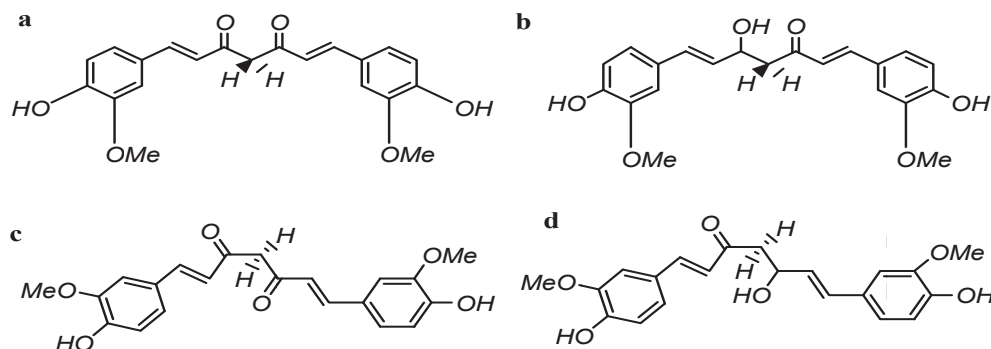


Figure1. Different isomers of curcumin

Results:

Some results of calculation such as computed energetics, and HOMO-LUMO gaps of the four isomers of curcumin in the gas phase and aqueous solution were shown in table 1, 2, respectively.

Table1. The computed energetics, and HOMO-LUMO gaps in the gas phase

isomer	Total energy(hartree)	HOMO	LUMO	HOMO-LUMO gap
a	-1263.2159	-0.2085	-0.0739	0.1346
b	-1263.2551	-0.1989	-0.07940	0.1195
c	-1263.2446	-0.2104	-0.0740	0.1364
d	-1263.2318	-0.1992	-0.0765	0.1227

Table2. The computed energetics, and HOMO-LUMO gaps in the aqueous solution

isomer	Total energy(hartree)	HOMO	LUMO	HOMO-LUMO gap
a	-1263.2419	-0.2133	-0.0813	0.1320
b	-1263.2781	-0.2040	-0.0904	0.1136
c	-1263.2692	-0.2150	-0.0844	0.1306

d	-1263.2571	-0.2036	-0.0864	0.1172
---	------------	---------	---------	--------

Conclusion:

As can be seen from Tables 1, 2, the syn enolic form was definitely found to be the ground state and the most stable form both in the gas phase and aqueous solution optimization of curcumin. This ground state both in the gas phase and in solution which are shown in Figure 2 have planar framework.

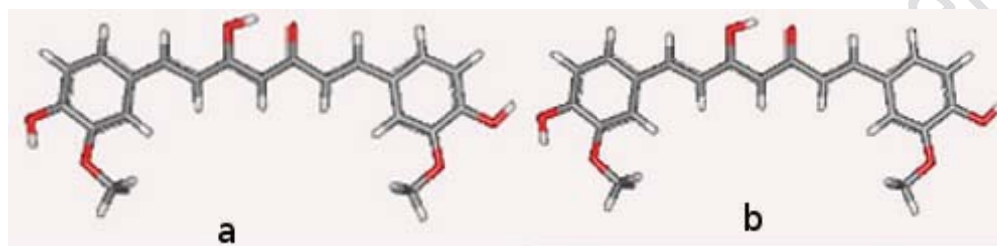


Figure 2. Final optimized structures of stable isomer of curcumin (a: gas phase, b: aqueous solution)

Reference:

- [1] K, BALASUBRAMANIAN, J. Agric. Food Chem. 2006, 54, 3512–3520
- [2] Y, Sun, H, Zhang, D, Chen and C, Liu, Org. Lett., 2002, 4 (17)
- [3] P, Denga, H, Zhange, J, Jianga, and Q, Jiang, J. At. Mol. Sci, 2011, 2(1), 51-57



Computational investigation on copper-assisted radioiodine exchange of Meta-iodobenzylguanidine in ammonium sulfate matrix

A. Vahidi Ferdowsi^{*a}

^a Research and Develop Branch, Nassimteb Corporation, Tehran, Iran.

Email: a.v.ferdowsi@gmail.com

Keywords : Meta-iodobenzylguanidine, Ammonium Sulfate, DFT , Thermodynamical Properties

Introduction:

Meta-iodobenzylguanidine contains a benzyl and a guanidine group. Neuroendocrine cells take up MIBG through an active mechanism and store it in the neurosecretory granules. Several methods for radioiodination of MIBG were investigated, based on nucleophilic isotopic exchange. These synthetic methods have produced varying radiochemical yields, which in some cases have been close to quantitative [1].

A new synthetic method by the simultaneous presence of copper and ammonium sulfate was used. In this method CuSO₄ and ammonium sulfate are simultaneously added to the reaction. A reducing agent isn't added directly to medium, but obtained iodine from reducing Cu²⁺ is reduced by productive SO₂ gas from thermal decomposition (deammoniation) of ammonium sulfate [2].

Furthermore, it is anticipated that the formation of complex from copper and ammonia at high temperature, the activation energy barrier decreases and favorable effects on yield and reaction rate does. In this claim with evidence of quantum mechanics is investigated and proven. Also, reaction mechanism by DFT computations has been carefully reviewed.

Methods:

The computed values of free energies were estimated by means of the B3LYP together with the standard mix basis sets for elements that yield potential energy barriers in good agreement



with the experiment. Transition states are characterized as having only one negative eigenvalue and absence of imaginary frequencies verifies that reactant and product structures are true minima. Frequency calculations were performed at the same theory level as the optimizations to obtain zero-point energies (ZPE) and to confirm the nature of the stationary points. The intrinsic reaction coordinate (IRC) path was traced in order to check the energy profiles connecting each TS to the two associated minima of the proposed mechanism.

Results and discussion:

We evaluated the relative concentrations of possible species in the reaction matrix. Our calculations show that desired carbocation is unstable and not formed. In presence iodide, previous structure are unstable and CuI the most desirable component. Thus, the S_N1 mechanism is not favorable. CuI may also combine with one molecule of H₂O to form CuI-H₂O and with increasing temperature, the ammonia molecule is added in the medium of reaction and the CuI-NH₃ combination is formed (-8.9 kcal/mol more stable than CuI-H₂O).

We explored the stable configuration of transition state in studied S_N2 mechanism. The transition states (TS1, TS2, TS3) for this reaction was located and confirmed by a frequency calculation to have an imaginary frequency. TS1 just contain of MIBG and CuI and TS2 has triangular planar geometry and TS3 has pseudo-tetrahedral geometry on copper atom with one and two NH₃ ligands, respectively.

We compared and evaluated base on the presence of ammonia in the medium of reaction. The energy of the intermediate, however, is lowered 164 kcal/mol, relative to the reactant energy. All the structural changes imply the formation of C-131I and Cu-I bonds and simultaneous weakening of relevant C-I and Cu-131I bonds.

Lowering of the free energy of activation by introducing additional NH₃ molecule amounted to *ca.* 32.29~ 5.41 kcal/mol, which made catalyzed reaction more facile than un-catalyzed one. Combining with their high activation barriers (32.3 kcal/mol), TS2 and TS3 are likely to be reactive transition state species in this copper-catalyzed reaction.

The $\Delta C-131I/\Delta C-I$ and $\Delta Cu-131I/\Delta CuI$ charge ratios by means of NBO analysis as measure of power transformation from reactants to products obtained. As a result, These ratios



demonstrated that the transition state changes to product in TS3 faster than TS2 and TS1, respectively. The computed FMOs prove S_N2 reaction and suggests that bonds are being formed and broken.

Conclusions :

Our thermodynamical and geometrical results show that TS3 with two molecules of ammonia are most favorable transition state. The present study would provide in-depth information about the influence of TS on the thermodynamic properties of reaction and highlight the crucial role of the ammonia ligand.

References:

- [1] H.H. Coenen and et al.; "Radioionidation Reactions For Pharmaceuticals"; Springer; 2006.
- [2] W. D. Halstead; "Thermal decomposition of ammonium sulphate"; Journal of Applied Chemistry; 20, 129–132, 1970.



A Theoretical Study on the Structural Features of Bisphosphonate Pharmaceuticals

M. Arabieh^{a,b}, M. Ghannadi-Maragheh^b, S.J. Ahmadi^b and M.H. Karimi-Jafari^{c*}

^a Department of Chemistry, Faculty of Sciences, Shahid Beheshti University, Tehran, Iran

^b Computational Chemistry Laboratory, NSTRI, Tehran, Iran

^c Department of Bioinformatics, IBB, University of Tehran, Tehran, Iran

Email: mhkarimijafari@ibb.ut.ac.ir

Keywords: Pamidronate, Bisphosphonate, Conformational search, Hydrogen bond

Introduction:

Bisphosphonates (BPs) are analogues of the naturally occurring inorganic pyrophosphate in which the oxygen in P-O-P has been replaced by a carbon, resulting in a metabolically stable P-C-P structure. These drugs represent a large contribution to the global pharmaceutical market and are widely used in treatment of a variety of bone disease such as osteoporosis, Paget's disease and hypercalcemia due to malignancy. Although these experimental studies shed some light on the structure-activity relationships of BPs, it is still an open theoretical question that how small structural modifications of BPs may lead to extensive alterations in their physicochemical, biological and toxicological characteristics. In this regard a detailed structural analysis of BPs under a well-defined theoretical frame-work is necessary for prediction of their activities. Thus the knowledge of conformational states of pamidronate is a prerequisite for study of its interaction and complexation with relevant metallic cations.

Computational details:

To explore conformational space of pamidronate, a systematic variation of all rotational degrees of freedom was performed. All bond lengths and bond angles are set initially to the equilibrium values obtained from a model-built structure that was optimized by PM6 semiempirical method. Semiempirically located minimum structures were then subjected to



further optimizations at the B3LYP/6-31+G* level of theory. Solvent effects were incorporated through the Conductor Polarized Continuum model (C-PCM). To increase the accuracy of relative conformational energies, single-point calculations were performed on the final structures at the MP2/6-311++G(2df,dp) level with and without C-PCM model.

Results and Discussions:

All stable gas-phase structures are of canonical form and solvation is necessary to stabilize charge-separated zwitterionic structures. Present calculations show that the H₃L form of pamidronate is mainly populated by a single conformer but the H₂L and HL protonation states are multi conformer systems in gas-phase and solution. In all protonation states the differences in electronic energy of conformers are small and thus ZPE and thermal corrections have significant effect on the energy ordering of different conformers. This effect is more pronounced for solvated structures as a result of smaller successive energy differences. It is found that values of P-O bond length are clustered in to two distinguishable distance ranges depending on the protonation of oxygen atom. Single P-O bonds are obviously longer and cover a range from 1.58 to 1.75 Å in gas-phase conformers. QTAIM analysis shows strongest hydrogen bonds are those occurred between phosphonate groups. In most conformations of pamidronate the alkyl amine side chain is folded on hydroxyl or phosphonate groups to participate in H-bonding with them. These nitrogen containing hydrogen bonds are weaker than inter-phosphonate H-bonds though play an important role on the relative stability of conformers.

Conclusion:

Full conformational space of pamidronate was searched for three protonation states relevant at physiological pH range. The spectrum of conformational energy is populated by many low lying structures. In gas phase and within an energy range of 5 kcal/mol higher than the most stable conformer there are 9, 15 and 8 conformers for H₃L, H₂L and HL protonation states, respectively. The best correlation was found to be a nearly linear relation between the



hydrogen-acceptor distance and the logarithm of electron density at hydrogen bond critical point.

References:

- [1] R. G. G. Russell, Bone 49 (2011) 2–19.
- [2] R. Chelli, F. L. Gervasio, C. Gellini, P. Procacci, G. Cardini, J. Phys. Chem. A 104 (2000) 11220–11222.
- [3] J. J. P. Stewart, J. Mol. Model. 13 (2007) 1173–1213.

15th Physical Chemistry Conference



Direct Ab Initio Dynamics Study on the Reaction of $\text{CF}_3\text{CHF}\text{CF}_3$ with Cl Atom

M. Arabieh and M. Zahedi*

Department of Chemistry, Faculty of Sciences, Shahid Beheshti University, Tehran, Iran

Email: m-zahedi@sbu.ac.ir

Keywords: $\text{CH}_3\text{CHF}\text{CF}_3$; Dual-level direct dynamics; Variational transition state theory (CVT)

Introduction:

Chlorofluorocarbons (CFCs) have been extensively used in many industrials and house usages. These compounds can involve in ozone destruction process via transferring from troposphere into stratosphere. Experimental and theoretical studies of kinetics of reaction of $\text{CF}_3\text{CFHCF}_3$ with different species such as H, O, and OH have been performed elsewhere. However; there are only a few experimental reports on reaction between $\text{CF}_3\text{CFHCF}_3$ and halogen atoms. Here we have theoretically studied both mechanism and kinetics of hydrogen abstraction reaction of $\text{CF}_3\text{CFHCF}_3$ by Cl atom. A dual-level direct dynamics approach is applied to investigate mechanism and kinetics nature of the titled reaction.

Computational methods:

The BB1K/6-31+G(d,p) level of theory was used as lower level of method for constructing initial potential energy surface (PES) where BB1K is one of hybrid meta density functional theory (HMDFT) methods proposed by Zhao et al. For higher level method, single point energy (SPE) calculations at BB1K/MG3S level of theory are implemented where MG3S denotes to semi-diffuse and modified version of G3Large basis set developed by Truhlar and et al.

Results and Discussions:

Fig-1 shows vibrational adiabatic potential energy curve (V_a^G) very smooth due to very low forward barrier height. In addition, it has two barriers, one barrier at the transition state [at $s=0$ ($\text{amu}^{1/2}\text{bohr}$)] and another one in entrance valley [at approximately $s = -0.64$ ($\text{amu}^{1/2}\text{bohr}$)]. As shown in Fig-2, following reaction path from reactants to products, all frequencies, except one, do not change significantly. The TST, TST/Wigner, CVT and CVT/SCT rate coefficients of reaction were calculated. The results showed the CVT rate constants are more close value to the available experimental data.

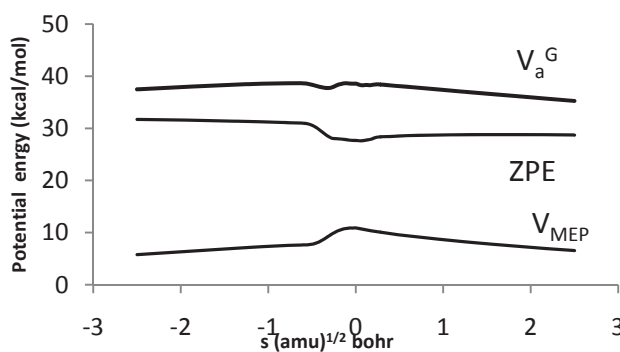


Figure -2

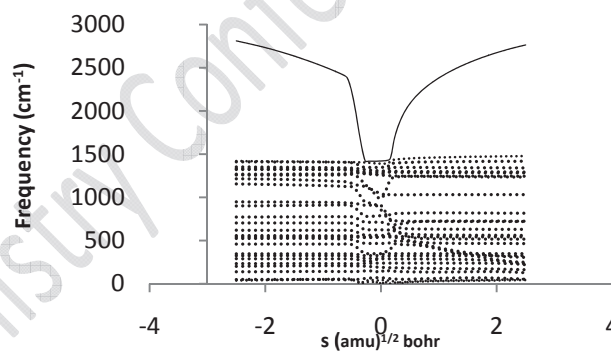


Figure- 1

Conclusion:

Using VTST-ISPE scheme, the rate coefficients are obtained at BB1K/MG3S//BB1K/6-31+G(d,p) quantum model built in a wide temperature range from 150 to 2000 K. Our results show for the title reaction both variational and tunneling effects are small. On the basis of present study it is expected our results are useful for prediction of rate coefficients of reaction in a wide temperature range where no experimental data is available.

References:

- [1] R. Atkinson, Chem. Rev. 86 (1986) 69-201.
- [2] Y. Zhao, D.G. Truhlar, J. Phys. Chem. A, 108 (2004) 6908-6918.
- [3] D.G. Truhlar, B.C. Garrett, J. Phys. Chem. 84 (1987) 365-369.

Quantum Chemical Modeling on Active Rutile TiO₂ Catalyst in Oxidative Coupling of Methane (OCM) Process

Mahtab Gharibi*, Bahareh Honarparvar, Ziba Hassanvand, and Leila Baharmand

National Petrochemical Company- Petrochemical Research & Technology Co. (NPC-RT),

Tehran Center, Iran, (m.gharibi@npc-rt.ir)

Key Words: Oxidative Coupling of Methane, TiO₂ Catalyst, Ab initio, DFT.

Introduction:

Methane is the most abundant component of natural gas, usually containing over 90% mole of the hydrocarbon fraction, and represents a possible raw material for the synthesis of more valuable products such as ethylene [1]. Formation of higher hydrocarbons from methane, which is the most abundant component of natural gas, is at the heart of several important industrial processes and the oxidative coupling of methane (OCM) represents the one viable route in this field. In recent years, several theoretical studies involving *ab initio* methods have been conducted to better elucidate the mechanism of OCM process [2]. These investigations aim at characterizing the ideal conditions for catalytic process:

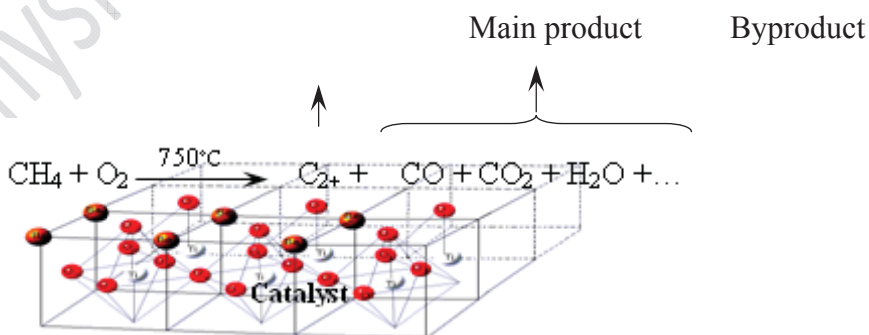


Figure 1. General representation of catalytic OCM process.

Effective catalysts for the reaction are largely rare earth, alkali and alkaline earth oxides; act as important catalysts in oxidative coupling of methane [3]. In this work, we reported ab initio cluster quantum chemical calculations of the modeling of titanium oxide catalyst to find the most proper cluster model for rutile structure of bulk titanium oxide and after identification of the active sites of catalyst surface.

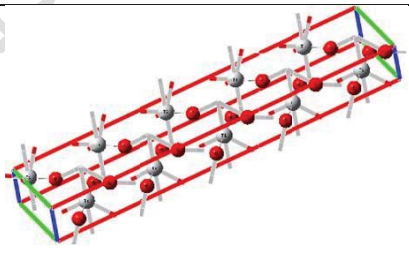
Materials and methods:

The computational techniques are described including the nature of the crystal models used in our calculations. The reactivity of the crystals with methane is discussed. Moreover, we theoretically estimated the interaction energies between hydrogen atoms of methane and oxygen of the catalyst at the level of B3LYP/TZVP in different distances and the graph of energy verses distance has been analyzed. The Gaussian 98 program package has been used for all calculations.

Result and discussion:

The results obtained demonstrate that the larger crystals didn't show any significant change in their relative energies and the best model has been observed in 3D lattice size (511) as a $\text{Ti}_{10}\text{O}_{20}$ molecular cluster with six atoms per unit cell. The less-coordinated lattice oxygen atom is more reactive and hemolytic fission of the C-H bond occurs on the surface of our catalyst. Also, the obtained result may reflect this fact that the values of relative energies in potential energy surface are highly sensitive to the size of simulation cells.

Table 1. The mechanism of interaction $\text{CH}_4 + (\text{TiO}_2)_{10}$ in OCM reaction

Optimized geometry: TiO_2 catalyst	Mechanism	Energy (E_h)
	<i>Hemolytic fission (Radical)</i>	- 1037. 392
	<i>Heterolytic fission-I (Anion)</i>	-1027.227
	<i>Heterolytic fission-II (Cation)</i>	-1027. 186



Conclusion:

The results show that the less-coordinated lattice oxygen atom is more reactive and hemolytic fission of the C- H bond occurs on the surface of our catalyst ($2\text{CH}_4 \rightarrow 2\text{CH}_3^\circ \rightarrow \text{C}_2\text{H}_6 \rightarrow \text{C}_2\text{H}_4$). A less-coordinated atom is usually more reactive, although an extremely high reactivity is often accompanied by a lower selectivity. We believe that the net atomic charge decrease with an increase in the coordination number.

References:

- [1] G. Wozny, H. Arellano-Garcia, *Chem. Eng. Trans.*, **21** (2010) 1399.
- [2] L. Olivier, S. Haag, H. Pennemann, C. Hofmann, C. Mirodatos, A. C. van Veen, *Catalysis Today* **137** (2008) 80.
- [3] M. S. Palmer and M. Neurock, *J. Phys. Chem B*, **106** (2002) 6543.

Adsorption of CO Molecules on Fullerene: A Density Functional Theory Study

M. Erfan. Zand^{a,b}, Hossen Mehdizadeh^{a,b}, Zahra feyli^c

^a Department of Chemistry, Payame Noor University, Shiraz, Iran

^b Padidavaran Co. Fars Science and Technology Park, Shiraz, Iran

^c Young Researchers Club, Hamedan Branch, Islamic Azad University, Hamedan, Iran
erfanzand@gmail.com

Keyword: CO, Fullerene, Adsorption, Density Functional Theory

Introduction:

Sensing gas molecules is critical to environmental monitoring, control of chemical processes, space missions, and agricultural and medical applications [1]. In the past few years, a new generation of gas sensors have been demonstrated using carbon nanotubes (CNTs) [2] and semiconductor nanowires [3]. It was reported that semiconducting CNTs could be used to detect small concentration of NH₃, NO₂, and O₂ with high sensitivity by measuring changes of the CNTs conductance upon exposure to the gases at room temperature [3]. Theoretical studies of gas molecular adsorption on the graphene surface have been reported recently, [27,28] which showed that NO₂, H₂O, NH₃, CO, and NO molecules are physically adsorbed on the pristine graphene.

In this task, using density functional theory (DFT) calculations, we study the adsorption of gas molecules on the different sites of fullerene surface. (see Figure 1)

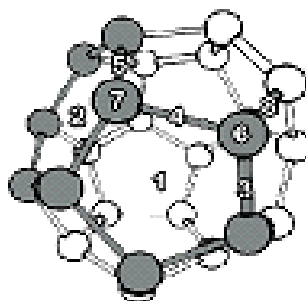


Figure 1. Labeling of C₂₄ fullerene surface sites used in this study.

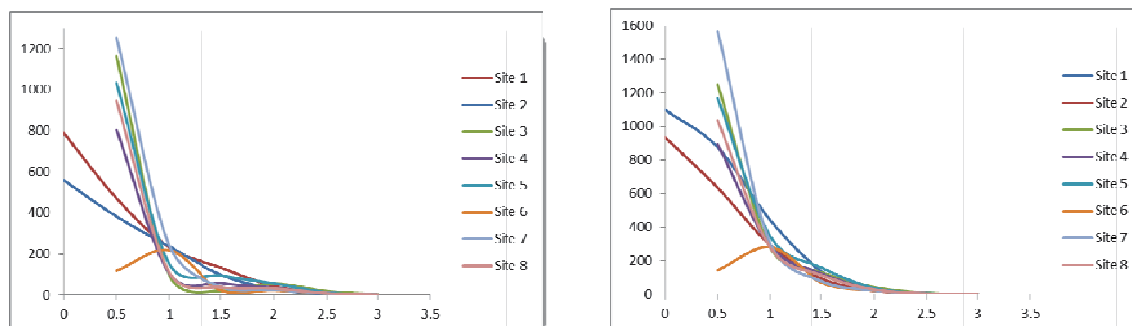


Figure 2. The graph of adsorption energy versus distance for different sites of fullerene from O (left) and C (right) heads.

Methods:

Density functional theory (DFT) calculations by Gaussian09 were performed in order to optimize both fullerene and CO using the hybrid B3LYP functional with 6-311++ g** basis set without any symmetry restrictions in the singlet ground state. Calculated vibrational frequencies without imaginary frequencies ensure the stable structures. Boys-Bernardi's counterpoise procedure (CP) to correct for the basis set superposition error (BSSE) was indicated that the so-called overcorrection of the BSSE by the counterpoise method is not large.

Results and Discussions

Binding energies were calculated via the difference in energy of fullerene /CO complexes from those of isolated fragments at different positions. The CO molecule could adsorb from Carbon or Oxygen heads (see Figure 2) at different distances ranges from 0 to 3 Å. In the most stable structure the CO molecules is separated on average by 1.5 Å.

Conclusion:

From these and some detailed consideration we can conclude that fullerene is a good candidate for adsorption of CO molecules.



References:

- [1] Special issue on Gas-Sensing Materials: MRS Bull. 1999, 24.
- [2] Kong, J.; Franklin, N. R.; Zhou, C.; Chapline, M. G.; Peng, S.; Cho, K.; Dai, H. Science 2000, 287, 622.
- [3] Wehling, T. O.; Novoselov, K. S.; Morozov, S. V.; Vdovin, E. E.; Katsnelson, M. I.; Geim, A. K.; Lichtenstein, A. I. Nano Lett. 2008, 8, 173.

15th Physical Chemistry Conference

Capacitive effect of C₂BN Bilayer Nanosheet by computational chemistry method

Narges bagheri ^{1*}, Mohammad Erfan Zand²

Department of Chemistry, Islamic Azad University, Firoozabad Branch, P. O. Box 74715-11745 Firoozabad ,
Fars, Iran

¹(nrgs.bagheri@gmail.com)

²(Erfanzand@gmail.com)

Keyword: Nanosheet, Capacitor, Density Functional Theory

Introduction:

More than ten years are passing from the time of verification of theory of presence of Bohrnithride nanotubs and then it has been identified different reports of its synthesis. Nowadays, it seems that it is necessary to know the chemistry of Bohrnitrid compound to preparation of composites and so on. These compounds have important application in nanoelectronic where the nanocarbonic compounds can't work effectively[1,2].

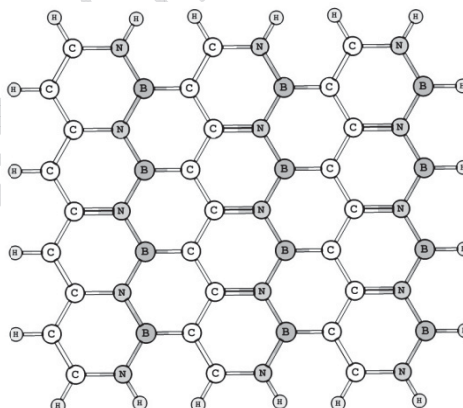


Fig 1: Structutr of C₂BN nano sheet

Computational method:

All calculations have been performed in gas phase using Density Functional Theory (DFT) level of B3LYP at 6-31G* standard basis set. All the calculations in this study have been performed by Gaussian 03 package[3].

Result and Discussion:

In this work, it has been investigated on the property of C₂BN bilayer nanosheets as nanocapacitor by using computational chemistry.

For investigation on capacitor character in these nanosheets, different fields parallel in z Cartesian axis: in different intensity are studied. These nanosheets include 148 atoms. In different distance of two sheets change of charge on any atoms, energy gap and total energy of system, the character of capacitor has with increasing of electric field, the charge of any atom are increased

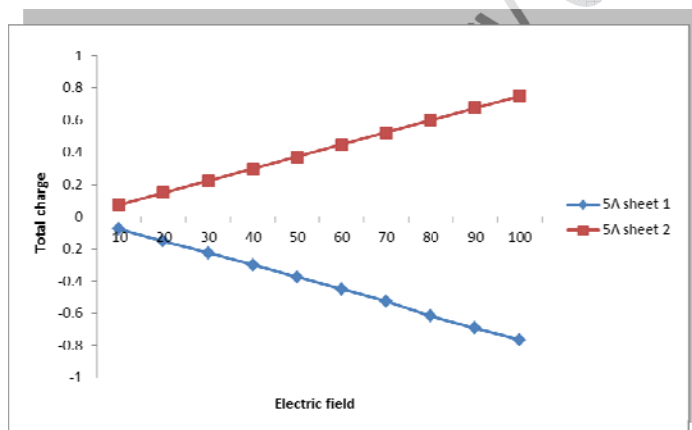


Fig 2: Charge difference between to layer

Conclusion:

In this study, the nanocapacitive properties of two-layered graphene sheets have been investigated within different distances and electric fields. The analysis of charges of each atom shows that these sheets can be used as capacitor. The capacitive properties depend on distances between two sheets and the applied electric field. It is shown that the nearer two sheets, the more stored charges. Also, the position of atoms in sheet is important. The atoms placed the outer edge of the sheet can store more charge. More in-depth investigation is in progress by the researchers of the present study.



References:

- [1] Kong, J.; Franklin, N. R.; Zhou, C.; Chapline, M. G.; Peng, S.; Cho, K.; Dai, H. *Science* 2000, 287, 622.
- [2] Wehling, T. O.; Novoselov, K. S.; Morozov, S. V.; Vdovin, E. E.; Katsnelson, M. I.; Geim, A. K.; Lichtenstein, A. I. *Nano Lett.* 2008, 8, 173
- [3] M. J. Frisch, G. W. Trucks, H. B. Schlegel, et al., GAUSSIAN 03, Revision B.04, Gaussian, Inc., Pittsburgh, PA, 2003.



Electrostatic Forces effects on aggregation behavior of CTAB surfactant around carbon nanotubes

M. Foroutan*, F. Mirzaie Milani

Department of Physical Chemistry, School of Chemistry, University College of Science, University of Tehran,
Tehran, Iran

Email: f.mirzaie.milani@khayam.ut.ac.ir

Keywords: Surfactant , Simulation , Carbon Nanotube , Salt.

Introduction:

Single-walled carbon nanotubes (SWCNTs) can be dispersed as individuals in water using surfactants. By controlling the intermolecular and surface forces of surfactant in water, it is possible to engineer the resultant VdW attraction between SWNTs [1]. On the other hand, one technique has been improved by Arnold *et al.* [2], who, using bile salts such as sodium cholate in addition to surfactants, demonstrated that it is possible to separate SWCNTs on the basis of their diameter and electronic structure. However, it is still not clear how surfactants self-assemble on SWCNTs in the presence of salt. A detailed understanding of the structure of surfactant aggregates adsorbed on SWCNTs in the presence of salt is the goal of this work.

Simulation details:

We used a canonical ensemble with undefined boundary conditions for considering the simulated volume were equals to infinite. The velocity form of Verlet algorithm method and the Nose-Hoover thermostat algorithm were used to integrate the equations of motion with a time step of 1.0 fs and temperature control of 300 K, respectively. Water molecules were modeled using the SPC/E model. Simulations were conducted for 3ns., for system containing 1153 water molecules, 25 surfactant CTAB molecules and (3, 12, 25, 50) salt NaCl molecules and a (5,5) CNT

Result and discussion:

In the present study, we performed a molecular dynamics (MD) simulation in a four-component system, including water, surfactant (CTAB), SWNTs and salt, to address the unresolved issue regarding the self-assembly structure of adsorbed CTAB surfactants onto SWNT surface in the presence of salt. Efforts have also been made to calculate the radial distribution function (RDF) and potential of mean force between two nanoscopic components, in order to shed new light on the dispersion and stability mechanism of SWCNT in aqueous CTAB solution in the presence of salt. To the best of our knowledge, this is the first simulation of complex interaction behavior on the atomic level in a four-component system. Figure 1 shows simulated system containing SWCNT, salt, surfactant and water.

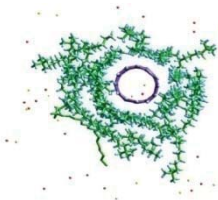


Figure 1- Front view of representative snapshot for (5,5) CNT covered by surfactants in the presence of salt molecules.

Water molecules are not shown for clarity. We calculated the radial distribution functions (RDFs) for all components of system including cation and anion of salt, carbon atoms of nanotube and different atoms of surfactant. Our results indicate that salt addition has a significant effect on the distribution of surfactant molecules around the carbon nanotube. Also the RDF between N of surfactant head groups and Cl⁻ atom of NaCl shows that when more Cl⁻ ions are located around the polar head group of surfactant, the tendency of surfactants for aggregating around CNT increases.

Conclusion:

In this work, we presented plots of the potential mean force in order to study the effects of salt addition on the behavior of aqueous solutions of CTAB surfactants in the presence and the absence of SWCNT. Results of salt concentration variations on systems including carbon



nanotubes did not show a regular pattern on stability of these systems and only resulted in increased stability in certain salt concentrations.

References

- [1] Y. Tan and et al;" Dispersion of single-walled carbon nanotubes of narrow diameter distribution"; Resasco, D. E. *J. Phys. Chem. B.*; 109, 14454-14460, 2005.
- [2] M. S. Arnold and et al;" Sorting carbon nanotube by electronic structure using density differentiation"; *Nat. Nanotechnol.*; 1, 60-65, 2006.



Theoretical study of the Substituent effects on O–H bond dissociation enthalpies of *trans*-resveratrol derivatives

Elyas Nazarpour, Mansour Zahedi

Department of Chemistry, Faculty of Sciences, Shahid Beheshti University,

G.C., Evin, 19839-6313, Tehran, Iran

E-mail: elyasnazarpour@yahoo.com

Keywords: Antioxidant, Resveratrol, BDE, Substituent Effect

Introduction:

In recent times, there has been a growing attention in selecting efficient and safety antioxidants from the natural compounds, such as flavonoids, vitamin E and other phenols [1]. One of the most closely considered compounds, *trans*-3,4',5-trihydroxystilbene, resveratrol (RES), found in red wine, grape products, berries, and peanuts, has established a wide variety of effectual biological properties [2,3].

Methods:

The DFT method with B3LYP functional and the 6-31G (d,p) basis set were used for geometry optimization of each compound and respective radical structure in the gas phase. Single point calculations have been carried out using 6-311++G (2d, 2p) basis set.

Results and discussion:

In this work, various electron-donating and electron-withdrawing groups were placed in X1, X2, X3 and X4 of *trans*-resveratrol (see Figure 1) and the Bond Dissociation Enthalpy (BDE) values of three hydroxyl groups (3OH, 5OH and 4'OH) in A and B-rings were calculated. The results show that the BDE of para position (4'OH) is lower by about 22-28 kJ mol⁻¹ than 3OH and 5OH for non-substituted resveratrol. Figure 2(A-D) is an illustration of the positive spin densities of above species' radicals after hydrogen abstraction. The BDE difference

between the 3OH and the 5OH in X1 position for studied substituents lies in the range 0.3–80.1 kJ mol⁻¹. For X2 position 5OH is in the ortho position and 3OH is in the para position. Various substituents are placed in this position (Figure 1) and BDEs and Δ BDEs are computed. As it is observed the substitution effect on ortho position is more significant and it is within the range of 1.0–88.4 kJ mol⁻¹. While for the para position the calculated BDEs are in the range of 1.5–35.9 kJ mol⁻¹. For X3 position the 4'OH is in meta position and The effect of EWG and EDG substituents on BDE and Δ BDE values was investigated. The highest values of BDE are found in the case of CHO (341.5 kJ mol⁻¹) and the lowest values of BDE are found in the case of OMe (316.2 kJ mol⁻¹). The difference between highest and lowest BDE values for *meta* substituents is 22.4 kJ mol⁻¹. The X4 substitutions are in ortho position of 4'OH group and have significant effect on its BDE values. The 4'OH BDE is decreased about 45.5 kJ mol⁻¹ in comparison with non-substituted structure in presence of NHMe (electron-donating group) and the lowest BDE (279.2 kJ mol⁻¹) was found for this structure. In the case of NH2 the BDE value (286.0 kJ mol⁻¹) decreases about 39.7 kJ mol⁻¹ and it shifts about 37.6 kJ mol⁻¹ in the presence of OH groups and reaches to 287.1 kJ mol⁻¹. The highest values of 4'OH BDE are found in the case of electron withdrawing groups such as NO2 (374.3 kJ mol⁻¹) and COOH (374.0 kJ mol⁻¹).

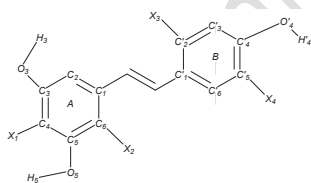


Figure 1. X1=H, X2=H, X3=H and X4=H (*trans*-Resveratrol)

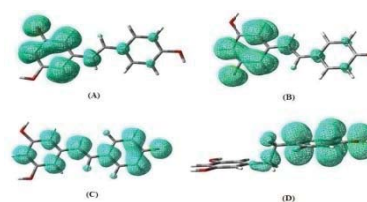


Figure 2. Positive Spin density and unpaired electron distribution

Conclusions:

Electron-donating and electron-withdrawing groups have been placed in available positions of *trans*-resveratrol and their effects on BDEs were investigated. The B-ring is more important than A from the BDE point of view, because the radical structure, after H abstraction from the 4'OH could be stabilized by the resonance between two rings. This OH group is also affected by the substitution groups of A-ring. Moreover, if an electron-donating group is placed in X4



position (the ortho position for 4'OH), the lowest BDEs are computed. Computed BDEs show that, the trans-resveratrol derivatives that have good spin density distribution, have the lowest BDEs.

References:

- [1] Halliwell, B.; Aeschbach, R.; Löliger, J.; Aruoma, O. *Food and Chemical Toxicology* **1995**, 33, 601-617.
- [2] Saiko, P.; Szakmary, A.; Jaeger, W.; Szekeres, T. *Mutation Research/Reviews in Mutation Research* **2008**, 658, 68-94.
- [3] Baur, J. A.; Sinclair, D. A. *Nature Reviews Drug Discovery* **2006**, 5, 493-506.



DFT/B3LYP study of the Antioxidant Properties of IRFI in the Gas Phase and DMSO solvent

Elyas Nazarpour, Mansour Zahedi

Department of Chemistry, Faculty of Sciences, Shahid Beheshti University, G.C., Evin, 19839-6313, Tehran, Iran
(Email: elyasnazarpour@yahoo.com)

Keywords: IRFI (IRFIOH), bond dissociation enthalpy (BDE), B3LYP

Introduction:

IRFI (IROH), a phenolic antioxidant originally designed for food preservation. It is both water and lipid soluble and has been studied chemically for its stabilizing radical-trapping activity and therapeutically for its capacity to limit myocardial infarction and prevent liver necrosis caused by lipid peroxidation.

Methods:

The hybrid B3LYP functional and the 6-31G(d) basis set was used for the optimization of all of the stationary points in the gas phase. Single point calculations have been carried out using 6-311+G(2d,2p) basis set. The solvent effect was taken into consideration in all of the calculations by employing the self-consistent reaction field (SCRF) method with a polarized continuum model (PCM). All calculations were performed with Gaussian 98 program.

Results and discussion:

A proposed mechanism which can be envisioned for sequential hydrogen abstractions from IRFIOH has been presented in Figure 1. The mechanism shown in Figure 1 involves the phenolic hydrogen (H1) and the acidic hydrogen (H2) abstractions from IRFI by hydroperoxyl radical. These data, together with the fact that the primary oxidation products of monophenolic compounds formed by hydroperoxyl are phenoxyl radicals, indicate that IRFIOH radical must

evolve chemically to the IRFIKD form through a series of intermediates starts with a hydrogen abstraction reaction of the IRFIO[•] radical to form a ketodiene, which is subsequently hydrolyzed to IRFI quinone, IRFIQ. By taking a look at Figure 2 and Figure 3, you can see that the abstraction reaction is a plausible mechanism for two HOO radical scavenging in DMSO, but the maximum barrier in vacuum, methanol or water is pretty high (almost twice the barrier in DMSO and the overall reaction is less exothermic). According to that, solvent effects are very important to decide whether hydrogen abstraction or an alternative mechanism is preferred to eliminate two HOO radicals.

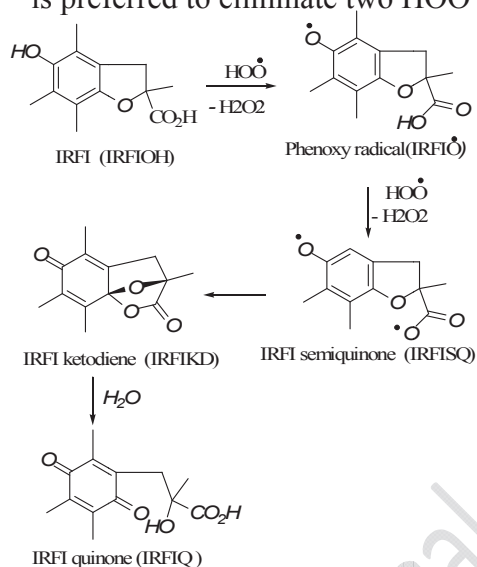


Figure 1

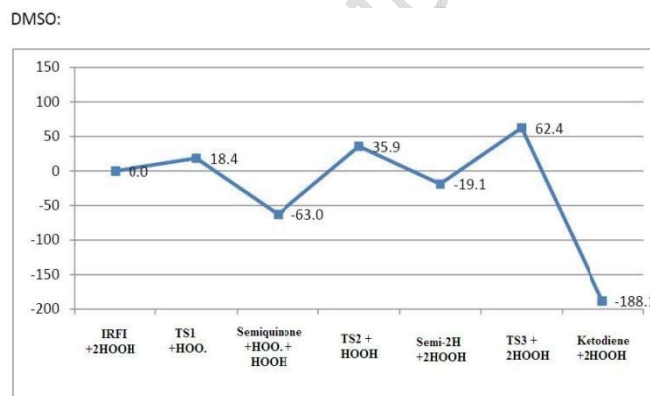


Figure 2

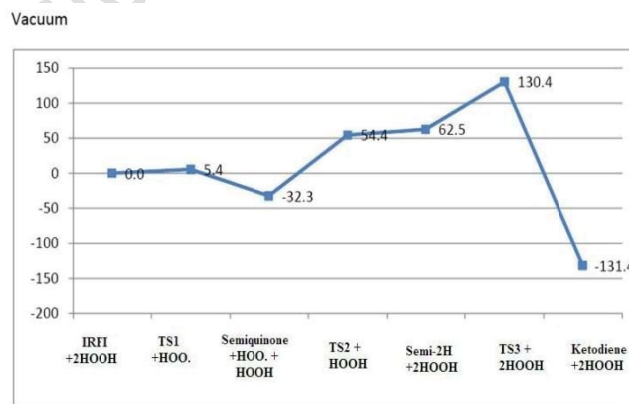


Figure 3



Conclusions:

The proposed mechanisms have been studied from both thermodynamics and kinetics points of view. The results show that the hydrogen abstraction from phenolic hydrogen is exothermic and will be carried out with high rate. As a result, the acidic H atom abstraction reaction is possible kinetically, but it is not predicted to occur from a thermodynamics point of view in the gas phase. But according to the spin density distribution of IRFIOH-2H and higher stability from ketodien formation, acidic H abstraction could be occurred. Solvent effects are very important to decide whether hydrogen abstraction or an alternative mechanism is preferred to eliminate two HOO radicals.

References:

- [1] J. W. Scott, W.M. Cort, H. Harley, J. Am. Chem. Soc. 51 (1974) 200.
- [2] D. Metodiewa, H. B. Dunford, Biochem. Int. 25(1991) 895.
- [3] M. J. Thomas, B. H. J. Bielski, J. Am. Chem. Soc. 111(1989) 3315.
- [4] K. Lee, P. Canniff, D. Hawel, , P. Silver, A. Ezrin, Gen. Pharmacol. Ther. 47(1990) 174.
- [5] T. Doba, G. W. Burton, K.U. Ingold, Biochim. Biophys. Acta. 899(1985) 76.
- [6] J. S. Wright, D. J. Carpenter, D. J. McKay, K. U. Ingold, J. Am. Chem. Soc. 119 (1997) 4245.
- [7] E. G. Bakalbassis, A. T. Lithoxoidou, A. P. Vafiadis, J. Phys. Chem. A. 107 (2003) 8594.



Molecular dynamics studies on the interaction of anionic surfactants with adenosine deaminase

N. Mahmoodabadi^{a*} and D. Ajloo^b

^a School of Chemistry, Damghan University, Damghan, Iran.

^b Institute of Biological Science, Damghan University, Damghan, Iran.

mahmoodabadi_n@yahoo.com, ajloo@du.ac.ir

Key words: Molecular dynamics, anionic surfactants, adenosine deaminase

Introduction:

Adenosine deaminase (E.C.3.5.4.4) is a monomeric protein (34.5 kDa), which catalyzes the deamination of adenosine and 20-deoxyadenosine nucleosides to their respective inosine derivative nucleosides and ammonia with a rate enhancement of 2×10^{12} relative to the nonenzymatic reaction [1]. The mechanism of denaturation is due to the binding of charged head groups of the surfactants to sites with opposite charge at the surface of the protein followed by unfolding and exposure of the hydrophobic interior and numerous hydrophobic binding sites [2,3]. The interaction of anionic surfactants with biomolecules has been studied earlier [4]. The aim of this work was to study the effects of anionic surfactants on the activity of adenosine deaminase by molecular dynamics.

Methods:

The structures of anionic surfactants were drawn using Hyperchem software. These structures were pre-optimized with Molecular Mechanics Force Field (MM+) and final geometries were obtained. For molecular dynamics simulation of ADA and surfactant, force field parameters and geometries were generated using PRODRG2 server. Then surfactant molecules were randomly added into the simulation box. The system was equilibrated for 20000 ps. All MD simulations were carried out using the GROMACS 3.3.1.

Results and Discussions:

In order to obtain complementary information about the structure of ADA and influence of surfactant on it, MD calculations were performed on ADA system using different chain length and concentration of anionic surfactants. The used surfactant include of sodium dodecyl sulfate sodium decyl sulfate (SDS), sodium octyl sulfate (SOS) and sodium hexadecyl sulfate (SHS). The radial distribution function (RDF) curves, existence probability of two particles around each other, between protein-surfactant (Fig. 1a) with different chain length and surfactant-surfactant (Fig. 1b) has been obtained. Fig. 1a shows RDF of surfactants with different chain length around protein. Fig. 2 shows surface area of protein in the presence of two surfactants with different chain lengths.

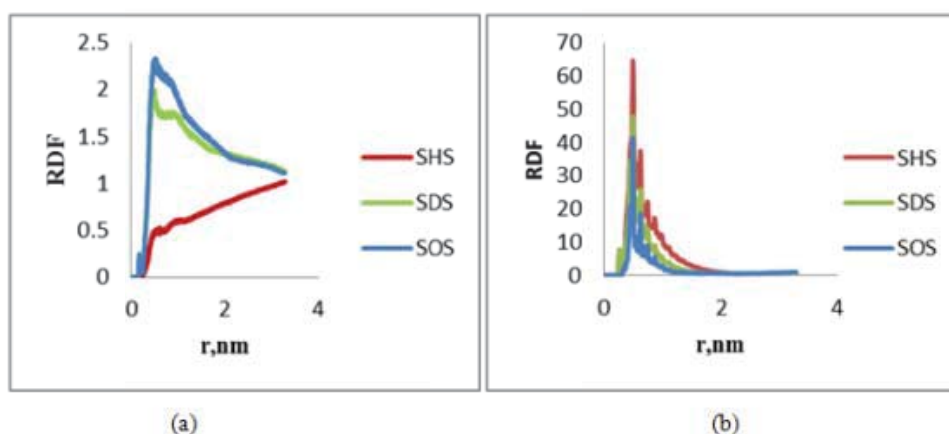


Fig. 1. Diagram of RDF a) between protein-surfactant with three different chain length.
b) between surfactant -surfactant with three different chain length

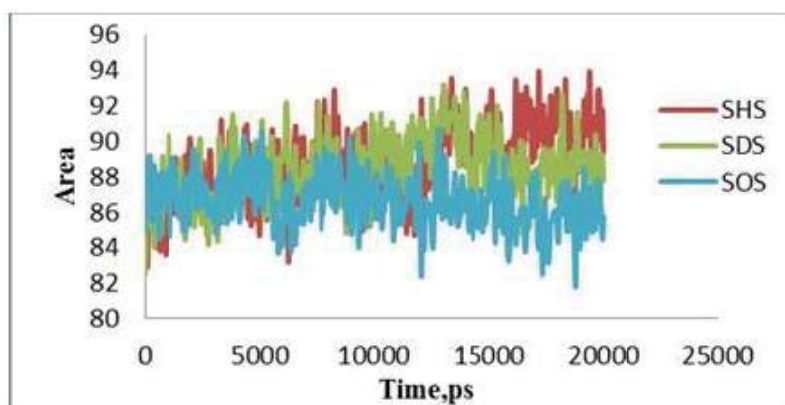




Fig 2. surface area of protein in the presence of two surfactants with different chain lengths.

Conclusion:

Figure 1 shows that With increasing concentrations of surfactant, The the presence of surfactants along the protein decreases. Figure 2 also complement this result, because according to this figure, with increasing concentration, the presence of surfactants together increases. According to Figure 3 with increasing chain length of surfactant, they aggregate more, as in Figure 4 is shown the presence of the surfactant -proteins is reduced.

References:

- [1] L. Frick, R. Wolfenden, E. Smal, DC. Baker. *Biochemistry*, (1986) .
- [2] *Food polymers: Gels and Colloids*, Royal Society of chemistry,. Jones, M.N .; Brass.; A, (1992).
- [3] J. Oakes, J. Chem. Soc. Faraday Trans.; 1 70 (1974) .
- [4] A.K. Bordbar, A.A. Moosavi-Movahedi, Bull. Chem. Soc. Jpn.; 69 (1996)

Computational study of aza-adamantanes as multivalent bases

H. Sabzyan*, B. Saed

Department of Chemistry, University of Isfahan, Isfahan 81746-73441, Iran

sabzyan@sci.ui.ac.ir / saed@chem.ui.ac.ir

Keywords: Azaadamantanes, Protonation, Multivalent Base, B3LYP, Isomerism

Introduction:

Multivalent bases are a group of compounds having high basic capacities [1] appropriate for the interaction with biopolymers (proteins and DNA) at appropriate PH [2]. So far, a number of compounds have been used as multivalent bases for the transfection of DNA to cytoplasm and cell nucleus [3]. In this report, we investigate properties of tetra-aza-adamantane (TAA), hexa-aza-adamantane (HAA) and deca-aza-adamantane (DAA) proposed as the core of a class of more stable and manageable multivalent bases.

Methods:

In the first step of this study, we have studied structure and bonding characteristics of TAA, HAA and DAA using density functional theory B3LYP method with the 6-311++G** basis set. The gas phase basicities of these compounds are also studied by step-wise protonation (according to Eq. (1) below) up to their maximum capacities, Figure 1.



Effects of protonation on the bond lengths, and angles, NBO atomic charges and electronic energies are analyzed. All possible stable isomers of these compounds at each protonation step are investigated. The routes of step-wise protonation for the TAA and HAA are unique as only one type of tertiary or secondary nitrogen atom is protonated over the whole route up to the complete protonation step. For the protonation of DAA, there are several possible routes. Two distinct routes are studied here, i.e. routes (a) and (b), in which only either the tertiary N atoms or the secondary N atoms are protonated sequentially. A deep intuition of the interplay between the added charge and structural relaxation can be visualized by the analysis of the

correlation between the distributed (fractional) differential group charges and the bond length elongations, as shown in Figure 2. The same sets of computations are carried out on TAM (tri-amino methane) as an un-caged reference multivalent base for this series of compounds.

Results and Discussion:

Results of this study show that the TAA, HAA and DAA have maximum proton abstraction capacity of four, five and four protons per molecule, respectively, with comparative basic strengths of $TAA \approx HAA > TAM > DAA$. Interestingly, in the protonation of DAA, charges of the unprotonated nitrogen atoms are increased more than the protonated nitrogen atoms. Because of minimum effect of the protonation on the skeletal C-N and N-N bond lengths, it can be said that the adamantane cage volume is not changed significantly upon protonation. The strange behavior observed at the last two points of the $\Delta R - \Delta Q$ correlation curves, (Figure 2) where the skeletal atoms charges do not increase (or even decrease) with the addition of the proton(s) while the bond lengths are constantly increasing, can possibly be attributed to the approach to the spherical symmetry of the charge distribution and repulsion of the skeletal charges which results in the spread of electric charges over the hydrogen atoms which are located farther from the molecular cage.

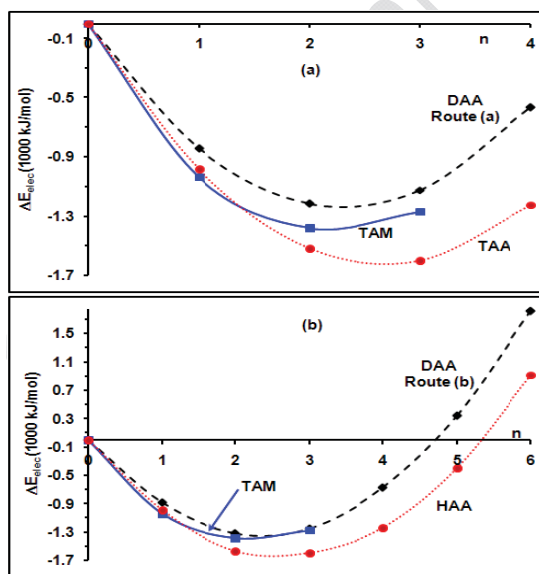


Figure 1. Protonation energies of TAA, HAA,

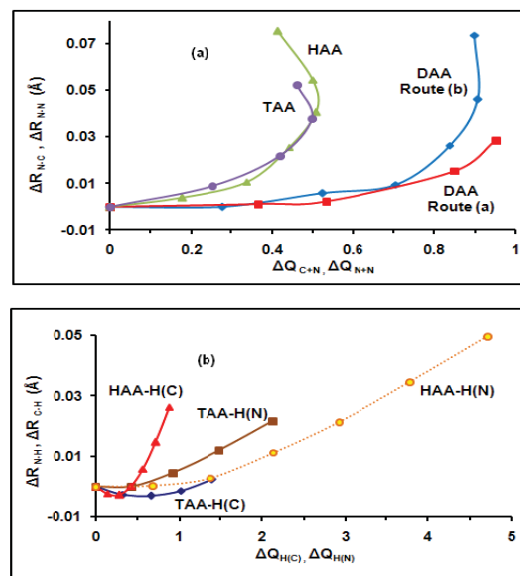


Figure 2. Correlation between charge and bond



DAA and TAM.

lengths of protonated TAA, HAA, DAA.

Conclusion:

Based on the results of this study, we propose TAA, HAA and DAA as multivalent basic cores for the synthesis of basic macromolecular or polymeric compounds to be prospectively used in biological systems.

References:

- [1] Singh A, Ganguly B (2008) New J Chem 32 (2):210-213.
- [2] Shim MS, Kwon YJ (2009) J Control Release 133 (3):206-213.
- [3] Midoux P, Breuzard G, Gomez JP, Pichon C (2008) Curr Gene Ther 8 (5):335-352.



Free energy Calculations of the Mutation in a Membrane Protein

Afsaneh Maleki^{*,a}, Seifollah Jalili^b, Mojdeh Akhavan^c

^a Islamic Azad University of Omidyeh, Khozestan, Iran

^b Department of Chemistry and Nanosciences Research Center, K. N. Toosi University of Technology, Tehran, Iran

^c School of Nano-Science, Institute for Studies in Fundamental Sciences (IPM), Tehran, Iran

*Email: maleki.afsaneh@gmail.com

Keywords: Amylin peptide, Free energy, DOPC bilayer, Molecular dynamics simulations, Mutation, thermodynamic integration.

Introduction:

Calculating the relative free energy difference has been one of major subjects in computational biophysics. It can help us to quantitatively understand solvation, drug binding, protein-protein interactions and so on. Our goal in this work is to develop a theoretical model that can accurately describe the difference in the energetics of insertion of native and mutated forms of the amyline peptide into the lipid bilayers.

Computational methods:

The initial configuration of amyline peptide was taken as the minimum energy structure from an ensemble of 30 structures determined by NMR, with the protein data bank (PDB) code of 2KB8. The starting configuration of the lipid bilayer (128 DOPC lipids + water molecules) was solvated with SPC (simple point charge) waters¹ and system-neutralizing sodium and chloride ions (corresponding to ~0.1 M NaCl) were added. The protein-lipid system was energy-minimized before MD, using ~50000 steps of the steepest descent method, to relax any steric conflicts generated during the setup. Briefly, in equilibration phase, after 1 ns NVT simulation at 323 K, the NPT simulation was performed for 1 ns at 323 K and 1 bar. Parameters from the Gromos96 53a6 parameter set² were applied to the peptide, water, and

ions in the system. Lipids were described by the parameters derived by Berger et al. After equilibration, restraints were removed from the peptide and the production phase began. All simulations were carried out using the GROMACS simulation package.

In the thermodynamic integration method, a coupling parameter λ is introduced in the Hamiltonian $H(\lambda)$ to connect two thermodynamic states, $H(\lambda=0)$ and $H(\lambda=1)$, which represent the initial and final states, respectively. Simulations are done for 20 different λ that change from 0 until 1. At each λ , free energy calculations for the protein in water solvent and in the membrane medium were performed for 2 and 5 ns, respectively.

Results and Discussion:

Free energy calculations can be illustrated using the thermodynamic cycle shown in Fig. 1.

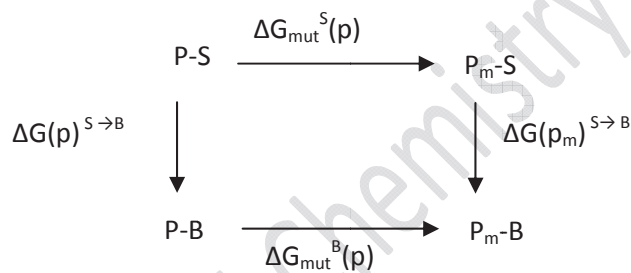


Figure 1. Thermodynamic cycle used to determine the relative free energy of the two molecules protein and mutated protein in solution and bilayer membrane.

In this picture, the superscripts S and B refer to the solvent and bilayer medium and subscripts P and p_m refer to the protein and the mutated protein. Each ΔG denote the free energy change between two connected states along the arrow direction.

$$\Delta\Delta G_{\text{mut}} = -\Delta G(p_m)^{S \rightarrow B} - \Delta G(p)^{S \rightarrow B} = \Delta G_{\text{mut}}^B(p) - \Delta G_{\text{mut}}^S(p) = 28.71 - 2.69 \text{ kJ/mol} = 26.05 \text{ kJ/mol}$$

Conclusions:

We have performed MD simulations of the protein in DOPC membrane and in water with amyline and mutated amyline where Ile26 was switched to a proline residue.



References:

- [1] Berendsen, H. J. C., J. P. M. Postma, W. F. van Gunsteren, and J. Hermans. 1981. Intermolecular Forces. Reidel, Dordrecht, the Netherlands.
- [2] Oostenbrink, C.; Villa, A.; Mark, A. E.; Van Gunsteren, W. F. A Biomolecular Force Field Based on the Free Enthalpy of Hydration and Solvation: The GROMOS ForceField Parameter sets 53A5 and 53A6. *J. Comput. Chem.* 2004, 25 (13), 1656–1676.

15th Physical Chemistry Conference



Calculation of Water-Ethanol Mixtures Autoprotolysis Constants using ab initio methods

F. Kiani^a, S. Sharifi^b, A. Bahadori^{*b}, F. Koohyar^a

^aDepartment of chemistry, Islamic Azad University, Ayatollah Amoli Branch, Amol, Iran.

^bDepartment of chemistry, Islamic Azad University, Arak Branch, Arak, Iran.

*E-mail: bahadori.az@gmail.com

Keywords: Autoprotolysis constant, Water-ethanol mixture, DFT Method

Introduction:

The aqueous organic solvent mixtures such as water-ethanol, has proven appropriate reaction media in different fields of chemistry due to specific properties and better ability to dissolve more compounds than pure solvents. Among the thermodynamics properties of solvent, autoprotolysis constant (pK_{ap}) is one of the most important properties and knowledge of this parameter is considered as fundamental concept in application of the solvent. The smaller the autoprotolysis constant, the greater the range of acid or base strengths that can exist in a solvent and the greater the likelihood that it will be a differentiating solvent. Hence, acid-base titrations are best carried out in solvents with small autoprotolysis constant values [1]. In mixtures of water and a miscible organic solvent such as ethanol, the dielectric constant of mixed solvent considerably changes with the proportion of ethanol. In respect of electrostatic interactions, the influence of dielectric constant of solvent can be used for elucidation of solvent composition effect on chemical equilibrium such as autoprotolysis constant [1].

Different methods were employed for the determination of pK_{ap} [2]. On the other hand, during the last two decades there has been much interest in developing a methodology enabling theoretical prediction of pK values, employing various quantum theoretical techniques [3]. Therefore, the objective of this study is the determination of autoprotolysis constant of different water-ethanol mixtures involving 10-90 volume percent of ethanol using DFT method, the determination of relationship between the calculated autoprotolysis constants with experimental autoprotolysis constants and dielectric constant of mixtures.

Computational method:

The structures of ethanol cation ($\text{C}_2\text{H}_5\text{OH}_2^+$), neutral molecule ($\text{C}_2\text{H}_5\text{OH}$), anion ($\text{C}_2\text{H}_5\text{O}^-$), and the practical numbering system adopted for performing the calculations. The initial geometries of the molecules by the semi empirical PM3 method are included in program CS Chem3D version 5.0. These geometries were optimized with the Gaussian program package using the B3LYP/6-31+G(d) method and the default convergence criteria. To analyze the solvent effects on all the specimens involved in the selected ionization reaction, the polarized continuum model (PCM) of Tomasi et al. was used [3]. All of the mentioned calculations were accomplished at different mixtures containing 10-90 % v/v of ethanol to calculate the autoprotolysis constants of water-ethanol mixtures.

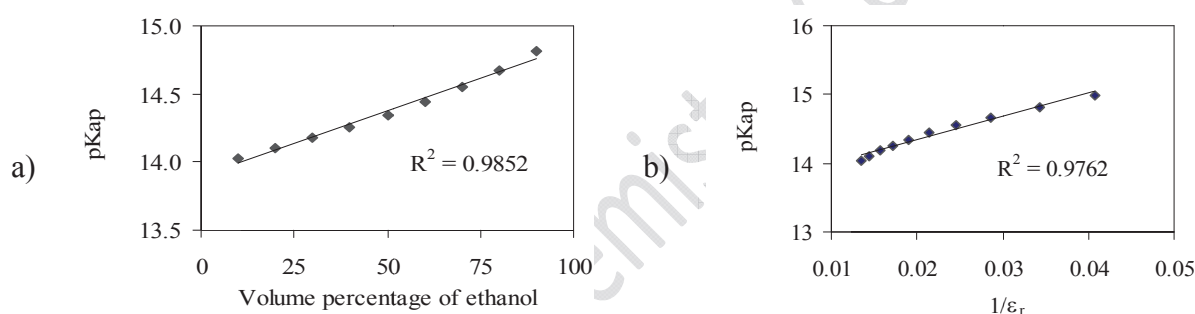


Figure 1. Illustration of pK_{ap} values versus: a) the volume percentage of ethanol, b) the reciprocal of the dielectric constant; in different mixed solvents.

Results and Discussion:

The ionization process in mixed solvent such as water-ethanol mixture can be presented by



where, RH_2^+ and R^- are solvated proton and produce ions of solvent respectively. Therefore the stoichiometric autoprotolysis constant of water-ethanol mixture will be according to equation (2):

$$\text{K}_{\text{ap}} = [\text{RH}_2^+][\text{R}^-] \quad (2)$$

K_{ap} , $[\text{RH}_2^+]$ and $[\text{R}^-]$ are the stoichiometric autoprotolysis constant, the concentration of solvated proton and the concentration of lyate ion, respectively. As pK equals $\Delta G/2.303 \text{ RT}$, where ΔG is a free energy change of the reaction either in a gas or solution, autoprotolysis

constant of a solvent can be determined by the ΔG value. Hence, the total free energy values calculated using the Tomasi's method at the B3LYP/6-31+G(d) level of theory for water-ethanol mixtures involving 0 to 90 volume percent of ethanol and the calculated autoprotolysis constants values, expressed in log unit, are plotted versus volume percentage of ethanol in Figure 1a. Relationships between pK_{ap} calculated of water-ethanol solutions and dielectric constant (ϵ_r) of the solvent were investigated. The values were plotted against the reciprocal of the dielectric constant of solvent mixture in Figure 1b. As the Figure 1b shows, a linear relationship with correlation coefficients of more than 0.97 is observed [4]

$$pK_{ap}(\text{cal.}) = 13.645 + 34.516 \times (1/\epsilon_r) \quad (3)$$

Therefore for each water-ethanol mixture in the range of 0-90 volume percentage of ethanol, the derived equation 3 can be effectively used to calculate pK_{ap} values. The linearity of the relationship indicates that, the electrostatic interaction in dielectric constant is an important parameter for elucidation of solvent effect over the whole range of this experimental solvent composition.

Conclusions :

The autoprotolysis constants theoretically show an suitable agreement with the autoprotolysis constants experimentally determined by potentiometric (Figure 2) [1]. However, the differences are mostly due to the different techniques, various ionic strengths with different background electrolytes. Also, the results indicate the pK_{ap} value of this media increases with addition of ethanol.

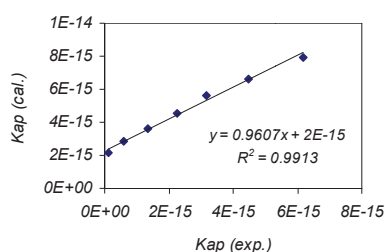


Figure 2. Comparison of calculated and experimental autoprotolysis constants in different mixed solvents.



References:

- [1] M. Faraji and et al.; "Determination of Water-Ethanol Mixtures Autoprotolysis Constants and Solvent Effect"; Journal of Applied Chemical Research; 9, 7-12, 2009.
- [2] K. Izutsu; "Electrochemistry in Nonaqueous Solutions"; Wiley; 2002.
- [3] F. Kiani and et al.; "Determination of Acidic Dissociation Constants of Glycine, Valine, Phenylalanine, Glycylvaline, and Glycylphenylalanine in Water Using ab Initio Methods"; Journal of Chemical and Engineering Data; 55, 2732–2740, 2010.
- [4] M. Yasuda; "Dissociation Constants of Some Carboxylic Acids in Mixed Aqueous Solvents"; Bulletin of the Chemical Society of Japan; 32, 429–432, 1959.



N-H...S and S-H...N intramolecular hydrogen bond in 4-amine-3-pentene-2-thial

Nowroozi^{b*}, M. Poorsargol^a

^a Department of Chemistry, Faculty of sciences, University of zabol, zabol, Iran

^b Department of Chemistry, Faculty of sciences, University of Sistan & Baluchestan, Zahedan, Iran

(Email: Poorsargol.mahdiye@yahoo.com)

Keywords: APT, Intramolecular hydrogen bond, resonance, AIM and NBO.

Introduction:

The intramolecular hydrogen bond, as an specific case, exist in numerous organic compounds and biomolecules, such as hormones, coenzymes and proteins. These kinds of intramolecular interactions are playing a key role in many areas of chemistry and can determine the most stable structure of many molecules [1-2]. 4-amine-3-pentene-2-thial (APT) involved in asymmetric N-H...S and N...H-S intramolecular hydrogen bonds which coupled with π -electron delocalization.

Computational details:

All of the computations in the present study were performed by Gaussian 98 series of programs. The geometry optimizations for all the possible conformations of APT were carried out by HF, B3LYP and MP2 methods with 6-311++G(d,p) basis set. Topological properties of HB critical point are the most important factors in discussing the RAHB properties in the chelated systems. The optimized structures at MP2/6-311++G (d, p) level of theory were used to obtained the appropriate wave function files for AIM and NBO analyses[3-4].

Results and Discussion:

Theoretically, APT has three classes of tautomers, Thialamine (TAA), Thioline (TOI) and Thialimine (TAI) which interconvert by tautomeric equilibriums. Our results show that the



TAA conformers group, by mean of average, is usually more stable than the TAI and TOI ones. This stability can be related to the various factors such as more basicity of N with respect to S, tautomeric equilibriums and π -electron delocalization energy. The geometrical parameters can be use for qualitative evaluation of HB strength of RAHB systems, TAA-1, TOI-11 and TOI-21. Consequently, we obtain the following IHB energy order (I):

$$E_{HB}(\text{TOI-21}) < E_{HB}(\text{TOI-11}) < E_{HB}(\text{TAA-1}) \quad (\text{I})$$

In order to have a deeper knowledge of the of the possible hydrogen bonds in APT conformers, a topological analysis of electronic charge density, ρ_{BCP} , and its Laplacian, $\nabla^2\rho_{BCP}$ were performed. It can be also observed that the electron density and its Laplacian at HB critical point increase from TOI-21 to TAA-1 and then TOI-11. Consequently, we obtain the following order (II):

$$E_{HB}(\text{ToI-21}) < E_{HB}(\text{TaA-1}) < E_{HB}(\text{ToI-11}) \quad (\text{II})$$

The results of NBO analysis also show that in hydrogen bonded structures, one or two lone pairs of proton acceptor and the proton donor antibonds are involved and the corresponding stabilization energy of TOI-11 and TAA-1 are about 22.88 and 26.31 kcal/mol, respectively. These results are in agreement with the order (I). Generally, beside the increasing of HB strength, the main consequences of the π -electron delocalization within the RAHB systems are as follows: (I) the decrease of total electronic energy or increase the stability of molecule; (II) the equalization of the analogous single and double bonds, such as C-C and C=C. These results reveal that the π -electron delocalization of TAA greater than the TOI. The greatness of resonance in TAA respect with TOI is mainly due to difference in charge transfer, especially $\pi\text{C}=\text{C} \rightarrow \pi^*\text{C}=\text{S}$, $\pi\text{C}=\text{C} \rightarrow \pi^*\text{C}=\text{N}$ and $\text{Lp}(\text{N}) \rightarrow \pi^*\text{C}=\text{C}$, $\text{Lp}(\text{S}) \rightarrow \pi^*\text{C}=\text{C}$. Finally, the results of NBO analysis proved that the π -electron delocalization is only superior factor which determined the tautomeric preference.

Conclusion:

The results of our theoretical study show that 20 stable conformer exist among 28 suggested conformers. As we expected, at all of the theoretical levels the TAA conformers have extra stability with respect to the TAI and TOI ones. The results population analysis of APT



conformer show that the origin of this tautomeric preference is mainly due to the π -electron delocalization, especially the charge transfer between the π C=C with π^* C=S and π^* C=N and lone pairs of N and S with π^* C=C .

References:

- [1] G.A.Jeffrey, W. Seanger; *Hydrogen Bonding in Biological Structures*; Springer, Berlin, 1991.
- [2] S. J. Grabowski, *Hydrogen Bonding- New Insights*, (Springer, Berlin, 2006).
- [3] F. Biegler-König, J. Schönbohm, D. Bayles; AIM2000-A Program to Analyze.
- [4] D. E. Glendening, A. E. Reed, J. E. Carpenter, F. Weinhold; NBO, Version 3.1.



Theoretical study of solvent effects on the conformational preference in β -Aminoacrolein and β -Thioaminoacrolein using PCM, IPCM and SCI-PCM methods.

A. Nowroozi^{b*}, M. Poorsargol^a

^a Department of Chemistry, Faculty of sciences, University of zabol, zabol, Iran

^b Department of Chemistry, Faculty of sciences, University of Sistan & Baluchestan, Zahedan, Iran

(Email: Poorsargol.mahdiye@yahoo.com)

Keywords: solvent effect, PCM, IPCM and SCI-PCM.

Introduction:

Hydrogen bonding is one of the most important concepts which play a key role in the chemistry of living systems. The intramolecular hydrogen bond, as an specific case, exist in numerous organic compounds and biomolecules, such as hormones, coenzymes and proteins. 3-aminoacrylaldehyde (AMAC) is the simplest molecule, which involved in O-H...N and N-H...O intramolecular hydrogen bonds and strongly coupled with π -electron delocalization [1]. Thioaminoacrolein (TAMAC) is the simplest thio derivative of AMAC which involved in asymmetric NH...S and SH...N intramolecular hydrogen bonds which coupled with π -electron delocalization [2]. Owing to the difference in polarity of the conformers, conformational preferences are very sensitive to solvent effects.

Computational details:

Solvent effects on conformational stability are examined by applying the PCM at the B3LYP/6-311++G (d,p) and MP2/6-311++G (d,p) levels of theory and all conformers have been fully optimized with $\epsilon=78.39$ using the Gaussian 03 series of programs [3]. Also single point computations in the IPCM and SCI-PCM methods with $\epsilon=78.39$ have been carried out at the MP2/6-311++G (d,p) level of theory. The NBO analysis was carried out on the MP2/6-311++G(d,p) wave function by using the NBO package [4] included in Gaussian 03 package.

Results and Discussion:

Theoretically, KA and TAA groups have four different planar conformers which all of these conformers were fully optimized by B3LYP and MP2 methods with 6-311++G(d,p) basis set and their energies are presented in Table I. Also the results calculated by PCM method and dipole moment at the same levels of theory are presented in this Table. Our results show that in the gas phase the TAA-1 and KA-1 conformers are more stable than the conformer ones. The increase stability of TAA-4 and KA-4 conformers in polar solvents could be related to the increase of dipole moments of these forms over the other forms. The results show that hydrogen bond strength for TAA-1 and KA-1 forms decreases in going from the gas phase to the solution one. This instability is due to the solute-solvent electrostatic interactions which is caused to hydrogen bond strength in the solution phase decrease. Because of the additional dipole moment induced by the solvent's reaction field, a polar molecule will have a larger dipole moment in a polar solvent than in the gaseous phase, which in turn will increase the stability of the molecular system.

Table I: Relative energies (E_r in kJ/mol) and dipole moment (Dip in Debye) of all the possible conformation of KA and TAA calculated at various levels of theory (kJ/mol).

	B3LYP		MP2	
	Gas ($\epsilon=1$)	H ₂ O($\epsilon=78.39$)	($\epsilon=1$)	($\epsilon=78.39$)
KA-1	0.00 (3.6827)	8.39 (5.5812)	0.00 (3.7339)	6.31 (5.5189)
KA-2	20.87 (5.4755)	10.94 (8.4220)	21.85 (5.3353)	11.48 (7.9517)
KA-3	30.37 (6.0549)	16.65 (9.4928)	27.21 (6.0055)	16.03 (9.4716)
KA-4	16.90 (6.5772)	0.00 (10.2183)	16.55 (6.7980)	0.00 (10.2908)
TAA-1	0.00 (4.5735)	10.27 (7.6965)	0.00 (4.8972)	3.12 (8.1880)
TAA-2	24.01 (6.3813)	13.02 (11.1959)	26.19 (6.2664)	12.05 (11.1692)
TAA-3	27.18 (6.5457)	14.74 (11.8319)	26.89 (6.7931)	14.18 (12.4551)
TAA-4	17.74 (7.2409)	0.00 (13.0063)	18.73 (7.3869)	0.00 (13.5336)

Conclusion:

The both PCM and IPCM methods predict that the stability of the KA-4 and TAA-4 conformers increases in going from the gas phase to the solution phase. The results both gas



and solution phase reveal that the contribution of resonance of KA-1 and TAA-1 are greater than the KA-4 and TAA-4. The results of NBO analysis shows that the electronic charge transfers of $Lp(S) \rightarrow \sigma^*NH$ and $Lp(O) \rightarrow \sigma^*NH$ interaction decreases in going from the gas phase to the solution one and clearly reflect the weakness of hydrogen bond in the solution phase.

References:

- [1] A. Nowroozi, H. Roohi, M. Sheibaninia, H. Raissi; Int. J. Quan. Chem. In press.
- [2] A. Nowroozi, H. Roohi, M. Poorsargol and et al; Int. J. Quan. Chem; 111, 3008-3016, 2011.
- [3] M. J. Frisch, et al. Gaussian 03, Revision A.7, Gaussian, Inc., Pittsburgh PA, 1998.
- [4] D. E. Glendening, A. E. Reed, J. E. Carpenter, F. Weinhold; NBO, Version 3.1.



Study of H₂ and CO₂ adsorption on bare and functionalized double-walled carbon nanotubes by molecular dynamics simulation

S. Jalili^a and A. Gorji*

^a Department of Chemistry, K. N. Toosi University of Technology, Tehran, Iran

(E-mail: cagorji@yahoo.com)

Keywords: Functionalized carbon nanotube, Adsorption, Self-diffusion coefficient.

Introduction:

Carbon nanotubes (CNTs) have been attracted a great interest due to their unique mechanical, electrical and chemical properties since their discovery. They are shown as one of the most promising materials for application in materials science and medicinal chemistry. As developing the nanotechnology, carbon nanotubes are one of the most famous materials used as a prototype of confinement systems to investigate by means of molecular dynamics simulation methods the adsorption properties of H₂O, H₂, CO₂ and other gases. H₂ is considered to be the most promising alternative energy carrier in the global energy balance of the future. The use of carbon-based fossil fuels for over a century seems to have caused measurable and catastrophic alterations to the earth's climate. It is widely hoped that the use of carbon-free energy carriers could reverse or decelerate the greenhouse phenomenon [1]. On the other hand, CO₂ is known as the most important fluid in biological, geological and chemical systems after water. Because it has an important role in cellular respiration, it is utilized by plants during photosynthesis, it can be produced by lots of human activities and it is one of the most important green house gases [2]. In this work, we performed a series of MD simulations on the adsorption of H₂ and CO₂ gases on functionalized CNT systems. Different functional groups (hydrophilic –COOH or hydrophobic –CH₃), and diameter effects were investigated.



Methods:

MD calculations were performed by GROMACS 4.0.5 molecular dynamics simulation package [2] in NVT ensemble using the Nosé-Hoover thermostat at 77 K up to 300 K. (6,6) and (16,16) single-walled nanotubes (SWNTs) and a (6,6)@(16,16) double-walled nanotube (DWNT) were chosen and functionalized at their open ends by $-\text{COOH}$ and $-\text{CH}_3$ groups. The OPLS all-atom force field was used. The volume of the rectangular simulation box was taken to be $50 \times 50 \times 150 \text{ \AA}$. During simulations, all carbon atoms in CNTs were fixed, while the functional groups were allowed to relax. The periodic boundary conditions were imposed in all three dimensions and Van der Waals cutoff was chosen 10 \AA . First, the initial configurations were energy minimized. Then, the system was equilibrated for 100 ps, followed by a 4 ns production run. The integration time step was 2 fs. The equations of motion were integrated by the leap-frog algorithm [3].

Result and discussion:

Adsorption coverage, binding energy, isosteric heat of adsorption, specific surface area and entropy were calculated for the adsorption on internal and external surfaces of carbon nanotube and in the inter-tube space of double-walled nanotube. Effect of pressure and temperature changes on above properties were investigated. Results were showed weak adsorption at room temperature, while in low temperatures and high pressures, adsorption coverage were increased. The trend of results was similar to other simulations and experimental data. Several classical adsorption models were examined for the obtained isotherms. Langmuir isotherms were shown to have the best fit in low temperature regions. The self-diffusion coefficient for hydrogen and carbon dioxide in pure and functionalized single-walled carbon nanotubes and double-walled carbon nanotubes were also investigated.

Conclusions:

We have investigated the adsorption of H_2 and CO_2 on carbon nanotubes as a function of temperature, functional groups and diameter of the nanotubes. Analysis of the radial



distribution function (RDF) plots demonstrates the pure physisorption behavior. The amount of adsorption was shown to be strongly influenced by the applied temperature, i.e. decreasing the temperature to 77 K results in higher adsorption. It is also found that adsorption energy is higher for nanotubes with smaller diameters.

Reference:

- [1] Gerasimos E. Ioannatos, Xenophon E. Verykios, International Journal of Hydrogen Energy 35 (2010) 622–628.
- [2] Alessio Alexiadis, Stavros Kassinos, Chemical Physics Letters 460 (2008) 512–516.
- [3] S. Jalili, A. Jaberi, M. G. Mahjani, M. Jafarian, International Journal of Nanoscience 8 (2009) 425.



Investigation of thermodynamic properties of Ni nanoclusters based on Molecular Dynamics Simulations

Hamed Akbarzadeh*

Department of Chemistry, Hakim Sabzevari University, Sabzevar, Iran
(akbarzadehhamed@yahoo.com)

Abstract:

We present an approach for the constant-pressure molecular dynamics simulation. This approach is especially designed for finite systems, for which no periodic boundary condition applies. Molecular dynamics, MD, simulation for Ni nanoclusters is used to calculate their p - v - T data for the temperature range $200 \text{ K} \leq T \leq 400 \text{ K}$, and pressures up to 600 kbar.

Keywords: Molecular-dynamics, Nickel nanocluster; Equation of state; Bulk modulus;

Introduction:

Three methods to apply pressure to nanosystems (using an auxiliary pressure transmitting medium) have been reported [1-3]. We present a new approach for the constant-pressure molecular dynamics simulation.

Method:

In our simulations, the pressure medium consists of particles that do not interact with each other, but do interact with the Ni atoms of in the crystal via a soft sphere potential of the form

$$U(r) = \varepsilon \left(\frac{\sigma}{r} \right)^{12} \quad (1)$$

We may use argon (or any other) ideal gas as pressure medium in these simulations. However, if one merely takes the interaction potential of equation 1 between each Ar atom and the nanocluster, the desired pressure would not be achieved. To overcome this problem, we may



assume that a small fraction of argon atoms interact with the nanocluster as follows, instead of equation 1.

$$V_{LJ} = 4\epsilon[(\frac{\sigma}{r})^{12} - (\frac{\sigma}{r})^6] \quad (2)$$

Result and Discussions, Conclusions:

We present a method for applying pressure in the computer simulation of nanoparticles, using an ideal gas as the pressure medium. This method is especially suitable for finite systems. We have compared the accuracy of three EoSs of solids, namely the Linear Isotherm Regularity-II (LIRII), Birch-Murnaghan (BM), and EOS III [4] by fitting their expressions into the simulation data and also zero pressure quantities used as an input data. The fact that the density range of our data is limited to less than 20% change, we haven't been able to compare the predictive power of the three EoSs. However, it is expected to do such comparison if the density range is large enough. For instance, it was found that EOSIII is very accurate even for very large pressure ranges. The values of B_0 and B'_0 for each isotherm with different sizes are calculated via the EoSs. An increase in bulk modulus with decrease in number of particles of cluster has been observed. As the cluster size decreases; large fraction of atoms are on the cluster surface. Surface atoms have less binding energy, compared to the bulk atoms, therefore when number of particles decreases, the compressibility is expected to decrease. Also, we have calculated the isobaric expansion coefficient for different cluster sizes at different temperatures via LIRII. An increase in isobaric expansion coefficient with decrease in number of particles has been observed; which may mean that the anharmonicity increases when cluster size reduces. Also, a decrease in isobaric expansivity with increase in temperature has been found.

References:

- [1] R. Martonak, C. Molteni, and M. Parinello, Phys. Rev. Lett. 84 (2000) 682.
- [2] B. J. Morgan, P. A. Madden, Nano Lett. 4 (2004) 1581.
- [3] M. Grunwald, C. Dellago, Molecular Physics 104 (2006) 3709.
- [4] G. A. Parsafar, H. V. Spohr, G. N. Patey, J. Phys. Chem. B 113(2009) 11977.



15th Physical Chemistry Conference



Sublimation Enthalpy of Nano-Sized Crystals of HMX: A Molecular Dynamics Simulation Study

Hamed Akbarzadeh*

Department of Chemistry, Hakim Sabzevari University, Sabzevar, Iran

(akbarzadehhamed@yahoo.com)

Abstract:

Molecular dynamics simulations of nanoparticles with 10- 100 molecules of HMX are carried out at 300 K. We have calculated sublimation enthalpy of HMX crystal polymorphs with different sizes. For the all sizes, the β – HMX is found to be the most stable phase, due to having the least total interaction energy. Also, α – HMX is more stable than δ – HMX. An increase in the sublimation enthalpy with the size of the nanoparticle can be seen.

Keywords: Molecular-dynamics, HMX nanoparticle, Structural stability, Sublimation enthalpy

Introduction:

There are four different crystal structures for HMX, three pure crystal phases, α , β and δ , and a hydrated phase γ . At ambient conditions, the relative stabilities of these bulk polymorphs are known to be $\beta > \alpha > \gamma > \delta$ [1].

Method:

We have made the bulk and nano-HMX with different sizes via Mercury 2.3. We have selected similar sizes for three phases of HMX (α , β , δ). A flexible force field used for HMX was developed by Smith and Bharadwaj [2]. In the present study, molecular-dynamics calculations were carried out by the DLPOLY 2.18 program. Simulations of the nanoparticles were done with the *NVE* ensemble with no periodic boundary conditions. A time step of 0.1 fs was used, and the total duration of the nanoparticle simulations was 2 ns, with the first 1 ns used for the equilibration. The electrostatic forces were directly calculated for the finite

number of nanoparticles. Ten sets of nanoparticle simulations, specifically with 10- 100 HMX molecules, were performed for the α , β , and δ HMX phases.

Result and Discussions, Conclusions:

The sublimation enthalpy, ΔH_{sub} , can be simply calculated as,

$$\Delta H_{\text{sub}} = H_{\text{gas}} - H_{\text{solid}} = RT + \Delta E_{\text{inter}} + \Delta E_{\text{intra}} \quad (7)$$

where R is the universal gas constant, ΔE_{inter} and ΔE_{intra} are the differences in intermolecular and intramolecular potential energies of HMX molecules in the ideal gas and corresponding crystal phases, respectively [3]. The calculated values of ΔH_{sub} are given in Table 1 at 300 K for different sizes of α -, β -, and δ - HMX.

N	$\Delta H_{\text{sub}}(\alpha)$	$\Delta H_{\text{sub}}(\beta)$	$\Delta H_{\text{sub}}(\delta)$
10	15.9	21.5	13.0
20	22.6	26.6	19.6
30	28.1	32.8	24.6
40	33.2	37.9	30.3
50	37.1	41.5	33.8
60	40.8	43.0	37.7
70	42.6	44.8	39.6
80	44.6	46.0	41.2
90	45.5	47.0	42.7
100	46.3	47.7	43.3
Bulk	46.5	47.6	43.5

As shown In Table 1, for all given sizes β – HMX is more stable than α – HMX, and α – HMX is more stable than δ – HMX. The experimental value for ΔH_{sub} of the bulk HMX is 44.16 and 42.04 kcal/mol for the β and δ phases, respectively [4] which are in good agreement with our MD results.

References:



- [1] F. Goetz, T. B. Brill, J. R. Ferraro, J. Phys. Chem. 82 (1978) 1912.
- [2] G. D. Smith, R. K. Bharadwaj, J. Phys. Chem. B 103 (1999) 3570.
- [3] D. Bedrov, C. Ayyagari, G. D. Smith, T. D. Sewell, R. Menikoff, and J. Zaug, , J. Comput.-Aided Mol. Des., 8 (2001) 77.
- [4] J. M. Rosen, C. Dickinson, J. Chem. Eng. Data, 14 (1969) 120.

15th Physical Chemistry Conference



Predicting the effects of basepair mutations in proline-rich homeodomain (PRH)-DNA complex by thermodynamic integration

L. Karami^{a*}, S. Jalili

Department of Chemistry, K. N. Toosi University of Technology, Tehran, Iran

E-mail: karami.leila1@gmail.com

Keywords: proline-rich homeodomain, MD simulations, Free energy, binding affinity

Introduction:

The PRH (Proline-Rich Homeodomain) protein [1] is a DNA binding protein having a key role in the regulation of gene expression in all eukaryotes. All types of the homeodomains interact with its conserved 5'-TAATNN-3' binding sequence. Homeodomains with glutamine at position 50, like PRH, recognize TAATTG, TAATTA or TAATGG sites. The complex between PRH and TAATTG were considered as a native complex. With mutation of the GC and TA base pairs in TAATTG to AT and GC, respectively, two mutated complexes (M1 and M2 complexes) were created. To predict of the effects of basepair mutations in PRH-DNA complexes, the binding free energy changes in each of two created mutations were investigated.

Methods:

The initial coordinates of the native PRH-DNA complex was taken from the superimposing the structure with PDB ID: 1IG7 on PRH structure with PDB ID: 2E1O. To obtain relative binding free energy ($\Delta\Delta G_{\text{bind}}$) of the mutations (GC \rightarrow AT and TA \rightarrow GC), the thermodynamic integration (TI) [2] method was used. To estimate $\Delta\Delta G_{\text{bind}}$ the thermodynamic cycle shown in Fig. 1 was applied. Since G is a state function, $\Delta\Delta G_{\text{bind}}$ can be written as $\Delta\Delta G_{\text{bind}} = \Delta G_3 - \Delta G_4 = \Delta G_1 - \Delta G_2$. The free energy change is then evaluated by $\Delta G = \int_0^1 \langle \frac{\partial G(\lambda)}{\partial \lambda} \rangle_\lambda d\lambda$ where $G(\lambda)$ is the potential energy of the system as a function of λ (coupling constant) and $\langle \frac{\partial G(\lambda)}{\partial \lambda} \rangle_\lambda$ is an

ensemble average at a given λ . Each mutation was broken up into 3 steps: first, discharging step, (ΔG_{dischg}), second, vdW-transformation step, (ΔG_{vdw}), and finally charging step, (ΔG_{chg}). All free energy simulations were performed using AMBER 10 [3] with ff99bsc0 force field. The following protocol was used for the free energy simulations: at first, 2000 steps steepest descent minimization followed by 300 ps equilibration at 310 K. Also, a 200 ps equilibration was carried out at 1 atm. Finally, 1500 ps production run was performed in NPT ensemble with time step of 2 fs.

Result and discussion:

To ensure having well equilibrated system, $dG/d\lambda$ versus time were investigated for the $\lambda = 0.1, 0.5$ and 0.9 for both of simulations (Fig. 2). Simulation systems in both mutations were reached the equilibrium after 500 ps of equilibration in both of free and bound states. Also, after the equilibration, 1500 ps of simulation is sufficient to calculate the binding free energy because cumulative average for all runs has converged.

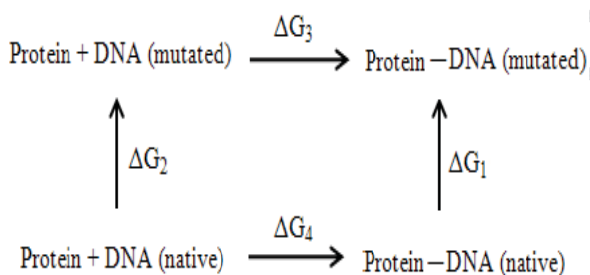


Fig.1. Thermodynamic cycle for computing the relative binding free energy in the PRH-DNA complex.

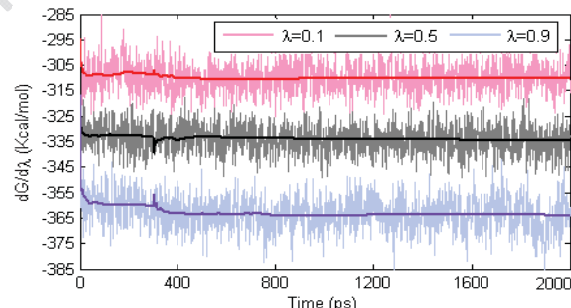


Fig. 2. $dG/d\lambda$ vs time for charging step of the TA→GC mutation in free state.

$\Delta\Delta G_{\text{bind}}$ values are summarized in Table 1. The overall relative binding free energy of GC→AT mutation is equal to 0.64 kcal/mol. Although this value is small, nonetheless contribution of the ΔG_{chg} is more than that of ΔG_{dischg} and ΔG_{vdw} , respectively. In the TA→GC mutation, the main contribution to the difference in binding free energies of 2 kcal/mol results from charging step.



Table 1 Binding free energy (in kcal/mol) results for GC → AT ^a and TA → GC ^b mutations				
Free energy	Free DNA ^a	PRH-DNA ^a	Free DNA ^b	PRH-DNA ^b
ΔG_{dischg}	266.81	266.14	163.08	162.17
ΔG_{vdw}	9.81	10.30	-0.84	0.28
ΔG_{chg}	-102.39	-101.57	-335.67	-333.87
ΔG_{total}	174.23	174.87	-173.43	-171.43
$\Delta \Delta G$	0.64		2	

Conclusions:

The relative binding free energy for GC → AT and TA → GC mutations was investigated. From data obtained, it can be deduced among three DNA sequence, native complex is more stable than two mutated complexes. The stability of the M1 complex is more than that of the M2 complex.

References:

- [1] M. Billeter, Homeodomain-type DNA recognition, Prog. Biophys. Mol. Biol. 66 (1996) 211–225.
- [2] J.G. Kirkwood, Statistical mechanics of fluid mixtures, J. Chem. Phys. 3 (1935) 300–313.
- [3] D.A. Case, T.A. Darden, 2008. AMBER 10. University of California, San Francisco, CA.



The effect of electric field on interaction of glycine with (6, 0) single-walled boron nitride nanotube

Davood Farmanzadeh*, Samereh Ghazanfary

Faculty of chemistry, University of Mazandaran, P. O. Box: 453, Babolsar, I. R. Iran

(E-mail: d.farmanzad@umz.ac.ir)

Keywords: Glycine, Density functional theory, Boron nitride nanotube, Electric field.

Introduction:

Since the discovery of carbon nanotubes, extensive studies have been performed on analogous tubular nanomaterials, such as boron nitride nanotubes (BNNTs). BNNTs possess many unique properties, therefore BNNTs have been proposed as more proper materials than the CNTs for application in the nano-devices [1]. Glycine is the simplest of α -amino acids, as an important model compound in chemical physics, biophysics and biochemistry [2]. The adsorption mechanism of amino acids and biological molecules on the nanotubes has attracted a lot of attention during the past years, since it is of great importance both from the fundamental and the applied point of view. On the other hand, modification of the structural and electrical properties by the applying external electric field (EF) is an important subject for designing nano-device. In this study, we investigated the effect of external EF on the interaction of glycine molecule with (6, 0) SWBNNT.

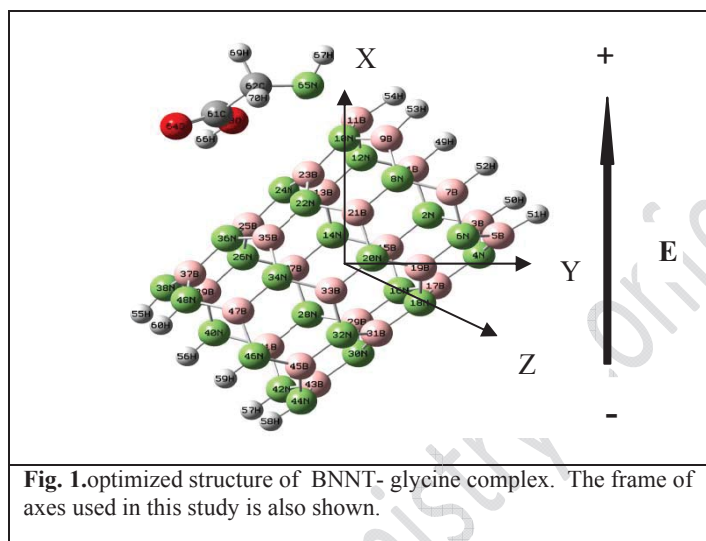
Computational details:

The quantum chemical calculations in this work were performed using Gaussian 03 program package. All structures were optimized by DFT/B3LYP method with the 6-31G* basis set. The numerical values of the applied static EF strengths are 50×10^{-4} and 100×10^{-4} a.u. (1 a.u. = 5.14224×10^{11} V/m).

Results and Discussion:

The optimized structure of the BNNT-glycine complex and the standard direction (+X) of the

external electric field are shown in Figure 1. The calculated values of the adsorption energy (E_{ad}), B-N bond length ($R_{B11-N65}$), band gap (eV), dipole moment (Debye) and charge transfer (Q) in the zero, 50×10^{-4} and 100×10^{-4} a.u. EF intensity are reported in Table 1.



These results show that stability, polarization and electro-conductivity of BNNT-glycine complex increases with increasing of EF intensity. We found that the electronic properties of the BNNT-glycine complex with increasing EF intensity modified.

Table 1. Calculated E_{ad} (in eV), band gap (in eV) of BNNT- glycine complex, B-N bond length $R_{B11-N65}$ (Å), transferred charge Q (in e) and dipole moment (in Debye), as function of external EF intensity.

External EF	E_{ad}	band gap	$R_{B11-N65}$	Q	Dipole moment
0	-2.237	5.027	1.726	0.331	8.179
50	-3.021	4.539	1.672	0.340	14.542
100	-4.126	4.041	1.663	0.343	22.657

Conclusion:



Through our calculations, EF could be an efficient method to control or improve the electronic properties of BNNT-glycine complex. This result may be useful in the application BNNT-glycine system under the EF effect to the design of biosensor devices.

References:

- [1] L. Jiang, W. Guo, *J. Mech. Phys. Solids* **59** (2011) 1204.
- [2] H. Kokten, S. Erkoc, *Mat. Sci. Eng.* **15** (2010) 012075.

15th Physical Chemistry Conference



The computational study on the effect of azobenzene linker on the dye

M. Kiasadegh^a, B. Sohrabi^{a*}, J. Beheshtian^b

^a Department of Chemistry, Surface Chemistry Research Laboratory, Iran University of Science and Technology,
P.O. Box 16846-13114, Tehran, Iran.

^b Department of Chemistry, Shahid Rajaee Teacher Training University, P.O. Box 16785-163, Tehran, Iran.

Email: Sohrabi_b@iust.ac.ir, sohrabi_b@yahoo.com

Key words: Solar cell, DFT, Linker.

Introduction:

The world energy demand steadily increases due to rising population in coming years, it is expected this demand will reach to several values. First, Gratzel et al. were produced solar cell via successful combination of nano-structured porous electrodes of TiO₂ and charge injector dyes with energy conversion efficiency of about 7% in 1991 and 10% in 1993 [1]. Organic and inorganic dyes anchored to semiconductor nanoparticles, have been found important applications as photosensitizers for solar cells and other optoelectronic systems. These dyes bind to the semiconductor nanoparticles surface by anchoring group. These types of solar cell form a donor- acceptor system, which dyes are donor and semiconductors are acceptor. Design a suitable linker, which contain a bridge between dye and anchoring group, is an important factor to improve efficiency of solar cells.

All linkers had surface activity and dye properties. Porphyrin and linkers had high resonance, so they could absorb wide spectra. Due to the high resonance of Zinc porphyrin dyes, they have good chemical stability in the solar cells. Azobenzene dyes with the nature of surfactant as linker were used for two main reasons: a) it seems that a linker with azobenzene dyes group increases the absorption ability of sunlight. b) Linkers with surface activity could convert the aggregation of dye from H-type to J-type and causes the red shift [2].



Computational Details:

Calculations were done using software Gaussian 98. First, dyes molecules were optimized the method DFT and base set 6-31G (d,p) in gas phase. The microscopic properties of molecules such as electron wave functions and molecular properties depend on nature of phase that those studies of molecules done on it. So, dyes optimization done in THF solvent using CPCM with quantum computing the method DFT and base set 6-31G (d, p). The UV-Vis spectra of dyes were computed by using the method DFT and base set 6-31G (d, p) in gas phase and THF solvent.

Results and Discussion:

Different functional groups effects were studied in the ability of linkers to absorption sunlight on Zinc porphyrin. The obtained results show that linker, contain a phenyl group as a functional group, adsorbed more sunlight wavelengths.

Conclusion:

Photo physical and photo electrical properties of dye depends on the functional groups of linkers. According to the results of our computations, donor functional groups improved photo physical and photo electrochemical properties more than acceptor groups.

Reference:

- [1] K. Bouzek and etal.; "Heat losses in Gratzel solar cells"; Solar Energy Materials & Solar Cells; 57, 359-371, 1999.
- [2] N. C. Maiti and etal.; "J- and H-Aggregates of Porphyrin and Surfactant Complexes; Time-Resolved Fluorescence and Other Spectroscopic Studies"; Journal of Physical Chemistry B; 102, 1528-1538, 1998.



Diameter effect on the adsorption of aqueous cetyltrimethylammonium bromide surfactant on carbon nanotube: A molecular dynamics simulations

N. Poorgholami-Bejarpasi, B. Sohrabi*

Department of Chemistry, Surface Chemistry Research Laboratory, Iran University of Science and Technology,
P.O. Box 16846-13114, Tehran, Iran.

Email: Sohrabi_b@iust.ac.ir, sohrabi_b@yahoo.com

Key words: Carbon nanotube, Cetyltrimethylammonium bromide (CTAB), Molecular dynamics simulation.

Introduction:

Carbon nanotubes (CNTs) are currently the focus of intense multidisciplinary research owing to their unique physical and chemical properties and their various potential applications [1]. However, an obstacle for the usage of CNTs is their affinity for one another, making it difficult to disperse them as individual tubes in aqueous solution. Dispersion of CNTs has been facilitated by covalently attaching polar or charged groups to CNT surfaces. However, this can alter the inherent properties of nanotube. Therefore, attention has turned toward the noncovalent adsorption of surfactants and polymers [2].

Among various surfactants, CTAB is commonly used to stabilize aqueous CNT dispersions.

In this study, the adsorption and the self-assembly of CTAB on (5, 7) and (10, 14) CNTs are investigated via all-atom MD simulations.

Computational Model:

Simulations of cetyltrimethylammonium bromide (CTAB) adsorption and the associated surface self-assembly on the CNT surface in aqueous solution were carried out using the Gromacs 4.5.3 software package. Two CNTs [(5, 7) and (10, 14)] with diameters of 0.818 and 1.635 nm, respectively, were considered. The carbon atoms within CNTs were treated as



Lennard-Jones (LJ) spheres and maintained fixed throughout the course of the simulations. The LJ parameters used to describe carbon-carbon interactions were adopted from the OPLS-AA force field family. Cetyltrimethylammonium ions and bromide ions in water, were modeled using the OPLS-AA force field.

Simulated Systems:

To study the adsorption of CTAB molecules on CNT, a single (5, 7) or (10, 14) nanotube was confined at the center of the simulation box, with its cylindrical axis oriented along the z-direction. Each system was equilibrated for 5 ns, and only the last 2 ns of simulation were used for data analysis.

Results and discussion:

Visual analysis indicates that the morphology of adsorbed aggregates depends on the CNTs diameter. Surfactant molecules on (5, 7) CNT lie parallel or antiparallel to each other and parallel to the nanotube axis. As the CNTs diameter increases most of the CTAB molecules still lie predominantly flat on the nanotube surface, however, some of adsorbed CTAB molecules wrap around the nanotube. This is because when one CTAB molecule wraps around a narrow tube, it has to bend, encountering an energetic barrier (CTAB is rather straight). As the nanotube diameter increases, it becomes easier and easier for the adsorbed CTAB to wrap around the CNTs.

Conclusion:

Stabilizing carbon nanotubes (CNTs) dispersed in diameter and chirality in aqueous and organic media remains elusive. Surfactants have proven useful for separating carbon nanotubes, but the molecular mechanism responsible for the effectiveness for such technique remains not completely understood. Because only limited experimental data are available to clarify these phenomena, we report here an all-atom molecular dynamics study on the morphology of cetyltrimethylammonium bromide (CTAB) aggregates adsorbed on (5,7) and (10,14) carbon nanotubes at room conditions.



References:

- [1] W. H. Duan and etal. "Dispersion of carbon nanotubes with SDS surfactants: a study from a binding energy perspective"; Chem. Sci.; 2, 1407–1413, 2011.
- [2] E. J. Wallace and etal. "Carbon Nanotube/Detergent Interactions via Coarse-Grained Molecular Dynamics"; Nano Lett., 7, 1923-1928. 2007.



Theoretical study of some aromatic compounds

A. Ashrafi^a

^a Department of Chemistry, Shiraz University, Shiraz, Iran

Keywords: Aromaticity, RCP and BCP properties, AIM, Polycyclic aromatic hydrocarbon

Introduction:

Aromaticity is an important concept in physical organic chemistry. Because of the importance of aromaticity, there have been many attempts to rationalize and quantify this property. Since it is not an observable quantity, there is not any generally accepted single quantitative definition of aromaticity. According to the most definition of Schleyer and co-workers [1], aromaticity is a manifestation of electron delocalization in closed circuits, results in energy reduction. Aromaticity is usually evaluated indirectly by measuring a physicochemical property that reflects the aromatic character of a molecule. Several criteria have been put forward in attempts to rationalize and quantify the concept of aromaticity. These can be divided into i) classical criteria, namely, energetic, structural, magnetic and reactivity based measures and ii) electronic properties. Here, we briefly introduce those indicators that are used in the current research. The present study is directed to show how the properties derived from the topological analysis of the electron density can be applied for description of different aromaticity indices.

Methods:

The molecular geometry of aromatic rings have been optimized at the B3LYP level of theory and 6-311++G** basis set with Gaussian 98 program [2]. The AIM2000 program [3] was used for topological analysis of electron density.

Results and Discussion:

In the last work[4], we have derived properties from topological analysis of electron density at the ring critical point, RCP, in aromatic rings. The present study is directed to study polyacenes and to show how the properties derived from the topological analysis of the



electron density can be applied for description of different aromaticity indices. In this research, the characteristics of the electron density at the critical points are analyzed as descriptors describing the aromaticity in aromatic rings. Molecules containing 1 to 4 six-membered rings have considered. We have calculated these properties and the values of HOMA, NICS(1), FLU, PDI, ATI, $\Delta \rho_6^{\pi}$ and SA indices of given rings (Table 1). Correlation between aromaticity indices were calculated (Table 2). The conclusions are illustrated that various aromaticity indices correlated in different manner.

Conclusions:

In this work, the characteristics of the electron density at the critical point are analyzed as descriptors describing the aromaticity in aromatic rings. The results obtained from the correlation between BCP properties and aromaticity indices for benzenoid aromatic hydrocarbons indicate that most of BCP properties have the best correlation with most of indices whereas HOMA and SA indices are found to be the best correlation with most of RCP properties.

	$\rho(r_c)$	$\nabla^2 \rho(r_c)$	$G(r_c)$	$H(r_c)$	\mathcal{E}	SA	HOMA	NICS(1)	FLU	PDI	ATI	SCI
Benzene ^a	0.309	0.215	0.100	-0.315	0.199	0.000	0.988	-20.510	0.000	0.103	1.395	0.027
^b	0.021	0.161	0.032	0.008	-1.189							
Naphthalene ^a	0.303	0.209	0.095	-0.304	0.186	0.001	0.782	-18.736	0.009	0.075	1.323	0.015
^b	0.021	0.153	0.031	0.007	-1.196							
Anthracene ^a	0.301	0.206	0.093	-0.300	0.181	0.001	0.628	-14.912	0.017	0.065	1.284	0.011
^a	0.299	0.204	0.092	-0.296	0.177	0.001	0.719	-23.516	0.013	0.032	1.256	0.010
^b	0.021	0.150	0.030	0.007	-1.197							
^b	0.020	0.147	0.030	0.007	-1.202							
Tetracene ^a	0.300	0.205	0.093	-0.298	0.178	0.002	0.537	-11.475	0.021	0.061	1.280	0.009
^a	0.298	0.202	0.091	-0.293	0.173	0.001	0.628	-24.656	0.016	0.061	1.239	0.008
^b	0.020	0.148	0.030	0.007	-1.197							
^b	0.020	0.145	0.029	0.007	-1.203							



Table 1. Properties of electron density at RCP and BCP and their calculated aromaticity indices of some polyacenes aromatic compound.

^a BCP properties

^b RCP properties

Table 2. Correlation between some of aromaticity indices

Index	SA	HOMA	NICS(1)	FLU	PDI	ATI	Δ_6^π
SA	1.0						
HOMA	0.755	1.0					
NICS(1)	0.571	0.658	1.0				
FLU	0.835	0.947	0.647	1.0			
PDI	0.629	0.863	0.500	0.879	1.0		
ATI	0.359	0.640	0.309	0.669	0.683	1.0	
Δ_6^π	0.734	0.898	0.467	0.937	0.927	0.726	1.0

References:

- [1] Schleyer, P. v. R. et al Chem. Rev. 105 (2005) 3842.
- [2] Frisch, M. J. et al Gaussian 98, Revision A.7, Gaussian, Inc., Pittsburgh PA, 1998.
- [3] Bader, R. F. W. AIM2000 Program, ver 2.0, Hamilton; McMaster University, (2000).
- [4] Mohajeri, A. Ashrafi, A. Chem. Phys. Lett. 458 (2008) 378.



15th Physical Chemistry Conference

Theoretical Study, Kinetics and Mechanism Investigation Of The Reactions Between Triphenylphosphite, Dialkylacetylenedicarboxylates And N-H Acid For Generation Of Phosphonate Esters

M. A. Kazemian, S. M. Habibi Khorassani*, M. T. Maghsoodlou, Y. Ghalandarzahi, O. Asheri

Department of Chemistry, University of Sistan and Baluchestan, P.O. 98135-674, Zahedan, Iran

Email: kazemean@yahoo.com

Keywords: Aniline; Dialkyl Acetylenedicarboxylates; Triphenylphosphite; Mechanism.

Introduction:

In the present work in gas phase, the variable mechanisms were investigated for the reaction between Triphenylphosphite (TPP), Dialkyl acetylenedicarboxylates (DMAD) in the presence of N-H acids such as Aniline for generation of Phosphonate Esters (Figure 1). Suitable mechanism was determined with respect to the potential energy surface. Phosphonate Esters are reactive systems which have a role in many valuable reactions of organic synthesis [1-2]. A facile synthesis investigated for the reaction between Triphenylphosphite **1**, dimethyl acetylenedicarboxylates **2** and Aniline (as NH-acid) [3-6].

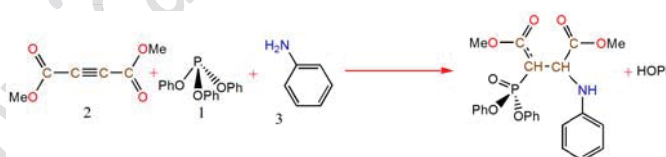


Fig.1 The reaction between TPP **1**, DMAD **2** and Aniline for generation of Phosphonate Esters **4**.

Methods:

All calculations were performed using Gaussian09 at HF/6-311G(d,p) level of theory. In addition, single point energy calculations were achieved at B3LYP/6-311+G(d,p) level. Two dimensional scanning techniques were applied to determine the transition state structures.

Results and Discussion:

Three proposed mechanism were theoretical studied for mentioned reaction. Only one of them was discussed as follows: Proposed mechanism **1**: In order to study this mechanism (Figure 2) all structures were drawn by guassview and the calculations were performed with Gaussian09 software. In the first step (step1-1) of proposed mechanism 1, **2** and **3** were considered together for investigation of probable interactions.

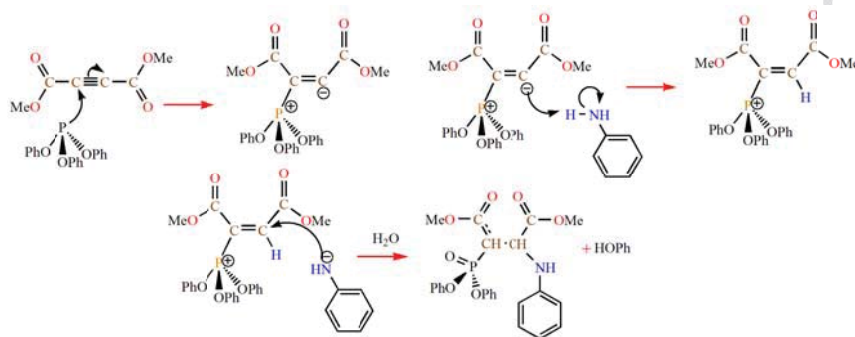


Figure 2 steps of proposed mechanism 1

Then intermediate p_1 was drawn and optimized at mentioned level. Under this condition P-C bond was longed in 0.1 \AA magnitudes step by step with full-scan. The results are shown in Figure 3 and amount of E_a , 34.91 kcal/mol, obtained for this stage. The procedure was then repeated for the second step in accord with the first step of the reaction mechanism. In this step (step1-2), hydrogen atom of Aniline is brought to carbon atom of intermediate 1 (p_1) to reduce the distance between the two atoms from 3.25 \AA to 1.00 \AA for generation of energy profile. As can be seen from Figure 4, the required energy for this step is about 36.17 kcal/mol. Because of the fast reaction between two ions in third step (step1-3), Transition State is not theoretically observed in this stage. Due to the some spices ionic are reacted together with no activation energy. With respect to the obtained activation energy for each step of proposed mechanism 1 overall activation energy was calculated about 70.08 kcal/mol. Hence the first step of the reaction is rate determent step for proposed mechanism 1 in comparison with second step. Same procedure was considered for the other probable mechanism (mechanism 2 and mechanism 3). The results indicated that probable mechanism 2 and 3 are rot consistent with the experimental data.

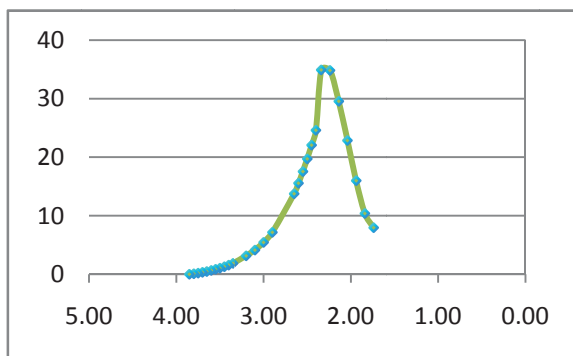


Figure 3: The changes of energy with respect to (C1-P9) distance and the transition states

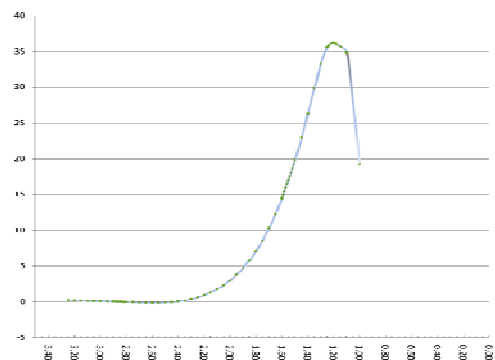


Figure 4: The changes of energy with respect to (C1-H2) distance and the transition states

Conclusion:

In our research work, three mechanisms of the reaction between TPP, DMAD and Aniline were theoretically studied in the gas phase. Two dimensional scanning techniques were employed to determine the transition state structures. The result can be summarized as follows: (1) proposed theoretical mechanism 1 was confirmed by the experimental mechanism, because the total activation energy was less than other probable mechanism 2 and 3.

References:

- [1] S.M. Habibi-khorassani, A. Ebrahimi, M.T. Maghsoodlou, M.A. Kazemian, M. Zakarianezhad; *Phosphorus, Sulfur Silicon Relat. Elem.* 184, 2959–2979, 2009.
- [2] G. Marandi; M.T. Maghsoodlou, N Hazeri., R. Heydari., S.M. Habibi-Khorassani, A. Ebrahimi, S. Mollaeipoor, H. Hosseini-Mahdiabadi, M. Nassiri, R. Kabiri; *Heteroatom Chem.* 4, 228–235, 2010.
- [3] S.M. Habibi-Khorassani, A. Ebrahimi, M.T. Maghsoodlou, S. Same-Salari, S. Nasiri, H. Ghasempour; *Magnetic Resonance in Chemistry* 49(5), 213-220, 2011.
- [4] S.M. Habibi-khorassani, A. Ebrahimi, M.T. Maghsoodlou, H. Saravani, M. Zakarianezhad, M. Ghahramaninezhad, M.A. Kazemian, M. Nassiri, Z. Khajehali; *Prog. Reaction Kinetics Mech.* 34, 261–288, 2009.
- [5] S. M. Habibi-Khorassani, M. T. Maghsoodlou, M. Zakarianezhad, M. Nassiri, M.A. Kazemian, P. Karimi; *Heteroatom Chem.* 19, 7-10, 2009.



15th Physical Chemistry Conference



Molecular dynamic simulation of dicationic ionic liquid: Effects of anion and cation type on the liquid structure and transport properties.

A. Soltanabadi, S. Yeganegi*, D. Farmanzadeh

Department of Physical Chemistry, Faculty of Chemistry, University of Mazandaran, Babolsar, Iran

Email: yeganegi@umz.ac.ir

Keywords: Geminal dicationic ionic liquid, Molecular dynamic Simulation, Radial distribution function, Diffusion coefficient

Introduction:

Geminal dicationic ionic liquids (ILs), a new category of IL family, have been developed recently and found to possess unique properties compared to conventional monocationic ILs [1-2]. In this work structures and dynamics of nine Geminal dicationic ionic liquids (DILs) $C_n(\text{mim})_2X_2$, where $n=3,6,9$ and $X=PF_6^-$, BF_4^- , Br^- , were studied by molecular dynamic simulations. Densities, detailed microscopic structures, mean-square displacements (MSD) and self-diffusivities for various ion pairs from MD simulations have been presented.

Computational details:

Molecular dynamic simulations have been carried out on nine DILs using DL-poly 2.20 code. The simulated fluids consist of 120–180 ionic complexes. Lopes et al [3]. force field was adopted for the simulations.

Results and discussion:

Densities of all nine DILs were calculated by NPT simulations at 450 K and 1 atm and results are shown in table 1. According to table 1, densities decrease with the number of carbon atoms. We investigated the liquid structure by calculating various radial distribution functions (RDFs or $g(r)$). The RDFs for anion-geometric center of imidazolium rings of cation, anion-anion and cation-cation center-of-mass correlations were calculated and shown Fig. 1a-i. The

simulated RDFs for the anions around geometric center of imidazolium rings in Fig 1a-c shows that the anion is very well organized around the cation rings. The self diffusion has been calculated in the time ranges of 3-8.5 ns, where the results are presented in Table 1. The calculated values of diffusion coefficients in table 1 are typically one order of magnitude smaller than that of a mono cationic ILs with a comparable molar mass.

Table 1 calculated density and self diffusion for all DILs

DILs	ρ (gr.cm ³)	D^+ (10 ⁻¹¹ m ² /s)	D^- (10 ⁻¹¹ m ² /s)
C ₃ (mim) ₂ (BF ₄) ₂	1.27 ₉	0.300	0.300
C ₆ (mim) ₂ (BF ₄) ₂	1.20 ₇	0.383	0.400
C ₉ (mim) ₂ (BF ₄) ₂	1.15 ₁	0.367	0.483
C ₃ (mim) ₂ (Br) ₂	1.48 ₈	0.012	0.015
C ₆ (mim) ₂ (Br) ₂	1.37 ₃	0.017	0.033
C ₉ (mim) ₂ (Br) ₂	1.27 ₅	0.050	0.083
C ₃ (mim) ₂ (PF ₆) ₂	1.47 ₉	0.067	0.050
C ₆ (mim) ₂ (PF ₆) ₂	1.38 ₁	0.100	0.107
C ₉ (mim) ₂ (PF ₆) ₂	1.31 ₃	0.100	0.150

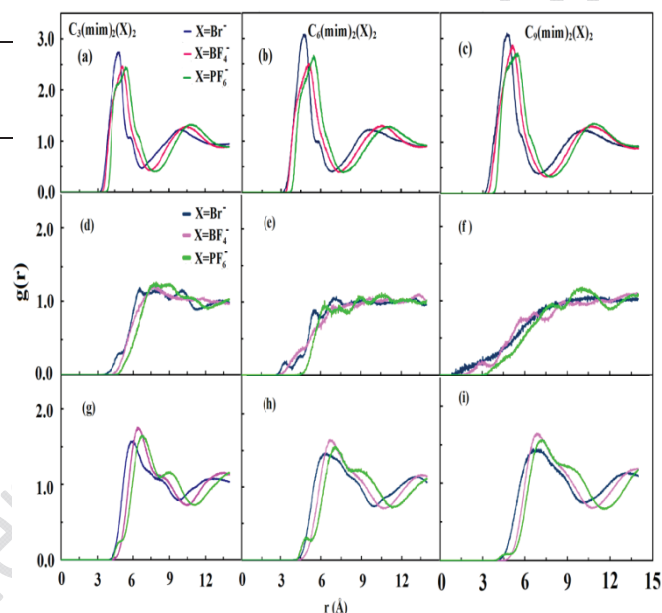


Figure 1. The calculated RDF for ring – anion (a, b, c), cation – cation (d, e, f) and anion – anion (g, h, i) correlations for all DILs at 450 K and 1 atm

Conclusion :

The molecular dynamic simulation of all DILs were carried out using Lopes et. al. force field [3]. The densities, microscopic structure, vaporization enthalpy, mean square displacement, self-diffusion coefficients are calculated. The calculated RDFs show that anions are very well organized around the cationic rings. The calculated values of diffusion coefficients show that the self diffusion for DILs are smaller than that of the mono cationic ILs.

References:

- [1] S. Mohamad et al.; “Conventional Study on Novel Dicationic Ionic Liquid Inclusion with β -Cyclodextrin”; Int. J.Mol. Sci; 12, 6329-6345, 2011.



- [2] X. Han et al.; "Using Geminal Dicationic Ionic Liquids as Solvents for High-Temperature Organic Reactions"; *Org. Lett.*; 7, 4205-4208, 2005.
- [3] J. Lopes et al.; "Modeling Ionic Liquids Using a Systematic All-Atom Force Field"; *J. Phys. Chem. B.* 2004, 108, 2038-2047.

15th Physical Chemistry Conference



445

15th Physical Chemistry Conference



Molecular structure and intramolecular hydrogen bonding of Orto Fetaleic Acid. A DFT study

F. Ghorbani Naieni^a, A. Bahmanei^a, L. Nassaji jahromi^b, F. Hodshahei^c, F. Bahrkazmei^c

^aMaster of Physical Chemistry, Basirat Research House student, Shahre-Rey Branch, Tehran, Iran

(E-mail: F_Ghorbani2010@yahoo.com)

^aMaster of Physics, Basirat Research House student, Shahre-Rey Branch, Tehran, Iran ^bMaster of Physical Chemistry, Education, Shahre-Rey Branch (Ray 2), Tehran, Iran

^cAshura High School, Shahre-Rey Branch (Ray 2), Tehran, Iran

Abstract:

All possible conformers of fetaleic acid were fully optimized at the B3LYP level of Density functional theory (DFT) with 6-31++G^{**} basis set, using Gaussian 03W software Package. The natural bond orbital (NBO) was applied as a powerful approach for evaluation of the hydrogen bond strength in the conformers.

Keywords: Intramolecular hydrogen bond, Density Functional Theory, Fetaleic acid, NBO

Introduction:

A hydrogen bond is the attractive interaction of a hydrogen atom with an electronegative atom, such as nitrogen, oxygen or fluorine, that comes from another molecule or chemical group [1]. The hydrogen must be covalently bonded to another electronegative atom to create the bond. These bonds can occur between molecules (intermolecularly), or within different parts of a single molecule (intramolecularly) [2]. This type of bond occurs in both inorganic molecules such as water and organic molecules such as DNA [3, 4, 5]. As the result of the effect of the intramolecular hydrogen-bonding interactions on the protein structure, it plays important roles in regulating the structure and the function of chemical and biological systems [6]. The information on intramolecular hydrogen bonding is, in particular, very useful to understand various molecular properties [7]. This research, deals with the existence of intermolecular

hydrogen bonding in orto fetaleic acid . Additionally, the strength of this bonding was studied in this research.

Computational methods:

All of the computations in the present study were performed by Gaussian 03 series of Programs[8]. The geometry optimizations were carried out by B3LYP method with the most popular basis set, 6-31++G(d, p). The modified bonds are calculated at the mentioned level in Å°. The charge distribution has also been investigated using natural bond orbital (NBO) analysis. The natural bond orbital (NBO) was applied as a powerful approach for evaluation of the hydrogen bond strength in the fetaleic acid conformers.



Figure1. The optimized molecular structure (a),(b) B3LYP/6-31++G**method and basis set

Table 1. hydrogen bonds length (Å°), and E_{HB} (kJ/mol) calculated at the B3LYP/631++G**

H-Bond	Bond Length	E_{HB} (kJ/mol)
O—H	0.99452	-33.0655
O...H	1.55071	-

Table 2.charge distributions at the B3LYP/631++G**

charge	H18	O17	O12	C11
orto	0.52001	-0.70642	-0.63435	0.82752
para	0.52251	-0.77961	-0.59953	0.79958



Results and discussion:

Our theoretical results show that *ortho* fetaleic acid conformer has extra stability respect to other forms and it is global minimum.

Evaluation of hydrogen bond energy by B3LYP method for O–H...O, clearly predicts that HB strength in *ortho* fetaleic acid.

Conclusion:

We have investigated the performance of popular computational method (B3LYP) for determination stability of the hydrogen bonds in *ortho* fetaleic acid. We have calculated hydrogen bonds of O – H.....O in *ortho* fetaleic acid (1.55071 \AA and $E_{\text{HB}} = -33.0655 \text{ kJ/mol}$). Also, the charge distribution analysis calculated prove to previous these stabilizations.

References:

- [1] Campbell, Neil A.; Brad Williamson; Robin J. Heyden (2006). *Biology: Exploring Life*. Boston, Massachusetts: Pearson Prentice Hall. ISBN 0-13-250882-6.
- [2] International Union of Pure and Applied Chemistry. "hydrogen bond". *Compendium of Chemical Terminology* Internet edition.
- [3] G.A. Jeffrey, W. Saenger, *Hydrogen Bonding in Biological Structures*, Springer- Verlag, Berlin, 1991.
- [4] G.A. Jeffrey, *An Introduction to Hydrogen Bonding*, Oxford University Press, New York, 1997.
- [5] G.R. Desiraju, T. Steiner, *The Weak Hydrogen Bond in Structural Chemistry and Biology*, Oxford University Press, New York, 1999.
- [6] Yosuke Hisamatsu, Yuki Fukumi, Naohiro Shirai, Shin-ichi Ikeda, Kazunori Odashima, *Tetrahedron Letters*, Vol.49, (2008) pp.2005–2009
- [7] L. Pauling, *the Nature of the Chemical Bond*, 3rd ed.; Cornell.
- [8] M.J. Frisch et al., *GAUSSIAN 03*, Revision E.01, Gaussian, Inc., Wallingford, CT, 2004.



A DFT Study on Intramolecular Hydrogen Bond in Orto Hydroxy Benzoic Acid

F. Ghorbani Naieni^{*a}, A. Bahmanei^a, L. Nassaji jahromi^b, Z. Tajekei^c, S.H. Naderpour^c

^aMaster of Physical Chemistry, Basirat Research House student, Shahre-Rey Branch, Tehran, Iran
(E-mail: F_Ghorbani2010@yahoo.com)

^aMaster of Physics, Basirat Research House student, Shahre-Rey Branch, Tehran, Iran

^bMaster of Physical Chemistry, Education, Shahre-Rey Branch (Ray 2), Tehran, Iran

^cAshura High School, Shahre-Rey Branch (Ray 2), Tehran, Iran

Abstract

Density functional theory (DFT) at B3LYP/6-31++G(d,p) level was employed to calculate intramolecular hydrogen bond in orthonitrobenzoic acid and O...H bond length. Also, we investigated the effect of the number of diethylether molecules present on the orthonitrobenzoic acid by determining the IHB energy.

Keywords: Orthonitrobenzoic acid, Density functional theory, Intramolecular hydrogen bond

Introduction:

Hydrogen bonding is a well-known phenomenon and a steering factor in many physical, chemical and biochemical processes [1, 2]. However, due to the variety of interactions classified as H-bonds, it is very difficult to indicate strictly their properties [3]. There is conventional X-H...Y- H bonds where X-H indicates the proton donating bond, Y is the proton acceptor, and both X and Y atoms are usually electronegative. Such meaning is in line with the definition of hydrogen bonding stated by Pauling [4]. Intramolecular hydrogen bonding (HB) is an interaction governing self-assembly and is responsible for the architecture and organization of molecular aggregates [5,9], and also ligand-receptor interactions that are responsible for the bioactivity of compounds [6]. Moreover, intramolecular HB has been found to govern the conformational preference of molecules [7]. In some of these systems,

especially in orto benzoic acid, the strength of hydrogen bond is solvent dependent. The aim of this work is study of solvent effects on the hydrogen bond strength in this system[8].

Computational Methods:

Considering the accuracy and conveniency of density functional theory (DFT) methods, B3LYP function on the basis set of 6-31++G(d,p) was employed in this letter to do calculations. The molecular geometries were optimized, B3LYP/6-31++G(d,p). As follows from this comparison, the bond lengths and angles calculated for title compound show quite good agreement with experimental values. The optimized geometries with atomic labels are shown in Figure 1. The typical intramolecular hydrogen bond is observed between two carbonyl oxygen atom and hydroxyl group hydrogen atom with graph-set notation (Table 1). To test the influence of solvent on the molecular structure, the geometry was optimized with the help of the self-consistent reaction field (SCRF), the scrf=(cpcm,solvent=diethylether) model.

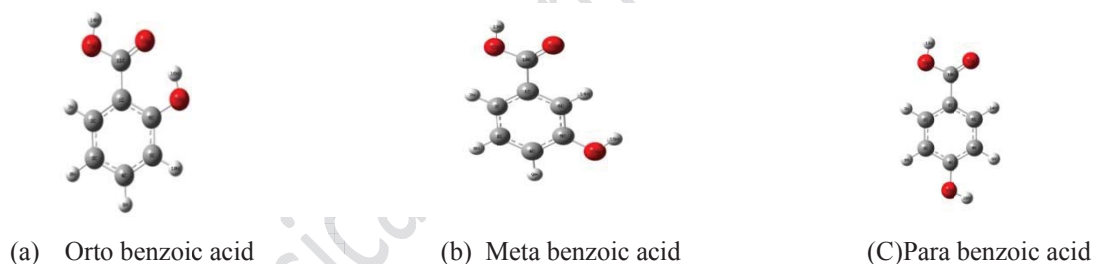


Figure1. The optimized molecular structure (a),(b),(c) B3LYP/6-31++G**method and basis set

Table 1. Hydrogen Bonding Geometry (A°) calculated by B3LYP/6-31++G** method and basis set

D—H---A	D—H	H---A
O15—H16---O12	0.98554	1.74776

Table2: The IHB energies for Orto benzoic acid form, calculated at B3LYP/6-31++G** level

$E_{HB(a.u)}$	$E_{HB(kcal/mol)}$	$E_{HB(kJ/mol)}$
-0.0086766	-5.4445665	-22.8671793



Table 3. Hydrogen Bonding Geometry (\AA^0) calculated by B3LYP/6-31++G** method and basis set and scrf=(cpcm,solvent=diethylether)

D—H---A	D—H	H---A
O15—H16---O12	0.98751	1.73609

Results and discussion:

The geometry of orto benzoic acid and the atom numbering system are given in Fig. 1. Some geometrical parameters and also E_{HB} are compared in Table 1, Table 2 and Table 3. According to Table 1 and Table 3 H-bond strength of orto benzoic acid is increased by solvent diethylether distance about 0.01 \AA^0 . This comparison, also confirm the mention theoretical and experimental result.

Conclusion:

The IHB energy (E_{HB}) for orto benzoic acid calculated at B3LYP/6-311++G** level of theory is 22.87 KJ/mol . This comparison, also confirm the mention theoretical and experimental result. The H-bond strength of orto benzoic acid is increased by solvent diethylether.

References:

- [1] G. A. Jeffrey, W. Saenger, Hydrogen Bonding in Biological Structures; Springer-Verlag: Berlin 1991.
- [2] G. A. Jeffrey, an Introduction to Hydrogen Bonding; Oxford University Press: New York, 1997.
- [3] G. R. Desiraju, T. Steiner, The weak hydrogen bond in structural chemistry and biology; Oxford University Press: New York, 1999.
- [4] L. Pauling, the Nature of the Chemical Bond, 3rd ed.; Cornell.
- [5] F. H. Beijer, H. Kooijman, A. L. Spek, R. P. Sijbesma, E. W. Meijer, *Angew. Chem., Int. Ed.* 1998, 37, 75–78.



- [6] J. R. Pinheiro, M. Bitencourt, E. F. F. da Cunha, T. C. Ramalho, M. P. Freitas, *Bioorg. Med. Chem.* 2008, 16, 1683–1690.
- [7] C. J. Duarte, M. P. J. Freitas, *Mol. Struct.* 2009, 930135-139.
- [8] G. L. Perlovich, S. V. Kurkov, A. N. Kinchin, A. Bauer- Brandl, Solvation and Hydration Characteristics of Ibuprofen and Acetylsalicylic Acid. *AAPS PharmSciTech* 2004, 6 (1), 1–9.
- [9] I. Rozas, I. Alkorta, J. Elguero, Intramolecular Hydrogen Bonds in ortho-Substituted Hydroxybenzenes and in 8-Substituted 1-Hydroxynaphthalenes: Can a Methyl Group Be an Acceptor of Hydrogen Bonds? *J. Phys. Chem. A* 105 (2001) 10462-10467.



Natural bond orbital (NBO) investigation of phase transition of confined water molecules inside carbon nanotubes: a multiscale method from MD simulation to DFT calculation

F. Taghavi^a, S. Javadian^{a*}, S. M. Hashemianzadeh^b

^a Department of Physical Chemistry, Tarbiat Modares University, Tehran, Iran.

^b Department of Chemistry, Iran University of Science and Technology, Tehran, Iran.

E-mail: javadian_s@modares.ac.ir

Key words: Confined water, Phase transition, Molecular dynamics (MD), NBO analysis.

Introduction:

After Koga et al. findings in 2001[1], there has been a great deal of interest in the study of freezing water inside carbon nanotubes [2, 3]. All simulation works and experimental investigations revealed the possible existence of new phase of water inside SCNTs in temperatures lower than room temperature. However, the fundamental understanding of the water freezing inside carbon nanotubes from the electronic feature is not still clear. In this paper, we gave insight into the electric mechanism of phase transition in water-filled SWCNTs by the use of joint methods of NBO analysis and molecular dynamic (MD) simulation. These studies can attract special interest because we could relate the molecular electronic configuration of water molecules inside SWCNTs to the phase transition as macroscopic phenomenon in spite of useful approximations that have been considered in DFT calculations.

Methods:

First, classical molecular dynamic (MD) simulations were performed with DL-POLY Classic molecular simulation package using AMBER force field. The MD calculations were carried out for SPC/E water molecules filling the interior part of an isolated armchair SWCNT (9,9) with a fixed length of 43 Å for canonical ensemble (NVT). MD simulation was first performed at high temperature 300 K and then, the temperature was decrease stepwise to 200 K (with the

temperature variation of 5 K at each run). The initial configurations for ab initio calculations were generated by averaging from equilibrium trajectory structures over the time interval. We just considered the water molecules encapsulated in five rings of carbon atoms in the middle of armchair SWCNT (9,9) and performed ab initio calculations on the water molecules inside the midsection of SWCNT at B3LYP /6-311++G** level of theory using G098W program package.

Result and discussion:

Figure 1A depicts an abrupt drop in the hyperconjugation interaction energies, $E_{n \rightarrow \delta^*}$ for two lone pairs of the oxygen atom about 275 K that could be referred to a sudden change in H-bond strength in this temperature or around it that could be related to the transformation from a disordered liquid-like structure at high temperature to n-gonal ice nanotube at low temperature, which means a first order phase transition. There is also a rapid diminishing in the amount of negative NBO charge on oxygen atom (Figure 1B) that reveals a sudden change in electric configuration of confining water molecules around 275 K.

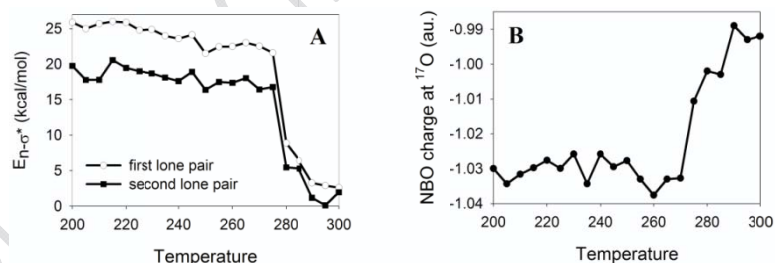


Figure 1: The temperature dependence of **A)** hyperconjugative interaction energies (Kcal/mol) for the first and second lone pairs **B)** NBO charges (au) at the target oxygen atom.

Conclusion:

NBO analysis showed that water molecules in confining structures exhibit exceptional intermolecular charge transfer during the phase transition phenomena. This is a very powerful finding, because an imperfect simple model yields a good deal of information from a complex phenomenon when it is interpreted in terms of a simple NBO analysis that is in agreement with experimental data.



Reference:

- [1] K.Koga et al.; “Formation of ordered ice nanotubes inside carbon nanotubes”; *Nature*; 412,802-805,2001.
- [2] H. Kyakuno et al.; “Confined water inside single-walled carbon nanotubes: Global phase diagram and effect of finite length”; *Journal of Chemical Physics*; 134,244501-244514, 2011.
- [3] Y. Maniwa et al.; “Ordered water inside carbon nanotubes: Formation of pentagonal to octagonal ice-nanotubes”; *Chemical Physics Letter*; 401,534-538,2005.



DFT calculations of IR and NMR properties of 4-(dimethyl amino)-1-(trimethylsilyl) pyridin-1-ium chloride

J.J. Sardroodi; M. Najafiasl; S. Afshare; J. Azamat*

Molecular Simulations Lab., Azarbaijan University of Tarbiat Moallem, Tabriz, Iran

E-mail: jafar.azamat@azaruniv.edu

Keywords: Ionic liquid, NMR, IR, DFT

Introduction:

Ionic liquids are salts of organic cations with melting points generally below 100 °C [1]. ILs are salts composed organic-based cationic parts and organic-based or inorganic-based anionic parts. Typical IL's have alkyl groups attached to cationic parts. Physicochemical properties of ILs are dependent to the length of alkyl group and anion position [2]. To rationalize interrelations between structure and properties of ILs, reliable data on the structure and bonding in ionic liquids are needed. Because X-ray structural elucidation of liquids is not routinely feasible, it is necessary to rely on spectroscopic methods. In this work used IR and NMR spectroscopy to the study of structures of ILs. We have investigated that conformation changes by DFT methods in combination with IR and NMR spectroscopy method.

Computational method:

All ab initio calculations were calculated using the GAMESS package [3]. All geometry optimizations in structural section employed DFT methods, the hybrid (B3LYP) method in combination with the Lee-Yang-Parr correlation functional[4] and 6-31G (d) basis set level were chosen and also in NMR section, Hartree-Fock and DFT methods have been used.

Result and discussion:

We discuss possible optimized geometries of ion pairs, and compare theirs which in stable structure. All structures have been optimized in Gas-Phase and PCM-Phase. The C-H

stretching vibration is a key band to characterize the H-bonds such as C-H · · · Cl and it can be used as a probe to reflect the interactions between cation and anion in ILs [5]. In the FTIR spectra, the pyridinium ring C-H stretching bands, centered around 3144.01, 3200.96, 3143.57, 3163.78 and 3177.12 cm⁻¹ in liquid state. As it is shown in Table 1, calculated ion-pair formation energies (EIL) and structural parameters are almost unchanged by the length of the alkyl chain. We compare experimental proton chemical shifts to protons chemical shifts calculated from absolute shielding's of by subtraction of a calculated reference (TMS). We demonstrated excellent correlations for isotropic shielding's obtained in Hartree-Fock GIAO calculations with both ¹H and experimental shielding data.

Table 1: Vibrational Spectra of 4-(dimethyl amino)-1-(trimethylsilyl) pyridin-1-ium chloride.

Exp.	1	2	3	4	Assignments
3032.30	3110.94	3110.28	-----	-----	v C-H st (PCM-Phase)
	2887.37	2830.39	-----	-----	v C-H st (Gas- Phase)
1605.04	1730.48	1705.27	1709.93	1705.43	v C-C _{Ring} (PCM-Phase)
	1708.15	1703.97	1710.05	1707.20	v C-C _{Ring} (Gas- Phase)
807.62	832.96	831.80	821.28	824.23	v CH ₂ (PCM- Phase)
	830.20	828.80	829.75	827.85	v CH ₂ (Gas- Phase)

In gas-phase Geometry optimizations have been carried out at the B3LYP level with the 6-31G (d) basis set. Structures optimized with both 6-31G (d) basis set and Hartree-Fock and DFT methods have been used in the calculation of and ¹H chemical shifts. In structures of [DMA TMSi P] [Cl] length of hydrogen-bonding by Hartree-Fock method is increase. In Table 2, we show the correlation between the calculated and experimental ¹H chemical shifts. The ¹H chemical shifts of the ring protons increase with the increasing H-bonding.

Table 2: Calculated and Experimental ¹H NMR Chemical Shifts of [DMA TMSi P][Cl]

	H Si(CH ₃) ₃	HCH ₂	H N loop	H loop	H N(CH ₃) ₂	
Gas-Phase						
Cation	0.3005	3.4057	8.1702	6.5978	3.1754	RHF/6- 31G(d)
ion-pair	0.1396	4.5363	9.7014	6.3649	2.9860	RHF/6- 31G(d)
Cation	0.2012	3.4200	8.2608	6.6609	3.2455	B3LYP/6- 31G(d)
ion-pair	0.1866	4.7934	10.1922	6.3689	3.0287	B3LYP/6- 31G(d)
PCM-Phase						
Cation	0.4975	3.7192	8.5760	7.0020	3.5552	RHF/6- 31G(d)
ion-pair	0.1133	4.3427	8.9994	6.4025	3.0072	RHF/6- 31G(d)
Cation	0.1802	3.4051	8.2616	6.6852	3.2402	B3LYP/6- 31G(d)
ion-pair	0.1429	4.5504	9.3901	6.4056	3.0524	B3LYP/6- 31G(d)
Experiment	0.1281	4.0727	8.3350	6.8816	3.2317	

Conclusion:

The results demonstrate that spectroscopy technique has the potential to become a more widely-used tool for the characterization of interactions in ionic liquids. For DFT, mean errors from a comparison of calculated and measured ¹H shift values are 0.8 ppm, which suggests that hydrogen-bonding play an important role for the molecules considered.

References:

- [1] X. Han, W. Armstrong, Acc. Chem. Res. 2007, 40, 1079-1086.
- [2] S. Tsuzuki, A. Ayusawa, J. Phys. Chem. B. 2008, 112, 7739-7747.



- [3] M.W. Schmidt, K.K. Baldridge, J. Comput. Chem. 1993, 14, 1347–1363.
- [4] C. Lee, W. Yang, Phys. Rev. 1988, B37, 785-789.
- [5] A. Katsyuba, E. Zvereva, J. Phys. Chem. A. 2007, 111, 352-370.

15th Physical Chemistry Conference



Barriers to permeation of ions through nanotubes

J.J. Sardroodi; J. Azamat*

Molecular Simulations Lab., Azarbaijan University of Tarbiat Moallem, *Tabriz, Iran*

E-mail: jafar.azamat@azaruniv.edu

Keywords: Molecular Dynamics simulations, nanotube, preferential permeation.

Introduction:

Ion channels are pore-forming proteins that help the establishment and control the voltage gradient across the plasma membrane of cells by allowing the flow of ions down their electrochemical gradient. They are present in the membranes that surround all biological cells. They are responsible for processes such as the effluence of nerve impulses and muscle contraction. Due to the comparable size of CNT to a biological ion channel [1], a CNT has been considered to have great potential for applications in biological nanosystems. BNNTs can be also find interesting applications in biological nanofluidic systems, because of their exciting properties. The permeation of ions across membranes enclosing living cells is an essential procedure that controls the electrical properties of the cells, such as, the action potential generation in nerves and muscles [2]. The cell membrane, however, is almost impassable to ions. Thus, an ion channel is needed to allow the transfer of ions in and out of the cell through the membranes. Each ion channel can be particular for a single ion or conduct a few or several ions. During the past decade, several nanotubes or nanochannels have been proposed as artificial ion channels to mimic the selectivity properties of biological ion channels.

Computational method:

We consider armchair carbon and boron nitride nanotubes. The considered nanotubes were optimized in the B3LYP level of theory with the 6-31G** basis set implemented in Gaussian03 [3]. Molecular dynamics simulations were performed using NAMD 2.7 [4]. The

one-dimensional potential of mean force (PMF) of the specific ion moving through the nanotube was determined.

Result and discussion:

In this work in order to obtain ionic current and ion-water radial distribution functions, the molecular dynamics simulations have been performed. Nevertheless the considered nanotube has a radius large enough to accept both magnesium and chloride ions, the results of MD simulations show that Mg^{2+} is permeated through (7, 7) nanotubes whiles Cl^- is permeated through (8, 8) nanotubes. The current-electrical field profile has been presented as Figure 1. This curve shows that the relation between the current and the electrical field is linear. Figure 2 includes profiles for PMF for the considered systems.

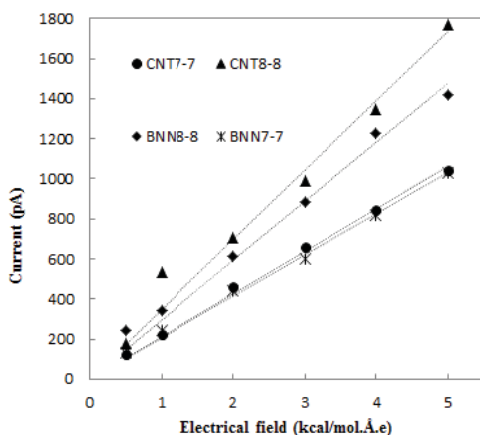


Figure 1: Current-electrical field profile

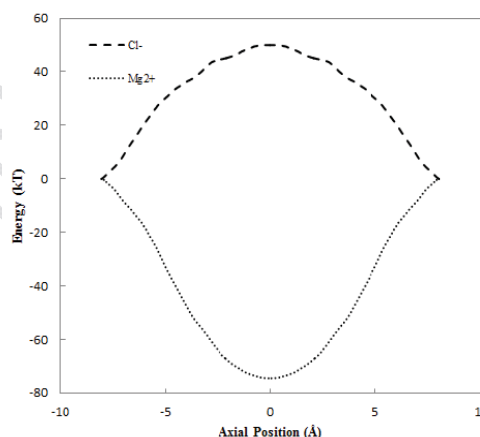


Figure 2: PMF for the considered systems

Conclusion:

The selective ion permeation via carbon and boron nitride nanotubes has been investigated by MD simulations. It was shown that the ion permeation through considered nanotubes happens in the presence of electrical field and is also selective. The results show that Mg^{2+} ions permeate through (7, 7) nanotubes whiles Cl^- ions permeate through (8, 8) nanotubes.

References:

- [1] M.S.P. Samson, P.C. Biggin, Nature 414 (2001) 156–159.



- [2] B. Hille, *Ionic Channels of Excitable Membranes*, Sunderland, MA, 1992.
- [3] M.J. Frisch, et. al. *Gaussian 03*, Gaussian Inc. Wallingford CT 2004.
- [4] L. Kale, *J. Comput. Phys.* 151 (1999) 283-312. <http://www.ks.uiuc.edu/Research/namd>.

15th Physical Chemistry Conference



Computational Studies of Fullerene Nano Structures

$C_{20}(I_h)$, $C_{24}(D_{6d})$, $C_{26}(D_{3h})$, as H_2 Adsorbent

F.R.Nikmaram*, M.Nami saee, J.Najafpour

Department of Chemistry, Faculty of science, Islamic Azad University Shahr-e-Rey Branch, Tehran, IRAN

namisaee@yahoo.com

Keywords: $C_{20}(I_h)$, $C_{24}(D_{6d})$, $C_{26}(D_{3h})$ Fullerenes, Thermodynamic analysis, AIM analysis

Introduction:

With a growing world population, an increasing standard of living in many developing countries, a limited supply of fossil fuels, and its adverse effect on the environment, the need for clean and sustainable energy has never been greater. Hydrogen, the simplest and most abundant element in the universe, has the potential to meet this energy need if numerous hurdles in its efficient and safe production, storage, and use in fuel cell vehicles can be overcome. In recent years fullerene structures have brought up steadily increasing attention both in academic and industrial researches. We study the simulations of H_2 adsorption on the fullerene surfaces, to determine the adsorption ability of $C_{20}(I_h)$, $C_{24}(D_{6d})$, $C_{26}(D_{3h})$ at 298K. We have examined what type of species on carbon surfaces may be able to adsorption of H_2 molecule by frequency and AIM analysis.

Computational method:

By Using frequency analysis, the relative energies, binding energies and change of thermodynamical properties are obtained for interaction of H_2 and $C_{20}(I_h)$, $C_{24}(D_{6d})$, $C_{26}(D_{3h})$ at 298K. The structures were fully optimized at B3LYP level of Quantum methods, in the 3-21g(d,p) basis set by Gaussian 03 package.

Also Atom In Molecules (AIM) quantum theory were carried out to study the interaction forces. QTAIM calculations have been done using AIM2000 package. The AIM analysis for the optimized structures has been performed to obtain the topological properties of the bonds,

such as the Bond Critical Points (BCP), Laplacian of ρ_b ($\nabla^2\rho_b$) at bond critical points, and density of total energy (H_b). H_b is sum of the kinetic energy density (G_b) and electronic potential energy density (V_b) at a BCP. As is known, $\nabla^2\rho_b$ identifies whether the charge of the region is shared interactions ($\nabla^2\rho_b < 0$ and/or $H_b < 0$) or closed shell interactions ($\nabla^2\rho_b > 0$ and/or $H_b > 0$). The former characterizes shared interactions (covalent bonds), where the electron density concentrates in the inter nuclear region, whereas the latter is typically associated with interactions between closed-shell systems (ionic bonds, hydrogen bonds, and van der waals molecules).

Conclusion:

The change of Charge at the interactions between H_2 and $C_{20(Ih)}$ and ΔH_{ads} , Binding Energy, ΔS_{ads} and ΔG_{ads} show that the ($C_{20(Ih)}$, H_2) structure may be more chemically stable than the $C_{24(D6d)}$ and $C_{26(D3h)}$ structures (Table1). All of the interactions between H_2 and $C_{20(Ih)}$, $C_{24(D6d)}$, $C_{26(D3h)}$ Fullerenes are van der Waals, because of values of $\nabla^2\rho_b > 0$, $H_b > 0$ and ρ_b order of 10^{-3} a.u (Table2).

Table1: The Thermodynamic results

Systems	$\Delta H_{(ads)}$ kcal.mol ⁻¹	$\Delta G_{(ads)}$ kcal.mol ⁻¹	$\Delta S_{(ads)}$ cal.mol ⁻¹	$\Delta charge$ (ads)	$E_{Binding}$ kcal.mol ⁻¹
$C_{20}H_2$	-0.794	-1.009	+0.718	+0.001	-2.313
$C_{24}H_2$	-0.275	+2.679	-9.910	0.000	-2.314
$C_{26}H_2$	-0.463	+2.467	-9.831	-0.004	-2.314



Fig1-a

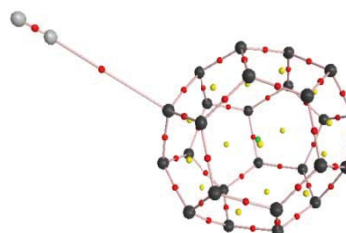
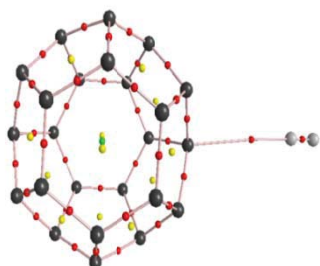


Fig 1-b

Fig1-c

Fig 1: The 3D molecular graph (MGs) of the **a)** C₂₀H₂ **b)** C₂₄H₂ and **c)** C₂₆H₂. (Bold points are Bond Critical Points: BCPs; Pale points are Ring Critical Points: RCPs. The lines are Bond Paths: BPs.)

results

Systems	ρ_b a.u	$\frac{1}{4} \nabla^2 \rho_b$ a.u	V_b a.u	G_b a.u	H_b a.u
C ₂₀ H ₂	+0.0045	+0.0030	-0.0020	+0.0025	+0.0005
C ₂₄ H ₂	+0.0031	+0.0024	-0.0012	+0.0018	+0.0006
C ₂₆ H ₂	+0.0040	+0.0028	-0.0017	+0.0022	+0.0005

Table2: The AIM

References:

- [1] FRISCH M.J., Trucks G. W., Schlegel H. B., Scuseria G. E., Robb M. A., Cheeseman J. R., and Pople J. A. 1998. *Gaussian 98, Revision A.7* Gaussian, Inc., Pittsburgh PA.
- [2] F. Biegler-König, J. Schönbohm, D. Bayles, AIM2000 - A Program to Analyze and Visualize Atoms in Molecules, J. Comp. Chem., 22, 545 ,2001.
- [3] Bosi, S. Eur.J.Med.Chem. 38, 913-923 ,2003.
- [4] Gharbi, N. Nano Lett 5, 2578-2585 ,2005.



- [5] Tim S. Jakubov, Adsorption 14, 727-732, 2008.
- [6] Morris Sylvan, Surface Chemistry (Adsorption), Sarup & Sons, New Dehli, 2005.

15th Physical Chemistry Conference



Theoretical study of Oxygen Adsorption on Ni(111) Surface

Amir N. Shamkhali* and Kobra Gharaghanabadi

Department of Chemistry, University of Mohaghegh Ardabili, Ardabil, Iran

56199-11367,

(Email: amir_n_shamkhali@yahoo.com)

Keywords: Adsorption, Vibrational frequency, DFT, Oxygen

Introduction:

Oxygen adsorption on Ni surface provides a model dissociative chemisorption system and a large number of studies of this system have been conducted using many kinds of techniques[1].

Computational method:

In this work the adsorption of oxygen on Ni(111) is investigated in p(2×2) configuration and oxygen atoms occupy 3-fold hollow sites on the unreconstructed Ni(111) surface corresponding to coverage value of 0.25 ML by Density Functional Theory (DFT) using ABINIT package. The exchange-correlation functional is treated within the generalized gradient approximation (GGA) and Perdew- Burke-Ernzerhof (PBE) functional is applied for the structural optimization and calculation of adsorptive bond stretching frequency[2].

A slab with 5 layers and 15 Å vacuum selected for these calculations as shown in Figure 1. Also the 4×4×1 and 6×6×1 k-point mesh are used for the structural optimization and frequency calculations, respectively. The plane waves with 45 Hartree cut off energy are used for all calculations. For Ni and O atoms, the Trouiller-Martins pseudopotentials are included in the calculations[3].

Results and discussion:

After structural optimization, the O-Ni bond length and the distance of O from the surface obtained 1.87 and 1.17 Å, respectively. The stretching frequency of adsorptive bond is

calculated by fitting of five points within harmonic and Morse oscillator models, respectively. Each of these points are calculated statistically by moving O atom around the minimum location along the z direction. potential models, for stretching frequency of adsorptive bond are comparable with experimental data [4].

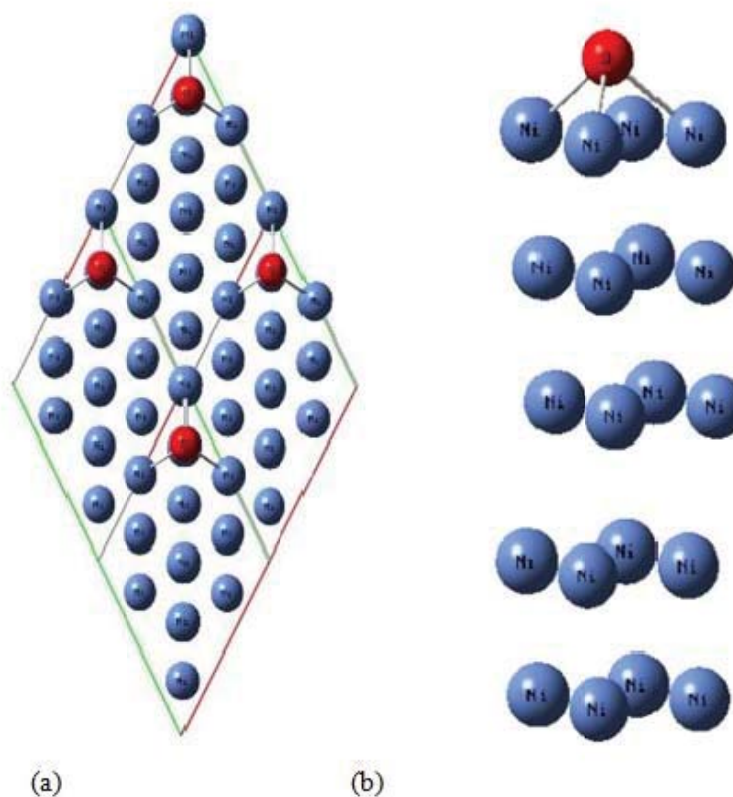


Figure 1: P(2×2) adsorption structure of O on Ni(111) surface (a), and the selected slab model for it (b).

Conclusion:

This method gives 484.1 and 487.9 cm^{-1} , respectively for harmonic and Morse potential models, for stretching frequency of adsorptive bond which is comparable with 514.5 cm^{-1} , obtained from experimental data [4]. The difference between harmonic and anharmonic frequencies for adsorptive bond of S atom on Ni(111) surface with the same configuration and coverage obtained 101.3 cm^{-1} [5]. These results show that the anharmonicity of adsorptive bond increases with the size of the atomic adsorbates for group VIA of the periodic table.



References:

- [1] S. Yamagishi, S.J. Jenkins, D.A. King, *Surface Science*. **543** (2003) 12.
- [2] J.P. Perdew K. Burke, M. Ernzerhof. *Phys. Rev. Lett.* **77** (1996) 3805.
- [3] See <http://www.abinit.org/downloads/psp-links/gga-fhi>.
- [4] J. E. Black, P. Bopp, K. Lutzenkirchen, and M. Wolfsberg. *J. Chem. Phys.* **76** (1982) 6431.
- [5] A. N. Shamkhali and K. Gharaghanabadi, 14th Iranian Physical Chemistry Conference, University of Tehran, Kish, February 25-28, 2011.



Investigation of solvation energy and intramolecular hydrogen bond of 1,3,4-Oxadiazole-2-thiol derivatives in different solvents

Maryam Yousofizadeh^{*a}, Mohammad Soleiman-Beigi^a

^aDepartment of Chemistry, Faculty of Science, Ilam University, P. O. Box 69315- 516, Ilam, Iran.

Email: yousofizadehm@yahoo.com

Keywords: 1,3,4-Oxadiazole-2-thiol, Density functional theory, Self-consistent reaction field, Dimethylformamide, Acetonitrile.

Introduction:

1,3,4-oxadiazole-2-thiol derivatives display various types of biological activity,^{1,2} including bactericidal, antimicrobial, anti-inflammatory, hypotensive, fungicidal and anticonvulsant activities.³ In addition, their derivatives represent an important group of heterocyclic compounds in the field of coordination chemistry because of their potential multifunctional donor sites, via either exocyclic sulfur or endo cyclic nitrogen atoms.^{4,5}

Method of calculations:

The Gaussian program was used for all quantum mechanical computations. The full geometry optimization were performed at B3LYP/6-311++G(d,p) with taking into account the polarity of medium in gas phase and in different solvents using self-consistent reaction field (SCRF) method by using SCIPCM solvent model.

Results and discussion:

Molecular geometry:

To ensure that hydrogen bonding with solvents of high polarity has a significant contribution in facilitating the formation of and stabilizing the thiol tautomer, we considered purposefully

the changes in bond lengths and angles of two tautomers. The values of C1=N4 and C2=N5

	E ^a		E ^b _{SSI}		E ^c _{HB}		E ^d _s		ΔE ^e _{HB}	ΔE ^f _s	^h μ	
	I	II	I	II	I	II	I	II			I	II
= 1ε	-891.5045327	-891.5219806	—	—	—	—	—	—	—	—	0.9773	1.7771
= 36.7ε	-891.5125739	-891.532338	- 891.5125695	-891.5323358	5.0432	6.4980	5.0459	6.4991	1.4548	1.4532	1.3208	2.3823
= 36.64ε	-891.5125732	-891.532345	-891.5125688	-891.5323396	5.0427	6.5004	5.0455	6.5039	1.4577	1.4584	1.3207	2.3838
24.2ε =	-891.5123820	-891.532098	-891.5123776	-891.5320928	4.9228	6.3455	4.9255	6.3485	1.4227	1.4230	1.3117	2.3699
8.39ε =	-891.5114328	-891.530870	-891.51142961	-891.5308670	4.3279	5.5764	4.3299	5.5779	1.2485	1.2480	1.2664	2.3012
= 2.38ε	-891.5082445	-891.526763	-891.5081894	-891.5267218	2.2946	2.9752	2.3292	3.0013	0.6806	0.6721	1.1266	2.0700

bond lengths experience maximum increment while the C2-S17, C1-O3, C2-O3 and S17-H18 bond lengths experience maximum decline in DMF as solvent in comparison with gas phase values for tautomer (I). It is believed that these changes are the consequences of hydrogen bond formation between tautomer (I) and dimethylformamide as solvent. Similar phenomenon is observed for tautomer (II) in acetonitrile proving the idea of solvent assistance for the tautomer selectivity. According to these findings, the tautomer (I) is preferred mostly to be formed in DMF as solvent. The structures of two possible tautomers of 1,3,4-oxadiazole-2-thiol(thione) are presented in Figure 1.

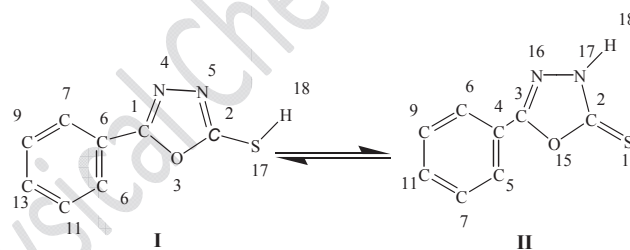


Figure 1 (The numbering system and the structure of I and II)

Energy Calculations:

The values of absolute energy and solvent-solute interaction energy indicates more stability for both tautomers in more polar solvents (Table 3). The highest solution energy values for tautomer (I) and (II) are in DMF and CH₃CN.

Table 1 (Calculated energies and dipole moments at the B3LYP level with 6-311++G**)

a) Energy (Hr), b) Solvent-solute interaction energy (Hr), c) Hydrogen bond strength (kcal/mol), d) solvation energy (kcal/mol), e) difference between the hydrogen bond strength



of I and II ($E_{HB} (II) - E_{HB} (I)$) in kcal/mol, f) difference between the solvation energies of I and II ($E_S (II) - E_S (I)$) in kcal/mol, h) dipole moment (debye).

Conclusion:

The influence of solvents on the progress of the reaction has been studied theoretically. DMF, as an accessible polar aprotic solvent, was found as most convenient medium to facilitate this process for the synthesis of 1,3,4-oxadiazole-2-thiols. Theoretical calculations using density functional theory (DFT) at B3LYP/6-311++G(d,p) level of theory confirmed that dimethylformamide (DMF) assisted the formation of only one of the expected tautomers (tautomer I) as the single observable product of the reaction.

References:

- [1] V. Mickevicius, R. Vaickelioniene, B. Sapijanskaite, Chem. Heterocycl. Comp. 2009, **54** 215.
- [2] G. Mekuskiene, P. Vainilavicius, A. Hetzheim, R. Shematovich, Chem. Heterocycl. Comp. 1993, **29**, 598.
- [3] H. Chen, Z. Li, Y. Han, J. Agric. Food. Chem. 2000, **48**, 5312.
- [4] M. Singh, R. J. Butcher, N. K. Singh, Polyhedron 2009, **28**, 95.
- [5] Y. T. Wang, G. -M. Tang, Inorg. Chem. Commun. 2007, **10**, 53.



Computational Study of 1-silaallene and 2-silaallene

S. Jameh-Bozorgi¹, A. Amiri², H. Soleymanabadi^{3*}, M. Nouraliei³

¹ Department of Chemistry, Toyserkan Branch, Islamic Azad University, Toyserkan, Iran

² Department of Chemistry, Central Tehran Branch, Islamic Azad University, Tehran, Iran

³ Young Researchers Club, Central Tehran Branch, Islamic Azad University, Tehran, Iran

(Email: soleymanabadi@hotmail.com)

Keywords: 1-silaallene; 2-silaallene; vibrational frequencies; normal modes; IR

Introduction:

Hydrogen Compounds with multiple bonds to silicon have attracted more and more interest since their first isolation in 1981, due to their unique properties compared to carbon analogs [1]. Although chemists have made and afford to synthesize compound which include a cumulenenic double bond to silicon [1], the first 1-silaallene was synthesized and isolated as a stable compound by West and co-workers in 1993. It was stabilized by an extremely large steric hindrance around the Si=C=C moiety and characterized by X-ray crystallography, revealing that it is slightly bent (173.5°) in contrast to the carbon analogue allene, which is linear [2]. Interpretation of an experimental IR spectrum of silaallenes is a difficult task due to the problems encountered in their synthesis and isolation [1-2].

Method:

The computations were performed using the Gaussian 03 program package. First of all, both structures (1-silaallene and 2-silaallene) were optimized at MP2/6-31G(d) level which is very successful in modeling for allenes. The vibrational frequencies of 1- and 2-silaallene were calculated at the MP2 levels of theory with 6-31+G(d,p) and 6-31+G(d,p) basis sets. The computational method helped us to determine the normal modes of 1- and 2-silaallenes. Agreement among the method is a useful indicator that the vibrational modes have been correctly assigned for silaallenes. Each motion (symmetrical stretching, antisymmetrical

stretching, scissoring, rocking, wagging, twisting) of normal modes were interpreted by means of visual inspection with help of GaussView program .

Result and discussion:

In The optimized structures of 1- and 2-silaallenes are shown in Figure 1. Although trisilaallene exhibit a very acute Si=Si=Si angle of 136.5° , the both studied molecules are linear with the bending angles of 179.9° and 179.5° at MP2/6-31G(d) level of theory, respectively. It is shows that the bond angles of 2-silaallene decreases slightly compared to 1-silaallene. The C=Si bonds on the 1- and 2-silaallenes are a little bit different from each other with 1.690 \AA and 1.697 \AA at MP2/6-31G(d) level of theory.

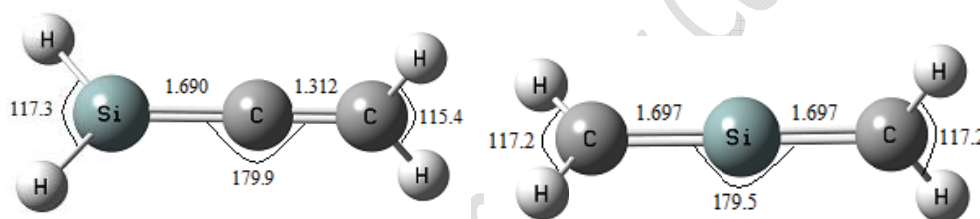


Figure 1. The optimized structures of 1-silaallene (*left*) and 2-silaallene (*right*) at MP2/6-31G(d) level of theory.

the calculated vibrational frequencies for 1- and 2-silaallenes at MP2 level of theory using the standard 6-31G(d) and 6-31+G(d,p) basis sets, respectively. For the calculated frequencies of 1- and 2-silaallenes, there are very little variations of vibrational frequencies in the different symmetries within each level of theory. We can see easily from the results, the procedure cause to trustable estimations. However, as a result of calculations which are several levels of theory, there are a bit difference on the data of vibrational frequencies and IR intensities on the same band. For instance, the calculated frequency of C=Si=C bend (V1) of 2-silaallene is 49.0 cm^{-1} at MP2/6-31G(d), whereas it is 78.6 cm^{-1} at MP2/6-31+G(d,p).

The Si-H group is readily identified by a strong band in the range 2280-2080. There is no interference from other bands in this part of group . In addition, the vibrational frequencies of C-H stretch, and C=C stretch are found, $3079, 1423 \text{ cm}^{-1}$ experimentally, respectively. There are very close results which are compared to experimental data in this study. For example, the



Si-H stretch, C-H stretch, and C=C stretch of 1-silaallene were calculated 2296.0 cm⁻¹, 3100.1 cm⁻¹, 1823.1 cm⁻¹ at MP2/6-31G(d), respectively.

Conclusion:

The normal mode geometries and corresponding vibrational frequencies in Cs symmetry were studied theoretically using the Gaussian 03W set of quantum chemistry codes. All normal modes were successfully determined in accordance with six of motion (symmetrical stretching, antisymmetrical stretching, scissoring, rocking, wagging, twisting) with help of a group of theoretical analysis. In addition to that infrared intensities are reported in this study. These findings would be helpful for further studies of 1- and 2-silaallenes.

References :

- [1] For reviews, see: (a) G. Raabe, J. Michl, in: S. Patai, Z. Rappoport (Eds.), *The Chemistry of Organic Silicon Compounds*, vol. 1, Wiley, Chichester (1989) Chapter 17
- [2] For reviews, see: (a) B. Eichler, R. West, *Adv. Organomet. Chem.* 46 (2001) 1; (b) J. Escudie, H. Ranaivonjatovo, L. Rigon, *Chem. Rev.* 100 (2000) 3639.



SO₃⁻² ion adsorption on (8, 0) zigzag Carbon Nano tubes

Khadijeh.Tavakoli hafshajani¹, Morteza Keshavarz², Ali Kazemi¹, M.H.Shahbazi²

¹Department of Chemistry, Faculty of Science, Islamic Azad University, Shahrekord Branch, Iran

²Department of Chemistry, Faculty of Science, Islamic Azad University, Shahreza Branch, Iran

Email: Tavakoli.khadijeh@yahoo.com

Abstract:

We studied the adsorptions of SO₃⁻² on the zigzag (8, 0) Carbon Nano tubes (SWCNT) by means of density functional theory (DFT) calculations. Our results show that binding energy corresponding to adsorption of SO₃⁻² on the C site in the (8, 0) carbon nanotube was calculated -2.25e. The calculated binding energies for SO₃⁻² in S-down orientation are higher than those in O-down orientation for the configurations.

Keywords: Carbon nanotube, Adsorption, binding energy, SO₃⁻², DFT

Introduction:

Since the discovery of carbon nanotubes (CNTs) [1], single-walled carbon nanotubes (SWCNTs) have attracted great interest owing to their physical and chemical properties [1–3] and applications as a fascinating novel material [4, 5]. SWCNTs have a wide range of applications in nanoelectronics, nanoscaling biotechnology, and biosensors [3, 6–9]. Because of their size, large surface area, and hollow geometry, SWCNTs are being considered as prime materials for gas adsorption [10–14]; biological, chemical, and electromechanical sensors; and nanoelectronic devices [15–17].

Computational methods:

The density functional theoretical method with the B3LYP functional and the 6-31G* basis set was used for all the calculations. In the first step, zigzag (8, 0) CNT (C80H16) have been

selected. The structure was allowed to relax by all atomic geometrical parameters in the optimization at the DFT level of B3LYP exchange functional and 6-31G* standard basis set.

The BE (binding energy) of SO_3^{-2} on the optimized nanotube model is calculated as follows:

$$\text{BE} = E_{\text{SO}_3^{-2}\text{-CNT}} - [E_{\text{CNT}} + E_{\text{SO}_3^{-2}}] \quad \text{Eq. (1)}$$

All the calculations were carried out by using the Gaussian 03 suite of programs [6].

Results and discussion:

For the adsorption of the SO_3^{-2} (S-down and O-down) on the CNT, we considered possible sites as described in Fig. 1. The notation S-down and O-down denotes an SO_3^{-2} perpendicular to the surface via S and O.

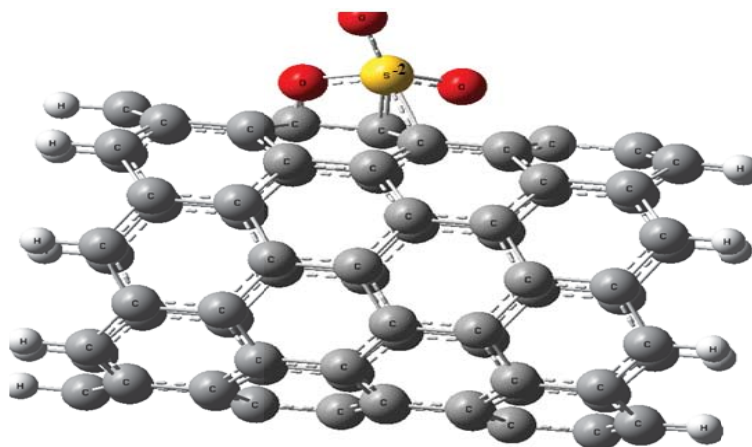


Fig. 1 SO_3^{-2} adsorption on the zigzag (8, 0) CNT

For the sites, we investigated the CNT/ SO_3^{-2} potential energy surface (PES). The binding energies (BE) of the SO_3^{-2} (S-down and O-down) at the two sites on the CNT are plotted in Fig. 2.

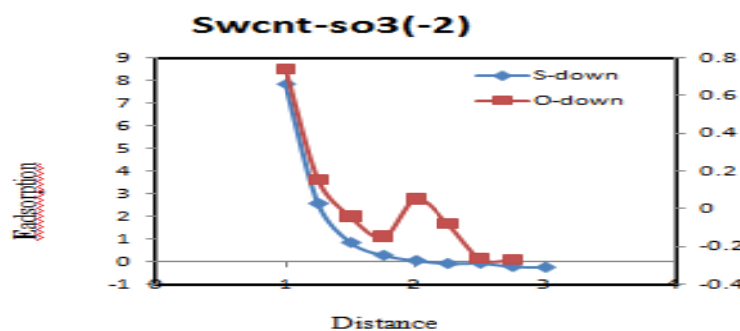


Fig. 2 Binding energy curves of SO_3^{-2} (S-down and O-down) adsorption



The binding energies (BE) obtained from these calculations showed that the most stable configuration of SO_3^{-2} adsorption on the zigzag (8, 0) CNT is the C site, also the calculated BE for SO_3^{-2} in S-down configuration is higher than that in O-down. The BE value for the C site (S-down) is -2.25 eV with rd of 2.0 Å. The results show that the zigzag (8, 0) CNT can significantly detect the SO_3^{-2} , because it can be adsorbed on the surface completely.

Conclusion:

We studied the adsorptions of SO_3^{-2} on the zigzag (8, 0) CNT by means of density functional theory (DFT) calculations. On the basis of our calculations, it seems that the pristine zigzag (8,0) CNT can be used as an SO_3^{-2} storage medium as long as SO_3 is adsorbed on the exterior walls of the CNT because of the high binding energy.

Acknowledgements With special thank full from Islamic Azad University Shahrekord Branch, that this article is resulting from research project published in this university.

References

- [1] Ijima S (1991) Nature 354:56
- [2] Derycke V, Martel R, Appenzeller J, Avouris P (2002) Appl Phys Lett 80:2773
- [3] Liu C, Fan YY, Liu M, Cong HT, Cheng HM, Dresselhaus MS (1999) Science 286:1127
- [4] Zurek B, Autschbach J (2004) J Am Chem Soc 126:13079
- [5] Nojeh A, Lakatos GW, Peng S, Cho K, Pease RFW (2003) Nano Lett 3:1187
- [6] Zhou O, Shimoda H, Gao B, Oh SJ, Fleming L, Yue G (2002) Acc Chem Res 35:1045
- [7] Zhen Y, Postma HWC, Balents L, Dekker C (1999) Nature 402:273
- [8] Baughman RH, Cui C, Zakhidov AA, Iqbal Z, Barisci JN, Spinks GM, Wallace GG, Mazzoldi A, Rossi DD, Rinzler AG, Jaschinski O, Roth S, Kertesz M (1999) Science 284:1340
- [9] Gao H, Kong Y, Cui D, Ozkan CS (2003) Nano Lett 3:471
- [10] Rawat DS, Calbi MM, Migone AD (2007) J Phys Chem C, 111:12980
- [11] Zhao J, Buldum A, Han J, Lu JP (2002) Nanotechnology 13:195
- [12] Gordillo MC (2007) Phys Rev B 76:115402



- [13] Choi YS, Park KA, Kim C, Lee YH (2004) J Am Chem Soc, 126:9433
- [14] Byl O, Kondratyuk P, Forth ST, Fitzgerald SA, Chen L, Johnson, JK, Yatesjr JT (2003) J Am Chem Soc 125:5889
- [15] Yang X, Lu Y, Ma Y, Liu Z, Du F, Chen Y (2007) Biotech Lett, 29:1775
- [16] Gowtham S, Scheicher RH, Ahuja R, Pandey R, Karna S (2007), Phys Rev B 75:033401
- [17] Froudakis GE, Schnell M, Muhlhaeser M, Peyerimhoff SD, Andriotis AN, Menon M, Sheetz RM (2003) Phys Rev B, 68:115435.

15th Physical Chemistry Conference



Adsorption properties of biatomic gases on (8,0) zigzag Single-walled carbon nanotubes: a density functional study

Khadijeh.Tavakoli hafshajani¹, Morteza Keshavarz², Ali Kazemi¹

¹Department of Chemistry, Faculty of Science, Islamic Azad University, Shahrekord Branch, Iran

²Department of Chemistry, Faculty of Science, Islamic Azad University, Shahreza Branch, Iran

Abstract:

The behavior of the biatomic gases (O_2 , CO_2) adsorbed on the external surface of H-capped (8,0) zigzag Single-Walled carbon nanotubes was studied by using density functional calculations. Geometry Optimizations were carried out at the HF, BLYP, B3LYP/3-21G, 6-31G, 6-311G level of theory using the Gaussian 03 suite of programs. We present the nature of the (O_2 , CO_2) surface interaction in selected sites of the nanotubes. Binding energies corresponding to adsorption of the biatomic gases are calculated to be in the range -0.08169- (0.34569) K.Cal.mol⁻¹. We provide the effects of (O_2 , CO_2) adsorption on the ,electronic properties (DOS) and bond gap (HOMO-LUMO) of the nanotubes.

Keywords: Nanotube, Adsorption, Binding energy, DFT, HOMO-LUMO

Introduction:

Synthesis of carbon nanotubes (CNTs) by Ijima [1] caused a burst of activity by both physical and chemical properties [1–3] and applications as a novel material [4,5]. The electronic properties of CNTs depend on their tubular diameter and chirality. SWCNTs are being considered as prim mater ialsfor gas adsorption [10–14], biological, chemical, and electromechanical sensors, and nanoelectronic devices [15–17].

Computational methods:

In the present work, adsorption behaviors of the (O_2 , CO_2) on the single-walled SWCNTs were studied by using the representative models of (8,0) zigzag single walled SWCNTs with four

molecular orientations, C- and O-down and parallel models in which the ends of the nanotubes are saturated by hydrogen atoms. The hydrogenated (8,0) zigzag single-walled SWCNTs have 67 (C₄₈H₁₆CO₂), 66 (C₄₈H₁₆O₂) atoms. In the first step, the structures were allowed to relax by all atomic geometrical optimization at the HF/3-21G, B3LYP/6-31G _ and B3LYP/6-311G methods. For pass of this problem, BSSE has been estimated for the calculated structures by B3LYP and HF methods. Using these methods, the binding energy (BE) of an CO₂ on the CNTs wall was calculated as follows:

$$BE = E_{\text{CNT-gases}} - (E_{\text{CNT}} - E_{\text{gas}}) + \delta_{\text{BSSE}}$$

Results and discussion:

An CO₂ molecule can approach the nanotube walls from outside (out), which is the most common case. Zigzag configurations of (8, 0) SWCNTs have two different state parallel and vertical adsorption of the CO₂ (C-down and O-down) and parallel models. The notation C down and O down denotes an CO₂ perpendicular to the surface via C and O. Comparison of the calculated BEs of obtained at the B3LYP/6-31G and B3LYP/6-311G levels of theory indicated that the calculated BEs for CO₂ in the B3LYP/6-31G _ method are more than that at B3LYP/6-311G method. We observed that when the CNTs diameter increases, the BE of the CO₂ also decreases at each particular site of the interaction very slightly (<3 kJ mol⁻¹).

1. Electronic properties:

To better understand the nature of interaction between the CO₂ and the CNTs, we studied the influence of CO₂ adsorptions on the electronic properties of the CNTs. When CO₂ is adsorbed on the CNTs, the interaction between them being weak, the electronic properties of these tubes are changed obviously and the band gaps are calculated as about 0.40, 0.29, and 0.35 eV. The DOS of these tubes show some significant changes due to CO₂ adsorptions in the gap regions of the TDOS plots. Therefore, the adsorption of CO₂ on the CNTs slightly decreases the energy gap of the pristine CNTs, and increases their electrical conductance. But for the O₂ on (8,0) zigzag SWCNTs, the interaction between O₂ and CNT is much further from the interaction of between O₂ and the CNTs. The DOS of the CNT show significant changes due

to O₂ adsorptions in the gap regions of the TDOS plots. Therefore, the band gap of the CNT-O₂ will change significantly.

Conclusion:

We have studied the adsorptions of O₂ & CO₂ on zigzag configurations of (8,0) SWCNTs by means of DFT and HF calculations. On the basis of our calculations, comparing all the BE curves of CO₂ interacting with all possible sites of adsorption on nanotube walls and in several structural configurations, it seems that the pristine CNTs cannot be used as an CO₂ storage medium. For the CNTs, the calculated BE for CO₂ in O-down is a little more than that in C-down. In all pathways for the zigzag configurations of (8,0), the CO₂ parallel to the CNTs are the most stable configurations.

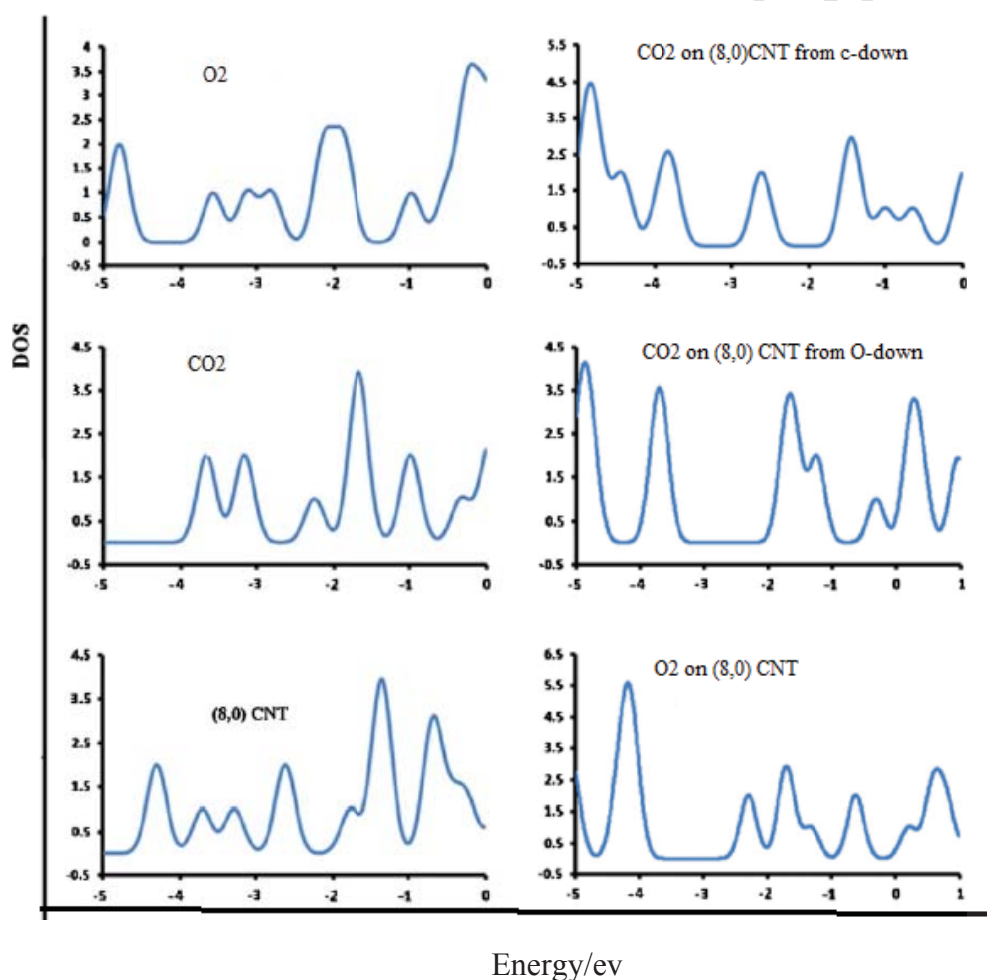


Fig 1; Total density of state (TDOS) for different models of the CNTs



References:

- [1] S. Ijima, Nature 354 (1991) 56–58.
- [2] V. Derycke, R. Martel, J. Appenzeller, Ph. Avouris, Appl. Phys. Lett. 80 (2002) 2773.
- [3] C. Liu, Y.Y. Fan, M. Liu, H.T. Cong, H.M. Cheng, M.S. Dresselhaus, Science 286 (1999) 1127.
- [4] B. Zurek, J. Autschbach, J. Am. Chem. Soc. 126 (2004) 13079–13088.
- [5] Das TP, Han EL (1958) Nuclear Quadrupole Resonance Spectroscopy. Academic Press, New York
- [6] Baei MT, Sayyed Alang SZ, Moradi AV, Torabi P (2012) J Mol Model 18:881–889
- [7] Baei MT, Moradi AV, Torabi P, Moghimi M (2011) Monatsh Chem, 142:783–788

Quantum mechanical study of interaction between 3-methyl-2-thioxoimidazolidin-4-one and I₂ in the gas phase.

T. Hadadi^a,

^aDepartment of Chemistry, Faculty of Science, University of Zabol, Zabol, Iran

Email: Tayebhehadad@yahoo.com

Keywords: Tautomer, Complex, Interaction, Hyperthyroidism

Introduction:

Interaction of organic molecules with iodine has been widely observed in biological systems [1] especially in human's thyroid [2]. In this category, imidazoline [3], and related compounds like thioimidazoline derivatives [4] are known as iodine absorbent in human's body [5]. Methimazole, as a most important member of this group, make powerful complex with iodine. This complex can prevent the first step of biosynthesis of thyroid's hormones to prevent hyperthyroidism. As a result, each compound with powerful complex with iodine can be used as a new drug in this category. By study of structures of previous hyperthyroidism drugs, 1-methyl-2-thioxoimidazolidin-4-one (T₁) was suggested to study of its structure and complexation properties to iodine in this research.



Materials and methods:

In our researches, geometry optimizations and frequency calculations were performed using B3LYP method and 6-31+G*, 6-31++G**, 6-31+G(2d,2p) and 6-31++G** basis sets and NBO analysis of all tautomers were calculated using B3LYP/6-31++G** level of theory. All optimizations, frequency calculations and NBO analyses were carried out using the Gaussian



03 program package. All results of frequency calculations have been corrected with appropriate scaling factor. AIM analyses were performed using AIM2000 program. This method has been presented useful information about intermolecular interactions and characterization of bonds through the analysis of the electron density.

In this research, molecular parameters, relative energies) and vibrational frequencies of DFT, AIM and NBO analysis of 3-methyl-2-thioxoimidazolidin-4-one and tautomers (T_1 - T_5) in Interaction with Iodine and its tautomer and the properties of their complexes with iodine have been calculated to determine the capability of this molecules in interaction with iodine and treatment of hyperthyroidism.

Result and discussion:

Calculated Gibbs free energy values showed that T_1 is the most stable tautomer in the gas phase. The NBO indicates that the sum of $E^{(2)}$ terms corresponding to the delocalization of N_2 and N_4 lone pairs to the NBO acceptors in the thione tautomer is greater than its value in the thione tautomer. As mentioned, the experimental results indicate that two T_1 (thione)- I_2 stereoisomeric complexes can be formed. The S-I distance in the planar complex (3.034) is shorter the perpendicular complex (3.156), Thus, as the I-I bond length increases the S-I distance decreases. In all methods show that the Gibbs free energy of the planar form is smaller than the perpendicular form of the thione tautomer. Therefore, the planar form is more stable than the perpendicular form of the thione tautomer in agreement with the experimental results. The result of the NBO analysis indicate that the occupation number of the $\delta^*(I-I)$ antibonding in the planar complex is greater than the perpendicular complex. In addition, it is expected that the $Lp(s)$ occupation number in the planar complex to be greater than the other complex. It seems that the second factor in the stabilizing of the planar complex with respect to the perpendicular is the interaction between S-bonded iodine lone pair with $\delta^*(N-H)$ antibonding.

Conclusion:

At the first sight, the results presented and discussed above indicate that all levels of theory the thione form of T_1 are the preferred tautomer in the gas phase. The most stable form of T_1 - I_2



(thione) complex is predicted to the planar form in agreement with the experimental results. The NBO analysis reveals that the two charge transfer interaction, $Lp(S) \rightarrow \delta^*(I-I)$ and $Lp(I) \rightarrow \delta^*(N-H)$, cause that the planar complex of T_1-I_2 to be preferred complex. AIM analysis shows that the charge density and its application at the S-I bond critical point of the planar complex are greater than the other complex. In addition, a critical point is observed at the NH-bond in the planar complex close to the hydrogen atom.

References:

- [1] H. Kohn, B. A. Kohn, M. L. Steenberg, J. P. Buckley, J. Med. Chem. 20 (1977) 158.
- [2] C. Laurence, M. J. El-Ghomari, M. Lucon, J. Chem. Soc., Perkin Trans. 2 (1998) 1159.
- [3] A. Taurog, J. Biochem. Biophys. 24 (1996) 330.
- [4] C. Laurence, M.J. El-Ghomari, J-Y. Le Questel, M. Berthelot, R. Mokhisse, J. Chem. Soc. Perkin Trans. 2 (1998) 1545.
- [5] B. Jemec, Acta Pathol. Microbiol. Scand. A 78 (1970) 151.



DFT, AIM and NBO analysis of 4-methyl-2-thioxoimidazolidin-4-one tautomers and their complexes with iodine

T. Hadadi^a,

^aDepartment of Chemistry, Faculty of Science, University of Zabol, Zabol, Iran

Email: Tayebhadad@yahoo.com

Keywords: Tautomers, Thioimidazoline, Iodine complex, DFT, NBO, AIM

Introduction:

Interaction of organic molecules with iodine has been widely observed in biological systems [1] especially in human's thyroid [2-4]. This phenomenon has also been studied computationally in pervious researches [5,6]. In this category, imidazoline [7] and related compounds like thioimidazoline derivatives [8,9] are known as iodine absorbent in human's body [10]. Methimazole, as a most famous member of this group, can make efficient complex with iodine. This complex can prevent the first step of biosynthesis of thyroid's hormones to prevent hyperthyroidism [8-10]. As a result, each compound with powerful complex with iodine can be considered as a new drug in this category. For example, carbimazoles and propylthiouracils are prevalent drug for hyperthyroidism [10]. Generally, treatment of hyperthyroidism is done by two different mechanisms. One mechanism is coordination to iodine and prevention of electrophilic substitution of iodine on thyrosine [10] and another is coordination to metal ionic center of thyrosine peroxide and deactivating it [10]. The first mechanism was considered in this study. So that, we decided to design new molecules with high ability in making complex with iodine that can be used as a new drug for hyperthyroidism.

Method:

In the first part of our study, the structures of all isomers were optimized using B3LYP/6-31+G** and B3LYP/6-31++G** levels of theory. To reduce calculations of T5 tautomer, only



Z geometric isomers were considered for OH group and two geometric isomers (E, Z) were considered only for SMe group. In addition, for the most stable isomer of each tautomer, its complex with iodine molecule was designed and optimized with both above levels of theory to find the most stable structure for each complex.

Result and discussion :

The relative stability (enthalpy and Gibbs free energy) of other tautomers and geometric isomers obtained from B3LYP/6-31++G** of theory is found to be as: T3Z>T3E>T2Z>T2E>T4Z> T5Z>T4E>T5E. Moreover, the relative stability of complexes is found to be as: T1-I2>T3-I2>T4-I2>T2-I2>T5-I2. These results show that although T4 isomers are less stable than T2 isomers, but a T4-I2 complex is more stable than T2-I2 complex. This observation is raised from the higher ability of thione tautomers (in T4) in formation of complex with iodine. One of the important results obtained from NBO calculations is orbital occupancies and another is acceptor-donor interactions.

Conclusion:

In the other words, the relative stability of tautomers found to be as: T1>T3Z>T3E>T2Z>T2E>T4Z>T5Z>T4E>T5E and also the relative stability of complexes is found to be as: T1-I2>T3-I2>T4-I2>T2-I2>T5-I2. Then, NBO calculations were done for tautomers and complexes to obtain atomic charges, occupation numbers and acceptor-donor interactions. These results confirm ability of MTIO tautomers in formation of complex and show that the planar complexes have more effective interaction than perpendicular complexes. Finally, The AIM analyses were done on complexes to prove them and obtain complexation properties. These calculations show the interaction between sulfur atom and iodine with low electron density and π bond character. The interaction of tautomers with iodine is more powerful in planar complexes versus perpendicular complexes.

References:

- [1] Kohn H., Kohn B.A., Steenberg M.L., Buckley J.P. J. Med. Chem. – 1977. – **20**, – P. 58–64.



- [2] Laurence C., Elghomari M.J., Lucon M. J. Chem. Soc. Perkin Trans. 2, – 1998. – P. 1159-1162.
- [3] Laurence C., Elghomari M.J., Berthelot M. J. Chem. Soc. Perkin Trans. 2, – 1998, – P. 1163-1167.
- [4] Laurence C., Elghomari M.J., Lequestel J.Y., Berthelo M, Mokhlisse R. J. Chem. Soc. Perkin Trans. 2, – 1998. – P. 1545-1551.
- [5] Roohi H., Ebrahimi A., Habibi S.M. THEOCHEM, – 2004. – **710**, – P. 77-82.
- [6] Papayannis D.K., Kosmas A.M. THEOCHEM, – 2008. – **851**, – P. 175-179.
- [7] Taurog A. J. Biochem. Biophys. – 1996. – **24**, – P. 330-337.
- [8] Raper E.S., Creighton J.R., Oughtred R.E., Nowell I.W. Acta Cryst. B, – 1983. – **39**, – P. 355-361.
- [9] Laurence C., Elghomari M.J., Lequestel J.Y., Berthelot M., Mokhlisse R. J. Chem. Soc. Perkin Trans. 2, – 1998. – P. 1553-1557.
- [10] Jemec B. Acta Pathol. Microbiol. Scand. A, – 1970. – **78**, – P. 151-155.



New grafted zigzag (10,0) carbon nanotubes with two phosphoramides

Z. Shariatinia*, E. Jalali Moghadam, Amir Ahmadi Ashtiani

Department of Chemistry, Amirkabir University of Technology (Polytechnic),

P. O. Box: 159163-4311, Tehran, Iran. (E-mail: shariati@aut.ac.ir)

Keywords: Phosphoramide, Carbon nanotube, ab initio calculations, NQR

Introduction:

Up to now, numerous studies have been carried out to investigate the various properties of carbon nanotubes (CNTs) [1]. Numerous computational and experimental studies have been dedicated to the investigations of the synthesis, properties and applications of the tubular structures of both carbon and non-carbon compounds [2]. Recently, the effect of one –OH group attached on the wall of the tube on electronic properties of SWCNT was studied using DFT method [3].

Computational details:

The structures of zigzag (10,0) carbon nanotube and compounds **1** and **2** were optimized in using Gaussian 98 program [4] at DFT (B3LYP and B3PW91) level of theory with standard 6-31G* basis set. The optimizations were followed by computations of the harmonic and the vibrational frequencies. Nuclear quadruple coupling constants (χ) were calculated from the equation $\chi = e^2 q_{zz} Q / h$, supposing that the electric quadrupole moments (Q) of ^2H , ^{17}O and ^{14}N nuclei are 2.860, -25.58 and 20.44 mb, respectively.

Results and discussion:

Herein, the structures of zigzag (10,0) carbon nanotube and compounds $\text{FP}(\text{O})(\text{NH}_2)_2$ (**1**) and $\text{F}_2\text{P}(\text{O})(\text{NH}_2)$ (**2**) were optimized at DFT (B3LYP and B3PW91) level of theory with standard 6-31G* basis set, Figure 1. The binding energies were measured from the equation $E(\text{bind}) = E(\text{molecule}) - \sum_i E(i)$, $i = \text{atom}$. Table 1 indicates the binding energies and dipole moments.

The results exhibit that the binding energies are more negative in grafted CNTs at both methods. Comparing the grafted CNTs with pristine CNT reveals that the hydrophilicity increases very much upon grafting. Besides, the NQCCs were computed for the ^2H and ^{14}N , ^{17}O atoms about 200-250 kHz and 4.0-5.0, 11.0 MHz, respectively.

Table 1. The stabilization energies and dipole moments of CNT and compounds **1,2**.

Compound	$\Delta E(\text{stabilization})/\text{kcal.mol}^{-1}$		Dipole moment/Debye	
	B3LYP	B3PW91	B3LYP	B3PW91
Zigzag (10,0)-CNT	-20858.599	-21314.291	1.495	1.942
FP(O)(NH₂)₂ (1)	-21521.037	-22006.711	8.915	9.351
F₂P(O)(NH₂) (2)	-21357.617	-21845.679	2.624	2.752

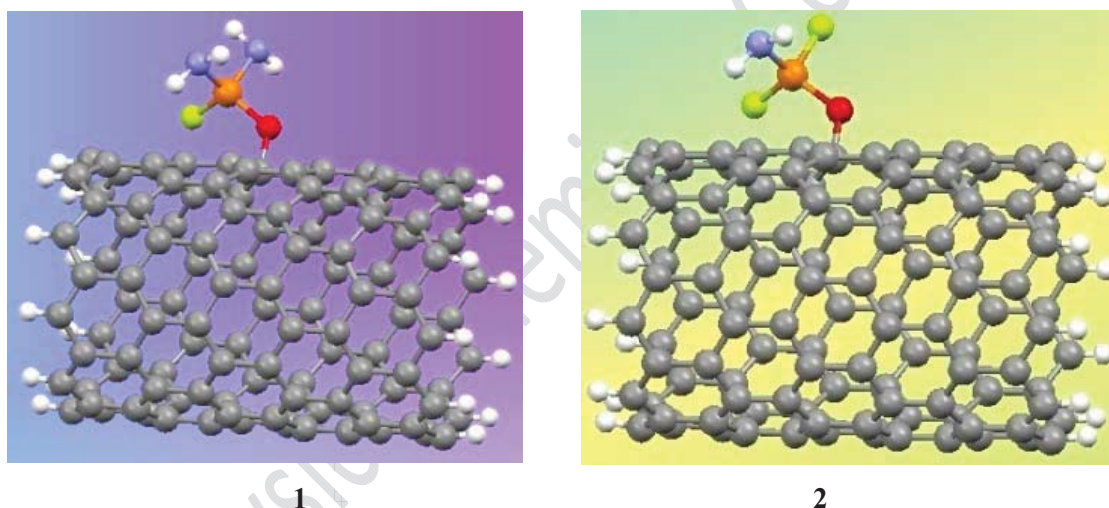


Figure 1. The optimized structures of compounds FP(O)(NH₂)₂ (**1**) and F₂P(O)(NH₂) (**2**).

Conclusion:

The structures of a zigzag (10,0) carbon nanotube and CNT-grafted phosphoramides **1** and **2** were optimized at DFT (B3LYP and B3PW91) level of theory with standard 6-31G* basis set. Results revealed that the grafted CNT becomes more stable and its hydrophilicity increases greatly. In addition, the NQCCs were computed for the ^2H and ^{14}N , ^{17}O atoms about 200-250 kHz and 4.0-5.0, 11.0 MHz, respectively.



References:

- [1] S.K. Smart, A.I. Cassady, G.Q. Lu, D.J. Martin, Carbon 44 (2006) 1034.
- [2] L. Adams, A. Oki, T. Grady, H.M. Whinney, Z. Luo, Physica E 41 (2009) 723.
- [3] H. Pan, Y.P. Feng, J.Y. Lin, Phys. Rev. B 70 (2004) 245425
- [4] M.J. Frisch, et al., Gaussian 98, Revision A9, Gaussian, Inc; Pittsburgh, PA (1998).



NQR study of two functionalized carbon nanotubes with phosphoric triamides

Z. Shariatinia*, E. Jalali Moghadam, Amir Ahmadi Ashtiani

Department of Chemistry, Amirkabir University of Technology (Polytechnic),

P. O. Box: 159163-4311, Tehran, Iran. (E-mail: shariati@aut.ac.ir)

Keywords: Carbon nanotube, Phosphoric triamide, Ab initio calculations, DFT

Introduction:

Carbon nanotubes (CNTs) are considered as the best one-dimensional model system offering excellent mechanical, electronic, and thermal properties [1]. In addition, they illustrate strong application potential in composite materials, sensing, electronics nanodevices and scanning probe microscopy. In contrast, their insolubility or poor dispersion in common solvents and polymeric matrixes is one of their disadvantages [2]. Introducing functional groups on the surface of CNTs through chemical covalent bonding is the best method to overcome these problems [3].

Computational details:

The structures of zigzag (10,0) carbon nanotube and compounds **1** and **2** were optimized using Gaussian 98 program [4] at DFT (B3LYP and B3PW91) level of theory with standard 6-31G* basis set. The nuclear quadruple coupling constants (NQCC or χ) were calculated from the equation $\chi = e^2 q_{zz} Q / h$, supposing that the electric quadrupole moments (Q) of ^2H , ^{17}O and ^{14}N nuclei are 2.860, -25.58 and 20.44 mb, respectively.

Results and discussion:

In this work, the structures of zigzag (10,0) carbon nanotube and compounds $\text{P(O)(NH}_2)_3$ (**1**) and $\text{P(O)[N(CH}_3)_2]_3$ (**2**) have been optimized using Gaussian 98 program [4] at DFT (B3LYP

and B3PW91) level of theory with standard 6-31G* basis set, Figure 1. The binding energies were measured from the equation $E(\text{bind}) = E(\text{molecule}) - \sum_i E(i)$, $i = \text{atom}$. Table 1 indicates the binding energies and dipole moments. It can be seen that at both methods the binding energies are more negative in grafted CNTs. Moreover, the hydrophilicity of phosphoric triamide grafted CNTs are enhanced greatly in comparison with pristine CNT. Furthermore, the NQCCs were computed for the ^2H and ^{14}N , ^{17}O atoms about 200-250 kHz and 4.0-5.0, 11.0 MHz, respectively.

Table 1. The stabilization energies and dipole moments of CNT and compounds **1,2**.

Compound	$\Delta E(\text{binding})/\text{kcal.mol}^{-1}$		Dipole moment/Debye	
	B3LYP	B3PW91	B3LYP	B3PW91
Zigzag (10,0)-CNT	-20858.599	-21314.291	1.495	1.942
P(O)(NH₂)₃ (1)	-21893.334	-22367.995	6.828	6.822
P(O)[N(CH₃)₂]₃ (2)	-23393.253	-23889.524	14.166	14.337

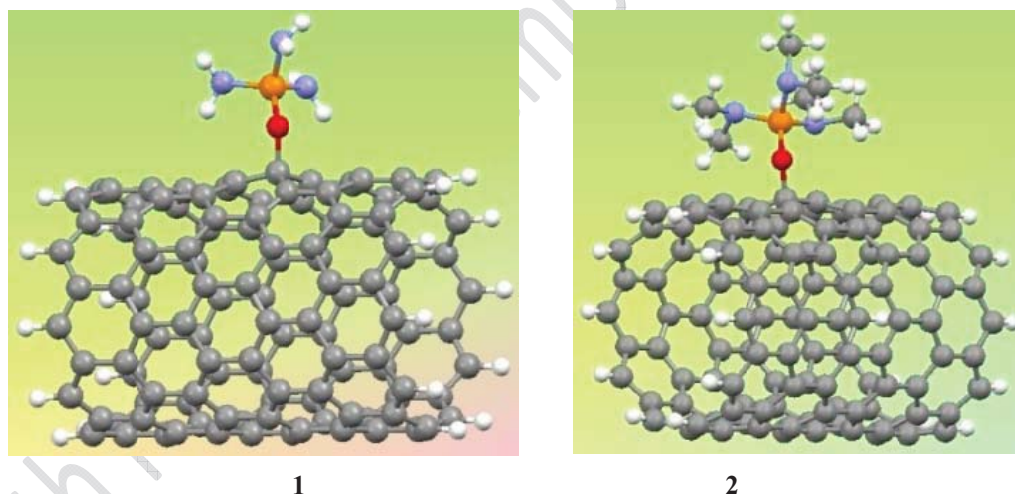


Figure 1. The optimized structures of compounds **P(O)(NH₂)₃ (1)** and **P(O)[N(CH₃)₂]₃ (2)**.

Conclusion:

The structures of a zigzag (10,0) carbon nanotube and phosphoric triamides **1** and **2** were optimized at DFT (B3LYP and B3PW91) method with 6-31G* basis set. Upon grafting, the binding energies became more negative and the hydrophilicity was enhanced greatly. Moreover,



the NQCCs were computed for the ^2H and ^{14}N , ^{17}O atoms about 200-250 kHz and 4.0-5.0, 11.0 MHz, respectively.

References:

- [1] S.T. Hu, T.W. Odom, C.M. Lieber, *Acc. Chem. Res.* 32 (1999) 435.
- [2] A. Thess, R. Lee, P. Nikolaev, H.J. Dai, P. Petit, J. Robert, C.H. Xu, Y.H. Lee, S.G. Kim, A.G. Rinzler, D.T. Colbert, G.E. Scuseria, D. Tomanek, J.E. Fischer, R.E. Smalley, *Science* 273 (1996) 483.
- [3] A. Hirsch, *Angew. Chem. Int. Ed. Engl.* 41 (2002) 1853.
- [4] M.J. Frisch, et al., *Gaussian 98*, Revision A9, Gaussian, Inc; Pittsburgh, PA (1998).



A DFT Study on Organic–Inorganic Hybrid Compound by NMR in Gas and Solvents

M. H. Ghorbani ^{a*}, R. Fazaeli ^a, A. Ghoorchian ^b

^a Department of Chemistry, Islamic Azad University - South Tehran Branch, Tehran, Iran

^b R&D Laboratory (cooperator of Institute of Standard and Industrial Research of Iran), Pakdasht Beton Company, Tehran, Iran
(Email: mh_ghorbani@azad.ac.ir)

Keywords: Hydrogen Bonding, NMR Study, Solvent Effect, Hybrid Compound.

Introduction:

As it is well known, Nuclear Magnetic Resonance (NMR) chemical shifts (δ) are closely relevant to understanding the electronic structure in a molecule. An intra- or intermolecular hydrogen bonding will result in a decrease in diamagnetic shielding around the hydrogen nucleus [1, 2]. The PCM procedure, one of the most widely used continuum dielectric methods [3] is applied to study the solvent effects on electronic structures. When using the PCM model and the DFT-based model, potential curves for electron emission can be obtained for all possible directions [4]. Inorganic compound can be introduced as ligand for organic as intermolecular complex. We investigated 1,2,4,5-Tetrazine- Sulphurous Acid (1:2) (T2SA) Complex by NMR tools (Fig 1. a) . T2SA complex is a type of the intermolecular complex between one aromatic compound and two sulphurous acid that stabilized by hydrogen bonds. We will report the NMR shielding for T2SA Complex in two solvents with the dielectric constant ranging from 1.00 to 46.70.

Methods:

The calculations carried out using Gaussian 09 program [5] with 6-311+G(d,p) basis set at the DFT method, with the Becke's three-parameter exchange functional with LYP correlation functional (B3LYP).

Results and discussion:

The formation of intermolecular hydrogen bonds, with four nitrogen atoms as donors, in the T2SA and support the behavior of the H(2), H(4), H(12) and H(13), as acceptors. In the gas phase, Methyl is donor group and strengthens hydrogen bond that realizable by nucleolus de shielding, also Fluorine is attractive group and to be shield nucleus (see Table 1.).

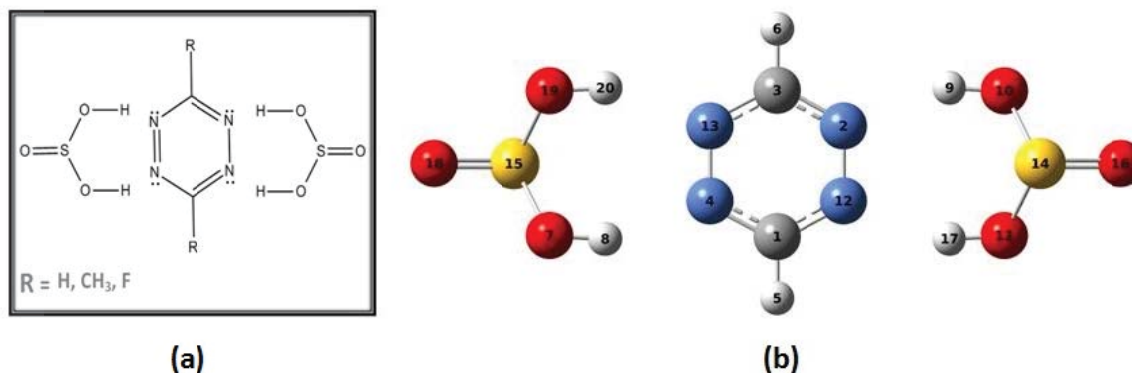


Fig 1. a) Schematic of T2SA Complex. b) Equilibrium structure of T2SA complex in the DMSO.

The dielectric constant of the solvent increases, H (8), H (9), H (17) and H (20) are more de shielded (solvent gives electrons in non-or anti- orbital of the atom and bond length is large). Note, in this all cases, two bonds are more de shielded i.e. these bonds is stronger bonds.

Table 1. Solvent Effects on nucleus shielding of T2SA complexes (ppm).

Substitution	Phase	□	H(8)	H(9)	H(17)	H(20)
H	Gas	1.00	6.3972	6.4046	6.4199	6.4289
	Benzene	2.25	7.6972	7.7437	7.7647	7.7689
	DMSO	46.70	9.0149	9.0156	9.0280	9.0292
CH₃	Gas	1.00	6.9244	6.9293	6.8819	6.8775
	Benzene	2.25	8.1283	8.1407	8.1588	8.1704
	DMSO	46.70	9.3332	9.3336	9.3703	9.3727
F	Gas	1.00	5.7015	5.7070	5.7133	5.7187
	Benzene	2.25	6.8624	6.9032	6.9228	6.8901
	DMSO	46.70	7.9216	7.9295	7.9403	7.9461



Conclusion:

The calculated results showed groups with higher donor properties strengthen the intermolecular hydrogen bond. The deshielding effects on four hydrogen of T2SA complex are referred to intermolecular force which is controlled by dielectric constants. We observed as dielectric constant increased, all of the nuclei participants in hydrogen bonds are more deshielded. When dielectric constant increases or donor group Substituted on aromatic ring, nucleus is de shield i.e. hydrogen bonds to be strengthen.

References:

- [1] A. Zielinska et al., J. Mol. Stru. 873 (2008) 109–116.
- [2] H. Zhao et al., J. Org. Chem. (2007) 72, 7071 7082.
- [3] Paulo J. Mendes et al., J. Mol. Stru. 946 (2010) 33–42.
- [4] G. Roos et al., J. Phys. Chem. A 109 (2005), 652-658
- [5] M.J. Frisch et al., Gaussian 09, Revision A.02-SMP, Gaussian Inc., (2009).

Resonance at Intramolecular Cyclization is Proven by Electron Density of Atom

M. H. Ghorbani ^{a*}, R. Fazaeli ^a, A. Ghoorchian ^b

^a Department of Chemistry, Islamic Azad University - South Tehran Branch, Tehran, Iran

^b R&D Laboratory (cooperator of Institute of Standard and Industrial Research of Iran), Pakdasht Beton Company, Tehran, Iran

(Email: mh_ghorbani@azad.ac.ir)

Keywords: Intramolecular Cyclization, Atomic Basin, Resonance, Electron Density, AIM.

Introduction:

Many researchers focused on chemistry and biological behaviors of 9H-pyrrolo(1,2-a)indol-9-one (fluorazone) and its derivatives [1]. Very recently, organic chemists have found that some 9H-pyrrolo(1,2-a)indole, directly obtained from 9H-pyrrolo(1,2-a)indol-9-one [2]. It is clearly that after and before cyclization, resonance of rings is changed. One important parameter is atomic electron density for resonance illustration. In this paper investigated AIM parameters of before and after fluorazone cyclization (Figure 1.).

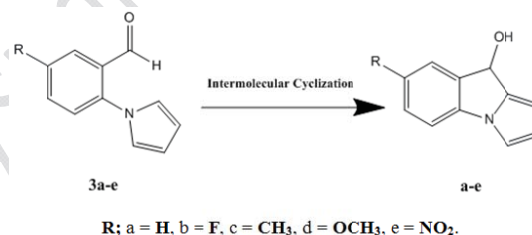


Fig 1. Schematic of cyclization reaction.

Methods:

At first, all structures has been optimized by density functional theory (DFT) method (B3LYP) and the 6-311++G** standard large basis set as implemented in the GAUSSIAN 09 [3]. Then AIM analysis has been calculated by AIM2000 [4].

Results and discussion:

The results of nitrogen atom at 3a-3e (before cyclization) and a-e (after cyclization) are presented in Table 1. When comparing the electron density of the atomic basins of nitrogen, it should be kept in mind that, this values depending on the number of aromatic rings or conjugated system. Before cyclization (3a-3e), Fluorine substitution act as donor group while Nitro substitution acts as inductive acceptor also the behavior of Methyl and Methoxy is donor. This result achieves from changes electron density respect to hydrogen substitution. Before cyclization, this discussion is very logical but all electron density values are unbalanced in after cyclization state; because between two aromatic rings, carbonyl groups does not exist. It is very self-explaining that between electron density, charge and Localization Index is excellent linear relationship.

Table 1. Results of Atomic Basin for nitrogen (before and after cyclization).

	Electron Density	Charge	Localization Index
3a	8.1898	-1.1898	6.2732
3b	8.1901	-1.1901	6.2729
3c	8.1923	-1.1923	6.2739
3d	8.1915	-1.1915	6.2750
3e	8.1896	-1.1896	6.2746
a	8.3148	-1.3148	6.4245
b	8.2079	-1.2079	6.3058
c	8.2094	-1.2094	6.3070
d	8.3145	-1.3145	6.4216
e	8.3152	-1.3152	6.4252

According to Figure 3 formation intermolecular cycle increase the electron density of nitrogen atom in all substitutions.

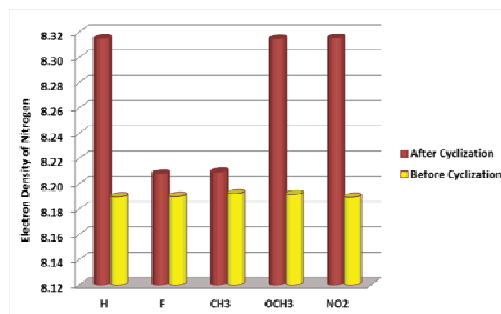


Fig 2. The Comparison Electron Density of nitrogen, Before and After Cyclization.

Conclusion:

Overall, have been investigated before and after intramolecular cyclization by atomic basin parameters, after cyclization electron density on atom is bigger i.e. resonance is stronger.

References :

- [6] V. Lisowsky et al., J. Med. Chem. 47 (2004) 1448.
- [7] F. Aiello et al. Tetrahedron 66 (2010) 274.
- [8] M.J. Frisch et al., Gaussian 09, Revision A.02-SMP, Gaussian Inc., (2009).
- [9] Biegler-Konig et al. J. AIM2000 2.0, (2002).



A novel nano Boron Nitrogen Carbon compound as an antibiotic carrier and DFT Study

H. Aghaie^a, P. Ardalan^{b*}

^a Department of Chemistry Science and Research Branch, Islamic Azad University, Tehran, Iran.

^b Science and Research Branch, Islamic Azad University, Tehran, Iran.

Email: pooran_ardalan@yahoo.com

Key words: Cefalxin, DFT Study, Antibiotic carrier, Nano Compound

Introduction:

Due to the similarity between B-N and C-C units, a lot of effort has been devoted to BN fullerene-like materials in recent years, which have excellent properties such as heat resistance, insulation, and structural stability. Several studies have been made on BN nanomaterials such as BN nanotubes, BN nanocapsules, and BN clusters since they have excellent properties such as heat resistance in air and insulation, and these nano-particles are expected to be useful as electronic devices, high heat resistance semiconductors, and insulator lubricants. From the experimental standard formation enthalpy, the energies of hybridized sp^2 and sp^3 B-N bonds are known to be stronger in comparison with those of B-B and N-N bonds, namely, 4.00, 2.32, and 2.11 eV, respectively. This research focuses on the Boron Nitrogen Carbon compound as a new compound for drug carrier.

Computational details:

The Boron Nitrogen Carbon compound and Cefalexin were geometrically optimized using GAUSSIAN 03 with density functional theory using B3LYP method and 6-31G, 6-31G** and 6-311G** basis sets. Relative energies (ΔE), enthalpies (ΔH), entropy (ΔS) and free Gibbs energies (ΔG) were calculated using thermodynamic analysis.

Result and Discussion:



In the present study, Boron Nitrogen Carbon nano compound with Cefalexin molecule is considered. All calculations were performed to study the relative stability of Boron Nitrogen Carbon nano compound especially thermodynamic properties. We selected a particular nano compound in this study. As follow antibiotic molecule was stuck to Boron Nitrogen Carbon nano compound through nitrogen atom. Then stability of these novel structures was reviewed. The values of the HOMO, LUMO, and HOMO–LUMO gap, for, nano carrier, Cefalexin and nano carrier / Cefalexin show that the Boron Nitrogen Carbon nano compound HOMO–LUMO gap value of 0.15887 decreasing by attach of Cefalexin.

Conclusion:

The interaction of Cefalexin, with Boron Nitrogen Carbon nano compound is investigated by DFT calculations at different basis sets in gas phase. Boron Nitrogen Carbon nano compound can act as a suitable drug delivery vehicle for internalization, transportation and translocation of Cefalexin within biological systems. Thermodynamical analysis indicates that the relative energies (ΔE), enthalpies (ΔH) and free Gibbs energies (ΔG) are negative for Boron Nitrogen Carbon nano compound / Cefalexin systems, but the calculated entropies (ΔS) are positive, suggesting thermodynamic favorability for covalent attachment of Penicillin and Cefalexin into Boron Nitrogen Carbon nano compound.

Reference:

- [1]. Chopra, N. G.; Luyken, R. J.; Herrey, K.; Crespi, V. H.; Cohen, M. L.; Louie, S. G.; Zettl, A. *Science*. **1995**, 269, 966.
- [2]. Blase', X.; Rubio, A.; Louie, S. G.; Cohen, M. L. *Europhys. Lett.* **1994**, 28L, 335.
- [3]. Chopra, N. G.; Luyken, R. J.; Cherrey, K.; Crespi, V. H.; Cohen, M. L.; Louie, S. G. *Science*. **1995**, 269, 966.
- [4] Zhukovskii, Y.; Sergei Piskunov, N.; Baiba, B.; Laima, T.; Stefano, B. *J. Phys. Chem. Solids* **2009**, 70, 796–803



B₅N₅C₈H₁₈ nano cluster as a novel material for drug delivery

P. Ardalan^{a*}

a Science and Research Branch, Islamic Azad University, Tehran, Iran.

Email: pooran_ardalan@yahoo.com

Key words: B₅N₅C₈H₁₈, Penicillin, DFT, Drug delivery.

Introduction:

Heterofullerenes became a subject of research interest soon after the establishment of fullerene research itself. The fullerenes containing boron and/or nitrogen atoms represent one distinguished class, though other elements have been combined with the fullerenes too. Boron nitride (BN) is a synthetic III-V compound with extraordinary mechanical, thermal, electrical, optical, and chemical properties widely applied for technological purposes. Since BN units are isoelectronic with hexagonal BN possessing a graphene-like layered structure, BN becomes the natural candidate to form heterofullerenes, which results in a certain isomorphism. BN crystalline samples were synthesized at room temperature and atmospheric pressure as structures containing hexagonal sp²-bonded sheets isomorphic with graphene.

Several studies have been made on BN nanomaterials such as BN nanotubes, BN nanocapsules, and BN clusters since they have excellent properties such as heat resistance in air and insulation, and these nano-particles are expected to be useful as electronic devices, high heat resistance semiconductors, and insulator lubricants. Since the thermodynamic conditions for growth of BN nanotubes from nuclei are still not well-defined, comprehensive theoretical simulations on these nanotubes continue to attract enhanced attention, and the lack of theoretical thermodynamic data precludes a more detailed analysis. This investigation focuses on the B₅N₅C₈H₁₈ cluster as a new material for drug delivery.

Computational details:

Calculations were performed using an all-electron linear combination of atomic orbitals Hatree–Fock (HF) and density functional theory (DFT) calculations using the Gaussian 03



package. We have geometric optimization calculation at the HF/6-31G, HF/6-31G**, HF/6-311G**. We have also performed a geometric optimization calculation at the B3LYP/6-31G, B3LYP/6-31G** and B3LYP/6-31G** level. The NMR isotropic shielding constants were calculated using the standard GIAO (Gauge-Independent Atomic Orbital) approach of Gaussian 03 program package.

Result and discussion:

We studied $B_5N_5C_8H_{18}$ cluster as a novel material for drug delivery. Before and after connecting the Penicillin to $B_5N_5C_8H_{18}$, NMR calculations were performed in electric field of charges.

The results show that Penicillin connect stronger to $B_5N_5C_8H_{18}$ cluster in negative charges than positive charge. Thus by creating negative field, Penicillin can be connected to the $B_5N_5C_8H_{18}$ cluster and delivered easily by using a positive field. So we found $B_5N_5C_8H_{18}$ is a novel material for drug delivery.

Conclusion:

The interaction of the penicillin molecule inside of the $B_5N_5C_8H_{18}$ have been investigated with density functional theory. We also analyze the electronic structure and charge Mulliken population for the energetically most favorable complexes. Our results indicate penicillin can form stable bindings with $B_5N_5C_8H_{18}$ via the nitrogen active site. Also the NMR shielding tensors have been investigated. Thus, we arrive at the prediction that the $B_5N_5C_8H_{18}$ can be implemented as a novel material for drug delivery applications.

Reference:

- [1] M. Monajjemi and et al; "Theoretical Description of Electromagnetic Nonbonded Interactions of Radical, Cationic, and Anionic $NH_2BHNBNH_2$ Inside of the $B_{18}N_{18}$ Nanoring"; Journal of Physical Chemistry. C ; 114, 15315–15330, 2010.
- [2] M. Monajjemi et al; " Interaction of Na, Mg, Al, Si with Carbon Nanotube (CNT): NMR and IR Study"; Russian Journal of Inorganic Chemistry; 54, 1465-1473, 2009.



[3]F. Zhukovskii F and etal;" Ab initio simulations on the atomic and electronic structure of single-walled BN nanotubes and nanoarches"; Journal of Physical Chemistry Solids; 70, 796-803,2009.

15th Physical Chemistry Conference



Theoretical studies on tautomerism of 4-Hydroxycoumarin derivatives in gas phase and solution

Zeinab dalirnasab^{a,b}, Ali Reza karimi^a, Sudabeh dalirnasab^c, Abbas Ali Nikseresht^d.

^a Department of chemistry, university of arak. Arak Iran.

^b Payamnoor university. Jahroom. Iran.

^c Department of chemistry, university of shiraz. Shiraz Iran.

^d department of Nasb niroo company.

Email: dalirnasab @gmail.com

Abstract:

The chemical properties of 4-Hydroxycoumarin derivatives have been extensively studied. The relative stability of three tautomers in the gas phase and solution (using PCM model) are evaluated by using DFT method. The variation of dipole moments and charges on atoms with change of solvent is also studied.

Key words: Tautomerism, 4-Hydroxycoumarin, DFT, PCM, NBO.

Introduction :

4-Hydroxycoumarin derivatives as warfarin, acenocoumarol and phenprocoumon have been the mainstay of oral anticoagulation therapy for 20 years [1]. Several coumarin derivatives have pronounced medicinal value as antibacterial and antifungal agents [2,3]. Others display antitubercular activity [4] or show insecticidal properties [5].

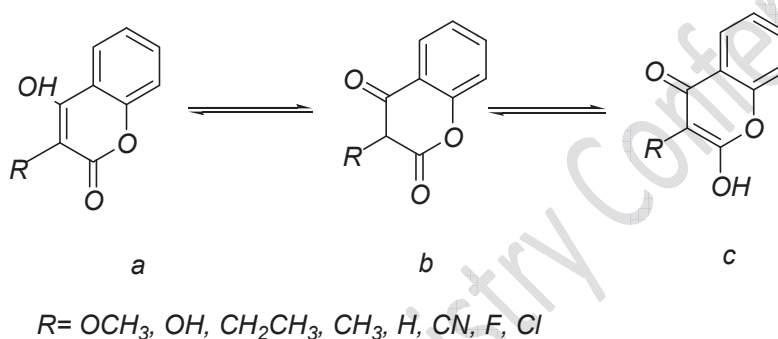
Computational details:

Full geometry optimizations are accomplished by means of hybrid functional B3LYP and the 6-31+G** basis set, as implemented in Gaussian 03. The tautomers were also optimized in polar solvents, and their effects have been considered by using a relatively simple self-consistent reaction field (SCRF) method based on polarizable continuum model (PCM) of

Tomasi. The electronic structures of stationary points were analyzed by the natural bond orbital (NBO) method.

Results and discussion:

Three tautomers of compounds a-c, presented in Fig.1 were considered in our study. 4-Hydroxycoumarin can exist as two tautomeric forms (E and K) in equilibrium.



The results of our calculations suggest that in the gas and solution phase the stability order is $a > b > c$. In addition this equilibrium depends on nature of substituents at position of 3. The order of dipole moments is $a < b < c$ in the gas phase and in solution.

Reference:

- [1] Hirsh, J.; Dalen, J. E.; Anderson, D. R.; Poller, L.; Bussey, H.; Ansell, J.; Deykin, D. *Chest* 8S.(2001) 119.
- [2] R. B. Moppett, *J. Med. Chem.* 7 (1964) 446.
- [3] G. Redighiero, C. Antonello, *Bull. Chim. Farm.* 97 (1958) 592.
- [4] C. R. Merchant, A. S. Gupita, P. J. Shah, S. S. Shirali, *Chem. Ind.* (1979) 351.
- [5] R. S. Mali, S. N. Yeola, B. K. Kulkarni, *Indian J. Chem.* 22B (1983) 352.



Calculation of Cl^- -Ar Potential Energy and Mobility of Cl^- Through Ar

A. Abedi^{*a}, M. Gharibi^b, L. Sattar^c

^a Islamic Azad University, Shahreza Branch, abedi@iaush.ac.ir

^b National Petrochemical Company-Research & Technology Co. (NPC-RT), m.gharibi@npc-rt.ir

^c Islamic Azad University, Shareza Branch, Young Research Club, sattar_l2000@yahoo.com

Keywords: Interaction potential, $\text{Cl}^- \dots \text{Ar}$ Complex, Ion Mobility

Introduction :

The interaction of halide ions with gaseous atoms or molecules is of considerable applied interest in the study of plasmas, gas discharges, transport of ions through the drift gas and photo dissociation in regions of the upper atmosphere. A clear understanding of such experiments requires accurate knowledge of the potential energy functions. Interactions between the closed-shell halide anions and the rare gas atoms are among the best-studied prototypes for understanding the details of ion-neutral forces [1-3]. In this work, the experimental measurements and theoretical calculations of the ion mobility coefficients of halide ions in noble gases are extended in a manner that allows comparison of theoretical and experimental mobility to serve the accuracy of ab initio potential data used in the calculations. The feasibility of these procedures is demonstrated with application of Cl^- halide ion in Ar noble gas.

Methods:

We calculated the $\text{Cl}^- \dots \text{Ar}$ potential energy curve at the CCSD(T)/different basis sets high level of theory by using the Gaussian 2009 package. Program PC is designed to work with uses a spline fit of the tabulated potentials for atomic ion-atom systems (Fig. 1) where it varies as the inverse fourth power and to calculate transport cross sections. The cross sections were calculated from the best data of interaction

potential energy and then were used in program GC (Gram-Charlier approach) to compute the transport coefficients for the ion mobility in an electrostatic field.

Results and discussions :

The ion mobility of chloride ion in argon drift gas was obtained via theoretical calculations was compared with the theoretical and experimental ion mobilities reported on different references in Fig. 2. According to the results the calculated ion mobilities from the level of theory CCSD(T)/aug-CC-pV5Z for $\text{Cl}^- \dots \text{Ar}$ had a good agreement with other references.

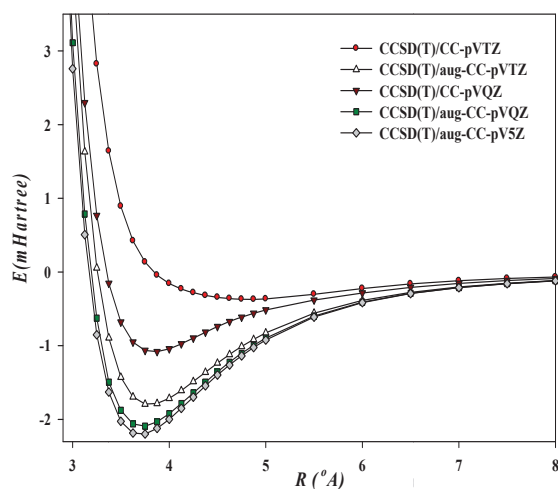


Figure 1: interaction potentials for $\text{Cl}^- \dots \text{Ar}$ systems

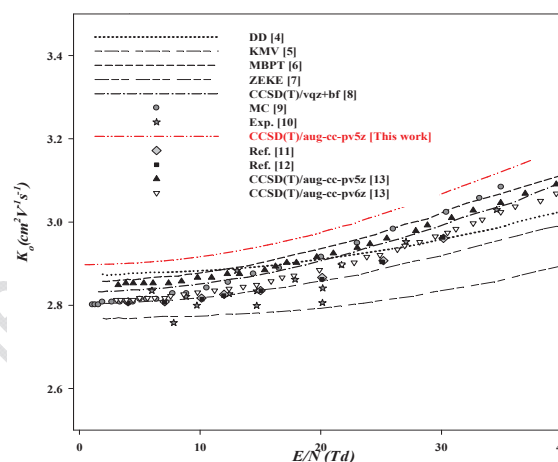


Figure 2: Ion mobility vs. E/N from this work and other references

Conclusions:

We calculated interaction potential potentials for the $\text{Cl}^- \dots \text{Ar}$ system by using several methods and basis sets. The potential curve was obtained by using of aug-CC-p V5Z basis set and coupled cluster CCSD(T) correlation method predicted ion mobility values that are comparable with experimental data. Excellent agreement between transport data derived from this potentials and experimentally reported values [4-13] has been demonstrated, leading us to conclude, the present potential is a good approximation for these systems.



References:

- [1] Kita, A.; Noda, K.; Inouye, H., J. Chem. Phys. 64 (1976) 3446.
- [2] Diercksen, G. H. F.; Sadlej, A. J.; Chem. Phys. Lett.; 156 (1989) 269
- [3] Bera, N. C.; Das, A. K.; Chem. Phys. Lett . 460 (2008) 319.
- [4] C. C. Kirkpatrick, L. A. Viehland, Chem. Phys. 98 (1985) 221-231
- [5] A. D. Koutselous, E. A. Mason, L. A. Viehland, J. Chem. Phys. 93 (1990) 7125-7136
- [6] V. Kellö, A. J. Sadlej Chem. Phys. 157 (1991) 123-133
- [7] T. Lenzer, I. Yourshaw, M. R. Furlanetto, G. Reiser, D. M. Neumark, J. Chem. Phys. 110(1999) 9578-9586
- [8] A. A. Buchachenko, R. V. Krems, M. M. Szcześniak, Y.D. Xiao, G. Chalasiński, J. Chem. Phys. 114 (2001) 9919-9928
- [9] Z. Lj. Petrović, J. V. Javonović, V. Stojanović, Z. M. Raspopović, Z. Ristivojević, Eur. Phys. J. D 48 (2008) 87-94
- [10] M. G. Thackston, F. L. Eisele, W. M. Pope, H. W. Ellis, I. R. Gatland, E. W. McDaniel, J. Chem. Phys. 70(1979) 3996-3997
- [11] W. Ellis, R. Y. Pai, E. W. McDaniel, E. A. Mason, L. A. Viehland, At Data Nucl. Data Tables, 17(1976) 177-210
- [12] H. W. Ellis, E. W. McDaniel, D. L. Albritton, L. A. Viehland, S. L. Lin, E. A. Mason, At. Data Nucl. Data Tables, 22 (1978) 179-217
- [13] C. D. Withers, T. G. Wright, L. A. Viehland, L. Grossman, C. C. Kirkpatrick, E. P. F. Lee, J. Chem. Phys. 135 (2011) 024312-024311



Stereoelectronic interaction effects on the conformational properties of 2-halo-2-oxo-1, 3, 2-dioxaphosphorinanes and their S, Se analogues

F. Azarakhshi^{*a}, N. Farhadyar^a, N. Masnabadi^b, E. Pournamdari^c

^aDepartment of Chemistry, Varamin-Pishva Branch, Islamic Azad University, Varamin, Iran

(E-mail address: fa_azarakhshi@iauvaramin.ac.ir)

^bDepartment of Chemistry, Roudehen, Branch, Islamic Azad University, Roudehen, Iran

^cDepartment of Chemistry, Islamshahr branch, Islamic Azad University, Islamshahr, Iran

Keywords: Dioxaphosphorinanes, NBO, Stereoelectronic, Anomeric effects, DFT, Conformational analysis

Introduction:

1, 3, 2-Dioxaphosphorinanes are an important class of organophosphorus heterocycles, which continue to attract considerable interest due to their unique stereochemical features and diverse potential biological applications. Six membered ring phosphates are interesting systems from the conformational point of view since there are several electronic effects, as the endo- and exo anomeric effects, that can play an important role in the conformational preferences of the substituents on phosphorus [1]. There is no published experimental or quantitative theoretical data about the donor-acceptor delocalization effects on the conformational properties of 2-halo-2-oxo-1, 3, 2-dioxaphosphorinanes. In this work, the stereoelectronic interaction effects, dipole-dipole interactions and also the conformational and structural properties of 2-flouro-2-oxo-1,3,2-dioxaphosphorinanes (1) [its analogues containing S (2) and Se (3) atoms], 2-choloro-2-oxo-1,3,2-dioxaphosphorinanes (4) [its analogues containing S (5) and Se (6) atoms] and 2-bromo-2-oxo-1,3,2-dioxaphosphorinanes (7) [its analogues containing S (8) and Se (9) atoms] have been investigated computationally using both ab initio MO and DFT methods.

Computational details:



Ab initio calculations were carried out using molecular orbital (MP2/6-311+G**) and density functional theory (B3LYP/6-311+G**) and (HF/6-311+G**) based methods with the GAUSSIAN 09 package of programs. An NBO analysis was performed for the axial and equatorial conformations of compounds 1-9 by the NBO 5.0 program contained in the PC-GAMESS interface.

Results and Discussion:

The methods used showed that these compounds exist predominantly in the axial chair conformation. The calculated Gibbs free energy difference (ΔG_{eq-ax}) values increase from compound 1 to compound 3, compound 4 to compound 6 and also from compound 7 to compound 9. There is good agreement between the calculated (ΔG_{eq-ax}) values by using B3LYP/6-311+G** and HF/6-311+G** levels of theory which is in agreement with reported NMR data [2, 3]. The NBO analysis of donor-acceptor interactions showed that the summations of the GAE and GE also increases from compound 1 to compound 3, compound 4 to compound 6 and also from compound 7 to compound 9. These findings led to the proposal that the calculated GAE values due to donor→acceptor hyperconjugation effects are more significant for the explanation of the conformational preferences of compounds that have been studied than the electrostatic interactions.

Conclusion:

The B3LYP/6-311+G** and HF/6-311+G** results showed the axial preference in these compounds. The DFT calculations reported and NBO analysis provided a reasonable picture from energetic, structural, bonding and stereoelectronic points of view for the conformational preference in compounds 1-9.

References:

- [1] W.G. Bentrude, E. Juaristi, Ed., *Conformational Behavior of Six Membered Rings. Analysis, Dynamics and Stereoelectronic Effects*; VCH: New York, 1995, 245–293.
- [2] Z. Domínguez, M. Galván, M.T. Cortez, M. Salas, R. Meza, M.A. Leyva-Ramirez and B. Gordillo, *Tetrahedron*, 2010, 66, 2066–2067.



[3] J. Herná'ndez, R. Ramos, N. Sastre, R. Meza, H. Hommer, M. Salas and B. Gordillo, *Tetrahedron*, 2004, 60, 10927–10941.

A study of the exchange and correlation energy of thiocyanate ion: DFT calculations within the symmetrized Kohn-Sham formalism

Gh. Ebrahimzadeh Rajaei^{a*}, M. Aghaie Khafri^b

^a Ph. D. student, Department of Chemistry, Research and Science Branch, Islamic Azad University, Tehran, Iran

^b Faculty of Chemistry, North Tehran Branch, Islamic Azad University, Tehran, Iran

Email: Farzad_Rajaei@yahoo.com

Keywords: Thiocyanate ion, DFT, Kohn-Sham theory, Exchange energy, Correlation energy

Introduction:

one of the most successful theories introduced in theoretical chemistry is density functional theory (DFT). Its foundations were established in the mid-1960s in two seminal articles by Hohenberg and Kohn [1] and Kohn and Sham [2]. The first proved rigorously that all physical observables-such as the ground state energy-can be written as functionals of the electronic density. This is a nontrivial statement and quite surprising at first sight. To completely describe the ground state of a many-body system one does not require knowledge of the complicated many-body wave function, but only that of a simple three-dimensional function: the density [3]. In the second article, Kohn and Sham introduced a scheme to obtain the density from the solution of a fictitious noninteracting electronic system.

Computational methods:

In this work we evaluated various energies of thiocyanate ion such as kinetic, exchange and correlation energy by using various density functional theory (DFT) applying the more cost-effective Pople-type basis set of 6-31G(d). The methods examined include the local density functional (SVWN), the pure gradient-corrected density functionals (BLYP and BPW91), and



the hybrid density functionals (B3LYP, B1LYP, B3PW91, BHandHLYP, B3P86, BPW91, BP86 and mPWP85).

Results and discussions:

We should clarify that there are inherent differences between the exchange-correlation energy that appears in the Kohn-Sham formalism and their namesakes, the exchange and correlation energies, as they are defined within the Hartree-Fock picture.

The Kohn-Sham exchange energy is given by:

$$E_x^{KS} = \frac{1}{2} \iint \frac{\rho_0(\vec{r}_1) h_x^{KS}(\vec{r}_1, \vec{r}_2)}{r_{12}} d\vec{r}_1 d\vec{r}_2 \quad (1)$$

where $\rho_0(r_1)$ and $h_x(r_1; r_2)$ are exact density and Fermi hole respectively. We know that E_{xc} as defined in the framework of Kohn-Sham theory also accounts for T_c , the difference between the kinetic energy of the real, T , and the kinetic energy T_s related to the non-interacting reference system, as below:

$$E_{xc}[\rho] = \{T[\rho] - T_s[\rho]\} + E_{ncl}[\rho] = T_c[\rho] + E_{ncl}[\rho] = E_x[\rho] + E_c[\rho] \quad (2)$$

The summarized computational results are shown in table 1.

Table 1. Energy components in hartrees for several methods

Functional	E_{total}	$E_x[\rho]$	$T_s[\rho]$	$E_{xc}[\rho]$
B3LYP	-491.0995	-0.7137	488.9584	-1.1163
BLYP	-491.0600	-1.2253	488.7594	-1.6279
SVWN	-489.5291	1.1100	488.0710	0.7074
BP86	-491.1289	-1.1737	488.7467	-1.5763
BPW91	-491.0906	-0.9597	488.7852	-1.3623
B3P86	-491.6480	-1.0164	488.9986	-1.4190
B3PW91	-491.0098	-0.4455	488.9677	-0.8481
mPWP85	-491.1337	-1.1342	488.7501	-1.5368
G96PW91	-491.1049	-0.8803	488.8289	-1.2829
BHandHLYP	-491.0246	-0.2134	489.3072	-0.6160
B1LYP	-491.0400	-0.6588	489.0354	-1.0614

Conclusion:

The obtained computational results indicated that usually the exchange contributions are significantly larger in absolute numbers than the corresponding correlation effects. Therefore,



an accurate expression for the exchange functional in particular is a prerequisite for obtaining meaningful result from density functional theory.

References:

- [1] P. Hohenberg and W. Kohn, Phys. Rev. 136, B864 (1964).
- [2] W. Kohn and L.J. Sham, Phys. Rev. 140, A1133 (1965).
- [3] I. I. Zakharov, Journal of Structural Chemistry, 52(3), 445-453 (2011).

15th Physical Chemistry Conference

Comparison of theoretical methods for ab initio and DFT calculations of the frequencies of normal vibrations of thiocyanate ion

Gh. Ebrahimzadeh Rajaei^{a*}, M. Aghaie Khafri^b

^a Ph. D. student, Department of Chemistry, Research and Science Branch, Islamic Azad University, Tehran, Iran

^b Faculty of Chemistry, North Tehran Branch, Islamic Azad University, Tehran, Iran

Email: Farzad_Rajaei@yahoo.com

Keywords: Thiocyanate ion, DFT, Kohn-Sham theory, Frequencies, Normal vibrations

Introduction:

Thiocyanate (also known as rhodanide) is the anion as SCN^- . It is the conjugate base of thiocyanic acid. Thiocyanate shares its negative charge approximately equally between sulfur and nitrogen. As a consequence, thiocyanate can act as a nucleophile at either sulfur or nitrogen [1]. The thiocyanate ion is represented by two resonance structures as below:



The actual structure of a molecule in the normal quantum state has the lowest possible value of total energy. This structure is called the "resonance hybrid" of that molecule. The resonance hybrid is the approximate intermediate of the contributing structures, but the overall energy is lower than each of the contributors, due to the resonance energy [2].

Computational methods:

The dependence of the quality of calculation of the frequencies of normal vibrations on the choice of the theoretical method and the basis set of Gaussian functions [3]. In this study we used several approximation methods such as the local density functional (SVWN), the pure gradient-corrected density functionals (BLYP and BPW91), and the hybrid density functionals

(B3LYP, B1LYP, B3PW91, BHandHLYP, B3P86, BPW91, BP86 and mPWP85) using the more cost-effective Pople-type basis set of 6-31G(d).

Results and discussions:

By the DFT and ab initio methods with a 6-31G(d) basis set the frequencies of normal vibrations of thiocyanate ion have been calculated and the results within theoretical error percentage are gathered in table 1.

Table 1. The frequencies of normal vibrations of thiocyanate ion applying 6-31G(d) basis set

Methods	Out of plane bending(cm^{-1})	S-C stretching(cm^{-1})	C \equiv N stretching(cm^{-1})	error % (ν_1)	error % (ν_2)	error % (ν_3)
B3LYP	477.44	731.57	2175.47	-1.6	1.6	-5.0
BLYP	459.07	707.59	2070.76	2.4	5.0	-0.2
SVWN	476.79	766.27	2139.14	-1.4	-3.0	-3.4
BP86	461.68	726.93	2081.07	1.8	2.2	-0.7
BPW91	462.75	731.38	2087.58	1.6	1.6	-1.0
B3P86	481.21	751.35	2186.56	-2.3	-1.1	-5.5
B3PW91	480.17	749.10	2183.15	-2.1	-0.8	-5.4
mPWP85	462.26	728.48	2083.86	1.7	2.0	-0.9
G96PW91	463.35	732.19	2088.69	1.4	1.5	-1.1
BHandHLYP	498.92	749.87	2302.45	-5.8	-0.9	-10.3
B1LYP	479.98	731.47	2192.97	-2.1	1.6	-5.8
MP2	442.16	751.55	2044.36	6.3	-1.1	1.1
HF	517.37	739.34	2439.99	-9.2	0.5	-15.3
experimental	470.00	743.00	2066.00	-	-	-

The results indicated that the calculated vibration frequencies using the 6-31G(d) basis set within the framework of any of the above theoretical methods agree with the experimental data.

Conclusion:

It has been concluded that the use of the basis set 6-31G(d) within the framework of these methods with allowance for the electron correlation for calculating the frequencies of normal vibrations of thiocyanate ion is most optimum in terms of the relation between the expenditure of time and the quality of the calculation.

References :



- [1] Greenwood, N. N.; Earnshaw, A. Chemistry of the Elements. Butterworth–Heinemann, Second Edition, p. 326-328 (1997).
- [2] Linus Pauling, The nature of the chemical bond - an introduction to modern structural chemistry, Cornell University Press, Third Edition, p. 10-13 (1960).
- [3] K. V. Berezin and V. V. Nechaev, Journal of Applied Spectroscopy, 71(2), p.164 (2004)

15th Physical Chemistry Conference



An analytical potential energy surface for P₂-He dimer from ab initio calculations

S. M. Atashzar^{a*}, A. Maghari^a, M. H. Karimi-Jafari^b, Z. Rezaei^a

^aDepartment of Physical Chemistry, College of Science, University of Tehran, Tehran, Iran

^bInstitute of Biochemistry and Biophysics, University of Tehran, Tehran, Iran.

(E-mail: Mahdi.atashzar@gmail.com)

Keywords: Van der Waals complex, Intermolecular forces, P₂-He dimer, CCSD(T)

Introduction:

A new potential energy surface (PES) for P₂-He has been calculated using the supermolecular method at the Coupled-Cluster level with Single and Double plus perturbative Triple excitations [CCSD(T)], using a large basis set supplemented with midpoint bond functions. The rigid molecule approximation has been used for P₂. Ab initio calculations of the PES of Van der Waals complexes initially reproduce the PES in the form of tables of numbers, which have to be interpolated or extrapolated for desired applications. To overcome the difficulties of apply a high level post Hartree-Fock method in conjunction with an extended basis set, application of bond functions located somewhere between monomers seems to be a wise solution. The CCSD(T) PES is characterized by a global minimum of -17.209 cm⁻¹ at $R_e = 3.417 \text{ \AA}$ and $\theta_e = 116$ degree.

Computational Method:

The geometry of the P₂-He complex, in which P₂ keeps linear, is described with the Jacobi coordinates (R, θ) , where R denotes the distance from the middle of P₂ bond to the helium atom, θ denotes the enclosed angle between the vector \mathbf{R} . The PES of P₂-He was first constructed at the CCSD(T)/ aug-cc-pVTZ level [1] and then calculations continued at MP4 level by aug-cc-pVQZ basis set of Woon and Dunning for all atoms [2] plus bond functions located at the center of vdW bond. The supermolecular approach was employed to produce the

intermolecular potential and the full counterpoise procedure [3] was used to correct for basis set superposition error.

Results and discussion:

The intermolecular interaction energy between two rigid linear molecules can be expanded as follows:

$$U(R, \theta) = \sum_{LM} V_{LM}(R) P_{LM}(\theta) \quad (1)$$

where $P_{LM}(\theta)$ represents the associated Legendre polynomial. The actual calculation of coefficients $V_{LM}(R)$ can be performed by calculating for a given value of R , integration over $U(R, \theta)$ which are weighted by Legendre polynomials. The potential $U(R, \theta)$ in a grid of points such that the integrations can be carried out by numerical quadrature. Thus, the ab initio calculations were performed in a 300 points Gauss-Legendre grid for θ . The full potential is obtained by fitting the radial coefficients over the grid of R points with the following general form:

$$V_{\lambda}(R) = e^{a-bR} \sum_k g_k R^k - \sum_n \frac{C_n}{R^n} F_n \quad (2)$$

Before complete exploration of the PES, the efficiency of different computational levels was investigated by some test calculations along an angular slice of PES. Accordingly, the best compromise between accuracy and computational cost is achieved at the CCSD(T)/aug-cc-PVTZ+b level of theory and Figure 1 is its 3D PES. Our investigation shows that the global minimum of the PES is corresponded to 3.417 \AA and $\theta_e = 116$ degree. Figure 2 shows the MEP on P_2 -He PES contour plot calculated at CCSD(T)/aug-cc-PVTZ+b level of theory.

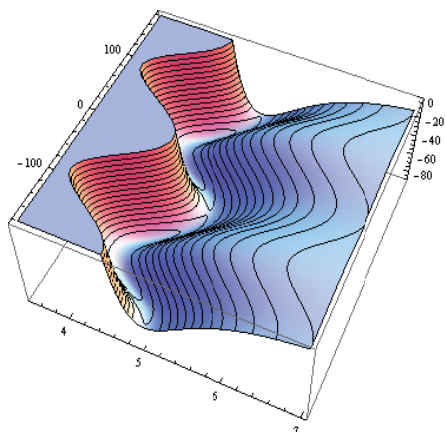


FIG. 1. PES of P₂-He.

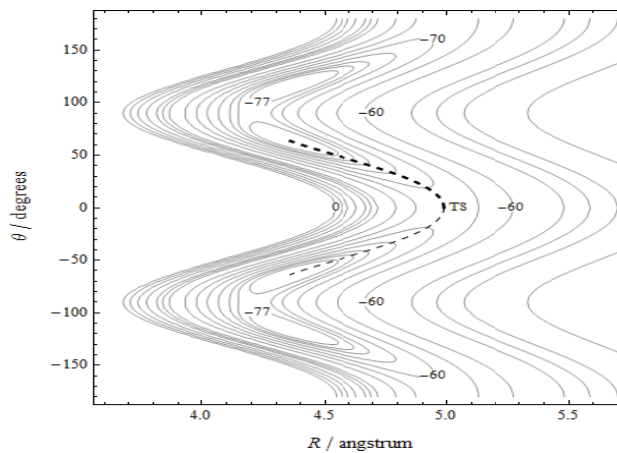


FIG. 4. MEP on contour plots for PES of P₂-He.

References :

- [1] K. Raghavachari, G. W. Trucks, J. A. Pople and M. Head-Gordon, *Chem. Phys. Lett.* **157**, 479 (1989).
- [2] D. E. Woon and T. H. Dunning, *J. Chem. Phys.* **98**, 1358 (1993).
- [3] S. F. Boys and F. Bernardi, *Mol. Phys.* **19**, 553 (1970).



Adsorption of parent nitrosamine on the nanocrystalline M-zeolite

H. Roohi, M. Jahantab*

Department of Chemistry, Faculty of Science, University of Guilan, Rasht, Iran

(E-mail: mahjoube.jahantab@yahoo.com)

Keywords: Nitrosamine, M-zeolites complexes, 10T cluster model

Introduction:

Development of modern industry causes increasingly serious pollution in the environment. Removing of pollutant materials has become important in recent years. Most of nitrosamines (NA) are carcinogenic compounds characterized with functional group of $-N=N=O$. They are widespread in environment such as cigarette smoke, bacon and diet [1-4]. In this paper, adsorption of parent nitrosamine on 10T cluster models of ZSM-5 has been investigated structurally, energetically, and topologically.

Methods:

The cluster models 10T, have molecular structure of $[AlSi_9O_{12}H_{20}]^-M^+$. In model clusters, an Al atom replaces a silicon atom and the resulting negative charge is compensated by H^+ , Li^+ and K^+ to produce M-zeolite (M = H, Li, and K) clusters. To mimic the geometry constrains of the real zeolite structure, the cartesian coordinates of boundary H atoms in clusters were held froze in all geometry optimization. The rest of the clusters have been optimized. The structures have been optimized at the B3LYP/6-311++G(d,p) level of theory using the Gaussian program package. The harmonic frequencies calculated at the same level of theory. The Zero-point vibrational energy correction (ZPE) has also been included.

Results and Discussion:

Two types of complexes have been predicted from the interaction between zeolite clusters and NA. In complexes A and B, nitrogen and oxygen atoms of NO group orient to the acidic H

atom of H-zeolite cluster, respectively. Also, the interaction between NA and M-zeolite cluster occur between O(N) atom of NA and Li(K) atom of clusters (see Fig. 1). The main interaction between NA and 10T cluster of H-zeolite occurs through hydrogen bonding. The direct interaction between the lone pair electron donor function of NA via the O and N atoms of the NO group and the electron pair acceptor function of the zeolite (i.e. H^+ , Li^+ , K^+) is the most important energetic contribution to adsorption.

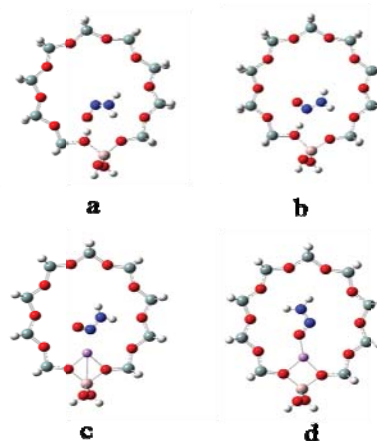
The calculated adsorption energies gathered in Table 1 as a difference between the energy of the complex and the sum of energies of its isolated constituents. As can be seen, the A complex is more stable than B in H-zeolite, while the reverse is true for M-zeolites. Also, the interaction between NA and H-zeolite is stronger than Li^+ and K^+ exchanged zeolites. On the other hand, it seems that the strength of adsorption of NA on the zeolite increases by changing from Li^+ to K^+ . Also, the zero-point and thermal binding energies correction decreases the binding energies (see Table 1).

Table 1. Binding energies ($kcal\ mol^{-1}$) at B3LYP/6-311++G(d, p) level

	ΔE_{elec}	ΔE_0^a	ΔE^b
H			
A(10T)	-16.11	-14.23	-12.07
B(10T)	-15.36	-13.33	-11.62
Li			
A(10T)	-6.59	-5.17	-2.85
B(10T)	-12.42	-10.92	-9.14
K			
A(10T)	-12.44	-10.82	-8.47
B(10T)	-12.51	-10.92	-8.62

$^a E_0 = E_{elec} + ZPE$. $^b E = E_0 + E_{thermal}$.

Fig. 1. The 10T cluster models for H-zeolite (a and b) and M-zeolites (M = Li, K) (c and d).



Conclusion:



Adsorption of nitrosamine on the ion-exchanged M–zeolites (M = H, Li and K) has been investigated using 10T cluster model at the B3LYP/6-31++G(d,p) level of theory. Two complexes were predicted from adsorption of nitrosamine on 10T cluster models of zeolites. The interaction between NA and H–zeolite is stronger than Li⁺ and K⁺ exchanged zeolites.

References:

- [1] P.N. Magee, J.M. Barnes; “The production of malignant primary hepatic tumours in the rat by feeding dimethylnitrosamine”; Br. J. Cancer; 10, 114-122, 1956.
- [2] H. Roohi, F. Akbari; “Adsorption of parent nitrosamine on the nanocrystalline H–zeolite: A theoretical study”; Applied Surface Science; 256, 7575–7582, 2010.
- [3] R.C. Shank, P.N. Magee; “Mycotoxins and N-nitroso Compounds: Environmental Risks”; CRC Press, Florida, 1, 1981.
- [4] W. Lijinsky, Mutat; “N-Nitroso compounds in the diet”; Mutat Res, 443, 129-138, 1999.



Theoretical investigation of Nitrogen mustards using quantum chemical calculation and neural network

E. Sedghamiz, E. Jamalizadeh, S.M.A. Hosseini

Department of Chemistry, Shahid Bahonar University of Kerman, Kerman 76175

Email: elahesedghamiz@yahoo.com

Keywords: Nitrogen mustards, quantum chemical study, neural network, sensitivity analysis

Introduction:

The use of chemicals to treat cancer in man began sometime around the end of World War II when it was found that nitrogen mustard and its derivatives had antitumor properties [1]. Nitrogen mustards, $\text{Cl}-\text{CH}_2-\text{CH}_2-\text{N}(\text{R})-\text{CH}_2-\text{CH}_2-\text{Cl}$, the oldest class of synthetic compounds shown to possess anticancer activity in man, have been used for the treatment of Hodgkin's disease, non-Hodgkin's lymphoma, leukemia, and multiple myeloma [2]. Neural networks and sensitivity analysis are versatile methods for a variety of tasks including analysis of structural chemical data and finding relation between them [3].

Computational details:

Molecular geometries of nine nitrogen mustard drugs that are Mechlorethamine, Melphalan, Chlorambucil, Bendamustine, Phosphoramide mustard, Cyclophosphamide, Ifosfamide, Spiromustine and Uracil mustard were fully optimized obtained at the B3LYP/6-31 ++G (d,p) level of the density functional theory in aqueous phase. All calculations are executed using the Gaussian 09 program [4]. Neural Network and Sensitivity Analysis were used to find the most correlated factor to $\log\text{GI}_{50}$ (concentration of compound needed for 50% growth inhibition). The structural and chemical properties of drugs are considered as inputs. For each drug $\log\text{GI}_{50}$ is considered as the output of the neural network.

Results and discussion:

LUMO, HOMO and E_t (total energy), dipole moments and also muliken atomic charges on Nitrogen and Chlorine atoms (atoms are shown in figure1) of drugs are obtained and also the average $\log GI_{50}$ values of them against leukemia cell lines were calculated. Because all of the drugs are widely used in chemotherapy of leukemia, leukemia cell lines were chosen to obtain average $\log GI_{50}$. Sensitivity analysis and R^2 values (correlation coefficients) reveal that E_t is the most correlated factor to $\log GI_{50}$ among other factors. To examine the results, eight sets of experimental data were fed into our model with the ninth left for assessment purposes. The near perfect match of the predicted $\log GI_{50}$ for Uracil mustard (experimental:-5.224, calculated:-5.399) meant the extrapolation of the linear model was allowed for, to extract results for the unknown quantities.

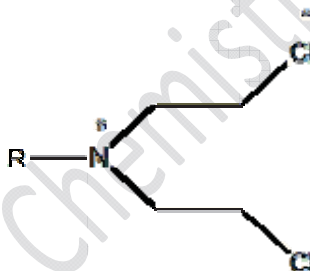


Figure 1. General structure of nitrogen mustards

Conclusion:

Quantum chemical calculations, scatter plots and sensitivity analysis show that E_t is the most correlated parameter with the cytotoxic activities ($\log GI_{50}$) of the Nitrogen mustards against leukemia cell lines compared to the other calculated and experimental data. It refers to steric effects of the drug's molecule and shows that smaller molecules are more effective drugs among Nitrogen mustard derivatives. Total energy of drug (E_t) can be used to predict the cytotoxic activity of drugs which are untested or to design a new drug which is more effective before drug synthesis in laboratory.

Reference:



- [1] J.D. Prejean and J. A. Montgomery, Structure-Activity Relationships in the Carcinogenicity of Anticancer Agents, *Drug metabolism reviews*, 15(3), 619-646 (1984)
- [2] James M. Allan, The molecular mechanisms of alkylating agent-related acute myeloid leukaemia, *Third International Symposium on Secondary Leukemias*, Rome, 3-4 November 2006
- [3] Lothar Terfloth and Johann Gasteiger, Neural networks and genetic algorithms in drug design, *genomics supplement*, DDT Vol. 6, No. 15 (Suppl.), 2001
- [4] Gaussian 09, Revision, M. J. Frisch et al, Gaussian, Inc., Wallingford CT, 2009.



Cytotoxic activity prediction of 2-chloroethylnitrosoureas using quantum chemical study and sensitivity analysis

E.Sedghamiz, E. Jamalizadeh, S.M.A. Hosseini

Department of Chemistry, Shahid Bahonar University of Kerman, Kerman 76175

Email: elahesedghamiz@yahoo.com

Keywords: 2-chloroethylnitrosoureas, quantum chemical study, neural network, sensitivity analysis

Introduction:

Alkylating agents are among the oldest class of anticancer drugs and are utilized to treat leukemia and solid tumors. They encompass a broad range of structurally diverse agents that includes nitrogen mustards, methylating agents, platinating agents and nitrosoureas[1]. Nitrosoureas differ from other members of this class in being relatively lipid soluble, non-ionized and therefore capable of crossing the blood-brain barrier. Computational biology and bioinformatics have the potential not only to speed up the drug discovery process, thus reducing the costs, but also to change the way drugs are designed [2]. Therefore, In this study, attempted has been made to expand the potential use of structural-chemical properties to the discovery of new anti-tumor agents and to use the structural-chemical properties to predict cytotoxic activity of untested drugs or design of better and more effective drugs.

Computational details:

Eight 2- Chloroethylnitrosoureas drugs that are Semustine , 88104 , Cis acid , Carmustine , PCNU , Chlorozotocin and Lomustine which have the same mechanism of action, were chosen and their molecular geometries were fully optimized, obtained at the B3LYP/6-31 ++G (d,p) level of the density functional theory in aqueous phase. All calculations were executed using the Gaussian 09 program [3]. The back propagation neural network is used here for sensitivity

analysis. The structural and chemical properties of drugs are considered as inputs. For each drug $\log GI_{50}$ (concentration of compound needed for 50% growth inhibition) is considered as the output of the neural network.

Results and discussion:

The HOMO, LUMO and E_t (total energies of drugs), dipole moments (μ) and also Muliken atomic charges of Nitrogen (q_N) and Carbon atom (q_C) (atoms are marked with * in figure 1) are obtained. In addition the chemical potential (μ), hardness (η) and electrophilicity (ω) of drugs were calculated.

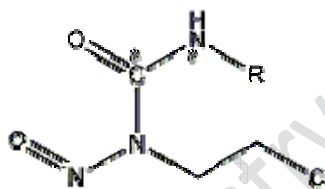


Figure1. Generic structure of 2-chloroethylnitrosoureas

Sensitivity analysis and R^2 values (correlation coefficients) reveal that muliken atomic charge on Carbon is the most correlated factor to $\log GI_{50}$ among other factors. To examine the results, six sets of experimental data were fed into our model with the seventh (Lomustine) left for assessment purposes. The near perfect match of the predicted $\log GI_{50}$ for Lomustine (experimental: -4.400, calculated: -4.337) meant the extrapolation of the linear model was allowed for, to extract results for the unknown quantities. Therefore for Nimustine which is untested in NCI, the $\log GI_{50}$ were predicted using this equation: $y = -1.069x - 4.014$

Where y is $\log GI_{50}$ and x is Muliken atomic charge on Carbon.

Conclusion:

Quantum chemical calculations, scatter plots and sensitivity analysis show that Muliken atomic charge on Carbon is the most correlated parameter with the cytotoxic activities ($\log GI_{50}$) of the 2-chloroethylnitrosoureas against central nervous system cell lines compared to the other calculated and experimental data. Muliken atomic charge on carbon can be used to predict the cytotoxic activity of drugs which are untested or to design a new drug which is



more effective before drug synthesis in laboratory. Therefore, these theoretical methods will be very profitable.

Refrence:

- [1] James M. Allan, The molecular mechanisms of alkylating agent-related acute myeloid leukaemia, Third International Symposium on Secondary Leukemias, Rome, 3-4 November 2006
- [2] Alberto Ambesi-Impiombato and Diego di Bernardo, Computational Biology and Drug Discovery, Current Bioinformatics, 2006, 1, 3-13
- [3] Gaussian 09, Revision, M. J. Frisch et al, Gaussian, Inc., Wallingford CT, 2009.

Evaluation the Anti-Bacterial Activity of Some 1,2,4-Triazole Derivatives through a Quantitative Structure Activity Relationship approach

Z. Rostami*^a and N. Afshari^a

^aDepartment of chemistry, Payame Noor University, Hamedan, Iran

E-mail: P_Rostami1978@yahoo.com

Keywords: QSAR, Genetic algorithms, MLR analysis, MIC, Triazoles derivatives

Introduction:

The steadily increasing bacterial resistance to existing drugs is a serious problem in antibacterial therapy and necessitates continuing research into new classes of antibacterials. There exist a number of 1, 2, 4 triazoles having a wide range of antibacterial activities, it following from the literature survey that depending on the type of substituent, the derivatives of triazole have a high potential for biological activity. Our study performed upon an extended series of 28 molecules of derivated of triazoles with certain minimum inhibitory concentration (MIC), that all of molecules have basic structure of triazoles but some differences in substitutions which has been shown in Figure 1 and also Table 1.

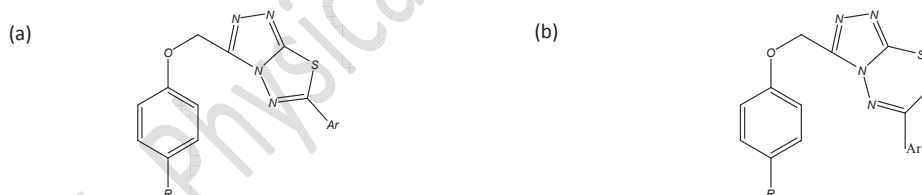


Figure 1: Basic Structures of 1, 2, 4 triazole molecules: a) 6a-s and b) 7a-i

Methods:

In the present study we aimed to develop Quantitative Structure Activity Relationship (QSAR) method for the antibacterial activity of triazoles. OPLS molecular mechanism quantum-chemical calculation was used to optimize the 3D geometry of the molecules using the HyperChem software. Dragon computer software was employed to calculate the molecular descriptors. Genetic algorithms (GA) were used as a variable selection method.



Results and Discussion:

Multiple linear regressions (MLR) were used to derive the QSAR equation. The three best QSAR models obtained with the descriptors are given below together with the statistical parameters of the regression:

Model (a):

$$\text{Log } X = -44.664 (\pm 5.864) + 3.858 (\pm 0.445) \text{ eeig11r} - 1.415 \text{ mor20e} (\pm 0.137) + 23.672 (\pm 3.043) \text{ belm2} - 1.502 (\pm 0.293) \text{ eeig12r} - 1.210 (\pm 0.373) \text{ mor18v} - 2.834 (\pm 0.879) \text{ ish}$$

$$N = 28, R^2 = 0.900, SE = 0.097, F = 28.414, Q^2 = 0.781$$

Table 1: Characterization data of compounds 1-28

compoun	Ar	R	Molecular	Molecular	Melting	Antibacteri	Antifungal	Antifunga
6a	C ₆ H ₅	SCH ₃	C ₁₇ H ₁₄ N ₄ O ₂ S	354	140	6.25	6.25	6.25
6b	2-ClC ₆ H ₄	SCH ₃	C ₁₇ H ₁₃ ClN ₄ O ₂ S	389	110	25	25	25
6c	4-CH ₃ C ₆ H ₄	SCH ₃	C ₁₈ H ₁₆ N ₄ O ₂ S	368	142	6.25	6.25	6.25
6d	4-OCH ₃ C ₆ H ₄	SCH ₃	C ₁₈ H ₁₆ N ₄ O ₂ S ₂	384	110	6.25	6.25	6.25
6e	4-NH ₂ C ₆ H ₄	SCH ₃	C ₁₇ H ₁₅ N ₅ O ₂ S	369	120	6.25	6.25	6.25
6f	2,3-(Cl) ₂ C ₆ H ₄	SCH ₃	C ₁₇ H ₁₂ Cl ₂ N ₄ O	371	106	6.25	6.25	6.25
6g	C ₆ H ₅ CH ₂	SCH ₃	C ₁₈ H ₁₆ N ₄ O ₂ S ₂	368	112	6.25	6.25	6.25
6h	C ₆ H ₅	SC ₂ H ₅	C ₁₈ H ₁₆ N ₄ O ₂ S	368	129	6.25	6.25	6.25
6i	2-ClC ₆ H ₄	SC ₂ H ₅	C ₁₈ H ₁₅ ClN ₄ O ₂ S	402	102	25	25	25
6j	4-CH ₃ C ₆ H ₄	SC ₂ H ₅	C ₁₉ H ₁₈ N ₄ O ₂ S	382	105	6.25	6.25	25
6k	4-CH ₃ O-C ₆ H ₄	SC ₂ H ₅	C ₁₉ H ₁₈ N ₄ O ₂ S ₂	398	98	25	25	25
6l	2-NH ₂ C ₆ H ₄	SC ₂ H ₅	C ₁₈ H ₁₇ N ₅ O ₂ S	383	120	25	25	25
6m	2,3-(Cl) ₂ C ₆ H ₄	SC ₂ H ₅	C ₁₈ H ₁₄ Cl ₂ N ₄ O	437	118	25	25	25
6n	2-OHC ₆ H ₄	SC ₂ H ₅	C ₁₈ H ₁₆ N ₄ O ₂ S ₂	384	185	25	25	25
6o	C ₆ H ₅	SO ₂ CH	C ₁₇ H ₁₄ N ₄ O ₃ S ₂	386	220	12.5	25	12.5
6p	2-ClC ₆ H ₄	SO ₂ CH	C ₁₇ H ₁₃ ClN ₄ O ₃	420	200	12.5	25	12.5
6q	3-ClC ₆ H ₄	SO ₂ CH	C ₁₇ H ₁₃ ClN ₄ O ₃	420	196	12.5	25	12.5
6r	CH ₂ C ₆ H ₅	SO ₂ CH	C ₁₈ H ₁₆ N ₄ O ₃ S ₂	400	170	12.5	25	12.5
6s	2,3-Dichloro-	SO ₂ CH	C ₁₇ H ₁₂ Cl ₂ N ₄ O	400	110	6.25	6.25	6.25
7a	2-OH-	SCH ₃	C ₁₉ H ₁₇ N ₅ O ₃ S ₂	427	180	25	25	25
7b	2,4-Dichloro-	SCH ₃	C ₁₈ H ₁₄ Cl ₂ N ₄ O	437	110	6.25	6.25	6.25
7c	4-ClC ₆ H ₄	SCH ₃	C ₁₈ H ₁₅ Cl ₂ N ₄ O	402	190	6.25	6.25	6.25
7d	2-OH-	SC ₂ H ₅	C ₂₀ H ₁₉ N ₅ O ₃ S ₂	441	175	6.25	6.25	6.25
7e	2,4-Dichloro-	SC ₂ H ₅	C ₁₉ H ₁₆ Cl ₂ N ₄ O	451	104	25	25	25
7f	4-ClC ₆ H ₄	SC ₂ H ₅	C ₁₉ H ₁₇ N ₅ O ₃ S ₂	416	116	25	25	25
7g	2-OH-	SO ₂ CH	C ₁₉ H ₁₇ N ₅ O ₃ S ₂	459	218	12.5	25	12.5
7h	2,4-Dichloro-	SO ₂ CH	C ₁₈ H ₁₄ Cl ₂ N ₄ O	469	110	12.5	25	12.5
7i	4-ClC ₆ H ₃	SO ₂ CH	C ₁₈ H ₁₅ ClN ₄ O ₃	434	180	25	25	25

Model (b):

$$\text{Log } Y = -38.305 (\pm 8.356) + 2.424 (\pm 0.307) \text{ eeig11r} - 1.271 (\pm 0.224) \text{ mor20p} + 31.289 \text{ belm2} (\pm 4.131) + 4.092 (\pm 0.704) \text{ rtm+} - 5.661 (\pm 1.068) \text{ behp5} - 8.462 (\pm 2.667) \text{ Mv}$$



$N = 28$, $R^2 = 0.896$, $SE = 0.112$, $F = 27.236$, $Q^2 = 0.825$

Model (c):

$\text{Log } Z = -40.190 (\pm 6.475) + 4.032 (\pm 0.436) \text{ eeig11r} - 0.755 (\pm 0.202) \text{ eeig09x} + 8.983$
 $(\pm 1.294) \text{ r6m} + 26.671 (\pm 4.565) \text{ r3u} + 19.182 (\pm 3.189) \text{ belm2} - 1.600 (\pm 0.305) \text{ eeig12r}$
 $N = 28$, $R^2 = 0.901$, $SE = 0.097$, $F = 28.839$, $Q^2 = 0.798$

In each model, N is the number of compounds, R^2 is the correlation coefficient, SE is the root mean square deviation, F is the Fisher ration, and Q^2 is the correlation coefficient of the cross-validation.

Conclusion:

As can be seen, the MLR models have good statistical quality with low prediction error and also the results indicated that the best model for the evaluating of anti-bacterial activity of some triazoles is found using the model (b).

References:

- [1] Karaba sanagouda, T; Vasudeva Adhikari, A; Suchetha Shetty, N; European Journal of Medicinal Chemistry, Vol. 42, 2007, pp 521-529.
- [2] Shiradkar, M; Venkata, G; Kumar, S; Dasari, V; Shah, A; European Journal of Medicinal Chemistry, Vol. 42, 2007, pp 807-816.
- [3] Tuzimski, T; Rzymowska, J; Pasternak, K; European Journal of Medicinal Chemistry, Vol. 43, 2008, pp 404-419.



Relative pK_b calculations of aniline derivatives in aqueous solution

B. Ghalami-Chooabar*, A. Ghiami-Shomami

Department of Chemistry, Faculty of Science, University of Guilan, P.O. Box: 19141, Rasht, Iran

E-mail address: a.ghiyami@gmail.com (A. Ghiami-Shomami)

Keywords: Computational methods, Relative pK_b , Anilines, PCM.

Introduction:

Theoretical determination of pK_a / pK_b of compounds in aqueous or non-aqueous solution have received a considerable attention in the recent years. In the previous works, we calculated absolute pK_a and pK_b values for benzoic acids and anilines, respectively [1-2]. At the present work, calculations of the relative pK_b values were performed on aniline derivatives. All calculations were carried out with the Gaussian98 program package. Gas-phase free energies were calculated at the B3LYP/6-31G(d,p) level of theory. Free energies of solvation were computed using the popular solvation model, polarized continuum model (PCM), at the same level of theory. Also, the results obtained were compared with the experimental pK_b data.

Method:

The relative pK_b values of anilines in aqueous solution were calculated in according to the following reaction 1 using of equation 2.



$$pK_b(B) = \frac{\Delta G_{aq}^\circ}{2.303RT} + pK_b(\text{Ref}) \quad (2)$$

Where ΔG_{aq}° indicates to the free energy of protonation in aqueous solution that was calculated basis of the proton exchange thermodynamic cycle (see figure 1). This cycle allows for further cancellation of errors in the gas-phase reaction free energy, especially when lower levels of theory (e.g. HF or DFT methods) are employed.

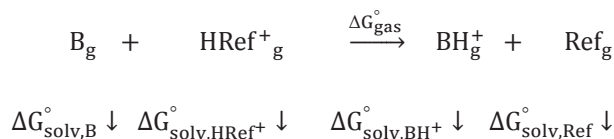


Figure1. The proton exchange thermodynamics cycle

With utilizing of the thermodynamic cycle, the ΔG_{aq}° values were calculated using equation 3, where aniline molecule is selected as reference molecule.

$$\Delta G_{aq}^\circ = \Delta G_g^\circ + \delta \Delta G_{solv}^\circ = G_g^\circ Ref + G_g^\circ BH^+ - G_g^\circ HRef^+ - G_g^\circ B = \Delta G_{solv}^\circ Ref + \Delta G_{solv}^\circ BH^+ - \Delta G_{solv}^\circ HRef^+ - \Delta G_{solv}^\circ B \quad (3)$$

Results and discussion:

The proton exchange method was applied to derive relative pK_b values. The results for all 10 bases were shown in Table 1. As shown in figure 2, there is a good correlation between the experimental and theoretical pK_b values with correlation coefficients 0.96, and the mean absolute deviations (MAD) equals to 0.57 units. It can be conclude that proton exchange method is an appropriate method for pK_b values calculation of anilines.

Table1. The Anilines together with its experimental and theoretical pK_b values

Compound	pK_b (Exp) ^a	pK_b (Theor)
Aniline ^b	9.13	-
4-Fluoro aniline	9.35	8.71
4-Bromo aniline	10.11	8.86
4-Cyano aniline	12.26	12.82
3-Ethoxy aniline	9.82	8.98
3-Chloro aniline	10.48	10.72
3-Bromo aniline	10.47	10.35
2-Fluoro aniline	10.80	11.28
2-Bromo aniline	11.47	11.58
2-Methyl aniline	9.55	8.66

a :The values taken from ref.[3]

b: Reference molecule

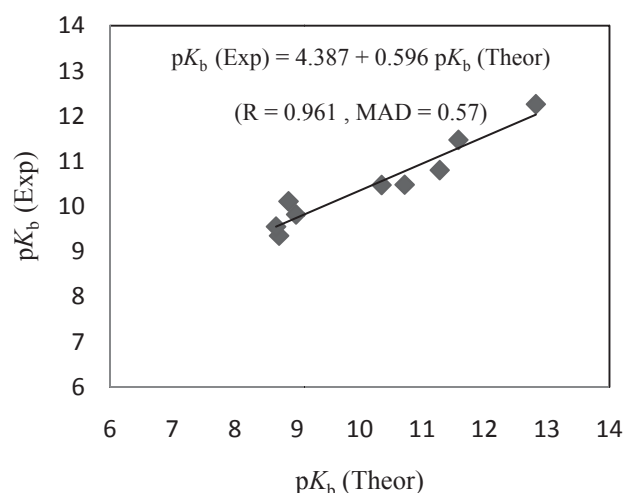


Figure2. Correlation between the experimental and theoretical pK_b values.



References:

- [1] B. Ghalami-Choobar, H. Dezhampanah, P. Nikparsa, A. Ghiami-Shomami, Theoretical Calculation of the pK_a Values of Some Drugs in Aqueous Solution, *International Journal of Quantum Chemistry*, 112 (2012) 2275–2280.
- [2] B. Ghalami-Choobar, A. Ghiami-Shomami, P. Nikparsa, Theoretical Calculation of pK_b Values for Anilines and Sulfonamide Drugs in Aqueous Solution, *Journal of Theoretical and Computational Chemistry*, 11(2012) 283-295.
- [3] R. D. Lide, *CRC Handbook of Chemistry and Physics*, 90th ed CRC Press/Taylor and Francis, 2010.



Interaction of Oxazepam drug and single-wall carbon nanotubes: A theoretical study

M. Nashtahosseini^a, M. Darvish Ganji^{b*} and S. Yeganegi^a

^a Faculty of science, Department of Chemistry, University of Mazandaran, Babulsar, Iran

^b Department of Chemistry, Qaemshahr Branch, Islamic Azad University, Qaemshahr, Iran

E-mail: ganji_md@yahoo.com

Keywords: Drug delivery, Oxazepam, Single wall carbon nanotubes, DFT.

Introduction:

Carbon nanotubes (CNTs) biomedical can be used in drug delivery systems because of their mechanical and chemical stability. There are a number of studies of nanostructures and their ability to distribute peptides, DNA fragments, and other substances [1,2]. Oxazepam [3] (serax; chemical name, (RS)-7-chloro-1,3-dihydro-3-hydroxy-5-2H-1,4-benzodiazepene-2, C₁₅H₁₁Cl N₂O₂) belongs to a group of drugs called benzodiazepines. It is used for the treatment of anxiety and insomnia. In this work, we investigated interaction between oxazepam and CNTs (7,0) / (4,4) with density functional theory. To evaluate the interaction between the CNTs and oxazepam, four active sites of oxazepam: Cl, hydroxyl oxygen, hydroxyl hydrogen and carbonyl oxygen groups as well as several sites of the exterior CNTs were considered. Adsorption energies, equilibrium distances, charge transfers, densities of states (DOS), for the performance of carbon nanotubes (7,0)/(4,4) as oxazepam carriers has been studied.

Computational methods:

We employed the *first-principles* approaches using numerical atomic orbitals as basis set to evaluate the structure and the energy of the CNTs-oxazepam complexes. Generalized gradient approximation (GGA) utilized to solve Cohn-Sham equations with PBE functional and DZP basis set selected for all atoms in this study. All the calculations carried out with SIESTA code.

Results and discussion:

The interaction of the oxazepam with the exterior wall of the (7,0) / (4,4) CNTs were studied by performing a series of single point energy (SPE) calculations. To further understand the adsorption properties of oxazepam on the CNTs we carried out the full structural optimization of the configurations with the minimum energy in the energy-distances plot of the oxazepam-CNTs (7,0) / (4,4). In the most stable configurations of oxazepam-CNT (7,0) and (4,4) combined systems, the Cl atom of the oxazepam were located 3 Å above the C-C and C-C zigzag bond of CNTs where their calculated binding energies were 1.93 and 0.96 KJ/mol, respectively.

To shed light on the binding nature of these systems, the density of states (DOS) for the most stable configurations of oxazepam-CNTs complexes were calculated and represented in Fig 1.

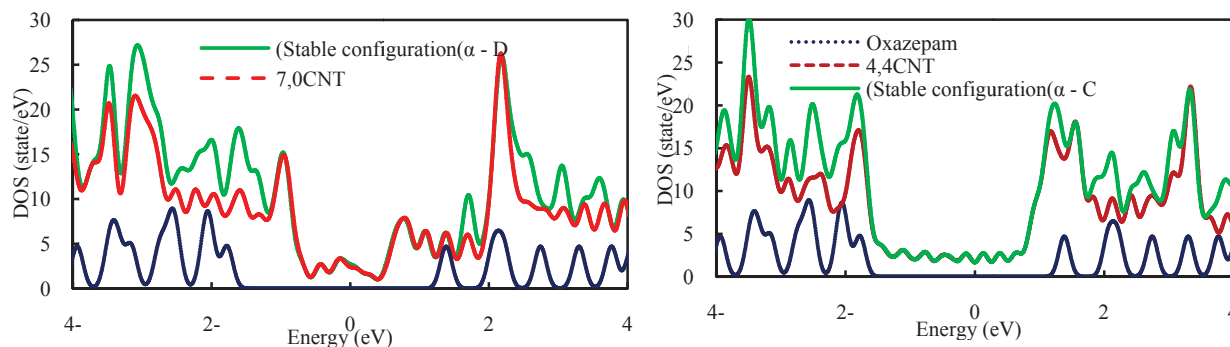


Fig. 1. Calculated density of states (DOS) for an isolated oxazepam, isolated CNTs, and the oxazepam/CNTs combined system of the two at equilibrium geometry. The Fermi level is localized in zero.

As clearly seen there is no evidence for hybridization between the CNTs and the oxazepam molecules and the DOS near the Fermi level is not affected by the adsorption of the oxazepam onto the carbon nanotubes. Also, charge analysis shows 0.01 *e* charge transfer from the oxazepam to the CNTs for the most stable oxazepam-CNTs complexes, which confirms that a very weak interaction takes place between the respective entities.

Conclusion:



Our results showed that clearly there aren't any significant interactions between oxazepam and carbon nanotubes (7,0)/(4,4). The obtained results indicated that CNTs (7,0)/(4,4) aren't good carrier for oxazepam.

References:

- [1] A Ochekepe, N.; O Olorunfemi, P.; C Ngwuluka, N. *Trop. J. Pham. Res.* **2009**, 8, 265.
- [2] Miyazaki, K.; Islam, N. *Technovation*, **2007**, 27, 661.
- [3] W. Sieghart, *J. Psychiatr Neurosci.* 1994, 19.



A computational study of the behavior bulk ionic liquid 1-n-propyl-4-amino-1,2,4-triazolium bromide

M. Foroutan*, M. A. Balazadeh

Department of Physical Chemistry, School of Chemistry, University College of Science, University of Tehran,
Tehran, Iran

Email: balazadeh@khayam.ut.ac.ir

Keywords: Ionic liquid, Molecular dynamic simulation, Bulk, Diffusion.

Introduction:

Ionic liquids (ILs) have attracted considerable attention in recent years, due to special properties such as low vapor pressure, high ionic conductivity, and ability to dissolve an enormous range of inorganic and organic materials. ILs consists of a large cation combined with a small size of anion. The physical properties of the IL depend on the choice of the cation and anion. So, the physical properties must be known before an IL can be used in application. In this field, Molecular dynamic (MD) simulations have been used by Tsuzuki et al. [1] to study bulk behavior of a series of ILs. Rey-Castro et al. [2] have analyzed the effect of temperature on some of the most relevant transport coefficients in ILs. In this work, we performed MD simulation for the IL 1-n-propyl-4-amino-1,2,4-triazolium bromide([part]⁺Br⁻). Our results clearly shows that bromide ions have lower diffusion coefficients compare to cations. The relationship between the ionic structure and transport properties of the IL is an important issue for designing new ILs for many applications.

Methods:

MD simulation has been performed using the Tinker software package in constant volume and temperature (NVT). To describing interatomic interactions, The OPLS-AA force field that developed by Lopes and co-workers was used. The force field parameters of cations and anions were adapted from Thompson's work [3]. The structure of the IL is shown in figure

1(a). We considered 69 IL molecules in $21 \times 21 \times 36 \text{ \AA}^3$ simulation box. The cutoff distance is 10 \AA and the temperature is fixed at 350 K. The partial mesh Ewald (PME) method was implemented to compute the electrostatic interactions.

Result and discussion:

The radial distribution functions (RDFs) provide quantitative information about ILs interactions. Figure 1(b) shows the RDFs of bromide anion around atoms of cation. These RDFs show that, the probability of finding Br^- surrounding the NT atom is higher than that of other atoms of cation. On the other hand, the intensity of the first peak for NT-Br is higher, suggesting stronger interactions between NT atom and Br^- anion.

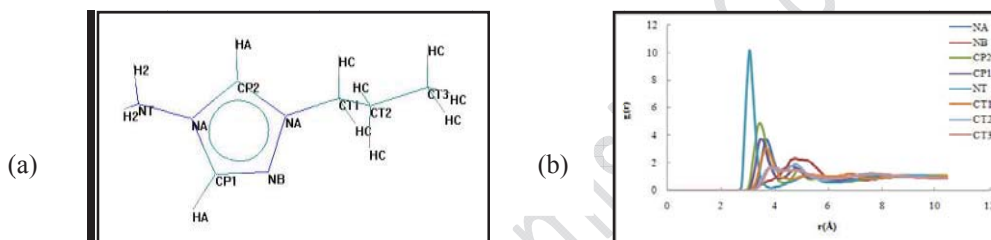


Figure1. (a) Schematic representation of the 1-n-propyl-4-amino-1,2,4-triazolium cation and (b) radial distribution functions between the cation atoms and bromide ion.

In figure 2, we present data the MSD of the cations and anions of bulk $[\text{part}]^+\text{Br}^-$. As figure 2 shows, the cations move faster than anions $\sim 800 \text{ ps}$ after equilibrium time.

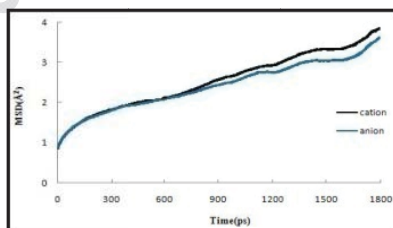


Figure2. Mean square displacement for cations (black solid) and anions (blue solid) in bulk $[\text{part}]^+\text{Br}^-$ at 350K.

Also diffusion coefficients (D) and transport numbers (T) of the cation and the anion are illustrated in Table 1. As shown in Table 1, the $[\text{part}]^+$ cation possess larger diffusion coefficient and transport number than the anion. The aromatic cations have board-shaped structures, which suggest that board-shaped structures of aromatic cations are important for the



large self-diffusion coefficients [2]. The large T_+ suggests that, the cation has a larger contribution to the ionic conductivity in bulk.

Table 1: diffusion coefficients and transport numbers calculated for ions in bulk $[\text{part}]^+\text{Br}^-$ at 350 K.

	D	T
cation	0.0022	0.51
anion	0.0021	0.48

Conclusion:

In this study, the self-diffusion coefficients demonstrate that IL cations have larger diffusion coefficient. Also, the cations diffuse more quickly and have a large contribution to the ionic conductivity than the anions.

References:

- [1] S. Tsuzuki and etal; "Molecular Dynamics Simulations of Ionic Liquids: Cation and Anion Dependence of Self-Diffusion Coefficients of Ions"; J. Phys. Chem. B; 113, 10641-10649, 2009.
- [2] C. Rey-Castro and etal; "Transport Properties of the Ionic Liquid 1-Ethyl-3-Methylimidazolium Chloride from Equilibrium Molecular Dynamics Simulation. The Effect of Temperature"; J. Phys. Chem. B; 110, 14426-14435, 2006.
- [3] S. Alavi and etal; "Simulations of the Solid, Liquid, and Melting of 1-*n*-Butyl-4-amino-1,2,4-triazolium Bromide"; J. Phys. Chem. B; 109, 18127-18134, 2005.



Molecular dynamic simulation of Water confined inside carbon nanotube

M. Foroutan*, M. A. Balazadeh

Department of Physical Chemistry, School of Chemistry, University College of Science, University of Tehran,
Tehran, Iran

Email: balazadeh@khayam.ut.ac.ir

Keywords: Carbon Nanotube, Molecular Dynamic Simulation, Water, Confined.

Introduction:

Single-wall carbon nanotubes (SWCNTs) have been studied intensively because of their unique chemical and physical properties. Also, during the last decade, the structural and dynamic properties of various fluids such as water inside SWCNTs have been widely studied [1,2]. So, information concerning the characteristic of water inside SWCNT is of primary importance. The behavior of confined water plays an important role in many relevant biological and geological systems. Aluru et al. [2] have shown that the chirality of a SWCNT has a significant influence on the single-file water structure and dynamics. Kassinos et al. [3] have calculated the density of water confined in CNTs of different sizes and chirality. In this work, we performed Molecular dynamic simulation to study the structural and dynamical properties of water confined inside (20,20) SWCNT.

Methods:

We considered a (20,20) armchair SWCNT that consist of 1240 carbon atoms and its length is 36.9 Å, containing 531 water molecules, which leads to a water density of 0.97 gr/cm³ in tube. The TIP3P model with an oxygen atom of -0.8340 e charge and two hydrogen atoms of +0.4170 e charge was used in this simulation. MD simulation was carried out at 350 K. The simulated system is performed in NVT ensemble in the Tinker (version 5.0) program package.

Result and discussion:

Figure 1(a) shows the snapshot of simulated system. The layering behavior of water structure is shown, which there is a good agreement with other studies[1]. Figure 1(b) presents the

interaction energy evolution for water confined in (20,20) SWCNT. The interaction energy is calculated using the following equation.

$$E_{\text{inter}} = E_{\text{nanotube-water}} - (E_{\text{nanotube}} + E_{\text{water}})$$

As figure 1(b) shows, the attractive interactions is observed for water confined in (20,20) SWCNT.

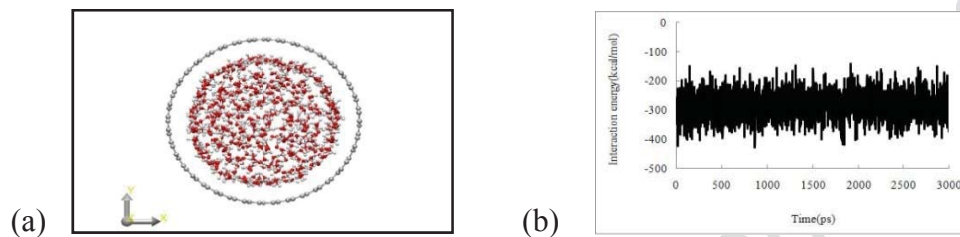


Figure1. (a) water confined inside (20,20) SWCNT and (b) interaction energy evolution for water confined inside (20,20) SWCNT during 3 ns.

Figure 2(a) depicts the radial distribution function (RDF) for water molecules, revealing stronger interactions O-O than between O-H and H-H. In the case of $g_{\text{O-H}}$, two characteristic maxima and one minimum can be discerned. In the case of $g_{\text{H-H}}$, one characteristic maximum and small second maximum is observed. Also, Figure 2 shows RDF for the hydrogen and oxygen atoms of the water around the SWCNT. Figure 2(b) shows that RDF for hydrogen atoms around carbon atom of SWCNT appears in lower distances. Because of the partial positive charge of the hydrogen atoms and the partial negative charge of the oxygen atoms, the orientation of water molecules at near the SWCNT is such that there is more attraction between carbon atoms of SWCNT and hydrogen atoms.

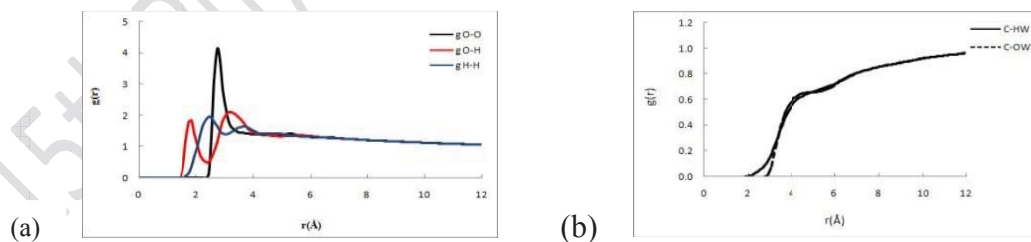


Figure2. (a) Radial distribution function for water molecules inside (20,20) SWCNT and (b) for the hydrogen and oxygen atoms of the water around the SWCNT.



Conclusion :

In summary, the aim of this study was to analyze the behavior of water confined in (20,20) SWCNT. It was found that RDFs for O-O have stronger interactions than RDFs between O-H and H-H.

References:

- [1] T. Nanok and etal; "Structure and Dynamics of Water Confined in Single-Wall Nanotubes"; J. Phys. Chem. A; 113, 2103-2108, 2009.
- [2] C. Y. Won and etal; "Effect of quantum partial charges on the structure and dynamics of water in single-walled carbon nanotubes" ; J. Chem. Phys; 125, 114701-114709, 2006.
- [3] A. Alexiadis and etal; "The density of water in carbon nanotubes" ; Chem. Eng. Sci; 63, 2047-2056, 2008.



Density functional theory investigation of interaction between single-walled carbon nanotube and amino acids

Farzaneh Tavousi^{a*}, Morteza Keshavarz^a, Neda Shakour^{a,b}

^aDepartment of Chemistry, Shahreza Branch, Islamic Azad University, Shahreza, Isfahan, Iran

^bDepartment of Chemistry, Faculty of Science, Zanjan University P.O. Box 45195-313 Zanjan, I.R. Iran

Email: f_tavousi@yahoo.com

Key words: Carbon Nanotube, Glycine, Histidine, Alanine, Adsorption, DFT

Introduction:

Single-walled carbon nanotubes (SWCNTs) have been shown to have unique electronic, thermal, optical, mechanical and transport properties, which play a important role in their interaction into nanotechnological devices [1-3]. Their interaction properties with other compounds are the main element in many applications involving CNTs such as biocompatible agents and functionalized elements. Interaction of biological molecules with CNTs shows their applications in the field of biomedical materials and devices special in drug delivery. These applications of carbon nanotubes depend upon the nature of interaction between CNTs with biological molecules. Covalent functionalization of carbon nanotube with alanine [4] were reported recently.

In the present work, we have investigated the interaction of a zig-zag single-walled carbon nanotube (6,0) with amino acids glycine, histidine and alanine by using density functional theory (DFT) calculations.

Computational methods:

The rich chemistry of carbon nanotubes and methods for their chemical modification have been reviewed previously [5-9]. The most methods can be used for the direct or indirect modification of carbon nanotubes with biomolecules. To investigate the structural and electronic properties of CNTs functionalized with amino acids glycine, histidine and alanine,



we were used DFT method. Initially the structure of amino acids and SWCNT were optimized separately. Then a complex between amino acids and SWCNT were fully optimized. Amino acids interact with nanotube with two different orientations; amine and carboxyl groups. Binding energy of the amino acids with CNT is calculated using the following relation:

$$E_b = E_{\text{CNT+amino acid}} - E_{\text{CNT}} - E_{\text{amino acid}}$$

All calculations were performed by Gaussian 03 program.

Result and discussion:

The amino acids are stabilized at a distance of 4Å (through the amine group of amino acid) and at a distance of 3.5Å (through the carboxyl group of amino acid) from the surface of the nanotube. Interaction of amino acids with nanotube is carried out with two different orientations of amino acids. The binding energies of the glycine for the both of orientations of glycine are comparatively lower than histidine and alanine. Obtained values of dipole moment for gly-CNT, his-CNT and ala-CNT complexes show that the adsorption of amino acids on nanotube surface doesn't change the metallic property of the nanotube.

Conclusion:

The adsorption of three amino acids glycine, histidine and alanine on nanotube surface have been investigated with two different orientations of them. The interaction between the amino acids and CNT are non-covalent that it's evident from small interaction energy. Also this interaction through the amine group of amino acids is the most favorable adsorption pathway.

Reference:

- [1] R.Satio; G.Dresselhause; M.Dresselhause; "Physical Properties of Carbon Nanotubes"; Imperial College Press: London, UK; 2003.
- [2] A.Jensen; J.Hauptmann; J.Nygaard; P.Lindelof; Phys. ReV.; B 72,035419,2005.
- [3] J.Nygaard; D.Cobden; M.Bockrath; P.McEuen; P.Lindelof; Appl. Phys.; A 69,297,1999.
- [4] W.Sun; Y.Bu and Y.Wang; J. Phys. Chem.; B 112,15442-15449,2008.



- [5] J.L.Bahr and J.M.Tour; "Covalent chemistry of single-wall carbon nanotubes"; J. Mater. Chem.; 12,1952–8,2002.
- [6] A.Hirsch; "Functionalization of single-walled carbon nanotubes"; Angew. Chem. Int. Edn; 41,1853–9,2002.
- [7] E.Katz and I.Willner; "Biomolecule-functionalized carbon nanotubes: applications in nanobioelectronics"; J. Phys. Chem.; 5,1085–104,2004.
- [8] S.Niyogi; M.A.Hamon; H.Hu; B.Zhao; P.Bhowmik; R.Sen; M.E.Itkis and R.C.Haddon; "Chemistry of single-walled carbon nanotubes"; Acc. Chem. Res.; 35,1105–13,2002.
- [9] C.V.Nguyen; L.Delzeit; A.M.Cassell; J.Li; J.Han and M.Meyyappan; "Preparation of nucleic acid functionalized carbon nanotube arrays"; Nano Lett.; 2,1079–81,2002.



Comparison of Hydrogen Bond interaction between Acetic and Propanoic acid Dimer with Density Functional theory calculation.

L. Nassaji jahromi^{*a}, F. Ghorbani Naieni^b, Z. Aljabori^c, M. Jafari^c, M. Habibi^c

^aMaster of Physical Chemistry, Education, Shahre-Rey (Ray 2), Tehran, Iran.

^bMaster of Physical Chemistry, Basirat Research House studentst, Shahre-Rey Branch, Tehran, Iran

^cAshura State High School, Shahre-Rey (Ray 2), Tehran, Iran

Corresponding Author E-mail: leila32nasaj@yahoo.com

Abstract:

Abinitio and density functional theory methods have been employed to study it. Molecular geometries and energetic of monomers and dimers in gaseous phase have been obtained using B3LYP level of theory, implementing 6 311++G(d,p) basis set. It was found that in comparison with Propanoic acid the strength of hydrogen bonding in Acetic acid decreased. The vibrational frequency shifts is reported. Natural population and atom in molecule analysis performed to predict electrostatic interactions in the cyclic H-bonded complexes and charges.

Key Words: Hydrogen bonding, Propanoic acid, Acetic acid, DFT calculation, NBO analysis.

Introduction:

Hydrogen bonding has been a very interesting issue for chemists for a long time since it can account for characteristics of many chemical and biological phenomena. Carboxylic acid is an organic compound whose molecules contain carboxyl group and have the condensed chemical formula $R-C(=O)-OH$ ¹⁻². The first character of carboxylic acid is acidity due to dissociation into H^+ cations and $RCOO^-$ anions in aqueous solution. Carboxylic acid is useful as a parent material to prepare many chemical derivatives due to the weak acidity of the hydroxyl hydrogen or due to the difference in electronegativity between carbon and oxygen. It is well

known that carboxylic acids form in the gas phase and solution cyclic structure with two very strong O-H...O=C hydrogen bonds³.

Computational Methods:

The ground-state properties of the monomers and the dimers of acetic acid and Propanoic acid have been calculated by using B3LYP method at 6-311++G(d,p) basis set level⁴⁻⁵. All computations have been performed on a personal computer using the Gaussian 03 program package and Gaussview molecular visualization program. Hydrogen bond energy is obtained according to the following

$$E_{\text{int}} = E_{X-Y} - E_X - E_Y$$

E_{X-Y} , respectively, which corresponds to the energy of the molecule Dimer and E_X and E_Y are considered relevant to the monomer molecule⁶. The shapes of molecules optimized with B3LYP/6-31++G** methods you can see the basic series⁴⁻⁶.

Result and discussion:

The structures Acetic acid and Propanoic acid are presented in Figure 1. A close look at the Table 1 indicates that complex formation induces a small elongation of the O-H and C=O bond lengths and decrease of C-O bond length. The results of calculated interaction energies for the acetic acid and Propanoic acid dimers are presented in the table 1. The results of vibrational frequencies of dimers and monomers in the Table 2. As you can see, all the vibrational modes in hydrogen bonding region show a shift to low wavelength as compared to the individual molecule⁷⁻¹⁰, a feature that may be attributed to the weakening of the individual bonds along with the charge separation on dimer formation. The calculated values NBO charges at optimized structures of acetic and Propanoic acid monomers and dimers in the gas phase are given in Table 2. It can be observed that, due to complexation, hydrogen atoms involved in hydrogen bonding gain more positive charges, the oxygen atoms acting as hydrogen acceptor gain more negative charges, and the charges on the oxygen atoms acting as hydrogen donor diminish as compared with monomers¹¹.



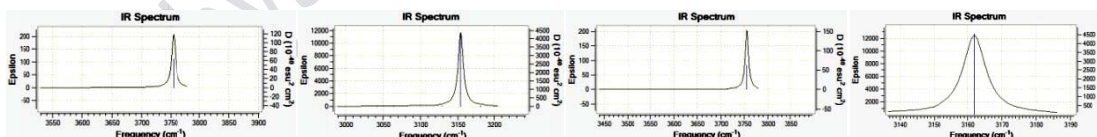
Figure 1. The structure and numbering of acetic acid and Propanoic acid.

Table 1. Some optimized geometrical parameters Geometry (A0) monomers and the dimers of acetic acid and Propanoic acid calculated at B3LYP/6-311++G(d,p)

	$E_{(a.u)}$	E_{int}	$E_{(kcal/mol)}$	$r(H...O)$	$r(C=O)$	$r(C-O)$	$r(H-O)$
CH ₃ COOH	-229.10592				1.21249	1.35948	0.97239
2CH ₃ COOH	-458.23789	-0.026044	-16.34286	1.63002	1.22346	1.31993	0.99777
CH ₃ CH ₂ COOH	-268.42373				1.21295	1.36009	0.97229
2CH ₃ CH ₂ COOH	-536.87318	-0.02572	-16.13955	1.6526	1.23336	1.32417	1.0049

Table 2. Selected calculated stretching vibrational frequencies (cm⁻¹) in the IR frequencies from monomers to dimers of acetic acid and Propanoic acid. And NBO charges for them calculated at the B3LYP/6-311++G(d,p) level.

		NBO		O...H		C=O	
		$\nu(OH)$	O	H	C	O	
1	CH ₃ COOH	3754.7332	-0.73215	0.51677	0.8096	-0.60423	
2	2CH ₃ COOH	3153.43	-0.72142	0.53192	0.84125	-0.67	
3	CH ₃ CH ₂ COOH	3755.3	-0.72579	0.51412	0.81417	-0.6103	
4	2CH ₃ CH ₂ COOH	3161.95	-0.71964	0.53158	0.84799	-0.6742	



Conclusion:

Our calculations show that With increasing carbon chain length in carboxylic acids hydrogen bonding strength increases and binding energy decreases then methyl groups in carboxylic acids reduces the acid strength and hydrogen bond will be weaker and the vibrational modes in hydrogen bonding region show a shift to low wavelength as compared to the individual



molecule and The calculated values NBO, the oxygen atoms acting as hydrogen acceptor gain more negative charges, and the charges on the oxygen atoms acting as hydrogen donor diminish as compared with monomers.

Reference:

- [1]. Scheiner, S. *Hydrogen Bonding*; Oxford University Press: New York, 1997.
- [2]. Jeffery, G. A. In *Introduction to Hydrogen Bonding*; Oxford University Press: New York, 1997.
- [3]. Hobza, P.; Havlas, Z. *Chem. Rev.* 2000, *100*, 4253.
- [4]. Frisch, M. J. *et al.*, Gaussian 03, Revision C.02, Gaussian Inc., Pittsburg, PA, 2003.
- [5]. Frisch, A.; Nielsen, A. B.; Holder, J. Gauss View User Manual, Gaussian.
- [6]. (a) Boys, S. F.; Bernardi, F. *Mol. Phys.* 1970, *19*, 553. (b) Boys, S. F.; Bernardi, F. *Reprinted in Mol. Phys.* 2002, *100*, 65.
- [7]. Young, C. *Computational Chemistry, A Practical Guide for Applying Techniques to Real-World Problems (Electronics)*; John Wiley and Sons, Inc.: New York, 2001.
- [8]. Anderson, P.; Uvdal, P. *J. Phys. Chem. A* 2005, *109*, 2937.
- [9]. Chermahini, A. N.; Ghaedi, A.; Teimouri, A.; Momenbeik, F.; Dabbagh, H. A. *J. Mol. Struct. (Theochem)* 2008, *78*, 867.
- [10]. Lewandowski, H.; Koglin, E.; Meier, R. J. *Vibrational Spectroscopy* 2005, *39*, 15.
- [11]. Glendening, E. D.; Badenhoop, J. K.; Reed, A. E.; Carpenter, J. E.; Weinhold, NBO Version 3.1, Theoretical Chemistry Institute, University of Wisconsin, Madison.



Effects of electronegative groups F, Cl, Br on Hydrogen Bond interaction in Propanoic Acid Dimer using QM.

L. Nassaji jahromi^{*a}, F. Ghorbani Naieni^b, F. Nezafat^c, S. Nalbandian^c, F. Alfaham^c

^aMaster of Physical Chemistry, Education, Shahre-Rey (Ray 2), Tehran, Iran.

^bMaster of Physical Chemistry, Basirat Research House studentst, Shahre-Rey Branch, Tehran, Iran

^cAshura State High School, Shahre-Rey (Ray 2), Tehran, Iran

Corresponding Author E-mail: leila32nasaj@yahoo.com

Abstract :

In this project we study hydrogen bonding in monomers and dimers Propanoic acid and its derivatives. The substituent effect can be analyzed by comparing the binding energies of propanoic acid and fluoro, chloro and Bromopropanoic acid monomers and dimers¹⁻³. We have been obtained binding energy and symmetrical dimer of propanoic acid calculated at B3LYP/6-311G (d,p) level was found as -16.14 kcal/mol and our calculations show that with replacing of one hydrogen with an electronegative substituent (1...1 F, Cl atom) hydrogen bonding strength decreases. But in the substituents (1...1 Br, 2...2 Cl, Br) hydrogen bonding strength increases. The calculated vibrational spectra of dimers give evidence of the formation of strong hydrogen bonds involving O-H...O=C. For the two dimers, elongation of O-H bonds results in downshift of the stretching vibrational frequencies that Br substituent exhibits a greater shift than F, Cl⁴⁻⁵. NBO analysis has been performed to calculate charges on atoms. Due to complexation, hydrogen atoms in hydrogen bonding gain more positive charges, the oxygen atoms acting as hydrogen acceptor gain more negative charges, and the charges on the oxygen atoms acting as hydrogen donor diminish as compared with monomers.

Key Words: Hydrogen bonding, Propanoic acid, DFT, electronegative groups F, Cl, Br, NBO analysis.

Introduction:

Carboxylic acid are important in biochemistry as well as in industrial fields. Higher chain compounds are used as components in metalworking fluids, surfactants, detergents, oiling

agents, emulsifiers, wetting agents textile treatments and emollients, intermediates for the manufacture of a variety of target compounds. Propanoic acid is a product of bacterial fermentation and is manufactured primarily for use as a preservative and anti-mold agent in animal feed and grain. Other uses for propionic acid include :Preservative and flavoring agent for baked goods and cheese, Food additives to prevent mold in bread, tortillas. It is used also as a solvent and in nickel-electroplating solutions, Chemical intermediate for herbicides, pharmaceuticals, dyes, textile and rubber products, plastics, plasticizers, cosmetics, and perfumes. Propanoic acid reacts as an acid to neutralize bases in exothermic reactions. Burns when exposed to heat, flame or oxidizers. At propanoic acid The two oxygen atoms are electronegatively charged and the hydrogen of a carboxyl group can be easily removed.

Computational Methods:

The calculations in this study hydrogen bonding in the structure of monomers and dimers Propanoic acid and its derivatives (electronegative substituent)⁶⁻¹⁰. In this structure the methyl group instead of hydrogen F, Cl and Br (0-0)-(1-1)-(2-2) is placed to the changes that occur in hydrogen-bond movements are about. Calculations with the B3LYP method with the Gaussian 03 software series was based. Hydrogen bond energy is obtained according to the following $E_{\text{int}} = E_{X-Y} - E_X - E_Y$

E_{X-Y} , respectively, which corresponds to the energy of the molecule Dimmer and E_X and E_Y are considered relevant to the monomer molecule. The shapes of molecules optimized with B3LYP/6-31++G** methods you can see the basic series.

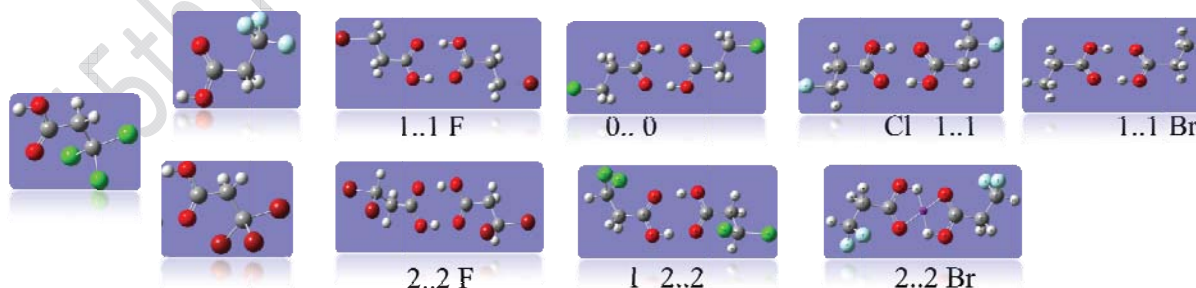


Figure 1. The structure and numbering of monomers and dimers Propanoic acid and substituent F, Cl, Br.

Result and discussion:

The geometry of monomers and dimers Propanoic acid and its derivatives (electronegative substituent) are given in Figure 1. Some geometrical parameters and stretching vibrational frequencies (cm⁻¹) in the IR frequencies And NBO charges monomers and dimers of Propanoic acid and electron-withdrawing substituent calculated at B3LYP/6-311++G(d,p) in Table 1, Table 2 and Table 3. In Figure 2. We Compare vibrational frequencies (cm⁻¹) in the IR frequencies from dimers and monomers of Propanoic acid and electron-withdrawing substituent F, Cl, Br.

Table 1. Some optimized geometrical parameters Geometry (Å) and stretching vibrational frequencies (cm⁻¹) in the IR frequencies And NBO charges monomers of Propanoic acid and electron-withdrawing substituent calculated at B3LYP/6-311++G(d,p)

SUBSTANCE	E(a.u)	r(C-X)	r(C=O)	r(C-O)	r(C-H)	r(H-O)	v(O-H)	NBO O...H		NBO C=O	
								O	H	C	O
CH ₃ CH ₂ COOH	-268.42		1.21295	1.36009	1.0972	0.97229	3755.3	-0.7258	0.5141	0.8142	-0.6103
CH ₂ FCH ₂ COOH	-367.66	1.4058	1.21384	1.35462	1.0961	0.97278	3750.55	-0.717	0.5176	0.814	-0.6087
CH ₂ ClCH ₂ COOH	-728.02	1.8154	1.21327	1.35451	1.0957	0.97276	3750.87	-0.7169	0.5181	0.8156	-0.6067
CH ₂ BrCH ₂ COOH	-2839.52	1.9689	1.21321	1.35449	1.0956	0.97286	3749.49	-0.7168	0.5181	0.8161	-0.7168
CHF ₂ CH ₂ COOH	-466.91	1.3766	1.21193	1.3512	1.0929	0.97309	3747.1	-0.7116	0.5203	0.8153	-0.6017
CHCl ₂ CH ₂ COOH	-1187.6	1.8029	1.20688	1.35846	1.0961	0.97253	3755.38	-0.7248	0.5204	0.8149	-0.5768
CHBr ₂ CH ₂ COOH	-5410.7	1.9596	1.20751	1.35697	1.0966	0.97254	3754.92	-0.7235	0.5206	0.8164	-0.579
CF ₃ CH ₂ COOH	-566.16	1.3533	1.20704	1.3553	1.0941	0.97281	3752.47	-0.7198	0.5225	0.8125	-0.5751
CCl ₃ CH ₂ COOH	-1647.2	1.8026	1.20658	1.35651	1.0944	0.97261	3754.88	-0.7216	0.5225	0.8169	-0.5763
CBr ₃ CH ₂ COOH	-7981.8	1.9702	1.20722	1.35573	1.0948	0.97266	3754.18	-0.7206	0.5221	0.8176	-0.5781

Table 2. Some optimized geometrical parameters Geometry (Å) dimers of Propanoic acid and electron-withdrawing substituent calculated at B3LYP/6-311++G(d,p). X represents a Halogen atom is substituted.

No. of X	E(a.u)	Eint	E(kcal/mol)	r(H...O)	r(C-X)	r(C=O)	r(C-H)	r(C-H)-X	r(H-O)
0....0	-536.873176	-0.02572	-16.13955	1.6526		1.23336	1.09723		1.0049
1...1 F	-735.343945	-0.025398	-15.93737	1.65394	1.40562	1.23452	1.09615	1.09285	1.00488
1...1 Cl	-1456.05805	-0.025383	-15.92802	1.65378	1.81537	1.23391	1.08939	1.08939	1.004925
1...1 Br	-5679.11408	-0.027681	-17.37008	1.64053	1.96575	1.23428	1.09585	1.08839	1.00622
2....2 F	-933.832081	-0.015803	-9.916571	1.65171	1.40562	1.22693	1.09493	1.09495	1.00499
2....2 Cl	-2375.22713	-0.031332	-19.66064	1.64419	1.803	1.22673	1.09595	1.08793	1.00531
2....2 Br	-10821.3455	-0.03527	-22.13199	1.62846	1.96322	1.23355	1.09119	1.08594	1.00815

Table 3. Selected calculated stretching vibrational frequencies (cm^{-1}) in the IR frequencies from dimers of Propanoic acid and electron-withdrawing substituent And NBO charges for them calculated at the B3LYP/6-311++G(d,p) level. X represents a Halogen atom is substituted

No. of X	NBO $\nu(\text{O-H})$	O...H		NBO C=O	
		O	H	C	O
0..0	3161.95	-0.71964	0.5316	0.848	-0.6742
1..1 F	3164.84	-0.70992	0.533	0.8491	-0.67517
1..1 Cl	3162.94	-0.70965	0.5334	0.8507	-0.67341
1..1 Br	3137.27	-0.70905	0.5332	0.8518	-0.67395
2..2 F	3166.4	-0.7147	0.5352	0.8497	-0.64613
2..2 Cl	3161.48	-0.7	0.5356	0.8528	-0.6716
2..2 Br	3108.19	-0.6983	0.5337	0.8544	-0.67238

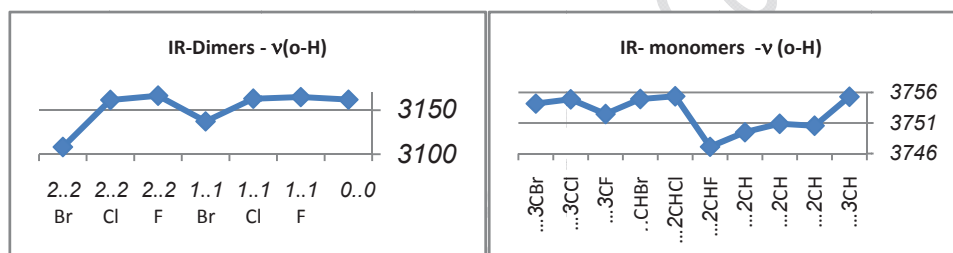


Figure 2. vibrational frequencies (cm^{-1}) in the IR frequencies from dimers and monomers of Propanoic acid and electron-withdrawing substituent F, Cl, Br.

Conclusion:

The hydrogen bond interaction of 1:1 and 2:2 complex has been analyzed by ab initio, B3LYP methods employing the 6-311++G(d,p) basis set. Calculations show that the methyl group in Propanoic acid instead of hydrogens atom are replaced electron-withdrawing substituent. Then bond length (H-O) and (C=O) increases and bond length (C-O) decreases. Frequency (O-H) is decreased. (This reduction in Dimer structure Br more than Cl, F). Several experimental studies such as IR spectroscopy,¹¹⁻¹² The dimerization leads to significant changes in the vibrational characteristics of the monomer unit. The large shifts of the most sensitive aggregation vibrations (O-H and C=O stretchings) confirmed the cooperative effect in the cyclic structures. NBO analysis shows electronegativity atoms¹³, (1..1) F, Cl electrons to the hydrogen being more positive than, but oxygen doesn't being more negative and an electron



withdrawing group leads to a decrease of strength of hydrogen bonding.. But when we replace Br because these group are less than electronegative F ,We expected hydrogen bonds are weaker and the bond length is longer. This predict does not view in Calculations. Due to the large radius of Br (1 .. 1) and prevented more space, shorter hydrogen bond length and bond energy increases. when ,Second electron-withdrawing substituent (2 .. 2) F be replaced instead of hydrogen due to higher Traction to both sides we are observed hydrogen bond more weaker . In this process don't observe at Br, CL (2 .. 2) Due to open space to prevent and hydrogen bonding energy is more negative.

Reference:

- [1] Scheiner, S. Hydrogen Bonding; Oxford University Press: New York, 1997.
- [2] Frisch, M.J. et al., Gaussian 03, Revision C.02, Gaussian Inc.,Pittsburg, PA,2003.
- [3]Frisch, A.Nielsen , A. B.Holder, J. Gauss View User Manual,Gaussian
- [4]. Jeffery, G.A. In Introduction to Hydrogen Bonding; Oxford University Press: New York, 1997.
- [5]. Hobza, P.; Havlas, Z. Chem. Rev. 2000, 100, 4253.
- [6].Chocholousova, J.; Vacek, J.; Hobza, P. J. Phys. Chem. 2003, 107, 3086.
- [7].Aquino, A. J. A.;Tunega, D.; Haberhauer, G.; Gerzabek, M. H. J. Phys. Chem. 2002, 106, 1862.
- [8]. Turi, L. J. Phys. Chem. 1996, 100, 11285.
- [9]. Lewandowski, H.; Koglin, E.; Meier, R. J. Vibrational Spectroscopy 2005, 39, 15.
- [10]. Wolfs, I.; Desseyn, H. O. J. Mol. Struct. (Theochem) 1996, 81, 360.
- [11]. Emmeluth, C.; Suhm, M. A. Phys. Chem. Chem. Phys. 2003, 5, 3094.
- [12]. Duarte, C. J.; Freitas, M. P. J. Mol. Struct. 2009, 930 135-139.
- [13]. Glendening, E. D.; Badenhoop, J. K.; Reed, A. E.; Carpenter, J. E.; Weinhold, NBO Version 3.1, Theoretical Chemistry Institute, University of Wisconsin, Madison.

Study of ionic liquid and a single- wall carbon nanotube mixtures using molecular dynamic simulations

M. Foroutan*, M. Mohammadi

Department of Physical Chemistry, School of Chemistry, University College of Science, University of Tehran,
Tehran, Iran

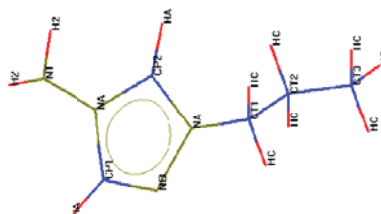
Email: Mohammadi_Morteza@khayam.ut.ac.ir

Keywords: Ionic Liquid, Carbon Nanotube, Solvated layer, Simulation.

Introduction:

Recently the mixture systems of ionic liquids and carbon nanotubes have attracted the attention of some results [1-2]. Single- and double- Walled CNTs solvated in the ILs are studied by Kim et al via MD computer simulations [1]. They demonstrated that cations and anions show smeared- out, cylindrical shell-like distributions outside of the nanotubes irrespective of the nanotube diameter, the smallest nanotube that allows solvent ion inside the tunnel is (7,7), and imidazole rings of cation in the first internal and external salvation shells are mainly parallel to the nanotube surface[1]. In this work, we consider a SWCNT that immersed in 1-n- propyl- 4- amino-1, 2, 4-triazolium bromide ($[part]^+[Br^-]$) IL. Our purpose is analyze the structure of the $[part]^+[Br^-]$ IL around the SWCNT by performing molecular dynamic(MD) simulations. Atomic labels of the $[patr]^+$ ion corresponding to the OPLS- AA force field is shown in Figure 1.

Figure1. Cation image of the ionic liquid solvent, atomic labels of the $[patr]^+$ ion corresponding to the OPLS- AA scheme.



Simulation details:

MD simulations were performed by using of Tinker molecular modeling package and OPLS-AA force field for the ([part]⁺[Br]⁻) IL and SWCNT molecules. The SWCNT molecules used in this work are (6, 6) with length of 15Å. After performed energy minimization, the MD simulations were performed at first NPT then NVT ensemble at 1 atm and 350.0K in the time scale of 3000 and 8000ps, respectively. We used from Ewald method, Beeman algorithm, periodic boundary conditions, Nose- Hoover thermostat and Berendsen barostat.

Results and Discussion:

Structural characteristics of carbon nanotube in ionic liquid were studied by using radial distribution functions (RDFs) (see figure 2) and it was revealed that the nearest IL cations to the carbon nanotube surface can approach it from three different positions.

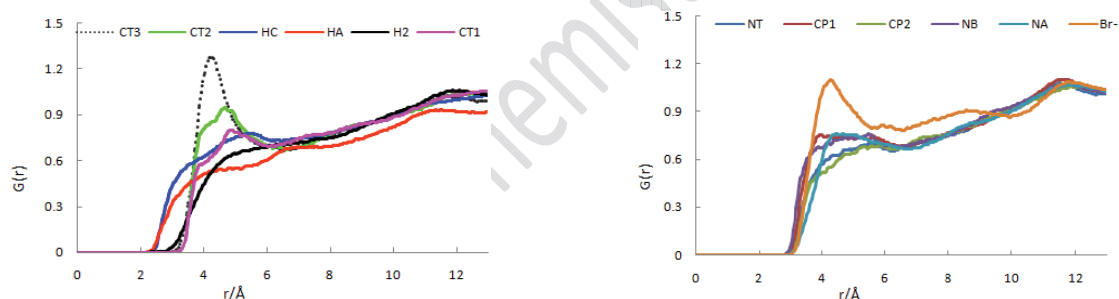


Figure2. Radial distribution functions of all species of the [part]⁺[Br]⁻ relative to species of the C_{SWCNT}.

Investigating of a single nanotube system immersed in ILs indicates that the diffusion of anion and cation into the inside of (6, 6) nanotube and were observed that aggregation of bromide anions at the two ends of nanotube molecule is more than the other places of simulation cell. In addition, it was found that because of existence the electron- rich C_{SWCNT} atoms and the possibility of producing of π – *stacking* interactions in the first solvated layer, IL cations get near to the nanotubes wall surface more than its anions. Indeed each of the interactions in system for example π – stacking, hydrogen bond, columbic and Van der waals interactions try to produce maximum attraction and minimum repulsion by mean of convenient orientation of molecules and ions. In close distance to nanotube, the π – stacking force is the determiner of



cation orientation relative to nanotube and in farther distance the other three forces are the determiner of it.

Conclusions:

It was found that: cations of IL orientated with three states in first solvated layer, larger density of anions around H_{SWCNT} than other space of simulation cell and the first solvated layer of cation is closer to SWCNT surface than to anion layer.

References:

- [1] Y. Shim and etal; " Solvation of Carbon Nanotubes in a Room- Temperature Ionic Liquid"; J. ACS Nano; 3, 1693–1702, 2009.
- [2] R. T. Kachoosangi and etal; " Carbon Nanotube–Ionic Liquid Composite Sensors and Biosensors" ; Anal. Chem.; 81,435-442, 2009.

Calculation of diffusion and transport coefficient for 1-n-propyl- 4- amino- 1, 2, 4- triazolium bromide ionic liquid

M. Foroutan*, M. Mohammadi

Department of Physical Chemistry, School of Chemistry, University College of Science, University of Tehran,
Tehran, Iran

Email: Mohammadi_Morteza@khayam.ut.ac.ir

Key words: Ionic Liquid, Carbon Nanotube, diffusion, simulation.

Introduction:

Between all physical properties of ionic liquids (ILs), transport properties are particularly important parameters that must be accounted for in the selection of a given IL for its applications as an alternative solvent or conductor. The relatively long equilibration times in the absorption of gases by ILs are a consequence of the low diffusivity of the solutes on a highly viscous medium [1]. The transport properties are also crucial when considering the reaction kinetics in a synthetic process or ion transport in an electrochemical device. Regarding the important role of ILs as reaction media, the significance of transport properties is manifested, among other things, in the fact that chemical reactions can be diffusion-limited even for highly soluble molecules [2]. In fact, most of current research for the development of new and more useful ILs is focused on the synthesis of products with improved transport properties (low viscosity, high electrical and heat conductivities, etc.). In this work we were studied and calculated mean square displacement (MSD), diffusion coefficient and transport coefficient for mixed systems of ILs and nanotube molecules. The structure and atomic partial charges of the IL cation are shown in figure 1.

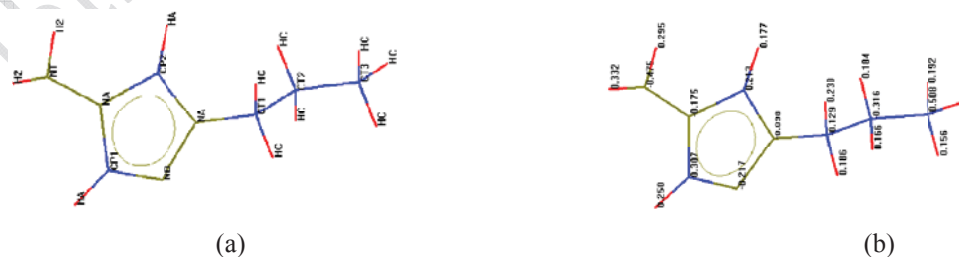


Figure1. Cation image of the ionic liquid solvent, (a) Atomic labels of the $[\text{patr}]^+$ ion corresponding to the OPLS- AA scheme. (b) Show the



partial charges for each atom.

Simulation details:

The OPLS-AA force field in TINKER molecular modeling package were used for performing the MD simulations studies on bundle, non- bundle and bulk IL. All the simulation systems after Minimize RUN, in order to obtain simulation data, at first were running in NPT ensemble and then continue in NVT ensemble in the time scale of 11ns. In our simulations, we used of Beeman algorithm, Nose- Hoover thermostat and Berendsen barostat in the temperature and pressure conditions of 350K and 1atm, respectively. The long- range electrostatic interactions were calculated by means of the Ewald method.

Results and Discussion:

MSD diagrams, self- diffusion coefficients and charge transport coefficients for cation and anion of each system were studied and calculated. The slopes of the MSD diagrams and the diffusive coefficient values indicated that in all simulation systems, despite of larger size of cation than to anion it is faster than anion. The comparison between diffusion coefficient of cation and anion for bundled system and similar non- bundled system shows that IL diffusion coefficient in bundled system is more than the other, and the IL bulk have least value diffusive of cation and anion. Since $MSD_i(t) \propto t^\beta$, we analyzed the β values by: $\beta(t) = \frac{d \log(MSD(t))}{d \log(t)}$. We understand from its data that the value of β is less than 1 ($\beta < 1$) for the cation and anion of all systems, this indicates that the dynamic of this IL is glassy and sub diffusive in the calculated time scales. It was determined that in these kinds of systems $t_+ > 0.5$ and this means that in these kinds of systems the ability of cation to charge transport and diffusion is more than anions, because the value of the distributed charge in the anion unit of surface is more than cations.

Conclusion:



In our studies, it is found that rate of the cation diffusion is more than anion; its ability in transport charge is more too, and also the $\beta < 1$ results for all systems indicate that dynamic of these systems is glassy and subdiffusive.

References:

- [1] L. J. Anthony and etal; " Solubilities and Thermodynamic Properties of Gases in the Ionic Liquid 1-*n*-Butyl-3-methylimidazolium Hexafluorophosphate" ; J. Phys. Chem. B; 106, 7315-7320, 2002.
- [2] C. Chiappe and etal; " Ionic liquids: solvent properties and organic reactivity"; J. Phys. Org. Chem; 18, 275- 297, 2005.



Mobility of gaseous ions in noble gases: comparison of potential models

A. H. Jalili ^{a*}, H. Behnejad ^b, G. Afsahi ^b, A. Abbaspour ^b, M. Gharibi ^c, L. A. Viehland ^d

^a Gas Science Department, Research Institute of Petroleum Industry, P.O. Box 14665-137, Tehran, Iran

(Email: jaliliah@ripi.ir)

^b School of Chemistry, University College of Science, University of Tehran, Tehran, Iran

^c Non-Polymeric Research Group, Petrochemical Research and Technology Company, National Petrochemical Company, P.O. Box 1435884711, Tehran, Iran

^d Science Department, Chatham University, Pittsburgh, Pennsylvania 15232, USA.

Key words: ion mobility, kinetic theory, ion-neutral interaction, potential model

Analysis of charged particle transport in dilute gases under the influence of electric fields has theoretical and practical applications in science and technology [1]. Investigation of ion mobility in gases is an important issue in applied fields such as plasma chemistry, atmospheric physics, and numerical simulations of industrial plasma [2-7]. There is now available on-line a large amount of data for such analyses [8]. Here, we compare ion mobilities calculated from the MSV-fitted INVERT potential [9-11], the classical (n,6,4) potential model [12], and the Lennard-Jones like (LJL) phenomenological potential recently proposed by Laricchiuta et al. [13] with the experimental data for monatomic, diatomic and triatomic ions in noble gases. The systems studied in this work are: a) HeO^+ and HeS^+ as examples of monatomic ions in atomic neutrals; b) ArO_2^+ and HeCO^+ as prototypes of diatomic ions in atomic neutrals; and c) He-SO_2^+ and Ar-SO_2^+ as examples of triatomic ions in atomic neutrals. The two-temperature theory of Viehland and Mason [14] has been employed to calculate the mobility of the ions in neutral gases. Results show that the MSV-fitted INVERT potential yields ion mobilities in best agreement with experimental data for atomic ions and diatomic ions in atomic neutral gases. However, in case of triatomic ions in atomic neutrals the (n,6,4) potential model shows the best agreement of calculated ion mobilities with experimental values. In all three cases, the



phenomenological LJJ potential due to Laricchiuta et al. [13] is less consistent with experimental ion mobility data than are the other two potential models studied in this work.

Acknowledgements:

We are thankful to the research council of the Research Institute of Petroleum Industry (RIPI) for their support of this work.

References:

- [1] E.A. Mason and E.W. McDaniel, *Transport Properties of Ions in Gases* (Wiley, New York, 1988).
- [2] F. M. Aghamir, N. S. Matin, A. H. Jalili, M. H. Esfarayeni, M. A. Khodaghali, R. Ahmadi, *Plasma Sources Sci. Technol.* **13**, 707, 2004.
- [3] N. Seyed Matin, A. H. Jalili, H. Savadkoobi, R. Ahmadi, M. Khodaghali, S. Vasheghani, *Proceedings of 17th International Symposium on Plasma Chemistry*, Toronto, Canada, August 7–12, 2005.
- [4] H. Savadkoobi, N. Seyed Matin, A. H. Jalili, R. Ahmadi, M. Khodaghali, H. R. Bozorgzadeh, *28th International Conference on Phenomena in Ionized Gases*, Prague, Czech Republic, July 15-20, 2007.
- [5] T. Hoffmann, G. Baldea, and U. Riedel, *Proc. Comb. Inst.* **32**, 3207, 2009.
- [6] H. Bozorgzadeh, A. Aziznia, N. Seyed-Matin, M. Baghalha, A. H. Jalili, *19th International Symposium on Plasma Chemistry*, Bochum, Germany, July 26-31, 2009.
- [7] N. Seyed Matin, A. H. Jalili, M. Hosseini-Jenab, M. Zekordi, A. Afzali, C. Rasouli, A. Zamaniyan, *Plasma Chem. Plasma Proc.* **30**, 333, 2010.
- [8] www.icecat.laplace.univ-tlse.fr
- [9] A. H. Jalili, N. Seyed-Matin, L. A. Viehland and M. Shahsavan, *Chem. Phys.* **365**, 94, 2009.
- [10] A. H. Jalili, A. Abbaspour, H. Behnejad, L. A. Viehland, *Mol. Phys.* **108**, 35, 2010.
- [11] M. Gharibi, L. A. Viehland, A. Abedi, A. H. Jalili, G. Afsahi, H. Behnejad, *Mol. Phys.* (submitted).



- [12] H. W. Ellis, R. Y. Pai, E.W. McDaniel, E. A. Mason, and L. A. Viehland, *At. Data Nucl. Data Tables* **17**, 177, 1976.
- [13] A. Laricchiuta, G. Colonna, D. Bruno, R. Celiberto, C. Gorse, F. Pirani, M. Capitelli, *Chem. Phys. Lett.*, **445**, 133–139, 2007.
- [14] L. A. Viehland, E. A. Mason, *Ann. Phys. (N.Y.)* **91**, 499, 1975.

15th Physical Chemistry Conference



Study Stability Complex Meso-tetra Arylporphyrinato Zinc & BF₃ With DFT Calculation results

M. Boostan ^{a*}, Ma. Boostan ^b, H. Yamola ^c

^a Shahr-E-Ray Branch, Islamic Azad University, Tehran. ^b Kashan University

^c Ph.D Student, Science and Research Branch, Islamic Azad University Tehran

Email: mhboostan@yahoo.com

Key words: Porphyrin ; DFT ; IR Spectra; Porphyrin–BF₃; Thermodynamic

Introduction:

Two important families of conjugated macrocycles exhibiting interesting optical and electronic properties are those of metaloporphyrins and sitting-atp complexes, both belonging to the general class of porphyrins [1]. Optimized structures of ligand and complex have been calculated, their structures parameters have been compared and thermodynamic parameters have been calculated for ligand and complex. The geometry optimizations and harmonic vibrational analyses were carried out without any symmetry restrictions. The nature of optimized geometries has been checked with harmonic frequency calculations. Finally the theoretical results have been compared to choosing the best method, basis set and structures for ligand and prepared complex [2-3]. Geometry calculation of molecular complexes of the metalloporphyrin Zinc and BF₃ by methods was mentioned above. All initial geometries were assumed as C₁ point group with no special symmetry constrain imposed. Only singlet spin states have been investigated.

Methods:

This systems also have been studied with theoretical methods at HF and B3LYP levels and 6-31g basis set for H, C, N, B and F and LANL2DZ basis set for metals with Gaussian 98. Thermodynamic calculations have been done in 289 K to resemble normal conditions in laboratory. Many studies have shown that DFT- B3LYP and HF method in combination with

6-31G basis set is able to figure out accurate energies, molecular structures, infrared vibrational frequencies that are very close to the experimental results.

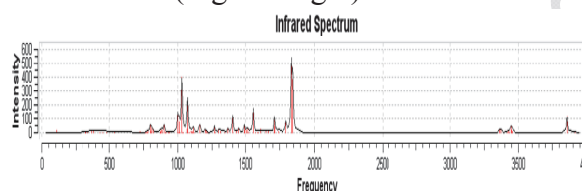
Result and discussion:

1-Geometric structures:

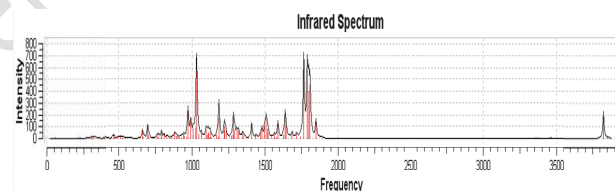
At first, it is necessary to examine their geometric structures before discussing various properties. All of optimized structures for the porphyrin ligand, 1:2 complex of porphyrin and BF_3 obtain at the B3LYP and HF method and using 6-31G basis set. Depict the final geometries contains selected bond lengths C=N, C-N and N-B. calculations show that demonstrating the strong donor-acceptor interaction between them also increase bond length C = N in 1:2 complex of porphyrin- BF_3 appointed the strong bond.

2-Infrared spectra:

It has a direct relation with the thermodynamic properties such as ΔH , ΔS and ΔG therefore; it is of great significance to calculate the IR spectra for the title compounds by B3LYP and HF/6-31G level. (Fig.1& Fig.2)



1. Frequency of ligand (B3LYP)



2. Frequency of complex 2BF3 (B3LYP)

Conclusion:

Finally optimized structures calculated ΔG & ΔH at level of 6-31G have been offered in Table 1, for porphyrin ligand, complex of porphyrin 1 BF_3 and complex of porphyrin 2 BF_3 (cis & trans).

Table1- Energies of porphyrin & complex 2 BF_3

HF/6-31G	Ligand	complex 1 BF_3	Co 2 BF_3 Cis	Co 2 BF_3 trans
$\Delta H(\text{kcal/mol})$	-616542.51	-819294.12	-1022022.02	-1022050.83



$\Delta G(kcal/mol)$	-616579.53	-819336.54	-1022070.28	-1022098.08
----------------------	------------	------------	-------------	-------------

References:

- [1] D.A. McQuarrie, Statistical Mechanics, University Science Books, California, 2000 .
- [2] J. J. Gajewski and P. Ngermeesri., Indiana UniVersity, Bloomington, Indiana 47401.
Received June 20, 2000 .
- [3] Hamid Reza Khavasi, Mansour Zahedi, Shant Shahbazian, Nasser safari, Seik Wenge Ng, Daryoush Mohajer, Chemical physics 301 ,2004 .



Study quantum mechanical calculations complex HABA^- and Li^+ With ab initio & Thermodynamic results

M. Boostan ^{a*}, Ma. Boostan ^b, H. Yamola ^c

^a Shahr-E-Ray Branch, Islamic Azad University, Tehran. ^b Kashan University

^c Ph.D Student, Science and Research Branch, Islamic Azad University Tehran

Email: mhboostan@yahoo.com

Key words: Phenyl azo dyes ; DFT ; IR Spectra; Ab initio methods; Thermodynamic

Introduction:

In this project anionic forms of ligand HABA^- and its complex of Li^+ by using quantum mechanical calculations with various theoretical methods and basis sets have been studied.. Azo dyes are most important classes of organic compounds, which have a number of application in different fields such as: eatable colors useful for foods, Plastic color dishes, solar sensors producing and electronic parts halograms, drugs and print ink. Pigments or Azo dyes are including aromatic rings which have been connected by chromophore group $-\text{N}=\text{N}-$ [1-2]. Optimized structures of ligand and complex have been calculated, their structures parameters have been compared and thermodynamic parameters have been calculated for ligand and complex. The geometry optimizations and harmonic vibrational analyses were carried out without any symmetry restrictions. The nature of optimized geometries has been checked with harmonic frequency calculations. Finally the theoretical results have been compared to choosing the best method, basis set and structures for ligand and prepared complex [3-4]. Geometry calculation of molecular complexes of the 2-(4- hydroxy phenyl Azo) benzoic acid and Li^+ by methods was mentioned above. All initial geometries were assumed as C1 point group with no special symmetry constrain imposed Only singlet spin states have been investigated.

Methods:

This systems also have been studied with theoretical methods at HF and B3LYP levels and 6-31 G 6-31 G* basis set for H, C, N, O and LANL2DZ basis set for metal with Gaussian 98. Thermodynamic calculations have been done in 27 °C to resemble normal conditions in laboratory. Many studies have shown that DFT- B3LYP and HF method in combination with 6-31G basis set is able to figure out accurate energies, molecular structures, infrared vibrational frequencies that are very close to the experimental results.

Result and discussion:

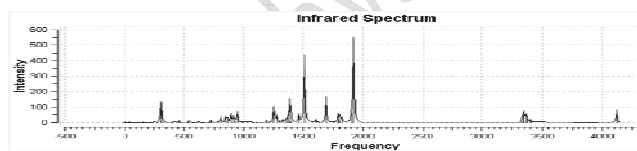
1-Geometric structures:

At first, it is necessary to examine their geometric structures before discussing various properties. All of optimized structures for HABA⁻ ligand, 1:1 complex of HABA⁻ and Li⁺ obtain at the B3LYP and HF method and using 6-31G & 6-31 G* basis set (fig.1).

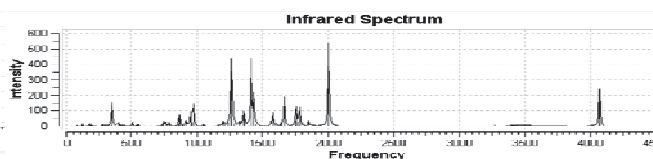


2-Infrared spectra:

It has a direct relation with the thermodynamic properties such as ΔE , ΔH , ΔS and ΔG therefore; it is of great significance to calculate the IR spectra for the title compounds by B3LYP and HF/ 6-31G & 6-31G* level. (Fig.2 & Fig.3)



2-Frequency of HABA⁻ (HF/6-31g *)



3- Frequency of complex HABA⁻ & Li⁺ (HF/6-31g *)

Conclusion:

Finally optimized structures calculated ΔG & ΔH at level of 6-31G and 6-31G* have been offered in Table 1, for HABA ligand, complex HABA⁻ and Li⁺.



Table1- Energies of complex HABA & Li⁺

	HF/6-31 G	HF/6-31 G *	B3LYP/6-31 G	B3LYP/6-31 G *
$\Delta E(\text{kcal/mol})$	-525808.627	-526021.514	-529047.894	-529185.725
$\Delta H(\text{kcal/mol})$	-525808.034	-526020.922	-529047.302	-529185.133
$\Delta G(\text{kcal/mol})$	-525845.083	-526058.247	-529085.341	-529223.433

References:

- [1] Singh, K., Singh, S. and Taylor, J.A., Dyes and Pigments, 54, p.189 (2002).
- [2] Towns, A.D., Dyes and Pigments, 42, p.3 (1999).
- [3] Hadadzadeh, H. and Rezvani, A.R., J. Crys. Min., 12, p.274 (2004).
- [4] H.Dabbagh, A. Teimouri, A. Najafi. spectrochimica Acta p A(2007).



Many-Body effects in some thermodynamic properties of CO₂, CO₂-Ar, and CO₂-CH₄ from molecular dynamics simulation

M. Abbaspour*, E. Nameni

Department of Chemistry, Hakim Sabzevari University, Sabzevar, Iran

(E-mail: abbaspour@sttu.ac.ir)

Keywords: HFD-like potential; Many-body interaction; Molecular dynamics simulation; Equation of state; Self-diffusion coefficient

Introduction:

Carbon dioxide has been widely studied via computer simulation techniques for the past few decades due to its importance in both industrial applications and environmental issues [1].

The purpose of the present paper is to perform Molecular dynamics (MD) simulation to obtain pressure and self-diffusion coefficient of fluid carbon dioxide using the two-body HFD-like potential of Abbaspour and Goharshadi [2]. We have also obtained pressure of CO₂-Ar and CO₂-CH₄ fluid mixtures at a given temperature and different densities using the 3A model of Hough and Howard [3] and ab initio potential of Oakley and Wheatley [4], respectively. To take many-body forces into account, three-body potential of Hauschild and Prausnitz [5] has been used with the two-body potentials of these systems. The MD simulation of carbon dioxide has been also used to determine a new equation of state.

Results and discussion:

The MD simulation has been performed to obtain pressure of fluid carbon dioxide using two-body HFD-like and total (two-body plus three-body) potentials using the three-body potential of Hauschild and Prausnitz [5].



Our results of pressure for fluid carbon dioxide in the NVT ensemble have been compared at different temperatures and densities (in the liquid state, vapor, and supercritical region) with the experimental data [6]. The results indicated that the three-body potential has improved the results and make them closer to the experiment. It is also expected and shown that the different potentials represent smaller deviations at lower densities and higher temperatures.

The MD simulation has been also used to determine carbon dioxide EOS using the total potential in better agreement with the NIST EOS [6] than others.

The calculated self-diffusion coefficient of carbon dioxide from the time-dependent mean-square displacement using two-body and total potentials has been shown good agreement with the experiment. It is also shown that the three-body potential of Hauschild and Prausnitz has increased the simulated values of diffusion to give better agreement with the experiment.

We have compared our simulated pressure results of CO₂-Ar and CO₂-CH₄ mixtures at constant temperature in the NVT ensemble and three different molar fractions and different densities using the two-body and total potentials with the experiment. The results indicated that the three-body potential has improved the results and make them closer to the experiment.

Conclusions:

The MD simulation has been performed to obtain pressure of pure CO₂, CO₂-Ar and CO₂-CH₄ mixtures using the two-body HFD-like potentials. To take many-body forces into account, three-body potential of Hauschild and Prausnitz [5] has been used with the two-body potentials.

For the first time, the three-body potential of Hauschild and Prausnitz extended as a function of density, temperature, and molar fraction and used with the two-body HFD-like potentials of CO₂, CO₂-Ar, and CO₂-CH₄ systems to improve the prediction of the pressures values without requiring an expensive three-body calculation. The MD simulation has been also used to determine a new equation of state which may be used as a reference for fluid carbon dioxide.

We have also simulated self-diffusion coefficient of fluid carbon dioxide using two-body and total potentials in good agreement with the experiment



References:

- [1] K. Yu, J.R. Schmidt, J. Chem. Phys. 136 (2012) 034503.
- [2] M. Abbaspour, E.K. Goharshadi, Chem. Phys. 330 (2006) 313.
- [3] A.M. Hough, B.J. Howard, J. Chem. Soc. Faraday Trans. 2 83 (1987) 191.
- [4] M.T. Oakley, H. Do, R.J. Wheatley, Fluid Phase Equilib. 290 (2010) 48.
- [5] T. Hauschild, J.M. Prausnitz, Mol. Simul. 11 (1993), pp. 177-185.
- [6] NIST Chemistry Webbook. Available at <http://webbook.nist.gov/chemistry/fluid>.

The effect of Mercapto acetic acid adsorption on Si₁₄ silicon quantum dot.

D. Farmanzadeh^{1*}; L. Tabari Shahandasht²

1, 2 Faculty of Chemistry, University of Mazandaran, Babolsar, Islamic Republic of Iran

E-mail: d.farmanzad@umz.ac.ir

Keywords: SiQDs, Mercapto acetic acid, DFT, CIS

Introduction:

Silicon quantum dots (SiQDs) are one of the most active frontiers in physics, chemistry, and biophysics because of being nontoxic and inexpensive which can be modified to achieve better properties by binding appropriate functional groups to terminate their surfaces[1,2,3]. In this work, we have studied the properties of hydrogenated and Mercapto acetic acid (MAA) capped Si₁₄QDs.

Methods:

The ground and excited state calculation are carried out with DFT/B3LYP and CIS method using the 6-31G* basis set respectively. The initial geometries of MAA-Si₁₄QDs were constructed starting from tetrahedral H-SiQDs, and then some H atoms were replaced by MAA groups. The optimized ground state geometries of hydrogenated and one of the MAA-terminated SiQDs are shown in Figure 1.

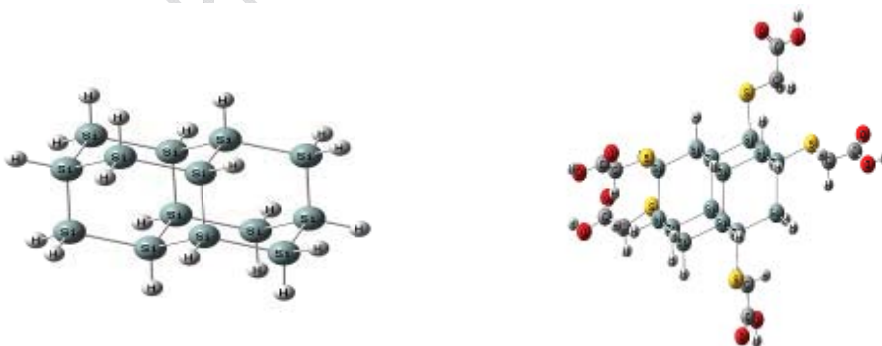


Figure 1: The optimized ground-state structures of $\text{Si}_{14}\text{H}_{20}$ and $\text{Si}_{14}\text{H}_{15}(\text{MAA})_5$

Results and discussion:

The calculated energies of the highest occupied molecular orbital (HOMO) and the lowest unoccupied molecular orbital (LUMO), HOMO-LUMO gaps and absorption and emission energies for H- Si_{14}QDs and selected MAA- Si_{14}QDs are reported in table 1. As can see from this table, adsorption of first Mercapto acetic acid reduces the optical gap and the absorption and emission energy but increasing the number of MAA molecule makes only a little change on these factors.

Table 1. The energies of HOMO and LUMO, and energy gaps (HLG) between HOMO and LUMO and the absorption (E_{abs}) and emission (E_{emi}) energies of Si_{14} and Si_{14}QDs which capped with MAA.

	HOMO (eV)	LUMO (eV)	HLG (eV)	E_{abs} (eV)	E_{emi} (eV)
$\text{Si}_{14}\text{H}_{20}$	-7.01	-0.99	6.02	6.67	4.81
$\text{Si}_{14}\text{H}_{19}(\text{MAA})_1$	-6.43	-1.32	5.11	5.63	4.49
$\text{Si}_{14}\text{H}_{18}(\text{MAA})_2$	-6.34	-1.58	4.76	5.49	4.48
$\text{Si}_{14}\text{H}_{17}(\text{MAA})_3$	-6.35	-1.60	4.75	5.49	4.48
$\text{Si}_{14}\text{H}_{16}(\text{MAA})_4$	-6.39	-1.62	4.77	5.49	4.47
$\text{Si}_{14}\text{H}_{15}(\text{MAA})_5$	-6.42	-1.66	4.76	5.49	4.48

Further investigation on the properties of MAA-capped Si_{14}QDs shows that the electronic excitation takes place by inner electron but not between HOMO and LUMO; for this reason, increasing amount of MAA has a few effects on the electronic properties.

Conclusions:

In conclusion, the surface MAA reduces the optical gap and enhances absorbance and fluorescence of Si_{14}QDs . Increasing the amount of MAA makes the small changes in the electronic and optical structure of the Si_{14}QDs . Our study shows that the Mercapto acetic acid is a good protecting molecule of SiQDs .

References:



- [1] X. Wang, R. Q. Zhang, T. A. Niehause, Th. Frauenheim, J. Phys. Chem, C 111(6), 2007, 2394.
- [2] J. H. Warner, A. Hoshino, K. Yamamoto, R. D. Tilley, Angew, Chem. Int. Ed, 44, 2005, 4550.
- [3] M. Nishida, J. Appl. Phys, 98, 2005, 023705.

15th Physical Chemistry Conference



Hybrid density functional theory study and natural bond orbital interpretation of conformational behavior of methanedithiol

E. Jalali^{a*}, H. Yahyaei^b

^a Chemistry Department, Science Faculty, Damghan branch, Islamic Azad University, Damghan, Iran

^b Chemistry Department, Zanzan Branch, Islamic Azad University, Zanzan, Iran

E-mail: ala.jalali@gmail.com

Keywords: methanedithiol , generalized anomeric effect , ab initio , NBO

Introduction:

The most dominant conformation-controlling factor in carbohydrate compounds is known as the *anomeric effect* (AE).¹⁻³ If a pyranose ring has an electronegative substituent at the anomeric carbon then this substituent is more likely to take the axial configuration than the equatorial configuration. This is a consequence of a general effect (the generalized anomeric effect, *GAE*) that in a chain of atoms X-C-Y-C, in which Y and X are atoms with nonbonding electron pairs (e.g. F, O, S, N), the synclinal conformation is more likely. Although the importance of the hyperconjugative interactions in some acyclic compounds has investigated, there is insufficient published experimental information about the stereoelectronic interactions in methanedithiol. In this work, the impacts of the generalized anomeric effect (*GAE*) associated with electron delocalizations,¹⁻³ steric and dipole-dipole interactions on the conformational and structural properties of methanedithiol were investigated computationally using hybrid-DFT and NBO interpretation.^{4,5}

Methods:

Hybrid DFT calculations were carried out using the B3LYP/6-311+G** levels of theory with the GAUSSIAN 03 package of programs.⁴ The main purpose of the present work was to study the impacts of the stereoelectronic interaction effects, dipole-dipole interactions on the



conformational preferences in methanedithiol. An NBO analysis was then performed for the axial and equatorial conformations of methanedithiol by the NBO 5.0 program contained in the PC-GAMESS interface.⁵

Results and Discussion:

Hybrid-density functional theory (B3LYP/6-311++G**) based methods and NBO interpretation were used to study the conformational behaviors of methanedithiol. The most stable conformations of methanedithiol were found by changing and scanning the dihedral angles H1-C2-S3-C3. The results obtained showed that the axial symmetrical (C₂) conformation of methanedithiol is more stable than its plane symmetrical (C_s) and unsymmetrical (C₁) conformations. The NBO analysis of donor-acceptor (LP→σ*) interactions showed that the generalized anomeric effect (GAE) value of the axial symmetrical (C₂) conformation is less than its corresponding plane symmetrical (C_s) conformation. Therefore, the rationalization of the conformation preference solely in terms of the GAE fails to account qualitatively for the of the axial symmetrical (C₂) conformation preferences in methanedithiol. On the other hand, the calculated dipole moment value of the plane symmetrical (C_s) conformation is greater than that of the axial symmetrical (C₂) conformation. There is a conflict between the GAE and electrostatic model in this case. Consequently, the electrostatic model succeeds to account qualitatively for the of the axial symmetrical (C₂) conformation preferences in methanedithiol. The correlations between the GAE, bond orders, ΔG, dipole-dipole interactions, structural parameters and conformational behaviors of methanedithiol have been investigated.

Conclusion:

The B3LYP/6-311++G** calculations reported above and NBO analysis provided a reasonable picture from energetic, structural, bonding and stereoelectronic points of view for the conformational properties of methanedithiol. Effectively, the B3LYP/6-311++G** results showed that the axial symmetrical (C₂) conformation of methanedithiol is more stable than its plane symmetrical (C_s) and unsymmetrical (C₁) conformations. There is a conflict between



the GAE and electrostatic model in methanedithiol and the electrostatic model succeeds to account qualitatively for the of the axial symmetrical (C₂) conformation preferences in methanedithiol.

References:

- [1] D. Nori-Shargh, H. Yahyaei, J. E. Boggs, *J. Mol. Graph. Model.* **2010**, 28, 807.
- [2] D. Nori-Shargh, J. E. Boggs, *J. Phys. Org. Chem.* 2010, doi:10.1002/poc.1728.
- [3] E. Juaristi, G. Cuevas, A. Vela, *J. Am. Chem. Soc.* 1994, 116, 5796 -5804.
- [4] M. J. Frisch, et al, Gaussian 03, Revision B.03, Gaussian, Inc., Wallingford CT, 2004.
- [5] E. D. Glendening, J. K. Badenhoop, A. E. Reed, J. E. Carpenter, J. A. Bohmann, C. M. Morales, F. Weinhold, Theoretical Chemistry Institute, University of Wisconsin, Madison, WI, 2004. NBO Version 5.0.



Ab initio study of intramolecular fluorine transfer in perfluoroguanidine

H. Sabzyan^{a*} and A. Enami^b

^a Department of Chemistry, University of Isfahan, Isfahan 81746-73441, I. R. Iran.

^b Department of Chemistry, Science and Research Branch, Islamic Azad University, Khuzestan, I. R. Iran.

sabzyan@sci.ui.ac.ir, azadeh.enami@yahoo.com

Keywords: Perfluoroguanidine, Fluorine Transfer, Proton Transfer, IRC, Transition State

Introduction:

Perfluoroguanidine (CF_5N_3 , **PFG**) a colorless liquid with molecular weight of 149.02 g/mol and boiling point of 44.4 °C contains one imino- and two amino- nitrogen atoms bonded to its only carbon atom, and five fluorine atoms attached to the nitrogen atoms (Fig. 1). **PFG** has eight hydrogen-bond acceptor and no hydrogen-bond donor. **PFG** forms several adducts with alcohols which are powerful explosives sensitive to impact, friction and heat. **PFG** is used also as a liquid rocket fuel oxidant. When heated to decomposition, **PFG** emits toxic fumes of F_2 . Characterization and interpretation of the chemical reactivity and physical behavior of **PFG** are necessary for its clever use in the desired applications. Computational methods can be considered as cost-effective and the most green methods for carrying out such characterization. In this work, the fluorine transfer reaction from the amine to the imine nitrogen atom (sigmatropic rearrangement) in the **PFG** molecule in the gas phase and the effect of protonation at the imino and amino nitrogen sites on this transfer have been studied computationally. The intrinsic reaction coordinate (IRC) of this intramolecular fluorine transfer in **PFG** passes through a symmetric intermediate and results in an identical structure.

Computational Method:

First, geometry optimization, vibrational and thermochemical analyses are carried out on the **PFG** and its two (imino- and amino-) protonated structures using B3LYP/6-311++G** method. Next, intramolecular fluorine transfer paths (IRC) and the corresponding TS

structures are calculated using QST2 approach. The transfer paths are characterized based on the NBO and Löwdin population analyses. The IRC curves obtained for the fluorine transfer reaction in **PFG** and its two imino- and amino- protonated species are shown in Fig. 1 (right). Numerical values of the TS and protonation energies calculated for **PFG** are listed in Table 1 where corresponding quantities for guanidine (**G**) are given for comparison.

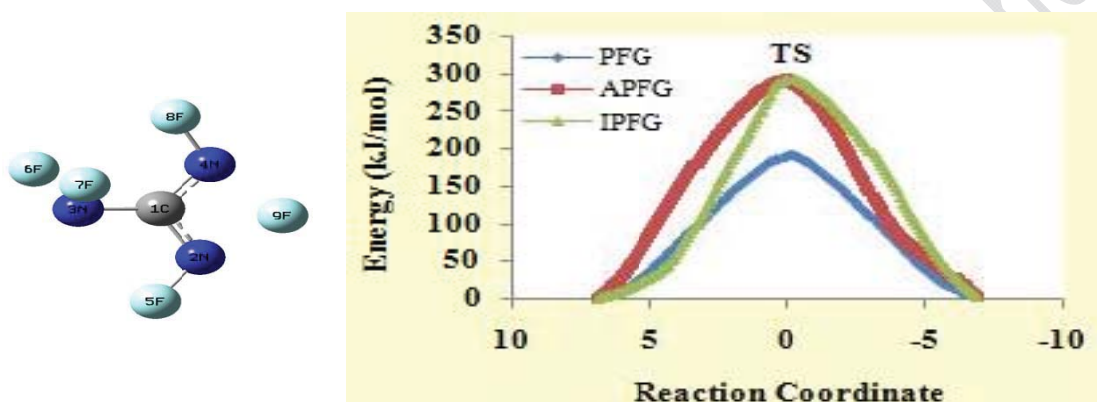


Fig. 1: Molecular structure of perfluoroguanidine (**PFG**) and its fluorine transfer IRC potential energy curves (left). The horizontal axis is scaled in terms of the number of IRC steps.

Results and Discussion:

Analyses of the calculated IRCs and the TS structures and energies obtained for **PFG** and its imino- and amino- protonated structures shows that the transition state energy in **PFG** is very high (much higher than proton transfer energies in **G** and **PFG**) and not accessible at room and intermediate temperatures. The TS energy is increased by protonation at both sites. At the TS point in the IRC of the three neutral, imino- and amino-protonated species, the transferring fluorine atom carries a small positive charge of 0.0003, 0.0472 and 0.0723.

The high energy fluorine transfer process, when occurring in solution phase, may be mediated by solvent molecules to become more feasible at ordinary temperatures, and therefore, explicit solvent molecules should be included in the quantum computations.

Table 1: Protonation (ΔE_p) and fluorine/proton transfer barrier (ΔE_{TS}) energies for perfluoroguanidine (**PFG**) /guanidine (**G**). For the proton transfer in **PFGH⁺(amino)**, ΔE_{TS} is calculated to be 144.3 kJ/mole.

Molecule	PFG	PFGH⁺(amino)	PFGH⁺(imino)	G	GH⁺(amino)	GH⁺(imino)
ΔE_{TS} (kJ/mol)	191.8	292.0	293.3	165.4	210.0	165.4
ΔE_p (kJ/mol)	-	-647.0	-711.3	-	-848.9	-1021.9

Conclusion:

The fluorine transfer reaction in the gas phase **PFG** has a large activation energy much higher than that of the proton-transfer reactions in similar guanidine systems. Protonation at both imino and amino nitrogen atoms of the **PFG** results in significantly higher TS barriers.

References:

- [1] T. Mezhenkova et al., Russ. J. Org. Chem., 46 (2010) 1418-1420.
- [2] T.V. Rybalova et al., J. Struct. Chem., 50 (2009) 741-753.
- [3] L.T. Kuhn et al., J. Phys. Chem. A., 110 (2006) 3521-3526.



A DFT study of hydrogen adsorption on Ln@B₁₆N₁₆ fullerene-like nanocluster (Ln: La, Gd and Lu)

Saeed Chashmniam, Vahideh Alizadeh, Mehdi D. Esrafil^{*}

Laboratory of Theoretical Chemistry, Department of Chemistry, University of Maragheh, Maragheh, Iran. (E-mail: esrafil@maragheh.ac.ir)

Key words: B₁₆N₁₆ fullerene-like nanocluster; Hydrogen adsorption; DFT; DOS.

Introduction :

It is well-known that the discoveries of fullerenes and carbon nanotubes have opened up new research area in condensed matter physics and materials science. The molecular structure of these carbon allotropes gives rise to a unique set of properties, suggesting a multitude of highly diversified application areas in, for instance, electronics and armor, etc [1]. As the isoelectronic counterparts to carbon cages, the structure and stability of boron nitrides (BN)_n as cages and nanotubes have been investigated extensively due to their potential electronic, optical and magnetic properties [2]. Earlier studies indicated that boron nitrides (BN)_n favor cage structures for $n > 10$ [3]. More recently, Strout [4] reported that the boron nitrides (B₁₃N₁₃, B₁₄N₁₄ and B₁₆N₁₆) with squares and hexagons are more stable than the corresponding fullerene-like structures containing pentagons and hexagons.

Hydrogen, the third most abundant element on earth, has the potential to meet the energy needs of the mobile industry. Its economical use as an alternate energy has considerable difficulties to overcome. Among these, the most difficult challenge is to find materials that can store hydrogen with large gravimetric and volumetric density and operate under ambient thermodynamic conditions. In this contribution, we report our DFT study of the stability and hydrogen adsorption behavior of alternate fullerene-like cage structures of Ln@B₁₆N₁₆, where Ln=La, Gd and Lu.



Computational aspects:

All DFT calculations were performed using Gaussian 03 program [5]. The geometries of the investigated Ln@B₁₆N₁₆ clusters were optimized at the B3LYP level employing 6-31G* basis set. As it is found in the literature, 46+4f *n* electrons of La³⁺, Gd³⁺ and Lu³⁺ ions were modeled by quasirelativistic effective core potentials (ECPs) of the Stuttgart group [6].

Results and discussion:

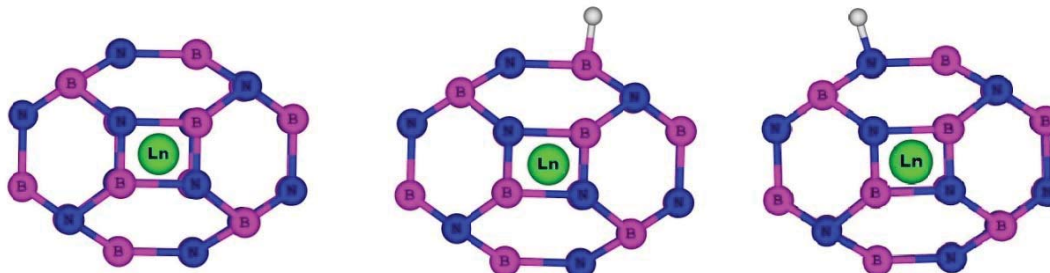
The optimized structures of pure and hydrogenated Ln@B₁₆N₁₆ clusters are shown in Figure 1. Our results indicated that there are two distinct sites for an H atom adsorption; the top of B atom and that of N one. Thus, to find the adsorption behavior of an H atom on the Ln@B₁₆N₁₆ cluster, H atom is put on the top site of B or N atom. The results show that this adsorption is site selective and H atom prefers to adsorb on the top site of the B atom with binding energy of -1.48, -1.44 and -1.41 eV for Ln=La, Gd and Lu, respectively. The corresponding length of newly formed H–B is 1.190, 1.189 and 1.186 Å, respectively, indicating that the interaction is very strong and a covalent bond is formed.

From density of states (DOS) analysis, it is revealed that the hydrogen adsorption on the B atom of Ln@B₁₆N₁₆ significantly affects the electrical properties of cluster. It is evident that the DOSs of this configuration near the valence band has a distinct change compared to that of the pristine cluster, so that local energy levels appear after the adsorption of hydrogen atom which would result in an electrical conductivity change of the cluster.

Concluding remarks:

Our results indicated that electron density of adsorbing atoms play an important role in the H adsorption. We showed that the H adsorption is thermodynamically feasible atop both the B and N atoms of cluster.

Figure 1- Optimized structures of pure and hydrogenated Ln@B₁₆N₁₆ clusters



References:

- [1] H. Shinohara, Rep. Prog. Phys. 63 (2000) 843.
- [2] Y. Saito, M. Maida, J. Phys. Chem. A 103 (1999) 1291.
- [3] D.L. Strout, J. Phys. Chem. A 105 (2001) 261.
- [4] D.L. Strout, Chem. Phys. Lett. 383 (2004) 95.
- [5] M. J. Frisch, *Gaussian 03*, revision E.; Gaussian, Inc.: Wallingford, CT, 2004.
- [6] M. Dolg, H. Stoll, H. Preuss, Theor. Chim. Acta. 85(1993) 441.



Dynamic Behavior of Boron Nitride Nanotube and Surfactant Complexes Mediated Molecular Dynamic Stimulation

M. Foroutan*, M. Fatemi

Department of Physical Chemistry, School of Chemistry, College of Science, University of Tehran, Tehran, Iran,
m.fatemi@khayam.ut.ac.ir

Keywords: Molecular Dynamics (MD) Simulation, Boron Nitride Nanotube (BNNT), Triton X100 (TX100) Surfactant, Carbon Nanotube CNT.

Introduction:

We used a molecular dynamics (MD) simulation approach to probe the behaviors of the BNNT with Triton X100 surfactant. So we assess nanotubes in different temperatures and diameter. The comparison of our results for BNNT-TX100 composites with those of the similar carbon nanotube CNT-TX100 composites, disclose that the BNNT-TX100 interactions are much stronger, which is the most significant result of this process.

Computational Procedure:

MD simulations were first carried out on a (5, 5) armchair CNT and (5, 5) armchair BNNT with a interacting with individual molecules of TX100. Using the AMBER99[1] force field and a canonical ensemble (constant NVT), the velocity form of Verlet algorithm method and the Nose-Hoover thermostat algorithm were used to integrate the equations of motion with a time step of 1.0 fs. Non-bonded van-der-Waals interactions were modeled by a Lennard-Jones potential with a cut-off distance of 1.2 nm. Our simulation is related to the behavior of the TX100 when they are close to the nanotubes in an “ideal” poor solvent.

Results and Discussion:

Figure 1 and 2 represent the snapshots of nanotubes wrapped by the TX100. Figure 3 represents the interaction energy for (5,5) nanotubes with TX100, as a function of simulation time. The interaction energies for BNNT_TX100 are much higher than those for the corresponding CNT-TX100, due to the large contribution of electrostatic interactions and π - π nature [2]. The stronger interfacial binding of TX100 to BNNTs is caused by the polarization of BNNTs [3], which directly gives rise to the strong electrostatic interactions between them. As Table 1 shows; with an increase in nanotube diameter, the interaction energy is increased, because the surface contact area between them increases accordingly. As Figure 4 shows; the attractive interaction of the TX100 with the nanotubes increasing only slightly with increasing temperature. Thus, the temperature dependence of the interaction energies can be considered negligible.

Conclusion:

Our work demonstrated that the composite materials of BNNTs and TX100 have a potential application in the preparation of fibers with mechanical strength much higher than that of composite materials of CNTs and TX100. So the BNNTs could be more efficient nanofillers than the CNTs for nanocomposite reinforcement applications.

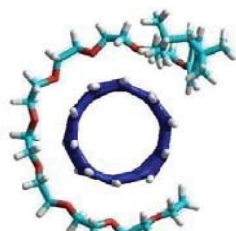


Fig.1: snapshot of (5, 5) CNT wrapping by TX100.

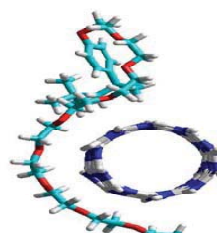


Fig. 2: snapshot of (5, 5) BNNT wrapping by TX100.

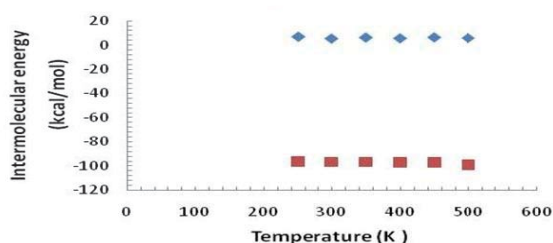
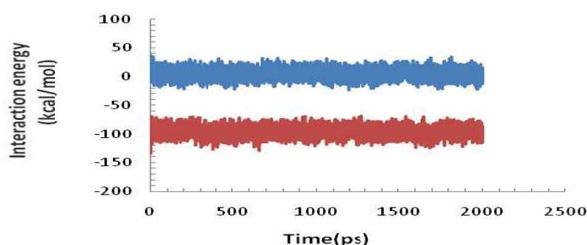




Fig.3: Interaction energy evolution for (5, 5) CNT-TX 100 and (5, 5) BNNT-TX100 composites respectively at 300 K.

Fig.4: Interaction energy of (5, 5) nanotube-TX100 composites as a function of temperature.

Table 1: Intermolecular interaction energy (kcal/mol) as a function of nanotubes diameter at 300 K.

Nanotube	diameter (Å)	interaction with TX_100
(5,5) CNT	6.68	5.82
(6,6) CNT	8.07	-44.49
(9,9) CNT	12.11	-56.82
(10,10) CNT	13.46	-58.31
(5,5) BNNT	6.95	-96.66
(6,6) BNNT	8.32	-101.52
(9,9) BNNT	12.45	-112.35
(10,10) BNNT	13.83	-124.62

Refrence:

- [1] N.L. Allinger.; Y.H. Yuh.; J.H. Lii.; J. Am. Chem. Soc. **1989**, 111, 8551.
[2] Chen, R. J.; Zhang, Y.; Wang, D.; Dai, H. J. Am. Chem. Soc. **2001**, 123, 3838.
[3] Won, C. Y.; Aluru, N. R. J. Phys. Chem. C **2008**, 112, 1812.



Molecular Dynamics Simulations Studies of surfactant -Wrapped Single - Walled Carbon Nanotubes surface

M. Foroutan*, M. Fatemi

Department of Physical Chemistry, School of Chemistry, College of Science, University of Tehran, Tehran, Iran,
m.fatemi@khayam.ut.ac.ir

Keywords: Molecular Dynamics (MD) Simulation, Carbon Nanotubes (CNT), Triton X100 Surfactant, Radius of Gyration (R_g).

Introduction :

We used a molecular dynamics (MD) simulation approach to probe the behaviors of the carbon nanotubes (CNT) with Triton X100 surfactant. So we assess nanotubes in different temperatures and diameter, according as the result of our simulations; the strong intermolecular interaction between CNT and TX100 that cannot be influenced by the temperature in the range we reported, and with an increase in nanotubes diameter, the interaction energy is increased.

Computational Procedure:

MD simulations were performed in the Tinker molecular modeling package (version 5.0)[1], using the AMBER99 force field, we used the (5,5), (6,6), (9,9), and (10,10) CNTs armchair with a length of about 25 Å. The diameter of CNTs ranges from 6.68 to 13.46 Å. Using a canonical ensemble (constant NVT), the velocity form of Verlet algorithm method and the Nose-Hoover thermostat algorithm were used to integrate the equations of motion with a time step of 1.0 fs. Non-bonded van-der-Waals interactions were modeled by a Lennard-Jones potential with a cut-off distance of 1.2 nm. Our simulation is related to the behavior of the TX100 when they are close to the CNT in an “ideal” poor solvent.

Results and Discussion:

Figure 1 and 2 represent the snapshots of CNT wrapped by the TX100. As figure 3 shows; with an increase in CNT diameter, the interaction energy is increased[2], because the surface

contact area between them increases accordingly, As Figure 4 shows; the attractive interaction of the TX100 with the CNT increasing only slightly with increasing temperature. Thus, the temperature dependence of the interaction energies can be considered negligible. As figure 5 shows, the radius of gyration (R_g) values of TX100 molecules increasing and show a fluctuation as the flexible hydrophilic polyethylene oxide chains wrap around the CNTs. As figure 6 shows, the R_g of TX100, when interaction with CNTs is higher than without CNTs, is caused by the intermolecular energy between TX100 and CNTs, which directly gives rise to the strong π - π interactions [3] with the nanotube surface, called “ π -stacking”[4] are responsible for the strong tendency of nanotubes to “stick together”, which is a major obstacle to their processing.

Conclusion:

Our simulation results showed that, the CNTs with larger diameter are suggested as better candidates compared to smaller CNTs in diameter for nanocomposite reinforcement applications, and the higher temperature and consequently higher kinetic energy does not have any significant effect on the total TX100 size.

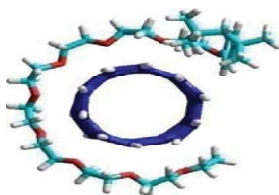


Fig. 1. Front view snapshot for a (5, 5) CNT Wrapping by TX100 surfactant.

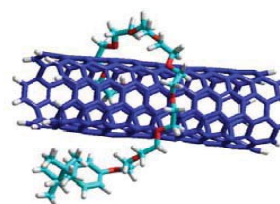


Fig. 2. Side view snapshot for a (5, 5) CNT wrapping by TX100 surfactant.

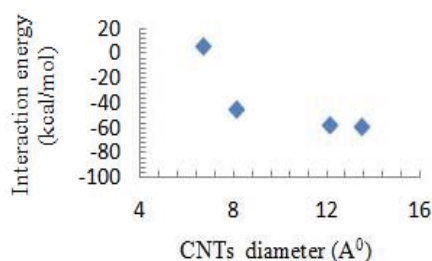


Fig. 3. Interaction energy as a function of CNT diameter at 300

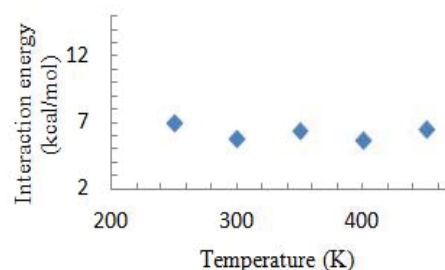


Fig. 4. Interaction energy as a function of temperature for CNTs.

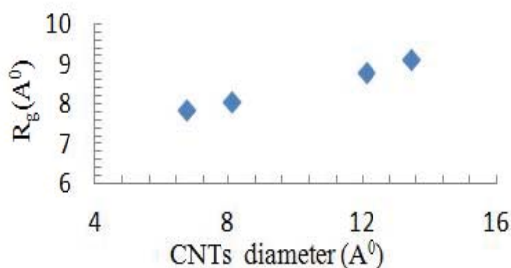


Fig.5. Change of (R_g) of the surfactant after the interaction with different CNTs in diameter.

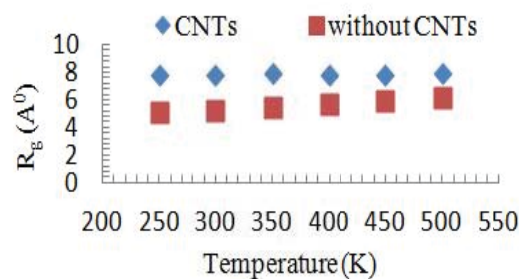


Fig.6. Change of (R_g) of TX100 after the interaction with and without CNTs as a function of temperature.

Reference:

- [1] Won, C. Y.; Joseph, S.; Aluru, N. R. J. Chem. Phys. **2006**, 125, 114701.
- [2] Jamie S. Quinton.; Adam J. Blanch.; Claire E. Lenehan. J. Phys. Chem. B **2010**, 114, 9805–9811.
- [3] Chen, R. J.; Zhang, Y.; Wang, D.; Dai, H. J. Am. Chem. Soc. **2001**, 123, 3838.
- [4] Tan, Y.; Resasco, D. E. J. Phys. Chem. B **2005**, 109, 14454.



Molecular modeling of 1-ethyl-3-methylimidazolium-based ionic liquids + H₂S complexes

Rozhin Fatehi ^{a,*}, Behrooz Adib^a, Amir H. Jalili^b

^a Department of Chemistry, Islamic Azad University – North Tehran Branch, Tehran, Iran,
(Email: r.fatehy@yahoo.com)

^b Gas Science Department, Research Institute of Petroleum Industry, P.O. Box 14665-137, Tehran, Iran

Key words: Ionic liquid, Interaction energy, *Ab initio* calculation, Gas solubility

Introduction:

Room temperature ionic liquids (RTILs) are a new class of compounds comprised of an organic cation and an anion. These compounds are liquid over a wide temperature range including ambient and due to strong electrostatic attraction between cation and anion, exhibit negligibly small vapor pressure [1]. Their tunable chemical structures make them adjustable solvents tailored to various practical and industrial applications. Nowadays, one of the active research areas is exploring ILs as a replacement to conventional alkanolamine (MEA, DEA, MDEA, etc.) solutions in natural gas sweetening processes [2]. A growing number of experimental data for solubility and diffusion of H₂S in various ILs have been generated in the past few years [3-10]. In this study we have focused on the application of some imidazolium-based ILs with different anions, i.e. [PF₆]⁻, [PF₅(CF₃)]⁻, [PF₄(CF₃)₂]⁻, [PF₃(CF₃)₃]⁻, in separation of H₂S from natural gas by employing a theoretical quantum chemical approach. This way the interaction of H₂S with the cation and anion of the IL is studied to gain a primary insight into the mechanism of dissolution of H₂S in the ILs and the results are compared with previously reported experimental and theoretical studies.

Method of Calculation:

Quantum chemical calculations were performed using Gaussian version 03 suite of programs. The geometries of isolated as well as supermolecules were optimized at the DFT/B3LYP level

of theory using the 6-311++G** basis set. The binding energies, E_{binding} calculated according to relation $E_{\text{binding}} = E_{\text{complex}} - (\sum E_{\text{monomer},i})$, where E_{complex} and $E_{\text{monomer},i}$ stand for the counterpoise-corrected optimized energy of the supermolecule (complex) and optimized energy of each of the monomers constituting the complex, respectively. For each of the complexes, several initial configurations were constructed for geometry optimization to explore the potential energy surface completely.

Results and Discussion:

The interaction energy of anions with 1-ethyl-3-methylimidazolium cation ($[\text{emim}]^+$) decreases as the number of $-\text{CF}_3$ substitutes in the anion increases. Due to our previous studies, this trend indicates that the density of the IL decreases from $[\text{emim}][\text{PF}_6]$ to $[\text{emim}][\text{PF}_3(\text{CF}_3)_3]$, which points out that probably the solubility of H_2S increases as the number of $-\text{CF}_3$ groups increase. The interaction energies of H_2S -anion complexes are in the range of 7-14 kcal/mol, indicating that these interactions are comparable in strength to traditional hydrogen bonds. In addition, the interaction energy of H_2S with the anion decreases as the number of $-\text{CF}_3$ substitutes increase, which further justifies the above-mentioned conclusion for the solubility of H_2S in the ILs studied in this work. Comparison of the interaction energy between cation and anion of the ILs studied in this work with previously studied ILs, indicates that $[\text{emim}][\text{PF}_3(\text{CF}_3)_3]$ is potentially a good candidate toward separation of H_2S from natural gas. Experimental measurements need to be performed to fix the problem.

References

- [1] Ionic Liquids in Synthesis; P. Wassercheid, T. Welton, Eds.; (Wiley-VCH: Verlag, 2002).
- [2] D. Camper, J. E. Bara, D. L. Gin, R. D. Noble, *Ind. Eng. Chem. Res.* **47**, 8496, **2008**.
- [3] F.-Y. Jou, A. E. Mather, *Int. J. Thermophys.* **28**, 490, 2007.
- [4] C. S. Pomelli, C. Chiappe, A. Vidis, G. Laurenczu, P. J. Dyson, *J. Phys. Chem. B*, **111**, 13014, **2007**.
- [5] A. H. Jalili, A. Mehdizadeh, M. Shokouhi, A. N. Ahmadi, M. Hosseini-Jenab, F. Fateminassab, *J. Chem. Thermodyn.* **42**, 1298, **2010**.



- [6] M. Shokouhi, M. Adibi, A. H. Jalili, M. Hosseini-Jenab, A. Mehdizadeh, *J. Chem. Eng. Data*, **55**, 1663, **2010**.
- [7] A. H. Jalili, M. Rahmati-Rostami, C. Ghotbi, M. Hosseini-Jenab, A. N. Ahmadi *J. Chem. Eng. Data*, **54**, 1844, **2009**.
- [8] H. Sakhaeini, A. H. Jalili, V. Taghikhani, A. A. Safekordi, *J. Chem. Eng. Data*, **55**, 5839, **2010**.
- [9] H. Sakhaeini, V. Taghikhani, A. H. Jalili, A. Mehdizadeh, A. A. Safekordi, *Fluid Phase Equilibria* **298**, 303, **2010**.
- [10] A. H. Jalili, M. Safavi, C. Ghotbi, A. Mehdizadeh, M. Hosseini-Jenab, *J. Phys. Chem. B* **116**, 2758, **2012**.



Assignment of Absolute Configuration of Fischerin by Computed NMR Chemical Shifts

Saeed K. Amini*

Chemistry and Chemical Engineering Research Center of Iran, Tehran, Iran

amini_s@ccerci.ac.ir

Fischerin, a biologically active components of fungi, which causes tremors and lethal peritonitis in mice, was extracted from *Neosartorya fischeri*.¹ Fujimoto and co-workers reported the partial configuration of fischerin.¹ They used NMR spectroscopic data to determine this partial configuration for the fused bicyclic moiety of this compound.¹ So, despite using powerful NMR techniques, Fujimoto and co-workers were not able to assign the relative configurations of the target molecule in the C19, C20, C21 and C22.¹

On the other hand, advanced methods in quantum chemistry facilitate the rapid, accurate, and reliable calculation of NMR chemical shifts. So, comparing the calculated and experimental chemical shifts will provide an efficient method in identifying and discriminating between the proposed diastereoisomers.²

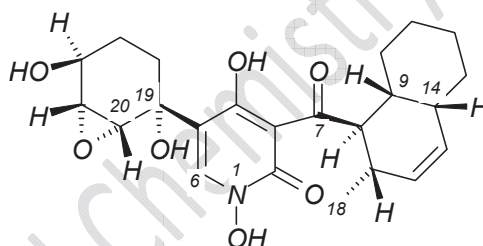
Considering the triangular fusion between C20 and C21 and assigned configuration of fused bicyclic moiety, four unassigned stereocenters allow for totally eight possible diastereomers for the target compound. They were used as probable structures of the target molecule in the quantum mechanical treatments. The first step in this treatment was their conformational analyses in order to find candidate conformers at room temperature which contribute to the experimental NMR spectra. In the next step, the postulated conformers, within a 3 kCal window of the lowest energy, were subjected to extensive geometry optimization followed by frequency calculations in order to confirm the nature of the optimized geometries as minima and provide their computed free energies. In the last step, among these extensively optimized structures, those within a 2.5 kCal window of the lowest energy were subjected to the chemical shielding calculations in dimethylsulfoxide solvent. In order to get accurate calculated chemical shieldings, Boltzman-weighted averaging based on relative free energies

of conformers at 298.15 K was used. The relative populations of conformers were computed as $\left(\frac{P_i}{P_j}\right) = \exp\left(\frac{-(E_i - E_j)}{RT}\right)$. Where P_x and E_x are the relative population and computed free energy of the x conformer, respectively.

In order to determine the correct configuration of the target molecule, the calculated chemical shifts were evaluated according to their largest and corrected mean absolute deviation (CMAD: $\left[\frac{1}{n}\sum_{i=1}^n |\delta_{calc} - \delta_{exp}|\right]$) in each configuration.

In order to confirm the conclusion of the CMAD analysis and get more confidence of which configuration is the correct one, the DP4 probability analysis developed by Smith and Goodman was also employed.²

Thus according to both the CMAD and DP4 analyses, structure, shown below, was found to be correct for the target molecule.



In this brief study the unassigned configurations of fischerin, extracted from *Neosartorya fischeri*, at C19, C20, C21 and C22 were assigned as R, R, R and S, respectively. In this assignment extensive conformational analysis and geometry optimization followed by frequency and chemical shielding calculations were employed in order to get the best computed chemical shifts compared to experimental ones. In these calculations solvent effects were also taken into account. The CMAD and DP4 analyses were employed together to get the correct configuration.

Keywords: Fischerin, Natural Product, Configuration, NMR, Ab Initio

References:

- [1] H. Jimoto, A. Keda, K. Amimoto, M. Yamazaki, *J. Nat. Prod.*, 1993 56, 8, 1268-1275.



[2] S. G. Smith, J. M. Goodman, *J. Am. Chem. Soc.* 2010, 132, 12946–12959 and references therein.

Configuration Assignment of 8 α -hydroxy-13-hydroperoxylabd-14,17-dien-19,16;23,6 α -diolide by Computed Chemical Shifts

Saeed K. Amini*

Chemistry and Chemical Engineering Research Center of Iran, Tehran, Iran

amini_s@ccerci.ac.ir

Some of terpenoids, which are bicyclic and mainly sesterpene lactones, were extracted from Iranian species.¹ Recently Matloubi and co-workers reported the partial configuration of a new sesterterpene, 8 α -hydroxy-13-hydroperoxylabd-14,17-dien-19,16;23,6 α -diolide.¹ They used their own X-ray determined configuration of norambereinelide-18,6 α -olide, a member of this family for the fused tricyclic moiety of this compound.¹

On the other hand, advanced methods in quantum chemistry facilitate the rapid, accurate, and reliable calculation of NMR chemical shifts. So, comparing the calculated and experimental chemical shifts will provide an efficient method in identifying and discriminating between the proposed diastereoisomers.²

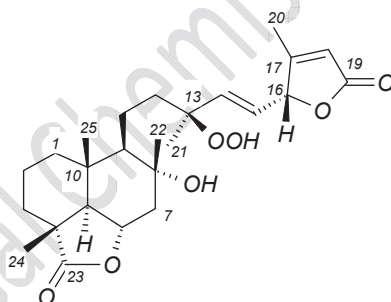
Considering the assigned configuration of fused tricyclic moiety, two unassigned stereocenters allow for totally four possible diastereomers for the target compound. They were used as probable structures of the target molecule in the quantum mechanical treatments. The first step in this treatment was their conformational analyses in order to find candidate conformers at room temperature which contribute to the experimental NMR spectra. In the next step, the postulated conformers, within a 3 kCal window of the lowest energy, were subjected to extensive geometry optimization followed by frequency calculations in order to confirm the nature of the optimized geometries as minima and provide their computed free energies. In the last step, among these extensively optimized structures, those within a 2.5 kCal window of the lowest energy were subjected to the chemical shielding calculations in dimethylsulfoxide

solvent. In order to get accurate calculated chemical shieldings, Boltzman-weighted averaging based on relative free energies of conformers at 298.15 K was used. The relative populations of conformers were computed as $\left(\frac{P_i}{P_j}\right) = \exp\left(\frac{-(E_i - E_j)}{RT}\right)$. Where P_x and E_x are the relative population and computed free energy of the x conformer, respectively.

In order to determine the correct configuration of the target molecule, the calculated chemical shifts were evaluated according to their largest and corrected mean absolute deviation (CMAD: $[(1/n) \sum_{i=1}^n |\delta_{calc} - \delta_{exp}|]$) in each configuration.

In order to confirm the conclusion of the CMAD analysis and get more confidence of which configuration is the correct one, the DP4 probability analysis developed by Smith and Goodman was also employed.²

Thus according to both the CMAD and DP4 analyses, structure, shown below, was found to be correct for the target molecule.



In this brief study the unassigned configurations of the 8 α -hydroxy-13-hydroperoxyabd-14,17-dien-19,16;23,6 α -diolide, extracted from Iranian salvia, at C13 and C16 were assigned as S and R, respectively. In this assignment extensive conformational analysis and geometry optimization followed by frequency and chemical shielding calculations were employed in order to get the best computed chemical shifts compared to experimental ones. In these calculations solvent effects were also taken into account. The CMAD and DP4 analyses were employed together to get the correct configuration.

Keywords: Salvia, Natural Product, Configuration, NMR, Ab Initio



References:

- [1] Matloubi Moghaddam, F.; Moridi Farimani, M.; Seirafi, M.; Taheri, S.; Khavasi, H. R.; Sendker, J.; Proksch, P.; Wray, V.; Edrada, R. *J. Nat. Prod.* 2010, 73, 1601–1605.
- [2] S. G. Smith, J. M. Goodman, *J. Am. Chem. Soc.* 2010, 132, 12946–12959 and references therein.



Adsorption properties study thiazole attached (6,0) zigzag single-walled boron phosphide nanotube

S. Zahra Sayyad-Alangi*, Hadi Sajjadi-Ghotbabadi

Department of Chemistry, Azadshahr Branch, Islamic Azad University, Azadshahr, Golestan, Iran

Email: zalangi_szalangi@yahoo.com

Key words: Boron phosphide nanotube, Adsorption, Thiazole, DFT

Introduction:

The thiazole ring and its derivatives present in the structure of many biologically active compounds such as thiamine, penicillin G, amphetamine drugs, vitamin B1 serves as an electron sink, and used an analytical reagent in analysis of heavy transition metals such as cadmium, lead, copper, and gold [1], as an active centre. Also, its coenzyme form is important for decarboxylation of α -ketoacids [2]. These heterocyclic compounds have been shown anti-inflammation [3], anti-hypertension [4], antibacterial [5], and anti-HIV [6] effects. The objective of the present work was to study thiazole adsorption on BPNT surfaces as a functional group in gas phase and thereby to establish a deeper understanding of the role of the BPNT in adsorption of thiazole on the BPNT surfaces.

Computational methods:

In the first step, the thiazole-attached (6,0) BPNT model was allowed to relax by all atomic geometrical parameters in the optimization at the DFT level of B3LYP exchange-functional and 6-31G* standard basis set in gas phase. Then, the binding energy (BE) of the thiazole - attached (6,0) BPNT model was calculated as follows:

$$BE = E_{\text{Thiazole-BPNT}} - [E_{\text{BPNT}} + E_{\text{Thiazole}}] \quad \text{Eq. (1)}$$

Where $E_{\text{Thiazole-BPNT}}$ was obtained from optimization of the thiazole- attached (6,0) BPNT model, E_{BPNT} and E_{Thiazole} are the energy of the optimized BPNT and thiazole structures. All calculations were carried out by using the Gaussian 03 suite of programs [4].

Results and discussion:

Thiazole can approach the nanotube walls with perpendicular orientation. We optimized the investigated model of the (6,0) *zigzag* BPNT at the B3LYP/6-31G* computational level. The values of the B-P bond distances indicated that the effects of the thiazole adsorption in the gas phase were important for the B-P bond distances close to the thiazole regions, whereas the values for other bonds did not show notable changes. Also, the results indicated that the average B-P bond lengths in thiazole-attached (6,0) BPNT complex were increased due to the influence of the thiazole adsorption on the (6,0) *zigzag* BPNT. In the complex, the average B-P bond length was increased from about 1.89 Å in the pristine model to about 2.00 Å in the thiazole -attached (6,0) BPNT complex. For evaluation the interaction of thiazole with the (6,0) *zigzag* BPNT model, the binding energy (BE) in the gas phase were studied. The binding energy (BE) for the thiazole- attached (6,0) BPNT model in the phase, was attractive, which characterizes a exothermic process. Also, Binding energy corresponding to adsorption of thiazole on the (6,0) BPNT was calculated as $-254.85 \text{ kJ mol}^{-1}$. The calculated BE of the thiazole- attached (6,0) BPNT indicated that thiazole can be absorbed significantly on the (6,0) BPNT.

Conclusions:

The thiazole adsorption on the external surface of H-capped (6,0) *zigzag* boron phosphide nanotube was studied by density functional theory (DFT) calculations in gas phase. Geometry optimizations were carried out at the B3LYP/6-31G* level of theory using the Gaussian 03 suite of programs. Our results shown that the pristine boron phosphide nanotube can significantly detect the thiazole. In gas phase, the binding energy for the thiazole - attached (6,0) BPNT model was attractive $-254.85 \text{ kJ mol}^{-1}$, which characterizes a exothermic process.



References

- [1] A.F. Pozharzskii et al; Heterocycles in Life and Society; Wiley, Chichester; 1997.
- [2] R. Breslow; J Am Chem Soc; 80, 3719, 1958.
- [3] F. Haviv et al; J Med Chem; 31, 1719, 1988.
- [4] W.C. Patt et al; J Med Chem; 35, 2562, 1992.
- [5] K. Tsuji et al; (Bioorg Med Chem Lett; 4, 1601, 1994.
- [6] F.W. Bell et al; J Med Chem; 38, 4929, 1995.

15th Physical Chemistry Conference



A DFT study of imidazole adsorption properties on (6,0) boron phosphide nanotube

S. Zahra Sayyad-Alangi*

Department of Chemistry, Azadshahr Branch, Islamic Azad University, Azadshahr, Golestan, Iran

Email: zalangi_szalangi@yahoo.com

Key words: Boron phosphide nanotube, Adsorption, Binding energy, DFT

Introduction:

Small and simple heterocyclic systems often have interestingly complex biological properties and belong to one of the most important classes of compounds in medicinal chemistry. Imidazole and their derivatives play a special role in medicinal chemistry because of their therapeutic properties [1] such as antineoplastic, immunosuppressive, anti-inflammatory [2], anti-bacterial, and anti-fungal activities [3]. The objective of the present work was to study imidazole adsorption on BPNT surfaces as a functional group in gas phase and thereby to establish a deeper understanding of the role of the BPNT in adsorption of imidazole on the BPNT surfaces.

Computational methods:

In the first step, the imidazole-attached (6,0) BPNT model was allowed to relax by all atomic geometrical parameters in the optimization at the DFT level of B3LYP exchange-functional and 6-31G* standard basis set in gas phase. Then, the binding energy (*BE*) of the imidazole-attached (6,0) BPNT model was calculated as follows:

$$BE = E_{\text{Imidazole-BPNT}} - [E_{\text{BPNT}} + E_{\text{Imidazole}}] \quad \text{Eq. (1)}$$

Where $E_{\text{Imidazole-BPNT}}$ was obtained from optimization of the imidazole- attached (6,0) BPNT model, E_{BPNT} and $E_{\text{Imidazole}}$ are the energy of the optimized BNNT and imidazole structures. All calculations were carried out by using the Gaussian 03 suite of programs [4].



Results and discussion:

Imidazole can approach the nanotube walls with perpendicular orientation. We optimized the investigated model of the (6,0) *zigzag* BPNT at the B3LYP/6-31G* computational level. The values of the B-P bond distances indicated that the effects of the imidazole adsorption in the gas phase were important for the B-P bond distances close to the imidazole regions, whereas the values for other bonds did not show notable changes. Also, the results indicated that the average B-P bond lengths in imidazole-attached (6,0) BPNT complex were increased due to the influence of the imidazole adsorption on the (6,0) *zigzag* BPNT. In the complex, the average B-P bond length was increased from about 1.86 Å in the pristine model to about 2.00 Å in the imidazole -attached (6,0) BPNT complex. For evaluation the interaction of imidazole with the (6,0) *zigzag* BPNT model, the binding energy (*BE*) in the gas phase were studied. The binding energy (*BE*) for the imidazole- attached (6,0) BPNT model in the phase, was attractive, which characterizes a exothermic process. Also, Binding energy corresponding to adsorption of imidazole on the (6,0) BPNT was calculated as -240.0 kJ mol⁻¹. The calculated *BE* of the imidazole- attached (6,0) BPNT indicated that imidazole can be absorbed significantly on the (6,0) BPNT.

Conclusions:

The imidazole adsorption on the external surface of H-capped (6,0) *zigzag* boron phosphide nanotube was studied by density functional theory (DFT) calculations in gas phase. Geometry optimizations were carried out at the B3LYP/6-31G* level of theory using the Gaussian 03 suite of programs. Our results shown that the pristine boron phosphide nanotube can significantly detect the imidazole. In gas phase, the binding energy for the imidazole - attached (6,0) BPNT model was attractive -240.0 kJ mol⁻¹, which characterizes a exothermic process.

References:



- [1] (a) G. Bertaccini et al; Journal of Pharmacy and Pharmacology; 16(7), 441, 1964 (b) J.G . Lambardino et al; J Med Chem; 17, 1182, 1974 (c) T. Maier et al; US Patent 820335 Chem Abstr ;111, 19494, 1989
- [2] D.W. Nebert et al; Annu Rev Biochem; 56, 945, 1987.
- [3] G.C. Porretta et al; Euro j Medic Chem; 23(4), 311, 1988.
- [5] M.J. Frisch et al; Gaussian 03, revision B03, Gaussian Inc., Pittsburgh, PA; 2003.



Ab initio studies on the reactivity and thermal decomposition of the CF₃OCH₂O radical

A. Reisi-Vanani*, S. Hoseinpour

Department of Physical Chemistry, Faculty of Chemistry, University of Kashan, Kashan, Iran

Email: areisi@kashanu.ac.ir

Keywords: Decomposition, HFE-143a, IRC, Canonical transition state theory

Introduction:

Due to the significant role played by haloalkoxy radicals formed from hydrofluoroethers in the destruction of a variety of organic compounds released into the atmosphere, studying the fate of CF₃OCH₂O formed from HFE-143a is needed from the viewpoint of understanding its role in atmospheric chemistry [1]. In the present investigation, we performed a computational study on the decomposition pathways of CF₃OCH₂O radical involving C-H and C-O bond scission as given by reactions (1), (2), (3a) and (3b) (shown in Figure) using high level accuracy methods. Rate constants for the above three considered channels are calculated by utilizing canonical transition state theory (CTST). Attempts have been made to search for transition states on the corresponding potential energy surfaces and the energy barriers are calculated. Existence of transition states is ascertained by making intrinsic reaction coordinate (IRC) calculation.

Calculation method:

The calculations have carried out in order to gain potential energy surface in two high accuracy levels CBS-Q and G2 theory method. Geometry of reactants, products and transition states has determined by MP2(full)/6-31G(d) and MP2/6-31G(d) in G2 and CBS-Q theory level, respectively. The vibration frequencies for optimized molecules by MP2/6-31G(d) in HF/6-31G(d) level which are in CBS-Q calculation. Zero point energies (ZPEs) in HF/6-31G(d) level have obtained for molecules which are optimized by HF/6-31G and MP2/6-31G(d) level in G2 and CBS-Q method respectively. Structures of the reactants and products

have no negative frequencies (NIMAG=0). Transition states are defined by the presence of only one virtual frequency (NIMAG=1). The existence of transition state on the potential energy surface is further ascertained by IRC calculation performed at the B3LYP/6-311G(d,p) level.

Results and discussion:

Optimizing reactants, products, and transition states has been done in MP2(full)/6-31G(d) and MP2/6-31G(d) level for G2 and CBS-Q method, respectively. Moreover the two proposed pathway by H. J. Singh et al. [2], we consider the reaction with atmospheric OH, elimination of H and migration of Hydrogen from Carbon to Oxygen then thermal decomposition. There were not any negative frequencies for reactants and products and for transition states only one negative frequency observed. For TS 1, 2, 3a and 3b the imaginary frequencies were attained as -2501, -1452, -2647 and -953, respectively. Transition states in potential energy surface have been determined by intrinsic reaction coordinate (IRC) calculation in B3LYP/6-311G(d,p) level. Energy barriers for pathways 1, 2, 3a and 3b are in the range of 0.1-2.2, 10-10.8, 25.0-25.9 and 21.1-22.1, respectively and for example in CBS-Q method, they are 2.2, 10.0, 25.0 and 21.1 kcal.mol⁻¹ for 1, 2, 3a and 3b pathway, respectively. The energy barrier diagrams for reactants, products and transition states in the CBS-Q level have plotted in Fig. 1. Rate coefficients for C₃F₇OCH₂O radical were calculated using the following equation:

$$k = \Gamma(T) \frac{K_B T}{h} \frac{Q_{TS}^\ddagger}{Q_R} e^{-\Delta E^\ddagger / RT}$$

Where $\Gamma(T)$ is the tunneling correction factor at temperature T that calculated by the expression given by Wigner [3], Q_{TS}^\ddagger and Q_R are the total partition functions for the transition state and reactant, respectively.

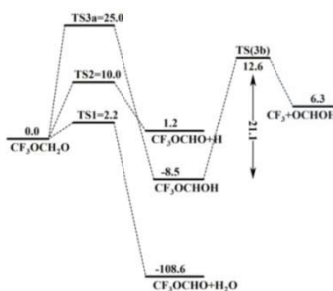




Fig. 1. Energy diagram in kcal mol⁻¹ for the reactivity and thermal decomposition of CF₃OCH₂O

Conclusion:

Ab initio studies on the reactivity and thermal decomposition of the CF₃OCH₂O radical considered by two high accuracy methods G2 and CBS-Q. In the line 1, 2, 3a and 3b the energy barriers were calculated as 2.2, 10.0, 25.0 and 21.1 kcal.mol⁻¹ by CBS-Q method, respectively. The rate constants for the considered pathways were 4.15×10^{11} , 2.47×10^5 and 1.22×10^{-6} s⁻¹ in 1 atm and 298.15 K. Therefore, line 1 was dominant pathway for reactivity of C₃F₇OCH₂O radical.

References:

- [1] Molina, M. J.; Rowland, F. S., Nature (1974) 249, 810.
- [2] Singh, H. J.; Mishra, B. K., J Mol Model (2010) 16, 1473.
- [3] Wigner EP., Z Phys Chem B (1932) 19, 203.



Theoretical studies of decomposition and reactivity of the $C_3F_7OCH_2O$ radical

A. Reisi-Vanani*, S. Hoseinpour

Department of Physical Chemistry, Faculty of Chemistry, University of Kashan, Kashan, Iran

Email: areisi@kashanu.ac.ir

Keywords: Decomposition, HFE-7000, IRC, Theoretical chemistry, PES

Introduction:

Hydrofluoroethers (HFEs) are a kind of compounds which have been developed to replace CFCs in applications such as the cleaning of electronic equipment, heat transfer agents for semiconductor and electronics manufacture and fluid carriers for lubricant deposition [1]. The atmospheric oxidation of $n-C_3F_7OCH_3$ (HFE-7000) will be initiated by reaction with OH radicals that the initial attack of OH radical on HFE-7000 leads to the formation of haloalkyl radicals [2], which in turn reacts with atmospheric O_2 to give peroxy radicals ($C_3F_7OCH_2O_2\bullet$). The reaction of $C_3F_7OCH_2O_2$ radical with NO, NO_2 and HO_2 in the troposphere finally causes the formation of haloalkoxy radicals ($C_3F_7OCH_2O\bullet$).

Calculation method:

Geometry optimization of the reactants, products and transition states have been obtained using B3LYP/6-311G(d,p) method. The vibration frequencies were attained in the same theory level for the optimized reactants, products and transition states. No virtual frequencies of all stationary points were identified (NIMAG=0). Transition states are defined by the presence of only one virtual frequency (NIMAG=1). To ascertain that the identified transition states connect reactants and products smoothly, intrinsic reaction coordinate (IRC) calculations were done at B3LYP/6-311G(d,p) level.

Results and discussion:

Two possible pathways have been detected for reactivity and decomposition for $C_3F_7OCH_2O$ radical. (1) $C_3F_7OCH_2O$ radical react with O_2 atmospheric to perform O_2H and C_3F_7CHO . (2) is thermal decomposition of $C_3F_7OCH_2O$ radical to C_3F_7O and CH_2O . The C-H bond length of TS1 will change from 1.105 to 1.227 Å (approx. 11%) the optimization structure of TS2, indicated that C-O bond increases from 1.344 to 1.981 Å (approx. 47%). The energy barrier for path (1) and (2) obtained 4.3 and 16.8 kcal mol⁻¹, respectively. These results reveal that the reactants and products in a stable minimum potential energy surface (PES) are marked only with positive vibrational frequencies. Transition states of TS1 and TS2 are characterized by a negative frequency, which are -1023 and -376 cm⁻¹, respectively. The existence of transition state on the PES is obtained by IRC calculation performed at B3LYP/6-311G (d, p) level. The IRC plots (Figure. 1) clearly showed a smooth transition from reactants to products on the PES.

Rate constants for $C_3F_7OCH_2O$ radical were calculated using the following equation:

$$k_{TST} = \frac{K_B T}{h} e^{-\Delta G^\ddagger / RT}$$

ΔG^\ddagger is the free energy of activation. The final rate coefficients were corrected using transmission coefficient by Wigner's method [3].

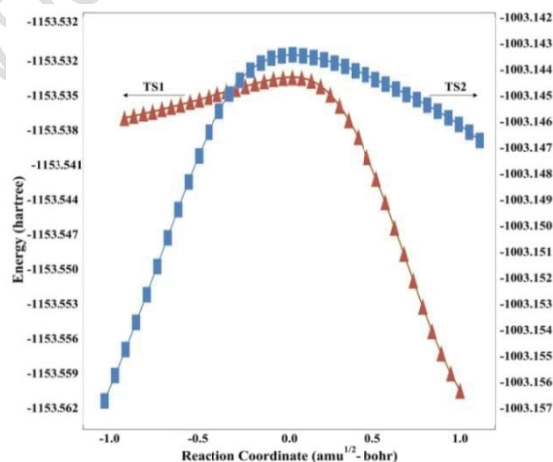


Fig. 1 IRC plots performed for transition states TS1 and TS2



The results showed that the rate constants for the C-H bond scission and C-O bond cleavage are 97.6 and 9.6 s⁻¹, respectively.

Conclusion:

Two important channels (C-H bond scission and C-O bond cleavage) are considered in detail that the C-H bond scission is found to be favorable for the C₃F₇OCH₂O radical reactivity. The energy barrier for C-H bond scission (TS1) and C-O bond cleavage (TS2) is 4.3 and 16.8 Kcal.mol⁻¹, respectively. The rate constants evaluated for the C-H bond scission and C-O bond cleavage are found to be 97.6 and 9.6 s⁻¹, respectively.

References:

- [1] Molina, M. J.; Rowland, F. S., Nature (1974) 249, 810.
- [2] Bravo, I.; Díaz-de-Mera, Y.; et al., Phys. Chem. Chem. Phys (2010) 12(19), 5115.
- [3] Houston, P. L., McGraw-Hill New York (2001).



Covalent hybridizations of carbon nanotubes – Graphene nanoribbons through peptide linkages: A density functional approach

Akbar Omidvara*, Nasser L. Hadipourb

a,bDepartment of Chemistry, Tarbiat Modares University, Tehran, Iran

*Corresponding author. Tel. +98 2182883488; fax: +98 2182889730. E-mail address:

Akbar.Omidvar.64@gmail.com (Akbar Omidvar)

To construct logic circuits based on Graphene nanoribbon (GNR) and Carbon nanotube (CNT) units, it is necessary to join them in particular ways. The GNRs and CNTs could be connected through the formation of new carbon-carbon bonds at the interface [1, 2]. Alternatively, chemical reactions could be applied to form covalent linkages between GNRs and CNTs and which do not introduce artificial damage [3, 4]. In the current research, we investigated covalent hybridizations of CNT-GNR through a peptide linkage by performing density functional theory (DFT) calculations. We have computationally investigated the properties of hybrid structures composed of GNRs and CNTs (Fig.1). The major goal of this study is to understanding the usage of peptide group in constructing the hybrid structures. Moreover, the parameters of nuclear magnetic resonance (NMR) spectroscopy have been evaluated to investigating the properties of the considered CNT - GNR hybrid structures through peptide linkages [5]. Density functional theory (DFT) calculations have been performed employing the B3LYP exchange-correlation functional and the 6-31G* standard basis set as implemented in the Gaussian 98 package.

Our calculations have yielded the stable hybrid structures of CNT – GNR counterparts. Moreover, the evaluated NMR parameters have indicated that the properties of hybrid structures are different from the original structures of isolated CNT and GNR. And as the final note, the properties of the CNT – GNR hybrids have revealed that the peptide group could play a dominant role in determining the characteristic properties of the investigated hybrids.

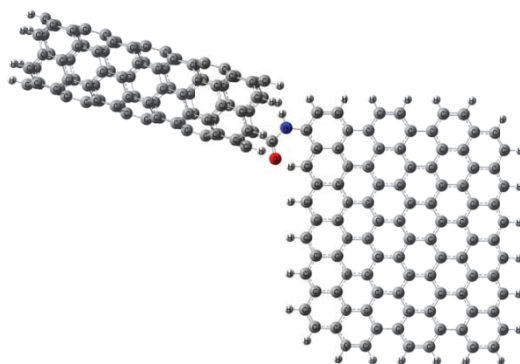


Fig.1: Hybrid of Carbon nanotube – grapheme nanoribbon.

Keywords: Carbon nanotube” Graphene” Peptide linkage “Density Functional Theory (DFT)

References:

- [1] M. Khazaei, S.U. Lee, F. Pichierri and Y. Kawazoe, **J. Phys. Chem. C** 111(2007) 12175.
- [2] F. Pichierri, M. Khazaei and Y. Kawazoe, **Mater. Trans.** 48 (2007) 2148.
- [3] S.U. Lee, M. Khazaei, F. Pichierri and Y. Kawazoe, **Phys. Chem. Chem. Phys.** 10 (2008) 5225.
- [4] Y.F. Li, B.R. Li and H.L. Zhang, **Nanotechnology** 20 (2009) 225202.
- [5] E. Zurek and J. Autschbach, **Computational and Theoretical Chemistry** 981 (2012) 47.



Theoretical study of complex formation constant between benzo-15-crown-5 and Mg^{2+} cation at different temperatures

Reza Behjatmanesh-Ardakani^{1*}, Mehdi Taghdiri¹, Fateme Bamdadi¹

¹Department of Chemistry, Payame Noor University, PO BOX 19395-3697 Tehran, Iran

E-mail: bamdad.nasim21@yahoo.com

Keywords: benzo-15-crown-5, Mg^{2+} cation, complex formation constant

Introduction:

Crown ether is compounds contains hydrogen, carbon and oxygen atoms. crown compounds is used as host-guest chemistry; crown ether is locked with the guest atoms in a solution. crown ethers are used in PTC (phase-transfer catalysts) system and contribute to the solubility of inorganic compounds in organic solvents in chemical reaction. "Host-guest" chemistry of crown ethers can be applied to develop new pharmaceuticals [1].

Computational and methods:

Complex formation constants of benzo-15-crown-5 with Mg^{2+} cation are predicted by ab initio methods in pure methanol solvent at different temperatures. In the present work, geometry optimizations have been done using Gauss View 5 and Gaussian 2009 [2]. Calculations in the gas phase were carried out at B3LYP level of theory with 6-311+g* basis set at different temperatures. For solution phase, PCM model [3] was used to introduce solvent interactions with the solute. The utilized expressions for the $\log K_f$ calculations are given below:

$$\Delta G_t = \Delta \Delta G_{solv} + \Delta G_g$$

$$\Delta G_t = -2.303 RT \log K_f$$

Results and discussion:



Results show that the change of the stability constant of $(B15C5.Mg)^{2+}$ complex with temperature is linear. The complex formation constant decreases with increasing temperature. Our calculated results are in good agreement with the results of conductometric data [4].

References:

- [1] J.D. Anderson, E.S. Paulsen, D.V. Dearden; "Alkali metal binding energies of dibenzo-18-crown-6: experimental and computational results"; *Int. J. Mass Spectrom.* 277, 63-76, 2003.
- [2] M.J. Frisch and etal, revision A-1, Gaussian; Inc. Walling ford CT, 2009.
- [3] J. Tomasi, B. Mennucci, R. Cammi; *Chem. Rev.* 105, 2999-3093, 2005.
- [4] G.H. Rounaghi, M. Mohajeri, M. Doaei, A. Ghaemi; " Solvent influence upon complex formation between benzo-15-crown-5 and Mg^{2+} , Ca^{2+} and Sr^{2+} cations in some pure and binary mixed solvents using conductometric method"; *J. Incl. Phenom. Macrocycl. Chem.* 67, 443-450, 2010.



Effect of aniline substitutions on polyaniline HOMO/LUMO band gap

M. S. Rahmanifar

Faculty of Basic Sciences, Shahed University, P. O. Box 19575-361, Tehran, Iran

Key words: Conducting polymer, Polyaniline, Band Gap

Introduction:

Polyaniline (PANI) is a typical organic semiconductor which has attracted great attention in fundamental science and industry, because its properties can be reversibly controlled by both oxidation/reduction of amine/imine groups and protonation/deprotonation. PANI has three redox forms, leucoemeraldin (LE), emeraldine (E) and pernigraniline (PG) that can be protonated and leading to drastic changes in different properties such as electrical, optical and etc. The rich electronic properties of PANI systems as well as their environmental stability and low cost make PANI an attractive material for applications in many areas such as rechargeable batteries [1], supercapacitors [2], sensors [3] and etc. The arisen properties are considerably affected by two groups of factors, first structural factors and second chemical factors that rearrange the intermolecular force. Here in, we establish a bridge between structural parameters of a substituted polyaniline with its conducting properties, then compare it with unsubstituted polymer.

Computational Details:

Geometries and band gaps of PANI and SO₃H, COOH and NH₂ substituted PANI oligomers up to octamer have been systematically calculated and analyzed using molecular mechanics and semiempirical methods, respectively, by GAUSSIAN 98 program. On the basis of fully optimized geometries of neutral and charged forms of PANI (substituted/unsubstituted) oligomers, excitation energies are calculated. Band gaps are also approximated by extrapolating the HOMO/LUMO difference and extrapolated to the band gap value of the infinite chain. The doped form of PANI (two positive charges per four aniline units) has been computed with band gap approximation from an extrapolation of the tetramer and octamer.

Results and Discussion:

It is indicated that the phenyl ring torsional angles and the pyramidity (the sum of the bond angles around a nitrogen atom) play an important role in determining structures of organic compounds containing an amine group. From the crystal structure study of diphenylamine (phenyl capping aniline dimer), the measured value of the interring dihedral angles are in the range of 23° -65°.

At the first, Geometries of all LE oligomers were optimized with MM method and the dihedral angles between phenyl rings calculated and compared with diphenylamine dihedral angles. Then HOMO/LUMO band gaps of oligomers were calculated by AM1 method. Fig. 1 represents the electronic levels of LE base oligomers, addition of every new aniline unit causes hybridization of the energy levels yielding more and more levels until a point is reached at which there are bands rather than discrete levels. Interaction between the electrons of neighboring molecules leads to a three-dimensional band structure. Extrapolated band gaps were obtained by plotting excitation energies from PANI oligomers calculations against the inverse number of aniline units and extrapolating to an infinite number of units as shown in Figure 2. The extrapolated band gap value of LE acid form is smaller than those of LE base oligomers, which may suggest that the LE acid form is more conjugated than LE base.

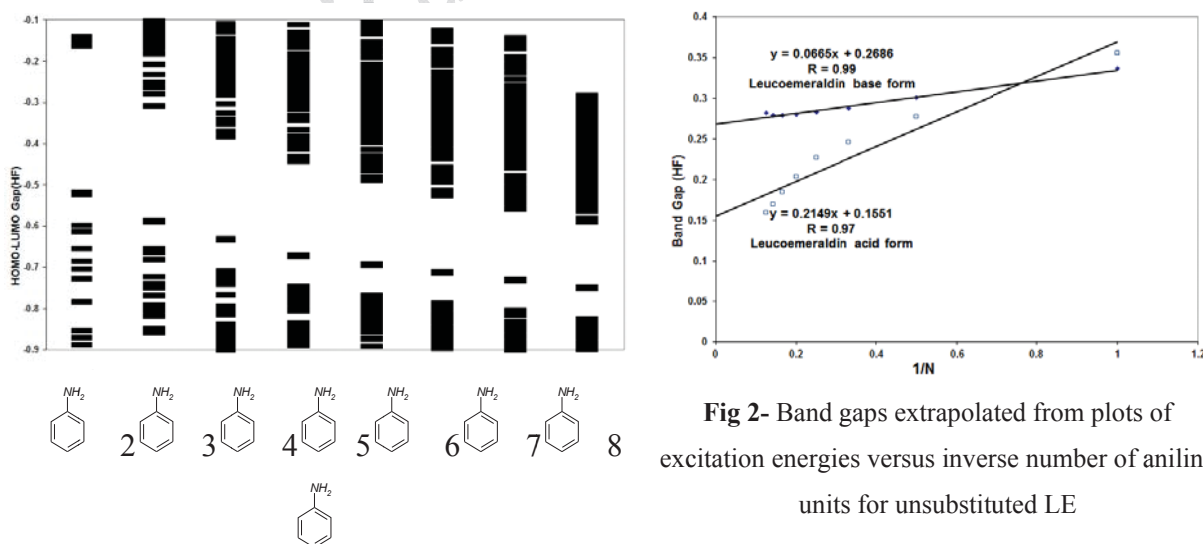


Fig 2- Band gaps extrapolated from plots of excitation energies versus inverse number of aniline units for unsubstituted LE



Fig 1- Calculated energy levels of oligoanilines

with $n = 1$ to 8 for LE

For PANI other forms, same calculation were carried out and band gaps were extrapolated. Table 1 shows the band gaps of PANI different redox forms in acid and basic states. This is very close to the experimental observation because insulator to conductor transition occurred for emeraldine protonated form of PANI. For this reason, in the case of substituted PANI only substituted emeraldine (protonated/deprotonated) form were considered. On the other hand, estimation of HOMO/LUMO band gap of substituted PANI only has done for substituted emeraldine and its protonated forms. For comparison of band gaps of substituted emeraldine with unsubstituted, relative values is shown in Table 2.

Table 1- Comparison of extrapolated Band Gaps (HF)
Between PANI different redox forms in acid and basic states

	Base form	Acid form
Leucoemeraldine	0.2686	0.1551
Emeraldine	0.2399	0.0055
Pernigraniline	0.2375	0.0672

Table 2- Comparison of HOMO/LUMO gap of
substituted/unsubstituted PANI fractions

	Base form	Acid form
SO ₃ H	0.60	14
COOH	0.55	4.3
NH ₂	0.98	26

Based on the results of table 2 can be concluded that substituted PANI in E acid forms has less conductivity than unsubstituted PANI. This can be related to the phenyl rings torsional angles connected to a nitrogen atom. When the π orbital of the phenyl rings is parallel to each other maximum conductivity is achieved, but substitution on ring cause distortion of the conjugation and band gap is increased.

References:

- [1] M. S. Rahmanifar and M. F. Mousavi, M. Shamsipur, M. Ghaemi, "What is the limiting factor in cycle life of Zn-polyaniline rechargeable batteries?" J. Power Sources, 132, 296-301, 2004.
- [2] H.R. Ghenaatian, M.F. Mousavi, M.S. Rahmanifar, "High performance battery-supercapacitor hybrid energy storage system based on self-doped polyaniline nanofibers", Synth. Met., 161, 2017-2023, 2011.



- [3] M. F. Mousavi, M. Shamsipur, S. Riahi, M. S. Rahmanifar, "Design of a new dodecyl sulfate-selective electrode based on conductive polyaniline", *Anal. Sci.*, 18, 137-140, 2002.

15th Physical Chemistry Conference



Computational mechanistic study of methanol and hydroperoxyl radical reaction.

K. Shayan^{*}, M. Vahedpour, F. Karami

Department of Chemistry, University of Zanjan, Zanjan, Iran

Email: k.shayan@znu.ac.ir

Key words: mechanistic study, hydroperoxyl radical, additive of fuels, H-abstraction

Introduction:

Methanol is one of the simplest oxygenated hydrocarbon compounds in this regard can be considered. Methanol's characteristics such as low pollution, fuel supply options fire safety, high performance and economically attractive are its advantage that make methanol as a gasoline replacement or at least be considered as the additive to fossil fuels. Under a wide range of experimental conditions, the methanol oxidation pathway involves successive dehydrogenations. Abstraction of H-atoms (dehydrogenation) from the alcohol can be accomplished by various radicals produced during combustion, such as the hydroperoxyl radical. [1-2]

In this work, we carried out the CH₃OH and HO₂ reaction on doublet potential energy surfaces (PES) by means of computational methods based on quantum theories to clarifying the reaction mechanism.

Theoretical method:

All the calculations were performed with the GAUSSSIAN 03 program [3]. The geometry optimizations were carried out using Møller–Plesset perturbation theory MP2 approach in connection with the 6-311++g (d, p) basis set. Single point calculations were performed for all species at the CBS-QB3 level.

Result and discussion:

Figure 1 shows the relative energy profile of methanol and HO₂ reaction. Total and relative energies for all species of reaction are tabulated in table 1 at MP2 and CBS-QB3 level of computations. We found two complexes formed between CH₃OH and HO₂ denoted as C1 and C2. The pre-reactive complex C1 is transformed to CP2 occurring via two transition states which are TS1 with the energy barrier of 25.441 kcal/mol and TS2 with the energy barrier of 26.833 kcal/mol. CP2 can be converted into the product P2 (CH₂OH+H₂O₂). Complex C2 is converted into CP1 via TS3 with the energy barrier of 27.852 kcal/mol. Then CP1 can directly convert to P1 (CH₃O+H₂O₂) without any transition state. CP2 is transformed into CP3 through TS4 with the energy barrier of 50.123 kcal/mol. After that CP3 can directly transform into P3 (CH₂OH+H₂OO). P2 is the most stable product in comparison with the others. So, it is the main product in thermodynamic approach. Structures of transition state (TS1 and TS2) are found H-abstraction on the methyl side while the H-attack on the OH group is found in TS3. Production of P2 from TS1 with the lowest energy barriers kinetically is the main reaction pathway.

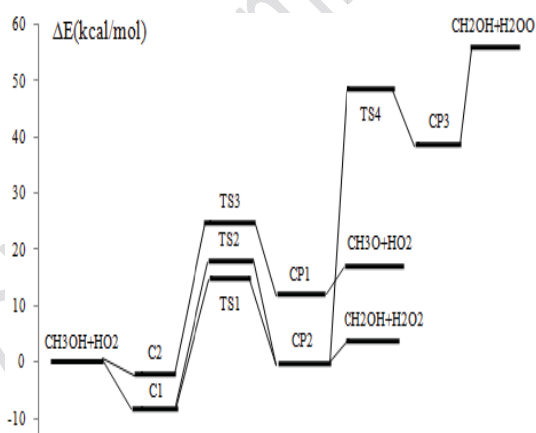


Figure 1. Doublet potential energy profiles of the CH₃OH + HO₂ reaction at MP2 level

Table 1: The total energies and relative energies (in parentheses) calculated for this reaction

Species	MP2	CBS-QB3	Species	MP2	CBS-QB3
R	-265.9725(0.0)	-266.2165(0.0)	TS2	-265.9438 (17.97)	
C1	-265.9866 (-8.86)	-266.2256(-5.77)	TS3	-265.9322(25.31)	-266.1842(20.23)
C2	-265.9765(-2.542)	-266.2181(-1.04)	TS4	-265.8932(49.76)	-266.1408(47.45)
CP1	-265.9533 (12.04)	-266.1963(12.64)	P1	-265.9453(17.03)	-266.1912(15.82)
CP2	-265.9731 (-0.36)	-266.2081(5.24)	P2	-265.9651(4.65)	-266.2038(7.93)
CP3	-265.9093 (39.63)	-266.1539(39.39)	P3	-265.8830(56.15)	-266.1259(56.80)
TS1	-265.9461(16.58)				



Conclusion:

The theoretical study carried out in this work lead to the following conclusions:

1. Reaction of CH_3OH with the HO_2 is produced three kinds of products after passing four transition state and five intermediate.
2. The pre-reactive complexes $^1\text{C1}$ and $^1\text{C2}$ are lying 8.86 and 2.54 kcal/mol below the original reactants and P2 is the main product both thermodynamic and kinetic approaches.

References:

- [1] [www.cdc.gov.niosh.ershdb](http://www.cdc.gov/niosh/ershdb), Emergency Response Card, NO:29750029.
- [2] M.Alecu et al; "Computational study of the reaction of methanol with the hydroperoxyl and methyl radicals. 1. Accurate thermochemistry..."; J. Phys. Chem. A; 115, 2811-2829, 2011.
- [3] Frisch et al; "GAUSSIAN 03, Revision B.03, Gaussian"; Inc., Pittsburgh, PA; 2003.



Evaluation of cyclic (amino)(phosphino)-, and cyclic (alkyl)(amino)carbene effects on the second generation of Grubbs' catalysts

Zahra Azizi*, Narges Karimi Setudeh Niasar

Department of Chemistry, Karaj branch, Islamic Azad University, Karaj, 31485-313, Iran

E-mail: Zahra.Azizi@Kiau.ac.ir; ZahraAzizi@yahoo.com

Keywords: Grubbs' catalyst, DFT calculation, NBO, QTAIM

Introduction:

There is abundant interest in *N*-heterocyclic carbenes (NHC) as a well-established class of new ligands in chemistry. Then metal complexes containing NHC ligands are emerged as catalysts for a variety of transformations. The exclusive features of the Metal-NHC bond by transition metal complexes are interested due to the importance of C-C bond formation in medicine, biology, and material sciences. Hence, intensive studies to understand of the Metal-NHC bond are developed by applying of advanced computational techniques. Grubbs' catalysts are ruthenium complexes that used as catalysts for olefin metathesis. [1]

Computational Methods:

In this study, equilibrium geometries and harmonic vibrational frequencies were first calculated at the DFT level with the B3LYP exchange-correlation functional theory. We used the 6-31+G* basis set for H, C, N, P and Cl atoms and the pseudopotential Stuttgart ECP28MWB basis set for the Ru [2,3] in the DFT optimization and frequency calculations. Then, single-point B3LYP calculations were performed with the cc-pVTZ (for H, C, N, P and Cl atoms) and cc-pVTZ-PP (for Ru) [4] basis sets at the above B3LYP geometries. Also, the NBO population and atoms in molecules (AIM) analyses of optimized structures are accomplished at B3LYP/cc-pVTZ B3LYP/QZVP levels, respectively. All calculations are carried out using the Gaussian 03 package.

Results and discussion:

High levels of DFT calculations are employed to examine the effects of cyclic (amino)(phosphino)carbene (CAPC), and cyclic (alkyl)(amino)carbene (CAAC) toward to saturated imidazolin-2-ylidene (H_2SI) on the second generation of Grubbs catalysts. Based on the AIM theory, ρ and its Laplacian ($\nabla^2\rho$) at the bond critical point (BCP) provide information about the strength and bond characteristic between the two atoms. Laplacian of ρ is calculated as $\nabla^2\rho = \lambda_1 + \lambda_2 + \lambda_3$, when λ_i is Hessian eigenvalue of the charge density. The large values of ρ and the values of $\nabla^2\rho < 0$, $|\lambda_1|/\lambda_3 > 1$ and $|\lambda_2|/\lambda_3 > 1$ are calculated for shared interactions or covalent bonds. On the contrary, the small values of ρ and the values of $\nabla^2\rho > 0$, $|\lambda_1|/\lambda_3 < 1$ and $|\lambda_2|/\lambda_3 < 1$ are correspond to closed-shell interactions (ionic, hydrogen bond, van der Waals bonds) [5].

Ligand	Bond Length (Å)		E_{HOMO} (eV)	$\Delta E_{HOMO-LUMO}$ (eV)	Bond Critical Point [3,-1] (a.u.)							
	R_{Ru-C}	R_{Ru-P}			Bond	ρ	λ_1	λ_2	λ_3	$\nabla^2\rho$	$ \lambda_1 /\lambda_3$	$ \lambda_2 /\lambda_3$
H_2SI	2.04	2.42	-5.81	4.02	Ru-C:	0.22	-0.27	-0.26	0.84	0.31	0.32	0.31
CAPC	2.01	2.45	-5.91	3.87	Ru-C:	0.23	-0.28	-0.27	0.84	0.28	0.34	0.33
CAAC	2.02	2.45	-5.85	3.88	Ru-C:	0.23	-0.28	-0.27	0.82	0.27	0.34	0.33

Ligand	Hybridization		Natural Atomic Orbital Occupancies					Atomic Charge		
	Ru in σ_{Ru-C}	C: in σ_{Ru-C}	π^* -backdonation		σ -donation			Ru	C:	P
			$p_z(C:)$	$d_{xz}(Ru)$	$p_x(C:)$	$d_{z^2}(Ru)$	$p_x(P)$			
H_2SI	$s^1p^{2.36}d^{2.11}$	$s^1p^{1.47}$	0.6750	1.8893	1.1294	1.1626	1.2524	-0.478	0.381	0.418
CAPC	$s^1p^{2.19}d^{2.04}$	$s^1p^{1.41}$	0.7188	1.8741	1.1922	1.1940	1.2606	-0.477	0.062	0.394
CAAC	$s^1p^{2.19}d^{2.07}$	$s^1p^{1.57}$	0.6474	1.8730	1.1288	1.1761	1.2641	-0.468	0.373	0.393

Conclusion:



In this study, we have analyzed the topology of the total charge density and its Laplacian, obtained by theoretical studies on the basis of the QTAIM method. While the HOMO energy level of free carbene of CAAC is higher than H₂SI, but HOMO energy level of the corresponding complex of CAAC is stabilized, and also its HOMO-LUMO energy gap is decreased. The analyses of data are shown that there is no difference between metal-carbene bond natures due to different of carbenic ligands in their corresponding complexes.

References:

- [1] C. Samojłowicz, M. Bieniek, K. Grela, *Chem. Rev.* **2009**, *109*, 3708–3742.
- [2] D. Andrae, U. Haeussermann, M. Dolg, H. Stoll, H. Preuss, *Theor. Chim. Acta.* **1990**, *77*, 123.
- [3] J. M. L. Martin, A. Sundermann, *J. Chem. Phys.* **2001**, *114*, 3408.
- [4] K.A. Peterson, D. Figgen, M. Dolg, H. Stoll, *J. Chem. Phys.* 2007, *126*, 124101.
- [5] R. F. W. Bader, *Atoms in molecules: A quantum theory*. Oxford University Press, Oxford, UK, **1990**.



Hydrolysis Reaction Mechanism of the Second Generation Anticancer Drug Carboplatin: An Ab-initio study

H. Saghafi^{*a}, R. Fazaeli^b, A.A. Salari^a

^a Department of Chemistry, Islamic Azad University Shahr-e Rey Branch, Tehran, Iran

^b Modeling and Optimization Research Center in Science and Engineering, Islamic Azad University-South Tehran Branch, Tehran, Iran

E-mail: r_fazaeli@azad.ac.ir

Keywords: Anti-cancer, DNA, Platinum, carboplatin, double-aquated

Introduction:

Platinum-based drugs are one of the most important parts of chemotherapy treatments of a variety of malignancies. The accepted mechanism of action of cisplatin is double stages. 1) intracellular activation by the hydrolysis of one chloride ligand, driven by the lower concentration of Cl⁻ anions in the cell, 2) formation of intra-strand cross-links in DNA through the covalent binding of the Pt complex to purine bases [1,2]. Despite the success reached by cisplatin in clinical application, several serious side-effects and acquired or intrinsic resistance of tumours are still unsolved problems. In order to overcome these limitations, a large number of platinum compounds such as carboplatin, have been screened in last decades [3].

Methods:

We carried out full unconstrained geometry optimization and frequency calculation for all distinct species at the B3LYP functional which includes the Beck's hybrid exchange and correlation functional of Lee, Yang, and Parr by using density functional theory (DFT) as implemented in the Gaussian03 quantum chemical program package. Also we applied the standard split valence basis set 6-31+G(d) for C, N, O and H atoms and employed the effective core potentials of Hay and Wadt with double-valence basis set (LanL2DZ) for describe Pt, and added polarization functions for Pt ($\zeta = 0.993$). In order to confirm proper convergence to

equilibrium and transition state geometries, vibrational frequency analysis were done based on analytical second derivatives of Hamiltonian at this level of theory.

Results and discussion:

Due to symmetric structure of carboplatin, we guessed that there is only one path for the hydrolysis process. The equilibrium structure obtained respectively hydrogen-bond calculation, as previously exposed; carboplatin is expected to undergo water degradation in a biphasic process: addition of the first water molecule connected to the ring-opening process followed by the release of the malonatoligand upon reaction with a second water molecule. The first studied reaction was the degradation of carboplatin in gas phase. In this reaction, as the water molecule approaches the Pt center, the platinum-oxygen (of the ligand) bond distance starts to increase until the transition state geometry is reached. The imaginary frequency observed in the transition state is about $209.4i \text{ cm}^{-1}$ in gas phase, and the analysis of this vibrational mode clearly indicates the rupture of the $\text{Pt-O}_{\text{ligand}}$ bond and the simultaneous formation of the $\text{Pt-O}_{\text{water}}$ bond. The activation barrier is 33.98 kcal/mol in gas phase. The reaction is endothermic by $+7.84 \text{ kcal/mol}$. In the next step, malonatoligand is lost, and second water molecule is coordinated to platinum. Also, the transition state geometry was optimized and yielded the follow data in gas phase: the imaginary frequency is about $195.6i \text{ cm}^{-1}$, and the animation of this vibrational mode clearly indicates the rupture of the $\text{Pt-O}_{\text{ligand}}$ bond and formation of the $\text{Pt-O}_{\text{water}}$ bond. The activation barrier is 34.02 kcal/mol and the reaction is endothermic by $+34.99 \text{ kcal/mol}$.

Conclusion:

With notice to symmetric structure of carboplatin, there is only one path for the hydrolysis process. According to the calculated results, double-aquated complex is expected to be species reacting with DNA.



References:

- [1] Andrea Melchior et al, *TheorChemAcc* **2011**, 128:627-638.
- [2] Hambly, T. W. *Coord Chem. Rev.* **1997**, 166, 181.
- [3] Matej Pavelka et al, *Chem. Eur. J.* **2007**, 13, 10108-10116.

15th Physical Chemistry Conference



DFT study of C₁₆ nano cluster as a novel material for antioxidant carrier

H. Aghaie^a, T. Ardalan^{*b}

^aDepartment of Chemistry, Science and Research Branch, Islamic Azad University, Tehran, Iran

^b Science and Research Branch, Islamic Azad University, Tehran, Iran

Email: tooran_ardalan_1363@yahoo.com

Key words: C₁₆ nano cluster, vitamin C, Thermodynamic, density functional theory.

Introduction:

Since the end of last decade nanotechnology has been grown at rapid pace and spread over many different fields out of the birthplace and material science. Now in medical science, nanotechnology is expected to open up the door to innovation method of treatment no one can imagine twenty years ago. In the past decade, the rapid development of nanotechnology has brought many fascinating ideas and opportunities to disease diagnosis and treatment. Fullerenes and their derivatives can serve as drug delivery vehicles, and in certain circumstances, as nano-drugs by themselves. Also extensive research has been focused on group-IVA elemental clusters C_n, Si_n, Ge_n, Sn_n and Pb_n in the past two decades for both fundamental and technological reasons while very limited experimental and theoretical investigations performed on binary A_mB_n or ternary A_lB_mC_n clusters (A, B, C= C, Si and Ge. In this work, interaction between C₁₆ nano cluster and vitamin C has been studied by using DFT employing B3LYP exchange correlation. Vitamin C is an electron donor, and this property accounts for all its known functions. Human diseases such as atherosclerosis and cancer might occur in part from oxidant damage to tissues. Oxidation of lipids, proteins and DNA results in specific oxidation products that can be measured in the laboratory. Epidemiological studies show that diets high in fruits and vegetables are associated with lower risk of cardiovascular disease, stroke and cancer, and with increased longevity.



Methodology:

In our model, vitamin C was attached covalently to C₁₆ nano cluster. The vitamin C and C₁₆ were geometrically optimized using 6-311G, 6-311G* and cc-pvdz basis sets with the Gaussian 03 by the B3LYP method. From the optimized structure, quantum-mechanical descriptors were calculated and compared. Also HOMO–LUMO gaps were calculated using DFT method by using the GAUSSIAN 03 software. The thermodynamic parameters also were calculated.

Results and discussion:

HOMO- LUMO energy analysis:

Values of HOMO, LUMO, HOMO–LUMO Gap energy C₁₆ nano cluster and C₁₆ nano cluster beside Vitamin C show that HOMO energy of vitamin C increases after connecting to C₁₆ nano cluster. Vitamin C is an electron donor (reducing agent or antioxidant), and probably all of its biochemical and molecular functions can be accounted for by this function. Also by increasing of HOMO energy for vitamin C beside C₁₆ nano cluster, it can act better as an electron donor and antioxidant.

Thermodynamic analysis:

calculated relative energies (ΔE), enthalpies (ΔH) and free Gibbs energies (ΔG) as well as entropy (ΔS) in gas phase, for C₁₆ nano cluster beside vitamin C at the physiological temperature show that C₁₆ nano cluster beside vitamin C has negative values of relative energies (ΔE), enthalpies (ΔH) and free Gibbs energies (ΔG) in gas phase. Also, our results in Table 2 that entropy (ΔS) for C₁₆ nano cluster beside vitamin C system has positive values. These observations can be related to the structural stability of the C₁₆ nano cluster beside vitamin C in gas phase.

Conclusion:

The physicochemical properties of a novel carbon cluster (C₁₆) and C₁₆ beside vitamin C have been evaluated using Density Functional Theory (DFT) calculation. HOMO and LUMO energy were calculated. Also thermodynamic analysis has been performed for C₁₆ cluster and C₁₆ beside



vitamin C. Thermodynamic results indicate that Vitamin C can form stable bindings with C₁₆ cluster via oxygen (O) active site. Also by increasing of HOMO energy for vitamin C beside C₁₆ nano cluster, it can act better as an electron donor and antioxidant.

References:

- [1] Monajjemi M, Lee VS, Khaleghian M, Honarparvar B, Mollaamin F (2010). Theoretical Description of Electromagnetic Nonbonded Interactions of Radical, Cationic, and Anionic NH₂BHNBH₂ Inside of the B₁₈N₁₈ Nanoring. J. Phys. Chem. C., 114: 15315-15330.
- [2] Monajjemi M, Chegini H, Mollaamin F, Farahani P (2011). Theoretical Studies of Solvent Effect on Normal Mode Analysis and Thermodynamic Properties of Zigzag (50)



C₇ Si₅Ge₃ Nano cluster for vitamin C carrier and DFT study

T. Ardalan^{a,*}

^aScience and Research Branch, Islamic Azad University, Tehran, Iran.

Email: tooran_ardalan_1363@yahoo.com

Key words: C₇ Si₅Ge₃, vitamin C, nuclear magnetic resonance, natural bond orbital, density functional theory.

Introduction:

Group-VA cluster such as BN nanomaterials are expected in extensive application due to the good stability at high temperatures with high electronic insulation in air. Despite the carbon nanotubes, BN nanotubes are constant band gap materials and thus provide an attractive opportunity for practical applications. The wide range of their electronic properties from metallic to wide-gap semiconductors, depending on their chemical composition, makes them suitable candidates for nanosize electronic devices. Due to the similarity between B-N and C-C units, a lot of effort has been devoted to BN fullerene-like materials in recent years, which have excellent properties such as heat resistance, insulation, and structural stability. Also extensive research has been focused on group-IVA elemental clusters C_n, Si_n, Ge_n, Sn_n and Pb_n in the past two decades for both fundamental and technological reasons while very limited experimental and theoretical investigations performed on binary A_mB_n or ternary AB_mC_n clusters (A, B, C=C, Si, and Ge). results reported on Ge_lSi_mC_n ternary clusters to date. In this work, interaction between C₇ Si₅ Ge₃ cluster and vitamin C has been studied by using DFT employing B3LYP exchange correlation.

Computational details:

In the present work, we optimized the C₇Si₅Ge₃ with 3 basis sets, 6-311G, 6-311G* and ccpvdz and C₇Si₅Ge₃ beside vitamin C with 2 basis sets, 6-311G, 6-311G* with the Gaussian 03 by the B3LYP method. The nuclear magnetic resonance (NMR) isotropic shielding



constants were calculated using the standard Gauge-Independent Atomic Orbital (GIAO) approach of GAUSSIAN 03 program package.

Results and discussion:

Nuclear magnetic resonance (NMR) calculation:

We studied about $C_7Si_5Ge_3$ as a novel material for vitamin C carriers. Before and after connecting the vitamin C to $C_7Si_5Ge_3$ NMR calculations were performed in electric field of charges. The remarkable feature in these calculations is observed in calculations of η . We can see completely symmetrical curves at various methods and basis sets. This symmetry does not exist after connecting to vitamin C. Although the maximum points are various in different methods but the symmetry is observed around the axis of zero charge. The results show that vitamin C connects stronger to $C_7Si_5Ge_3$ cluster in positive charges than negative charge. Thus by creating a positive field vitamin C can be connected to the $C_7Si_5Ge_3$ cluster and delivered easily by using a negative field.

Natural bond orbital (NBO) analysis:

The concepts of NBO analyses are useful for distributing electrons into molecular orbitals used for the one electron density matrix to define the shape of the atomic orbitals in molecular environment and then derive molecular bonds from electron density between atoms. At each considered coordination, the bonding and antibonding coefficients of s and p orbital of Si-C were 0.5 and 0.8 for $C_7Si_5Ge_3$ cluster at B3LYP/6-311G, B3LYP/6-311G* and B3LYP/cc-pvdz level of theory. But this order does not exist for $C_7Si_5Ge_3$ cluster inside vitamin C.

Conclusion:

In the present study, structural properties of $C_7Si_5Ge_3$ cluster and interaction between this cluster and vitamin C have been studied extensively utilizing density functional theory (DFT) employing B3LYP exchange correlation. Nuclear magnetic resonance (NMR) properties are calculated. Also natural bond orbital (NBO) analysis has been performed for $C_7Si_5Ge_3$ cluster



and $C_7 Si_5 Ge_3$ inside vitamin C. Our results indicate that vitamin C can form stable bindings with $C_7 Si_5 Ge_3$ cluster through oxygen (O) active site.

Reference:

- [1] M. Monajjemi M and etal.; "Interaction of Na, Mg, Al, Si with Carbon Nanotube (CNT): NMR and IR Study" ; Russian Journal of Inorganic Chemistry; 54, 1465-1473, 2009.
- [2] M. Monajjemi M and etal.; "Theoretical Description of Electromagnetic Nonbonded Interactions of Radical Cationic, and Anionic $NH_2BHNBNH_2$ Inside of the $B_{18}N_{18}$ Nanoring";. Journal of Physical Chemistry C; 114, 15315-15330, 2010.
- [3] M Corso and etal.; "Boron Nitride Nanomesh"; Sciences; 303, 217-220, 2004.



A QM/MM study of catalytic mechanism of human Glyoxalase I

M. Irani^{*a}, S. Jafari^a

^a Department of Chemistry University of Kurdistan, Sanandaj, Iran

Email: m.irani@uok.ac.ir

Keywords: Glyoxalase, QM/MM, Reaction mechanism

Introduction:

The glyoxalase system catalyzes the glutathione-dependent conversion of toxic methylglyoxal to D-lactate. The system consists of two enzymes, glyoxalase I (GlxI) and glyoxalase II. GlxI converts a hemithioacetal, formed from methylglyoxal and glutathione, to *S*-D-lactoylglutathione, whereas glyoxalase II converts the latter to D-lactate and glutathione.

The catalytic mechanism of GlxI has been studied by two different groups [1,2]. In general, it is accepted that the mechanism is initiated by abstracting a proton from substrate and then the reaction proceeds via an enediolate intermediate. Based on the X-ray structure of GlxI [2], the proton can be abstracted either by Glu172 or Glu99. Also, Glu172 and Glu99 are in best positions to abstract proton from *S* and *R* diastereomers of substrate, respectively. In the active site of this enzyme the Glu172 and Glu99 are trans to each other, but they are not coordinated symmetrically to Zn atom. Glu172 is displaced from Zn atom (the Zn–O distance is 3.3 Å).

In this work, we look for a reasonable mechanism by hybrid quantum mechanical and molecular mechanical (QM/MM) calculations, including full account of the surrounding protein.

QM/MM calculations:

The QM/MM calculations were carried out with the ComQum program. The QM calculations employed the TPSS density functional method and the def-SV(P) basis set. The MM calculations were done with the sander module in Amber software using the Amber 99SB force field. The calculations were based on crystal structure of Glx I (PDB ID 1QIN) [2].

To have model of the active site of GlxI, the inhibitor molecule was changed to the substrate by removing iodine atom, removing five carbon atoms of benzene ring and replacing the nitrogen atom that is connected to the phenyl group with a carbon atom.

Results and discussion:

The mechanism is initiated by transferring H1 to O6 in the substrates (the nomenclatures are according to Figure 1). Calculated QM/MM energy barrier for this step is 10 kJ mol⁻¹. After transferring H1 to O6 there are two possibilities for continuing the reaction, transferring H1 from O6 to C1 or transferring H1 from O6 to O1. In later one after removal of the bond restraint from the final structure, H1 returns to O6. In another word H1 does not like to be on O1. Therefore, the first two steps of the mechanism is transferring H1 from C2 to O6 and then transferring H1 from O6 to C1. While transferring H1 to C1, H2 moves from O2 to O4. During this move, the C–C bond in Glu99 rotates to bring H2 in a good position to transfer it to O1. Now, the product can dissociate from the enzyme and it can take H2 or another proton from the environment to complete the valance of O1. Figure 2 shows the energy barrier for these steps. It indicates a barrier of 50 kJ mol⁻¹ and a reaction energy close to 0 kJ/mol.

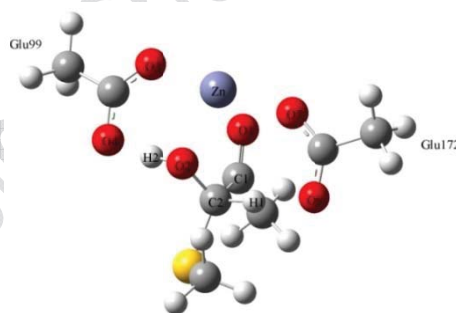


Figure 1. QM/MM optimized structure of a part of active site in reactant state

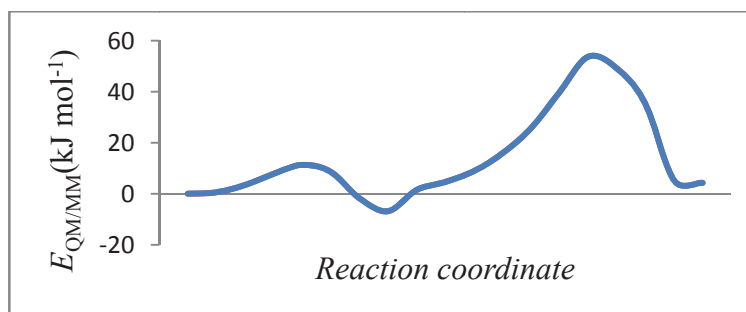




Figure 2. QM/MM energy barrier of proton abstraction and proton delivery steps.

References

- [1] Himo, F; Siegbahn, E. M. *J. Am. Chem. Soc.* **2001**, *123*, 10280.
- [2] Cameron, A. D.; Ridderström, M.; Olin, B.; Kavarana, M. J.; Creighton, D. J.; Mannervik, B. *Biochemistry* **1999**, *38*, 13480.

15th Physical Chemistry Conference



Quantitative structure-activity relationship study of dihydropyridine derivatives by methods topological descriptors and chemometrics

Ali Niazi, Ali khalili*, Ahmad Akrami, Samaneh ghaneinasab

Department of Chemistry, Faculty of Science, Islamic Azad University-Arak Branch, Arak, Iran

Email: ali.khalili.66.a@gmail.com

Key words: OSC, PLS, Mean-centering, dihydropyridine

Introduction:

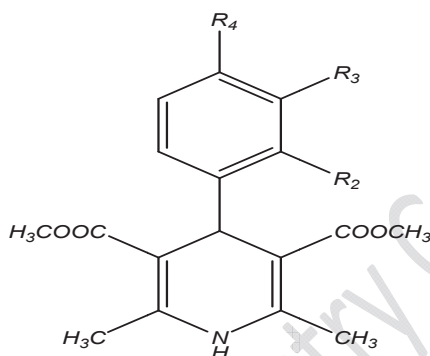
A quantitative structure-activity relationship (QSAR) study is suggested for the prediction of structure of dihydropyridine (DHP). Ab initio theory was used to calculate some quantum chemical descriptors including electrostatic potentials and local charges at each atom, HOMO and LUMO energies, etc. One of the challenges in the field of quantitative structure-activity relationship (QSAR) analysis is the correct classification of a chemical compound to an appropriate model for the prediction of activity.

The aim of this model is to obtain information from one class of numerical descriptors that describe molecular structure. Using information that is provided a relation between structure and biological activation has occurred. Structure of these compounds first design in ChemDraw software and improve in Chem3D software with AM1 semi experimental war. By helping improved structure catch great amount of Dragon software descriptor. Related descriptor deleted taking advantage of PCA. With methods PLS, Mean-centering- PLS, OSC-PLS and Mean-centering-OSC-PLS tried to achieve best score and loading plot.

Computer hardware and software:

The derivation of theoretical molecular descriptors proceeds from the chemical structure of the compounds. In order to calculate the theoretical descriptors, molecular structures were run on

a computer processor with windows XP operating system. The ChemDraw software was used for drawing the molecular structures. Hyperchem (version 6.03, Hypercube, Inc.) and Dragon 5.4 software were used for geometric optimization of the molecules and calculation of the quantum chemical and topological descriptors [2-4]. All programs needed for OSS variable selection and PLS modeling were written in MATLAB (version 6.5, MathWork, Inc.). The parent structure of DHP derivatives is shown in Figure 1.



Result and discussion:

The PLS model was run twice. In the first run (run a), all the calculated descriptors were considered in modeling; while in the second run (run b), after preprocessing by OSC. After preprocessing by OSC, were considered in the modeling procedure. However, modeling of all the descriptors by PLS needs some increased number of factors. The optimal number of factors for this data by PLS and OSC-PLS models were obtained 7 and 5, respectively. OSC-PLS model was established to predict the inhibitory of some DHP derivatives. A proper model with high statistical quality and low prediction errors was obtained. The model could predict the solubility not existed in the modeling procedure accurately.

Conclusion:

The quantum chemical, WHIM and GETAWAY descriptors concerning to the whole molecular properties and those of individual atoms in the molecule were found to be important factors controlling the inhibitory behavior. Moreover, the electrostatic potential was found to be more informative than the local charge in this study.



Reference:

- [1] A. Niazi, *J. Braz. Chem. Soc*, 17 (2006) 1020.
- [2] A. Niazi, J. Ghasemi, M. Zendehtdel, *Talanta*, 74 (2007) 247.
- [3] H.Y. Yu, X.Y. Niu, H.J. Lin, *Food Chemistry*, 113 (2009) 291.
- [4] M. Kompany-Zareh, Y. Akhlaghi, *J. Chemometrics*, 21 (2007) 239.

15th Physical Chemistry Conference



A comparative study of B3LYP in predicting of stability of N'-benzylidene-2,4-dichlorobenzohydrazide

Ali. Dehghan Tazargani a*, Saeedeh. Hashemian b

a,b Department of chemistry, Faculty of sciences, Islamic Azad University, Yazd, Iran

Email: dehghan1362@yahoo.com

Key words: DFT, HOMO-LUMO, NBO, N'-benzylidene-2,4-dichlorobenzohydrazide (BDCBH)

Introduction:

Schiff base are important class of compounds in medicinal and pharmaceutical field. Hydrazide derivatives are Schiff base and have been claimed to possess antimicrobial [5], anti micro bacterial, anti tumor, anti malaria and anti HIV activities. Hydrazide analoges also possess other biological activities like anticancer, and anti depressant [1, 2]. Density functional theory (DFT) has become very popular in recent years. This is justified based on the pragmatic observation that it is less computationally intensive than other methods with similar accuracy [3].

Materials and methods:

In the present work, the $C_{14}H_{10}Cl_2N_2O$ structure was allowed to relax by all atomic geometrical parameters in the optimization at the DFT level of B3LYP exchange-functional method and 6-311++G** basis set.

Result and discussion:

Selected bond lengths, bond angles and dihedral angles are listed in table 1 and Second order perturbation theory analysis of Fock matrix in NBO (E(2)- hyperconjugative energy) basis in table 2. There is the optimized molecular structure in fig 1, IR spectra in fig 2, Atomic orbital composition of the frontier molecular orbital in fig 3.

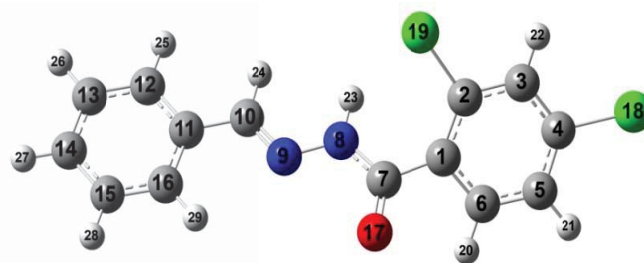


Fig. 1. Optimized molecular structure of N'-benzylidene-2,4-dichlorobenzohydrazide

Table 1. Calculated geometrical bond distance for the BDCBH (bond length in Å, bond angles in Å°)

The bond lengths in B3LYP / 6-311++G**							
Parameters	(Å)°	Parameters	(Å)°	Parameters	(Å)°	Parameters	(Å)°
C1-C2	1.4005	C7-N8	1.3777	C1-C7	1.5141	C2-C3	1.3934
C2-Cl19	1.7657	N8-N9	1.3582	C7-O17	1.2128	C3-C4	1.3886
C4-Cl18	1.7522	N9-C10	1.2805	C10-C11	1.4634	C4-C5	1.3919
The bond angles in B3LYP / 6-311++G**							
C3-C2-Cl19	115.8891	O17-C7-N8	123.895	C10-C11-C12	119.0972	C1-C2-C3	121.7738
C3-C4-Cl18	119.1139	N8-N9-C10	116.9048	C12-C11-C16	119.0716	C2-C1-C6	117.1604
C1-C7-O17	120.7546	N9-C10-C11	122.087	C11-C16-C15	120.1212	C1-C6-C5	122.2411

Table 2. Calculated Second order perturbation theory analysis of Fock matrix in NBO basis (in (Kcal/mol))

Donor	Acceptor	E(2)	Donor	Acceptor	E(2)	Donor	Acceptor	E(2)
π^* C2-C1	π^* C6-C5	143.93	π C6-C5	π^* C4-C3	23.33	π C11-C12	π^* C13-C14	19.7
π^* C4-C3	π^* C6-C5	115.04	π C15-C16	π^* C13-C14	21.01	π C4-C3	π^* C2-C1	19.54
π^* N9-C10	π^* C11-C12	70.95	π C6-C5	π^* C2-C1	19.97	π C2-C1	π^* C4-C3	19.47
π^* C2-C1	π^* C7-O17	64.86	π C11-C12	π^* N9-C10	19.76	π C11-C12	π^* C15-C16	18.65

- Other E(2) between 18.54 (Kcal/mol) – 0.51 (Kcal/mol)

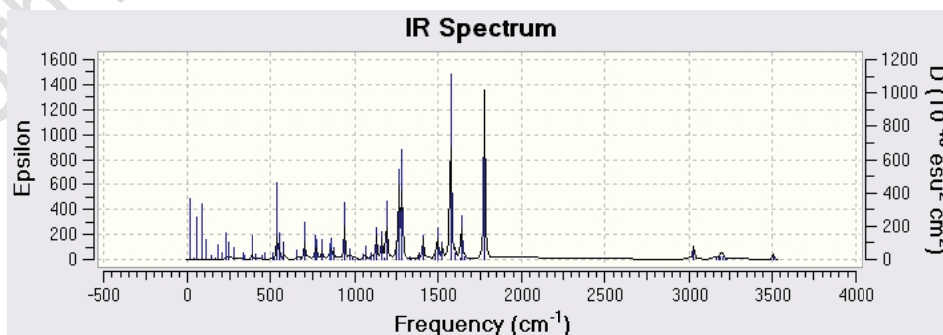
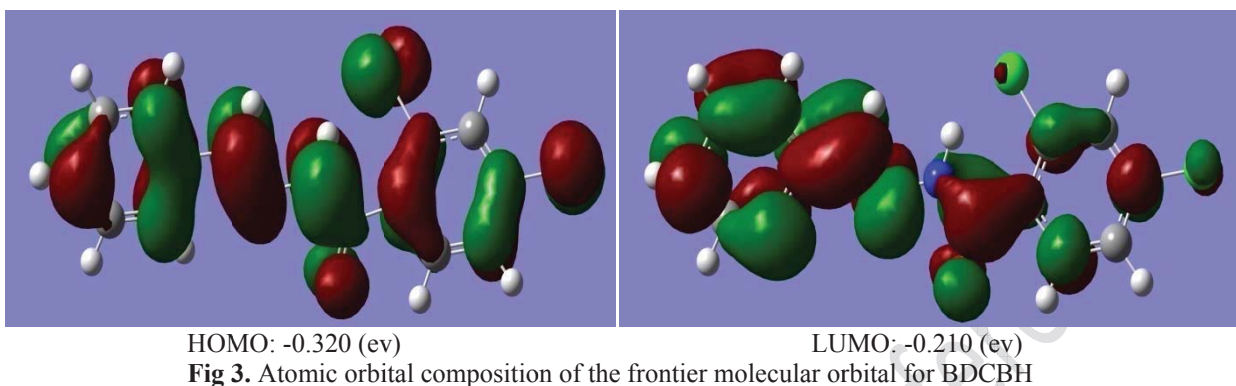


Fig 2. IR spectra of N'-benzylidene-2,4-dichlorobenzohydrazide



Conclusion:

Bond parameters and vibrational frequencies were calculated at B3LYP/6-311++G(d,p) level and computed values compared with experimental spectral frequencies. Novelty of the compound was also studied and compared with available literatures. The NBO analysis reveals that the maximum energy during the molecular interactions. Energy gap of the molecule have predicted, when compare with previous study, BDCBH possesses high energy gap (0.11 eV). Charges of every atom have calculated and it was illustrated by Mullikens plot.

Reference:

- [1] F. Sheikhshoae, W. Belaj, M.F. Fabian, *J. molec. Strut.* 794 (2006) 244.
- [2] D.A. Atwood, M.j. Harvey, *Chem. Rev.* 101 (2001) 37.
- [3] M. J. Frisch, G. W. Trucks, H. B. Schlegel, G. E. Scuseria, M. A. Robb, J. R. Cheeseman, J. A. Montgomery, Jr., T. Vreven, K. N. Kudin, J. C. Burant, J. M. Millam, S. S. Iyengar, J. Tomasi, V. Barone, B. Mennucci, M. Cossi, G. Scalmani, N. Rega, G. A. Petersson, H. Nakatsuji, M. Hada, M. Ehara, K. Toyota, R. Fukuda, J. Hasegawa, M. Ishida, T. Nakajima, Y. Honda, O. Kitao, H. Nakai, M. Klene, X. Li, J. E. Knox, H. P. Hratchian, J. B. Cross, C. Adamo, J. Jaramillo, R. Gomperts, R. E. Stratmann, O. Yazyev, A. J. Austin, R. Cammi, C. Pomelli, J. W. Ochterski, P. Y. Ayala, K. Morokuma, G. A. Voth, P. Salvador, J. J. Dannenberg, V. G. Zakrzewski, S. Dapprich, A. D. Daniels, M. C. Strain, O.



Farkas, D. K. Malick, A. D. Rabuck, K. Raghavachari, J. B. Foresman, J. V. Ortiz, Q. Cui, A. G. Baboul, S. Clifford, J. Cioslowski, B. B. Stefanov, G. Liu, A. Liashenko, P. Piskorz, I. Komaromi, R. L. Martin, D. J. Fox, T. Keith, M. A. Al-Laham, C. Y. Peng, A. Nanayakkara, M. Challacombe, P. M. W. Gill, B. Johnson, W. Chen, M. W. Wong, C. Gonzalez, and J. A. Pople, Gaussian, Inc., Pittsburgh PA, 2003.

15th Physical Chemistry Conference



A comparative study of B3P86 in predicting of stability of N'-benzylidene-4-(dimethylamino)benzohydrazide

Ali. Dehghan Tazargani*, Saeedeh.Hashemian

Department of chemistry, Faculty of sciences, Islamic Azad University, Yazd, Iran

Email: dehghan1362@yahoo.com

Key words: DFT, IR Spectra, NBO, N'-benzylidene-4-(dimethylamino)benzohydrazide (BDMABH)

Introduction:

Quantum chemical methods are ideal tool for investigating these parameters and are able to provide an insight into the inhibitor–surface interaction. Density functional theory, which connects some traditional empirical concepts with a quantum mechanical interpretation, is very reliable in explaining the hard and soft acid-base behavior of inhibitor molecules introduced by Pearson [1-3].

Materials and methods:

In This work, the $C_{16}H_{17}N_3O$ structure was allowed to relax by all atomic geometrical parameters in the optimization at the B3P86 exchange-functional method and 6-311++G** basis set.

Result and discussion:

The optimized molecular structure of (BDMABH) is shown in Fig 1. Selected bond lengths, bond angles and dihedral angles of title compound are listed in Table 1 and second order perturbation theory analysis of Fock matrix in NBO (E(2)- hyperconjugative energy) basis in Table 2. IR, Raman and NMR spectra of (BDMABH) is shown in Fig 2 and molecular orbital (HOMO – LUMO) is shown in Fig 3.

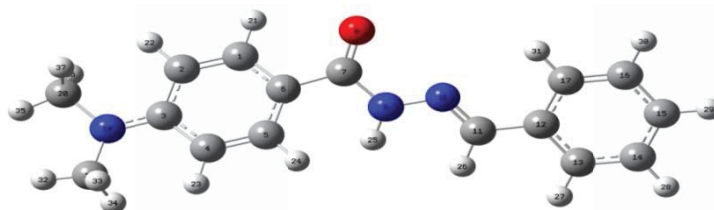


Fig. 1. Optimized molecular structure of N'-benzylidene-4-(dimethylamino)benzohydrazide (BDMABH)

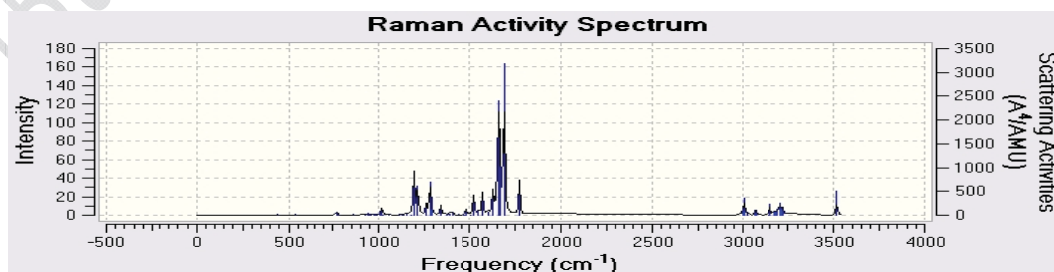
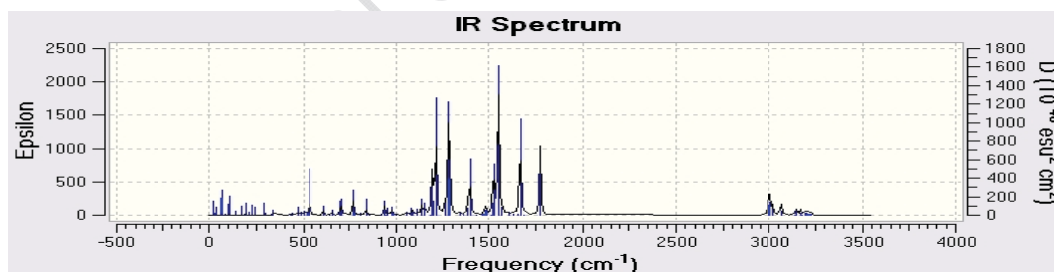
Table 1. Calculated geometrical bond distance for the BDCBH (bond length in Å, bond angles in °)

The bond lengths in B3P86 / 6-311++G**							
Parameters	(Å)°	Parameters	(Å)°	Parameters	(Å)°	Parameters	(Å)°
C11-C12	1.458	N9-N10	1.343	C6-C7	1.485	C1-C6	1.397
C11-N10	1.278	C7-N9	1.388	C7-O8	1.212	C3-N18	1.373
The bond Angles in B3P86 / 6-311++G**							
C12-C11-N10	121.834	N9-C7-C6	114.200	C2-C3-N18	121.320	C20-N18-C19	118.789
C11-N10-N9	117.521	C6-C7-O8	123.198	C3-N18-C20	119.792	O8-C7-N9	122.595

Table 2. Calculated Second order perturbation theory analysis of Fock matrix in NBO basis (in (Kcal/mol))

Donor	Acceptor	E(2)	Donor	Acceptor	E(2)	Donor	Acceptor	E(2)
π^* C5-C6	π^* C7-O8	192.43	LP N9	π^* C7-O8	45.02	π C5-C6	π^* C1-C2	22.58
π^* C3-C4	π^* C1-C2	189.94	LP N9	π^* N10-C11	30.62	π C1-C2	π^* C3-C4	22.54
π^* N10-C11	π^* C12-C13	78.43	LP O8	π^* C7-N9	29.31	π C16-C17	π^* C14-C15	20.96
LP N18	π^* C3-C4	46.26	π C3-C4	π^* C5-C6	26.29	π C14-C15	π^* C12-C13	20.36

- E(2) is between 192.43 (Kcal/mol) – 0.50 (Kcal/mol)



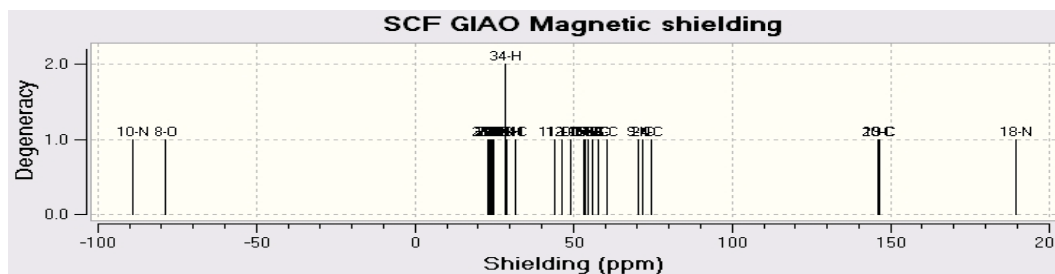
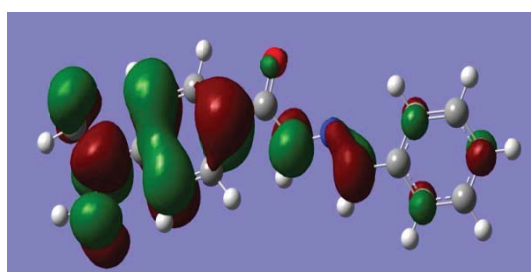
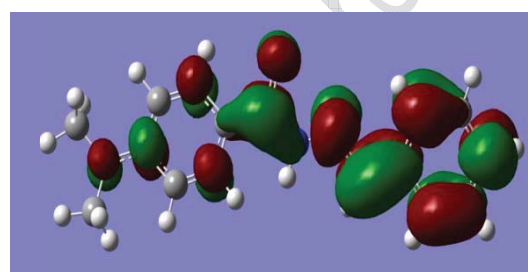


Fig 2. IR, Raman and NMR spectra of N'-benzylidene-4-(dimethylamino)benzohydrazide (BDMABH)



HOMO: -0.302 (ev)



LUMO: -0.209 (ev)

Fig 3. Atomic orbital composition of the frontier molecular orbital for (BDMABH)

Conclusion:

The geometry of the title compound was optimized with DFT (B3P86) method using 6-311++G(d,p) basis set. The complete molecular structural parameters and thermodynamic properties of the optimized geometry of the compound have been obtained. The vibrational frequencies of the fundamental modes of the compound have been precisely assigned and analyzed. The NBO analysis reveals that the maximum energy during the molecular interactions. Energy gap of the title molecule have predicted, when compare with previous study, BDMABH possesses high energy gap (0.93 eV). Charges of every atom have calculated and it was illustrated by Mullikens plot.

Reference:

- [1] R.G. Pearson, J. Am. Chem. Soc. 85 (1963) 3533.
- [2] R.G. Pearson, Proc. Nat. Acad. Sci. 83 (1986) 8440.
- [3] R.G. Pearson, Inorg. Chem. 27 (1988) 734.

Investigation of substituent effects phenyl on the intramolecular hydrogen bond of methyl 3-oxo-3-phenyl propanoate (MOPP)

S. Salem^{a*}, F. Bahry^a

^aChemistry Department, Hakim Sabzevari University Sabzevar Iran Email: f_s_bahry@yahoo.com

Key words: electron-withdrawing group, electron donating group, intramolecular hydrogen bond, β -diketones

Introduction:

β -diketones are capable of keto-enol tautomerism. The cis-enol forms of β -diketones are stabilized by a strong intramolecular hydrogen bond.

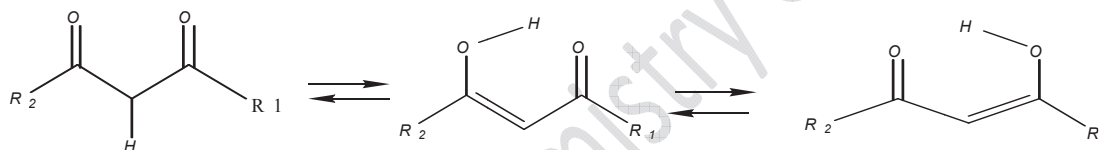


fig1: Tautomerism in β -diketones $\beta\uparrow$ $\alpha\uparrow$ $\beta\uparrow$

The hydrogen bond formation leads to an enhancement of the resonance conjugation of the π -electrons, which causes a marked tendency equalization of the bond order of the valence bonds in the resulting six member chelated ring.

Therefore, it seems that any parameter that affects the electron density of the chelated ring will change the hydrogen bond strength. It is well known that substitution in α or β position drastically changes the hydrogen strength.

Method:

Geometrical calculations are performed by using GAUSSIAN (98) programs (B3LYP 6311G basis set).

Results and discussion:

several experimental data suggest that the strength of such bridge decreases when an electron-withdrawing group replaces the group in position β , and it increases when an electron donating group replaces in this position.

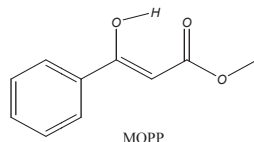
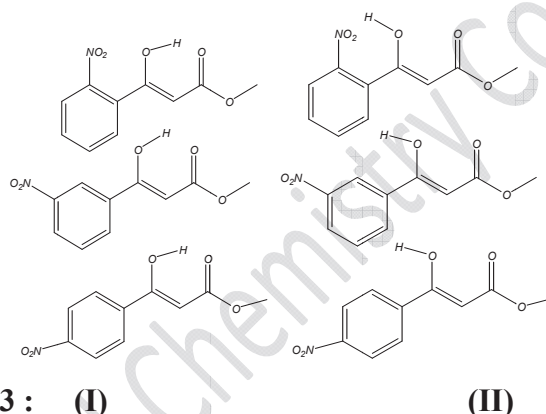


fig2: the most stable conformer of MOPP

We put substituent (CH₃, Cl, NO₂, CN, NH₂) in position orto, meta and para of phenyl ring of MOPP for example:



The hydrogen bond strength, EHB, the energy difference between chelated(I) and open(II) structures are shown in fig3

Energy (hartree)	CH3(I)	CH3(II)	Cl(I)	Cl(II)	CN(I)	CN(II)	NH2(I)	NH2(II)	NO2(I)	NO2(II)
orto	-652.0206	-651.98891	-1072.2990	-1072.2748	-704.9356	-704.9106	-668.0484	-668.0142	-817.1252	-817.0935
meta	-652.0239	-651.99949	-1072.3032	-1072.2784	-704.9403	-704.9147	-668.0571	-668.0329	-817.1708	-817.1460
para	-652.0237	-651.99942	-1072.3085	-1072.2833	-704.9407	-704.9152	-668.0580	-668.0335	-816.9629	-816.9356

	Orto EHB(kcal mol ⁻¹)	Meta EHB (kcal mol ⁻¹)	Para EHB (kcal mol ⁻¹)
CH3	19.93	15.34	15.27
Cl	15.15	15.59	15.80
CN	15.69	16.08	16.02
NH2	21.42	15.19	15.37
NO2	19.87	15.54	17.13



Conclusion:

The electron-withdrawing group (Cl, CN, NH₂) in para position makes MOPP more stable than meta and ortho position but electron donating group (NH₂, CH₃) in ortho position makes MOPP more unstable and the difference of cis and trans forms is a lot, therefore the hydrogen bond in ortho position is stronger than meta or para position.

Reference:

- [1] S.F. Tayyari, S. Salemi, M. Zahedi Tabrizi, M. Behforouz, J. Mol. Struct. 694 (2004) 91–104
- [2] S.F. Tayyari, J.S. Emampour, M. Vakili, A.R. Nekoei, H. Eshghi, S. Salemi, M. Hassanpour, J. Mol. Struct. 794 (2006) 204–214

Investigation of intramolecular hydrogen bond and study of conformers of methyl 3-oxo-3-phenyl propanoate (MOPP)

S. Salem^{a*}, F. Bahry^a

^aChemistry Department, Hakeem Sabzevar University Sabzevar Iran

Email: f_s_bahry@yahoo.com

Key words: β -diketones, intramolecular hydrogen bond, transfer proton, tautomerism

Introduction:

The tautomerism between the keto and enol form of β -diketones can be represented as follows:

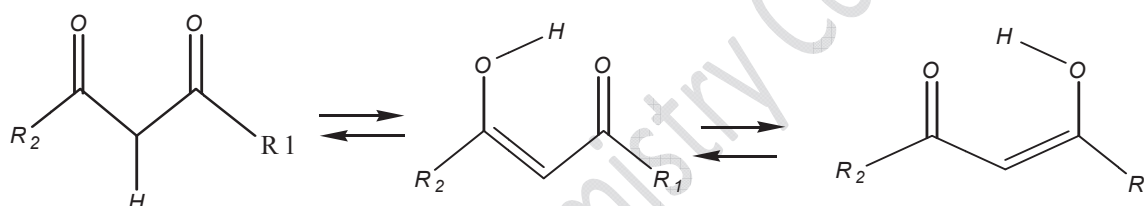


fig1: tautomerism

it is well known that the cis-enol form of β -diketones is characterized by a strong intramolecular hydrogen bond. A complete conformational analysis of the keto and chelated enol forms of MOPP. The hydrogen bond strength of the most stable conformer is compared with acetylacetone (AA).

Method:

Geometrical calculations are performed by using GAUSSIAN programs. Geometries of the cis enol forms of MOPP and their corresponding open structures and fully optimized with MP2 using 6311G** base set.

Results and discussion:

Two different isomeric cis-enol forms are distinguishable in the case of unsymmetrical β -diketones an inter conversion occurs by transfer of an enol proton from one oxygen atom to the other.

From the theoretical point of view, four enol conformers can be drawn for the MOPP molecule; the structures of M7 and M8 are not stable and under optimization turn to the M3 and M4 conformers, respectively. the structures of these conformers, their relative stabilities and their hydrogen bond strength, EHB, the energy difference between chelated(I) and open(II) structures are shown in fig2

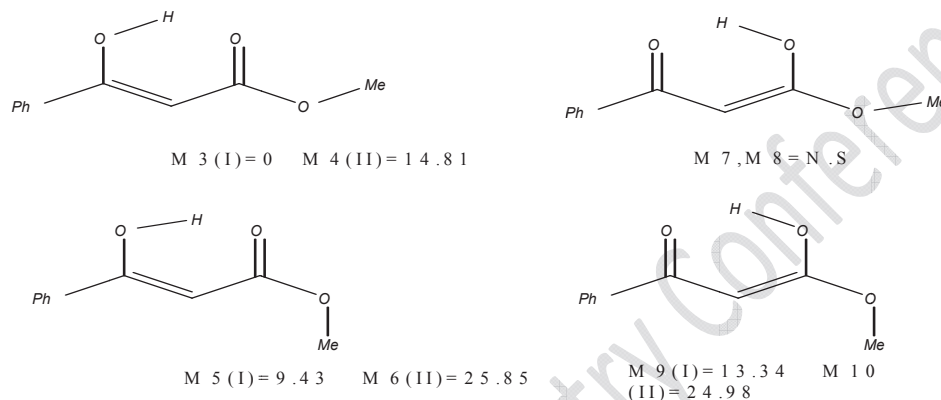


fig 2: the structures of enol conformers

Geometrical parameters of the enol ring of the most stable conformer MOPP is compared with AA.

Bond distances	AA	MOPP
O...O	2.52	2.701
O—H	1.013	0.98
C—O	1.325	1.38
C=C	1.374	1.36
C—C	1.442	1.45
C=O	1.252	1.267

Conclusion:

Thirty eight possible conformer of MOPP fully optimized. Comparison of the structural parameters of MOPP with those of AA reveals a considerably weaker H-bond in MOPP than that in AA.

According to the table bond lengths O...O in AA was shorter than in MOPP and O-H bond in AA was longer than in MOPP.



Reference:

- [1] S.F. Tayyari, S. Salemi, M. Zahedi Tabrizi, M. Behforouz, J.Mol Struct. 694 (2004) 91–104
[2] S.F. Tayyari, J.S. Emampour, M. Vakili, A.R. Nekoei, H. Eshghi, S. Salemi, M. Hassan pour, J.Mol Struct 794 (2006) 204–214

15th Physical Chemistry Conference

Conformational stability, molecular structure, and Intramolecular hydrogen Bonding of (Z) -4, 6-dioxo-6-phenylhex-2-enoic acid [ZDPEA]

S. Salemi^{a*}, F. Nateghi^a

^a Chemistry Department, Hakim Sabzevari University, Iran

Email: Siroussalemi@gmail.com

Key word: Intramolecular hydrogen bonding, β -Dicarbonyl, molecular conformer, (Z) -4, 6-dioxo-6-phenylhex-2-enoic acid

Introduction:

β -Dicarbonyl compounds are capable of keto-enol tautomerism; the tautomers exist in equilibrium with each other (Fig. 1). The position of the keto-enol equilibrium for this class of compounds differs according to electronic characteristics of the substituents. The cis-enol form of β -dicarbonyl compounds are stabilized by a strong intramolecular hydrogen bond (IHB) with a double minimum character.

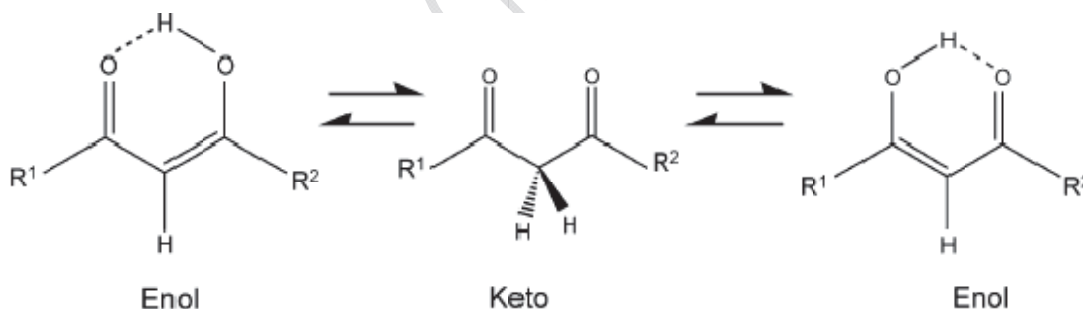


Fig. 1. The keto-enol tautomerization of β -dicarbonyls

Methods:

All the computations in the present study were performed using GAUSSIAN 98W program suite. All possible enol and keto conformations of (Z) -4,6-dioxo-6-phenylhex-2-enoic acid [ZDPEA] were fully optimized at the B3LYP level using 6-311++G** basis set.

Result and discussion:

A β -dicarbonyl compound predominantly exists as conjugated cis-enol, stabilized by an intramolecular hydrogen bond. From the theoretical point of view, seventy eight enol conformers can be drawn for the ZDPEA molecule. Depending on the position of the enolated proton, the occurrence of two classes of cis-enol forms is possible. Among these forms, only six of them are engaged in a six-member ring intramolecular hydrogen bonded system with E_{HB} (Kcal/mol): 14.39, 15.75, 14.54, 15.75, 17.11, 15.17, for them. The A (phenyl group in C-OH side) conformers are considerably more stable than B(CO₂H-C=C- fragment in C-OH side) conformers. The full optimized geometrical parameters of ZDPEA (most stable conformer), BA (benzoylacetone), and AA (acetylacetone) are compared in Table 1. According to Table 1, substitution of phenyl group in C-OH side, ZDPEA(A) conformer, increases the C=C and C=O bond lengths by 0.010 and 0.014 Å, respectively, while the C-C bond length decreases by 0.024 Å. These changes in the bond lengths indicate that the Π -electron delocalization in the enol ring slightly increases by phenyl substitution in the hydroxyl side. We observed that not stable H-O bond with Substitution of CO₂H -C=C- fragment in the C-OH side (B conformer). The O...O distance of ZDPEA (A) 2.520 Å, is longer than the corresponding for BA, 2.513 Å, which indicates stronger hydrogen bond in BA than that in ZDPEA (A). It is noteworthy that the O-H bond order correlates with the calculated O...O distance, by increasing the hydrogen bond strength, reducing the O...O distance, the O-H bond order decreases. E_{HB} for ZDPEA (A), AA, BA, compared in Table 1 and the following trend in hydrogen bond strength is concluded: ZDPEA < AA < BA

Table 1. The geometrical parameters of the cis-enol forms of BA And ZDPEA calculated at the B3LYP level with 6-311++G** Basis set

Bond lengths (Å)	BA	ZDPEA(A)	AA
O...O	2.513	2.52	2.544
C-O	1.326	1.32	1.326
C=O	1.250	1.26	1.246
O-H	1.010	1.002	1.003
H...O	1.585	1.614	1.633
C-C	1.439	1.420	1.444
C=C	1.378	1.380	1.370
E_{HB}	16.07	14.34	15.87

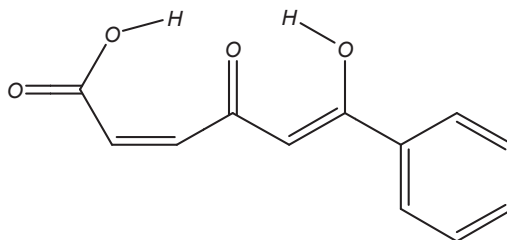


Fig.2. The most stable conformer of ZDPEA

Conclusion:

Among seventy eight possible enol conformers of ZDPEA, only six conformers have the chelated IHB. The DFT calculations show that only six conformers are stable. According to the theoretical (Table1) the hydrogen bond strength in ZDPEA is weaker than BA and AA.

Reference:

- [1] S.F. Tayyaria, S. Salemi, M. Zahedi Tabriz, M. Behforouz .Journal of Molecular Structure 694 (2004) 91–104
- [2] S.F. Tayyari, J.S. Emampour a, M. Vakili, A.R. Nekoei, H. Eshghi, S. Salemi, M. Hassanpour .Journal of Molecular Structure 794 (2006) 204–214
- [3] M. Vakili, S.F. Tayyari, A. R. Nekoei, H. Miremad, S. Salemi, R.E. Sammelson. Journal of Molecular Structure 970 (2010) 160–170
- [4] S.F. Tayyari, H. Rahemi , A.R. Nekoei, M. Zahedi-Tabrizi, Y.A. Wang .Spectrochimica Acta Part A 66 (2007) 394–404.



Density functional study of ternary B-C-N compounds by NMR spectroscopy and NBO analysis

Elham Pournamdari^{*1}, Fatemeh Azarakhshi²

¹Department of chemistry, Islamshahr branch, Islamic Azad University, Islamshahr, Iran

²Department of Chemistry, Varamin-Pishva Branch, Islamic Azad University, Varamin, Iran

E-mail: epournamdar@iiu.ac.ir

Keywords: DFT, NBO, NMR spectra, B-C-N materials

Introduction:

Ternary BCN compounds have recently attracted increased interest due to their attractive properties as super-hard materials [1] and as semiconductors with various band gap energies [2]. The preparation of BCN materials with a wide range of compositions and a corresponding range of properties offers many opportunities for materials science research [3]. B-C-N materials have been investigated both theoretically [4-6] and experimentally [7-9], and various methods have been used to the synthesis of the graphite-like B-C-N compounds, such as nitriding of solid-phase at high temperatures [10], chemical vapor deposition (CVD) [11, 12], solvothermal method [13], chemical process [14], etc. In this theoretical work the structure of $H_{20}B_4C_9N_4$ is studied by ab initio using the density functional method. The results of calculations are compared between different methods with NMR spectroscopy of $H_{20}B_4C_9N_4$. Our recent theoretical and experimental work reveals that the ternary B-C-N system may have many kinds of structures, showing different characteristics.

Computational details:

In our calculation optimization of $H_{20}B_4C_9N_4$ geometry as well as calculation of NMR spectra and NBO analysis was carried out using the DFT method (B3P86, B3PW91 and PG96LYP) with 6-31G basis set which are implemented by the GAUSSIAN 98 program package.



Result and discussion:

Theoretical information on chemical shifts will increase the accuracy and characteristic of BCN structures and extend the applicability of NMR spectroscopy to ever larger systems. In addition NBO analyses of ternary BCN compounds have been done. It could be concluded that the most polar band in this structure which has got the most resonance energy (E_2) is N (3)-C (10) bond and it has got the highest voltage difference which is confirmed by NMR spectra. Moreover the results of stereoelectronic interactions are due to hyperconjugation effects, which are significant for the explanation of the conformational properties of this compound as semiconductors.

Conclusion:

The optimized structures parameters, dipole – dipole interaction, donor-acceptor electronic delocalization and electric potential data of ternary BCN compounds are discussed. In this letter, we represented the quantum-chemical simulation of structure, NBO analysis and NMR spectra.

References:

- [1] E. Knittle, R.B. Kaner, R. Jeanloz, M.L. Cohen: Phys. Rev. B **51**, 12 149 (1995)
- [2] M.O. Watanabe, S. Itoh, K. Mizushima, T. Sasaki: Appl. Phys. Lett. **68**, 2862 (1996)
- [3] V.S. Teodorescu¹, A. Luches², R. Dinu³, A. Zocco², M.F. Ciobanu⁴, M. Martino², V. Sandu¹, M. Dinescu³ Appl. Phys. A 69 [Suppl.], S667–S670 (1999)
- [4] Liu AY, Wentzcovitch RM, Cohen ML (1989) Phys Rev B 39:1760
- [5] Mazzoni MSC, Nunes RW, Azevedo S, Chacham H (2006) Phys Rev B 73:073108
- [6] Pan ZC, Sun H, Chen CF (2006) Phys Rev B 73:214111
- [7] Badzian AR (1981) Mater Res Bull 16:1385
- [8] Nicolich JP, Hofer F, Brey G, Riedel R (2001) J Am Ceram Soc 84:279.
- [9] Yamada K (1998) J Am Ceram Soc 81:1941.
- [10] Andreev YG, Lundstrom T (1994) J Alloys Compd 210:311.



- [11] Kaner RB, Kouvetakis J, Warble CE, Sattler ML, Bartlett N (1987) *Mater Res Bull* 22:399.
- [12] Kouvetakis J, Sasaki T, Shen C, Hagiwara R, Lerner M, Krishnan KM, Bartlett N (1990) *Synth Met* 34:1.
- [13] Huang FL, Cao CB, Xiang X, Lv RT, Zhu HS (2004) *DiamRelat Mat* 13:1757.
- [14] Hubacek M, Sato T (1995) *J Solid State Chem* 114:258.

15th Physical Chemistry Conference



Evaluation of the Host-Guest Inclusion Complex Formation of Cucurbit [7,8]uril with trans- $[\{PtCl(NH_3)_2\}_2(\mu-NH_2(CH_2)_8NH_2)]^{2+}$ Anticancer Drug

M. Abboud poura, Z. Mahdavi farb

^aDepartment of chemistry, Islamic Azad University, Khozestan science and research branch, ahvaz, Iran

^bDepartment of chemistry, Faculty of Science, Shahid Chamran University, Ahvaz, Iran

Email: maryamabbodpoor@yahoo.com

Keyword: Inclusion Complex, DFT, Anticancer drug, Cucurbit[n]uril

Introduction:

Multinuclear platinum complexes developed by farrell and co-workers have shown considerable promise as anti-cancer agents[1]. The mechanism of these drugs is through the chemical bindings with DNA molecules which destroys the cancer cells. Recently the researchers encapsulated of multinuclear platinum complexes by cucurbit[n]uril could reduce their toxicity and protect them from binding by thiol containing proteins[1,2].

Method:

Quantum mechanical calculations, were carried out by Gaussian 03 software in order to study the host-guest inclusion complex formation of trans- $[\{PtCl(NH_3)_2\}_2(\mu-NH_2(CH_2)_8NH_2)]^{2+}$ with CB[7,8]. All the structures were optimized with B3PW91 method and LanL2DZ basis set. The inclusion complexes were simulated by putting the drug at the end of CB[7,8] cavity and allowing it to pass through the CB cavity by steps. The energy of complexes in different position of the guest molecules was calculated. In addition, the most stable position of drug in the cavity of the CB[n] was optimized.

Results and Discussion:

The potential energy surfaces of the complexes of CB[7,8] with anticancer drug vs the z coordinate are shown in Fig 1. The stabilization energy of the complex formed(ΔE),

electrophilicity (ω), highest occupied molecular orbital (HOMO), lowest unoccupied molecular orbital (LUMO), energy gap and the electronic chemical potential (μ) are also calculated. These results are summarized in Table 1

$$\Delta E = E_{\text{complex}} - (E_{\text{CB}} + E_{\text{drug}}), E_{\text{LUMO}} - E_{\text{HOMO}}, \mu = (E_{\text{HOMO}} + E_{\text{LUMO}})/2, \omega = \mu^2/2\eta$$

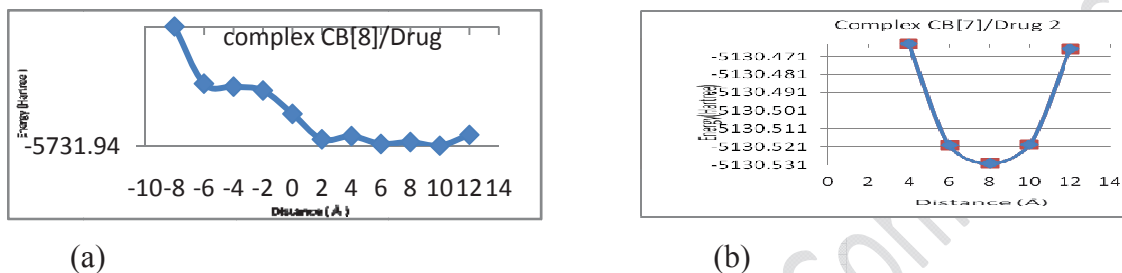


Fig. 1: Graphic diagram for emulation of the inclusion complexation of (a) Drug into CB[8] and (b) Drug into CB[7]

Table 1: Electronic energies and HOMO, LUMO, Gap energy, electronic chemical potential (μ) and electrophilicity (ω) of the inclusion complexations of CB[7,8] and Drug of the DFT/lanl2dz optimized structures

Type	ΔE (Kcal/mol)	HOMO (eV)	LUMO (eV)	Gap Energy (eV)	μ (eV)	ω (eV)
Drug	-	-11.341	-6.403	4.938	-8.872	15.940
CB[7]	-	-6.772	0.479	7.251	-3.146	1.364
CB[8]	-	-6.827	0.460	7.288	-3.183	1.390
CB[7]/Drug	-102.224	-9.491	-4.493	4.997	-6.992	9.781
CB[8]/Drug	-100.624	-9.405	-4.271	5.133	-6.838	9.107

The results of stabilization energy indicate that CB[7]/Drug complex has a more negative value than that CB[8]/Drug, which means that this complex is stable than that one. The results of HOMO-LUMO energy gap show that the complex CB[7] with drug can transfer electron from HOMO to LUMO easily than complex CB[8] with drug.

Conclusion:

The results of DFT calculations of CB[7,8]/Drug complexes indicate that CB[7]/drug is more stable than CB[8]/drug.



Reference:

- [1] Mark S. Bali, Damian, J, Royal. Soci. Chem. 2006, 5337-5339
- [2] Nial j. Wheate, J, Inorg, Biochem. 2008, 2060- 2065

15th Physical Chemistry Conference



Theoretical Calculations of the Host-Guest Inclusion Complex Formation of Cucurbit[n]urils with Multinuclear Platinum Anticancer Agent

M. Abboud pour^a, Z. Mahdavi^b

^aDepartment of chemistry, Islamic Azad University, Khoozestan science and research branch, Ahvaz, Iran

^bDepartment of chemistry, Faculty of Science, Shahid Chamran University, Ahvaz, Iran

Email: maryamabbodpoor@yahoo.com

Key Words: Inclusion Complex, DFT, Anticancer, Platinum, Cucurbituril

Introduction:

In the 40 years since the discovery of cisplatin, hundreds of new platinum(II) and platinum(IV) – based complexes have been synthesized and tested as anticancer drugs. Nowadays important improvements in platinum-based chemotherapy causes application of di- and trinuclear platinum drugs. The mechanism of these drugs is through the chemical bindings with DNA molecules which destroys the cancer cells. The drug is destructed as entering body by blood plasma proteins. The researchers have used a group of macromolecules named cucurbit[n]urils (CBs) as drug encapsulation. CBs protect the drugs from degradation[1,2].

Method:

Quantum mechanical calculations of Host-guest inclusion complex formation of trans- $[\{PtCl(NH_3)_2\}_2 \mu-N_4\text{-spermidine-}N_1, N_8\}^{3+}]^{3+}$ (BBR3571) with Cucurbit[7,8] were studied. All the structures were optimized with B3PW91 method and LanL2DZ basis set by Gaussian 03 and 09 software. The inclusion complex was simulated by putting the drug at the end of CB[7,8] cavity and allowing it to pass through the CB cavity by steps. The energy of complex in different distances was calculated and the most stable position of drug was optimized. The complex formation energy, electronic potential, structural properties of molecules, NBO, hydrogen bonding, complexation and interaction energies were calculated.

Result and discussion:

The results of stabilization energy indicate that CB[8] /Drug complex has more negative value than other complex, which means that this complex is more stable than that one. The results of the Natural Bond Orbital (NBO), the energy deformation and interaction calculations show that the complex between CB[8] and drug has more interaction than other. (Table and Fig 1).

Table1. Complexation and interaction energies (ΔE , $E_{\text{interaction}}$) (kcal/mol) for complexes CB[7,8]/Drug

Complex	E_{Complex}	$E_{\text{CB in Complex}}$	$E_{\text{Drug in Complex}}$	$E_{\text{interaction}}$	ΔE
CB[7]/Drug	-3229740.01	-2641077.06	-587810.18	-852.75	-146.11
CB[8]/Drug	-3607168.57	-3018484.85	-5877091.93	-891.77	-180.22

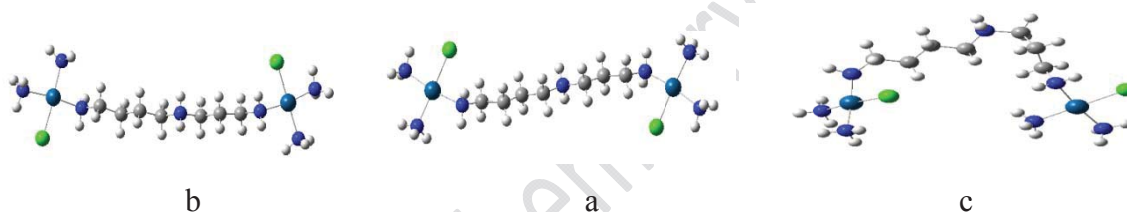


Fig.1. The geometries of the drug (a) before complex formation, (b) deformation after complex formation CB[7]/Drug, (c) deformation after complex formation CB[8]/Drug

Conclusions:

The complex processes of BBR3571 as guest with CB[7,8] as hostes were studied by DFT method. The results calculations of CB[7,8] /Drug complexes indicate that CB[8] /Drug is more stable than CB[7]/Drug.

Reference:

- [1] Nial j. Wheate, Journal, Inorg, Biochem. 2008, 2060- 2065
- [2] Madi Fatiha. Journal, Molecular liquids. 2010, 15



Application of linear and nonlinear QSAR methods for prediction of antitrypanosomal drugs activities of some 1, 2-dihydroquinolin-6-ols and their ester derivatives

N. Goudarzi, M. Arab Chamjangali, H. Rameh*

Faculty of chemistry, Shahrood University of Technology, Shahrood, Iran

Email: hasan_chemistry@yahoo.com

Key words: QSAR, ANN, GA-ANN, SR-ANN, Antitrypanosomal

Introduction:

Trypanosome or sleeping sickness is a swelling of the brain caused by parasites that live in infected tsetse flies. When a tsetse fly inserts the parasite into the human body by means of its sting, the parasite is diffused into the person's blood stream. Some of drug compounds such as anti-trypanosomal can be effective for this type of sleeping sickness. QSAR methods are power tools for prediction of pIC₅₀ drug compounds such as 1, 2-dihydroquinolin-6-ols and their ester derivatives. In the present work, we used stepwise regression (SR) and genetic algorithm (GA) as variable selection methods and ANN as modeling technique to predict of anti-trypanosomal activity of 1, 2-dihydroquinolin-6-ols and their ester derivatives.

Materials and Methods:

The dataset used in this work, contains pIC₅₀ of 48 anti-trypanosomal drug compounds. Sketching and optimization of the molecules were done by Hyperchem software. Totally 1481 descriptors were calculated for each molecule using Dragon software. In addition to decrease in redundancy of the descriptors within data matrix, the descriptors' correlation with each other and with the pIC₅₀ of the molecules was examined. In the next step, was used this correlation to predict the validation and test series. We employed a two-layer network with a sigmoid transfer function as an ANN construction. Then, some parameters such as number of epochs,

momentum and the number of nodes in input and hidden layers were optimized. Descriptors were selected by GA and SR as input of ANN for prediction of pIC50.

Result and Discussion:

The data set including 48 compounds was split randomly into a training set (28 compounds), a test set (10 compounds), and a validation set (10 compounds). In this work, we selected 6 descriptors by using stepwise regression (SR) method. Then, we selected 6 descriptors by genetic algorithm (GA). The plot of predicted pIC50 against experimental of these values (test set) and (validation set) for SR-ANN and GA-ANN are shown in Figure 1. The mean square errors (MSE) of validation and test sets were obtained by SR-ANN and GA-ANN models are 0.0276, 0.0678, 0.125, and 0.185 respectively.

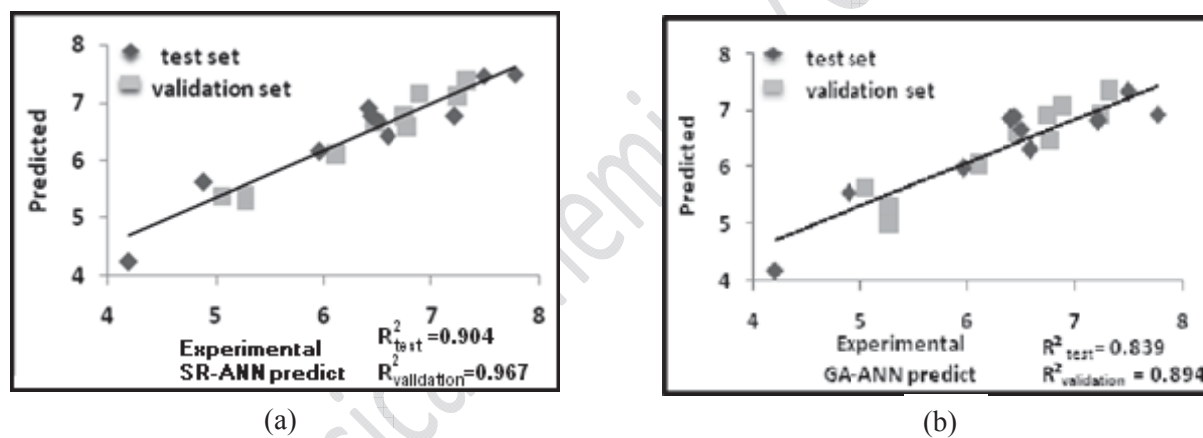


Figure1: Plot of calculated pIC50 against experimental value for a) SR-ANN and b) GA-ANN

Conclusion:

These results illustrate the suitable ability of these models to predict pIC50 of anti-trypansomal activity of some 1, 2-dihydroquinolin-6-ols and their ester derivatives. Two methods, stepwise regression (SR) and genetic algorithm (GA) were used as variable selection techniques. The results obtained reveal the superiority of SR-ANN over the GA-ANN model

References:

- [1] A. Werbovets, M. Kaiser, V. Mahasenan., *J. Med. Chem.* 2010, 53, 966–982.



- [2] N. Goudarzi, M. Goodarzi, M. C. U. Araujo and R. K. H. Galvao., *J. Agric. Food Chem*, 2009, 57, 71553.
- [3] N. Goudarzi and M. Goodarzi., *Mol. Phys*, 2009, 107, 1065.

15th Physical Chemistry Conference



QSAR study of p38 MAP kinase inhibitors activity of some pyridopyridazin-6-one derivatives using SR-ANN and GA-ANN

N. Goudarzi, M. Arab Chamjangali, H. Rameh*

Faculty of chemistry, Shahrood University of Technology, Shahrood, Iran

Email: hasan_chemistry@yahoo.com

Key words: QSAR, SR-ANN, GA-ANN, Pyriopyridazin-6-one, P38 MAP kinase inhibitors

Introduction:

P38 MAP kinases are a class of p38 mitogen- activated protein kinases that are responsive to stress stimuli, such as cytokines, ultraviolet irradiation, heat shock, osmotic shock, and are involved in cell differentiation and apoptosis. The aim of the present article is to propose a model for prediction of pIC₅₀ of p38 MAP kinase inhibitors based on the large space of theoretically calculated molecular descriptors. Also, in this work we used stepwise regression (SR) and genetic algorithm (GA) as variable selection methods.

Materials and Methods:

One important step in QSAR investigation is the numerical representation of the chemical structure (often called molecular descriptor). The built model performance and accuracy of the results are strongly dependent on the way that descriptor is performed. The chemical structure of the 42 studied molecules was drawn with the Hyperchem software. The Dragon software was used to calculate the descriptors in this research and a total of 1481 molecular descriptors were calculated for each molecule. In addition to decrease of redundancy existing in the descriptor data matrix, the descriptors correlation with each other and with the pIC₅₀ of the molecules was examined. In the next step, data set was split into three parts of training, validation and test series. We employed a two-layer network in this study. Also, training functions transfer function, the number epochs, momentum on the number of nodes in hidden layers.

Result and Discussion:

In this work, the QSAR model was generated using a training set of 24 molecules. The both test and validation set of 9 molecules with regularly distributed pIC₅₀ values were used to assess the predictive ability of the QSAR model produced in the artificial neural network. The number of molecular descriptors selected by SR and GA is 8 and 6 descriptors respectively. The plot of predicted pIC₅₀ against experimental of these values (test set) and (validation set) for SR-ANN and GA-ANN are shown in Figure 1. The mean square errors (MSE) of validation and test sets were obtained by SR-ANN and GA-ANN models are 0.0285, 0.0338, 0.0665, and 0.1176, respectively.

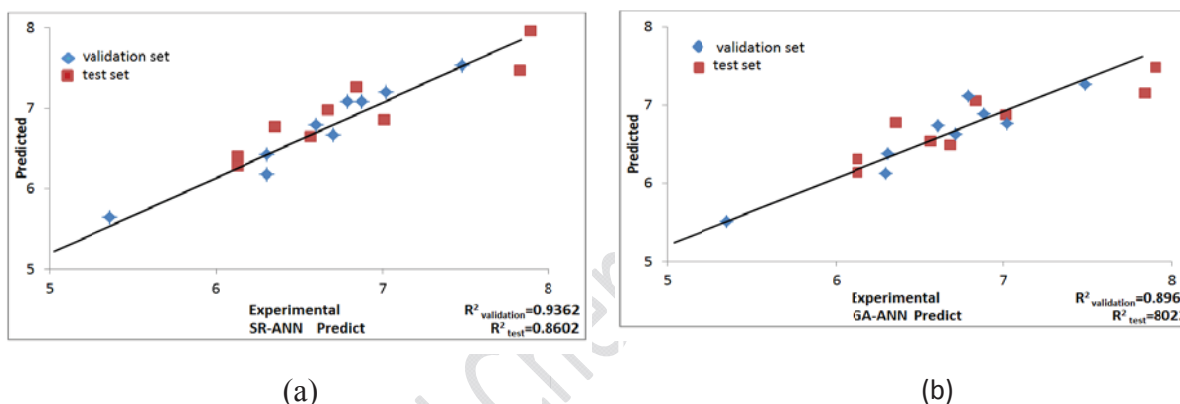


Figure 1: Plot of calculated pIC₅₀ against experimental value for a) SR-ANN and b) GA-ANN

Conclusion:

In the present work we used two methods of SR-ANN and GA-ANN to predict of pIC₅₀ of p38 MAP kinase inhibitors' activity of some pyridopyridazin-6-one derivatives. The obtained results show the superiority of SR-ANN over GA-ANN for prediction of pIC₅₀ of these compounds.

Reference:

- [1] M. Tynebor a, R. Natarajan., *Bioorganic & Medicinal Chemistry Letters*, 2011, 21, 411.
- [2] N. Goudarzi, M. Goodarzi, M. C. U. Araujo and R. K. H. Galvao., *J.Agric. Food Chem*, 2009, 57, 71553.
- [3] N. Goudarzi and M. Goodarzi., *Mol. Phys*, 2009, 107, 1065.



Simulation of N₂-CO mixture using an *ab initio* potential and study of thermodiffusion phenomena

H. Fallah^a, M. R. Toosi^{*b}, M. H. KarimiJahfari^c, R. Cheraghali^a

^a Department of Chemistry, Saveh Branch, Islamic Azad University, Saveh, Iran

^b Department of Chemistry, Qaemshahr Branch, Islamic Azad University, Qaemshahr, Iran

^c Computational Chemistry Laboratory, Nuclear Science and Technology Research Institute, Tehran, Iran.

Keyword: Simulation, Ab Initio Potential, Molecular Dynamic, Transport Property

Introduction:

Introducing the molecular mechanism, for instance through non-equilibrium molecular dynamics simulations, has significantly changed our knowledge of the transport properties of dense fluids [1]. The effect of systematic variation of molecular parameters on the thermal diffusion factor in some mixtures of real gases and alkanes has been investigated by some authors [2]. By utilizing the results of molecular dynamics, an explanation in terms of contributions to the microscopic heat fluxes has been proposed.

Method:

The MD simulation of nitrogen was performed by a NVE ensemble of equimolar mixture of nitrogen and carbon monoxide using the AR potential as an *ab initio* potential [3]:

$$U(R, \omega) = \sum_{\Lambda} V_{\Lambda}(R) \Gamma_{\Lambda}(\omega)$$

The energy flux of NEMD calculation for simulated system was considered as the Irving-Kirkwood formalism:

$$\mathbf{J}_{U,CV} = \frac{1}{V} \sum_{i \in CV} \left\{ \left[\frac{1}{2} [m_i (\mathbf{v}_i - \mathbf{v})^2 + I_i \omega_i^2] + U_i \right] (\mathbf{v}_i - \mathbf{v}) - \frac{1}{2} \sum_{j=1}^N [(\mathbf{v}_i - \mathbf{v}) \mathbf{F}_{ij} + \omega_i \mathbf{T}_{ij}] \mathbf{r}_{ij} \right\}$$



The first and second terms represent the kinetic and potential energy fluxes, respectively and the third term is the intermolecular energy transferred due to the motion of a particle moving in the field of other particles.

Results and discussion:

The results showed that the thermal diffusion factor was very sensitive to the anisotropy of potential in the angular part of potential. Based on obtained data, a phenomenological description of calculated transport property was presented.

References:

- [1] P.-A. Artola, B. Rousseau, Phys. Rev. Lett., 98 (2007), 125901.
- [2] G. Galliero, Fluid Phase Equilib., 224 (2004), 13.
- [3] M. H. Karimi-Jafari, A. Maghari, and A. Farjamnia, J. Phys. Chem. A, 115 (2011) 1143.



A quantum chemical study on the structural and electronic properties of 4-Bromo-2-[(2, 4-dichloro-phenyl imino)-methyl]-phenol

A. Soltani^a, R. Mashkoor^{b*}, M. Moradian^b, A.D. Khalaji^b

^aYoung Researchers Club, Gorgan Branch, Islamic Azad University, Gorgan, Iran

^bDepartment of Chemistry, Qaemshahr Branch, Islamic Azad University, Qaemshahr, Iran

^cDepartment of Chemistry, Faculty of Science, Golestan University, Gorgan, Iran

Email: rezamashkoor@yahoo.com

Key words: BDPMP, DFT, HOMO-LUMO, Quantum molecular descriptors

Introduction:

Schiff bases have been of growing interest these years, they having imine groups (-C=N-) and phenyl rings. because the design of the supramolecular compounds is highly influenced by several factors such as the central atom's coordination geometry, and the structural characteristics of the ligand. [1-2]. In this work, we have investigated the electronic properties of this molecule of the 4-Bromo-2-[(2, 4-dichloro-phenylimino)-methyl]-phenol (BDPMP) compound was also performed at B3LYP/6-31G* level.

Computational details:

The DFT calculation has been performed via Gaussian 03[3] program package at the B3LYP method with standard 6-31G* basis set for geometry optimization of the title. The electrophilicity concept was stated initially in 1999 by Parr et al. μ is defined according to the following equation: $\mu = (E_{\text{HOMO}} + E_{\text{LUMO}})/2$. $\eta = (E_{\text{LUMO}} - E_{\text{HOMO}})/2$. S and ω are defined as the following equations, respectively [4]. $S = 1/2\eta$, $\omega = (\mu^2/2\eta)$

Results and Discussion:

The HOMO represents the ability to donate an electron and LUMO as an electron acceptor that are main orbitals taking part in chemical stability [4]. The HOMO and LUMO energy gap

and quantum molecular descriptors computed by DFT/B3LYP in different basis sets are summarized in Table 1.

Table 1 Quantum molecular descriptors of BDPMP in gas phase.

Property	$-E_{HOMO}/\text{eV}$	$-E_{LUMO}/\text{eV}$	Gap/eV	μ/eV	η/eV	ω/eV	S/eV
BDPMP	6.06	1.95	4.11	-0.4	2.05	0.04	0.24

The electronic transition absorption corresponds to the transition from the ground to the first excited state and is mainly described by an electron excitation from HOMO to LUMO (see in Fig. 1).

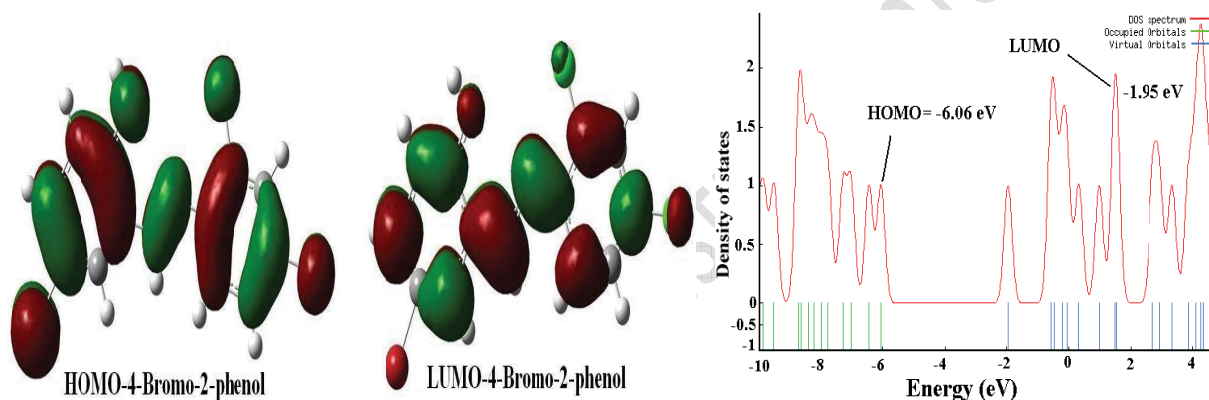


Fig.1. Orbital depiction of HOMO, LUMO, and DOS in BDPMP system.

The HOMO are more localized on the C=N and C-C bonds and also is on oxygen, brom, and chlore orbitals; while HOMO→LUMO transition implies an electron density transfer from benzen ring to C-C and C-N bonds and is slightly on oxygen and chloro orbitals.

Conclusion:

In this present investigation the electronic properties and the HOMO- LUMO energy gap analysis of the BDPMP have been studied using ab initio DFT/B3LYP/6-31G* computation.

Refrence:

- [1] A. D. Khalaji, G. Grivani, S. J. Akerdi, H. Mighani, Struct Chem 21 (2010) 995.
- [2] A. D. Khalaji, M. Weil, G. Grivani, S. J. Akerdi, Monatsh Chem 141 (2010) 539.



- [3] M.J. Frisch et al., Gaussian 03, Revision B03, Gaussian Inc., Pittsburgh, PA, 2003.
- [4] Nabanita Saikia, Ramesh C. Deka, Comput. Theo. Chem. 964 (2011) 257.

15th Physical Chemistry Conference



Determination of Acidic Dissociation Constants of 5'-GMP and 5'-AMP in Water using ab initio Methods

H. Rahmania,^{*} F. Kianib, A. Babanegada, and F. Ashrafia

^aDepartment of Physical chemistry University of Payam Noor, Mazandaran, Iran

^bDepartment of chemistry, Islamic Azad University, Ayatollah Amoli Branch, Amol, Iran.

^{*}E-mail: Mrrahmanirahmani@gmail.com

Abstract:

The basic component of biological nucleic acids is the nucleotide, each of which contains apurine or pyrimidinenucleobase (sometimes termed *nitrogenous base* or simply *base*), a pentosesugar, and a phosphate group. The substructure consisting of a nucleobase plus sugar is termed a nucleoside [1]. Guanosine monophosphate (GMP) and **Adenosine monophosphate** (AMP) are nucleotide that is found in RNA. they are an ester of phosphoric acid with the nucleoside guanosine and adenosine[2]. The acid-base behavior of nucleotides, nucleosides, bases, and polynucleotides is essential to deduce the speciation and the possible conformational changes with pH in solution [3]. Kinds of polarizable continuum models have been applied to calculate free energy differences for cations, neutral compounds and their anions. On the basis of solvation free energies, the pKa values were obtained for the compounds in question by using thermodynamic equations; involving the combined experimental and calculated data [4]. This paper deals with the influence of factors such as the SCRF model applied, choice of a particular thermodynamic equations, atomic radii used to build a cavity in the solvent(water), optimization of geometry in water, inclusion of electron correlation, and the dimension of the basis set on the solvation free energies and on the calculated pKa values. In this study, pKa values of GMP and AMP were determined in aqueous solution by ab initio method and temperature 25°C.

Keywords: Dissociation constant, GMP, AMP, DFT method, solvation free energy



Computational method:

The initial geometries of the molecules by the semi empirical PM3 method are included in program CS Chem3D version 7.0. These geometries were optimized with the Gaussian 98 program packages using the B3LYP/6-31+G(d) methods and the default convergence criteria. To analyze the solvent effects on the specimen involved in the selected ionization reaction, the polarized continuum model (PCM) of Tomasi et al. was used [4].

Results and discussion:

The acid-base behavior of a nucleotide is its most important physical characteristic. It determines its charge, its tautomeric structure, and thus its ability to donate and accept hydrogen bonds, which is the key feature of the base:base recognition[5]. The bases are uncharged in the physiological range pH. It should be noted that purine or purine derivatives undergo self-association due to stacking of their nucleic base-ring systems [6]. The release of the first proton from H₃GMP⁺ and H₃AMP⁺ occurs at very low PH. A fourth proton is released from H⁺ (N-1) in GMP in the alkaline PH range and from the ribose group in AMP (PH>13).

Conclusion:

In order to explain the acidic dissociation constants obtained, we investigated the molecular conformations and solute-solvent interactions of the cation, anion and neutral species of GMP and AMP using ab initio and density functional theory (DFT) methods. According to the Gaussian calculations based on the quantum mechanics principals, the values of total energy and dissociation constants of GMP and AMP are investigated and the results are listed in Table 1.



Table 1. Values of pKa for the protonation of GMP and AMP obtained using the Tomasi method at the B3LYP/6-31+G(d) level of theory, at 298.15 K.*

Selected equations	GMP		AMP	
	pKa (calculated)	pKa(experimental) [8]	pKa(calculated)	pKa(experimental) [8]
$\text{H3NMP}^+ + \text{H}_2\text{O} \rightleftharpoons \text{H2NMP} + \text{H}_3\text{O}^+$	0.7	0.3 (I=0.1, NaClO ₄)	0.4	0.4 (I=0.1, NaClO ₄)
$\text{H2NMP} + \text{H}_2\text{O} \rightleftharpoons \text{HNMP}^- + \text{H}_3\text{O}^+$	2.9	2.4 (I=0.1, NaClO ₄)	3.6	3.8 (I=0.1, NaClO ₄)
$\text{HNMP}^- + \text{H}_2\text{O} \rightleftharpoons \text{NMPH-12}^- + \text{H}_3\text{O}^+$	6.2	6.2 (I=0.1, NaClO ₄)	6.1	6.2 (I=0.1, NaClO ₄)
$\text{NMPH-12}^- + \text{H}_2\text{O} \rightleftharpoons \text{NMPH-23}^- + \text{H}_3\text{O}^+$	9.6	9.4 (I=0.1, NaClO ₄)		

*N represents nucleosides of guanosine and adenosine.

References:

- [1] H. Sigel et al.; J. Am. Chem. Soc.; 116 , 2958–2971, 1994.
- [2] Ahluwalia GS et al. Metabolism and action of amino acid analog anti-cancer agents, in Pharmac. Ther. (1990) 46: 243-271
- [3] D..E..Metzler; "Biochemistry: The Chemical Reaction Living Cells"; Academic Press; 2001.
- [4] F. Kiani et al.; J. Chem. Eng. Data; 55, 2732–2740, 2010.
- [5] M. Blackburn et al.; "Nucleic Acids in Chemistry and Biology"; RSC; 2006
- [6] Sigel H. Biol. Trace Elem. Res. 1989; 21:49.
- [7] H. Sigel H et al.; J. Am. Chem. Soc.; 116, 2958, 1994.
- [8] F. Gharib et al.; Can. J. Chem. 84: 1534–1540, 2006.



Vibrational Frequencies of halo-derivatives of aniline: A DFT Study

M. Rezaei Sameti, S. Yaghoobi

Department of Physical Chemistry, Faculty of Sciences, Malayer University, Malayer, Iran

E-mail address: mrsameti@malayeru.ac.ir

Key words: DFT, aniline derivatives, IR, Vibrational frequencies.

Introduction:

Aniline and its derivatives have been subjected to many different types of scientific studies up to now [1–2]. They have been widely used in a variety of industrial and commercial purposes, including dyestuff, pesticide and pharmaceuticals manufacturing. Some of the *para*-substituted derivatives of anilines are local anesthetics and the amino group in these molecules plays an important role in the interaction with the receptor. The inclusion of a substituent group in aniline leads to the variation of charge distribution in the molecule and consequently this greatly affects the structural, electronic and vibration parameters. Molecular geometry changes due to enhanced interaction between the aromatic ring and the amino group [3]. This paper is a continuation of our earlier work related to the study of ab initio for predicting the experimental parameters [5–6]. In this work a theoretical study of vibrational frequencies for fluoro aniline, chloro aniline, bromo aniline derivatives at substituted of *orto*, *meta*, *para*, {(2,3), (2,4), (2,5), (2,6), (3,4), (3,5)} di halo aniline and {(2,3,4), (2,3,5), (2,4,5)} tri halo aniline, {(2,3,4,5), (2,3,4,6), (2,3,5,6)} tetra halo aniline and {(2,3,4,5,6)} penta halo aniline have been done at B3LYP employing the 6-31G(d), 6-31G(d, p), 6-31++G(d, p), and 6-311++G(d,p) basis sets. The optimized structural parameters were used for calculation of vibrational frequencies.

Results and discussion:

The geometrical parameters (bond length and angles) of all halo aniline derivatives, such as fluoro aniline, chloro aniline and bromo aniline at substituted of {*orto*, *meta*, *para*} mono

halo aniline , $\{(2,3), (2,4), (2,5), (2,6), (3,4), (3, 5)\}$ di halo aniline , $\{(2,3,4), (2,3,5), (2,4,5)\}$ tri halo aniline , $\{(2,3,4,5), (2,3, 4,6), (2,3,5,6)\}$ tetra halo aniline and $\{(2,3,4,5,6)\}$ penta halo aniline are optimized and the geometry parameters are given in supplementary data. The comparison of the frequencies calculated at the DFT using B3LYP 6-311++G (d,p) level and scaled data with experimental values for all fluoro aniline derivatives are given in Table 1. The calculated and experimental IR spectra and optimized structures of the title compound are shown in the Figure 1. As it can be seen in this figure, there is a good correlation between the experimental and calculated frequencies for these components. The trends of vibrational frequencies are depended of the substitute of halogen, the number of halogen and electronegativity of halogen in aniline ring.

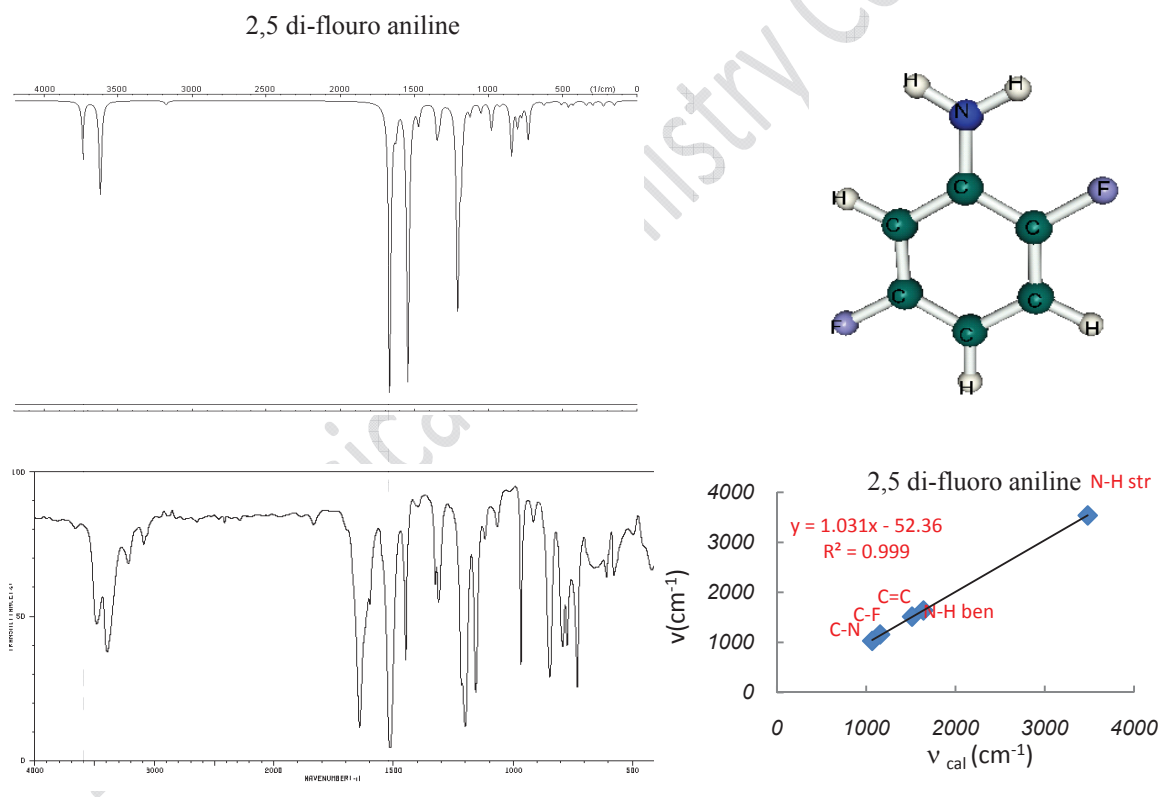


Fig. 1. A : Theoretical IR spectra, optimized structure by DFT/ ((B3LYP//6-311++G(d,p)) and B: experimental IR spectra of para fluoro aniline and 2,5 di- fluoro aniline derivatives.



References:

- [1] Kurt, M. ; Yurdakul , M. ; Yurdakul, S. J. Mol. Struct. (Theochem.) 2004,711, 25.
- [2] Kanungo, M.; Kumar, A. ; Contractor, A.Q. J. Electroanal. Chem. 2002, 528, 46.
- [3] Sundaraganesan, N.; Priya, M. ; Meganathan, C. ; Dominic Joshua, B. ; Cornard, J.P. Spectrochim. Acta A 2008, 70, 50.
- [4] Rezaei-Sameti, M. J. Mol. Struct. (Theochem.) 2008, 867, 122.
- [5] Mooney, E.F. Spectrochim. Acta 1963,19, 877.



DFT study on the mechanism of the Formation of Monodentate Acetate Complex of Palladium(II)

A. Morsali^a, S. A. Beyramabadi^a and F. Rezazadeh^{* a}

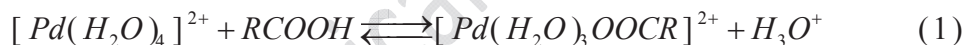
^a Department of Chemistry, Mashhad Branch, Islamic Azad University, Mashhad, Iran

(Email: faeze.rezazade@yahoo.com)

Keywords: Monodentate Acetate Complex, Mechanism, Palladium, Density functional theory

Introduction:

There are few investigations of reactions between square planar Pd(II) centers and carboxylic acids/carboxylates in aqueous solution. Shi and Elding [1] described studies of equilibria and kinetics for complex formation between $[Pd(H_2O)_4]^{2+}$ and acetic, propionic, and glycolic acids, with the aim to elucidate the reaction mechanism. Kinetics and equilibria for reversible formation of 1:1 monodentate complexes between $[Pd(H_2O)_4]^{2+}$ and acetic, propionic, and glycolic acid (RCOOH) according to the equation (1) were studied as a function of temperature and pressure in an aqueous medium [1]:



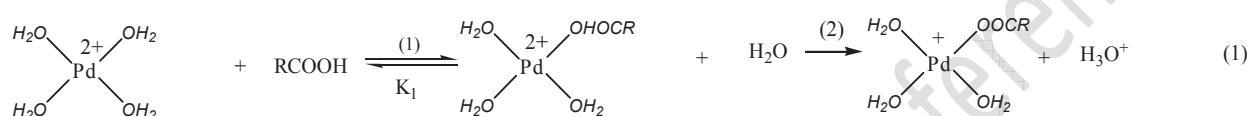
In this work, the mechanism of the Formation of Monodentate Acetate Complex of Palladium(II) has been studied using density functional methods..

Computational details:

All of the present calculations have been performed with the B3LYP [2] hybrid density functional level using the G09 package. The 6-311+G(d,p) basis set was employed except for Pd atom, in which the LANL2DZ [3] basis set was used with including effective core potential functions. The gas phase optimized geometries used to apply the solvent effects, where the valuable PCM [4] model was employed.

Results and discussion:

The following mechanism (Eq.(1)) for the Formation of Monodentate Acetate Complex of Palladium(II) was proposed which is compatible with experimental evidence. In this mechanism, a fast equilibrium step (with equilibrium constant K_1) will result in the formation of complex $[Pd(H_2O)_3OHOCR]^{2+}$ which will be converted into $[Pd(H_2O)_3OOCR]^+$ and $[H_3O]^+$ during a slow process.



The optimized structure of transition state obtained from step2 has been shown in Fig. 1. By taking Solvent effects into consideration, $E_a = 15.8 kcal/mol$. This shows that the model presented in this research is a suitable model for the Formation of Monodentate Acetate Complex of Palladium(II).

Conclusion:

Using quantum mechanical method, mechanism of the Formation of Monodentate Acetate Complex of Palladium(II) was investigated and ultimately a model was presented in which $[Pd(H_2O)_3OHOCR]^{2+}$ form is produced in the rate determining step and in continuation is converted into products.

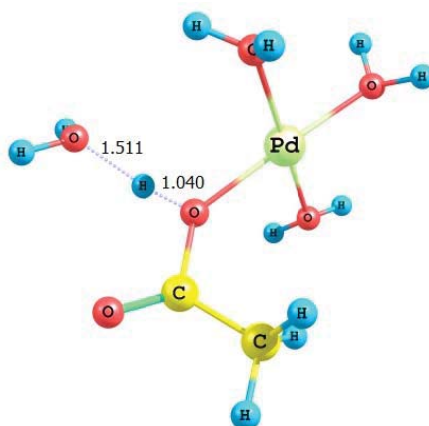


Fig 1. Optimized structure of the TS (step 2)



References:

- [1] T. Shi, L. I. Lars, *Inorg. Chem.* 35 (1996) 735.
- [2] A.D. Becke, *Phys. Rev. A*, 38 (1988) 3098.
- [3] P.J. Hay, W.R. Wadt, *J. Chem. Phys.* 82 (1985) 299.
- [4] S. Miertus, E. Scrocco, J. Tomasi, *Chem. Phys.* 55 (1981) 117.

15th Physical Chemistry Conference



Use of ab initio methods to predict excess molar enthalpies by using thermodynamics models for binary mixture of acetonitrile + water

M. Mehrara*, H. Zarei

Faculty of Chemistry, Department of Physical Chemistry Bu-Ali Sina University

Email: mehrara.mahshid@gmail.com

Key words: Excess molar enthalpies, gaussian03, NRTL and Wilson model, acetonitrile and water.

Introduction:

An important challenge in applied thermodynamic is the prediction of mixture properties without the use of any experimental data [1]. In this study ab initio quantum mechanic methods are used to compute intermolecular interaction energies by determining the minimum-energy in all configurations between pairs of molecules in the cluster. The computed interaction energy were used to predict excess molar enthalpies of binary mixture of acetonitrile and water by using NRTL and Wilson models.

Ab initio calculations of intermolecular interaction energies:

All ab initio calculations in this work were carried out with the Gaussian03 software package [2].

Ab initio calculations of inter molecular interaction energies were performed in a cluster composed of ten molecules, five of each species. All structures were full optimized at HF/6-31G and HF/6-311G level of theory. Then intermolecular interaction energy parameters for two activity coefficient NRTL [3] and Wilson [4] were calculated to predict excess molar enthalpies. The results of these calculations are compared with experimental data [5]. They are represented in figures 1 and 2.

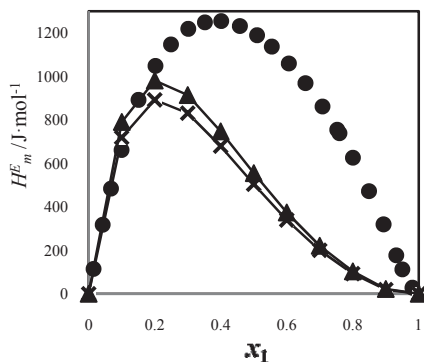


Figure 1. Excess molar enthalpies for acetonitrile (2) + water (1) at NRTL model [(×) HF/6-31G, (▲) HF/6-311G]

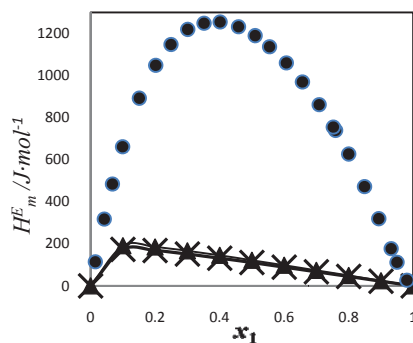


Figure 2. Excess molar enthalpies for acetonitrile (2) + water (1) at WILSON model [(×) HF/6-31G, (▲) HF/6-311G]

Result and discussion:

The intermolecular interaction energy of acetonitrile, water and their mixture were used to compute intermolecular interaction energy parameters of NRTL and Wilson models. The NRTL and Wilson models were used to predict excess molar enthalpies. Figures 1 and 2 show the predicted excess molar enthalpies and experimental data. The predicted values with the NRTL model are in better agreement with the experimental data than the Wilson values.

References:

- [1] Amadeu K. Sum, Stanley I. Sandler. Use of *ab initio* methods to make phase equilibria predictions using activity coefficient models, *Fluid Phase Equilibria* 158–160 (1999) 375–380
- [2] Gaussian 03, Revision B.04, M.J. Frisch, G.W. Trucks, H.B. Schlegel, G.E. Scuseria, M.A. Robb, J.R. Cheeseman, J.A. Montgomery, Jr., T. Vreven, K.N. Kudin, J.C. Burant, J.M. Millam, S.S. Iyengar, J. Tomasi, V. Barone, B. Mennucci, M. Cossi, G. Scalmani, N. Rega, G.A. Petersson, H. Nakatsuji, M. Hada, M. Ehara, K. Toyota, R. Fukuda, J. Hasegawa, M. Ishida, T. Nakajima, Y. Honda, O. Kitao, H. Nakai, M. Klene, X. Li, J.E. Knox, H.P. Hratchian, J.B. Cross, C. Adamo, J. Jaramillo, R. Gomperts, R.E. Stratmann, O. Yazyev, A.J. Austin, R. Cammi, C. Pomelli, J.W. Ochterski, P.Y. Ayala, K.



- Morokuma, G.A. Voth, P. Salvador, J.J. Dannenberg, V.G. Zakrzewski, S. Dapprich, A.D. Daniels, M.C. Strain, O. Farkas, D.K. Mal-ick, A.D. Rabuck, K. Raghavachari, J.B. Foresman, J.V. Ortiz, Q. Cui, A.G. Baboul, S. Clifford, J. Cioslowski, B.B. Stefanov, G. Liu, A. Liashenko, P. Piskorz, I. Komaromi, R.L. Martin, D.J. Fox, T. Keith, M.A. Al-Laham, C.Y. Peng, A. Nanayakkara, M. Challacombe, P.M.W. Gill, B. Johnson, W. Chen, M.W. Wong, C. Gonzalez, J.A. Pople, Gaussian, Inc., Pittsburgh, PA, 2003
- [3] H. Renon, J. M. Prauznitz. local compositions in thermodynamic excess functions for liquid mixtures, *A. I.Ch. J.* 14 (1968) 135-144.
- [4] G.M. Wilson, Vapor-Liquid Equilibrium. XI. A New Expression for the Excess Free Energy of Mixing, *J. Am. Chem. Soc.* 86 (1964) 127-130
- [5] A. Wakisaka, H. Abdoul-Carime, Y. Yamamoto and Y. Kiyozumi. "Water-methanol and water-acetonitrile from the viewpoint of clustering structure". *J. Chem. Soc, Faraday T rans.* 94(3) (1998) 369-374



Binding energy calculation and complex formation constant prediction of some aza-crown ethers with Cd^{+2}

R. Behjatmanesh-Ardakani^a, M. Taghdiri^a and F. Pourroustaei-Ardakani^{a*}

^aDepartment of Chemistry, Payame Noor University, P.O. Box 19395-3697 Tehran, Iran

* Email: porosta@yahoo.com

Keywords: Complex formation constant, Ab initio calculation, DFT, Binding energy, 1-aza-18-crown-6.

Introduction:

In recent years, density functional theory (DFT) calculations have been used extensively for estimating molecular properties. In this paper, B3LYP level of theory is used to perform theoretical calculation on the structure, binding energies and complex formation constants for four ligands in CH_3CN at 298.15 K (Figure 1).

Calculation methods:

GaussView 5.0 program [1] has been used to build Gjf inputs for free and complexed Ligands. Semiempirical pre-optimized structures were used as initial inputs for further optimization at B3LYP/LANL2DZ level of theory. During the calculations, number of imaginary frequencies (NIMAG) were checked to be zero to ensure the structures are stationary points in potential energy surface. In addition to gas phase properties, solvation free energy of studied species have been calculated by polarizable continuum model (PCM). All calculations were carried out with Gaussian 09 set of programs [2].

Ligand1: $\text{R}_1=\text{NO}_2$, $\text{R}_2=\text{OCH}_3$, $\text{R}_3=\text{ACE}$

Ligand2: $\text{R}_1=\text{NO}_2$, $\text{R}_2=\text{R}_3=\text{ACE}$

Ligand3: $\text{R}_1=\text{N}(\text{CH}_3)_2$, $\text{R}_2=\text{OCH}_3$, $\text{R}_3=\text{ACE}$

Ligand4: $\text{R}_1=\text{N}(\text{CH}_3)_2$, $\text{R}_2=\text{R}_3=\text{ACE}$

ACE=1-aza-18-crown-6

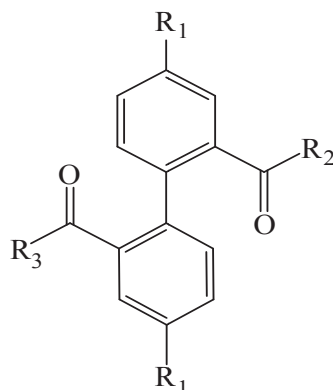


Figure1: The structures of four Ligands studied in this work

Result and discussion:

In the gas phase, a complex formation reaction between a Ligand and Cd^{+2} can be considered as following reaction: $\text{Ligand} + \text{Cd}^{+2} \longrightarrow \text{Ligand-Cd}^{+2}$ (1)

where, binding energy of complexation between the Ligand and Cd^{+2} in the gas phase is defined by: $\Delta E (\text{Ligand-Cd}^{+2}) = E (\text{Ligand-Cd}^{+2}) - E (\text{Cd}^{+2}) - E (\text{Ligand})$ (2)

The definition of $\log K_f$ is:

$$\log K_f = \frac{\Delta G^\circ_{\text{soln}}}{2.303RT} \quad (3)$$

Where $\Delta G^\circ_{\text{soln}}$, $\Delta G^\circ_{\text{gas}}$ and $\Delta \Delta G^\circ_{\text{solv}}$ is:

$$\Delta G^\circ_{\text{soln}} = \Delta G^\circ_{\text{gas}} + \Delta \Delta G^\circ_{\text{solv}} \quad (4)$$

$$\Delta G^\circ_{\text{gas}} = G^\circ_{\text{gas}}(\text{Ligand-Cd}^{+2}) - G^\circ_{\text{gas}}(\text{Ligand}) - G^\circ_{\text{gas}}(\text{Cd}^{+2}) \quad (5)$$

$$\Delta \Delta G^\circ_{\text{solv}} = \Delta G^\circ_{\text{solv}}(\text{Ligand-Cd}^{+2}) - \Delta G^\circ_{\text{solv}}(\text{Ligand}) - \Delta G^\circ_{\text{solv}}(\text{Cd}^{+2}) \quad (6)$$

Standard states in above equations are 1 atm and 298.15 K for the gas phase and 1 M and 298 K for the solution phase. Converting $\Delta G^\circ_{\text{gas}}$ reference state (24.46 L at 298.15 K) from 1 atm to 1 M requires introduction of $RT \ln (24.46)$ in to above equation:

$$\Delta G^\circ_{\text{gas}} (1\text{M}) = \Delta G^\circ_{\text{gas}} (1\text{atm}) + RT \ln(24.46) \quad (7)$$

By this correction we have:

$$\log K_f = \frac{-(\Delta G^\circ_{\text{gas}} + \Delta \Delta G^\circ_{\text{solv}} + 1.89)}{1.3644} \quad (8)$$



Table 1 contains zero point energy and BSSE corrected of binding energy, $\Delta G^{\circ}_{\text{gas}}$, $\Delta \Delta G^{\circ}_{\text{solv}}$ and calculated $\log K_f$.

Table 1

Name of species	$\Delta E^{\text{ZPE+BSSE}}_{\text{binding}}$ (kcal/mol)	$\Delta G^{\circ}_{\text{gas}}$ (kcal/mol)	$\Delta \Delta G^{\circ}_{\text{solv}}$ (kcal/mol)	$\log K_f$ (calc)	$\log K_f$ (exp) ^a
Ligand 1-Cd ⁺²	-279.99	-274.84	263.70	6.78	2.09 ± 0.02
Ligand 2-Cd ⁺²	-299.22	-291.94	288.74	0.96	2.473 ± 0.005
Ligand 3-Cd ⁺²	-298.97	-292.13	286.09	3.04	2.27 ± 0.01
Ligand 4-Cd ⁺²	-330.68	-322.70	316.74	2.95	1.98 ± 0.01

^aData taken from Ref.[3]

Conclusion:

Data show strong interaction between Ligands and ion. PCM estimated complex formation constant are nearly in good line with experimental data.

References:

- [1] R. Dennington et al.; GaussView, Version 5; *Semichem Inc*, Shawnee Mission KS; 2009.
- [2] M.J. Frisch et al.; Gaussian 09, Revision A.01. Inc., Wallingford CT, 2009.
- [3] A.M. Costero et al.; "Conformationally regulated fluorescent sensors. Study of the selectivity in Zn⁺² versus Cd⁺² sensing"; *Tetrahedron*; 60, 6327-6334, 2004.



Electron density analysis of noncovalent P...N interactions

R. Dashtpeyma K. Eskandari*

School of Chemistry, Damghan University, Damghan, Iran

(Email: r_dashtpeyma_ch@yahoo.com, eskandari@du.ac.ir)

Keywords: Noncovalent Interaction, Atomic Multipole Moment, QTAIM

Introduction:

Noncovalent interactions play important roles in different areas of chemistry and biochemistry. Generally, this type of interactions encompasses hydrogen bonds, halogen bonds, van der Waals interaction, steric repulsion, and London dispersion. Recently, Scheiner and co-workers found a new class of interactions between the N atom of HSN and the P atom of phosphine [1]. They also found that when PH_3 is paired with NH_3 , the P and N atoms face one another directly and form a $P \cdots N$ interaction [2]. According to their calculations, although these interactions are generally weak, their binding energy can be enhanced if the H atom of the phosphine is replaced by Cl or F atoms [3]. In the current work, quantum theory of atoms in molecules (QTAIM) is used for some $P \cdots N$ interactions to gain a deeper understanding of the nature of these bonds. Our focus will be on the electrostatic aspect of these bonds.

Methods:

Molecular geometries and their electronic wave functions were optimized at the MP2/aug-cc-pVDZ level using Gaussian 09 program. We used Quantum Theory of Atom in Molecules (QTAIM) to calculate electric atomic multipole moments. Integration over atomic basins was carried out using standard mode of AIMAll program.

Result and Discussion:

As stated by Scheiner, the $P \cdots N$ interactions are mainly electrostatic in nature. So we decided to evaluate the electrostatic potential around P atom in PH_3 , PH_2F , PHF_2 and PF_3 monomers

to compare their ability in forming $P \cdots N$ bonds. Indeed, The multipole expansion (ME) of electrostatic potential at a given point, N , in a vicinity of a molecule is given by:

$$V_N = \sum_i \frac{q_i}{r_{i,N}} + \sum_i \frac{(\mathbf{m}_i \cdot \mathbf{r}_{i,N})}{r_{i,N}^2} + \sum_i \frac{(\mathbf{r}_{i,N} \cdot \mathbf{Q}_i \cdot \mathbf{r}_{i,N})}{2r_{i,N}^3}$$

In which, q_i , \mathbf{m}_i and \mathbf{Q}_i are, respectively, the atomic monopole moment, atomic dipole moment vector and the atomic traceless quadrupole moment of i -th atom. $r_{i,N}$ and $\mathbf{r}_{i,N}$ are the distance between atom i and the point N and the unitary vector pointing from atom i to point N , respectively. Since this equation deals with vectors, the chosen orientation of the molecules is important. So, in PH_3 and PF_3 molecules, their C_3 symmetry axis has been chosen as Cartesian z axis, while in PH_2F and PHF_2 molecules, one of the $P - F$ bonds has been oriented along the y axis. The values of components of dipole and quadrupole moments of the P atom have been listed in Table 1.

Table 1. Dipole and quadrupole moment components (in a.u.) of P atom.

	m_x	m_y	m_z	Q_{xx}	Q_{yy}	Q_{zz}
PH_3	0.00	0.00	-1.14	1.86	1.86	-3.71
PH_2F	-1.02	0.34	0.00	-2.60	1.39	1.20
PHF_2	0.76	0.00	-0.59	-1.22	2.72	-1.50
PF_3	0.00	0.00	0.00	2.12	2.12	-4.24

Conclusion:

Clearly, the $P \cdots N$ interactions can be regarded as Lewis acid-base interactions; the P and N atoms are acceptor and donor, respectively. So, a positive (or at least, less negative) potential around the P atom is needed for formation of these interactions. The values of components of atomic dipole and quadrupole moments in Table 1 reveal that for all of these molecules, the most positive value for V_N should be along the y axis; in which both m_y and Q_{yy} are positive. In other words, the $P \cdots N$ interaction is formed along y axis, that is perpendicular to the C_3 symmetry axis in PH_3 and PF_3 or along $P - F$ bonds in PH_2F and PHF_2 molecules. This is in agreement with calculated geometries of Scheiner's papers.



References:

- [1] M. Solimannejad, M. Gharabaghi, S. Scheiner, J. Chem. Phys. 134 (2011) 024312.
- [2] S. Scheiner, J. Chem. Phys. 134 (2011) 094315.
- [3] S. Scheiner, Chemical Physics, 387(2011) 79.

15th Physical Chemistry Conference



A comparison of some properties of C=S and C=Se bond

V. Hadigheh Rezvan^{a*}, A. Kianroodi^b

Department of chemistry, Ardabil Branch, Islamic Azad University, Ardabil, Iran

Email: a_k_ch@yahoo.com

Key words: Thiocarbonyl group, selenocarbonyl group, charge distribution, force constants.

Introduction:

There are significant and interesting differences between compounds with thiocarbonyl and selenocarbonyl groups. The C=Se bond length ($\sim 1.8 \text{ \AA}$) is considerably longer than C=S ($\sim 1.6 \text{ \AA}$) [1]. As a result, one would expect the bond strengths to differ significantly. The π -bond also might be expected to be strongly affected in view of the orbital size mismatch between second and third row atoms. On the other hand, selenoamides are known to have larger rotational barriers than thioamides, where the barrier arises from the interaction nitrogen with the adjacent C=S or C=Se group [2].

Computational methods:

The geometry optimizations for the ground state and, transition states, were carried out using Gaussian 03 program with B3LYP level of theory in combination of 6-311G (d, p) Basis set. Frequency calculation were performed for all stationary points on the potential energy surfaces to verify whether they are minima or transition states there are imaginary frequencies but for global and local points there are real frequencies. We have studied frequencies of all stationary points.

Result and discussion:

Bond strength:

One of the most important quantities that characterize a bond is the strength. This can be expressed either as the bond dissociation energy or the force constant for stretching the bond.

The first refers to complete cleavage, and the latter to the effects of small deviations from the equilibrium geometry.

Force constants:

Vibrational force constants are usually obtained via a normal coordinate analysis or a calculation of the vibrational frequencies. This presents problems because there is always coupling between the C=S (or C=Se) vibration with other vibrational modes. Fitting the data to a third order polynomial gave the force constant and also the cubic term. The harmonic terms along with the corresponding bond lengths are given in Table 1.

Charge distributions:

There is considerable no difference in electronegativity between selenium and sulfur [3], and therefore the charge distribution should be no different between selenocarbonyl and thiocarbonyl compound. The charges thus calculated are given in Table 2.

Table1

Compound	K ₂	r C=S,Se (Å)
NH ₂ CSCH ₃	2.66	1.662
N(CH ₃) ₂ CSCH ₃	4.46	1.657
N(CH ₂ CH ₃) ₂ CSCH ₃	2.44	1.677
N(CN) ₂ CSCH ₃	6.87	1.624
NH ₂ CSeCH ₃	2.30	1.813
N(CH ₃) ₂ CSeCH ₃	4.12	1.829
N(CH ₂ CH ₃) ₂ CSeCH ₃	2.56	1.833
N(CN) ₂ CSeCH ₃	7.97	1.733

Table2

Compound	S	Se	C=S	C=Se
NH ₂ CSCH ₃	-0.202	—	-0.060	—
N(CH ₃) ₂ CSCH ₃	-0.241	—	-0.024	—
N(CH ₂ CH ₃) ₂ CSCH ₃	-0.242	—	-0.018	—
N(CN) ₂ CSCH ₃	0.0302	—	-0.065	—
NH ₂ CSeCH ₃	—	-0.275	—	0.045
N(CH ₃) ₂ CSeCH ₃	—	-0.306	—	0.071
N(CH ₂ CH ₃) ₂ CSeCH ₃	—	-0.305	—	0.077
N(CN) ₂ CSeCH ₃	—	-0.205	—	0.021

Conclusion:

Relatively high level computational methods are able to satisfactorily reproduce the available experimental data for selenocarbonyl and thiocarbonyl derivatives. They also allow the estimation of data that are currently not available. Other quantities such as the charge distribution may also be derived from the results of these calculations and are useful in explaining the differences between these compounds.



Reference:

- [1] Rindorf, G.; Carlsen, L. *Acta Cryst.* 1979. B35, 1179.
- [2] Wiberg, K. B.; Rablen, P. R. *J. Am. Chem. Soc.* 1995, 117, 2201.
- [3] Allred, A. L.; Rochow, E. G. *J. Inorg. Nucl. Chem.* 1958, 5, 264

15th Physical Chemistry Conference

Structural and energetic aspects of adsorbed CH₄ on different single-walled carbon nanotubes, A DFT study

Aidin Bahrami^a, Sirous Yourdkhani^a and Minoo Sadri^{*b},

^a Department of Chemistry, Tarbiat Modares University, Tehran, Iran

^b Department of Biology, Malek ashtar University of Technology, Tehran, Iran

E-mail: mnsadri@yahoo.com

Key words: Single-walled carbon nanotube, methane, density functional theory

Introduction:

The discovery of carbon nanotubes has opened an extraordinary field in the front of scientists to use them as a powerful tools in so many applications. One of the most attractive applications is the gas adsorption. However, the details of the adsorption mechanism has not been well understood [1]. In this paper we have studied the energetic aspects of physisorption of CH₄ molecule with the various molecular orientations on external surface of (4,0), (5,0), (5,5) and (6,6) single-walled carbon nanotubes (SWNTs) using the DFT methods.

Methods of calculations:

Full geometry optimizations were performed using Gaussian 09 suite of programs and M06 hybrid density functional, which provides the better description of dispersion interactions and of the physical adsorption, and 6-31+G* basis set. To find the adsorption behavior, the three different molecular orientations of CH₄ on (4,0) SWCNT (“Line”, “Point” and “Face”) have been considered (Figure 1).[2]

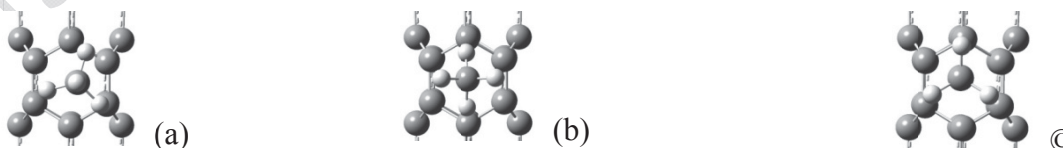


Fig. 1. CH₄ adsorption with three different molecular directions (a:Face, b:Line, c:Point) on (4,0)SWCNT.

Result and discussion:

According to our results (Table 1), all of the orientations of CH₄ on (4,0) SWCNT reoriented to Face state after optimization. Whereas, face state is more stable than the other directions, we have used the Face direction of CH₄ to investigate the adsorption behavior on (5,0), (5,5) and (6,6) SWCNTs. The results for zigzag and armchair tubes with different diameters are shown in Table 2. The binding energies clearly show that the adsorption depends on tube diameter. Also, in the case of armchair CNTs, the stability of tube-CH₄ decreases as their diameter increases. In addition to, equilibrium Distances and dipole moments are significantly increased that can be understood by considering the polarization of the conducting electrons due to physisorption. In the case of zigzag tubes, the results indicate that as the diameter increases, the binding energy of CH₄ molecule increases.

Table 1. Calculated Adsorption Energies E_b , Equilibrium Distances R and Dipole Momenta of the CH₄ adsorbed on (4,0)SWCNT.

Parameter	$E_b(\text{meV})$	$R (\text{\AA})$	Dipole moment(D)
Face	-78.9	3.18	0.21
Line	-76.2	3.28	0.32
Point	-74.4	3.28	0.21

Table 2. Calculated structural parameters of the adsorbed CH₄ on (4,0), (5,0), (5,5) and (6,6)SWCNT.

Parameter	$E_b(\text{meV})$	$R (\text{\AA})$	Dipole moment (D)
CH ₄ + (4,0)	-78.9	3.18	0.21
CH ₄ + (5,0)	-182.3	3.15	0.19
CH ₄ + (4,4)	-123.7	3.28	0.15
CH ₄ + (5,5)	-101.4	3.44	0.17



Conclusion:

The results have been proved that CH₄ molecule is weakly bound to the nanotubes. Therefore, it seems that the tube-CH₄ interactions are physical adsorption. Also, the orientations of CH₄ and diameter of nanotubes play a significant role in this kind of adsorption.

References:

- [1] R. Saio, M. Fujita, G. Dresselhaus: Appl. Phys. Lett. 60 (1992) 2205
- [2] Yoshio AKAI and Susumu SAITO: Jpn. J. Appl. Phys. 42 (2003) 640-644

Theoretical Study of Cooperative effects in α -glycylglycine clusters

Aidin Bahrami ^a, Mehdi D Esrafil ^b, Sirous Yourdkhani ^a and Nasser L Hadipour ^{* a},

^a Department of Chemistry, Tarbiat Modares University, Tehran, Iran

^b Department of Chemistry, University of Maragheh, Maragheh, Iran

E-mail: hadipour@modares.ac.ir

Key words: Hydrogen-bonding, cooperativity, DFT, Glycylglycine, NQR, NBO.

Introduction:

An important concept in the theory of hydrogen bonding matters is hydrogen bond cooperativity that can be considered computationally using ab initio and DFT methods. The most studies have been focused on small molecules as models. However, little information is available on the real biologically systems [1-2]. α -glycylglycine (α -glygly) as a important dipeptide, which plays a considerable role in the protein structures, can prove the existence of the cooperative effects in the NC=O...H-N interaction. This paper reports some structural and spectroscopic parameters about H-bonding cooperativity effect in linear crystalline α -glygly clusters such as H-bonds lengths, Nuclear Quadruple Resonance (NQR) and Natural Bond Orbitals (NBO).

Methods of calculations:

Molecular orbital calculations were performed using DFT methods by Gaussian 03 program. The geometry Optimization, (Fig. 1) NBO and NQR calculations were performed using the B3LYP method with 6-31+G*, 6-311++G** basis sets.

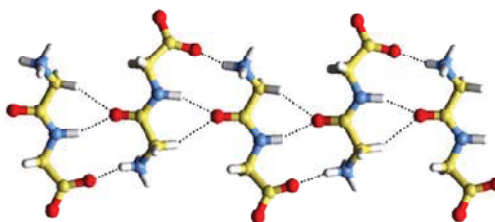


Fig. 1. Hydrogen-bonding network of (α -glygly)₅ cluster optimized at B3LYP/6-31+G* level.

Result and discussion:

According to our results, all the N–H bonds acting as H-donors and the C=O bonds acting as H-acceptors are almost elongated ($r_{C=O} = 0.939 r_{N-H} + 0.282$ ($R^2 = 0.964$)) relative to the isolated α -glygly molecule (1.019 Å). On the other hand, a regular decrease in r_{C-N} is generally observed from dimer to pentamer. The calculated delocalization energies of $n_O \rightarrow \sigma_{NH}^*$ interaction from dimer (28.9 kcal/mol) to pentamer (49.6 kcal/mol) are increased that they are in accordance with other evidences for intermolecular hydrogen bond strength increase. It is worth mentioning that the $n_O \rightarrow \sigma_{NH}^*$ electron density transferring, is often used to explain the elongations and down-shift of $C_Q(^{14}N)$ values in N-H...O. According to our calculations, the $C_Q(^{14}N)$ value decreases from 2.64 MHz for the monomer to 1.14 MHz in the pentamer (43%), at the B3LYP level.

Conclusion:

This work reports DFT, NBO and NQR theories to investigate properties of cooperativity effects in α -glygly₍₂₋₅₎ clusters. The results are proved that the cooperativity is increased with cluster size. Such cooperative effects help us to rationalize the common occurrence of H-bonding interactions in biosystems.

Reference:

- [1] van Mourik T, Dingley AJ (2007) Characterizing the cooperativity in H-bonded amino structures. J Phys Chem A 111:11350-11358.
- [2] Xantheas SS (2000) Cooperativity and hydrogen bonding network in water clusters. Chem Phys 258: 225-231

Interaction of the Alkali Metals with Graphene Sheet

Maryam, Nayebyzadeh¹; Seifollah, Jalili^{1,*}

¹ Department of chemistry, K.N. Toosi University of Technology, Tehran, Iran

Email: Nayebyzadeh.maryam@yahoo.com

Key Words: Graphene, DFT, Coronene, Density of State, Band Gap.

Introduction:

Graphene is a single layer of Carbon atoms disposed in a honeycomb lattice and it is predicted to be a very promising material for future electronics due to several useful properties such as high mobility of the charge carriers and high crystal quality. The electrical and chemical properties of graphene ($C_{24}H_{12}$) were studied. The optimized, energy gap and electronic structure for this proposed carbon 2D models are reported. It was found that through hydrogenated process, the graphene have semiconductor behavior. In this paper we investigate the interaction of alkali metals elements such as lithium, sodium and potassium with graphene sheet. We have determined the structural and electronic properties of graphene before and after of interaction with the adatoms. This is important because of the adsorption of alkali metals increase the conductivity on the graphene sheet [1-4].

Materials and Methods:

as a graphene surface model, a graphene sheet ($n=7$, where n means numbers of hexagonal rings of carbon) were examined in the present study, Figure (1). First each of atoms was put on the center-of-mass of graphene surface, and then the structures of metal-graphene system were optimized, the calculation were performed in the framework of DFT/B3LYP theory along with 6/3-11++ g (d) basis set was used for all the atoms.

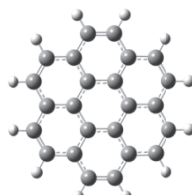


Figure (1): the optimized structure of grapheme (coronene)

Apparatus:

all DFT calculations were carried out using Gaussian 03 program package. We drew the Coronene structure with gauss view software then performed optimization and energy calculation for isolated graphene and the complex system (graphene with the metals adatoms) by using the Gaussian 03, after structure optimization and receive to the optimum interaction energy, then visualized the electronic structure to calculate the energy band gap throughout the Gausssum software.

Results and Discussion:

According to our calculation, the structure of graphene (Coronene) behaves as a semiconductor material, with gap energy of 4 eV. Due to the interaction between the alkali metals and graphene sheet, we defined the adsorption energy as ($E_{\text{ads}} = E_{\text{ag}} - E_{\text{g}} - E_{\text{a}}$), Where E_{ag} is the total energy per adatoms, E_{a} is the total energy of isolated atom, and E_{g} is the total energy of isolated graphene. The table (1) shows the verity of adsorption energy for each complex system:

Table (1): the adsorption energy and the Distance of different metals from graphene sheet.

ATOM	Dis (Å)	E_{ads} (ev)	Ads site
Li	1.8	1.87	H
Na	2.7	1.29	H
K	3.2	0.87	H

We realized that, lithium atoms have a minimum distance from the graphene sheet after adsorption and maximum adsorption energy.

To study the electronic structure and conductivity of the systems, we depicted the density of states diagrams for each system and compared them with each other. For example Fig (2) shows the DOS diagram for potassium the band gap energy for spin up after interaction decreased to 0.55 eV. Therefore, the conduction increases in coronene sheet.

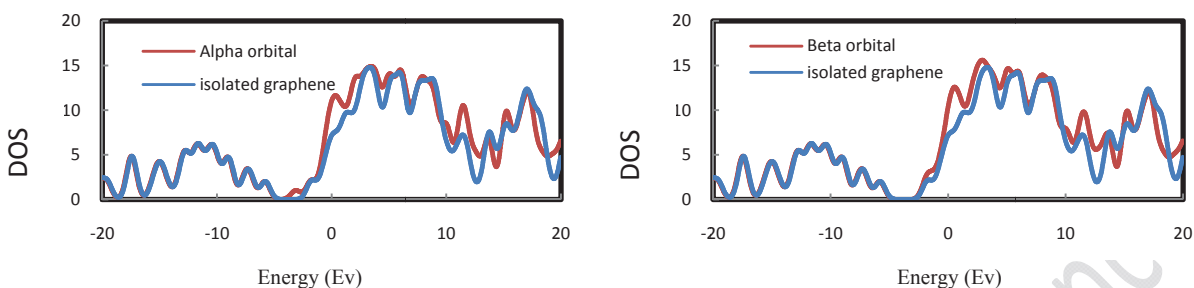


Figure (2): DOS diagram of potassium on coronene

Conclusion:

adsorption of alkali metals is closet to ideal ionic bonding. For spin up, we observed the strong interaction for K which shows a decline in band gap. Consequently, the conduction in this system increased. The H site is favorite adsorption site.

Reference:

- [1] T. Pankewitz, W. Klopper, Chem. Phys. Vol 498, 345-348, (2010).
- [2] T. Pakewitz and W. Klopper, J. Phys. Chem. Vol 111, 18917-18926, (2007).
- [3] D. A. Firsov, A. M. Tolmachev, Russian Journal of Physical Chemistry, Vol 81, 2035-2039, (2007).
- [4] K. T. Chan, J. B. Neaton. Phys. Rev. Vol 77, 235430, (2008).



Calculation of ^{13}C NMR parameters of 3-anilino-2-nitrobenzo[b]thiophenes and Comparison with experimental

M. Rezaei Sameti, N. Ali Safarzadeh

Department of physical Chemistry, Faculty of science, Malayer University, Malayer, 65157, Iran

mrsameti@malayeru.ac.ir

Key word: DFT, ^{13}C NMR, NMR, thiophenes

Introduction:

The last decade has seen significant improvements in both theoretical techniques in the field of quantum chemistry and in computer hardware that allow us to calculate accurate magnetic, as well as other properties of molecules [5-6]. The calculation of NMR shielding constants using ab initio techniques has become a challenging and important problem, because NMR spectroscopy is one of the most sensitive probes of molecular structures and electronic states. A number of papers have recently appeared in the literature concerning the calculation of NMR chemical shift (c.s.) by quantum-chemistry methods [1-3].

Computational details:

The molecular structures of the title compounds of figure 1 in the ground state are optimized by B3LYP with 6-31++G (p, d) basis set. ^{13}C NMR chemical shifts have been measured for structures of some substituted 3-anilino-2-nitrobenzo[b]thiophenes containing (OH, NH_2 , OMe, Me, Et, H, F, Cl and Br). The molecular structures were fully optimized using B3LYP/6-31G (d, p). The calculation of the ^{13}C shielding tensors employed the GAUSSIAN 03 implementation of the (GIAO) and (CSGT) by using 6-31G (d, p), 6-31++G(d,p) and 6-311++G(d,p) basis set methods at density functional levels of theories (DFT). Excellent linear relationships have been observed between experimental and calculated ^{13}C NMR chemical shifts for all derivatives.

Results and discussion :

Initially, the optimized molecular structure of 2o derivatives is shown in figure 1. Then, GIAO and CSGT of ^{13}C chemical shielding calculations of the title compounds (A-I) have been made by using B3LYP method with 6-311++G(d,p) basis set. The calculated chemical shifts for the most stable gas phase conformers, δ_{calc} , gives the following relationship:

$$\delta_{\text{calc}} = a\delta_{\text{exp}} + b \text{ ppm}$$

a and b are a slope and intercept of linear regression respectively. The correlation between the experimental values in solvent DMSO-d_6 and CDCl_3 of the ^{13}C chemical shifts and those calculated using GIAO and CSGT for the carbons of compound (G) of 3-anilino-2-nitrobenzo[b] thiophenes (2o) are shown in Figure 1. It is seen that the isotropic shielding for the carbons agree quite well with the experimental values. The slopes are in the range of 0.981 - 1.708, and the correlation coefficients are 0.952 - 0.992.

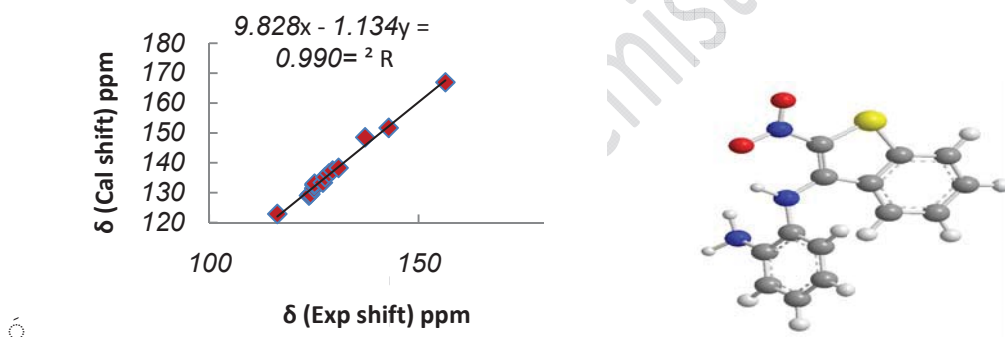


Fig. 1. The optimized molecular structure of two series of ortho substituent (OH, NH_2 , OMe, Me, Et, H, F, Cl and Br) of 3-anilino-2-nitrobenzo[b] thiophenes, comparison experimental and calculation.

References:

- [1] J. Gauss, J.F. Stanton, Adv. Chem. Phys. 123 (2002) 355
- [2] C. Michael .A. Bohm , Chemical Physics 342 (2007) 1–15
- [3] M. Tagashira, S.Yamazaki, S. Yamanaka, Computational Materials Science 14 (1999) 248-253
- [4] Y. Atalay, A. Basoglu, D. AvcıSpectrochimica Acta Part A 69 (2008) 460–466



A DFT study of Ga-doped in armchair and zigzag models of boron phosphide nanotubes

M. Rezaei-Sameti, F. Khaje Joushaghani

Department of Applied Chemistry, Faculty of Science, Malayer University, Malayer, 65174, Iran

E-mail address: mrsameti@malayeru.ac.ir

Key word: BPNTs, DFT, Ga-doped, NMR

Introduction:

In the last years, the significant research efforts have been done to synthesize and theoretical study of nanometer-scale tubular forms of various materials [1-2]. Among these materials, semiconductors of group III and V: boron nitride (BN), aluminum nitride (AlN), gallium nitride [3-4]. In particular, the BPNTs have attracted much attention, due to their unique properties and promising applications, optical, mechanical properties, electronics and optoelectronics applications and nano composites that can be operated at extreme environment such as high temperature, high power and radiation, and in harsh environments. In this project the electrical properties and NMR parameters of the pristine and Ga-doped structures of two representative (8, 0) zigzag and (4, 4) armchair model of boron phosphide nanotubes (BPNTs) have been investigated. In this work the HOMO and LUMO structures of undoped and doped model of BPNTs determined and the difference of band gap energies between the pristine and Ga-doped in the armchair model is larger than the zigzag model.

Computational methods:

In this computational research, all models are individually optimized by using density functional theory (DFT) at B3LYP level of theory with using the Gaussian 03 set of programs. The calculated CS tensors in principal axes system converted to measurable NMR parameters, chemical shielding isotropic and chemical shielding anisotropic:

$$CSI(ppm) = \frac{1}{3}(\sigma_{11} + \sigma_{22} + \sigma_{33}) \quad , \quad CSA(ppm) = \sigma_{33} - (\sigma_{22} + \sigma_{33}) / 2$$

Results and discussions:

The electronic structure properties of armchair and zigzag models of BPNTs and doping of Ga in the B nuclei have been investigated. The geometrical structures results show that by doping Ga; 1) the values of band gap energies in armchair model (see fig.1) is decreased and in zigzag model is increased; 2) the band gap energy of the zigzag model (see fig 2) was larger than the armchair because of interaction between d_{xy} orbital of gallium and p orbital of phosphorus atoms ; 3) The CSI and CSA values of two models of BPNTs at neighbor site of doping are decreased and other sites increased; 4) The results show that CSI values are directly proportional to the electronic density at the atomic sites; 5) it is worth noting that the electronic densities at the atomic sites of nanotubes are very important for interactions occurring between nanotube and other molecules or atoms.

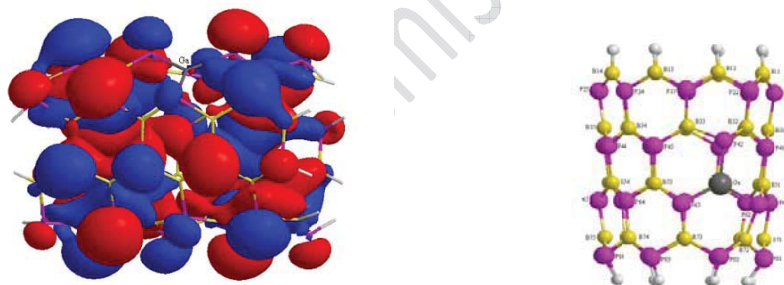


Fig.1 plot of HOMO and LUMO structures of the undoped and Ga doped of armchair and zigzag models of BPNTs.

References:

- [1] M.W. Zhao, Y.Y. Xia, D.J. Zhang, L.M. Mei, Phys. Rev. B 68 (2003) 235415.
- [2] S. M. Lee, Y.H. Lee, Y.G. Hwang, J. Elsner, D. Porezag, Th.Frauenheim, Phys. Rev. B 60 (1999) 7788.
- [3] M. Mirzaei, M. Mirzaei / Solid State Sciences 13 (2011) 244e250
- [4] M. Rezaei-Sameti, Arabian. J. Chem. (2011) in press
- [5] M. Rezaei-Sameti, Physica E. 43 (2010) 588–592
- [6] M. Rezaei-Sameti, J. Mol. Struc.(THEOCHEM) 867 (2008) 122–124.



A computational NMR study of BN-doped SiC nanotubes

M. Rezaei-Sameti^{*1}, S. Darabi

Department of Applied Chemistry, Faculty of Science, Malayer University, Malayer, 65174, Iran

^{*1} Corresponding author : E-mail: mrsameti@gmail.com, mrsameti@malayeru.ac.ir Tel/Fax: 98-851-3339843

E-mail address: mrsameti@malayeru.ac.ir

Key word: SiCNTs, NMR, DFT, BN-doped

Introduction:

In the past decade, after the discovery of CNTs by Iijima has raised great interest to synthesize tubular structures of SiC nanotubes (SiCNTs) and to characterize the properties of this novel material [1-2]. Recently, significant numbers of researches have prepared new one-dimensional SiC nano structures such as nano rods, nano whiskers, nano wires, nanotubes, hollow nano spheres, nano flowers, nano springs [3-4], due to their unique electrical, optical, mechanical properties and nano composites that can be operated at extreme environment such as high temperature, high power and radiation, and in harsh environments [4-5].

Computational methods:

In this new project the isotropic and anisotropic chemical shielding parameters (CSI and CSA) of ²⁹Si and ¹³C have been calculated based on DFT theory to investigate the electrostatic properties of the armchair (4, 4) SiCNTs and four models of BN-doped in Si and C nuclei (SiCNTs). The structures of all compounds were optimized at the level of B3LYP using 6-31G* basis set. The calculated CS tensors in principal axes are converted to measurable NMR parameters, chemical shielding isotropic (CSI) $CSI(ppm) = \frac{1}{3}(\sigma_{11} + \sigma_{22} + \sigma_{33})$ and chemical shielding anisotropic (CSA) by using equations $CSA(ppm) = \sigma_{33} - (\sigma_{22} + \sigma_{33})/2$ [4]. The evaluated NMR parameters of the sites of ²⁹Si, ¹³C, ¹¹B and ¹⁵N nuclei are presented in Tables 2 and 3.

Results and discussions:

The electronic structure properties of SiCNTs and four models of doping N and B in Si and C nuclei have been investigated (see Fig.1). The geometrical structures results show that bond length for the Si_BC and Si_NC models in Si41 site are smaller than other bond lengths. The comparisons of the CSI parameters in four doped models reveal that the most significant changes occur in the Si_NC and SiC_N, because of the large electronegativity of nitrogen. On the other hand the NMR parameters of ¹³C between undoped model and four doped models show that the CSI values of sites, which are directly connected to B or N atoms show significant decrease and so the bond length of (B or N – C31) is smallest. The results show that CSI values are directly proportional to the electronic density at the atomic sites. It is worth noting that the electronic densities at the atomic sites of nanotubes are very important for interactions occurring between nanotube and other molecules or atoms.

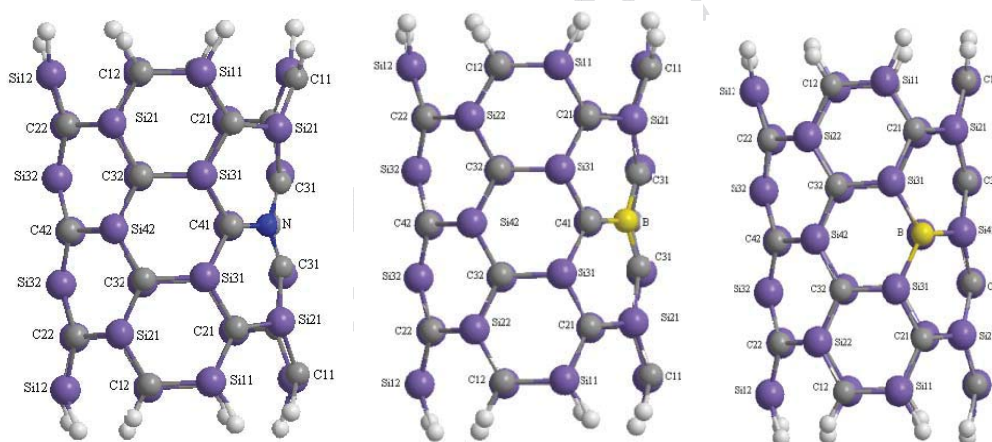


Fig.1

References:

- [1] Becke, A. D., 1993. J. Chem. Phys. 98, 5648-5652.
- [2] Ditchfield, R., Hehre, W. J., Pople, J. A., 1972. J. Chem. Phys. 54, 724-728.
- [3] Mirzaei, M., Mirzaei, M., 2010. Monatsh Chem. 141, 941-943.
- [4] Rezaei-Sameti, M., 2010. Physica E, 43, 588-592.
- [5] Taguchi, T., Igawa, N., Yamamoto, H., Shamoto, S., Jitsukawa, S., 2005. Physica E. 28, 431-438.



Molecular dynamics simulation study on the interaction of metalated tetra sulphonated phthalocyanine with adenosine deaminase

Seyyed Morteza Fazeli^{*a}, Davood Ajloo^{a,b}, Taghi Lashkarbolouki^{b,c}

^a School of Chemistry, Damghan University, Damghan, Iran

^b Institute of Biological Science, Damghan University, Damghan, Iran

^c School of Biology, Damghan University, Damghan, Iran

Email: fazelim44@yahoo.com, ajloo@du.ac.ir

Keywords: Molecular dynamics simulation, Phthalocyanine, Thermal stability.

Introduction:

The aromatic macrocycles phthalocyanines (Pcs) [1] are one of the best known synthetic porphyrin analogues. They are highly versatile and stable chromophores with unique physicochemical properties that make them ideal building blocks in the construction of molecular materials having special electronic and optical properties. Interestingly, owing to their extended flat hydrophobic aromatic surface, these macrocycles can interact with each other by attractive π - π stacking interactions [2], leading to aggregation in solution. Adenosine deaminase (ADA) is a cytosolic enzyme, which has been the object of considerable interest, mainly because a congenital defect in the enzyme causes severe combined immunodeficiency disease (SCID) in humans. ADA is an aminohydrolase (EC 3.5.4.4) which participates in the purine metabolism where it degrades either adenosine or 2'-deoxyadenosine producing inosine or 2'-deoxyinosine, respectively [3]. The product of human ADA gene consists of 363 aminoacids (41 kDa) and there is a high degree of amino acids sequence conservation amongst species. The enzyme contains a parallel α/β barrel motif with eight central β strands and eight peripheral α helices, which is a common structure found in 1/10 of all known enzymes [4]. ADA is involved in some diseases such as: tuberculosis [5].

Materials and methods:



Molecular Dynamics Simulation was carried out using the GROMACS (4.5.4) package with the GROMOS96 force field. The resulting system of MD models contains an enzyme, about 22,000 water molecules and 6, 12 and 18 molecules of tetra sulphonated nickel (II) phthalocyanine (NiPcTS) in a box dimension of $9.105 \times 9.105 \times 8.666 \text{ nm}^3$. The force field parameters of ligands were generated using the PRODRG web server. Then, NiPcTS were randomly distributed around the ADA enzyme. We used the crystal structure of enzyme (pdb code; 1VFL) downloaded from the protein data bank. The system was equilibrated for 20 ns at constant pressure (1 atm) and temperature of 300 K. MD calculations were performed during 20 ns. Finally, structure parameters of RMSD, RDF, $CD_{222\text{nm}}$, content were calculated.

Results and Discussion:

Accessible surface area (ASA), circular dichroism at 222 nm ($CD_{222\text{nm}}$), midpoint of transition temperature (T_m), number and distance of hydrogen bond, radial distribution function and other physical parameters were obtained from analyzing the trajectory of molecular dynamics. Results of calculated heat capacity at constant pressure (C_p) showed that transition temperature increases by increasing the NiPcTS concentration. Mid-point of temperature transition (T_m) obtained as 350 and 365 K in the absence and presence of 0.014 M of NiPcTS, respectively. Thus two peaks will be observed in the plot of C_p versus temperature.

Conclusion:

Self-aggregation of NiPcTS and interaction with ADA enzyme increases with increasing concentration. Results of calculated heat capacity at constant pressure (C_p) and radial distribution functions showed that NiPcTS behaves like osmolytes at low concentration that increases the beta form and so increases the enzyme stability.

Reference:

- [1] C.C. Leznoff, A.B.P. Lever (Eds.), Phthalocyanines: Properties and Applications; 1–4, VCH Publishers, New York; 1989, 1993, 1996.



- [2] C. A. Hunter, J. K. M. Sanders; "The nature of π - π interactions"; J. Am. Chem. Soc; 112, 5525-5534, 1990.
- [3] N. Spencer, D. Hopkinson, H. Harris; "Adenosine deaminase polymorphism in man"; Ann. Hum. Genet; 32, 9-14, 1968.
- [4] M. Kaisemann, A. Kritski, M. Pereira, A. Trajman; "Pleural fluid adenosine deaminase detection for the diagnosis of pleural tuberculosis"; J. Bras. Pneumol; 30, 549-556, 2004.
- [5] G. Farber, G., Petsko ; "The evolution of alpha/beta barrel enzymes"; Trends Biochem. Sci; 15, 228-234, 1990.



The effect of cationic and anionic phthalocyanines on the adenosine deaminase structure, molecular dynamics and docking studies

Seyyed Morteza Fazeli^a, Davood Ajloo^{a,b}

^aSchool of Chemistry, Damghan University, Damghan, Iran

^bInstitute of Biological Science, Damghan University, Damghan, Iran

Email: fazelim44@yahoo.com, ajloo@du.ac.ir

Keywords: Docking energy, Molecular dynamics simulation, Structural parameters.

Introduction:

Phthalocyanines (Pcs), both metalated (MPcs) and metal-free (H₂Pc), are metal-organic semiconductors that have been applied as chemiresistive sensors [1-3]. MPc sensitivity to vapor-phase molecules may be tuned by manipulation of the metal center and by substitution of functional groups on the organic ring [1-4]. It has been reported the optical absorption spectra of phthalocyanine films are insensitive to substitutions for the central metal atom [5]. Adenosine deaminase (ADA) is a cytosolic enzyme, which has been the object of notable interest, mainly because a congenital defect in the enzyme causes severe combined immunodeficiency disease (SCID) in humans. ADA is an aminohydrolase (EC 3.5.4.4) which participates in the purine metabolism where it degrades either adenosine or 2'-deoxyadenosine producing inosine or 2'-deoxyinosine, respectively [6]. The crystal structure also revealed that ADA is a metalloenzyme that complexes one mole of Zn²⁺ per mole of protein [7]. ADA is involved in some diseases such as: tuberculosis [8], brain tumor [9].

Materials and methods:

Molecular Dynamics Simulation was carried out using the GROMACS (4.5.4) package with the GROMOS96 force field. The resulting system of MD models contains a protein, about 22,000 water molecules and 6 molecules of tetra sulphonated phthalocyanine (PcTS) and tetrakis [2- (trimethylammonium) ethoxy] phthalocyanine (PcTme) in a box of



$9.105 \times 9.105 \times 8.666 \text{ nm}^3$. The force field of ligands was generated using the PRODRG web server. Then, two phthalocyanines were randomly distributed around the ADA. We used the crystal structure of enzyme (pdb code; 1VFL) downloaded from the protein data bank. MD calculations were performed during 20 ns. Then structure parameters of RMSD, RDF and $CD_{222\text{nm}}$, were calculated. We want to determine computationally whether two phthalocyanines will interact or bind to enzyme, and if so, we would like to compare the binding energy of them, as well as the affinity of the binding or interaction and Gibbs energy of interaction. AutoDock 3.0.5 software was used for the ligand-protein docking studies.

Results and Discussion:

Accessible surface area (ASA), circular dichroism at 222nm ($CD_{222\text{nm}}$), number of hydrogen bond, radial distribution function (RDF), radius gyration (R_g) and other physical parameters were obtained from analysing trajectory of molecular dynamics. Results showed that ADA accessible surface area and R_g parameters increased and number of hydrogen bond, circular dichroism at 222nm ($CD_{222\text{nm}}$) decreased in the presence of PcTme. Value of binding free energy (ΔG_{bind}) for cationic and anionic phthalocyanine is -3.90 and -4.89 kcal/mol respectively.

Conclusion:

Self-aggregation of PcTS and PcTS decrease in comparison with PcTme and PcTme, but their interaction with ADA increases. Results of calculated radial distribution functions showed that PcTS locate near ADA in comparison with PcTme at 0.014M concentration. Docking energy showed that binding energy with ADA of anionic is negative than cationic phthalocyanine and dimerization free energy for PcTme is negative than PcTS, Therefore enzyme denaturation is more than in presence of PcTS.

Reference:

[1] A.W.Snow, W.R., Barger; Phthalocyanine Films in Chemical Sensors. In Phthalocyanines: Properties and Applications, New York; 1, 341, 1989.



- [2] D. Eley; *Nature*; 162, 819, 1948.
- [3] R. D. Gould; *Coord. Chem. Rev.*; 156, 237–274, 1996.
- [4] G. Guillaud, J. Simon, J. Germain; *Coord. Chem. Rev.*; 178, 1433–1484, 1998.
- [5] B. H. Schechtman, W. E. Spicer; *J. Mol. Spectrosc.*; 33, 28, 1970.
- [6] N. Spencer, D. Hopkinson, H. Harris; *Ann. Hum. Geit.*; 32, 9-14, 1968.
- [7] D. K. Wilson, F. B. Rudolph, F. A. Quirocho; *Science*; 252, 1278, 1991.
- [8] M. Kaisemann, A. Kritski, M. Pereira, A. Trajman; *J. Bras. Pneumol.*; 30, 549, 2004.
- [9] S. Manjula, A. Raja, S. Rao, A. Aroor, A. Rao; *Acta Neurochir.*; 121, 149, 1993.

Quantum mechanical investigation of the catalytic mechanism and inhibition of the dinuclear zinc metallo- β -lactamase by penicillin

Mina Ghiasi*^a, Bahare Noohi^a and Mansour Zahedi^b

^a Department of Chemistry, Faculty of Science, Alzahra University, Vanak, Tehran, ghiasi@alzara.ac.ir, ^b

Department of Chemistry, Faculty of Science, Shahid Beheshti University, G. C., Evin, 19839-63113, Tehran, Iran .

baharenoohi@yahoo.com

Key words: Metallo β -lactamase, Penicilline, Catalytic Mechanism, QM calculations.

Introduction:

It is known that bacterial resistance to β -lactam antibiotics stems from the expression of the β -lactamase that catalyzes the hydrolytic cleavage of the substra amid bond. Metallo- β -lactamase contains zinc and other divalent cations as cofactors. The active site includes two zinc ions, both of which are required for full catalytic activity, bringing hydroxide ion, Figure 1. Since the initial discovery of inhibitors, a number of new inhibitors of metallo- β -lactamase, antibiotics, have been discovered [1, 2]. Besides the large amount of experimental work, a few theoretical studies on the dinuclear zinc metallo- β -lactamase have reported. Therefore, in the present study the coordination structure of active site dizinc center, catalytic mechanism and inhibitor (penicillin) binding based on quantum calculations have investigated.

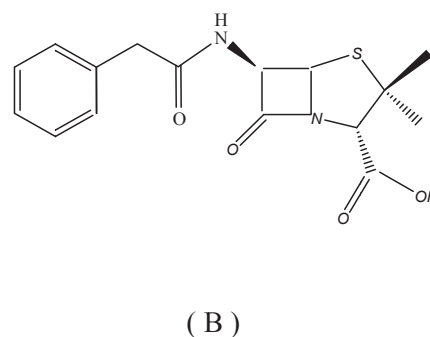
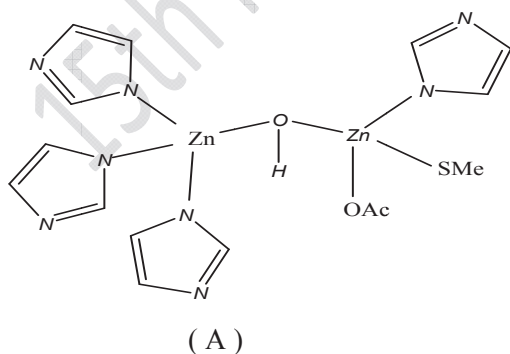


Figure 1. Model system for the (A) dinuclear zinc cluster and (B) penicillin inhibitor.

Computational methods:

Ab initio calculations were carried out with the Gaussian program series 2003. All geometries were fully optimized employing a B3LYP/6-31G method. The harmonic vibrational frequencies were computed to confirm that an optimized geometry correctly corresponds to a local minimum. QST2 method was used to search for transition state. Transition state geometry was double-checked by using IRC and FREQ calculations. The solvent effects on the conformational equilibrium have been investigated with a PCM method for water solvent.

Results and Discussion:

The results of quantum calculation of the metallo- β -lactamase in complex with penicillin shows that the substrate β -lactam group interacts with active site zinc ions. The structural and energetic features of the binding of penicillin inhibitor show that penicillin can deactivate the dinuclear zinc center through a two-step reaction mechanism involving two transition states and three intermediates, Figure 2. The energetic and mechanistic features of an active site model indicate that the two zinc ions play a significant role in catalysis.

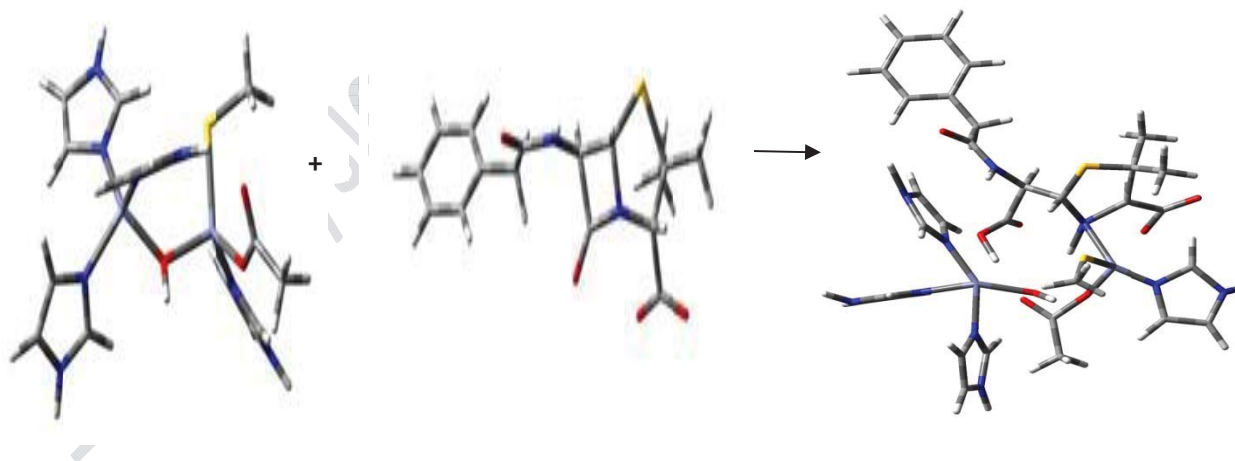


Figure 2. complexation of penicillin and dinuclear zinc metallo- β -lactamase.

References:

- [1] A. Carfi, E. Duee, M. Galleni, J. Frere, O. Dideberg, Acta Crystallogr. 1998, 54, 313-323.
- [2] H. Park, E. N. Brothers, K.M. Merz J. Am. Chem. Soc., 2005, 127, 4232-4241.



15th Physical Chemistry Conference



A DFT study of ^{17}O NMR parameters of Benzyl ethers Components

M. Rezaei Sameti^{*1}, A. Kazemi, V. Mousa Zadeh

Department of physical Chemistry, Faculty of science, Malayer University, Malayer, 65157, Iran

* Tel.: +98 851 3339983; fax: +98 851 3339843.

E-mail address: mrsameti@malayeru.ac.ir

Key word: DFT, ^{17}O , NMR, Benzyl ethers

Introduction:

Nuclear Magnetic Resonance (NMR) is a useful technique for studying the structure of chemical and biological systems, from small molecules to complicated structures such as nucleic acids and proteins. Chemical shifts and spin-spin coupling serve to recognize the molecular conformation, composition and environment of the moiety. However, the investigation and understanding of the relationships between molecular structure and measured NMR parameters can sometimes be quite difficult, and need the support of theoretical calculations [1]. Theoretical methods for the prediction of the nuclear magnetic resonance (NMR) parameters of molecules have become a useful quantum chemical tool. A number of papers have recently appeared in the literature concerning the calculation of NMR chemical shift (CS.) by quantum-chemistry methods [2-5].

Computational methods:

The entire calculations were performed at density functional (DFT) levels on a Pentium using Gaussian 03. The geometry of the title compounds in (Fig. 1) is fully optimized and ^{17}O NMR chemical shielding are calculated with GIAO and CSGT approach by applying B3LYP method at the 6-31G (d,p), 6-31++G(d,p) and 6-311++G(d, p) basis sets. The obtained shielding tensors were referenced against to an absolute shielding reference $\sigma_{\text{ref}} = 287.5$ ppm

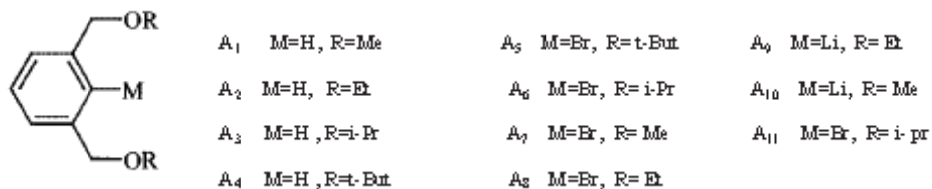


Fig. 1

Results discussions

The results show that in the compounds A₁ and A₂, A₄ and A₇ the GIAO method by 6-31++G(d,p), in compound A₃ and A₆ the CSGT method by 6-31++G(d,p) and 6-31G(d,p) respectively and in the compounds A₅ and A₁₁ the GIAO method by 6-31G(d,p) are in a good agreement with experimental. Fig.1, Table 1

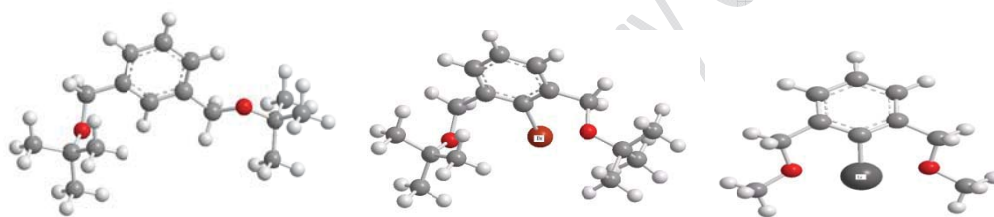


Fig. 1 Optimized of structures of Benzyl ethers derivatives

Table 1. Theoretical chemical shift and experimental chemical shift of Benzyl ethers ¹⁷O NMR spectra (ppm), deviation error $\Delta\delta = \delta_{EXP} - \delta_{calc}$ with B3lyp/6-31++G(d,p).

Compounds	GIAO	CSGT	Exp. ^a	$\Delta\delta_{GIAO}$	$\Delta\delta_{CSGT}$
A1	-18.0	-2.7	-14.0	4.0	-11.3
A2	4.3	17.7	9.6	5.3	-8.1
A3	29.3	38.0	39.0	9.7	1.0
A4	35.4	39.5	49.0	13.6	9.5
A5	52.2	56.5	40.1	-12.1	-16.4
A6	34.3	44.2	33.0	-1.3	-11.2
A7	-21.3	-5.9	-20.0	1.3	-14.1
A8	2.5	16.2	-		
A9	14.1	20.3	-		
A10	52.0	-5.3	-		



A11	52.1	57.9	33.5	-18.6	-24.4
-----	------	------	------	-------	-------

References

- [1] A. Wong, K. J. Pike, R. Jenkins, G. J. Clarkson, T. Anupold, A. P. Howes, D. H. G. Crout, A. Samoson, R. Dupree, M. E. Smith, 2006. *J. Phys. Chem. A* 110: 1824-1835.
- [2] C. Silly, J. Y. Legein, F. Calvayrac, 2004. *Solid State Nuclear Magnetic Resonance* 25: 241-251.
- [3] C. Johnson¹, E. A. Moore, M. Mortimer, *Solid State Nuclear Magnetic Resonance*, 27, 155-164 (2005).
- [4] D. A. Forsyth, A. B. Sebag, 1997. *J. Am. Chem. Soc* 119: 9483-9494.
- [5] E. Virtanen, A. Valkonen, J. Tamminen, E. Kolehmainen, 2003. *J. Mol. Structure* 650 : 201-212.



Configurational and conformational properties of 1,3,7,9-tetrastanna-cyclododeca-1,2,7,8-tetraene. A hybrid density functional study and natural bond orbital interpretation

Mitra Keshavarz¹, Seiedeh Negar Mousavi¹, Hooriye Yahyayi² and Davood Nori-Shargh

(Email: keshavarzm53@yahoo.com)

¹Chemistry Department, Arak Branch, Islamic Azad University, Arak, Iran

²Chemistry Department, Zanjan Branch, Islamic Azad University, Zanjan, Iran

Keywords: DFT, NBO, allenic compounds

Introduction:

Allenes are an important class of unsaturated hydrocarbons which contain two double bonds in an orthogonal geometry.^{1,2} Ring constraints bend and twist the normally linear perpendicular allene and engender substantial strain and resultant kinetic reactivity.³ Monocyclic medium ring diallenes with the allene groups in a ring that has more than nine members appear to be fairly stable. Simple monocyclic diallenes possess two chiral centers and should exist in two diastereoisomeric forms, one diastereoisomer being racemic and the other a meso compound.⁴ In this work, we have investigated computationally the structural, conformational properties of 1,3,7,9-tetrastanna-cyclododeca-1,2,7,8-tetraene, by hybrid density functional based method (B3LYP/Def2-TZVPP) and natural bond orbital interpretation, using the GAUSSIAN 03 package of programs.^{5,6} In addition, the allenic bonds nature (population and bonding orbital deviation) and the stability of various conformations of (\pm) and meso configurations of 1,3,7,9-tetrastanna-cyclododeca-1,2,7,8-tetraene, was systematically and quantitatively correlated using NBO analysis.⁶

Computational details:

DFT calculations were carried out using B3LYP/Def2-TZVPP level of theory for the *meso* and *dl* structures of 1,3,7,9-tetrastanna-cyclododeca-1,2,7,8-tetraene with the GAUSSIAN 03



package of programs.⁵ Manually constructed appropriate Z-matrix files of initial geometries of the *meso* and *dl* structures of 1,3,7,9-tetrastanna-cyclododeca-1,2,7,8-tetraene were used as input files for optimization at the B3LYP/Def2-TZVPP level of theory. Energy minimum molecular geometries were located by minimizing the energy, with respect to all geometrical coordinates without imposing any symmetry constraints. An NBO analysis was then performed for the *meso* and *dl* structures of 1,3,7,9-tetrastanna-cyclododeca-1,2,7,8-tetraene by the NBO 5.G program contained in the PC-GAMESS interface.⁶

Results and Discussion:

The results concerning an investigation employing the hybrid density functional theory (DFT) method to calculate structural optimization and conformational interconversion pathways for the two diastereoisomeric forms, *dl* and *meso* configurations of 1,3,7,9-tetrastanna-cyclododeca-1,2,7,8-tetraene are reported in this work. Two axial symmetrical conformations are found for the *dl* configuration of this compound. The unsymmetrical *meso*-TBBC form is found to be the most stable geometry, among the various conformations of *meso* configuration. B3LYP/Def2-TZVPP results showed that between the two most stable conformations of *dl* and *meso* configurations, *meso*-TBBC is more stable than (\pm)-TB. Using NBO (Natural Bond Orbital) analysis, π and π^* allenic-like bonding and anti-bonding orbital occupancies and also the deviations of σ and π bonding orbitals of allenic moieties were investigated. NBO results revealed that in the most stable form of *dl* configuration [(\pm) -TB], the sum of the π^* allenic antibonding orbital occupancies ($\Sigma\pi^*$ occupancy) is greater than *meso* configuration [*meso*-TBBC]. In addition, NBO results indicated that in the *meso*-TBBC conformer, the sum of σ and π allenic-like moieties bonding orbital deviations, from their normal values, is lower than in the (\pm)-TB form. All these facts could explain the relative more stability of *meso*-TBBC conformer, as compared to the (\pm)-TB form.

Conclusion:

The results obtained showed that by the *meso*-TBBC conformer d is more stable than (\pm)-TB. The greater sum of the π^* allenic antibonding orbital occupancies ($\Sigma\pi^*$ occupancy) and the



greater sum of σ and π allenic-like moieties bonding orbital deviations explain the relative more stability of *meso*-TBBC conformer, as compared to the (\pm)-TB form.

References:

- [1] A. Greenberg, J.F. Liebman, *Strained Organic Molecules*, Academic Press, New York, 1979.
- [2] M. Traetteberg, P. Bakken, A. Almenningen, *J. Mol. Struct.* 70 (1981) 287.
- [3] R.P. Johnson, *Chem. Rev.* 89 (1989) 1111.
- [4] D. Nori-Sgargh, N. Saroogh-Farahani, S. Jameh-Bozorghi, F. Deyhimi, M.-R. Talei Bavi, F.R. Ghanizadeh, *J. Chem. Res. (S)* (2003) 384.
- [5] M.J. Frisch, et al, Gaussian 03, Revision B.03, Gaussian, Inc., Wallingford CT, 2004.
- [6] E.D. Glendening, J.K. Badenhoop, A.E. Reed, J.E. Carpenter, J.A. Bohmann, C.M. Morales, F. Weinhold, Theoretical Chemistry Institute, University of Wisconsin, Madison, WI, 2004. NBO Version 5.G.



NMR parameters of Boron and Nitrogen doped in nano-size of Fullerene (C60)

M. Rezaei-Sameti, R. Rami, E.S. Dadfar

Department of Applied Chemistry, Faculty of Science, Malayer University, Malayer, 65174, Iran

E-mail address: mrsameti@malayeru.ac.ir

Key word: Fullerene (C60), NMR, DFT, N- and B- doping

Introduction:

In the present work, we investigate the influence of N- and B-doping on the electrostatic structure properties and NMR parameters of nano-size of the Fullerene (C60) model. The calculations are performed at the level of density functional theory (DFT) using Gaussian 03 package of program. Since the discovery of fullerene 26 years ago [1], numerous investigations have been done that C60 undergoes various types of reactions, such as hydrogenation, reduction, nucleophilic addition, radical addition and cyclo addition reactions [2-3]. Regarding theoretical studies on stable structures of hetero fullerenes, the quantum molecular-dynamics calculations have shown the possibility to synthesize C59N and C59B, C58N2 and C58B2 or for example C12B24N24 [4-6].

Computational details:

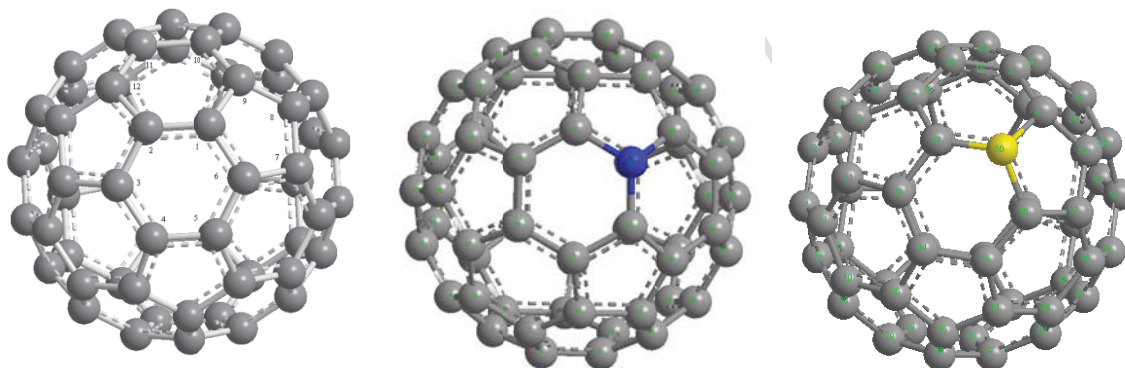
The structures of three models of C60 were firstly optimized by hybrid density functional theory and B3LYP functional based method and 6-31G(d) standard basis set and then the chemical shielding (CS) tensors at the sites of ^{13}C nuclei are calculated based on the gauge included atomic orbital (GIAO) approach. The calculated CS tensors in principal axes system are converted to measurable NMR parameters, chemical shielding isotropic (CSI) and chemical shielding anisotropic (CSA) by using equations (1) and (2), respectively. The evaluated NMR parameters at the sites of ^{13}C nuclei in the pristine and N, B-doped models (n and b) are presented in Table 2.

$$CSI(ppm) = (\sigma_{11} + \sigma_{22} + \sigma_{33})/3 \quad (1)$$

$$CSA(ppm) = \sigma_{33} - (\sigma_{11} + \sigma_{22})/2 \quad (2)$$

Results and discussions:

The optimized bond lengths reveal that when B and N atom are substituted in fullerene, the bond lengths of C-B are increased and C-N are decreased. The results show that the value of the bond angles (6-7-8 and 6-7-8) placed at sides of N and B-doped are decreased largely from 120° to 108° and the bond angle (11-12-2) in two models increased from 108° to 120°. The comparison between N-doped and B-doped models shows that, the values of CSI and CSA for N-doped model undergo more remarkable changes than B-doped model because of the lone pair of electrons in the nitrogen valence shell.



References:

- [1] H.W. Kroto, J.R. Heath, S.C.O'Brien, R.F. Curl, R.E. Smalley, *Nature.*, **318**, 162 (1985).
- [2] W. Krätschmer, L.D. Lamb, K. Fostiropoulos, D.R. Huffman, *Nature.*, **347**, 354 (1990).
- [3] R.E. Haufler, J. Conceicao, L.P.F. Chibante, Y. Chai, N.E. Byrne, S. Flanagan, M.M. Haley, S.C.O'Brien, C. Pan, *J. Phys.Chem.*, **94**, 8634 (1990).
- [4] K. Winkler, A. de Bettencourt-Dias, A.L. Balch, *Chem. Mater.*, **12**, 1386 (2000).
- [5] Y. Chen, C.H. Tsai, *J. Appl. Polym. Sci.*, **70**, 605 (1998).
- [6] R. Borghi, L. Lunazzi, G. Placucci, *J. Org. Chem.*, **61**, 3327 (1996).



Computational Study on the interaction between $B_{12}H_{12}^{2-}$ and $Ca(C_6H_6)_2^{2+}$.

Mehdi Bayat^{*,a}, Yazdan Maghsoud^a, Yasin Gholiiee^a, Fatemeh Zamanian^b, Sadegh Salehzadeh^a

^a Faculty of Chemistry, Bu-Ali Sina University, Hamedan, Iran (Email: mehdi806@gmail.com)

^b Department of Chemistry, Faculty of Science, Malayer University, Malayer, Iran

Key words: Theoretical Study, Boran Hydrides, non-covalent interactions, NBO Analysis

Introduction:

Supramolecular chemistry, the chemistry of non-covalent interactions, is a highly active interdisciplinary field with important implications in biology, chemistry, physics and engineering[1,2]. It is well known, that non-covalent interactions (anion... π , lone pair(lp)- π , C-H... π , cation... π , π - π , “conventional” and “non-conventional” H-bonds) have attracted considerable attention [3] since they play a pivotal role in various biological and chemical systems. Among these weak interactions, the C-H... π interaction is considered as one of weak hydrogen bonds, in which the C-H and π -system acts as a soft acid and a soft base, respectively. The C-H... π interaction has particular importance in influencing molecular recognition, conformational preference, biological processes, and the structure of biomacromolecules[4]. On the other hand, it can be similar interactions between B-H functions in boran hydrides (or in carborans) and π -cation/anion systems at first sight. However, there are some difference between the C-H... π and B-H... π interactions, as regards to the electronegativity of carbon is more than the boron atom. So far, interaction between B-H functions in $B_{12}H_{12}^{2-}$ and π system in $Ca(C_6H_6)_2^{2+}$ has not investigated. In this computational work, the latter interactions and their likeness with C-H... π (cation/anion) interactions have been investigated.

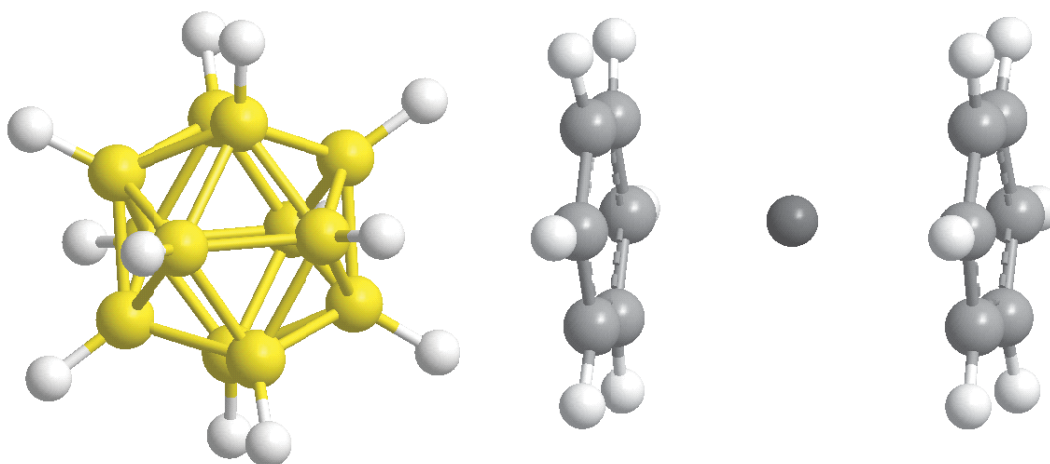
Computational details

The structures of the complexes $B_{12}H_{12}^{2-}$, $Ca(C_6H_6)_2^{2+}$ and $[B_{12}H_{12}^{2-}][Ca(C_6H_6)_2^{2+}]$ in the gas phase were fully optimized at standard 6-31++G** basis set by B3LYP level of theory using

the Gaussian 09 set of programs. Vibrational frequency analysis, calculated at the same level of theory, indicates that optimized structures are at the stationary points corresponding to local minima without any imaginary frequency. The natural bonding orbitals (NBO) calculations were performed using NBO 3.1 program as implemented in Gaussian 03 package at the same level.

Result and discussion:

The results showed that there are $-208.909 \text{ kcal.mol}^{-1}$ interaction between the B-H function in $\text{B}_{12}\text{H}_{12}^{2-}$ and π -system in $\text{Ca}(\text{C}_6\text{H}_6)_2^{2+}$.



Conclusion:

The interaction between B-H functions in $\text{B}_{12}\text{H}_{12}^{2-}$ and π system in $\text{Ca}(\text{C}_6\text{H}_6)_2^{2+}$ was investigated. The studied π -system has strong bonding interactions with B-H functions in $\text{B}_{12}\text{H}_{12}^{2-}$.

Reference:

- [1] S. Leininger, B. Olenyuk, P. Stang, J. Chem. Rev. 2000, 100, 853.
- [2] J. M. Lehn, Supramolecular chemistry. Concepts and Perspectives. Weinheim, Germany: Wiley-VCH; 1995.



- [3] H. J. Schneider, *Angew. Chem., Int. Ed.* 2009, 48, 3924.
- [4] M. Nishio, Y. Umezawa, S. Tsuboyama, H. Takahashi, *Pept. Sci.* 1999, 36, 61–64.

15th Physical Chemistry Conference



Complete Gas-Phase Proton Microaffinity Analysis of Two Aliphatic Linear Pentaamine Ligands.

Yazdan Maghsoud^a, Yasin Gholiee^a, Sadegh Salehzadeh ^{*a}, Mehdi Bayat^a, Shiva Khodaveisi^b,
Marzieh Bayat^b,

^a Faculty of Chemistry, Bu-Ali Sina University, Hamedan, Iran (Email: Saleh@basu.ac.ir)

^b Department of Chemistry, Faculty of Science, Malayer University, Malayer, Iran

Keywords: Theoretical Study, Proton Microaffinity, Proton Macroaffinity, Proton Overallaffinity, Linear Pentaamines.

Introduction:

The proton affinity of a monobasic neutral ligand at 0 K is defined as the negative of the electronic energy difference between HL^+ and L together with a correction for difference in zero point energies [1,2]. For each polybasic molecule there may be several ways for protonation depending on which site is protonated. Protonation of different sites will release different amounts of energy. Recently we introduced three new defined proton affinities for polybasic molecules in the gas phase: proton microaffinity, proton macroaffinity and proton overallaffinity [3-5]. We showed that there is a good correlation between the calculated gas-phase proton macroaffinities of some polyamine ligands with corresponding protonation macroconstants in solution[3]. Herein we want to report a theoretical study on complete gas phase proton microaffinities of two aliphatic linear pentaamine ligands with formula: $NH_2(CH_2)_2NH(CH_2)_2NH(CH_2)_2NH(CH_2)_2NH_2$ (2222-pent); and $NH_2(CH_2)_3NH(CH_2)_2NH(CH_2)_2NH(CH_2)_3NH_2$ (3223-pent).

Computational details:

The geometries of all species in the gas-phase were fully optimized at DFT (B3LYP and BP86) level of theory using the GAUSSIAN 09 set of programs. The standard 6-31G** basis

set was used for all calculations. Vibrational frequency analyses, calculated at the same level of theory, indicate that optimized structures are at the stationary points corresponding to local minima without any imaginary frequency.

Results and discussion:

After calculation of proton microaffinities (Fig.1, left), the proton macroaffinities and proton overall affinity for studied molecules were calculated using Eqs. (1) and (2) [3,4].

$$\overline{PA}_n = \frac{\sum_{j=1}^l \sum_{i=1}^m PA_{n,i} \times R_{i,j} \times S_{n,j}}{\sum_{j=1}^l \sum_{i=1}^m R_{i,j} \times S_{n,j}} \quad \text{Eq (1)} \quad \text{where} \quad R_{n,j} = \sum_{i=1}^K R_{n-1,i} \times S_{n-1,i}$$

$$\overline{PA}_{ov} = \sum_{n=1}^m \overline{PA}_n \quad \text{Eq (2)}$$

The results show that the variations of proton macroaffinities of both 2222-pent and 3223-pent is similar to variations of their protonation macroconstants in solution (Fig. 1, right).

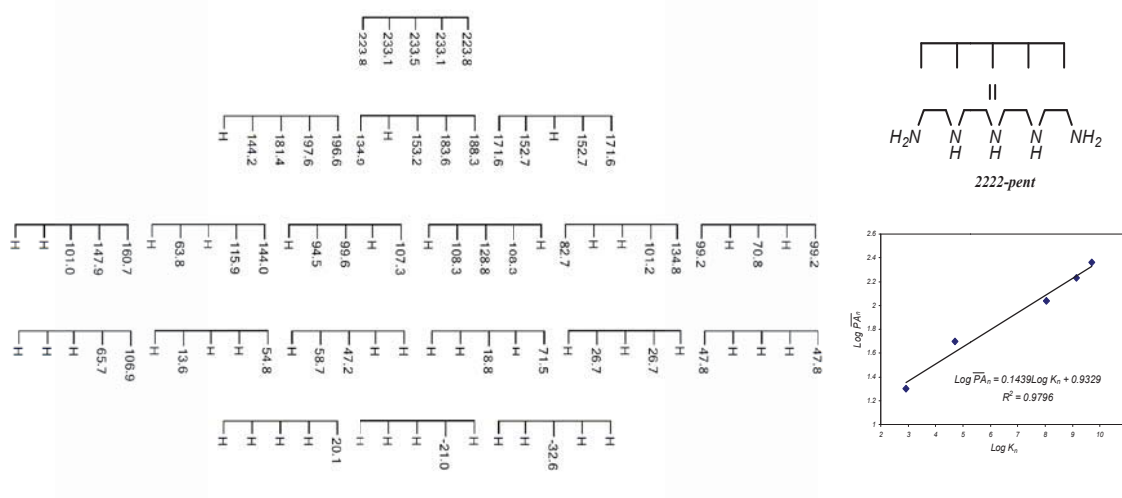


Fig 1. Left: Illustration of full protonation steps of 2222-pent. Numbers show the proton microaffinity of each basic site (kcal/mol). Right: the correlation between the $\log \overline{PA}_n$ and $\log K_n$ for 2222-pent.

Conclusion:



The reliable theoretical calculation of the gas-phase proton macroaffinities and proton overallaffinities of linear pentaamine ligands according to the complete proton microaffinity analysis is potentially possible.

References:

- [1] J. R. Rusted, D. A. Dixon, J. D. Kubicki, A. R. Felmy, J. Phys. Chem. A 2000, 104, 4051.
- [2] D. Kaur, R. P. Kaur, R. Kohli, J. Mol. Struct. TheoChem 2009, 913, 90.
- [3] S. Salehzadeh, M. Bayat, Chem. Phys. Lett. 2006, 427, 455.
- [4] S. Salehzadeh, M. Bayat, M. Hashemi, J. Phys. Chem. A 2007, 111, 8188-8192.
- [5] S. Salehzadeh, M. Bayat, M. D. Ward, J. Phys. Chem. A 2008, 112, 4090-4094.



Theoretical study on the mechanism of urea hydrolysis catalyzed by Pd(II)

A. Morsali^a, S. A. Beyramabadi^a and Z. Zare^{* a}

^a Department of Chemistry, Mashhad Branch, Islamic Azad University, Mashhad, Iran

(Email: faranak.zare@gmail.com)

Keywords: Urea hydrolysis, Mechanism, Palladium, Density functional theory

Introduction:

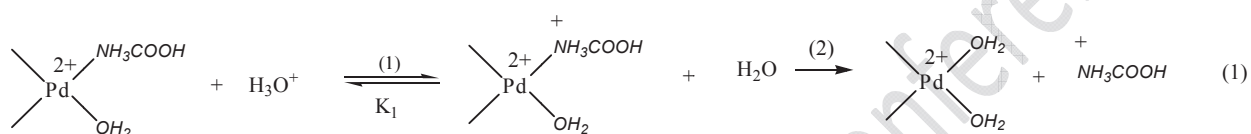
Four palladium(II) aqua complexes catalyze hydrolytic decomposition of urea into carbon dioxide and ammonia [1]. The reaction catalyzed by $[Pd(en)(H_2O)_2]^{2+}$. The following steps in the mechanism of this reaction are studied experimentally by Kaminskaia and Kostic [1]: binding of urea to the catalyst, formation of carbamic acid (H_2NCOOH) coordinated to palladium(II) via the nitrogen atom, and conversion of this intermediate into carbon dioxide and ammonia. Although the simple palladium(II) complexes are very different from the enzyme urease, which contains nickel(II) ions, the decomposition of urea catalyzed by both kinds of agents involves carbamic acid as the intermediate (rate determining step). In this work, the mechanism of conversion of this intermediate into carbon dioxide and ammonia has been studied using density functional methods. Mechanistic studies with metal complexes contribute to the understanding of the enzymatic mechanism.

Computational details:

All of the present calculations have been performed with the B3LYP [2] hybrid density functional level using the G09 package. The 6-311+G(d,p) basis set was employed except for Pd atom, in which the LANL2DZ [3] basis set was used with including effective core potential functions. The gas phase optimized geometries used to apply the solvent effects, where the valuable PCM [4] model was employed.

Results and discussion:

The following mechanism (Eq.(1)) for the rate-determining step was proposed which is compatible with experimental evidence. In this mechanism, a fast equilibrium step (with equilibrium constant K_1) will result in the formation of complex $[Pd(H_2O)_3NH_3COOH...H_2O]^{3+}$ which will be converted into $[Pd(en)(H_2O)_2]^{2+}$ and $[NH_3COOH]^+$ during a slow process. Thereafter, during a fast reaction, $[NH_3COOH]^+$ will be converted into reaction products ($NH_4^+ + CO_2$).



The optimized structure of transition state obtained from step2 has been shown in Fig. 1. By taking Solvent effects into consideration, $E_a = 23.8 kcal/mol$. This shows that the model presented in this research is a suitable model for the rate determining step of urea hydrolysis catalyzed by palladium(II) complex.

Conclusion:

Using quantum mechanical method, urea hydrolysis catalyzed by palladium(II) complex was investigated and ultimately a model was presented in which $[NH_3COOH]^+$ form is produced in the rate determining step and in continuation is converted into products.

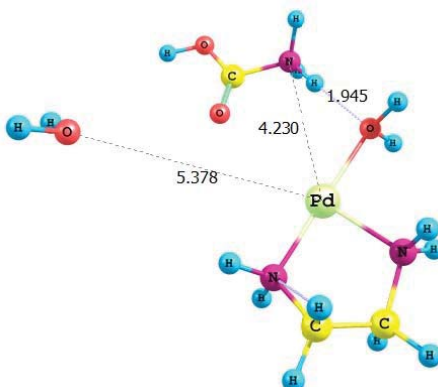


Fig 1. Optimized structure of the TS (step 2)

References:

- [1] N.V. Kaminskaia, N.M. Kostic, Inorg. Chem. 36 (1997) 5917.
- [2] A.D. Becke, Phys. Rev. A, 38 (1988) 3098.
- [3] P.J. Hay, W.R. Wadt, J. Chem. Phys. 82 (1985) 299.
- [4] S. Miertus, E. Scrocco, J. Tomasi, Chem. Phys. 55 (1981) 117.



Effects of electron donating and electron withdrawing substituents on the nature of C=N bond in *Z* and *E* isomers of R-CH=N-R' compounds: A computational study

Farahnaz Maleki, Samaneh Hokmi, Mehdi Bayat, Sadegh Salehzadeh*

Faculty of Chemistry, Bu-Ali Sina University, Hamedan, Iran. Email: Saleh@basu.ac.ir

Keywords: Theoretical study, Imine, Electron donating and electron withdrawing substitutions, Interaction energy, NBO analysis, AIM analysis.

Introduction:

Imine compounds, characterized by the >C=N- functional group, have been the subject of numerous investigations, both experimentally and theoretically [1–2] since the C=N group has been found widespread application on organic synthesis and in many biological processes. As well-known, the substituent effect on physical and chemical properties of compounds has been an important focus of interest in chemistry [3]. The ability of to mediate structure and *E/Z* inversion isomerization was reported by experimental and theoretical investigations on some imine compounds [4], suggesting possibility to regulate isomerization process through substituent modification. In this work, we will focus on the substituent effect on C and N atoms in *E* and *Z* isomers of R-CH=N-R' compounds. For this purpose we consider the t-Bu and CF₃ substituents as electron donating and electron withdrawing groups, respectively, in a series of compounds with general formula R-CH=N-R' (R, R'=Me, CF₃, t-Bu).

Computational methods:

Calculations were performed using the Gaussian09 program. The structures of R-CH=N-R' (R, R'=Me, CF₃, t-Bu) have been optimized at the density functional theory (B3LYP, M06) levels with 6-311++G** and def2-TZVP basis sets. Then harmonic vibrational frequency was calculated at the same levels to confirm that the optimized structures are at local minima. All

frequencies in the compounds are real. The interaction energy was calculated with the formulas of $\Delta E = E_{AB} - (E_A + E_B)$, where E_{AB} is the energy of the compound $R-CH=N-R'$ and E_A and E_B are the energies of the $R-CH$ and $N-R'$ fragments. The NBO analysis was performed at the B3LYP and M06 levels with 6-311++G** and def2-TZVP basis sets for all of compounds by the NBO 3.1 program included in the GAUSSIAN 03 package of programs. Bader's Atoms in Molecules (AIM) method was used to analyze the chemical bonding in all molecules. AIM analyses were carried out for $X=Y$ bond with all of methods and basis sets.

Result and discussion:

For all of E and Z conformers of $R-CH=N-R'$ compounds a starting molecular mechanics structure for the DFT calculations was obtained using the HyperChem 8.08 program. The optimized structures are shown in Fig. 1. Wiberg bond indices of C=N bond and natural charge of C and N atoms in $R-CH=N-R'$ compounds were calculated using by NBO analysis. It was shown that the electron donating and electron withdrawing substituents do not affect considerably the Wiberg bond indices of C=N bond and natural charges of C and N atoms. Also, AIM calculations showed that the electron density (ρ) values of bond critical points in C=N bond are almost constant in the series of studied compounds. The results showed that the interaction energy between $R-CH$ and $N-R'$ fragments in E isomers are more than those in Z isomers. It seems that if the electron donating substituent is connected to the C atom and the electron withdrawing substituent is connected to the N atom of C=N bond, then the amount of interaction energy will be maximum. Thus (E)-Me-CH=N-CF₃ and (E)-(t-Bu)-CH=N-CF₃ compounds have largest and (Z)-(t-Bu)-CH=N-(t-Bu) has smallest interaction energies.

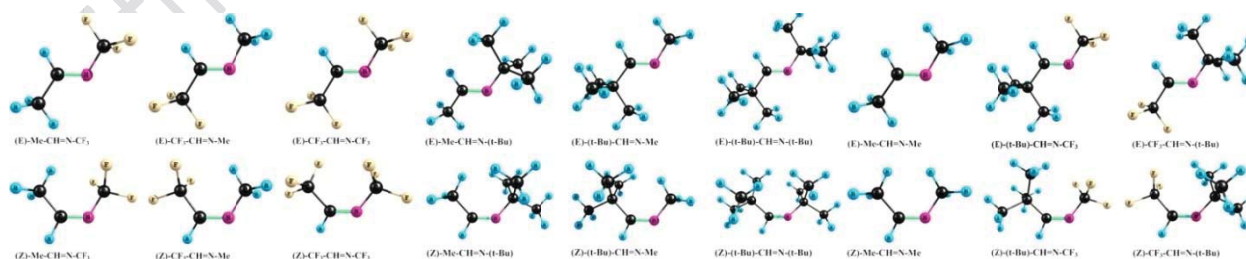


Fig 1. The optimized structures of $R-CH=NR'$ ($R, R' = CF_3, t-Bu, Me$) molecules at M06/def2-TZVP level

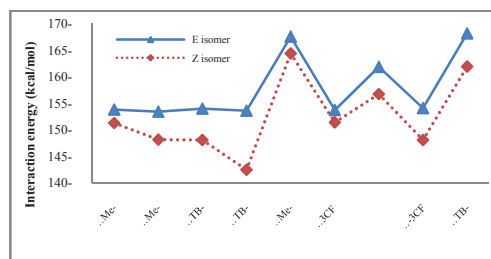


Fig 2. Interaction energy between R-CH and N-R' fragments in R-CH=N-R' compounds at M06/def2-TZVP level.

Table 1. Natural charge of C and N, Wiberg bond indices and ρ values of bond critical points of C=N bond in R-CH=N-R' compounds at M06/def2-TZVP level.

Compound	Natural charge		Wiberg bond indices of C=N bond	ρ of C=N bond
	C	N		
(E)Me-CH=N-Me	0.15	-0.41	1.96	0.40
(E)Me-CH=N-CF ₃	0.21	-0.50	1.94	0.39
(E)-CF ₃ -CH=N-Me	0.03	-0.34	1.91	0.41
(E)-CF ₃ -CH=N-CF ₃	0.09	-0.43	1.96	0.40
(E)-Me-CH=N-(t-Bu)	0.14	-0.42	1.92	0.40
(E)-(t-Bu)-CH=N-Me	0.17	-0.42	1.92	0.40
(E)-(t-Bu)-CH=N-(t-Bu)	0.16	-0.43	1.92	0.40
(E)-CF ₃ -CH=N-(t-Bu)	0.03	-0.36	1.96	0.40
(E)-(t-Bu)-CH=N-CF ₃	0.23	-0.51	1.87	0.39

Reference:

- [1] S. Salehzadeh, S. M. Nouri, H. Keypour, M. Bagherzadeh, Polyhedron; 24, 1478–1486, 2005.
- [2] W.M.F. Fabian, L. Antonov, D. Nedeltcheva, F.S. Kamounah, P.J. Taylor, J. Phys.Chem. A 108, 7603, 2004.
- [3] X.M. Pu, N.B. Wong, G. Zhou, J.D. Gu, A.M. Tian, Chem. Phys. Lett. 408, 101, 2005.
- [4] H. Yamataka, S.C. Ammal, T. Asano, Y. Ohga, Bull. Chem. Soc. Jpn. 78, 1851, 2005.

A theoretical study on the Diels–Alder reaction of 2-nitroindolizines

Mehdi Bayat^{*}, Fereshteh Yaghoobi, Samaneh Hokmi, Sadegh Salehzadeh^{*}

Faculty of Chemistry, Bu-Ali-Sina University, Hamedan, Iran (e-mail: Saleh@basu.ac.ir)

Key words: Theoretical study, Diels-Alder, Activation barriers

Introduction:

Since its discovery in 1928 [1] by otto Diels and kurt Alder, the Diels-Alder (D-A) reaction has become one of the most powerful tools in organic synthesis. The Diels-Alder (DA) reaction is perhaps the most widely used synthetic methodology for construction of a six-membered ring. In this work, we report a theoretical study on the Diels–Alder (DA) reactions of 1-methyl-3-(methoxycarbonyl)-2-nitroindolizine with R-1,3-butadiene (RCHCHCHCH₂) (R=F, Cl, CH₃, SiH₃)[2]. For this reaction, we considered two possible different pathways (Fig 1) in the presence and absence of methylaluminium dichloride as a catalyst. The relative energies and activation barriers of all model DA reactions in the gas phase and in methylene chloride were computed.

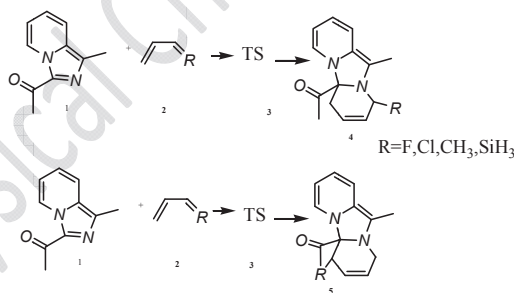


Fig.1

Computational methods:

All of the DA reactions were computed at the DFT (B3LYP/6-31+G**) level using GAUSSIAN 09 package.

Results and discussion:

The results show that the compound **4** is more stable than **5** when we use electron donating substituents. On the other hand, the compound **5** is more stable than **4** when we use electron

withdrawing substituents. The final results show us that both the electron donating and electron withdrawing substituents on 1,3-butadiene decrease the formation enthalpy of both compounds 4 and 5 in comparison with 1,3-butadiene[3]. As shown in Fig 2, in the presence of methylaluminium dichloride the co-ordination of organoaluminium reagent to the carbonyl oxygen increases the activation barrier compared to that for the uncomplexed 2-nitroindolizine.

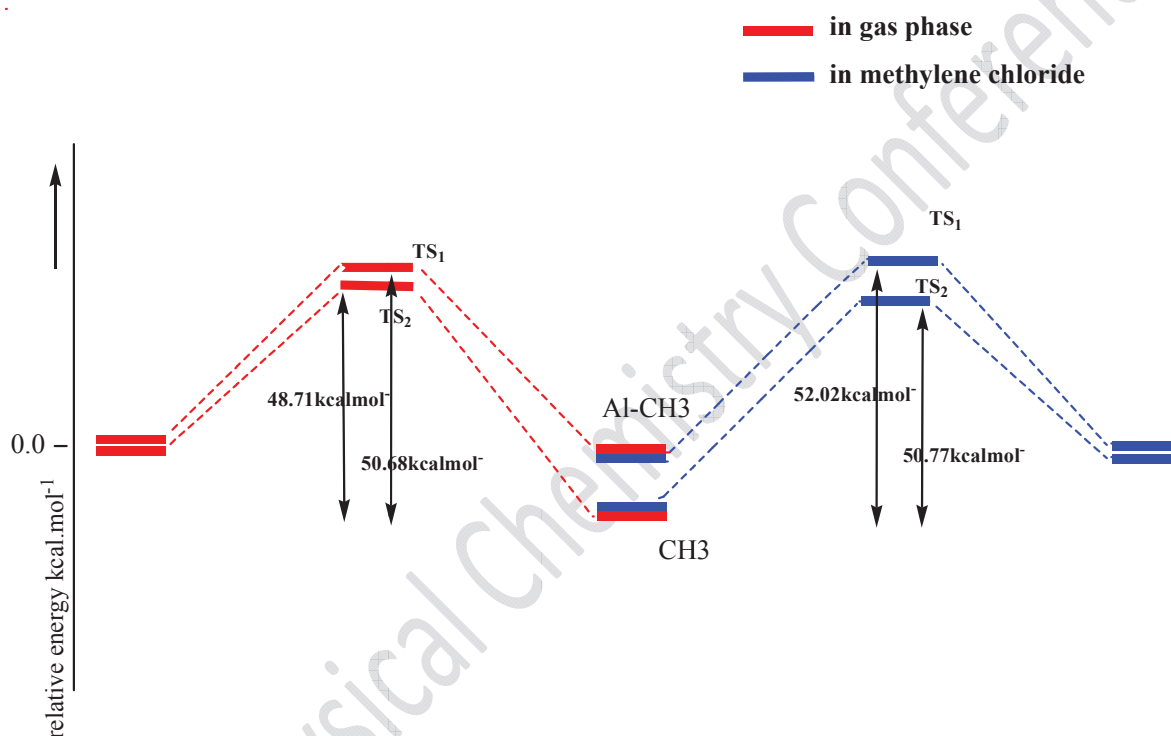


Figure 2. Activation barriers for the DA reactions of 2- nitroindolizine complexes calculated at B3LYP/6-31+G level.

Conclusion:

The results show that in the presence of electron donating substituents the compound **4** is more stable than **5** but when we use electron withdrawing substituents the compound **5** is more stable than **4**.



References:

- [1] O. Diels, K. Alder, *Ann*, 460 (1928) 98.
- [2] Bansal, R. K.; Gupta, N.; Kumawat, S. K. *Tetrahedron* 2006, 62, 1548.
- [3] R.K. Jangid, N.Gupta, G.Frenking, *Tetrahedron Letters* 52 (2011) 1721–1724

15th Physical Chemistry Conference



Ion-pairs formed in ([Mim⁺][N(CN)₂⁻]) ionic liquid: A quantum chemistry Study

H. Roohi ^{*a}, Sh. Khyrkhah ^b

^aDepartment of Chemistry, Faculty of Science, University of Guilan, Rasht, Iran.

Email: hroohi@guilan.ac.ir

^bDepartment of Chemistry, Faculty of Science, University of Guilan, Rasht, Iran.

Key words: Quantum chemistry, Methyl imidazolium dicyanamid, Ionic liquid

Introduction:

Ionic liquids are room temperature molten salts which have recently attracted much interest due to some of their unique properties such as non-volatility, high ionic conductivity, nonflammability, high thermal stability, wide electrochemical window, etc [1-3]. The ionic liquids generally consist of a large asymmetric organic cation and an inorganic/organic anion. They can be used as solvents for a wide range of organic and inorganic reactions and their unique properties make them important candidates for the so-called “green chemistry” [4-5].

Methods:

All the structures studied in this work were fully optimized, without symmetry restrictions using B3LYP, MP2, M052X and M062X methods in conjunction with 6-311++G(2d,2p) basis set. All calculations were performed using the Gaussian 03 program package. The NBO analysis was carried out on the MP2/6-311++G(2d,2p) wave functions using version 3.1 of NBO package included in Gaussian 03 program package.

Result and discussion:

The ionic liquid modeled herein is the cation Mim⁺ (methyl imidazolium) coupled with the anion N(CN)₂⁻. The equilibrium structures obtained from interaction between ion pairs are depicted in Fig. 1. The Mim⁺ has various sites available for hydrogen bond formation. As can

be seen in Fig. 1, $\text{N}(\text{CN})_2^-$ can be placed in five regions in vicinity of Mim^+ . In **A** and **B** ion pairs, two N atoms of $\text{N}(\text{CN})_2^-$ act as proton acceptors and N–H and C–H bonds of Mim^+ as proton donors. In **C**, **D** and **E** ion pairs, instead of N–H, the C–H bonds in Mim^+ acts as proton donors. The **A** and **B** complexes are the most stable ones at all levels of theory. BSSE and ZPVE corrected BEs of **A** to **E** ion pairs at all levels of theory are ordered as

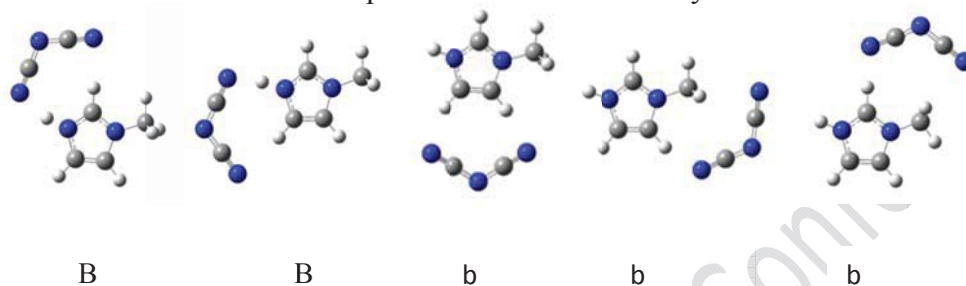


Fig. 1. Optimized structures of Mim^+ and $[\text{Mim}+\text{N}(\text{CN})_2^-]$ ion pairs.

Binding energies (kcal/mol) calculated for $[\text{Mim}+\text{N}(\text{CN})_2^-]$ ion pairs at various levels of theory

Ion pair	Method	Basis set	BSSE	BE_e	$\text{BE}_e^{\text{BSSE}}$	BE_0	$\text{BE}_0^{\text{BSSE}}$
A	M062X	6-311++G(2d,2p)	0.29	-93.84	-93.6	-93.4	-93.1
	MP2		2.65	-95.24	-92.6	-90.6	-87.9
B	M062X	6-311++G(2d,2p)	0.29	-89.4	-89.1	-89.3	-89.0
	MP2		2.39	-91.0	-88.6	-86.8	-84.4
C	M062X	6-311++G(2d,2p)	0.22	-78.8	-78.6	-78.2	-78.0
	MP2		1.98	-79.6	-77.6	-74.9	-72.9
D	M062X	6-311++G(2d,2p)	0.22	-78.1	-77.9	-77.2	-77.0
	MP2		2.03	-78.3	-76.3	-73.5	-71.5
E	M062X	6-311++G(2d,2p)	0.24	-81.3	-81.0	-80.2	-80.0
	MP2		2.10	-82.2	-80.1	-77.7	-75.6

$\text{BE}_e^{\text{BSSE}}$ = Electronic binding energy (BE_e) + BSSE, $\text{BE}_0 = \text{BE}_e + \Delta\text{ZPE}$, $\text{BE}_0^{\text{BSSE}} = \text{BE}_0 + \text{BSSE}$.

A > **B** > **E** > **C** > **D**. Lowering of energy for **A** and **B** complexes is attributed to N–H...N and C–H...N interactions. The N–H and C–H bonds of Mim^+ ring involved in interaction are elongated and C–H bonds of methyl group are shortened upon complex formation. Population analysis shows that the charge transfer taking place from $\text{N}(\text{CN})_2^-$ to Mim^+ upon complex formation.

Conclusions:



Five cyclic complexes are predicted with two hydrogen bonds involved in each of them. The BE of $[\text{Mim}^+ \text{N}(\text{CN})_2^-]$ complexes changes depending on the binding site. Our results show that ion pair **A** is more stable than others in gas phase.

References:

- [1] A. Triolo, O. Russina, B. Fazio, G.B. Appetecchi, M. Carewska, S. Passerini, J. Chem. Phys. 130 (2009) 164521.
- [2] L. Gong, W. Guo, J. Xiong, R. Li, X. Wu, W. Li, Chem. Phys. Lett. 425 (2006) 167.
- [3] N.R. Dhumal, Chemical Physics 342 (2007) 245.
- [4] P. Wasserscheid, T. Welton (Eds.), Ionic Liquids in Synthesis, Wiley-VCH, Weinheim, 2003.
- [5] A. Triolo, O. Russina, B. Fazio, G.B. Appetecchi, M. Carewska, S. Passerini, J. Chem. Phys. 130 (2009) 164521.

Cis-enol tautomerism of Ethyl-2, 4-dioxo-4-phenyl butanoate: A theoretical study

S. Salemi^a, E.S. Banihashemi^{a*}

^a Department of chemistry, Hakim Sabzevari University, Sabzevar, Iran

Email: e77_banihashemi@yahoo.com

Key words: Cis enol tautomerism, Ethyl-2, 4-dioxo-4-phenylbutanoate, Density function theory, proton transfer

Introduction:

It is well known that the cis-enol form of β -diketones is characterized by a strong intramolecular hydrogen bond [1-4]. Ethyl-2,4-dioxo-4-phenyl butanoate (EDPB) is stabilized by a relatively strong intramolecular hydrogen bond (IHB). Two different isomeric cis-enol forms are distinguishable in EDPB. The EDPB1 is the most stable conformer of EDPB. An inter conversion occurs by transfer of enol proton from one oxygen atom to the other atom [5] (Fig1).

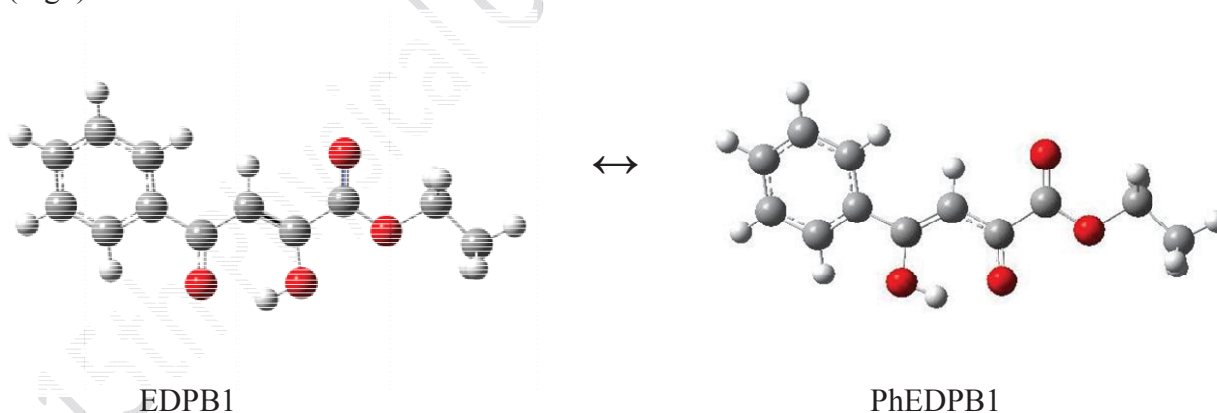


Fig.1: inter conversion by transfer of enol proton between phEDPB1 and EDPB1

Methods:



We applied the methods in Gaussian program package by means of density function theory at B3LYP/6-311++G** level of theory.

Result and discussion:

From the theoretical point of view, fifty enol forms can be drawn for EDPB molecule of which thirteen of them are engaged in six-member ring intramolecular hydrogen bond. The energy of EDPB1 is lower than phEDPB1 by 0.18 kcal/mol. Free energy difference $\Delta G_{298}^0 = (G_{\text{phEDPB1}}^0 - G_{\text{EDPB1}}^0) = -0.065$ kcal/mol. Hydrogen bond energy, E_{HB} (the energy difference between the chelated and trans enol rotamers) is 14.51 and 10.21 kcal/mol for phEDPB1 and EDPB1, respectively. This conclusion is well supported by the theoretical O-H stretching frequency in 3035.67 and 3079.17 cm^{-1} for phEDPB1 and EDPB1, respectively. Substitution of phenyl group in C-OH side, phEDPB1 conformers, increases the C=O and C=C bond lengths by 0.007 and 0.017 Å, respectively, while the C-C bond length decreases by 0.025 Å. These changes in the bond lengths indicate that the π -electron delocalization in the enol ring slightly increases by phenyl substitution in the hydroxyl side. Substitution of phenyl group in the carbonyl side only increases the C=O bond length and changes in the other bond length are negligible. The result suggests that in phEDPB1 conformer, the phenyl group is conjugated only with the C=O group [5].

Conclusion:

According to DFT calculations the EDPB1 \leftrightarrow phEDPB1 equilibrium in EDPB should be shifted towards EDPB1. The hydrogen bond in phEDPB1 is stronger than that in EDPB1. This effect is due to the increase in π -electron delocalization in the chelated ring by the phenyl group. The electron-withdrawing group (such as COOEt) in the β -position weakens the IHB while increasing the enol content.

References:

- [1] A.H. Lowery, C. George, P.D. Antonio, J. Karle, J. Am. Chem. Soc. 93 (1971) 6399.
- [2] R.S. Brown, A.T. Nakashima, R.C. Haddon, J. Am. Chem. Soc. 101 (1979) 3175.
- [3] J. Emsley, Structure and Bonding, 2, Springer, Berlin, 1984



- [4] F. Hibbert, J. Emsley, Hydrogen bonding and Chemical Reactivity, Advanced in Physical Chemistry, 26, Academic Press, London, 1990, p. 255.
- [5] S.F. Tayyari, J.S. Emampour, M. Vakili, A.R. Nekoei, H. Eshghi, S. Salemi, M. Hassanpour. J. Mol. Struct. 794 (2006) 204.

15th Physical Chemistry Conference



The conformational and vibrational assignment studies of ethyl-2, 4-dioxo-4-phenyl butanoate

S. Salemi, E.S. Banihashemi^{a*}

^a Department of chemistry, Hakim Sabzevari University, Sabzevar, Iran

Email: e77_banihashemi@yahoo.com

Key words: Ethyl-2, 4-dioxo-4-phenylbutanoate, Intramolecular hydrogen bond, Density function theory, Conformational analysis

Introductions:

β -dicarbonyls are capable of keto-enol tautomerism. The cis-enol form of β -dicarbonyl compounds are stabilized by a strong intramolecular hydrogen bond with a double minimum character [1-4]. Ethyl-2, 4-dioxo-4-phenyl butanoate (EDPB) has two β -substituted groups with different electron-withdrawing strength. This compound is consisting of conformers with six-member chelated ring and seven-member chelated rings that only six-member is engaged in intramolecular hydrogen bond (IHB) system. The hydrogen bond strength of the most stable conformer of EDPB is compared with that of dimethyl oxaloacetate (DMOA) [5].

Methods:

We applied the calculation in Gaussian program package. The chelated cis-enol and the corresponding open conformers of EDPB optimized at B3LYP levels by using 6-311G and 6-311++G^{**} basis set and MP2/6-311G level. The vibrational frequency calculations were carried out for the most stable conformer at the B3LYP/6-311++G^{**} level of theory.

Results and discussion:

EDPB has two β -substituted groups with different electron-withdrawing strength. Depending on the position of the enolated proton, the occurrence of two classes of cis-enol form is

possible. From the theoretical point of view, fifty enol and twenty-four keto conformers can be drawn for EDPB molecule of which thirteen of them are engaged in six-member ring intramolecular hydrogen bond. EDPB1 (Fig.1) is the most conformer of EDPB molecule. The calculated hydrogen bond energy for EDPB1 is about 32.67 kJ/mol, calculated at MP2/6-311G level of theory. The O...O distance for EDPB1 is about 2.53 Å which indicate the hydrogen bond in EDPB is stronger than that in DMOA (2.62 Å). The effect of the phenyl and COOEt groups on the π -delocalization in the chelated ring could be explained in terms of the Gilli's symmetry coordinates (Q , q_1 , q_2 and λ) [6]. These parameters also compared with DMOA which that suggests that the π -systems such as phenyl group increase the H-bond strength through conjugation with the enol ring. O-H stretching frequency and out-of-plane bending appear in 3079.11 and 913.34 cm^{-1} which confirm the hydrogen bond in EDPB is stronger than of the DMOA.

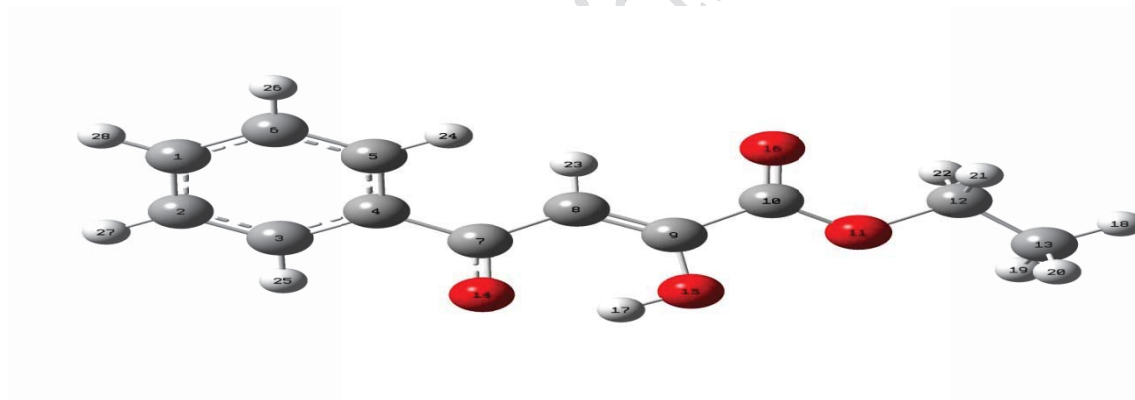


Fig. 1. The most stable conformer (EDPB1) and atomic numbering system.

Conclusion:

According to the calculation, the IHB stabilizes the cis-enol form of EDPB by 49.11 kJ/mol, which is 18.01 kJ/mol more than that for DMOA. Substitution of OMe group in DMOA by phenyl group increases the hydrogen bond strength. Comparison of the vibrational spectra and structural parameters of EDPB with those of DMOA reveals a stronger H-bond in EDPB than that in DMOA. From the DFT calculations, we understand enol conformers that are



engaged in IHB system are more than stable of their keto forms and enol conformers don't have IHB are less than stable of their keto forms.

References:

- [1] A.H. Lowery, C. George, P.D. Antonio, J. Karle, J. Am. Chem. Soc. 93 (1971) 6399.
- [2] R.S. Brown, A.T. Nakashima, R.C. Haddon, J. Am. Chem. Soc. 101(1979) 3175.
- [3] J. Emsley, Structure and Bonding, 2, Springer, Berlin, 1984.
- [4] R. Boese, M.Y. Antipin, D. Blaser, K.A. Lyssenko, J. Blaser, Chem. B 102 (1998) 8654.
- [5] S.F. Tayyari, S. Salemi, M. Zahedi-Tabrizi, M. Behforouz, J. Mol. Struct. 694 (2004) 91.
- [6]. V. Bertolasi, P. Gilli, V. Ferretti, G. Gilli, J. Am. Chem. Soc. 113 (1991) 4917.



Determination of acidic Dissociation Constant of L-Alanyl-L-Alanine in water Using ab initio Methods

Nesa Shafiei ^{a*}, Farhoush Kiani ^b, Mahmoud Tajbakhsh ^c, and Fereydoon Ashrafi ^a

^a Department of Chemistry, Faculty of Science, University of Payamnoor, Sari, Iran

^b Department of Chemistry, Faculty of Science, Islamic Azad University, Ayatollah Amoli Branch, Amol, Iran

^c Department of Organic Chemistry, Faculty of Chemistry, University of Mazandaran, Babolsar, Iran

Email: n_shafiee_ch@yahoo.com

Keyword: pK_a, Solvation free energy, Ab initio methods, L-Alanyl-L-Alanine.

Introduction:

Peptides are increasingly attractive as therapeutics give their diverse biological functions and potentially high potency and target specificity.¹ Proton transfer reactions constitute an important class of chemical reactions and have been studied extensively over a long period of time.² Studies of the acidity of organic compounds are of the fundamental importance and play a very important role in the evaluation of activity, reaction mechanisms and structure of organic compounds.^{3,4} As pK_a equals $\Delta G/2.303RT$, where ΔG is a free energy change of the dissociation reaction either in a gas or solution, activity of compound can be determined by the ΔG values.⁶

Computational method:

In this study structures were optimized by the semi empirical PM3 method in program Hyperchem version 8.0.8 for windows. All calculations were performed using Gaussian 98w version 5.2. DFT calculations were done using the hybrid exchange – correlation functional of Becke, Lee, Yang, and Parr (B3LYP) and the Gaussian 6-31G (d) basis set was used.

To analyze the solvent effects on all species involved in the selected ionization reaction, the polarized continuum model (PCM) of Tomasi et al. was used.⁵

Results and Discussion:

The acidic dissociation constants of L-Alanyl-L-Alanine have been determined using potentiometric technique. The method of determining acidic dissociation constant was previously described and its values are used in this work. These values are listed in Table 1 together with the calculated values using the Tomasi's method at the B3LYP/6-31+G(d) level of theory.

Table 1. Values of pK_a for Protonation of L-Alanyl-L-Alanine Obtained Using the Tomasi Method at the B3LYP/6-31+G(d) level of theory, at 298.15 K

Species	Selected Equations	pK _a (Calculated)	pK _a (Experimental)
L-Alanyl-L-Alanine	$H_2L^+(H_2O)_2 \rightleftharpoons HL(H_2O):UZ + H_3O^+$	3.2570	3.30 (I=0.1, NaClO ₄)
	$HL(H_2O)_3:UZ + H_2O \rightleftharpoons L^-(H_2O)_3 + H_3O^+$	8.0361	8.14 (I=0.1, NaClO ₄)

I. ionic strength.

UZ. unzwitter form.

Conclusions:

In this paper, pK_a values of L-Alanyl-L-Alanine were successfully calculated with high accuracy by using ab initio methods. The B3LYP/6-31+G(d) is employed and found to be sufficiently accurate in predicting the gas – phase acidities. The calculated results show very good agreement with experimental data in all studied solvents. The regression calculated results are as follows:

$$Y=1.0160X-0.4946$$

References:

- [1] Chereau, P.; Allary, C. Therapeutic Peptides under the Spotlight. *Eur. Biopharm. Rev.* **2005**, 88– 91.



- [2] Aue, D. H.; Bowers, M. T.; in: Bowers, H. T. (Ed). *Gas Phase Ion Chemistry*. Academic Press: New York. Chapter 9. **1979**, 2.
- [3] March, J. *Advanced Organic Chemistry: Reactions, Mechanisms, and Structure*, 2nd ed.; McGraw-Hill Book Co.: New York, **1977**.
- [4] Cram, D.J. *Fundamentals of Carbanion Chemistry*; Academic Press: New York, **1965**.
- [5] Kiani, F.; Rostami, A. A.; Sharifi, S.; Bahadori, A.; Chaichi, M. J. Determination of Acidic Dissociation Constant of Glycine, Valine, Phenylalanine, Glycylvaline, and Glycylphenylalanine in Water Using ab initio Methods. *J. Chem. Eng. Data*. **2010**, 55, 2732-2740.



Prediction of retention index of atmospheric volatile organic compounds dataset using QSPR methods.

N. Goudarzi, S. Mesgaran Karimi *, M. Arab chamjangali

Faculty of Chemistry, Shahrood University of Technology, P.O.Box 316, Shahrood, Iran

Email: S.mkarimi@yahoo.com

Key words: Volatile organic compounds, QSPR, SR-ANN, GA-ANN

Introduction:

Volatile organic compounds (VOCs) are organic chemical that have high vapor pressure at ordinary, room temperature conditions. Their high vapor pressure results from a low boiling point, which causes large numbers of molecules to evaporate or sublime from the liquid or solid form of the compound and enter the surrounding air. Many VOCs are dangerous to human health or cause harm to the environment. Also, VOCs play an important role in communication between plants [1]. Therefore, it is necessary to measurement of VOCs in ambient air. Quantitative structure-property relationship (QSPR) studies are the most extensively used methods in computational chemistry. In this study, we used from nonlinear QSPR method of ANN to predict of retention index of some atmospheric volatile organic compounds (VOCs).

Material and Methods:

The dataset was used in this work, containing retention indices of 60 volatile organic compounds. Firstly, by using stepwise regression method we selected descriptors and then ANN were used for building of nonlinear models to predict of retention index. Descriptors were selected by this method including; G1, mor09m, RDF035v, GATS3v, RDF045u, BEHm3, moro6v. In the second part, we used genetic algorithm as variable selection tools. The best descriptors were selected by GA including; G1, H2u, x2sol, RDF035v, mor09v, mor09m, H2m. Then, these descriptors were used for building model to predict of RI by ANN method.

Results and Discussion:

Dataset randomly was divided in to three section including training (36 compounds), validation (12 compounds) and test (12 compounds) sets. The important parameters that affect on modeling power of ANN such as transfer function, training function, the number of epoch, momentum and the number of nodes in input and hidden layers were optimized. The obtained results show the superiority of SR-ANN than GA-ANN to predict of RI of these compounds. The determination coefficients (R^2) and mean squared error (MSE) for SR-ANN model and GA-ANN model are 0.999, 0.998, 36.29 and 41.55 respectively.

The plot of the predicted values of RI against experimental for SR-ANN model are shown in Figure 1. Also, the Figure 2 represent the distribution of residual versus experimental values of RI.

Figure 1: The plot of predicted values of RI against experimental

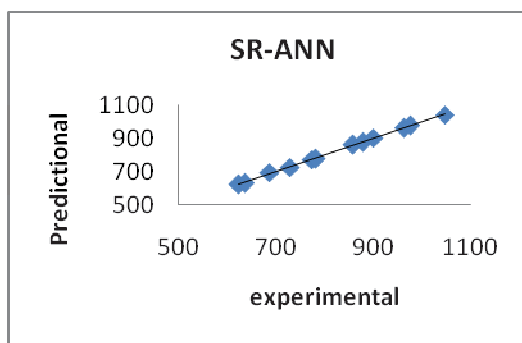
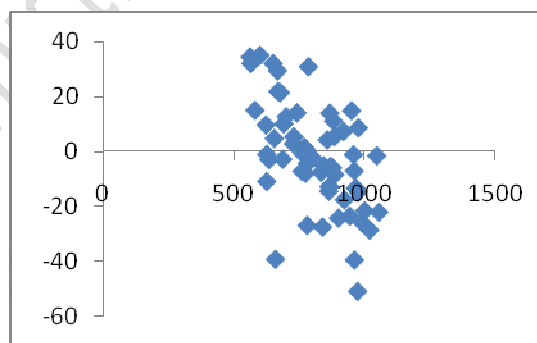


Figure 2: distribution of residual versus experimental values of RI



Conclusion:

ANN is used as feature mapping technique for predict of retention index of some atmospheric volatile organic compounds. Two methods, stepwise regression (SR) and genetic algorithm (GA) were used as variable selection techniques. The results obtained reveal the superiority of SR-ANN over the GA-ANN model. Descriptors appearing in these QSPR models provide information related to different molecular properties, which can affect the retention index of a compound in GC separation.

References:



- [1] Directive 2008/50/EC. Directive 2008/50/EC of the European Parliament and of the council of 21 May 2008 on ambient air quality and cleaner air for Europe. Official Journal of the European Communities 2008; L152:1.
- [2] N. Goudarzi, M. Goudarzi, (2009) *Molecular Physics* 107:1739-1744
- [3] N. Goudarzi, M. Goudarzi, Araujo M.C.U, Galvao R.K.H, (2009) *J. Agric. Food Chem.* 57:7153-7158

15th Physical Chemistry Conference



Electron Density Analysis of Unusual Oxygen-Oxygen Bonds in Benzoyl Peroxide

Sara Ranjbar^b, Sara Fakhraee^{*,a}

^a Department of Chemistry, College of Sciences, Payame Noor University, Shiraz, Iran.

^b Department of Chemistry, College of Sciences, Azad University, Marvdasht, Iran.

*Email: fakhraee@pnu.ac.ir

Key words: Atoms in molecules, benzoyl peroxide

Introduction:

Benzoyl peroxide (BPO) is an organic compound consists of two benzoyl groups bridged by a peroxide link. This compound has important application in improving flour, bleaching hair and teeth, polymerizing polyester and many other uses [1]. The O-O bond in peroxides is so weak and BPO readily undergoes homolysis (symmetrical breaking) forming free radicals $C_6H_5CO_2^{\bullet}$ [2]. The reactivity of BPO and its derivatives is directly affected by the properties of O-O bond. In this work, nature of O-O bond in BPO in the present of electron donor and acceptor substituents is investigated at ortho, meta and para positions. The atoms in molecules (AIM) analyses are applied to evaluate the bond properties of O-O.

Theoretical method:

The BPO structure with two perpendicular benzoyl groups was considered as a reference structure. This structure is more stable than the planar structure in energy. The Br, OH, Cl, CN, COOH and phenyl (Ph) groups are substituted symmetrically in para, meta and ortho positions of two benzoyl rings of peroxide. Geometry optimization, energy and wave function calculations were performed at B3LYP/6-311++G** level of theory by using Gaussian.03W program. Frequency analysis was performed to ensure that all structures are in energy minima. The AIM analysis on wave functions was carried out by the AIM2000 program.

Results and discussion:

The AIM graphs, critical points (CP) and bond critical points (BCP) have been demonstrated in Fig.1. Table 1 represents the AIM parameters of CP 3 correspond to O₂-O₃ bond in peroxide groups. The positive values for $\nabla^2\rho$ and negative values for H_b indicate partially covalent and partially electrostatic nature of O₂-O₃ bond in BPO and all its derivatives. Two different types of substituents including activating and deactivating towards the aromatic rings were considered in ortho, meta and para positions. Groups with unshared pairs of electrons are strongly activating like OH. Halogens possess unshared pair of electrons. But, since halogens are substantially more electronegative than carbon, they draw electron density away from the pi system deactivate ring. The non-halogen groups with atoms that are more electronegative than carbon, such as CN, COOH and also Ph groups draw substantial electron density from the pi system. These groups are also deactivating groups. It is expected that the activating and deactivating groups show different behavior in substitution on BPO.

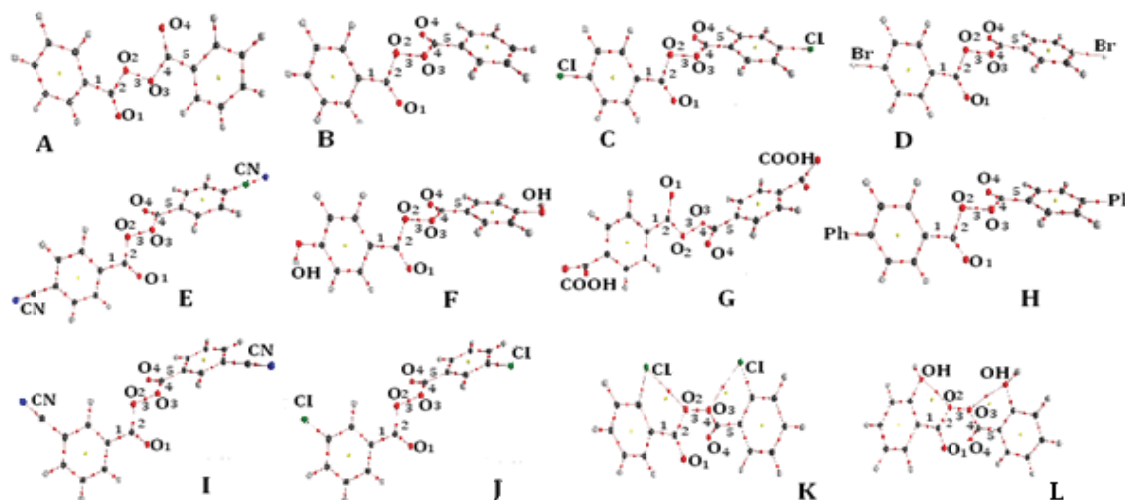


Figure 1: AIM graph, critical points, bond critical points, for structures in Table 1.

Table 1: Bond length, electron density, laplacian of electron density and kinetic and potential and total electronic energy of the critical point 3 in O-O peroxide bond. (M), (O) and (P) refer to meta, ortho and para substitutions, respectively.

	<i>Molecules</i>	<i>Bond length</i>	ρ_b	$\nabla^2 \rho_b$	G_b	V_b	H_b
A	BPO (Planar)	1.435	0.2875	+0.0328	0.2030	-0.3978	-0.1948
B	BPO (Vertical)	1.427	0.2928	+0.0268	0.2087	-0.4106	-0.2019
C	BPO-Cl (P)	1.426	0.2932	+0.0248	0.2088	-0.4118	-0.2030
D	BPO-Br (P)	1.426	0.2932	+0.0252	0.2088	-0.4113	-0.2025
E	BPO-CN(P)	1.427	0.2931	+0.0252	0.2087	-0.4111	-0.2024
F	BPO-OH(P)	1.426	0.2934	+0.0244	0.2089	-0.4117	-0.2028
G	BPO-COOH(P)	1.425	0.2942	+0.0224	0.2094	-0.4133	-0.2039
H	BPO-Ph (P)	1.427	0.2929	+0.0264	0.2087	-0.4108	-0.2021
I	BPO-Cl (M)	1.427	0.2932	+0.0259	0.2088	-0.4111	-0.2029
J	BPO-CN(M)	1.427	0.2934	+0.0240	0.2089	-0.4117	-0.2028
K	BPO-Cl (O)	1.441	0.2817	+0.0680	0.2036	-0.3903	-0.1867
L	BPO-OH(O)	1.436	0.2863	+0.0492	0.2053	-0.3983	-0.1930

But, according to Table 1, substitutions on para and meta positions, regardless of their activating or deactivating properties towards the aromatic ring, keeps the bond length and AIM parameters almost unchanged respect to reference BPO (vertical). But, applying Cl and OH substituents in ortho position creates two new bond paths with electrostatic (closed shell) character between substituents and O₂ or O₃ atoms in peroxide. The resulting O-Cl halogen bond in K and O-O bond in L structures decrease the ρ_b and increase the bond length of O₂-O₃. This reduces the covalent and increases the electrostatic character of the oxygen-oxygen bond of peroxide to the level of planar molecule.

Conclusion:

Oxygen-oxygen bond nature of benzoyl proxide is highly affected by ortho substitutions bonds of peroxide regardless of the activating or deactivationg types of substituents.

References:

- [1] Brodie, B. C. (1858), Ann. Chem. **108**, 79–83.
- [2] Li, Hui, III (1998), Synthesis, Characterization and Properties of Vinyl Ester Matrix Resins, Ph.D. Dissertation, University of Vermont, Chapter 2.



Evaluation of Chemical and physical properties of copper ions in boron nitride nanotube

M. Seyed Hosseini

Department of Chemistry, Science and Research Branch, Islamic Azad University, Tehran, Iran

Key words: boron nitride , Chemical and physical properties, copper ions

Introduction:

A variety of subjects of BNNTs have been investigated by theoretical methods, including hydrogen storage ,magnetism [1], phonon characteristics [2], stability [3],molecular dynamics, field-electron emission [4], scanning tunneling microscopy simulation , electron transport , symmetry breaking [5], work function , spin-splitting and thermodynamics of yield. Since there are no synthesis techniques to control chiral angles and diameters of CNTS, BNNTs are considered to be better suited for some electronics applications in which the uniform electronic property is desirable . The electronic structures of boron nitride (BN) nanotubes under a transverse and perpendicular electric field were investigated with theory (DFT) calculations [6].

Computational methods:

In order to analyze the molecular interaction potential of the nanotubes interacting with Cu cations we have carried out calculations on Hartree–Fock (HF) wavefunction with lanl2dz basis set. The first, we have optimized a (4,4) armchair nanotube $B_{16}N_{16}$ and also performed a single point calculation at the HF/lanl2d_z for nanotubes $B_{16}N_{16}(Cu^{2+}, Cu^{+})$.

Result and discussion:

1. Energy:

The total energy of molecule, including all forms of kinetic motion (translation, vibration, and rotation) and all forms of potential energy (electrostatic interaction between charges, magnetic



interactions between spinning charges, and potential energy of bonds), determines the reactivity and stability of a molecule

2. Electrical Potential:

We calculated the potential difference for boron and nitrogen atoms in the nanotube with the central ions and reported in terms of various properties such as total energy, dipole moment, quadrupole moment, changes of gap energy.

3. Investigation on Crystal Field Theory and Jahn Teller distortion:

After hydrogen bonding and strong electrostatic interactions (e.g., charge–charge, charge–dipole, and dipole–dipole), the most significant non covalent interactions in biological applications are probably those involving aromatic p systems. Orbital energy splitting in the field of nano-tubes for Cu^{2+} , Cu^+ cations shown in Figure.

Conclusion:

In splitting of d-orbitals, because probably the d_z^2 –orbital located on z axis, so this states is more stable and has the lowest energy. Splitting orbitals in the $\text{B}_{16}\text{N}_{16}$ (Cu ions) nanotube field is almost similar to the square-planar field. It seems that Jahn Teller distortion in the nanotube field is slightly different from the usual field. We compared difference Electrical potential in Cu-ions in table.

Reference:

- [1] J.B. Wu, W.Y. Zhang, Solid State Communications 149 (2009) 486.
- [2] I. Savic, N. Mingo, D.A. Stewart, Physical Review Letters 101 (2008) 165502.
- [3] G.Y. Gou, B.C. Pan, L. Shi, Journal of Physical Chemistry C 112 (2008) 19353.
- [4] V. Meunier, C. Roland, J. Bernholc, M.B. Nardelli, Applied Physics Letters 81 (2002) 46.
- [5] M. Ishigami, J.D. Sau, S. Aloni, M.L. Cohen, A. Zettl, Physical Review Letters 97 (2006) 176804.
- [6] Claudio Attaccalite, 1, Ludger Wirtz^{1, 2}, Andrea Marini³, and Angel Rubio, phys. stat. sol. (b) (2007) 244, No. 11, 4288–4292 .



Investigation NMR and NBO properties of B₁₂N₁₂ nanotube

M. Seyed Hosseini

Department of Chemistry, Science and Research Branch, Islamic Azad University, Tehran, Iran

Key words: NBO, NMR properties, B₁₂N₁₂ nanotube

Introduction:

Boron nitride (BN) is one of the most interesting III–V compounds due to its unique properties, such as low density, high thermal conductivity, excellent mechanical strength wear resistance, stability at high temperatures, and possibility of easy doping with silicon (n-type) and beryllium (p-type). Thus, the material appears as a good alternative for carbon-related materials in several applications[1-3]. BN is a structural equivalent of carbon. It is mostly found in the same phases and produces similar nanostructures. This is probably because the B–N bonding tends to be dipolar and average the number of electron per atom to 2 in the 2P layer as for carbon. (carbon is 2P², nitrogen is 2P³, boron is 2P¹). Armchair nanotubes are formed when $n = m$ and the chiral angle is 30°. All other nano tubes, with chiral angles intermediate between 0° and 30°, are known as chiral nanotubes[4].

Computational Details:

The geometry of nanotubes B₁₂N₁₂ has been optimized by Beck's hybrid three-parameter exchange functional and the nonlocal correlation functional of the Lee, Yang, and Parr (B3LYP) method with the EPR-II basis sets of Baron[5]. The Gaussian quantum chemistry package was used for all calculations. EPR-II is a double-basis set with a single set of polarization functions and an enhanced S part, for H and for B-F.

Result and discussion:

1. Natural Bond Orbital (NBO) Analysis:

The concepts of natural atomic orbital (NAO) and NBO analyses are useful for distributing electrons into atomic and molecular orbitals used for the one-electron density matrix to define



the shape of the atomic orbitals in the molecular environment and then derive molecular bonds from electron density between atoms.

2. Analysis of Chemical Shift and Chemical Shielding in NMR:

In the standard convention, the principal components of the chemical shift tensor, $(\delta_{11}, \delta_{22}, \delta_{33})$, are labeled according to the IUPAC rules [6]. NMR shielding constants and corresponding parameters for BNNT's are shown in Table.

Conclusion:

In the nanotube $B_{12}N_{12}$, coefficients orbitals is between 0.4600 to 0.5070 for boron and 0.8619 to 0.8879 for nitrogen. Our results in NBO calculation indicate that average the number of electron per p orbital in BNNT's $B_{12}N_{12}$ is $p^{1.64}$ for B atoms, and $p^{2.17}$ for N atoms respectively. NMR shielding constants and corresponding parameters calculated and reported for BNNTS.

Reference:

- [1] D. Golberg, Y. Bando, M. Mitome, (2002) Physica B 323, 60.
- [2] R. Zedlitz, M. Heintze, M.B. Schubert, (1996) J. Non-Cryst. Solids 198, 403
- [3] A. Zettl, (1996) Adv. Mater. 5, 443.
- [4] [13] Masa Ishigami, Shaul Aloni, and A. Zettl (2003) 12th international conf. American Institute of Physics.
- [5] Lee, C.; Yang, W.; Parr, R. G. (1998) Phys. Rev. B, 37, 785.
- [6] M. Mehring, (1983) Springer Verlag: Berlin Principles of High Resolution NMR in Solids, 2nd ed. H. W. Spiess, (1978) Springer Verlag, Berlin In NMR Basic Principles and Progress; P. Diehl, E. Fluck, R. Kosfeld, Eds: Vol. 15.



Interaction between selenium analogues of methimazole and M^{z+} (Na^+ , Li^+ , K^+ , Be^{2+} , Ca^{2+} and Mg^{2+}): A quantum chemical study

H. Roohi ^{*a}, P. Fakour^b

^aDepartment of Chemistry, Faculty of Science, University of Guilan, Rasht, Iran

^bDepartment of Chemistry, University of Payame Nour, Abhar, Iran

Email: hroohi@guilan.ac.ir

Keywords: selenium analogues, **MSeI** complexes, binding energy

Introduction:

The methimazole as an anti-thyroid drug and its selenium analogue (3-methyl-1H-imidazole-2(3H)-selenone) (**MSeI**) has been a focus of many investigations [1]. Roy et al. [2] have studied the structural activity correlation of the anti thyroid drugs by using a number of sulfur and selenium analogues. Anti-thyroid drugs can interact with the electron acceptors such as cations [3]. Owing to the vast biochemical activity of anti-thyroid drugs, different experimental and theoretical investigations have been performed on these molecules [4]. In the present work, interaction between M^{z+} (Li^+ , Na^+ , K^+ , Mg^{2+} , Ca^{2+} and Be^{2+}) and **MSeI** has been investigated at various levels of theory.

Method:

All calculations were performed using Gaussian 03 program package. The geometry of the monomers and dimmers **MSeI** was optimized at MP2/6-311++G(2d,2p) level of theory. The counterpoise procedure was used to correct the basis set superposition error (BSSE) in the calculation of the interaction energies.

Results and discussion:

Two planar and non-planar (Fig. 1) complexes were found on the potential energy surface of interaction between **MSeI** and M^{z+} cations. The binding energies for **MSeI**- M^{z+} complexes calculated at the MP2/6-311++G(2d,2p) are given in Table 1. It is found that the non-planar

forms are more stable than planar ones. The binding energy of **MSeI**– M^{z+} complexes changes depending on the type of cation. Among the cations, Be^{2+} complexes have the strongest binding strength while K^+ complexes have the weakest. Alkaline metal cations are more stable than alkali ones. As can be seen in Table 1, BSSE corrected binding energies are smaller than uncorrected ones at the same level of theory.

Table 1. Calculated binding energies (kJ/mol) of the MSeI– M^{z+} complexes at MP2/6–311++G(2d,2p) level

M^{z+} Complexes	ΔE_e	ΔE_e^{BSSE}
Li(plan)	-194.55	-189.53
Li(perp)	-201.52	-196.16
Na(plan)	-140.98	-136.92
Na(perp)	-147.35	-143.17
K(Plan)	-108.86	-106.28
K(Perp)	-112.68	-109.96
Be(plan)	-998.04	-987.22
Be(perp)	-1027.16	-1016.23
Mg(Plan)	-605.74	-599.18
Mg(Perp)	-634.38	-627.72
Ca(plan)	-409.13	-404.70
Ca(perp)	-421.83	-417.29

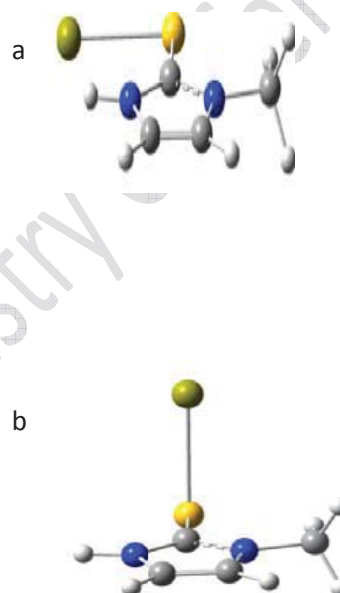


Fig. 1. (a) Planar and (b) non-planar structures of complexes

Conclusions:

Based on the binding energy, stability of **MSeI**– M^{z+} complexes increases in the following order: $K^+ < Na^+ < Li^+ < Ca^{2+} < Mg^{2+} < Be^{2+}$. For alkali and alkaline metal cations increase in the atomic number within the same group of elements is accompanied with the decrease in the binding energy. In other world, as the size of cation decreases, binding strength increases.



References:

- [1] H.Roohi, S.Baghery; "Theochem" 910, 41, 2009.
- [2] G.Roy, D.Das, G.Mugesh; "Inorg.Chem.Acta" 360, 303, 2007.
- [3] S.F.Boys, F. Bernardi; " Mol. Phys" 19, 553, 1970.
- [4] H.Roohi, A.Ebrahimi, S.M.Habibi; " J. Mol. struct" 710, 77, 2004.

15th Physical Chemistry Conference



Tautomeric properties of a Schiff base derived from thiosemicarbazide and 5-chloro salicylaldehyde : NBO and AIM analyses

R. Behjatmanesh-Ardakani^a, H. Kargar^a, B. Daieakbari^{*a}

^aDepartment of Chemistry, Payame Noor University, P.O. Box 19395-3697 Tehran, IRAN

*Email: b.daieakbari@yahoo.com

Keywords: AIM, NBO, Intramolecular hydrogen bond, Tautomer.

Introduction:

Hydrogen bond interaction is one of the non-covalent interaction which plays an important role in solvation process, supramolecular chemistry and in the properties of various materials. The proper hydrogen bond is represented as X-H...Y, where X and Y are electronegative atoms. There is an interaction between Lone pair orbitals of the proton acceptor "Y" with the antibonding orbitals of the proton donor "X" and this can be explained using Weinhold's natural bond orbital (NBO) analysis [1].

Computational methods:

Geometry optimization for the three tautomers of the titled compound were performed with Gaussian 09 program [2] applying the B3LYP/6-311++G(2d,2p) theoretical level. Analyses of data were done with AIM2000 [3] and NBO programs [4].

Result and discussion:

Figures 1, 2 and 3 show optimized geometry structures of the three tautomeric forms of (E)-1-(5-chloro-2-hydroxy benzylidene).

Data in table 1 shows that there is an strong intramolecular interactions between N₄...H₁₅-O₃ in all three tautomers.



Figure 1. Structure of tautomer 1

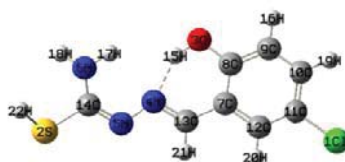


Figure 2. Structure of tautomer 2



Figure 3. Structure of tautomer 3

Table 1. Calculated topological properties for selected critical point of studied tautomers

Tautomer	E	ρ	$E^{(2)}$	∇^2	Δ
tautomer 1	-883282.37	14.77	0.038	0.103	0.54
tautomer 2	-883273.83	19.94	0.045	0.102	0.59
tautomer 3	-883266.68	14.95	0.038	0.104	0.54

According to table 1, the electron density (ρ) and second-order perturbation energy $E^{(2)}$ shows that hydrogen bond in tautomer 2 is stronger than the others. This result is confirmed by comparing NBO charges on N₄ atom that are -0.33, -0.39, -0.31 for tautomer 1, tautomer 2, and tautomer 3, respectively.

Conclusion:

All three tautomers have strong intramolecular hydrogen bonds. Among above structures, tautomer 2 has higher $E^{(2)}$ and electron density at hydrogen bond critical point.

References:

- [1] P. Kolandaivel, V. J. Nirmala, Mol. Struct ; 694, 33-38, 2004.
- [2] M.J. Frisch et al., Gaussian 09, Revision A.02, Gaussian, Inc., Pittsburgh PA, 2009
- [3] F. Biegler-König, J. Schönbohm, D. Bayles, AIM2000- A program to analyse and visualize atoms in molecules, J. Comput. Chem ; 22, 545, 2001.
- [4] E.D. Glendening, A.E. Reed, J.A. Carpenter, F. Weinhold, NBO version 3.1.

Methoxy position effects on donor and acceptor interactions in schiff bases derived from 5-amino-thiadiazole-2-thiol.

R. Behjatmanesh-Ardakani^a, H. Kargar^a, H. Habibi^{a*}

^aDepartment of chemistry, Payame Noor University, PO BOX 19395-3697 Tehran, IRAN

*Email: habibeh.habibi@yahoo.com

Keywords: AIM, NBO, Hydrogen Bonding, BCP.

Introduction:

The azole compounds are of significant importance to medicinal chemistry because of their biological and pharmaceutical properties. The azole group is present in various drugs such as omeprazole, mebendazole, astemizole, and emedastine difumarate [1]. The molecules under study have a O—H···N intramolecular hydrogen bond (see Fig. 1).

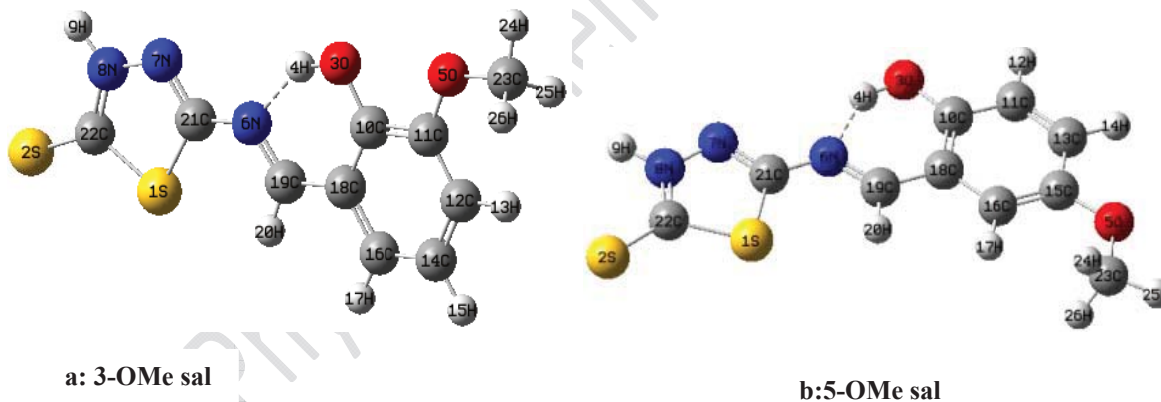


Fig.1. The structure of compounds with hydrogen bonds.

Methods:

All calculations were done with B3LYP/6-311++G(2d,2p) level of theory with Gaussian 09 [2]. Topological parameters at bond critical points (BCP) have been analyzed by Bader's 'Atoms in molecules' AIM theory. The natural bond analyses (NBO) were applied for evaluation of the hydrogen bond strength in the title compounds.

Result and discussion:

1. AIM analysis:

The "atom in molecules" of Bader [3] is a very useful method for the estimation of hydrogen bond energy. The Bader theory is based on topological properties of electron density (ρ), Laplacian ($\nabla^2\rho$), kinetic energy (G), total energy (H) and potential energy (V) at the bond critical points (BCP). The topological parameters of the titled compounds are shown in table 1.

Table 1: Topological parameters of the investigated molecules.

	$\rho(r)$	$\nabla^2(\rho)$	$G(r)$	$V(r)$	$H(r)$	
a	0.044	0.1064	0.032	-0.037	0.005	0.58
b	0.043	0.1056	0.031	-0.026	0.005	0.41

2. NBO analysis:

The NBO analysis was carried out using version 3.1 of NBO package [4]. The results of NBO analysis show $n(N6) \rightarrow n^*(H4)$ charge transfer with energy of 29.61 and 31.8 kcal/mol for compounds a and b, respectively

Conclusion:

Data show that there are strong hydrogen bonds in both compounds. However comparing AIM and NBO results show that methoxy group in para position gives rise to stronger hydrogen bond.

Reference:

- [1] T. Sakai, T. Hamada, N. Avada, J. Watanabe, *Pharmabiol. Dyn.* (1989) 530.
- [2] M.J. Frisch, et al.; *Gaussian 09*, Revision A.02.
- [3] R.F.W. Bader, *Chem. Rev.* 91 (1991) 893.
- [4] E.D. Glendening, A.E. Reed, J.E. Carpenter, F. Weinhold, *NBO*, Version 3.1, Gaussian, Inc., Pittsburgh, PA, 1992.

Application of a two-dimensional potential function for calculating tunneling frequency of tropolone

M. Rasouli, M. Zahedi-Tabrizi

Department of Chemistry, Faculty of Science, Alzahra University, Tehran, Iran

Email: zahedi@alzahra.ac.ir

Keywords: Potential energy surface, Two-dimensional potential function, Tunneling frequency, Tropolone.

Introduction:

Tropolone and related molecules are one of the best known species where proton transfer occurs through a tunneling mechanism. Those molecules have been extensively studied both from the experimental and the theoretical points of view. Tropolone (TRN) is a seven-membered pseudoaromatic notable for its hydrogen-atom tunneling in a symmetric double minimum potential well. The intramolecular hydrogen bond in tropolone (TRN) has been studied extensively over the last two decades as it offers a model system in which to study proton transfer (PT) in the ground (S_0) and first excited singlet $\pi\pi^*$ (S_1) states.

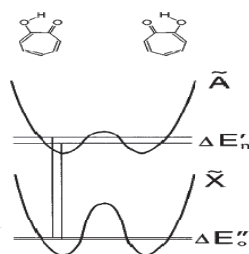


Fig.1. Tropolone molecule and its schematic potential curve.

Methods:

All ab initio calculations in this work were performed using the GAUSSIAN 03W. The optimization also performed at B3LYP/6-31G**, B3LYP/6-31G*, MP2/6-31G** and G96LYP/6-31G* levels. To explore two-dimensional proton tunneling, we have varied the

O–H distance in TRN from 0.9 to 1.3 Å and the COH angle from 25 to 50° and calculated the energies at all above levels by fixing all other parameters at their optimized equilibrium positions at the same levels. The potential energy surfaces obtained at these levels were fitted to the following anharmonic two-dimensional potential function:

$2V = K_s X^2 + K_{ss} X^4 + K_b Y^2 + K_{ssb} X^2 Y$ Where K_s and K_{ss} represent the quadratic and quartic force constants in the X (stretching) direction respectively, K_b represents the quadratic force constant in Y (bending) direction and K_{ssb} represent the interaction between stretching and bending modes. The obtained Hamiltonian matrix, then, was diagonalized. We calculated coefficients of two dimensional potential function equation by SPSS16.0 and MAPLE12.0 programs. Also we depicted contours of this potential function via MAPLE program. Furthermore we used this coefficient to calculate tunneling frequency and barrier height by FORTRAN POWER STATION 4 program.

Results and discussions:

Table 1 summarizes the transition frequencies for various cutoffs imposed on the potential energy of the hydrogen motion (i.e. the restriction imposed on the amplitude of hydrogen motion).

Table 1. Transition frequencies calculated at different levels.

	$ 0,0\rangle_+ \rightarrow 0,0\rangle_-$		$ 0,0\rangle_- \rightarrow 0,1\rangle_+$		$ 0,0\rangle_+ \rightarrow 0,1\rangle_-$		$ 0,0\rangle_- \rightarrow 1,0\rangle_+$		$ 0,0\rangle_+ \rightarrow 1,0\rangle_-$		$ 0,0\rangle_- \rightarrow 0,2\rangle_+$	
	H	D	H	D	H	D	H	D	H	D	H	D
MP2/6-31G**	3.0	0.1	1380.0	1074.5	1457.8	1079.0	2238.3	1809.0	2477.7	1834.9	2762.1	2120.5
G96LYP/6-31G*	11.0	0.7	1118.0	931.6	1322.4	957.3	1959.1	1559.1	2351.0	1696.5	2527.3	1877.2
B3LYP/6-31G**	6.1	0.3	1293.8	1037.7	1429.2	1049.2	2128.6	1725.2	2432.1	1783.7	2679.4	2027.6
B3LYP/6-31G*	5.4	0.3	1295.0	1034.9	1420.5	1045.0	2125.0	1722.6	2415.9	1774.3	2661.9	2019.2

Conclusion:

A simple two-dimensional potential function was applied to calculate the hydrogen-bond transition frequencies in TRN. In this method, ab initio programs were used to generate a two dimensional potential energy surface, which correctly predicted the equilibrium molecular



geometries. The results are in excellent agreement with experimental tunneling frequency that is 0.9 and 0.1 cm⁻¹ for light and deuterated systems respectively.

Reference:

- [1] R. Casadesus et.al., Chem. Phys. Lett., 405 (2005), 187-192.
- [2] D. Murdock, L.A. Burns, P.H. Vaccaro, Chem. Phys. , 12 (2010), 8285-8299.
- [3] R.L. Redington, J. Chem. Phys., 113(2000), 2319-2335.



Quantum study of effect of inhibition some Schiff base compounds in the mild steel corrosion in Sulfuric acid environment

M. Hamadani*, M. H. Hadizadeh

Department of Chemistry, Faculty of Science, University of Kashan, Kashan, Islamic Republic of Iran

E-mail: hadizadeh.mh@gmail.com

Keywords: “Quantum study, Schiff base, Corrosion, Inhibitors ”

Introduction:

Mild steel is widely used as a substantial material in many industries such as power plants, petroleum industries and etc [1], due to its low cost and good mechanical properties [2-3]. Acid solutions such as Hydrochloric acid are widely used for the removal of rust, industrial cleaning, acid pickling, petrochemical processes and acid descaling of ferrous alloys and steel. Schiff bases, are organic compounds that due to the presence of the $-C=N-$ group, electronegative nitrogen, oxygen and/or sulfur atoms in the molecule, have been reported to be efficient inhibitors of corrosion for steel and alloys in acid media. Although experimental means are useful to investigation the corrosion inhibition but they are often time consuming and costly.

Methods:

Among quantum chemical methods, the DFT has some merits, one of which is the inclusion of the relativistic effect as an electron correlation term. So far, a hybrid version of DFT and Hartree Fock (HF) methods, i.e. B3LYP, has been introduced as one of the most accurate methods for energy calculation [4-5].

Results and discussion:

The new Schiff base structures of SB1 to SB17 were investigated as corrosion inhibitors of mild steel. Possible correlations between experimental inhibition efficiencies and quantum

chemical parameters such as dipole moment (μ), highest occupied (E_{HOMO}) and lowest unoccupied (E_{LUMO}) molecular orbitals were investigated. The models of the inhibitors were optimised with the Density Functional Theory formalism (DFT) using hybrid B3LYP/6-311G** as a higher level of theory. The Quantitative Structure Activity Relationship (QSAR) approach has been used and composite index of some quantum chemical parameters were constructed in order to characterize the inhibition performance of the tested molecules. To reduce the difference between theoretical and experimental values, a corrected equation was used that based on Inhibition efficiency is determined with more precision. In order to study the corrosion inhibition of the Schiff base structures, the basic structure (SB) was optimized using DFT at the B3LYP/6-311G** basis set level. Then each of the agent groups CH₃, OH, F, NO₂ were replaced in four different positions instead of hydrogen atoms and the optimization procedure was performed for sixteen Schiff base structures. It should be noted that in order to facilitate the naming, the position of agent groups in the primary structure, is displayed with letters R1, R2, R3, R4 (Fig 1). Furthermore, obtained relationships were used for different Schiff base structures from various articles and all of them acknowledged that corrected inhibition efficiency is closer to values of the experimental efficiency.

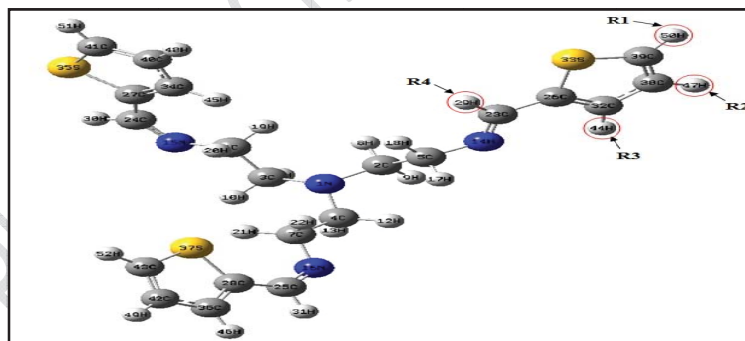


Fig. 1. The position of agent groups in the primary structure (SB) shown with R1, R2, R3, R4

Conclusions:

Although the Quantitative Structure Activity Relationship (QSAR) approach as a famous model has been used to determine the inhibition efficiency in many papers nevertheless still



there is a clear difference between theoretical and experimental values. Using the equation of corrected inhibition efficiency presented in this article this difference is lowest. It is interesting that this equation encompasses a wide range of Schiff base structures, this means that corrected Inhibition efficiency is more accurate than non-corrected.

References:

- [1] G. Schmitt, Br. Corros. J. 19 (1984) 165.
- [2] A.Y. Musa, A.A.H. Kadhum, M.S. Takriff, A.R. Daud, S.K. Kamarudin, N. Muhamad, Corros. Eng. Sci. Tech., doi: 10.1179/147842208X386359.
- [3] A.Y. Musa, A.A. Khadom, A.A.H. Kadhum, A.B. Mohamad, M.S. Takriff, J. Taiwan Inst. Chem. Eng. 41 (2010) 126.
- [4] N. Lopez, F. Illas, Ab initio modeling of the metal–support interface: the interaction of Ni, Pd, and Pt on MgO (1 0 0), J. Phys. Chem. B 102 (1998) 1430–1436.
- [5] A. Ignaczak, J.A.N.F. Gomes, Interaction of halide ions with copper: the DFT approach, Chem. Phys. Lett. 257 (1996) 609–615.



Computational Insights of Gas Phase Cluster Ions: Chloride Ion with (CH_{4-m} Cl_m) (m=0-4)

A. Abedi*¹, M. Gharibi², M. Barat³

¹Islamic Azad University, Shahreza Branch, abedi@iaush.ac.ir

²National Petrochemical Company- Petrochemical Research & Technology Co. (NPC-RT), m.gharibi@npc-rt.ir

³ Islamic Azad University, Shareza Branch, mahsa.barat@yahoo.com

Key Words: Halomethanes, Calculation Study, Basis Set, Interaction Energy, Halide Ion.

Introduction:

The interest in gas phase ion-molecule complexes has produced in recent years a large result on binding energies and affinity scales. Such in the case, the bond energies for the cluster ions of halides ion X⁻ with organic molecules would give the fundamental information about structures, thermochemical stabilities, binding energies, and charge transfer of complexes [1-4].

The study of small haloalkanes has broad-reaching implications in the understanding of atmospheric chemistry. Methane, CH₄, is abundant at mid stratospheric levels, while CH₃Cl is one of the most abundant halogenated methane in nature. The relative strengths of carbon-halogen bonds also have other important atmospheric consequences. In this study we performed density-functional-theory (DFT) and higher levels of ab initio calculations on Cl⁻ with methane and chloromethanes (CH_{4-m} Cl_m) (m=0-4) to assess the experimental bond energies. All calculations have been carried out by using the Gaussian 98 program.

Method:

Geometries of Cl⁻ ...CH₄ and Cl⁻ ... (CH_{4-m} Cl_m) (m=1-4) were optimized using the B3LYP, MP2, and other higher ab initio calculations at different basis sets such as 6-311++g (d,p) . The diffuse functions (+) are indispensable to describing properly anionic systems. Subsequent

vibrational analyses were made to check whether the bonding geometries are correctly at the energy minimum and obtain the zero-point vibrational energies (ZPEs). To evaluate electronic energies of ion clusters accurately, we made single point calculations on optimized geometries at QCISD and CCSD (T) levels.

Results and discussions:

The interactions of Cl^- with neutral molecules H-R range from hydrogen bond to electrostatic bond. The B3LYP results include partially the electron-correlation effect and the suitable geometry of $\text{Cl}^- \dots \text{CH}_4$ and $\text{Cl}^- \dots (\text{CH}_{4-m} \text{Cl}_m)$ ($m=1-4$) clusters are in good agreement with experimental data. According to the results, in terms of energy levels of molecular orbitals, CHCl_3 is a good electron acceptor (electrophile) and the most stable complex was formed between CHCl_3 molecule and Cl^- ion because of large dipole moment of this molecule. Also, the methane molecule is bounded very weakly to Cl^- halide ion (Fig. 1).



Figure 1. The optimum geometries of Cl^- with a) CH_4 , b) CHCl_3 molecules.

Conclusions:

The study of small haloalkanes is important in the understanding of atmospheric chemistry. Interaction of these molecules with ions has effect on ozone layer. In this work standard high-level theoretical methods were used to predict the optimized geometries, energies and other properties of $\text{Cl}^- \dots \text{CH}_4$ and $\text{Cl}^- \dots (\text{CH}_{4-m} \text{Cl}_m)$ ($m=1-4$) clusters ions. Our calculations show



that there is a good agreement between the calculated thermochemical stabilities, binding energies, and charge transfer in this work and those obtained experimentally.

References:

- [1] W. S. McGivern, A. Derecskei-kovacs, S. W. North, J. Phys. Chem. 104 (2000) 436-442.
- [2] J. Novoa, M. Whangbo, Chem. Phys. lett. 180 (1991) 241-248.
- [3] J. Novoa, M. Whangbo, Chem. Phys. lett. 177(1991) 483-490.
- [4] A. Bagno, A. Dono, S. Martinucci, Int. J. Mass Spectrom. 179/180 (1998) 349-357.

DFT/B3LYP Study of the Substituent and Solvent Effects on the Reaction Enthalpies of Homolytic and Heterolytic N–H Bond Cleavage in Melatonin Derivatives

Meysam Najafi, Davood Farmanzadeh*

Department of Physical Chemistry, Mazandaran University, Babolsar, Iran

(Email: d.farmanzad@umz.ac.ir, najafimm@yahoo.com)

Keywords: Natural Antioxidant, Melatonin, Solvent Effect, Reaction Enthalpy, Substituent.

Introduction:

Melatonin is an animal and plant hormone, its ability to scavenge hydroxyl radicals was discovered and scavenges free radicals [1]. The reaction between free radicals and antioxidants can follow different mechanisms (HAT, SET-PT and SPLET) [2]. The reaction enthalpy of the first step of HAT, SET-PT and SPLET mechanism corresponds to the BDE, IP and PA, respectively [3]. Understanding the role of different structural features and preparation of new compounds with enhanced antioxidant property is of great interest. Melatonin structure (Figure 1) represents the basic structure. Various substituents such as electron-withdrawing groups (EWG) and electron-donating groups (EDG) were located in three available positions on the aromatic ring (Figure 1). We have investigated the substituent effect on reaction enthalpies of homolytic (HAT mechanism) and heterolytic two-step (SPLET and SET-PT) mechanisms of N–H bond cleavage for mono-substituted melatonins in gas phase and water.

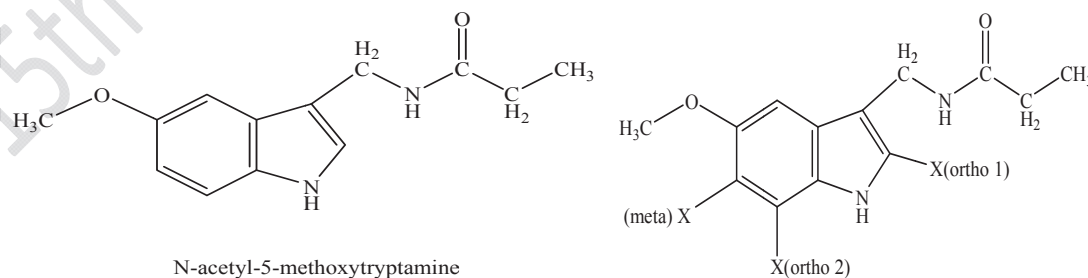


Figure 1. Structure and substituted of melatonin (X = Br, Ethyl, CH=CH₂, CCH, CF₃, Me, Cl, CN, COMe, COH, COOH, F, NMe₂, NHMe, NH₂, NO₂, OMe, OH, Ph, t-Bu).



Computational details:

The geometry optimization of the molecules and respective radicals, radical cations and anions was performed using DFT method with B3LYP functional and the 6-31G (d, p) basis set in the gas-phase and water. Single point calculations were performed for 6-311++G (2d, 2p) basis set [4]. Solvent contribution to the total enthalpies was computed employing integral equation formalism IEF-PCM method [5]. Total enthalpies were calculated for 298.15 K and 1.0 atmosphere pressure with Gaussian 03 program package.

Results and Conclusions:

In this article, the reaction enthalpies of the individual steps of three antioxidant action mechanisms, HAT, SET-PT and SPLET, for various mono-substituted melatonins were calculated in gas-phase and water. Obtained results indicate that electron-donating substituents induce rise in PAs, whereas electron-withdrawing groups cause increase in the reaction enthalpies of the processes, where electron (IPs) or hydrogen atom is abstracted (BDEs). Substituents placed in *ortho* positions show larger effect on reaction enthalpies in comparison to the same groups in *meta* position. Water attenuates the substituent effect on all reaction enthalpies. In gas-phase, BDEs are lower than PAs and IPs, i.e. HAT represents the thermodynamically preferred pathway. On the other hand, SPLET mechanism represents the thermodynamically favored process in water. IP and BDE values can be correlated with the length of indolic $R(N-H)^{+}$ bond length and partial charge on the indolyl radical nitrogen, $q(N)$, of the studied molecules successfully. Calculated results reveal that in the case of EWG-substituents, E_{HOMO} values become more negative, while the presence EDG-substituents results in less negative E_{HOMO} values. Therefore, melatonins with strong electron-donating groups are better electron donors. It has been also found that PA and IP values for substituted melatonins can be estimated from their E_{HOMO} values. This fact may be useful for the development of new melatonin based antioxidants.

References:

- [1] G. W. Burton, M. G. Traber, *Annu. Rev. Nutr.* **1990**, 10, 357-382.
- [2] G. Litwinienko, K.U. Ingold, *J. Org. Chem.* **2004**, 69, 5888-5896.



- [3] M. C. Foti, C. Daquino, C. Geraci, *J. Org. Chem.* **2004**, 69, 2309–2314.
- [4] A. D. Becke, *J. Chem. Phys.* **1993**, 98, 5648–5652.
- [5] E. Cancès, B. Mennucci, J. Tomasi, *J. Chem. Phys.* **1997**, 107, 3032–3041.

15th Physical Chemistry Conference



The influence of aliphatic amino acid side groups on the acidity of Lysine by density functional theory

Zeinab Shabani^{a*}

Mohammad Reza Bozorgmehr^a, Mohammad Momen Heravi^a

*zeinabshabani66@gmail.com

^a Department of chemistry, Faculty of science, Mashhad Branch, Islamic Azad University, Mashhad, Iran

key words: Lysine, Acidity constant, solvation free energies, DFT.

Introduction:

The peptides are an amazing class of compounds. Although they are all constructed from relatively simple building blocks (the amino acids), they exhibit a remarkable range of biological properties; because of their medicinal properties that the study of peptides has become one of the most active area of current research [1]. Lysine is an essential amino acid, which means that the human body cannot synthesize it and must obtain it through food sources. The concepts of acidity (K_a , $pK_a = -\log K_a$) and proton transfer are essential to physical and structural chemistry [2]. Oftentimes pK_a values can be measured quite easily experimentally; however, many times chemists are interested in the pK_a values of molecules that have not been synthesized or for which experiments are not straightforward. For instance, amino acids that are part of a polypeptide chain have pK_a values that very based on their local environment, which are difficult to determine [3]. In this study we performed a theoretical calculation for determination of side group exchange effects on the Lysine acidity.

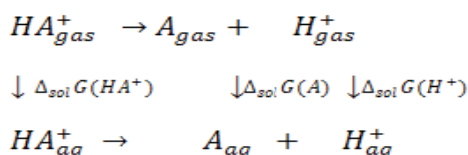
Methodology:

According to the most common thermodynamic cycles have been used to calculated pK_a values of lys^+ (denoted as HA^+) equals $pK_a = \frac{\Delta G_{aq}}{RT \ln 10}$, where $\Delta G_{aq} = \Delta G_{gas} + \Delta \Delta G_{sol}$ is free

energy change of the dissociation reaction either in a gas or solution, acidity of a compound can be determined by the ΔG value.

Apparatus:

The Gaussian 03[4] tool using B3LYP method and the standard 6-311++G (d,p) basis sets has been applied for optimization and frequency calculations for all structures. The polarized continuum model (PCM) [5] was used to describe the solvent effects.



Result and discussion:

According to our calculation solvated free energies and pK_a values at the standard condition are reported in table below. Based on this result we can propose the following acidity order for the dipeptides:



Kcal/mol	$\Delta_s G(AH^+)$	$\Delta_s G(A)$	$\Delta_a G$	pK_a
$\text{Lys}^+ \rightarrow \text{lys}$	-61.3654	-13.8830	12.6553	9.2760
$\text{Met-lys}^+ \rightarrow \text{met-lys}$	-52.7465	-17.3650	07.5625	5.5688
$\text{Cys-lys}^+ \rightarrow \text{cys-lys}$	-64.1076	-17.7201	05.5357	4.0884
$\text{Gly-lys}^+ \rightarrow \text{gly-lys}$	-59.4660	-16.3241	06.9110	5.0890

Conclusion:

In this study we have calculated the acidity constant (pK_a) of lysine in Lysine – Aliphatic (methionine, cysteine, glycine) amino acid dipeptides using the Density Functional Calculation and continuum solvation methods. Based on our results $\Delta_s G$ values are located between -13.8830 and -64.1076 kcal mol⁻¹ which are related to Lys and Cys-Lys⁺ respectively. According to our calculations pK_a values are between 4.0884 and 9.2760 that belong to Cys-Lys⁺ and lys⁺ forms, respectively.



Reference:

- [1] F. Kiani, A. Rostami, S. Sharifi, A. Bahadori, Journal of Molecular Structure: THEOCHEM 2010 ,956(20-25)
- [2] T.N. Brown, N.M. Diez, Journal of Physical Chemistry 2006,110(9270-9276)
- [3] K.S. Alongi, G.C. Shields, Theoretical Calculations of Acid Dissociation Cnstants :A Review Article, John Wiley and Sons, New York,2005
- [4] M. J. Frisch, G. W. T., H. B. Schlegel, G. E. Scuseria, M. A. Robb, J. R. Cheeseman, J. A. Montgomery, T. Vreven, K. N. Kudin, J. C. Burant, J. M. Millam, S. S. Iyengar, J. Tomasi, V. Barone, B. Mennucci, M. Cossi, G. Scalmani, N. Rega, G. A. Petersson, H. Nakatsuji, M. Hada, M. Ehara, K. Toyota, R. Fukuda, J. Hasegawa, M. Ishida, T. Nakajima, Y. Honda, O. Kitao, H. Nakai, M. Klene, X. Li, J. E. Knox, A. D. Daniels, M. C. Strain, O. Farkas, D. K. Malick, A. D. Rabuck, K. Raghavachari, J. B. Foresman, J. V. Ortiz, Q. Cui, A. G. Baboul, S. Clifford, J. Cioslowski, B. B. Stefanov, G. Liu, A. Liashenko, P. Piskorz, I. Komaromi, R. L. Martin, D. J. Fox, T. Keith, M. A. Al-Laham, C. Y. Peng, A. Nanayakkara, M. Challacombe, P. M. W. Gill, B. Johnson, W. Chen, M. W. Wong, C. Gonzalez, J. A. Pople, Gaussian 03, Revision B.03; Gaussian. Inc.Wallingford, CT, U.S: 2004.
- [5] S. Miertus, E. Scrocco, Tomasi, J. Chem. Phys. 1981, 55, 117.
- [6] Hudáky, P.; Perczel, A., The Journal of Physical Chemistry A 2004, 108 (29), 6195-6205.



DFT study of interaction of nitrosamine with single-walled BN nanotubes

M. Zakarianezhad^{a*}, B. Makiabadi^b, S. Zareei^a, P. Mohammaddadi^a

^aDepartment of Chemistry, Payame Noor University, Tehran, Iran

^bIran Department of Chemical Engineering, Sirjan University of Technology, Sirjan, Iran

E-mail: mzakarianezhad@pnu.ac.ir

Keywords: Functionalization, Electronic Properties, BN43zz nanotube, Formamide

Introduction:

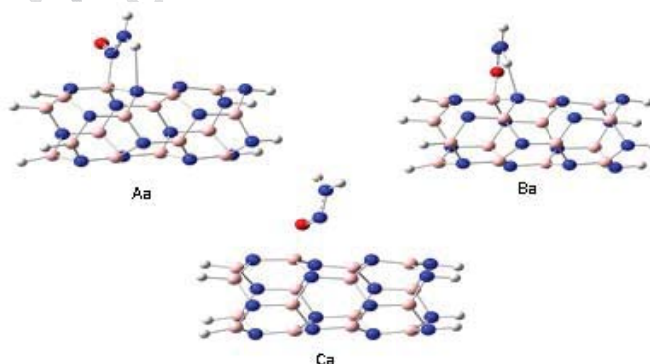
Boron nitride nanotubes are semiconductors with a wide band gap (5.5 eV), weakly depending on the diameter, the helicity, and the number of tube walls [1]. The functionalized or doped BNNTs, which exhibit dramatic changes in electronic properties with respect to their pristine counterparts, further enlarge the application in nanomolecular range. Many studies have been performed on the adsorption of various molecules on the boron nitride nanotubes. Nitrosamines constitute a family of potent carcinogens and mutagens compound which are formed readily from a diverse set of nitrogen compounds and nitrites or its derivatives [2]. Nitrosamines occur as contaminants in different food categories and beverages [3]. The aim of this study is to investigate the adsorption of nitrosamine on single wall boron nitride nanotube. We studied the reactivities of NH_2NO toward BNNTs and effect of that upon electronic and structural properties of BNNTs.

Computational methods:

For the study of interactions between NH_2NO molecule and BN43zz nanotube, DFT computations were carried out using B3LYP hybrid density functional method and the 6-311++G (d) basis set. In our calculations, BN43zz nanotubes were chosen. The first and second numbers in the label represent the number of hexagonal rings around the circumference of the tube and along the tube axis, respectively.

Result and discussion:

To investigate the adsorption of a NH_2NO molecule on middle ring of BN43zz nanotube, we have considered all the possible sites including the site on top of B and N atoms, and at the bridge sites of B-N bonds. We find that three different configurations (A, B and C) are possible for the adsorption this molecule. We assume that each of the configurations A and B is further divided into four subconfigurations a, b, c and d whereas, the configurations C is further divided into two subconfigurations a and b (scheme 1). Totally, we found ten minima structures on the potential energy surface in the adsorption of NH_2NO on middle ring of BN43zz nanotube. In A configuration, N and H atoms of NH_2NO are involved in the adsorption, resulting in one five-membered ring in A1-A3 and two seven-membered in A4 involving the adsorb molecule. Whereas in configuration B, O and H atoms of NH_2NO are involved in the adsorption, resulting in one six-membered ring in B1-B3 structures and two eight-membered in B4 involving the adsorb molecule. In configuration C, O atom of NH_2NO is involved in the adsorption. The calculated binding energies for these configurations at B3LYP/6-311++G(d) level of theory indicate that in all three configurations the most and less stable subconfigurations is a and b, respectively. The most stable subconfigurations are shown in Fig 1. In A, B and C configurations the stability of subconfigurations decreases in the order $a > d > c > b$, $a > c > d > b$ and $a > b$, respectively.



Scheme 1

Reference:

- [1] A. Rubio, J.L. Corkill, M.L. Cohen; "Theory of graphitic boron nitride nanotubes"; Phys. Rev. B; 49, 5081-5086, 1994.



[2] F. Murad; "Discovery of Some of the Biological Effects of Nitric Oxide and Its Role in Cell Signaling"; *Angew. Chem*; 38, 1856-1868, 1999.

[3] H. Biaudet, T. Mavelle, G. Debry "Mean daily intake of *N*-nitrosodimethylamine from foods and beverages in France in 1987–1992", *Food Chem; Toxicol*; 32, 417-421, 1994.

15th Physical Chemistry Conference



Investigation of the addition-cyclization reaction between dialkylacetylenedicarboxylates and thiourea: A theoretical study

M. Zakarianezhad^{a*}, B. Makiabadi^b, P. Mohammaddadi^a, Asyeh Barkhoda^a

^aDepartment of Chemistry, Payame Noor University, Tehran, Iran

^bDepartment of Chemical Engineering, Sirjan University of Technology, Sirjan, Iran

E-mail: mzakarianejad@pnu.ac.ir

Keywords: Reaction mechanism, Rate constant, Thiourea, Dialkylacetylenedicarboxylate

Introduction:

Organosulfur compounds are important materials in chemistry and many of them have found general application in organic synthesis. Thiazole skeleton compounds are important heterocycles in bio-organic chemistry and are present in many pharmaceuticals. Many studies have been reported on the synthesis of the thiazole ring structure [1]. They are prepared by diverse synthetic methods using different starting materials. Synthesis of some bioactive compounds, are prepared through the addition of thiols to electron-deficient olefins. One-pot Streoselective synthesis of E-2-(2-imino-4-oxo-1,3-thiazolane-5-yliden) acetates have been reported earlier [2]. To get further insight to the reaction mechanism, a theoretical study performed at B3lyp/6-311++g(2d,2p) and B3lyp/aug-cc-pVDZ level of Theory.

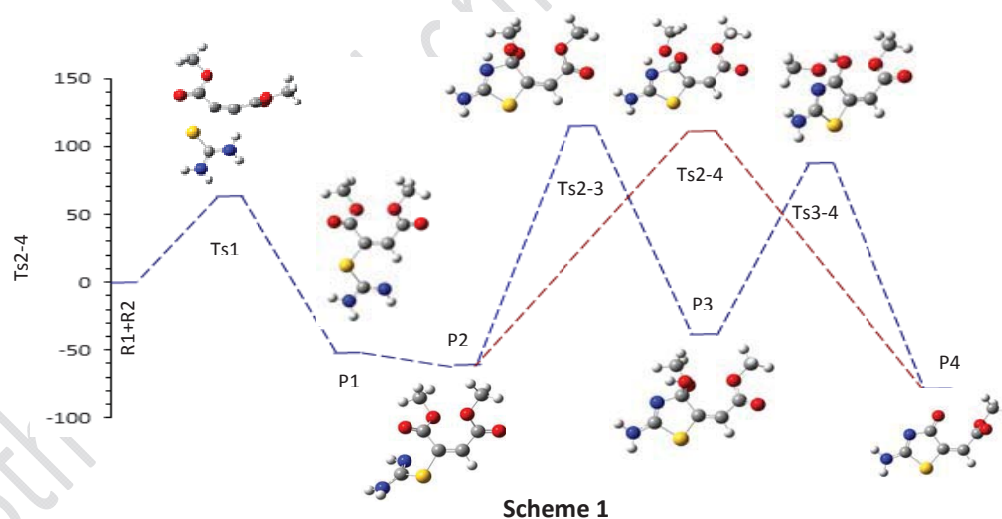
Methods:

Quantum chemical computations were carried out with the Gaussian 03 series of programs. Full geometry optimization of stable species and transition states (TS) were performed in the gas phase by employing the hybrid density functional B3LYP with the 6-311++g(2d,2p) and aug-cc-pVDZ basis sets. To take into account condensed-phase effects, single-point calculations were also performed on the gas-phase-optimized geometries using the polarizable continuum model (PCM) of Tomasi et al. To establish the connection between the transition

state structures and corresponding equilibrium structures, intrinsic reaction coordinate (IRC) analysis was carried out at B3LYP/6-311++g(2d,2p) level of theory.

Results and Discussion:

The reaction was initialized by addition of thiourea to the acetylenic ester and concomitant protonation of the 1:1 adduct by thiourea. Then intermediate P2 alters to P2 with rotation on C-S bond. Reaction proceeds with two parallel paths and produces the product with elimination of one methanol or ethanol molecule. The first pathway contains formation of N-C=O bond while the hydrogen atom transfers to MeO group to produce intermediate P3. The second reaction path includes two steps. In the first step, with formation of N-C=O bond, the hydrogen atom transfers to O atom in carbonyl group at the same time to produce P3. In the second step, intermediate P3 converts to P4 with transformation of hydrogen atom to MeO group and elimination of methanol. Two directions have been investigated as a best direction to nucleophilic attack (scheme 1).



Conclusions:

Results indicate that, in the presence of dimethyl acetylenedicarboxylate, the reaction is preferable both dynamically and thermodynamically but, both differences in energy surface are negligible in both directions. In both competitive pathways, in the path with one transition state, reaction proceed with higher rate constant. AIM data reveal the partially covalent nature



of C^{...}S interaction and electrostatic nature of C^{...}H-N interaction in transition state. In the presence of diethyl acetylenedicarboxylate, the covalent nature and electrostatic nature of both interaction increase. Increase of the covalent nature of C^{...}S is more than electrostatic nature of C^{...}H-N interaction.

References:

- [1] T.H. Kim, M.H. Cha; "Efficient synthesis of 2-methylaminothiazolines via Mitsunobu reaction of *N*-(2-hydroxyethyl)-*N'*-methyl-thioureas"; Tetrahedron Lett.;40,3125-3128, 1999.
- [2] A.Ramazani, S.A.Hossaini-Alemi; "A new and high efficient one-pot synthesis of alkyl E-2-(2-imino-4-oxo-1,3-thiazolan-5-yliden) acetates"; Phosphorus, Sulfur and Silicon;176 237, 2001.



Adsorption of formamide on single-walled BN nanotubes: A DFT study

B. Makiabadi^{a*}, M. Zakarianezhad^b, M. Zareei^b

^aDepartment of Chemical Engineering, Sirjan University of Technology, Sirjan, Iran

^bDepartment of Chemistry, Payame Noor University, Tehran, Iran

Email: bmakiabadi@sirjantech.ac.ir

Keywords: Functionalization, Electronic Properties, BN_{43zz} nanotube, Formamide

Introduction:

BNNTs are found to be wide band gap semiconductors, typically independent of on the diameters and chirality of the tube [1]. The functionalized or doped BNNTs, which exhibit dramatic changes in electronic properties with respect to their pristine counterparts, further enlarge the application in nanomolecular range. Many studies have focused on functionalization of BN nanotubes with more reactive substances [2-3]. Formamide is one of the simplest molecules usually chosen as model for studying biological systems exhibiting the peptide type of bonding and DNA structures. Focus of this study is to investigate the reactivity of NH₂COH toward BNNTs and effect of that upon electronic and structural properties of BNNTs.

Methods:

The full geometry optimizations and property calculations on the BN_{43zz} with and without a NH₂COH molecule were performed using B3LYP/6-311++G(d) level of theory. The NBO and AIM analysis were carried out for all complexes on the B3LYP/6-311++G(d) wave functions.

Result and discussion:

We considered all sites for adsorption of a formamide molecule on middle ring of BN_{43zz} nanotube. The A and B configurations were obtained from the adsorption of NH₂COH molecule on the SWNT. Each of the configurations A and B is investigated in four regions a, b,



c and d. We found seven minima structures on the potential energy surface in the adsorption of NH_2COH on middle ring of BN43zz nanotube. The calculated binding energies indicate that in A and B configurations the stability of structures decreases in the order $a > c > b > d$, respectively. Important conclusions arise from the analysis of the dipole moments. In the gas phase, it is generally found that the conformer with the larger dipole moment has the larger electrostatic energy, and an increased overall energy. The amount of dipole moment increases upon adsorption of NH_2COH on SWNT. The value of dipole moment for the B model is more than A one. Thus in polar solvent, it is expected that the solubility of B model to be greater than A one. In the B model, the value of dipole moment decreases in the order of $c > a > b > d$. Our calculations show that after attachment of NH_2COH , energy gap between the highest occupied molecular orbital and the lowest unoccupied molecular orbital decreases which would result in increases of conductivity of the nanotube upon adsorption of the NH_2COH molecule. According to NBO analysis, adsorption of a formamide molecule on the SWNT leads to charge transfer of nanotube to formamide molecule. The results show that in each of regains, value of charge transfer for the A model is more than B one. The results of AIM show that O...B and N(C)...H interactions in A and B configurations have nature of partially covalent and electrostatic, respectively.

Conclusions:

In summary, we have investigated the structural and electronic properties of chemically modified BN43zz nanotube with NH_2COH molecule. The A and B configurations were obtained from the adsorption of this molecule on middle ring of SWNT. After attachment of functional group, energy gap between the HOMO and the LUMO decreases which would result in increase of conductivity of the nanotube upon adsorption of the NH_2COH molecule. Also the amount of dipole moment increases upon adsorption. It is expected that the solubility of these configurations increases in polar solvents. The results of AIM show that O...B and N(C)...H interactions in A and B configurations have nature of partially covalent and electrostatic, respectively.



References:

- [1] A.Loiseau, F.Willaime, G.Hug, H.Pascard; "Boron Nitride Nanotubes with Reduced Numbers of Layers Synthesized by Arc Discharge"; Phys. Rev.Lett; 76, 4737-4742, 1996.
- [2] X.Wu, W.An, X.C, Zeng; "Chemical Functionalization of Boron–Nitride Nanotubes with NH₃ and Amino Functional Groups"; J. Am. Chem. Soc; 128, 12001-12006, 2006.
- [3] R.Wang, R.Zhu, D.Zhang;"Adsorption of formaldehyde molecule on the pristine and silicon-doped boron nitride nanotubes";Chem. Phys. Lett; 467, 131–135, 2008.



Interaction between different cations with tautomeric forms of thiocytosine

B. Makiabadi^{a*}, M. Zakarianezhad^b, Z. Ahmadinejad^b, M. Zareei^b

^a Department of Chemical Engineering, Sirjan University of Technology, Sirjan, Iran

^b Department of Chemistry, Payame Noor University, Tehran, Iran

E-mail: bmakiabadi@sirjantech.ac.ir

Keywords: Thiocytosine, Tautomerization, Cation-heteroatom, Bidentate

Introduction:

The metal ions are involved in almost all biological processes, such as the regulation of enzyme, stabilization and function of nucleic acids. Therefore further investigations on how metal cations interact with biological molecules and how these interactions affect or control the functions of biological molecules are essential. The study of the tautomerism of nucleobases is important due to the effects on base pairing, base stacking and formation of H-bonded complexes [1]. Thiocytosine is an analog of the natural nucleic acid base cytosine whose oxygen atom is substituted by sulfur atom. Thiocytosine has been found in tRNA molecules in *Escherichia coli* [2]. Tautomerism of thiocytosine has been studied as that of cytosine [3]. In this work we investigated interaction between tautomer forms of thiocytosine with metal cations Ca^{+2} and Mg^{+2} . The aim of the present work is to find the influence of metal cations on the structural and energetic properties of different tautomers of thiocytosine.

Method:

Geometry optimization were done using B3LYP/6-311++G(2d,2p) level of theory. Harmonic vibrational frequencies were computed to verify the nature of minima and transition states. The AIM analysis was carried out in B3LYP/6-311++G(2d,2p) level of theory.

Result and discussion:

For thiocytosine, there are seven isolated tautomers C1- C7 on the process of tautomerization. Sixteen complexes were obtained from the interaction between metal cations Ca^{+2} and Mg^{+2} with different tautomers of thiocytosine. In cation-heteroatom complexes, in which an X^{2+} , lying in the same plane as the ring structures of a thiocytosine, interacts directly by flanking the heteroatom. The cations could form more than one cation-heteroatom complex with the same tautomer form due to more than one possible binding site in an isomer. Thus, eight optimized structures of X^{+2} -heteroatom complexes were obtained for each metal cation. The most stable complexes always correspond to bidentate species. The analysis of the energies is shown that all $[\text{X-thiocytosine}]^{+2}$ complexes are more stable than isolated tautomers. Also in comparison with $[\text{Ca-thiocytosine}]^{+2}$ complexes, in the same positions, the binding energies in $[\text{Mg-thiocytosine}]^{+2}$ complexes are greater. And the binding distances in the $[\text{Mg-thiocytosine}]^{+2}$ complexes are smaller than that in $[\text{Ca-thiocytosine}]^{+2}$ one. This conclusion is in agreement with the greater binding energy obtained for $[\text{Mg-thiocytosine}]^{+2}$ complexes. The HOMO and the LUMO energies were also computed for the most stable conformer. The results show that the most stable complex in each two type of cation-heteroatom complex is C5. The results of AIM calculation shows that the electronic density $\rho(r)$, in the same bond critical points of $\text{X}^{+2} \dots \text{thiocytosine}$ in $[\text{Mg-thiocytosine}]^{+2}$ complexes are greater of $[\text{Ca-thiocytosine}]^{+2}$ ones.

Conclusion:

In the present report, the different tautomers of $[\text{X-thiocytosine}]^{+2}$ ($\text{X}=\text{Mg}, \text{Ca}$) complexes were optimized by DFT method. Eight optimized structures of X^{+2} -heteroatom complexes were obtained for each metal cation. The effect of cations size on the stability of $[\text{X-thiocytosine}]^{+2}$ complexes has been also investigated and order of stability was found to be $\text{Mg}^{+2} > \text{Ca}^{+2}$. The bidentate species of $[\text{X-thiocytosine}]^{+2}$ complexes was found be most stable. The results of AIM shows that the $\rho(r)$, in the same bond critical points of $[\text{X} \dots \text{thiocytosine}]^{+2}$ complexes in $[\text{Mg-thiocytosine}]^{+2}$ complexes are greater of $[\text{Ca-thiocytosine}]^{+2}$ ones.



Reference:

- [1] A.Muller, J.A.Frey; "Hydrogen-bond vibrations in the $S_1 \leftrightarrow S_0$ spectra of a nucleobase pair"; J. Phys. ChemA; 109, 5055-5059, 2005.
- [2] J.Carbon, H.David, M.H.Studier; "Thiobases in Escherchia coli Transfer RNA: 2-Thiocytosine and 5-Methylaminomethyl-2-thiouracil"; Science; 161, 1146-1147, 1968.
- [3] Y.Podolyan, L.Gorb, A.Blue, J.Leszczynski; "A theoretical investigation of tautomericequilibria and proton transfer in isolated and hydrated thiocytosine"; THEOCHEM; 549, 101-109, 2001.



A DFT study of the structure and electronic properties of Benzoxazole

A. Soltani^a, S. Ghafouri Raz^{b*}, S. M. Vahdat^b, S. Bagheri^b

^aYoung Researchers Club, Gorgan Branch, Islamic Azad University, Gorgan, Iran

^bDepartment of Chemistry, Ayatollah Amoli Branch, Islamic Azad University, Amol, Iran

Email: ghafouri_shima@yahoo.com

Key words: Benzoxazole, DFT, HOMO-LUMO, Quantum molecular descriptors

Introduction:

In recent years of Benzoxazole and their by-products have been studied due to structure properties such high quantum yields, high non-linear optical effectiveness, biological activities, photo-stable properties and capabilities to ligate transition metals [1-2]. Therefore, benzoxazole compounds and their derivatives have been widely applied for use in chemistry and medicine. In this paper, we have studied the thermodynamic and electronic properties of this molecule of the title compound was also performed at B3LYP/6-31G* level.

Computational details:

The density functional theory computation has been performed with the Gaussian 03[3] program package at the B3LYP level with standard 6-31G* basis set for geometry optimization of Benzoxazole. The electrophilicity concept was stated for the first time in 1999 by Parr et al. μ is defined according to the following equation: $\mu = (E_{\text{HOMO}} + E_{\text{LUMO}})/2$. χ is defined as the negative of μ , as follows: $\chi = -\mu$. $\eta = (E_{\text{LUMO}} - E_{\text{HOMO}})/2$. S and ω are defined as the following equations, respectively [4]. $S = 1/2\eta$, $\omega = (\mu^2/2\eta)$

Results and Discussion:

The HOMO and LUMO are the main orbital take part in chemical stability [4]. The HOMO represents the ability to donate an electron and LUMO as an electron acceptor. The HOMO

and LUMO energy gap and quantum molecular descriptors computed by DFT/B3LYP in different basis sets are summarized in Table 1.

Property	$-E_{HOMO}/\text{eV}$	$-E_{LUMO}/\text{eV}$	Gap/eV	μ/eV	η/eV	ω/eV	S/eV
Benzoxazole	6.57	0.77	5.8	-3.67	2.9	2.32	0.17

The electronic transition absorption corresponds to the transition from the ground to the first excited state and is mainly described by an electron excitation from HOMO to LUMO (see in Fig. 1).

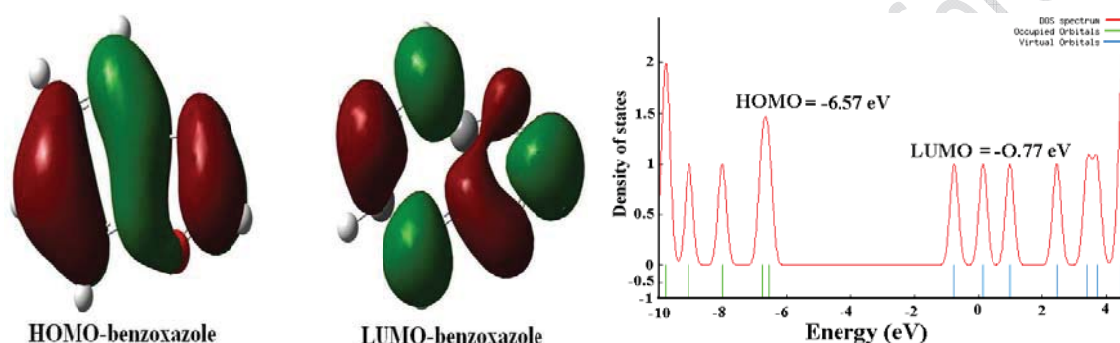


Fig.1. Orbital depiction of HOMO and LUMO and DOS in Benzoxazole system.

The HOMO are more localized on the C-C and C-N bonds and also is on oxygen orbital; while HOMO→LUMO transition implies an electron density transfer from benzen ring to C-O and C-N orbitals and is slightly on carbon atom.

Conclusion:

In this present investigation molecular structure, HOMO, LUMO analysis of Benzoxazole have been studied using ab initio DFT/B3LYP/6-31G* computation.

Refrence:

- [1] J.G. Małecki, Polyhedron 31 (2012) 159-166.
- [2] W.A. Skinner, F. Gualtieve, G. Brody, A.H. Fieldsteel, J. Med. Chem. 14 (1971) 546.
- [3] M.J. Frisch et al., Gaussian 03, Revision B03, Gaussian Inc., Pittsburgh, PA, 2003.
- [4] Nabanita Saikia, Ramesh C. Deka, Comput. Theo. Chem. 964 (2011) 257-261.



15th Physical Chemistry Conference



A DFT study of the structure and electronic properties of 4-Bromo-2-(2, 5-dichloro-phenylimino)-methyl]-phenol

A. Soltani^a, S. Ghafouri Raz^{b*}, A. Dehnokhalaji^c, R. Mashkoor^b

^aYoung Researchers Club, Gorgan Branch, Islamic Azad University, Gorgan, Iran

^bDepartment of Chemistry, Ayatollah Amoli Branch, Islamic Azad University, Amol, Iran

^cDepartment of Chemistry, Faculty of Science, Golestan University, Gorgan, Iran

^bDepartment of Chemistry, Qaemshahr Branch, Islamic Azad University, Qaemshahr, Iran

Email: ghafouri_shima@yahoo.com

Key words: BDPMP, DFT, HOMO-LUMO, Quantum molecular descriptors

Introduction:

Schiff base compounds have been of growing interest for many years, because they play an important role in the extensive of coordination chemistry. They having imine groups ($-C=N-$) and phenyl rings [1-2]. Therefore, Schiff base compounds and their derivatives have been widely applied for use in chemistry and medicine. In this paper, we have reported the thermodynamic and electronic properties of this molecule of the title compound was also performed at B3LYP/6-31G* method.

Computational details:

The density functional theory computation has been performed with the Gaussian 03[3] program package at the B3LYP level with standard 6-31G* basis set for geometry optimization of the BDPMP. For Quantum molecular descriptors, μ is defined according to the following equation: $\mu = (E_{\text{HOMO}} + E_{\text{LUMO}})/2$. χ is defined as the negative of μ , as follows: $\chi = -\mu$. $\eta = (E_{\text{LUMO}} - E_{\text{HOMO}})/2$. S and ω are defined as the following equations, respectively [4]. $S = 1/2\eta$, $\omega = (\mu^2/2\eta)$.

Results and Discussion:

The HOMO and LUMO are the main orbital take part in chemical stability [4]. The HOMO and LUMO energy gap and quantum molecular descriptors computed by DFT/B3LYP in different

basis sets are summarized in Table 1.

Property	$-E_{HOMO}/\text{eV}$	$-E_{LUMO}/\text{eV}$	Gap/eV	μ/eV	η/eV	ω/eV	S/eV
Benzoxazole	6.17	2.05	4.12	-4.11	2.06	4.10	0.24

The electronic transition absorption corresponds to the transition from the ground to the first excited state and is mainly described by an electron excitation from HOMO to LUMO (see in Fig. 1).

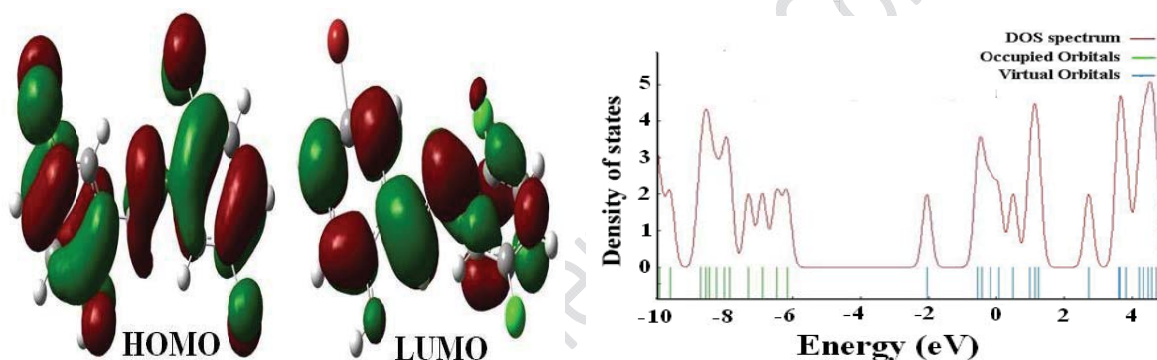


Fig.1. Orbital depiction of HOMO and LUMO and DOS in BDPMP system.

The HOMO are more localized on the C-C and C-N bonds and also is on oxygen and chloro orbitals; while HOMO→LUMO transition implies an electron density transfer from benzen ring to C-O and C-C orbitals and is slightly on oxygen atom.

Conclusion:

In this present investigation molecular structure, HOMO and LUMO analysis of the BDPMP have been studied using ab initio DFT/B3LYP/6-31G* computation.

Refrence:

[1] J.G. Małecki, Polyhedron 31 (2012) 159-166.



- [2] W.A. Skinner, F. Gualtieve, G. Brody, A.H. Fieldsteel, J. Med. Chem. 14 (1971) 546.
- [3] M.J. Frisch et al., Gaussian 03, Revision B03, Gaussian Inc., Pittsburgh, PA, 2003.
- [4] Nabanita Saikia, Ramesh C. Deka, Comput. Theo. Chem. 964 (2011) 257-261.

15th Physical Chemistry Conference



Investigation on the Ability of Different Generations of Density Functionals to Predict the Structural Properties of VO(Salen) Complex

Amir Nasser Shamkhali*, Abolfazl Bezaatpour, Abbas Yousefi Veleni

Department of Applied Chemistry, Faculty of Sciences, University of Mohaghegh Ardabili, Ardabil, P. O. Box:
56199-11367, Iran

*Email: shamkhali@uma.ac.ir

Key words: VO(Salen), Vibrational frequency, LSDA, GGA, HGGA, MHGGA.

Introduction:

Vanadyl complexes of Schiff base ligands have two attractive properties. One is the possession of the d^1 configuration which is important to biological systems because it allows EPR to probe ligand bio-environments. The other is catalytic reactivity towards organic substrates, in particular the oxidation of organic substrates such as alkenes and sulfides [1]. It is clear that chemical activity of a compound is directly related to its electronic structure. However, electronic structure calculation for transition metal complexes is a challenging area of computational chemistry, due to the strong electron correlation in transition metals [2]. In recent years, Density Functional Theory (DFT) is widely used for all types of materials which can give reliable results with lower computational cost in comparison with post/Hartree-Fock methods. In this work we examine the ability of different types of density functionals to predict the structural properties of [vanadyl (N,N'-salicylideneethylendiamine)] {VO(Salen)} complex by selected functionals from common generations of them to examine their performance for these types of materials.

Computational method:

In this work four types of density functionals are selected: Local Spin Density Approximation (LSDA), Generalized Gradient Approximation (GGA), Hybrid-GGA (HGGA), and Meta-HGGA. For LSDA group, SVWN5 functional is selected. Also, PBEPBE and BLYP

functionals are selected from GGA group. Similarly, PBE0 and B3LYP HGA functionals are chosen, and finally, M06 MHGA functional is selected [2]. For all of the calculations, SBKJC basis set with effective core potentials (ECPs) is included in structural optimization and frequency calculations of VO(Salen) complex [3]. The LSDA, GGA, and HGA calculations are performed by Firefly (PC-GAMESS) software and GAMESS-US package is used for M06 functional. The results of optimization and frequency calculations are given in Table 1. Also, the optimized structure of VO(Salen) complex is shown in Figure 1.

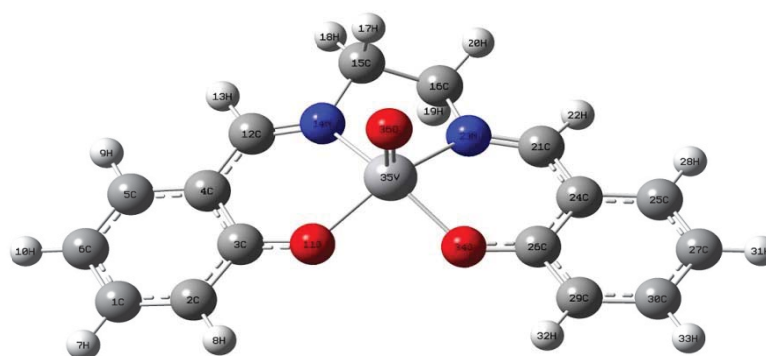


Figure 1: Optimized structure of VO(Salen) complex.

Table 1: Some of important bond lengths and vibrational frequencies of VO(Salen) complex calculated by different types of density functionals. The atomic labels are compatible with Figure 1.

Bond length (Å)	B3LYP	PBE0	BLYP	PBEPBE	LSDA
C12=N14	1.32206	1.31623	1.33659	1.3323	1.33577
C21=N23	1.32827	1.32219	1.34347	1.33954	1.34725
C3-O11	1.34496	1.33495	1.35878	1.34938	1.34844
C26-O34	1.34042	1.33083	1.35461	1.34622	1.35014
V35-N14	2.08396	2.06487	2.09672	2.07686	2.04808
V35-N23	2.08737	2.06859	2.0965	2.07254	2.02224
V35-O11	1.94139	1.92968	1.96017	1.94672	1.88169
V35-O34	1.95164	1.94004	1.97214	1.95811	1.88623
V35=O36	1.61577	1.60414	1.63733	1.62694	1.61635
$\nu(\text{C}=\text{N})$ (cm ⁻¹)	1612.15	1651.87	1554.33	1568.41	1574.67
$\nu(\text{V}=\text{O})$ (cm ⁻¹)	1034.85	1058.13	979.53	1000.06	1023.64



Results and discussion:

It is obvious from Table 1 that the bond lengths are not considerably sensitive to the type of density functional. However, vibrational frequencies are more dependent to the different types of density functionals. The experimental data for C=N and V=O stretching frequencies are 1636.8 and 999.9 cm^{-1} , respectively [4]. On the basis of Table 1, HGGA functionals give more reliable results for C=N stretching frequency. However, GGA functionals give better results for V=O stretching frequency. It seems that combination of Hartree-Fock exchange with pure exchange functionals is suitable for organic molecules. But this is not the case for transition metals. Also, there is many convergence problems for M06 MHGGA functional when it used for VO(Salen) complex. This problem can be created from various reasons. One of them can be as a result of possible bugs in coding process of GAMESS program. The other important reason can be due to the incorrect analytic gradients which were designed for M06 functional due to the fact that many of functionals are parameterized by experimental or high level post-HF thermodynamic data for a wide range of molecules and usually organic molecules are more used for such parameterizations [5]. Therefore, it seems that transition metal compounds are needed to more attention in construction of new types of density functionals.

Conclusion:

In overall view, it seems that various types of density functionals do not considerably affect structural properties and one can use each of them or structural optimization without important differences. However, vibrational frequencies are more depend on the type of performed density functional, in such a way that the selection of appropriate functional is related to the type of chemical bond and existence of transition metals or other atoms with highly correlated electrons.

References:

- [1] E. Kiss, A. Benyei, T. Kiss, *Polyhedron*, **22** (2003), 27-33.
- [2] N. E. Schultz, Y. Zhao, D. G. Truhlar, *J. Phys. Chem. A*, **109** (2005), 4388-4403.



- [3] W. J. Stevens, M. Krauss, H. Basch, and P. G. Jasien, *Can. J. Chem.*, **70** (1992) 612-630.
- [4] Y. Yang, S. Hao, Y. Zhang, Q. Kan, *Soild State Sci.* **12** (2011), 1938-1942.
- [5] H. L. Schmider and A. D. Becke, *J. Chem. Phys.*, **108** (1998) 9624-9631.

15th Physical Chemistry Conference



Theoretical Study of a Di-Copper(I) Macrocyclic Complex Bearing Bromide Bridges

Amir Nasser Shamkhali*, Marjan Abedi, Mahnaz Mardian

Department of Applied Chemistry, Faculty of Sciences, University of Mohaghegh Ardabili, P. O. BOX: 56199-11367, Ardabil, Iran

*Email: shamkhali@uma.ac.ir

Key words: Di-copper(I) complexes, DFT, Macrocyclic, Frequency.

Introduction:

Synthetic chemists have long been attracted to the design and synthesis of macrocyclic ligands and their metal complexes; as such complexes show enhanced thermodynamic and kinetic stabilities and characteristic properties that are inaccessible for complexes of the corresponding open-chain chelate ligands [1].

In recent years, Density Functional Theory (DFT) has been widely used to study the electronic structure of all types of materials such as single molecules and solids, due to its reliable results and lower computational cost in comparison with high level ab initio methods. However, construction of appropriate functionals applicable for materials with strongly correlated electrons, is a challenging area of computational and quantum chemistry [2]. In this work we examine selected functionals from their various generations to predict the structural properties and vibrational frequencies of a $\text{Cu}_2\text{L}_2\text{Br}_2$ complex which L is a [2+2] macrocyclic Schiff base ligand with N_4 donors.

Computational method:

All of the calculations were performed by Firefly (PC-GAMESS) program. For Local Spin Density Approximation (LSDA), SVWN5 functional is selected. Also for Generalized Gradient Approximation (GGA) group, BLYP functional with Becke 88 exchange and Lee-Yang-Parr correlation is chosen. Finally, the B3LYP three parameter hybrid-GGA (HGGA)

functional is selected for calculations [2]. Also, the second order Möller-Pleasant perturbation (MP2) method is used to compare with DFT calculations. All of the calculations were performed by the SBKJC basis set which included effective core potentials for inner shell electrons of heavy atoms [3]. Before using SBKJC basis set a B3LYP calculation with TZVP basis set was done to examine the validity of SBKJC results and there is no considerable difference between the results of two mentioned basis sets [4]. Therefore we can use SBKJC basis set with reliable accuracy and lower computational cost. For all of the DFT and MP2 methods, structural optimization and vibrational frequency calculations is performed. The optimized structure of Cu₂LBr₂ complex is shown in Figure 1. Also the results for bond lengths and C=N stretching frequencies in comparison with experimental data are given in Tables 1 and 2, respectively. Finally, the differences between HOMO and LUMO energies (ΔE_{gap}) for all of mentioned methods are given in Table 2.

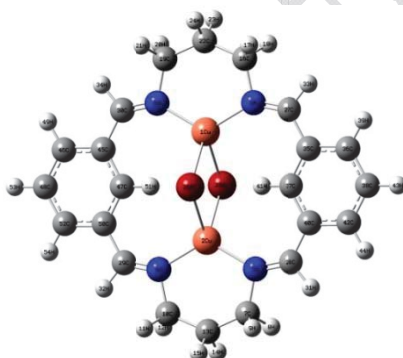


Figure 1: The optimized structure of Cu₂LBr₂ complex. The labels of atoms are compatible with the data of Tables 1 and 2.

Table 1: Selected bond lengths for Cu₂LBr₂ complex.

Bond Length (Å)	SVWN5	BLYP	B3LYP	MP2	Experimental [1]
Cu1-N5	1.9222	1.9942	2.0123	2.0172	2.0439
Cu2-N3	1.9222	1.9943	2.0124	2.0171	2.0403
Cu1-Br25	2.5462	2.6803	2.6573	2.5626	2.4928
Cu2-Br25	2.5462	2.6803	2.6573	2.5626	2.6082
Cu1...Cu2	3.4700	3.4763	3.3830	3.2762	3.098
Br25...Br26	3.7272	4.080	4.0987	3.9413	4.055

Table 1: C=N stretching frequencies (cm⁻¹) and ΔE_{gap} (nm) for Cu₂LBr₂ complex.



Method	C=N	HOMO-LUMO gap
Experimental [1]	1616	-----
MP2	1599.9	200.8 ($n \rightarrow \pi^*$)
B3LYP	1605.9	457.1 ($n \rightarrow \pi^*$)
BLYP	1517.3	1169.67 ($n \rightarrow \pi^*$)
SVWN5	1580.5	1166.7 ($n \rightarrow \pi^*$)

Results and discussion:

On the basis of data of Table 1, B3LYP and MP2 methods give better results for ligand-metal bond lengths (Cu-N bonds). However, there is not considerable difference for structural results among the various functionals. Since the ligand-metal interactions have the most important role in the chemical properties of transition metals complexes, one can use B3LYP functional to obtain better results. This advantage of B3LYP method is obvious in C=N stretching frequencies and ΔE_{gap} which are given in Table 2. It is clear that LSDA and GGA functionals give wrong results for ΔE_{gap} , due to the fact that this complex has yellow-orange color [1]. Therefore, MP2 method also gives wrong result for ΔE_{gap} value which its result is over estimated.

Conclusions:

In an overall point of view, B3LYP and MP2 methods give reliable results for structural properties of Cu_2LBr_2 complex. However, B3LYP gives more accurate results for electronic structure and molecular orbitals of the mentioned complex.

References:

- [1] A. A. Khandar, R. J. Butcher, M. Abedi, S. A. Hosseini-Yazdi, M. Akkurt, M. Nawaz Tahir, *Polyhedron*, **30** (2011), 942-946.
- [2] N. E. Schultz, Y. Zhao, D. G. Truhlar, *J. Phys. Chem. A*, **109** (2005), 4388-4403.
- [3] W. J. Stevens, M. Krauss, H. Basch, and P. G. Jasien, *Can. J. Chem.*, **70** (1992) 612-630.



A Reliable Simple Correlation for prediction of the flash point of aliphatic amines from molecular contributions

Somayeh Moradi

Department of Chemistry, Malek-ashtar University of Technology, Shahin-shahr, Islamic Republic of Iran

Email: mrd_smyh@yahoo.com

Abstract:

The flash point is an important indicator of the flammability of liquids and solids. Many methods of estimating the flash point of pure chemicals have been published, but these methods either rely on accurate thermodynamic data. This work introduces a simple method for prediction of the flash point of different classes of flammable amines, which are important for safety measures in industrial processes. Different amines include aliphatic amines such as primary, secondary, tertiary. The proposed correlation is based on the contribution of some specific molecular moieties and functional groups, which can easily be used for any types of aliphatic amines. Elemental composition is used as a original function. Intermolecular forces are important in this method, which are counted by a correcting function. The predicted flash point for different classes of aliphatic amines including 83 diverse compounds are in good agreement with the measured values such that the root mean square (rms) and average absolute deviations are 18 and 14.9 K, respectively. The estimated flash points for 5 further amines containing complex molecular structures and multifunctional chemicals have been compared with one of the best available predictive methods, which give much lower values of the rms and average absolute deviations.

Keywords: Flash point; flammability amine; derivative; molecular moiety; safety

Results and discussion:

The study of various types of amines has shown that the presences of some specific polar functional groups and molecular fragments as well as elemental composition are important

parameters for prediction of flash points of amino derivative compounds. A careful examination of the flash points of many amine derivatives with general formula CHNOCl given in Table 1 reveals their strong dependence on the number of carbon (n_C), hydrogen (n_H) and nitrogen (n_N) atoms, which can be given as follows:

$$FP_{\text{original}} = 226.6 + 18.35n_C - 5.392n_H + 47.64n_N \quad (1)$$

To derive Eq. (1), a multiple linear regression method was used in which its coefficient of determination or the r^2 -value is equal to 0.725 [1]. As seen in Eq. (1), the coefficients of n_C and n_N have positive sign, which increase the flash point of amines by high values of them (especially n_N). In contrast, the contribution of coefficient of n_H is small and negative that shows opposite effect. In order to improve the reliability of Eq. (1), it was found that the effects of some specific polar groups and molecular moieties may be considered. The existence of some structural parameters can increase or decrease the predicted flash point on the basis of elemental composition. For some amine derivatives, the flash point depends on the number of highly polar groups such as hydroxyl group as well as the attachments of certain substituents to nitrogen atom. However, Eq. (1) can be re-optimized by considering the effects of two correcting functions as increasing (IP) and decreasing (DP) parameters through experimental data given in Table 1 as:

$$FP = 207.2 + 23.43n_C - 7.363n_H + 49.41n_N + FP_{\text{correcting}} \quad (2)$$
$$FP_{\text{correcting}} = 64.79ISP - 62.96DSP$$

The coefficients of elemental compositions in Eq. (2) have close values to those corresponding coefficients given Eq. (1). $FP_{\text{correcting}}$ corresponding two correcting functions ISP and DSP in Eq. (2) have been estimated from structural moieties on the basis of deviations of FP_{original} from the measured values. They are equal to zero if the conditions for giving them various values are not met.

Conclusions:

A simple reliable correlation on the basis of molecular moieties has been introduced to predict the flash points of different amine derivative organic compounds such as aliphatic amines including primary, secondary. Eq. (1) has shown that the number of carbon, hydrogen,



nitrogen atoms has the major contribution to predict flash point of different amine derivatives. Eq. (2) has correcting functions $FP_{correcting}$, which can be easily predicted according to some specific molecular fragments. As compared to Eq. (1) and Rowley *et al.* [2] method, it was indicated that Eq. (2) provides more reliable results for nine amine derivatives with complex molecular structures. Thus, the novel method provides a quick and reliable pathway to predict flash points of different classes of amine derivatives with any complex molecular structure.

References

- [1] W. J. Palm III, Introduction to Matlab for Engineers, McGraw-Hill, 2005, p. 328 and p. 394
- [2] J. R. Rowley, R. L. Rowley, W. V. Wilding, Estimation of the flash point of pure organic chemicals from structural contributions, Process Saf. Prog. 29 (2010) 353-358.



Electron donating and electron withdrawing groups effects at β -position of seven membered ring C_6H_7MX ($M=C, Si, Ge, Sn, Pb$) using computational method.

M. Nikoorazm^{a*}, E. Vessally^b, H. Ghoudarzi Afshar^a and Eynollah abolfathi^a

^aDepartment of Chemistry, University of Ilam, Ilam E-mail: e_nikoorazm@yahoo.com

^b Payame Noor University, Department of Science, P. O. Box: 19395-4697 Tehran, Iran

Keywords: Gaussian, Carbenes, β -Position, Computational method

Introduction:

The chemistry of the divalent Carbenes, Silylenes, Germylenes, Stanylenes and Plumblylenes has been extensively discussed[1]. Since, these compounds are unstable for experimental analysis studies on the carbenes and their analogues have been carried out by theoretical calculation chemistry[2]. For this purpose, the density functional theory (DFT) calculation were carried out to study the substitution effect at β -position on the singlet-triplet splitting C_6H_7MX ($X = -NH_2, -OH, -CH_3, -H, -Br, -Cl, -F, -CF_3, -NO_2$ and $M = C, Si, Ge, Sn, Pb$). Other geometrical parameters such as bond lengths, bond angles, Mulliken charge at atoms, HOMO and LUMO energies, dipole Moment (D) and dihedral angle was calculated.

Computational methods:

Geometry optimization were performed by B3LYP method with the used of the 6-311++G ** basis set and Gaussian 98 package[3].

Results and Discussion:

The DFT calculation indicate that the energy difference between singlet and triplet states $\Delta G_{(t-s)}$, $\Delta E_{(t-s)}$ and $\Delta H_{(t-s)}$ at C_6H_7MX ($M = C, Si, Ge, Sn, Pb$) is increased from $M = C$ to $M = Ge$ and slightly decreased from $M = Ge$ to $M = Pb$. This trend can be explained base on the

atomic radius of hetero atoms. with increasing the atomic radius of hetero atoms the repulsive force between the non-bonding electrons in the singlet states and triplet states is decreased with the result both states become more stable (Table 1). The energy difference from M=Ge to M=Pb is decreased due to pressure angle convention.

Table 1. Thermal energy differences, $\Delta E(t-s)$, enthalpy differences, $\Delta H(t-s)$, and free energy differences, $\Delta G(t-s)$, between the singlet and triplet states of C_6H_8M calculated at the B3LYP/6-311++G** level

M	C	Si	Ge	Sn	Pb
ΔE_{t-s} (Kcal/mol)	0.49	1.83	28.53	20.62	19.11
ΔH_{t-s} (Kcal/mol)	0.49	1.83	28.53	20.62	19.11
ΔG_{t-s} (Kcal/mol)	-0.26	1.12	27.69	18.69	16.86

The ΔG_{t-s} between singlet and triplet states of β -substituted C_6H_7MX ($X = -NH_2, -OH, -CH_3, -H, -Br, -Cl, -F, -CF_3, -NO_2$ and $M = C, Si, Ge, Sn, Pb$) were measured at B3LYP/6-311++G** level in the orders of :

$M = C \quad CH_3 > OH > CF_3 > NH_2 > F > Br > Cl > H > NO_2$

$M = Si \quad NO_2 > Br > F > Cl > CF_3 > OH > CH_3 > NH_2 > H$

$M = Ge \quad CF_3 > Br > Cl > F > OH > CH_3 > H > NO_2 > NH_2$

$M = Sn \quad NO_2 > CH_3 > OH > Br > F > Cl > CF_3 > NH_2 > H$

$M = Pb \quad Br > Cl > F > CH_3 > OH > NO_2 > CF_3 > NH_2 > H$

From free energy gap (ΔG_{t-s}), it was found that the singlet states of C_6H_7MX is more stable than their corresponding triplet states. The presence of electron donating and electron withdrawing group at β -position of C_6H_7MX ring increase the stability of rings.

Conclusion:

Calculated energy difference $\Delta E_{(t-s)}$, $\Delta H_{(t-s)}$ and $\Delta G_{(t-s)}$ at B3LYP/6-311++G** level for β -substituted divalent of seven membered ring C_6H_7MX ($X = -NH_2, -OH, -CH_3, -H, -Br, -Cl, -F,$



-CF₃, -NO₂ and M=C, Si, Ge, Sn, Pb) indicated that the singlet states of C₆H₇MX is more stable than their corresponding triplet states due to the presences of electron donating and electron withdrawing groups the stability of rings was increased.

Reference:

- [1] Kuhl, O. Coord. Chem. Rev, 248, 411-427(2004)
- [2] E.vessally, M.Nikoorazm, F. Esmaili, E.Freyduni, j. Organomet. Chem. 696:932-939 (2011)
- [3] M. J. Frisch, G. W. Trucks, H. B. Schlegel, et al., Gaussian 98, Revision A.6 (Gaussian Inc., Pittsburgh, PA, 1998).



Steric effects on the Singlet–Triplet Energy Gaps of Seven Membered Ring $R_2C_6H_6M$ ($M=C, Si, Ge$).

E. Vessally^a, H. Ghoudarzi Afshar^b, M. Nikoorazm^{b*} and Eynollah abolfathi^b

^a Payame Noor University, Department of Science, P. O. Box: 19395-4697 Tehran, Iran

^b Department of Chemistry, University of Ilam, Ilam E-mail: e_nikoorazm@yahoo.com

Keywords: Steric effects, energy gaps, α -Position, DFT method

Introduction:

Divalent carbenes and their analogues are strongly reactive and their derivatives have played important roles as transient intermediate and powerful reagents [1-2]. the singlet-triplet energy splitting could be related to several effects. The singlet state should be stabilized by substituents that are electronegative and/or have electron pairs that can be donated via hyperconjugation to the empty σ orbital. The triplet state, on the other hand, should be stabilized by substituents that are bulky and/or electropositive. The sterically demanding groups may be employed as a stabilizer for a variety of highly reactive heavy carbenes [3]. Follow up on our work [4], the density functional theory (DFT) calculation were carried out to study the Steric effects at α -position on the singlet-triplet splitting $R_2C_6H_6M$ ($R = -H, -CH_3, i\text{-Pr}, t\text{-Bu}$, and $M = C, Si, Ge$). Other geometrical parameters such as bond lengths, bond angles, Mulliken charge at atoms, dipole Moment (D) and dihedral angles were calculated and discussed.

Computational methods:

Full geometry optimizations of $R_2C_6H_6M$ are carried out by the DFT method using the 6-311++G** basis set of the GAUSSIAN 98 system of programs.

Results and discussion:

Thermal internal energy gaps, ΔE_{t-s} ; enthalpy gaps, ΔH_{t-s} ; Gibbs free energy gaps, ΔG_{t-s} , between triplet(t) and singlet(s) states of $R_2C_6H_6M$ ($M = C, Si, \text{ and } Ge$) were calculated at

B3LYP/6-311++G** level of theory (Table 1). DFT calculations indicated that all the triplet states $R_2C_6H_6C$ are more stable than the related singlet states. The ΔG_{t-s} between the singlet and triplet states of $R_2C_6H_6C$ were increased at B3LYP/6-311++G** level in the order (in kcal/mol): $R = t\text{-Bu}$ (-8.08) > $i\text{-Pr}$ (-4.55) > $-\text{CH}_3$ (-3.77) > $-\text{H}$ (-0.26) (table1).

Whether the stability of the triplet state or instability of the singlet state is responsible to decrease the ΔG_{t-s} , could be explained by comparison of the relative energies between the singlet state and those corresponding triplet states.

Table1. Thermal internal energy gaps, ΔE_{t-s} ; enthalpy gaps, ΔH_{t-s} ; Gibbs free energy gaps, ΔG_{t-s} , between singlet (s) and triplet(t) states of $R_2C_6H_6M$ ($R = -\text{H}$, $-\text{CH}_3$, $i\text{-Pr}$, and $t\text{-Bu}$; $M = \text{C}$, Si , and Ge) at B3LYP/6-311++G** level of theory, kcal/mol									
R	ΔE_{t-s}	ΔH_{t-s}	ΔG_{t-s}	ΔE_{t-s}	ΔH_{t-s}	ΔG_{t-s}	ΔE_{t-s}	ΔH_{t-s}	ΔG_{t-s}
	M = C			M = Si			M = Ge		
H	0.49	0.49	-0.26	1.83	1.83	1.12	28.53	27.69	28.61
Me	-2.66	-2.66	- 3.77	0.03	0.03	0.03	20.22	20.25	20.41
i-Pr	- 4.19	- 4.19	- 4.55	0.03	0.03	0.03	20.57	20.57	21.25
t-Bu	- 7.76	- 7.76	-8.08	0.02	0.02	0.02	20.12	20.12	18.34

The ΔG_{t-s} between the singlet and triplet states of $R_2C_6H_6\text{Si}$ and $R_2C_6H_6\text{Ge}$ were increased at B3LYP/6-311++G** level in the order (in kcal/mol): $-\text{H}$ (1.12) > $-\text{CH}_3$ (0.03) > $i\text{-Pr}$ (0.03) > $t\text{-Bu}$ (0.02) and $-\text{H}$ (28.61) > $i\text{-Pr}$ (21.25) > $-\text{CH}_3$ (20.41) > $t\text{-Bu}$ (18.34) (Table 1). The calculated ΔG_{t-s} for of $R_2C_6H_6\text{Si}$ and $R_2C_6H_6\text{Ge}$ indicated that the singlet states of $R_2C_6H_6\text{Si}$ and $R_2C_6H_6\text{Ge}$ were destabilized when the bulky substituent ($R = t\text{-Bu}$) was used.

Conclusion:

The ΔG_{t-s} between singlet and triplet states of $R_2C_6H_6M$ was determined. The calculated ΔG_{t-s} for $R_2C_6H_6C$ indicated that the triplet states of $R_2C_6H_6C$ were stabilized when the bulky substituent ($R = t\text{-Bu}$) was used. While, the ΔG_{t-s} for $R_2C_6H_6\text{Si}$ and $R_2C_6H_6\text{Ge}$ indicated that



the triplet states of both $R_2C_6H_6Si$ and $R_2C_6H_6Ge$ were instabilized when the bulky substituent ($R = t\text{-Bu}$) was used. The stability of the singlet state of $R_2C_6H_6M$ with replacement of the heavy atom (from $M = C$ to $M = Ge$) could reasonably be explained by atomic radius of heteroatom. The higher atomic radius of a heteroatom (M) decreases the none pair electron repulsion in singlet state and hence increases the stability of the singlet state.

Reference:

- [1] Fontis Medica, S.A. Carbene chemistry : From Fleeting Intermediate to Powerful Reagents, Marcel Dekker : Newyork (2002)
- [2] M. D. Sefcik and M. A. Ring, J. Organometall. Chem. 59, 167 (1973)
- [3] N. Tokitoh, H. Suzuki, R. Okazaki, and K. Ogawa, J. Am. Chem. Soc. 115, 10428 (1993).
- [4] E. Vessally, M. Nikoorazm, and A. Ramazani, Chin. J. Inorg. Chem. 24, 631 (2008)



HOMO-LUMO Energy and NBO Analysis on Chemical Reactivity Description of Some Derivatives of 1-Pyrazolines

M. Izadyar, A. Mansuri, M. R. Hosaindokht

Department of Chemistry, Faculty of sciences, Ferdowsi University of Mashhad, Mashhad, Iran
izadyar@um.ac.ir

Keywords: Natural Bond Orbital (NBO); Chemical reactivity; Transition State (TS), HOMO-LUMO energy

Introduction:

Natural bond orbital analysis provides an efficient method for studying intra and intermolecular bonding and interaction among bonds, and also provides a convenient basis for investigating charge transfer or conjugative interaction in molecular systems. Some electron donor orbital, acceptor orbital and the interacting stabilization energy resulted from the second-order micro-disturbance theory are reported. As a part of a research program which devoted to the study of elimination reactions of 1-pyrazolines (Figure1) by the theoretical procedures with the aim of the reaction analysis from the kinetic and mechanism point of view, we decided to perform a comprehensive examination of NBO and HOMO-LUMO analysis in the gas phase. In order to allow comparison between the theoretical and the experimental results, computational data with the Crawford and Mishra results [1] are presented.

Computational Methods:

The quantum chemical calculations have been performed using Gaussian 09 program [2]. Full geometry optimizations and frequency calculations of the fundamental vibrational frequencies of all possible methyl substituted on 3,3 and 4,4 and 3,5 positions of 1-pyrazoline derivatives (R1,R2,R3) have been carried out employing density Functional theory (B3LYP) with 6-

311++G(d,p) basis sets. The stationary points found on the molecular potential energy hyper-surfaces were characterized using standard analytical harmonic vibrational analyses. For further investigation of the substituent effects, the frequency calculations as well as their corresponding thermochemical parameters including thermal energies, and entropies, Gibbs free energies and entropies of the methyl derivatives of 1-pyrazolines have been performed to find the most stable candidate. Plots of the frontier molecular orbital of the molecules (HOMO and LUMO) were obtained to analyze the main atomic contributions for these orbitals. The importance of observing these plots was to determine the chemical reactivity of 1-pyrazolines

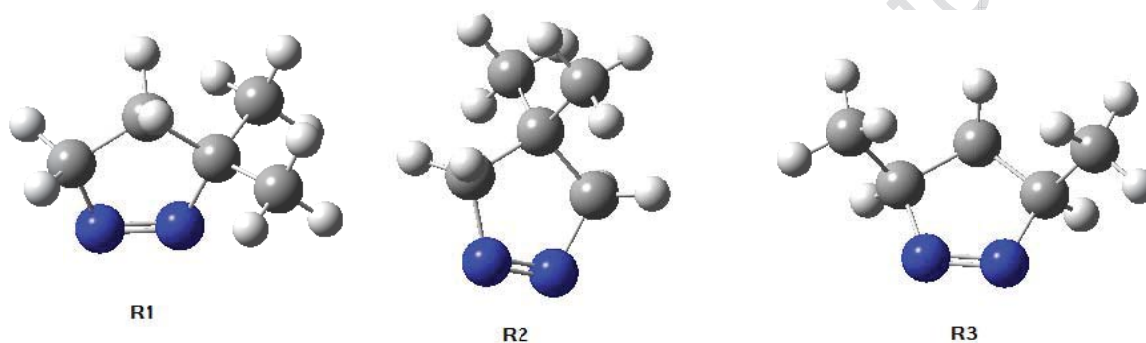


Figure 1. Optimized structures of methyl substituted of 1-pyrazolines

derivatives. Finally, natural bond orbital (NBO) analysis has been carried out to explore the distribution of electrons into atomic and molecular orbitals and thereby derived molecular bonds are then based on these data the graphs of %P orbitals of some nuclei for different bonds of considered reactants have been plotted and analyzed using DFT approach.

Results and Discussion:

The HOMO energy characterizes the ability of electron giving; LUMO energy characterizes the ability of electron accepting. The energy gap between HOMO and LUMO characterizes the molecular chemical stability and it is a critical parameter in determining molecular reactivity. Relatively large LUMO–HOMO energy gap of the studied molecule indicates that it can be considered as kinetically stable. In addition, energy of the HOMO is directly related to the ionization potential, while energy of the LUMO is directly related to the electron affinity. The energy gaps are largely responsible for the chemical and spectroscopic properties of the



molecules. LUMO–HOMO energy gap in gaseous phase is accordance to $R1 > R3 > R2$. These trend is accordance to experimental activation energies, E_a $R1 < R3 < R2$. NBO result reflects the charge transfer between the C–C and N–N group. C–H...N–N hydrogen-bond-like weak interaction which plays a weakly role in stabilization of the reactants are exposed in the NBO analysis. NBO analyses also confirm the intermolecular charge transfer which can be an indicator for C–N bond splitting at the TS.

References:

- [1] R.J. Crawford, A. Mishra, J. Am. Chem. Soc., 87 (1966) 3963,
- [2] Gaussian, Inc., Wallingford CT, Gaussian 09, Revision A.02 (2009).



Kinetic Isotope Effects Investigation on the Mechanism of Nitrogen Extrusion from 3-Methyl-1-Pyrazoline

M. Izadyar, A. Mansuri, M. R. Hosaindokht

Department of Chemistry, Faculty of sciences, Ferdowsi University of Mashhad,

Mashhad, Iran

izadyar@um.ac.ir

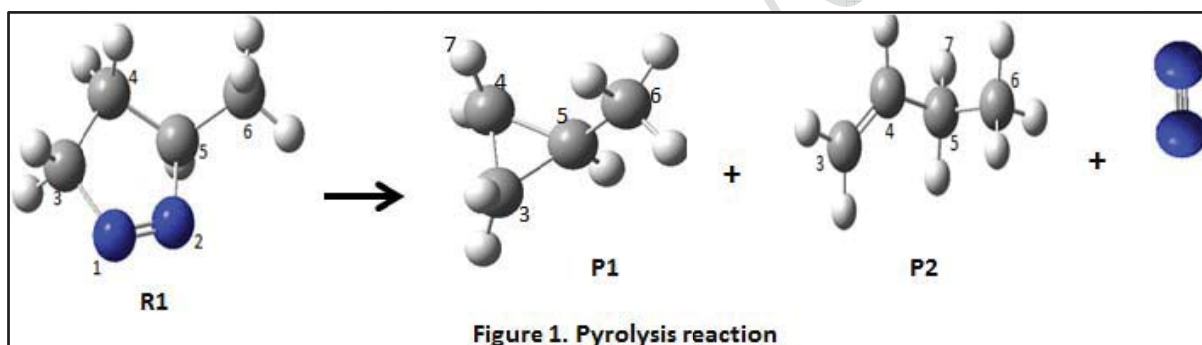
Keywords: Mechanism; Computational; 3-Methyl-1-pyrazoline; Transition State; DFT

Introduction:

Currently determining the transition state (TS) of reactions in the gas and liquid phases becomes more interesting using the femto-second pulses from the experimental point of view. Theoretically, recent progress in computing devices such as CPUs and motherboards of computers in addition to computing softwares is the second factor which accelerates the kinetic and mechanistic studies. One class of the interesting reactions which may be occurred in the gas phase is the elimination reactions. For example nitrogen elimination from substituted 1-pyrazolines in the gas phase is a unimolecular reaction in which two probable trajectories can be compete. This pyrolysis reaction is synthetically important because the corresponding products are clean and further purifications is not needed. Since in this type of pyrolysis H transfer may be take place in the TS, kinetic isotope effects investigation is of importance to determine the real mechanism. Due the course of reaction, secondary deuterium kinetic isotope effect and k_H/k_D value were evaluated to determine which one of the proposed mechanisms is dominant. As the secondary deuterium kinetic isotope effect offers a powerful method for characterization of the bond breaking at the transition state (TS) of the pyrolysis reactions, the presented research employs the deuterium isotope instead of hydrogen atoms on some specific situations of the reactant.

Computational details:

Full geometry optimizations were performed with the Gaussian09 program[1] using the 6-311++G(d,p) basis set and the B3LYP, B3PW91, PBE/PBE hybrid density functional and MP2 method. Based on our previous experience[2,3] use of the DFT and MP2 approaches properly describes the energetic and kinetics features of volatile organic compounds such as pyrazolines reactions. Unrestricted calculations were used for open shell systems. Frequency calculations were carried out for all the stationary points and local minima and transition states were identified by the number of imaginary frequencies (NIMAG = 0 or 1, respectively). Intrinsic reaction coordinate (IRC) calculations were carried out at the B3LYP level of theory to confirm that the transition state structures connect the proper RCs and products. Rate constants were calculated using the conventional transition state theory.



Results and discussion:

Figure 1 shows the nitrogen extrusion from the 3-methyl-1-pyrazoline in the gas phase. We have been examined two paths for the reaction, including the molecular and the radical mechanisms. The molecular mechanism consists of two cyclic transition states, the six-centered cyclic TS and the four-centered cyclic TS. Computed kinetic and activation parameters in the presence and absence of specific deuterium atoms for all mentioned mechanisms of the pyrolysis reaction in the gas phase implies that the reaction is followed by a stepwise radical mechanism. We estimated k_H/k_D values to find out the role of hydrogen atom transfer in the reaction based on the equation 1: $\log k_H/k_D = n\Delta(\Delta G^\ddagger)/(2.303RT)$ (1)



Values of the secondary kinetic isotope effect per α -deuterium on C3 for radical mechanism at the B3LYP, B3PW91, PBEPBE and MP2 are 1.21, 1.22, 1.24 and 1.20, respectively. These values are not accordance to experimental ones. k_H/k_D values For β -deuterium in which D atom is attached to the central methylene are 1.40, 1.45, 1.55 and 1.50, respectively, which are accordance to experiments. In this scenario a new situation similar to hyper-conjugation interaction is born which plays an important role in the stabilization of activated species and enhances the β -deuterium isotope effect. Therefore we concluded that hydrogen atom migration in the TS2 (β -position) plays an important role in the reaction progress while it is less important in the TS1 (α -position). AIM analysis confirmed the obtained results of kinetic isotope effects.

References:

- [1] Gaussian 09 references, Inc., Pittsburgh PA, (2009).
- [2] M.R. Gholami, M. Izadyar, J. Mol. Struct. (Thochem). 672 (2004) 61.
- [3] M. Izadyar, N. Zamani, M.R. Gholami, Chem. Phys. 330 (2006) 394.



A Density Functional Theory and QTAIM-Based Study of the Physical Properties of $[M(\text{dipic})(\text{H}_2\text{O})_3]$, ($M=\text{Fe}, \text{Co}, \text{Ni}, \text{Zn}$) Complexes

Zahra Aghamirzayi, Masoud Arabieh and Mansour Zahedi*

Department of Chemistry, Faculty of Sciences, Shahid Beheshti University, Tehran, Iran

E-mail: m-zahedi@sbu.ac.ir

Key words: Dipic, Transition metals, QTAIM

Introduction:

The formation of complexes between the series transition metals of the first row in their +2 oxidation state and dipic (pyridine-2,6-dicarboxylic acid) have been studied using computational chemistry methods. Dipicolinic acid is one of the very important ligands because its ability to form stable chelates, with various coordinate modes such as bidentate, meridian, or bridging. The B3LYP functional in conjugation with triple- ζ valence quality basis sets, 6-311++G(d,p) have been used for all of the calculations. Initially the obtaining results with their CIF's were compared to determine the ability of B3LYP/6-311++G(d,p). Then the charge distribution was evaluated using NPA and QTAIM analysis in the gas phase, as well as in solvent simulated by incorporating the PCM of Tomassi and co-workers. Finally, based on the topology of the electron density and a number of bond descriptor at bond critical point (bcp) of each system, the nature of interactions in the isolated ligands and that between the ligands and the metal ions have been characterized.

Computational Details:

All the structures were energy-minimized at the B3LYP/6-311++G(d,p) level. In addition to performing minimizations in vacuo, we also performed minimizations in a simulated environment with self-consistent reaction field (SCRF) techniques. The topological properties of the electron density in these complexes were calculated with QTAIM using AIM2000. All calculations were performed using Gaussian09 on a linux workstation.

Results and Discussion:

As the complexes of $[M(II)(H_2O)_3(Dipic^{2-})]$ found in the Cambridge Structural Data-Based (CSD) have the three coordinated H_2O ligands, two H_2O in axial and one in equatorial, we have defined our calculations to these structures. A comparison of the mean DFT and crystallographic bond lengths for the M-O(H_2O) and M-O(dipic) bonds and bond angles \angle O-M-O(dipic) show a reasonable agreement between the computed and the solid state bond lengths and bond angles. The binding energy increases in the order $Fe^{2+} < Co^{2+} < Ni^{2+} > Zn^{2+}$ (-1.08528, -1.21312, -1.25008 and -1.12448). Based on the topological properties of the electron density, $\rho(r)$, QTAIM, there is a correlation between the M-O(dipic) and M-O(H_2O) bond lengths and the electron density at the bcp, this is a reverse correlation (i.e. M-O(dipic) and M-O(H_2O) bond lengths are 2.148 and 2.28 and their charge densities are 0.057 and 0.04 respectively for Fe), correlations are also observed between the electron charge density ρ_b and its Laplacian, $\nabla^2\rho_b$, with the total energy density H_b , indicating that both ρ_b and $\nabla^2\rho_b$ can be used as a measure of bond strength (for example : for M-O bond in Fe, ρ_b , $\nabla^2\rho_b$, H_b are 0.057, 0.24, 0.006, respectively). The average value of ρ_b at $M-OH_2$ bcp is always smaller than the average value at dipic M-O bcps; hence the aqua ligands form weaker bonds with metal ions than do the dipic oxygen donors. The ellipticity, $\varepsilon_b = |\lambda_1|/|\lambda_2| - 1$, is always positive for all of complexes because $\lambda_1 < \lambda_2 < 0$, (i.e. for M-O bond in Fe: $\lambda_1 = -0.072$ and $\lambda_2 = -0.06$) and a large value of its at a bcp is known to reflect structural instability. The values of ε_b for $M-OH_2(ax)$ within each complex are very similar and different from ε_b for $M-OH_2(eq)$. (i.e. for Fe: 0.68 and 0.597).

Conclusion:

We have carried out geometry optimization on a series of complexes containing $Dipic^{2-}$ and three H_2O molecules as coordinating ligands and selected transition metals. The results show that the high-spin divalent metal ions are ground electronic states in incorporating a polarized continuum medium. The structures are in good agreement with those observed from available crystal structure data. Complex formation always results in charge transfer from the ligands to



metal. This suggests that the ability of the ligands to transfer charge density to metal is an important factor influencing complex stability. Based on a QTAIM analysis we have shown that the $M - OH_2$ bond are intermediate between covalent and ionic bond.

References:

- [1] P. R. Varadwaj, A. Vardwaj, H. M. Marques , J. Phys. Chem. A 115 (2011) 5592-5601.
- [2] P.R. Vararwaj, I. Cukrowski, C.B. Perry, H. M. Marques , J. Phys. Chem. A 115 (2011) 6629-6640.
- [3] P. Laine, A. Gourdon, J.-P. Launay , Inorg. Chem. 34 (1995) 5129-5137.



Study Stability Novel Complex of Diimine and Boron Triploids With DFT Calculation results

Ma. Boostan ^{a*}, H. Yamola ^b, M. Boostan ^c

^a Kashan university Chemistry Department, Iran,

^b Ph.D Student, Science and Research Branch, Islamic Azad University, Tehran, Iran

^c Shahr-E-Ray Branch, Islamic Azad University, Tehran, Iran

Email: mhboostan@yahoo.com

Key words: diimine; boron trifluoride; DFT; IR spectra. Thermodynamic

Introduction:

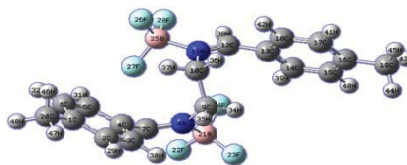
Imine families are important groups in organic chemistry. The classical synthesis of imines involves a condensation of a carbonyl compound with amine. [1]. Optimized structures of ligand and complex have been calculated, their structures parameters have been compared and thermodynamic parameters have been calculated for ligand and complex. The geometry optimizations and harmonic vibrational analyses were carried out without any symmetry restrictions. The nature of optimized geometries has been checked with harmonic frequency calculations. Finally the theoretical results have been compared to choosing the best method, basis set and structures for ligand and prepared complex [2-3].

Methods:

Many studies have shown that DFT-B3LYP method in combination with 6-31G basis set is able to figure out accurate energies, molecular structures, infrared vibrational frequencies that are very close to the experimental results. In this paper, formation of dative bonds between boron and nitrogen of diimines have been widely studied with Gaussian-98 program at the B3LYP and HF level using by 3-21G, 6-31G Basis sets.

Result and discussion:

1-Geometric structures:



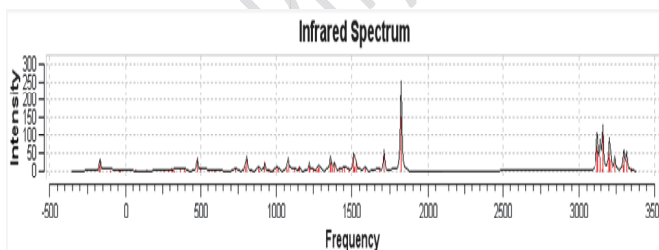
At first, it is necessary to examine their geometric structures before discussing various properties. All of optimized structures for the diimine ligand, 1:2 complex diimine and BF_3 obtain at the B3LYP method and using 6-31G basis set. Depict the final geometries contains selected bond lengths C=N, C-N and N-B. The N-B bond lengths in this complex 1.598 Å is which corresponds to the sum of covalent radii of N – B atoms 1.6 Å, that demonstrating the strong donor-acceptor interaction between them also increase bond length C = N in 1:2 complex diimine – BF_3 appointed the strong bond.

2-Infrared spectra:

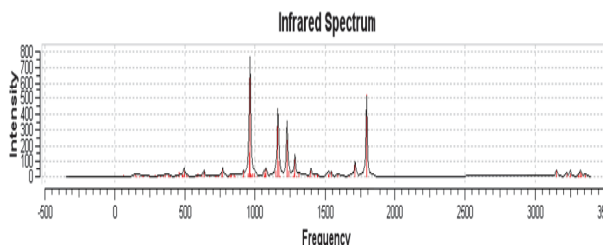
It has a direct relation with the thermodynamic properties such as ΔH , ΔS and ΔG therefore; it is of great significance to calculate the IR spectra for the title compounds by B3LYP and HF/6-31G level. Based on obvious shift is observed in bond C = N of range 1840 cm^{-1} to 1800 cm^{-1} advertised dative bonds between boron and nitrogen.. Table 1.

Conclusion:

Final optimized structures calculated ΔG at level of B3LYP– 6-31G have been offered in Table 2. Finally look at this table also reveals the fact that complex diimine 2 BF_3 stable diimine ligand in studied DFT Ab initio also are drawn their charts.



1-ligand(B3LYP)



2-complex (B3LYP)



Table1- Frequency diimine & complex $2BF_3$

B3LYP/6-31G	Frequency
C = N(diimine)	1840
C = N($2-BF_3$)	1800

Table2- Energies of diimine & complex $2BF_3$

B3LYP/6-31G	ΔG (kcal/mol)
diimine	-506355.61
complex	-913622.86

References:

- [1] La Macchia, G; Li Manni, G; Todorova, T. K; Brynda, M.; Aquilante, F.; Roos, B. O.; Gagliardi, L. *Inorg. Chem.* 2010, *49*, 5216-5222.
- [2] J Volbeda, A Meetsma, and M W. Bouwkamp; *Organometallics*. American Chemical Society .2009, *28* 209–215
- [3] Bouwkamp, M. W.; Lobkovsky, E.; Chirik, P. J. *J. Am. Chem. Soc.* 2005, *127*, 9660.



Application of Transition Metal Substitutions in Biosensors

A. H. Pakiari* , S. Shariati

Chemistry Department, College of sciences, Shiraz University, 71454 Shiraz (Iran)

Email: sabashariati@yahoo.com

Key words: Reduction potential, Quinones, Biosensor

Introduction:

The role of transition metals on redox potential in biosensors is not well-known yet. Quinones are a class of compounds that have widespread importance in sensors or biosensors [1-4]. Their biological action is often linked to their electron transfer rates and redox potentials. In this research we have studied the effect of three transition metals (Cu, Ag, Au) on two-electron reduction potential of quinones.

Method:

The general theory here is to calculate reduction potential using an isodesmic reaction:



The two-electron reduction potential ($E_{Q'}$) in this method can be calculated through:

$$E_{Q'} - E_Q = - \frac{\Delta G_{rxn}}{|Z|F} \quad (2)$$

Where E_Q is the experimental electrode potential of reference molecule, $|Z|$ is the number of electrons transferred (here equals two) and F is the Faraday constant.

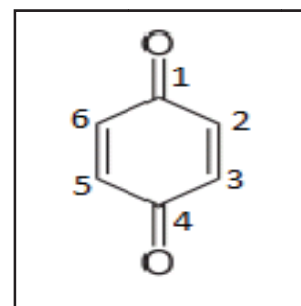
All calculations have been performed with Gaussian 09 program. The geometries have been optimized at B3LYP level of theory and 6-31+G** basis set for all atoms except metals and LANL2DZ for metals. The same method and basis set have been used to perform frequency calculations. All reduced and oxidized structures have been passed the frequency job to obtain Gibbs free energy of each molecule.

Results and discussion:

All of the molecules in our research are quinones containing one or more transition metals. Selection of Cu, Ag and Au is due to their interaction with biological compounds [5] that makes them suitable for biosensors. We tried to understand the effect of these metals, with or without other functional groups, on two-electron reduction potential of quinone. The primary results show that these transition metal substitutions decrease the two-electron reduction potential of quinones, and the trend is $E_{Cu} < E_{Ag} < E_{Au} < E_{unsub.}$, where $E_{unsub.}$ is the experimental two-electron reduction potential of un-substituted quinone, 0.7 volt. A decrease of maximum 66% in potential value is obtained. Some of the results have been shown in Table 1.

Table 1. Two-electron reduction potential values of
Some of the molecules. (units in volt)

	<i>Cu</i>	<i>Ag</i>	<i>Au</i>
3,6-OH-2,5-M-Q	0.238	0.238	0.370
5-OH-2-M-Q	0.444	0.459	0.554
6-OH-2-M-Q	0.473	0.481	0.568
3-OH-2-M-Q	0.507	0.516	0.585
3,6-Cl-2,5-M-Q	0.516	0.519	0.664
5-CH ₃ -2-M-Q	0.528	0.541	0.627
6-CH ₃ -2-M-Q	0.540	0.553	0.64
3-CH ₃ -2-M-Q	0.547	0.555	0.634
6-Cl-2-M-Q	0.584	0.597	0.684
2-M-Q	0.592	0.599	0.687



M=Cu, Ag, Au

Conclusions:

It is found that substitution of transition metals (Cu, Ag, Au) on quinone decreases the reduction potential values. Using these metals together with other functional groups as a substitution on quinones provides a wide range of potential which is suitable for different sensors due to our needs.



Reference:

- [1] P. Wang a, S. Amarasinghe , J. Leddy , M. Arnold. J. S. Dordick, polymer, 39 (1998) 123
- [2] A. Ghindilis, V. Gavrilova, A. Yaropolov, Biosens. Bioelectron. 7 (1992) 127.
- [3] B. Piro, S. Reisberg, V. Noel, M.C. Pham, Biosensors and Bioelectronics 22 (2007) 3126.
- [4] N. Mogharrab, H. Ghourchian, J. Elec. Commun. 7 (2005) 466.
- [5] A. H. Pakiari, M. Jamshidi, J. Phy. Chem. 111 (2007) 4391.



Intermolecular Forces in Imidazolium-based Ionic liquids: QTAIM and NBO Analysis

Z. Rezaei*, A. Maghari and S. M. Atashzar

Department of Physical Chemistry, University of Tehran, Tehran, Iran

Email: zrezaei@ut.ac.ir

Keywords: ILs, Intermolecular forces, $[\text{Bmim}]^+[\text{I}]^-$, $[\text{Bmim}]^+[\text{Br}]^-$, QTAIM, NBO

Introduction:

Ionic liquids (ILs) have become a hot research area with a wide range of applications in recent years [1], due to their potential uses as green solvents and possible replacements for normal volatile organic solvents. In order to design ionic liquids, it is necessary to make a link between the fundamental properties of the system such as electronic structure and inter-molecular force and specific macromolecular properties [2]. In room-temperature ILs there is a complex interplay of forces, including coulombic, dipole-dipole, dipole-induced dipole, dispersion and hydrogen bonds, which has yet to be unraveled. In this work, to interplay the nature of bonds the QTAIM and NBO analysis has been performed as useful reference point for an analysis of the charge distribution and charge transfer in 1-butyl-3-methylimidazolium bromide $[\text{Bmim}]^+[\text{Br}]^-$ and iodide $[\text{Bmim}]^+[\text{I}]^-$ B3LYP optimized structures.

Method:

Different structures and the bmim^+ cation (Figure 1) separately, in the level of density functional theory (DFT) and the pseudopotential-based augmented correlation-consistent basis sets, aug-cc-pVDZ-PP, based on the small core relativistic pseudopotentials (PPs) of Figgen et al, on Br^- and I^- , and the Pople 6-31++G(d,p) basis set on 1-butyl-3-methylimidazolium $[\text{bmim}]^+$, Were fully optimized.

Furthermore, a total optimization at MP2 level with the same basis set was performed, the results as an accurate source to comparing the results of the rest methods were used. These calculations have been done using Gaussian 03 suite of programs. To reveal the nature of bonds, QTAIM and NBO analyses were carried out on the B3LYP optimized structures.

Results and Discussion:

Geometry optimization started by placing anion near the active sites of cation which were selected based on the results of AIM software (Figure 2) and previous researches on ILs with the $[\text{bmim}]^+\text{halogen}^-$ structures and five positions for the anion around the 1-butyl-3-methylimidazolium, was selected and all studies were performed for all conformers in both the ionic liquid.^[3] Conformers exhibited in Figure 3.

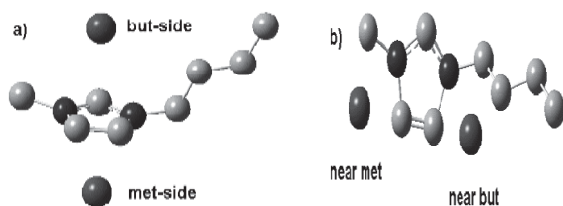


Figure 3. Location of primary cation-anion interaction sites for $[\text{Bmim}]\text{I}$ and Br : a) anion out-of-plane b) anion in-plane

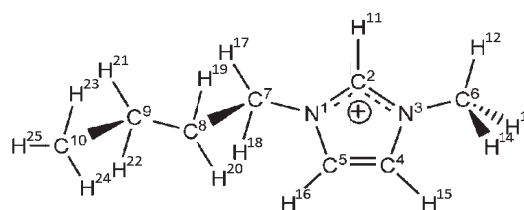


Figure 1. The 1-butyl-3-methylimidazolium cation

The relative stability of the structures was compared: near m < near b < m side < b side < opt. In both molecules a distinct structure, which is named opt (a structure in which the anion is placed out of the imidazolium ring plane and over the center of positive charge) as a stable state was selected. Maximum BSSE values were detected for structures with the most molecular orbital interaction.

Primary delocalization interaction occurs from anion to cation were evaluated according to molecular orbital graphs. In all structures, graphs and charge transfers show interactions in same orbitals. (Table 1 and Figure 3 show results for $[\text{Bmim}]^+[\text{Br}]^-$ in opt conformer)

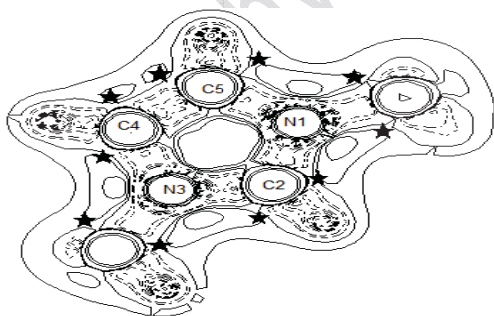


Figure 2. Contour map of the Laplacian projected onto the N1-C2-N3 Plane of imidazolium cation. Lines are positive and dashes are negative. Star signs indicate regions of local acidity.

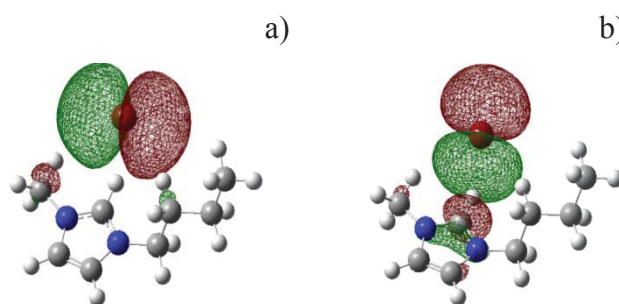


Figure 4: a) HOMO-1 and b) HOMO-2 of opt $[\text{Bmim}]^+[\text{Br}]^-$ MOs, isosurfaces calculated at 0.02.



Table 1. Primary delocalisation interactions of [Bmim]⁺[Br]⁻ in opt conformer, occur from the orbitals in the “From” column to the orbitals in the “To” column.

From	To	2 nd order energy [kJ mol ⁻¹]
Br _{lp}	$\sigma_{C_2-H_{11}}^*$	29.51
Br _{lp}	$\pi_{C_2-N_3}^*$	1.94
Br _{cr}	$\sigma_{C_2-H_{11}}^*$	1.01
Br _{lp}	$\sigma_{C_6-H_{12}}^*$	0.62
Br _{op}	$\sigma_{C_8-H_{19}}^*$	0.56

Reference:

- [1] M.J.Earle and K.R.Seddon. *Pure Appl. Chem.* **72** (2000) 1391.
[2] B.L. Bhargava and S.Balasubramanian. *Chem. Phys. Lett.*, **417** (2006) 486.
[3] P.A.Hunt, B.Kirchner and T.Welton, *Chem. Eur. J.*, **12** (2006) 6762.



Tautomerism of new azo-azomethine ligand in the gas phase and in solution: TD-DFT study of the electronic spectra and thermodynamic parameters

Hamid Khanmohammadi*, Mahshid Saberinasab

Faculty of science, Department of Chemistry, Arak University, Arak 38156-8-8349, Iran

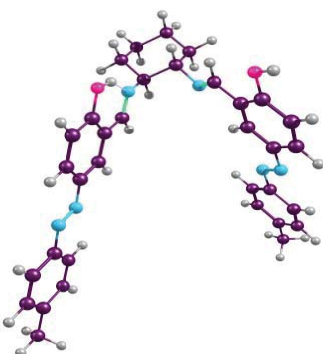
E-mail: h-khanmohammadi@araku.ac.ir

Key words: Tautomerism, TD-DFT, Azo- Azomethine, Thermodynamic studie

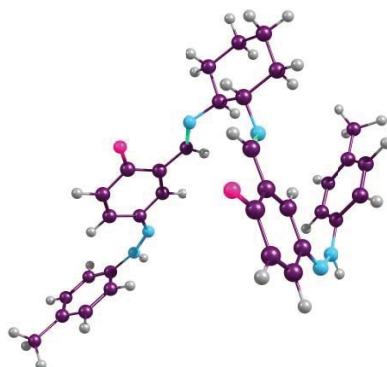
Introduction:

During the past decade, considerable attentions have been paid to the study of tautomerism of azo-azomethine ligands containing hydroxyl groups [1]. The presence of azo/imino, phenol/imino and hydrazone/azo-enaminone tautomerism in these ligands may influence considerably in their unique photo-physical and photo-chemical properties, which is in turn strongly influenced by several factors. As the matter of fact, the tautomerism phenomena of azo-azomethines have been studied theoretically during recent years [2]. Also, Time-dependant density functional theory (TD-DFT) is one of the most accurate methods for the investigation of large organic molecules and for the calculation of excitation energies and oscillator strengths and has recently witnessed a certain success in the investigation of molecular systems with bulk solvation effects [3]. As a new inquiry, in this study three main tautomers comprising of mentioned mixture have been assessed and studied in diverse aspects. Meanwhile, the time-dependant density functional theory (TD-DFT) was used for azo-azomethine tautomers in various media and gas phase, to characterize the excited-state energetic and associated electronic density distribution in H₂L ligand.

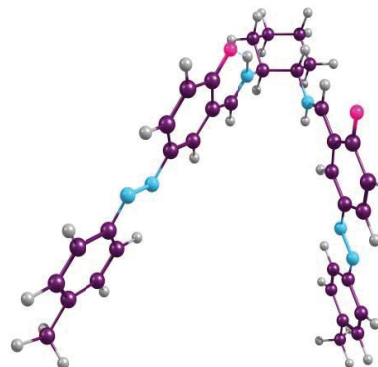
Tautomer I (enol-imine)



Tautomer II (hydrazon)



Tautomer III (enaminone)



Computational details

All calculations were performed using G03 package. Ground state geometry optimizations of H₂L gas and liquid phases (DMSO and CHCl₃) were performed exploiting the analytical gradient technique of density functional theory (DFT) with B3LYP, implementing the modest 6-31G* basis set. Also, geometry vibrational frequencies were calculated analytically to ensure it to be a true local minimum (no imaginary frequencies). All assessments in solvent were done based on Tomasi's polarized continuum model (PCM) [4].

Result and discussion:

The thermodynamic parameters E, U, H and G of each tautomer were calculated at the mentioned level of theory by employing the self-consistent reaction field theory (SCRF). One of the most imperative factors determining the tautomer distribution in the material is the environment. Considering this, the calculated results corroborated that enamine tautomer is the most stable one in liquid phase and the interaction of the solvent with the molecular system caused the stability of tautomers decreased in the sequence : III > I > II. In contrast to liquid phase, in the gas phase the dienol form is more stable and relative stability is: I > III > II. Furthermore, to fully understand the designed compound, maximum absorption wavelength (λ_{max}), Oscillator strengths (f), excitation energy (E_{ex}), configuration and assignment of electronic transition for each tautomer utilizing TD-DFT method at B3LYP/6-31G* level were investigated. The calculated λ_{max} in various media confessed that media causes a red shift of



λ_{max} for I and III to high oscillator strengths for I and lower oscillator strengths for III. The λ_{max} of I is mainly determined by the $\pi \rightarrow \pi^*$ electronic transition of HOMO-1 \rightarrow LUMO in solvent. Also the dominate emission bands for III are found to be associated with HOMO-1 \rightarrow LUMO+1 electronic transition.

Conclusion:

In the present work, the obtained azo-azomethine ligand and its three possible stable tautomers were studied based on theoretical investigation. The results showed that enamine is the most stable one in different media. In addition, geometries of all tautomers were optimized using DFT method at the B3LYP/6-31G* level. In the matter of electronic transitions, for all tautomers UV-Vis spectra have been predicted with PCM-TD-DFT calculation. The λ_{max} of the adsorption spectra of each tautomer is mainly determined by $\pi \rightarrow \pi^*$ electronic transition while intermolecular charge transfer is also involved.

References:

- [1] P. I. Nagy, W. M. F. Fabian, *J. Phys. Chem. B*, 110 (2006) 25026-25032
- [2] E. Hadjoudis, A. Rontoyianni, K. Ambroziak, *J. Photochem. Photobiol. A* 162 (2004) 521
- [3] D. Guillaumont and S. Nakmura, *Dyes and Pigments*, 46 (2000) 85
- [4] M. Cossi and V. Barone, *J. Chem. Phys.*, 112 (2000) 2427

Investigation of vibrational modes and intramolecular hydrogen bonding in Quinizarin

S. Dehghannejad, M. Zahedi-Tabrizi*

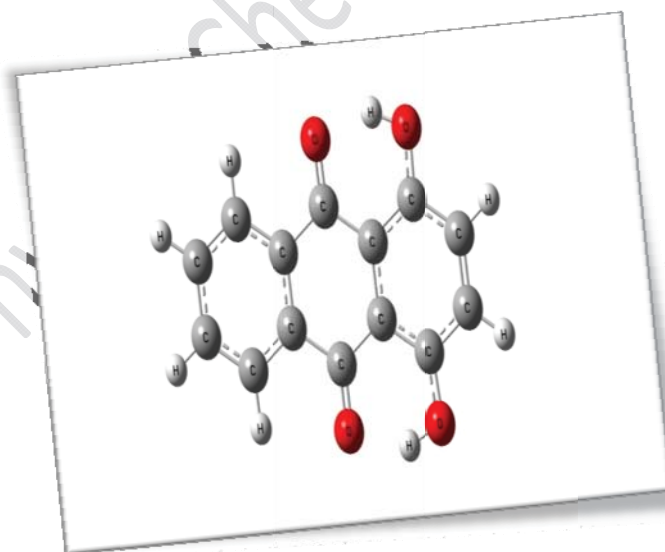
Department of chemistry, Faculty of sciences, Alzahra University, Tehran, Iran

Email: zahedi@alzahra.ac.ir

Keywords: 1,4 – dihydroxy – 9,10 – anthraquinone, Quinizarin, Intramolecular hydrogen bonding, Vibrational assignment, DFT, NBO.

Introduction:

Quinizarin (1,4 – dihydroxy – 9,10 – anthraquinone), one of the anthraquinone dihydroxy derivatives, is the simplest molecule showing the chromophore framework peculiar to several compounds of biological and pharmaceutical interest. This compound is present in some antitumor drugs as doxorubicin, daunorubicin, and adriamycin.



Since Quinizarin exhibits two intramolecular hydrogen bonds due to the resonance-assisted effect, it can be investigated by vibrational spectroscopy [1-4].



Computational methods:

All calculation within the study were carried out using Gaussian 03 program package and using Density Functional Theory (DFT) with B3LYP hybrid functional in combination with the 6-31G(d,p) and 6-311++G(d,p) basis sets.

Results and discussion:

The full geometry optimization, O...H and O...O hydrogen bond distances, and intramolecular hydrogen bond strength (difference between cis-enol and trans-enol forms) were calculated.

¹H-NMR spectra was identified and the chemical shift for H atom attached to oxygen measured from TMS in gas phase was 13.15 ppm and in CDCl₃ solvent was 13.19 ppm.

The calculation of vibrational frequencies and the assignment of vibrational modes of Quinizarin and its spectral behaviors upon deuteration were performed in the 3300-50 cm⁻¹ region.

In addition, OH/OD stretching and out-of-plane bending frequencies in hydrogen bond strength were calculated.

Conclusion:

By comparing these parameters with corresponding parameters in Naphthazarin, it was cleared that the intramolecular hydrogen bond strength in Quinizarin was more than Naphthazarin.

The resonance effect due to delocalization of the π electrons over the three rings is responsible for increasing the hydrogen bond strength in Quinizarin compare with Naphthazarin.

Reference:

- [1] M. B. Gholivand et al, J. Med. Chem. 46 (2011) 2630-2638.
- [2] M. L. Ferreira, J. Rodríguez-Otero, J. Mol. Struct. (Theochem) 542 (2001) 63-77.
- [3] K. Ishii et al, J. Chem. Phys. 131 (2009) 044512-1-044512-9.
- [4] T. B. Nasrallah et al, J. Solid State Chem. 106 (1993) 388-399.



H-bonded complexes of uracil with 1 nitrosopyrrolidin – 2 ol

H. Roohi^a, R. Nokhostin^a

^aDepartment of Chemistry, Faculty of Science, University of Guilan, Rasht, Iran

Email: hroohi@guilan.ac.ir

Key words: Uracil, Nitrosamine, Hydrogen bonds, Quantum chemistry study

Introduction:

Uracil (U) plays a fundamental role in basic biological processes. The quantitative analysis of uracil is very essential and medically significant in some instances [1,2]. Uracil contains many consecutive hydrogen-bond donor and acceptor groups, which makes it ideal for studying hydrogen-bond interactions. N-nitrosamines (NA) compounds are one important class of naturally occurring carcinogens. N-nitrosamines are latent carcinogens and require cytochrome P450 mediated α -oxidation for their conversion into the active carcinogens [3]. The structure, stability and proton transfer in H-bonded complexes formed from interaction between uracil (U) and (NA) have been investigated.

Computational details:

All the structures studied in this work were optimized by using B3LYP, M062X, M052X and MP2 methods in conjunction with the 6-311++G(2d,2p) basis sets.

Results and discussion:

The equilibrium structures obtained from interaction between uracil (U) and NA are depicted in Fig. 1. As can be seen in Fig. 1, NA can be placed in four regions R1–R4 in vicinity of U. All systems analyzed here are coupled through double hydrogen bonds.

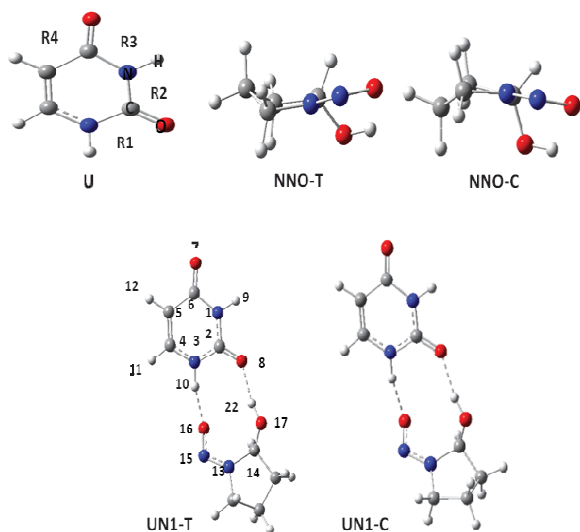


Fig. 1. Optimized structures for free monomers and complexes UN1 at MP2/6-311++G(2d,2p) level.

Table 1: Calculated interaction energies (kJ/mol) of the UN1–4 complexes

	ΔE^a	ΔE^b	ΔE^c	ΔE^a	ΔE^b	ΔE^c
		UN1-			UN1-C	
B3LYP	-	-46.2	-	-	-47.2	-
M052X	-	-51.9	-	-	-53.3	-
M062X	-	-51.5	-	-	-52.9	-
MP2	-	-48.4	-	-	-49.8	-
		UN2-			UN2-C	
B3LYP	-	-31.4	-	-	-32.3	-
M052X	-	-38.7	-	-	-39.7	-
M062X	-	-39.2	-	-	-40.3	-
MP2	-	-5.7	-	-	-36.9	-
		UN3-			UN3-C	
B3LYP	-	-33.8	-	-	-34.6	-
M052X	-	-40.3	-	-	-41.5	-
M062X	-	-40.5	-	-	-41.7	-
MP2	-	-37.1	-	-	-38.4	-
		UN4-			UN4-C	
B3LYP	-	-26.0	-	-	-27.0	-
M052X	-	-30.6	-	-	-31.5	-
M062X	-	-30.5	-	-	-31.3	-
MP2	-	-29.6	-	-	-30.3	-

ΔE^a = electronic interaction energy, $\Delta E^b = \Delta E^a + \text{BSSE}$, $\Delta E^c = \Delta E^b + \text{DZPVE}$

As mentioned above, in each region, U–NA complexes can adopt both cis and trans forms. Among the eight optimized complexes, the highest IE at all levels of theory is predicted for UN1. Consequently, relative stability order of cis and trans complexes is UN1 > UN3 > UN2 > UN4. From Table 1, the IE calculated by DFT functionals is smaller than MP2 method. Although zero-point vibrational energy (ZPVE) correction has a significant effect on the IE of complexes, but inclusion of ZPVE does not change the stability order of complexes. Thus, BSSE and ZPVE corrected IEs of complexes are ordered as UN1 > UN3 > UN2 > UN4.

Conclusions:

IE of U–NA complexes changes depending on the interaction site. The UN1 complex is the most stable one at all levels of theory.

References:

- [1] J.S. Singh, J. Mol. Struct. 876 (2008) 127.
- [2] H. Susi, J.S. Ard, Spectrochim. Acta Part A: Mol. Spectrosc. 27 (1971) 1549.
- [3] Yang, C. S.; Smith, T. J. Adv. Exp. Med. Biol. 1996, 387, 385.



15th Physical Chemistry Conference



A Density Functional Theory (DFT) Study on the Tautomerism of 2-Amino-6-methyl Pyrimidine-4-one: Solvation Effect and NBO Analysis

Majid Khodaei-Tehrani^{*1}, Mohsen Hajibeygi², Meisam Shabanian³ and Ali Esmaeili¹

¹Department of Chemistry, Arak Branch, Islamic Azad University, Arak, Iran

²Department of Chemistry, Varamin-Pishva Branch, Islamic Azad University, Varamin, Iran

³Young Researchers Club, Arak Branch, Islamic Azad University, Arak, Iran.

E-mail: m.khodaei.tehrani@gmail.com

KeyWords: DFT study, NBO analysis, Pyrimidine, Tautomerism, PC model

Introduction:

Amino-imino tautomerization processes facilitated by intramolecular proton transfer in heterocycles have been the subject of a number of studies [1-2]. These processes are relevant to many areas of biological chemistry and have been invoked in mechanisms of radiation-induced damage in DNA [3]. The physical-chemical properties of the aminopyridine and their biochemical importance have received considerable attention from both experimental and theoretical approaches [4-5], due to the understanding for many fundamental biochemical processes. This study employs density functional theory (DFT) on the investigation of those structures and to present a complete analysis of their relative stabilities in the gas phase and deferent solution. This work includes variation of dipole moments and NBO charges on atoms in the solvents and gas phase.

Methods:

All calculations were carried out on a Pentium personal computer by means of GAUSSIAN03 program package.

Results and discussion:

A Density Functional Theory (DFT) study is used to calculate structural data of tautomers of 2-Amino-6-methyl pyrimidine-4-one (AMPO) in the gas phase and selected solvents (benzene, tetrahydrofuran (THF) (polar aprotic solvent) and methanol (protic solvent), Dimethyl



sulfoxide (DMSO) (polar aprotic solvent) and water) by using PC model. All tautomers are optimized at the B3LYP/6-31++G(d,p). The results show that the tautomer AMPO1 (nonaromatic, containing NH₂ and carbonyl group) is more stable than the other tautomers especially in water. In addition, stability of the tautomers in different solvents shows interesting results and variation of dipole moments and NBO charges on atoms in the solvents are studied. In the gas phase AMPO6 (aromatic, containing NH₂ and OH group) form is more stable than the other forms. The major difference between AMPO6 and the other forms in gas phase was found for AMPO3 (nonaromatic, containing =NH and OH group) with 25.08 kcal mol⁻¹.

Conclusions:

In this work a DFT study is used to calculate structural data of tautomers of 2-Amino-6-methyl pyrimidine-4-one (AMPO) in gas phase and selected solvents from non-polar to polar aprotic. In the gas phase AMPO6 form was more stable than the other tautomers. In the solution the stability of some tautomers is different than gas phase and stability of tautomers were affected by different solvents. Also the dipole moments of all compounds are affected by solvent. With increase of the polarity of solvents the dipole moments of all tautomers were increased and the charges on all six positions were affected by solvents. In addition with increase of dielectric constant a variation was found.

References:

- [1] Cantor P R & Schimmel P R, Biophysical Chemistry, vol. 2, W.H. Freeman, San Francisco, CA, **1980**.
- [2] Kasha M, *J Chem Soc*, 2, **1986**, 2379.
- [3] Sheiner S, *J Phys Chem A*, 104, **2000**, 5898.
- [4] Ishikawa H, Iwata K & Hamaguchi H, *J Phys Chem A*, 106, **2002**, 2305.
- [5] Hung F, Hu W, Li T, Cheng C & Chou P, *J Phys Chem A*, 107, **2003**, 3244.



Theoretical Investigation of Solvent Effect on Aromaticity of 7-Azaindole

Sara Fakhraee^{*,a}, Maryam Souri^b

^aDepartment of Chemistry, Payame Noor University, Kherameh, Iran

^bDepartment of Chemistry, Payame Noor University, Kangan, Iran

Email: fakhraee@pnu.ac.ir

Key words: Aromaticity, HOMA, NICS, Azaindole

Introduction:

Aromaticity and reactivity are two deeply connected concepts. Although aromaticity cannot be directly measured, but, there are different methods to describe it quantitatively. In this study, two different criteria was applied to investigate the aromaticity of 7-azaindole (7AI) via complexation with solvent: The geometry based; HOMA (Harmonic Oscillator Model of Aromaticity) index and magnetic based; NICS (Nucleus- Independent Chemical Shifts). The effect of several protic and aprotic solvents on this context has been evaluated.

Theoretical Method:

The Formamide (FM), formic acid (FA), methanol (MeOH), pyridine (PY) and 7AI solvents were selected to form complexes with 7AI molecule in gas phase. Geometry optimization and vibrational frequency calculations were carried out at B3LYP/6-311++G** level of theory using Gaussian 03 program. BSSE correction has been applied to wave function and energy calculations based on Boys and Bernardi counterpoise method [1]. Gauge invariant atomic orbitals (GIAO) method implemented in Gaussian package was applied to estimate the magnetic tensor shielding within the same level of theory [2].

Results and Discussion:

Figure 1. represents the optimum structures of complexes constructed from 7AI molecule and formamide (7AI-FM), formic acid (7AI-FA), methanol (7AI-MeOH), pyridone (7A-PY), 7AI

(7AI-7AI), as (a), (b), (c), (d) and (e) complexes, respectively. HOMA indices were calculated for complexes by applying Kruszewski and Krygowski [3] definition as:

$$HOMA = 1 - \frac{\alpha}{n} \sum_{i=1}^n (R_{opt} - R_i)^2 \quad (\text{Eq. 1})$$

where n is the number of bonds considered, R_{opt} is the bond length of fully aromatic system and α is an empirical constant. Moreover, Schleyer et al. [4] efforts lead to a useful method to calculate the chemical shift not just at every nucleus NICS(0) but also at any point in the space in the vicinity of molecules NICS(n). To determine a pure measure of π aromaticity without the shielding effects of the framework of σ electrons, calculations have been also done at points 1 Å above the center, as NICS(1) [5]. The out of plane (zz) component of the magnetic shielding tensor is considered as a better descriptor of aromaticity for cyclic π electrons delocalization [6]. Table 1 summarizes the evaluated HOMA and NICS(n) indices for five- and six-membered rings of 7-AI in complex with the solvents compared with 7AI monomer.

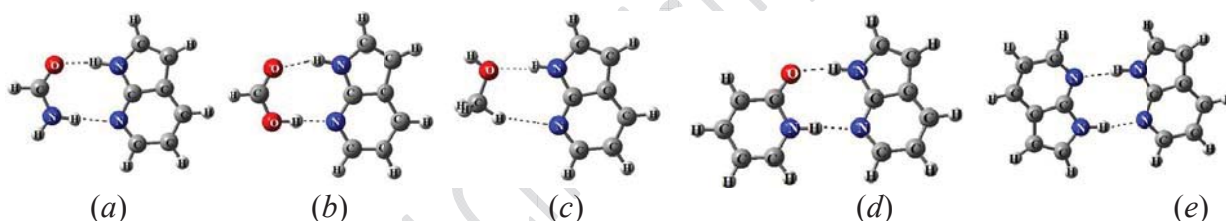


Figure 1: Optimum structures of (a) 7AI-FM, (b) 7AI-FA, (c) 7AI-MeOH, (d) 7AI-PY, and (e) 7AI-7AI complexes.

Table 1. Calculated HOMA and NICS indices for pentagonal and hexagonal rings of 7AI in complex and monomer.

Species	Pentagonal ring				Hexagonal ring			
	NICS(0)	NICS(1)	NICS(1) _{zz}	HOMA	NICS(0)	NICS(1)	NICS(1) _{zz}	HOMA
7AI	-12.391	-10.251	-28.220	0.769	-8.490	-10.681	-29.230	0.960
7AI-FM	-12.658	-11.087	-28.590	0.792	-8.596	-10.843	-28.182	0.956
7AI-FA	-12.870	-10.668	-29.182	0.789	-8.611	-10.475	-28.332	0.959
7AI-	-12.507	-10.528	-28.871	0.782	-8.431	-10.566	-28.893	0.954
7AI-PY	-12.783	-10.746	-29.317	0.795	-8.421	-10.331	-28.127	0.953
7AI-7AI	-12.553	-10.532	28.628	0.792	-8.264	-10.208	27.760	0.956

The NBO analyses of the complexes fulfill the NICS and HOMA results in Table 1. Electron transition from oxygen lone pair (or nitrogen in 7AI) of solvent to σ^*_{N-H} of 7AI increases the aromaticity of pentagonal ring of 7AI, while the $n_N \rightarrow \sigma^*$ transition from 7AI to solvent



decreases the hexagonal ring aromaticity via double H-Bond formation. This trend is totally supported by NICS(1)_{zz} values for pure π delocalized electrons.

Conclusion:

The double H-bond formation between 7AI and protic or aprotic solvents has a diverse effect on the aromaticity and reactivity of five and six membered rings of 7AI.

References:

- [1] Boys, S. F.; Bernardi, F. Mol. Phys. 1970, 19, 553.
- [2] K. Wolinski, J.F. Hilton, P. Pulay, J. Am. Chem. Soc. 112 (1990) 8251.
- [3] J. Kruszewski and T. M. Krygowski, Tetrahedron Lett. 13, 3839 -1972.
- [4] P.v.R. Schleyer, C. Maerker, A. Dransfeld, H. Jiao, N.J.Hommes, J. Am. Chem. Soc. 118 (1996) 6317
- [5] P.v.R. Schleyer, M. Manoharan, Z.X. Wan, B. Kiran, H. Jiao, R. Puchta, N.J. Hommes, Org. Lett. 3 (2001) 2465.
- [6] M. S. Miranda, M. A. R. Matos, V. M. F. Morais, J. F. Liebman, J. Chem. Thermodynamics 50 (2012) 30–36.



Interactions of Glutathione tripeptide with gold cluster: Influence of intramolecular hydrogen bond on complexation behavior

Zahra Aliakbar Tehrani^a, Zahra Jamshidi^{b*}, Marjan Jebeli Javan^a, Alireza Fattahi^{a*}

^a Department of Chemistry, Sharif University of Technology, P.O. Box: 11365-9516, Tehran, Iran,

^b Chemistry and Chemical Engineering Research Center of Iran P.O. Box: 14335-186, Tehran, Iran

Email: fattahi@sharif.edu, jamshidi@ccerci.ac.ir

Key words: Glutathione tripeptide, Gold nanocluster, Intramolecular hydrogen bond, AIM theory, NBO analysis

Introduction:

Understanding the nature of interaction between metal nanoparticles and biomolecules has been important in the development and design of sensors. Among various nanoparticles, gold nanoparticles have attracted much attention in chemistry and material science because of their good biocompatibility, facile synthesis, and conjugation to a variety of bimolecular ligands. Glutathione -modified gold nano surfaces were considered for specific protein binding. Ligand exchange between the Glutathione -Au nanoparticles with thiolated oligonucleotides has been examined by Kornberg and co-workers. Recently, the development of a nanoparticle-based drug delivery and release system using Glutathione as the releasing agent has been shown to be viable. However, interparticle interactions of glutathione and metal particles remain elusive.

Computational method:

Geometries of glutathione complexes in neutral and anionic forms with Au₃ cluster were fully optimized using DFT calculations with B3LYP method employing the Spartan programs. The 6-31+G** basis set was used for the atoms in glutathione, while for gold cluster Lanl2DZ basis set was applied. Natural bond orbital and quantum theory of atoms in molecules analyses were carried out on optimized structures to reveal the nature of bonds.



Result and discussion:

Binding of glutathione with gold cluster is governed by two different kinds of interactions: Au-X (X = N, O, and S) anchoring bond and Au...H-X nonconventional hydrogen bonding. To gain insight on the role of intramolecular hydrogen bonding on gold- glutathione interaction, we compared interaction energies of gold- glutathione complexes with those of cysteine and glycine components. Our results demonstrated that in spite of the ability of cysteine to form highly stable metal-sulfide interaction, complexation behavior of glutathione is governed by its intramolecular backbone hydrogen bonding. The QTAIM and NBO have also been applied to interpret the nature of interactions in gold- glutathione complexes. Based on the positive value of $\nabla^2 \rho(r)$ and negative value of $H(r)$ for Au-X bond, interaction of Au₃ cluster with active site of glutathione ligand is partially covalent and partially electrostatic. However, the positive values of both $\nabla^2 \rho(r)$ and $H(r)$ indicate that Au...H-X interaction of Au₃ cluster with of glutathione ligand is electrostatic in nature. Finally, conformational flexibility of glutathione during complexation with Au₃ cluster was investigated by means of monitoring Ramachandran angles.

Conclusion:

Interactions of glutathione (in neutral and anionic forms) with gold cluster have been described in the geometrical and energetic aspects using the DFT-B3LYP approach with 6-31+G**,-LANL2DZ mixed basis set. It is believed that anchoring bonds Au-X, and nonconventional Au...X-H hydrogen bonds to be responsible for the inter particle interaction of gold particles and glutathione. In spite of the ability of thiol-containing biomolecules to formation of metal-sulfide interaction (such as cysteine amino acid), complexation behavior of glutathione tripeptide is governed by its backbone intramolecular hydrogen bonding. The new insight into the pH and chemical tenability of the inter particle hydrogen bonding interaction of glutathione on gold nanoparticles have implications to the exploitation of glutathione - nanoparticle systems as fictional nanoprobes for biological detection and biosensors.



Reference:

- [1] W. Wang et al.; J Am Chem Soc, 127, 15949-15958, 2005.
- [2] C. Burda et al.; Chem Rev, 105, 1025-1102, 2005.
- [3] A.H Pakiari, Z. Jamshidi, J Phys Chem A, 111, 4391-4396, 2007.
- [4] Z. A. Tehrani et al.; J Phys Chem A, 116, 4338-4347, 2012.
- [5] P.K Sudeep et al.; J Am Chem Soc, 127, 6516-6517, 2005.

15th Physical Chemistry Conference



Conformational aspects of Glutathione tripeptide: electron density topological & natural bond orbital analyses

Zahra Aliakbar Tehrani, Alireza Fattahi*

Department of Chemistry, Sharif University of Technology, P.O. Box: 11365-9516, Tehran, Iran

Email: fattahi@sharif.edu

Key words: Glutathione tripeptide, Ramachandran map, Intramolecular hydrogen bond, AIM theory, NBO analysis

Introduction:

Glutathione (GSH) is an unusual tripeptide (γ -glutamyl-cysteinyl- glycine) with a peptide bond between the amine group of cysteine and the carboxylic group of the glutamic acid side chain. GSH is one of the most abundant ligands in living systems, with an almost ubiquitous presence from bacteria to human cells. The interest in the study of GSH is due to the fact that, despite its structural simplicity, it exhibits a number of roles in detoxification of heavy metal ions, in preventing oxidation stress damages and as a shuttle in transport of metal ions and complexes. It can exist in its neutral form either as neutral, zwitterionic, cationic and anionic forms. The latter form predominates in the condensed phase. The lowest-energy zwitterionic structures of GSH have been calculated at the semi-empirical AM1 and PM3 levels and compared to the experimental crystal structure. The modeling of the tripeptide underlines the question of whether fundamental understanding of protein conformation can be obtained on the level of substituent amino acids.

Computational method:

Initial search of minima on the potential energy surface for neutral, anionic, cationic, and zwitterionic forms of GSH at the relative energy range 10 kcal/mol were carried out using the MMFF force field with Spartan software. The most stable structures were optimized by DFT-B3LYP-6-31+G (d,p) method. Intramolecular hydrogen bonds in these structures were



identified and characterized in details by topological parameters such as electron density $\rho(r)$ and Laplacian of electron density $\nabla^2 \rho(r)$ from Bader's atom in molecules theory. Charge transfer energies based on NBO analysis are also considered to interpret intramolecular hydrogen bonds energies.

Result and discussion:

Structural properties, relative energies and thermodynamic quantities of the lowest energy conformers of GSH in neutral, cationic, anionic and zwitterionic forms in the gas phase were investigated in this report. Our results revealed that conformation of each amino acid in GSH depends on its orientation within the peptide sequence in addition to the conformation of other amino acids within the chain. The effects of intramolecular hydrogen bonds and side-chain orientations on the relative stabilities of these structures were analyzed. Our results show that these hydrogen bonds are partially electrostatic and partially covalent in nature, in which the covalent contribution increases as the stabilization energy of hydrogen bond increases.

Conclusion:

We investigated a detailed DFT study with B3LYP/6-31+G (d,p) basis set to probe conformational analysis of neutral, zwitterionic, cationic and anionic forms of GSH. Our results revealed that glutathione is very flexible molecule and does not adopt a strongly preferred conformation at any ionic form. Moreover, some interesting features concerning backbone and side chain conformations of these structures have been investigated. Comparison of structural parameters of zwitterionic form of GSH with solid state crystallographic structures of GSH and its oxidized forms shows that crystal packing forces the glutathione skeleton into a confirmation that is not seen in this study. Moreover, intramolecular hydrogen bonds in various ionic forms of this mole molecule have been characterized by means of AIM and NBO analyses. Results show that these hydrogen bonds are partially electrostatic and partially covalent in nature.



Reference:

- [1] D.A Dickinson et al.; Biochem. Pharmacol, 64, 1019, 2002.
- [2] M. Nicotra et al.; Biochemistry, 37, 3020, 1998.
- [3] A. Rauk et al.; Can J Chem 79, 405, 2001.
- [4] S.A McCallum et al.; Biochemistry, 39, 7343, 2000.
- [5] W.D Arnold et al.; J Am Chem Soc, 122, 12835, 2000.
- [6] R.F.W Bader, Atoms in Molecules: A. Quantum Theory, Clarendon Press, Oxford, UK, 1990.

15th Physical Chemistry Conference

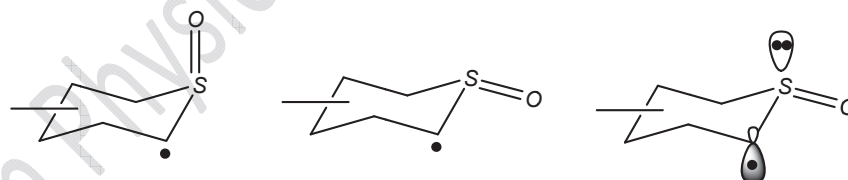
Stereoelectronic interaction effects on the structural and configurational properties of radicals derived from thiacyclohexane 1-oxide selenacyclohexane 1-oxide. A Hybrid density functional theory study and natural bond orbital interpretation

Fatemeh Delshad

Department of Chemistry, Arak Branch, Islamic Azad University, Arak, Iran

Introduction:

The saturated heterocyclic compounds comprise a large segment of organic and inorganic chemistry and are quite widespread in nature (e.g., in alkaloids, carbohydrates, plant growth regulators, etc.), the knowledge about the impacts of the stereoelectronic, steric and electrostatic interactions on the conformational properties of heterocyclic compounds is of very general interest. In 1991, Renaud examined the reactivity of radicals derived from thiacyclohexane 1-oxide with the sulfinyl group in the axial and equatorial positions. While preferential radical reactions syn to the S=O bond in the former was explained in steric terms, the high stereoselectivity observed for the deuteration of the latter was rationalized as the result of a stereoelectronic effect orienting the attack at the radical center anti to the lone pair of the S-atom (see Scheme 1).¹



Scheme 1: Schematic representation of the structures of radicals derived from thiacyclohexane 1-oxide with the sulfinyl group in the axial and equatorial positions

Although the importance of the hyperconjugative interactions in the reactivity of radicals derived from thiacyclohexane 1-oxide (**1**) has mentioned,¹ there is no published experimental or quantitative theoretical data about the donor-acceptor delocalization effects on the structural



and configurational properties of radicals derived from thiacyclohexane 1-oxide (**1**) and selenacyclohexane 1-oxide (**2**). In this work, the contributions of the total dipole moments, steric effects and the anomeric effect (*AE*) associated with the electron delocalization on the configurational and structural properties of radicals **1** and **2** were investigated by means of molecular orbital (ROHF/6-31G*) based method and natural bond orbital (NBO) interpretation (see scheme 1).²⁻⁴

Computational details:

Ab initio molecular orbital calculations were carried out using the ROHF/6-31G* level of theory with the GAUSSIAN 03 package of programs.²⁸ The main purpose of the present work was to study the impacts of the hyperconjugation, electrostatic interactions and steric effects on the structural and configurational behaviors of radicals **1** and **2**. In order to estimate quantitatively the magnitude of the plausible donor-acceptor hyperconjugative interactions in the axial and equatorial conformations of radicals **1** and **2**, we conducted NBO analyses for these compounds.

Results and Discussion:

Although the absolute values of the thermodynamic properties certainly can not be calculated at the accuracy level used in this work; however, the quantities of interest here are the relative values of the thermodynamic functions for different conformations of the same molecule. Accordingly, the errors in such differences will be very small and that even the corresponding errors between the different closely related compounds will be minimal. The smooth variation among the calculated values supports this expectation.²⁷⁻²⁹

Based on the ROHF/6-31G* results (with fully geometry optimization), the stabilities of the various configurations of radicals **1** and **2** are as follow:

radical **1**: **1-cis-eq** > **1-trans-eq** > **1-trans-ax** > **1-cis-ax**

radical **2**: **1-cis-eq** > **1-trans-ax** > **1-trans-eq** > **1-cis-ax**

Interestingly, the NBO analysis of donor-acceptor (bond-antibond) interactions showed that the anomeric effect (*AE*) associated with the donor-acceptor electron delocalizations has no



significant impact on the configurational properties of radicals **1** and **2** but have influences on their structural parameters.

Conclusion:

Effectively, ROHF/6-31G* results revealed that the *cis*-eq configurations of radicals **1** and **2** are more stable than the other forms. The smaller dipole moments of these configurations rationalized the more stability of these forms compared to the *trans*-eq, *trans*-ax and *cis*-ax configurations.

References

- [1] Renaud, P. *Helv. Chim. Acta*, 1991, 74, 1305-1309.
- [2] Frisch, M. J.; et al, *Gaussian 03*, Revision B.03, Gaussian, Inc., Wallingford CT, 2004.
- [3] Hehre, W. J.; Radom, L.; Schleyer, P. V. R.; Pople, J. A. *Ab initio molecular orbital theory*, Wiley: New York, NY, 1986.
- [4] Glendening, E. D.; Badenhoop, J. K.; Reed, A. E.; Carpenter, J. E.; Bohmann, J. A. C.; Morales, M.; Weinhold, F. *Theoretical Chemistry Institute*, University of Wisconsin, Madison, WI, 2004. NBO Version 5.G.



Calculation of the pK_b values of some Aniline derivatives in DMSO solution

B. Ghalami-Choobar* , H. Dezhampanah, M. Fereidoonzadeh

Department of Chemistry, Faculty of science, University of Guilan

E-mail: setar_1386@yahoo.com

Key words: pK_b , non-aqueous solvents, aniline derivatives, DMSO solution,

Introduction:

The tendency of a compound to transfer a proton is a fundamental property to understand many chemical and biochemical processes; consequently a good knowledge of the corresponding dissociation constants in various solvents is essential for the study of the general reactivity of a chemical compound. Although most experimental pK_b values have been determined in water, the increasing importance of the chemistry in non-aqueous solvents has promoted the determination of the basicity constants in them [1]. In the present work, a computational method has been developed to determine of values for some aniline derivatives in dimethylsulfoxide (DMSO) solution. The results were compared with experimental data of pK_b .

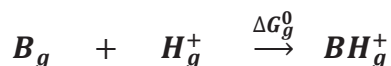
Computational method:

The gas-phase basicity (ΔG) is defined as the Gibbs free energy change of the following equilibrium:



$$\Delta G_g^0 = G_g^0(BH^+) - G_g^0(B) - G_g^0(H^+) \quad (2)$$

Here, the value of Gibbs free energy of the proton in the gas phase, $G_g^0(H^+)$, is -6.28 kcal/mol. Absolute determination of Gibbs free energy of protonation in DMSO solution, $\Delta G_{\text{DMSO}}^\circ$, are based on the following thermodynamic cycle: [2]



$$\downarrow \Delta G_{solv,B}^0 \quad \downarrow \Delta G_{solv,H^+}^0 \quad \downarrow \Delta G_{solv,BH^+}^0$$



Scheme 1: Thermodynamic cycle

The pK_b values can be calculated in according to equation (3)

$$pK_b = \Delta G_{DMSO}^0 / RT \ln 10 \quad (3)$$

Results and Discussion:

All of calculations in gas-phase and solution were made on aniline and its derivatives using Gaussian 98 software. Several basis sets at HF and B3LYP methods were used to obtain the optimized level of theory. The results showed that the B3LYP/6-31+G(d,p) was in good agreement with experimental data. Free energies of solvation were computed using the polarizable continuum model (PCM), conductor-like polarizable continuum model (CPCM) and the integral equation formalism-polarizable continuum model (IEFPCM) with single radii (bondi) at the same level which have been used for geometry determination in the gas-phase (table 1).

Table 1 The calculated pK_b values using PCM, CPCM and IEF-PCM

anilines	PCM	CPCM	IEF-PCM	$pK_b(\text{exp})$
2-fluoro	5.68	5.19	4.53	6.3
3-fluoro	4.74	4.39	3.85	6.6
4-fluoro	3.41	2.93	2.28	4.3
4-MeSO ₂	8.67	8.17	7.61	9.4
MAD	1.02	1.48	2.08	

It can be concluded which PCM with bondi radius in comparison with CPCM and IEFPCM provide satisfactory results. In addition, Single-point electronic energies were calculated at the B3LYP/6-311++G(2d,2p) level of theory and were used to determine of the pK_b values. The results obtained were listed in table 2,



Table 2. single point energy calculation at B3LYP/6-311++G(2d,2p) level of theory

anilines	$\Delta G(\text{gas})$	$Pk_b(\text{calc})$	$Pk_b(\text{exp})$	ΔpK_b
2-Fluoro	-199.463486926997	7.55	6.3	1.25
3-Fluoro	-198.8066131199025	6.41	6.6	0.19
4-Fluoro	-200.73274160754	4.98	4.3	0.68
4-MeSO ₂	-193.0201848679155	10.12	9.4	0.72
MAD				0.71

References:

- [1] J. Jover, et al; QSPR Prediction of pK for Aliphatic Carboxylic Acids; QSAR & combinational Science 2008 No. 10, 1204 – 1215
- [2] A. Trummal, et al; IEF-PCM Calculations of Absolute pKa for Substituted Phenols in Dimethyl Sulfoxide and Acetonitrile Solutions; J. Physical Chemistry. A. 2009, 113, 6206-6212



Influence of Multiple & Cooperative Hydrogen Bonding on the Acidity of Polyhydroxylated Piperidines: Electron Density Topological Analysis

Marjan Jebeli Javan & Alireza Fattahi*

Department of Chemistry, Sharif University of Technology, Tehran, Iran

Email: fattahi@sharif.edu

Key words: Polyhydroxylated piperidines, Hydrogen bonding, Gas-phase acidity, pK_a , Dimethyl sulfoxide.

Introduction:

Iminosugars (“azasugars”) are structural analogues of sugars in which the ring oxygen atom is replaced by a nitrogen atom. In recent years, there has been much interest in synthetic and naturally occurring iminosugars. The biological properties of iminosugars arise because they interfere with the function of carbohydrate processing enzymes. Naturally occurring sugars mimics with a nitrogen atom in the ring are classified into five structural classes: polyhydroxylated piperidines, pyrrolidines, indolizidines, pyrrolizidines, and nortopanes. Polyhydroxylated piperidines (“azasugars”) have received a great deal of attention recently. These alkaloidal sugar mimics contain the same dense stereochemical information as the common hexoses, and many of them exhibit potent biological activity. Also, azasugars have been postulated as possible therapeutics including the treatment of viral infections,⁶ diabetes,⁷ and cancers,⁸ and as invaluable tools in the study of enzyme mechanism.⁹ The interesting behavior of intramolecular hydrogen bonds both from the practical and theoretical points of view have received increased attention in recent years. This can be attributed to the fact that the value of hydrogen bond energy is only a few kilocalories per mole and can be readily perturbed by any change in its environment. Although, hydrogen bonding interactions are usually weaker than classical chemical bonds, they play an important role in chemical and physical properties in both intramolecular and intermolecular interactions. The capacity of



organic molecules to form hydrogen bonds affects very significantly a wide range of their physical properties and is thus directly linked to many important properties, including aqueous solubility, boiling, and melting points, viscosity, solvatochromism, and lipophilicity. Furthermore, acid-base reactions are ubiquitous in nature and play a critical role in a myriad of chemical transformations. Hydrogen bonds are served as templates for proton transfer reactions and organization of three-dimensional structures of O-H and N-H containing compounds. They also lead to an easier gas-phase deprotonation of alcohols. In our previous work [1] we measured gas-phase acidity and pK_a of a series of polyols in dimethyl sulfoxide and our results indicate that multiple hydrogen bonds to a single charged center lead to greatly enhanced acidities.

Result and discussion:

The gas-phase acidity (GPA) of polyhydroxylated piperidines was studied by means of MP2/6-311++G(d,p)//B3LYP/6-311++G(d,p) method. For each structure, deprotonation of the various primary and secondary hydroxyl groups was considered. The quantum theory of atoms in molecules (QTAIM) and natural bond orbital (NBO) analyses have also been applied to understand the nature of the hydrogen bonding interactions in compounds. The results show that the addition of each hydroxyl group decreases ΔH_{acid} in gas phase (it becomes less endothermic) and lowers pK_a value in the solution phase. Therefore, intramolecular hydrogen bonds lead to enhance the acid strength. In both gas phase and solution phase, the β -Nojrimycin-OH₂ (β -1-OH₂) was found to be the most acidic compound with calculated gas-phase acidity (GPA) of 349.4 kcal.mol⁻¹ and the pK_a value of 22.0 (8.0 pK_a units more acidic than 1-propanol). It was also shown; employing the polarized continuum model (PCM), there is a good linear relationship between the gas phase acidities (GPAs) of polyhydroxylated piperidines and their calculated pK_a (DMSO) values.

Computational Methods:

Systematic conformational search as implemented in Spartan 10 software was carried out using MMFF level. The lowest energy structures (those within 10 kcal.mol⁻¹ of the most



favorable conformer) were then optimized using density functional theory (DFT) calculations with a nonlocal hybrid B3LYP (Becke-Lee-Parr) exchange-correlation functional and the 6-311++G (d,p) atomic basis set. Natural bond orbital (NBO) analysis was carried out using the B3LYP functional and the 6-311++G (d,p) basis set. We calculated the electron density topological properties of our systems using the AIM2000 program.

Conclusion:

The MP2/6-311++G(d,p)//B3LYP/6-311++G(d,p) method gives reliable absolute gas-phase acidities. NBO analysis confirms that the various effects (negative charge, *exo*- and *endo*-anomeric) and hyperconjugation are responsible for the hydroxyl orientations. In case of piperidine-diols, QTAIM (quantum theory of atoms in molecules) analysis was also used to elaborate the nature of the hydrogen bonding interactions. The pK_a values of studied compounds in DMSO were computed via a thermodynamic cycle, utilizing Gibbs free energies of dissociation in DMSO solution as computed by MP2/6-31+G(d,p)//B3LYP/6-31+(d) method. The range of pK_a is between 30.7 and 22.0 kcal.mol⁻¹. With this protocol, systematic studies of diverse types of polyhydroxylated piperidines in DMSO were conducted. The results show that GPA and pK_a values decrease with the addition of each hydroxyl group and thus the acid strength increases as anticipated based upon our gas-phase computations.

Reference:

- [1] Tian, Z.; Fattahi, A.; Lis, L.; Kass, S. R. *J. Am. Chem. Soc.* **2009**, 131, 16984–16988
- [2] Pakiari, A. H.; Eskandari, K. *Journal of Molecular Structure (THEOCHEM)*, **2006**, 759, 51-60.
- [3] Cramer, C. J.; Truhlar, D. G. *J. Am. Chem. Soc.* **1993**, 115, 5745-5753.
- [4] Mulroney, B.; Peel, J. B.; Traeger, J. C.; Stone, B. A. *J. Mass Spectrom.* **1999**, 34, 544-553.



A NMR study of Ge and As-doping in (4, 4) Armchair and (8, 0) Zigzag forms of boron phosphide nanotubes

Mahdi Rezaei-Sameti, M. Farahani Farvazi

Department of Applied Chemistry, Faculty of Science, Malayer University, Malayer, 65174, Iran

E-mail address: mrsameti@malayeru.ac.ir

Key word: BPNTs, NMR, DFT, Ge and As- doping

Introduction:

Nanoscience and nanotechnology are opening up a new era of integrated fundamental research at the nanoscale, a more coherent science and engineering education, economic nanoscale manufacturing of products, and an enabling foundation for improving human capabilities and societal outcomes in the long term [1-2]. After publication of Iijima's 1991 paper considerable efforts have been done to introducing other kinds of nanotubes consisting of other atoms such as third (III) and fifth (V) groups (III: boron, aluminum, and gallium; V: nitrogen, phosphorous, and arsenic) of the periodic table of elements due to play an important role in techniques, engineering, electronics, optoelectronics, chemistry, and biochemistry [3-5]. In this new work the NMR parameters and electronic structure of the (4, 4) armchair and (8, 0) zigzag models of boron phosphide nanotubes (BPNTs) with the effect of Germanium and Arsenic doping on it are investigated by density functional theory (DFT).

Computational methods:

In this computational work (4,4) armchair and (8, 0) zigzag models of boron phosphide nanotubes (BPNTs) with Ge- and As-doped in above two models are carried out using density functional theory (DFT) at the B3LYP [37-40] level of theory using the Gaussian 03 set of programs[41]. The standard 6-31G* basis set was used for all models.

The calculated CS tensors in principal axes system (PAS) ($\sigma_{33} > \sigma_{22} > \sigma_{11}$) are converted to measurable NMR parameters: chemical shielding isotropic (CSI) and chemical shielding anisotropic (CSA) using equation 1 and 2 [4].

$$CSI(ppm) = (\sigma_{11} + \sigma_{22} + \sigma_{33})/3 \quad (1)$$

$$CSA(ppm) = \sigma_{33} - (\sigma_{11} + \sigma_{22})/2 \quad (2)$$

Results and discussions:

The results of bond lengths reveal that when Ge and As atoms are substituted in BPNTs, the bond lengths are increased. The bond angles of near Ge and As doping are decreased. Due to the donor electron effects of Ge and As doped in stead of boron the calculated CSI and CSA values undergo significant changes and the neighbor of atoms doping the CSI values for B and P nuclei in two models are increased and charge density electron at this sites are bigger than other sites.

Table 2. The NMR parameters of the ¹¹B and ³¹P nuclei in (4, 4) armchair BPNTs

B-15 nuclei	CSI (ppm)			CSA (ppm)	P-31 nuclei	CSI (ppm)			CSA (ppm)
B11	36 ^b	43	40	86 ^b 120 121	P11	414 ^b	436	115 ^b	87 92
B12	36	41	42	86 122 123	P12	414	431	115	93 93
B21	35	38	40	85 69 74	P21	360	375	124	291
B22	35	37	36	85 64 58	P22	360	382	124	290
B31	40	35	34	73 102 104	P31	358	378	233	94
B32	40	43	45	73 99 97	P32	358	382	233	97
B41	42	-	-	91 - -	P41	359	405	139	279
B42	42	42	39	91 50 44	P42	359	383	139	286
B51	42	59	63	82 47	P51	359	321	238	195



				40			380		105	
B52	42	41	37	82	42	P52	359	377	238	112
				35			385		102	
B61	40	47	46	89	107	P61	358	399	124	275
				106			396		272	
B62	40	42	37	89	103	P62	358	381	124	277
				104			383		272	
B71	35	41	43	99	70	P71	360	383	235	94
				75			385		113	
B72	35	40	38	99	60	P72	360	382	235	84
				51			383		106	
B81	36	39	42	112	105	P81	414	430	103	155
				106			440		140	
B82	36	36	32	112	104	P82	414	433	103	156
				106			433		159	
Ge- As	1403-	1538		800 -	303					

References:

- [1] P.J.F. Harris, Carbon Nanotubes and Related Structures. Cambridge University Press, Cambridge, 1999.
- [2] X. Chen, J. Ma, Z. Hu, Q. Wu, Y. Chen, J. Am. Chem. Soc. 127 (2005) 17144.
- [3] A. Loiseau, F. Willaime, N. Demoncey, N. Schramcheiko, G. Hug, C. Colliex, H. Pascard, Carbon
- [4] M. Rezaei-Sameti / Physica B 407 (2012) 22–26
- [5] M. Rezaei-Sameti, Arabian Journal of Chemistry (2011), doi:10.1016/j.arabjc.2010.10.035 (in press)



Heavy metal (Co^{2+} , Cr^{3+} , Ni^{2+} , Pb^{2+} , Zn^{2+}) complexation by Calixarene, supramolecular nano organic material: chemometric analysis

Afsaneh Amiri*¹, Fatemeh Pirouzi¹, Mohsen Najafi Rodbary²

¹Department of Chemistry, Islamic Azad University, Central Tehran Branch, Tehran, Iran.

²Department of Chemistry, Tarbiat Modare University, Tehran, Iran.

Email: afsaamiri@gmail.com

Keywords: Calixarenes, DATAN, Benesi-Hildebrand, Nonlinear least square, chemometrics

Introduction:

Numerous attempts have been made to design new host systems which can selectively interact with the target guest and perform intriguing molecular recognition processes [1].

Fine control of the size of calix[n]arenes, by changing the value of n and the introduction of various functional groups makes. Calixarenes are of interest in chromatography, slow release of drugs, transport across membranes, ion channels and many other applications [2, 3].

In this research study, stability constants of metal cations and calix[4]arene and calix[6]arene in chloroform-methanol (50%-50% v/v) were determined at 25°C using spectrophotometric technique.

Materials and methods:

Chemicals: The para-tert-butyl-calix[4]arene and para-tert-butyl-calix[6]arene were synthesized. The solvent, chloroform and methanol (from Merck, p.a.), was used without further purification. Zinc and nickel sulfate, cobalt nitrate, chromium chloride and lead acetate as the cations sources were dried under vacuum at room temperature for 48 h before use. 1.5 cm³ solution of ligand was titrated with stepwise addition of an cation solution both in chloroform-methanol solution. The UV-vis spectrum of the mixture undergoes small changes at 260–300 nm.



Results and discussions:

complex formation between the para-tert-butyl-calix[4] arene and some transition metal ions in organic solvent. Principle component analysis (PCA) was used for determination of the number of components in the absorbance data matrix and the formation constant of complex was obtained using by DATAN on the spectrophotometric data and compared with other methods. All ligands have been shown to form exclusively 1: 1 (metal ion to ligand ratio) complexes with cations in our experimental conditions. LogK_f of metal- calix[4] arene complexes are 5.03±0.10, 4.68±0.11, 5.32±0.11, 5.41±0.10 and 4.70±0.11 for Co²⁺, Cr³⁺, Ni²⁺, Pb²⁺ and Zn²⁺ respectively.

It has been used three methods for determination of stability constant for complexes: DATAN, Benesi-Hildebrand, Nonlinear least square curve fitting with Microsoft excel solver. Principle component analysis (PCA) was used for determination of the number of components in the absorbance data matrix and the formation constant of complex was obtained using by DATAN on the spectrophotometric data and compared with two another other methods. and after that we Spectrophotometric titration plots and determin the complex stoichiometry.

Conclusion:

The interesting curve resulting from the spectrophotometric titrations of the ligand by metal cations shows the absorbance increase within a very small range and no significant break in complexation curve, indicating the formation of low stability constant. However, the spectrophotometric titration curve of the ligand by metal cations displays a more continuous variation in the absorbance with concentration ratio.

Although the ligands present two potential complexation sites, the complex stoichiometry was found to be 1 : 1 (each calixarene : each alkali cation). This behavior may be explained by a negative allosteric effect, which has been found in complexing systems containing two conformationally related subunit. Benesi-Hildebrand and Nonlinear least square curve fitting with Microsoft excel solver are soft metod and DATAN is the collection of soft and hard method therefore daten is beter than two method.



References:

- [1] Volker Böhmer. Calixarenes 2001, Johannes Gutenberg-Universität, Mainz, Germany (2001).
- [2] Li Wang, Xian-Fa Shi, Zhong-Liang Zhu; *Molecular and Biomolecular Spectroscopy*, 67 (789-792) 2007
- [3] C. Ruckebusch, L. Duponchel, J.P. Huvenne, A. Caudron, L. Boilet, J.P. Cornard, J.C. Merlin, A. de Juan *analytica Chimica Acta*, 544 (337-344) 2005



Configurational behavior of 1,2-diphenyldistibene. A hybrid-density functional theory study and natural bond orbital interpretation

Vahid Moradi^{*,a}, Seiedeh Negar Mousavi^a and Hooriye Yahyayi^b

^aChemistry Department, Science Faculty, Arak branch, Islamic Azad University, Arak, Iran

^b Chemistry Department, Zanzan Branch, Islamic Azad University, Zanzan, Iran

(Email: v.moradi328@gmail.com)

Keywords: 1,2-diphenyldistibene, Stereoelectronic effect, Molecular modeling, Ab initio, NBO

Introduction:

Numerous effects have been proposed to rationalize the observed preferred conformation of organic compounds. These have included the anomeric effect, hyperconjugation, dipole-dipole interactions, resonance, steric repulsions, and others. It is known that the maximization of an interaction between the best donor lone pair and the best acceptor bond results in the preferred geometry of many molecules [1]. In this work, the impacts of the hyperconjugation, electrostatic model associated with the dipole-dipole interactions and steric hindrances on the configurational and structural properties of (*E*)- and (*Z*)- 1,2-diphenyldistibene have been investigated using the complete basis set composite method hybrid-DFT based methods and natural bond orbital (NBO) interpretations [2].

Computational details:

Hybrid density functional theory calculations was carried out using the B3LYP/Def2-TZVPP level of theory with the GAUSSIAN 98 package of programs [2]. The NBO analyses were performed for the *E* and *Z* configurations of 1,2-diphenyldistibene by using GAMESS program suite. Accordingly, the magnitude of the donor-acceptor hyperconjugative interactions in *E* and *Z* configurations of 1,2-diphenyldistibene can be quantitatively estimated.



Results and discussion:

The results obtained showed the Gibbs free energy difference ($G_E - G_Z$) values (i.e. ΔG_{E-Z}) at 298.15 K and 1 atm between the E- and Z-configurations of 1,2-diphenyldistibene is by about 2.91 kcal mol⁻¹. The NBO analysis of donor-acceptor ($LP \rightarrow \sigma^*$ and $\sigma \rightarrow \sigma^*$) interactions showed that the *generalized anomeric effect* (i.e. $GAE_{total} = GAE_E - GAE_Z$) associated with the $LP_{M1} \rightarrow \sigma^*_{M2-Cphenyl}$ and $\sigma_{M1-Cphenyl} \rightarrow \sigma^*_{M2-Cphenyl}$ is -0.34 kcal mol⁻¹. Therefore, the rationalization of the configurational preference solely in terms of the *generalized anomeric effect* fails to account for 1,2-diphenyldistibene. Obviously, other factors (steric effect and dipole-dipole interactions) have determinant impacts on the conformational preferences in 1,2-diphenyldistibene. Using the dipole moments a “ Δ ” parameter was defined as $\Delta\mu_{Z-E}$. $\Delta\mu_{Z-E}$ value for 1,2-diphenyldistibene is by about 1.7063 Deby. Therefore, the *electrostatic model* associated with the dipole-dipole interactions [3-5] justifies the more stability of the E configuration of 1,2-diphenyldistibene compared to its Z configuration. The correlations between the *generalized anomeric effect*, *electrostatic model*, ΔG_{E-Z} , bond orders, structural parameters and configurational behavior of 1,2-diphenyldistibene have been investigated.

Conclusions:

The B3LYP/Def2-TZVPP calculations reported above and NBO interpretations provided a reasonable picture from energetic, structural, bonding and stereoelectronic points of view for the configurational preferences in (E)- and (Z)- 1,2-diphenyldistibene. The results obtained showed that the *generalized anomeric effect* fails to account for the configurational behavior of 1,2-diphenyldistibene but the *electrostatic model* succeeded in this system.

References:

- [1] N.D. Epiotis, R.L. Yates, R.J. Larson, C.R. Kirmayer, F. Bernardi, Directional effects of . sigma. Conjugation on geometrical isomerism, J. Am. Chem. Soc. 99 (1977) 8379-8388..
- [2] M.J. Frisch, et al., GAUSSIAN 98 (Revision A.3) Gaussian Inc. Pittsburgh, PA, USA, 1998.



- [3] Y. Mo, Computational evidence that hyperconjugative interactions are not responsible for the anomeric effect, *Nature Chemistry* 2 (2010) 666-671.
- [4] Liu SB, Steric effect: A quantitative description from density functional theory, *J. Chem. Phys.* 126 (2007) 244103(1-5).
- [5] Y. Huang, A.-G. Zhong, Q. Yang, S.B. Liu, Origin of anomeric effect: A density functional steric analysis, *J. Chem. Phys.* 134 (2011) 084103(1-9).

15th Physical Chemistry Conference

The role of L-histidine in the activation of carbonic anhydrase enzyme: A quantum mechanical approach

Mina Ghiasi*^a, Mona Taheri^a and Mansour Zahedi^b

^aDepartment of Chemistry, Faculty of Science, Alzahra University, Vanak, Tehran, ^b

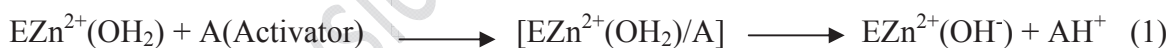
ghiasi@alzara.ac.ir, mona.taheri67@yahoo.com

Department of Chemistry, Faculty of Science, Shahid Beheshti University, G. C., Evin, 19839-63113, Tehran, Iran .

Key words: Carbonic anhydrase, Activator, Transition State, QM calculation.

Introduction:

The carbonic anhydrase (CA) comprise a family of ubiquitous zinc metalloenzymes that catalyze a very simple physiological reaction, the interconversion between carbon dioxide and the bicarbonate ion [1, 2]. All known isozymes of carbonic anhydrase contain a single Zn²⁺ ion, which is essential for catalytic activity, Figure 1. In order to regenerate the catalytically active form, a proton transfer reaction must occur from the water bounded to Zn(II) within the enzyme active site to the external medium. In the presence of activators, an enzyme/activator complex form, eq 1.



In this work, we studied the mechanism of interaction between L-histidine, as an efficient amine activator with active center of CA enzyme by using quantum mechanical calculations.

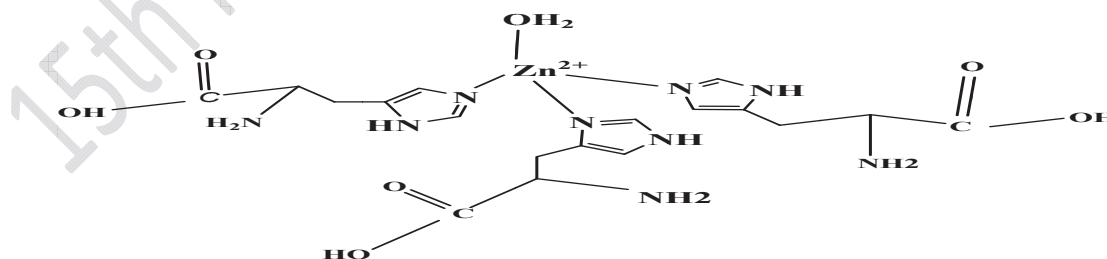


Figure 1. Presentation of active center of Carbonic anhydrase enzyme.

Computational methods:

Ab initio calculations were carried out with the Gaussian program series 2003. All geometries were fully optimized employing a B3LYP/6-31G* method. Full optimizations were performed without any symmetry constraints. The harmonic vibrational frequencies were computed to confirm that an optimized geometry correctly corresponds to a local minimum. QST2 method was used to search for transition state. Transition state geometry was double-checked by using IRC and FREQ calculations.

Results and Discussion:

The results of calculations indicate that L-histidine is a potent activator for CA enzyme. L-Histidine binds within the CA active site, without interacting with the metal center. In fact, we propose this binding site of activators as the important binding site in CAs, after the metal center. The mechanism of action for activators suggests a facilitation of the rate-determining proton transfer reaction between the active site and the reaction medium, Figure 2.

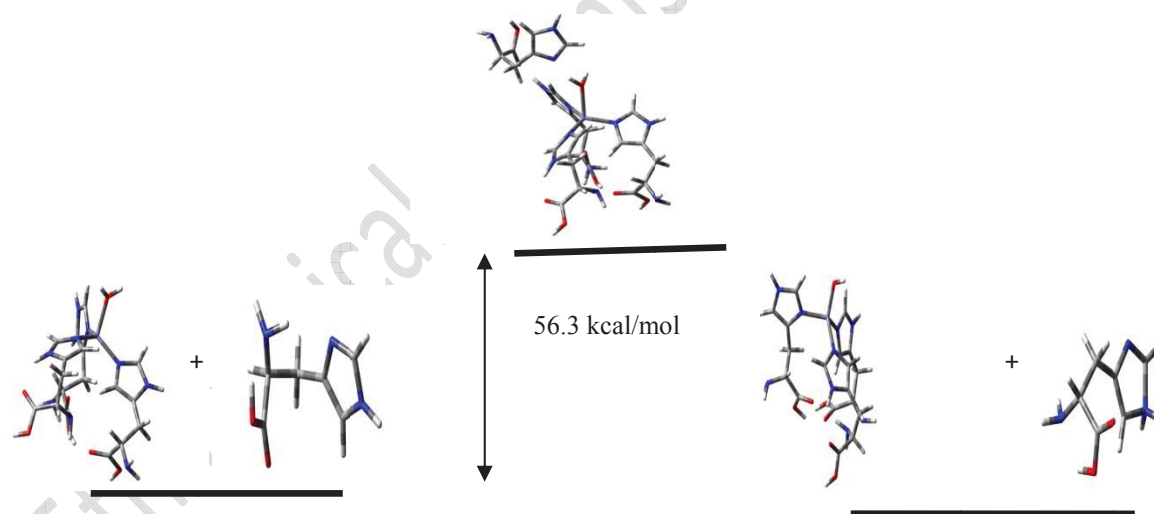


Figure 2. Potential energy profile for the complexation of L-histidine and CA active site.

References:

- [1] G. Behravan, B.H. Jonsson, S. Lindskog, Eur. J. Biochem. 1990, 190, 351-357.
- [2] C. Temperini, A. Sozzafava, C.T. Supuran, Bioorg. Med. Chem. Lett., 2005, 15, 5136-5141.



A QTAIM study on carbon-doping at different sites of (8,0) BNNTs

Firouzeh Zarinfar^a, Mehdi D. Esrafil^{*,b}

^a Department of Chemistry, Tabriz Branch, Islamic Azad University, Tabriz, Iran;

^b Laboratory of Theoretical Chemistry, Department of Chemistry, University of Maragheh, Maragheh, Iran

(esrafil@maragheh.ac.ir)

Key words: (8,0) BNNT; QTAIM; Bond critical point; Carbon-doping.

In recent years, many research interests were focused on boron nitride nanotubes (BNNTs), as isomorphous analog of the carbon nanotubes (CNTs), due to their unique and important properties ideal for structural and electronic applications [1]. There are many similarities between CNTs and BNNTs, the main difference being that BNNTs are viewed as always being semiconductors with almost constant band gap nearly independent of tubular diameter and chirality [1], while CNTs can present metallic or semiconductor behavior [2].

Many studies have demonstrated that the electronic and structural properties of BNNTs can be significantly influenced by dopant atom [3]. Although doped BNNTs have been realized experimentally [4], it is very hard task to verify the ordering and distribution of dopant atoms over the atomic sites of a BNNT. It is fundamentally of importance to technology how the electronic structure of BNNTs can be modified through suitable doping. Here we determine the influence of C-doping on different sites of a representative model of zigzag (8,0) BNNT.

Computational aspects

All molecular orbital calculations were performed using Gaussian 03 program [5]. The geometry of the investigated pristine and C-doped BNNTs was optimized at the B3LYP level employing 6-31G* basis set. Quantum theory of atoms in molecules (QTAIM) analysis for the optimized structures was performed at B3LYP/6-31G* level of theory using AIM2000 package [6].

Results and discussion

The optimized pristine and C-doped (8,0) BNNTs are shown in Figure 1. The pristine model (Figure 1a) stands for the original structure of the BNNT consisting of B and N atoms. There are two nonequivalent B-N bonds in the pristine (8,0) BNNT: axial B-N bonds parallel to the longitudinal direction of the tube (e.g., the bond between the B1 and N2 layers in Figure 1a) and zigzag B-N bonds (e.g., the bond between the B1 and N1 layers in Figure 1a). In general, the B-N bond lengths are not significantly changed upon C-doping in the considered models. However, different B-C and C-N bond distances are evident where the latter is slightly shorter than the former one. Although our estimates of C-B and B-N contacts in doped (8,0) BNNTs agree well with (within 0.5%) earlier work [7], our evaluated bond lengths of C-N bonds deviate by up to 4-5%. Figure 2 indicates the molecular graph of pristine (8,0) BNNT in its equilibrium geometry. One of the most striking features of these results is the fact that all calculated ρ_{BCP} values in B-N of pristine (8,0) BNNT are predicted to be in a range of 0.190–0.194 au, whereas the values of $\nabla^2\rho_{\text{BCP}}$ are all positive, ranging from 0.288 to 0.337 au. These values are within the common accepted values for closed-shell interactions [6].

Concluding remarks

B3LYP/6-31G* calculations indicated that the values of B-N bond lengths are not changed due to the C-doping. Based on QTAIM results, it can be concluded that all B-N interactions in the pristine (8,0) BNNT have a negative H_{BCP} value, thus indicate partially covalent character. However, a covalent interaction is evident for the B-C and N-C doped bonds.

Figure 1. The molecular models of investigated (8,0) BNNT

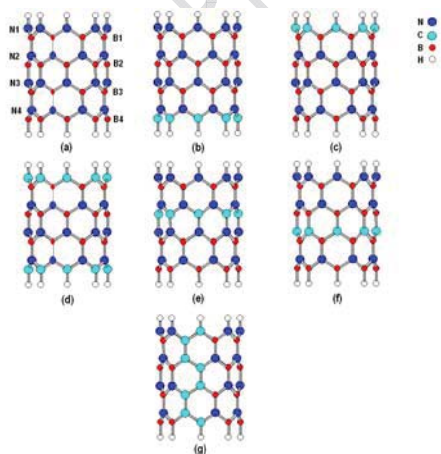
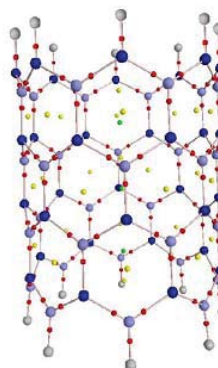


Figure 2. Molecular graph of pristine BNNT





References:

- [1] A. Rubio, J. L. Corkill, M.L. Cohen, Phys. Rev. B 49 (1994) 5081.
- [2] N. Hamada, S. Sawada, A. Oshiyama, Phys. Rev. Lett. 68 (1992) 1579.
- [3] C. Tang, Y. Bando, Y. Huang, and D. Golberg, J. Am. Chem. Soc. 127 (2005) 6552.
- [4] J. Liu, R. Czrew, D.L. Carroll, J. Mater. Res. 20 (2005) 538-543.
- [5] M. J. Frisch, *Gaussian 03*, revision E.; Gaussian, Inc.: Wallingford, CT, 2004.
- [6] F. Biegler-Konig, J. Schonbohm, and D. Bayles, J. Comput. Chem. 22 (2001) 545.
- [7] J.X. Zhao, Y. Tian, B.O. Dai, J. Chin. Chem. Soc. 52 (2005) 395.



Molecular dynamics simulation and free energy perturbation to calculate free energy of solvation for carbon nanotube

Khalil Ghafarian(MS)* , Ali Khanlarkhani(PhD) , Mansour Kianpour-Rad(PhD)

Materials and Energy Research Center, P.O. Box 31787-316

Karaj , Iran

*Khalil_earth@yahoo.com

Keyword : free energy , solvation , carbon nanotube , molecular dynamics

Introduction :

Solvation of carbon nanotubes and functionalized carbon nanotube is crucial parameter in most of their applications. to quantify this parameter we used Gibbs energy of solvation which provides a measure of the solubility of a substance in a solvent. The more negative the energy of solvation, the higher the degree of solubility. Negative values of the solvation energy from thermodynamic consideration denote that the process is spontaneous .

When the results of molecular dynamics simulation conjugated with appropriate statistical mechanics method like thermodynamics integration (TI) or free energy perturbation (FEP), one can predict difference free energy between two states.

in FEP, the difference in free energy between two states, a and b is expressed by:

$$\Delta A_{a \rightarrow b} = -k_B T \ln \left\langle \exp \left[-\frac{\mathcal{H}_b(\mathbf{r}, \mathbf{p}) - \mathcal{H}_a(\mathbf{r}, \mathbf{p})}{k_B T} \right] \right\rangle_a$$

wherein k_B is the Boltzmann constant and T is the kinetic temperature .

note that this formula is valid only when the difference between two states is small enough.

Materials and Methods :

All simulations performed on (5,5) single wall carbon nanotube with 20 Å length .

To build initial configuration we used Packmol package that provide a nanotube surrounded with water molecules. we also put some water molecules to inner space of carbon nanotube. MD simulations at 25 C and 1 atm were carried out using the NAMD 2.8 software package. To analyze the results of simulations, we used two pathways. In the first one (multiple stages) we solvate carbon nanotube layer by layer in water because of the essence of FEP method. It means series of simulations performed and total free energy comes from adding these steps. In the second pathway (single stage) we solvated carbon nanotube completely in one stage. Finally we compare our results with TI method with almost similar carbon nanotube that we found in literature.[1]

Results and discussion :

With multiple stage method we got these results that suggest 415 kcal/mol for free energy of solvation of carbon nanotube.

layer	Number of carbon atoms	ΔH_{solv} (kcal/mol)
1	180	60
2	160	60
3	140	60
4	120	60
5	100	60
6	80	60
7	60	60
8	40	71
9	20	6

Total

415

The result of one stage method is 23 kcal/mol but since multiple stage method produce more accurate results than one stage method so we think 23 Kcal/mol is underestimated.

on the other hand one group[1] report this number for almost similar nanotube (6.1 Å diameter and 28.6 Å length) about 216 Kcal/mol, the deviation of these results may related to effect of length.

References :



- [1] Patrick S. Redmilla, Shannon L. Capps, Peter T. Cummings, Clare McCabe, A molecular dynamics study of the Gibbs free energy of solvation of fullerene particles in octanol and water, Vanderbilt University, Nashville, USA, 2009
- [2] J. Robles, M.J. López, and J.A. Alonso, Modeling of the functionalization of single-wall carbon nanotubes towards its solubilization in an aqueous medium, Universidad de Valladolid, 47011 Valladolid, Spain, 2010

15th Physical Chemistry Conference



CHARMM General Force Field Parameterization for Curcumin

Z. Alimohammadi Keyvani^{*a}, M. Zahedi^b, M.H. Karimi-Jafari^c

^c Department of Bioinformatics, Institute of Biochemistry and Biophysics, University of Tehran, Tehran, Iran.

^{a,b} Department of Chemistry, Shahid Beheshti University, Tehran, Iran

Email: zalimohammadi_k@yahoo.com

Key words: Curcumin, CGenFF, CHARMM, Force Field

Introduction:

Curcumin is the principle ingredient of the Indian turmeric which has various medical and pharmaceutical properties such as Antitumor, Antioxidant, Anti-inflammatory and Anti-microbial [1]. Classical simulations based on Empirical Force Fields (FF) are valuable tools for study of the function of biomolecules. Applying simulation methods to biological processes involving several types of biomolecules requires the use of parameters that belong to the same FF for all types of molecules. Accordingly, most FF developers have extended their FF to wide range of biomolecules and also molecules interacting with them. In this regard, CGenFF was developed to be a general FF for drug-like molecules compatible with the CHARMM all-atom additive biomolecular FF [2]. The present work attempts to create an accurate CHARMM-compatible FF for Curcumin and its derivatives in agreement with CGenFF protocol.

Methodology:

Each model compound, was optimized at MP2/6-31G(d) level. To exactly determine the global structure, complete conformational analysis was done at PM6 and MP2/6-31G (d) levels. Parameters were validated and optimized with respect to QM target data. The whole procedure of FF development was conducted by PARAMATICA package that provides interfaces with MOPAC, GAMESS, Firefly and NAMD programs for necessary semiempirical, *ab initio* and molecular mechanical calculations.

Results:

Two model compounds, Dehydrozingerone (**b**) and 1,6-heptadiene-3,5- dione (**c**) were considered for Curcumin fragments (Figure 1).

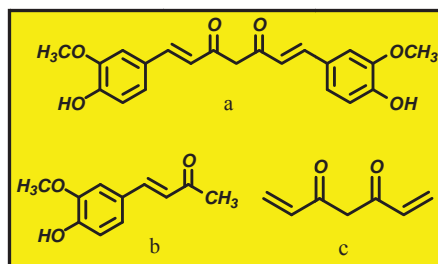


Figure 1. (a) Curcumin, (b) Dehydrozingerone, (c) 1,6-heptadiene-3,5- dione.

Due to the good agreement between MP2/6-31G (d) force constants with available parameters in CGenFF, they were used as initial estimates of missing parameters (Figure 2, Table 1).

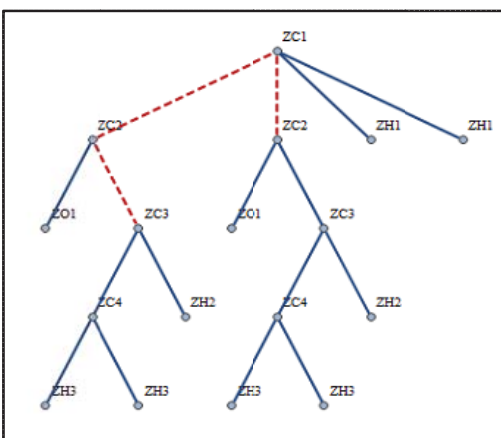


Figure 2. Molecular graph of (c) with atom type labels. Red dashed lines represent missing angle parameters.

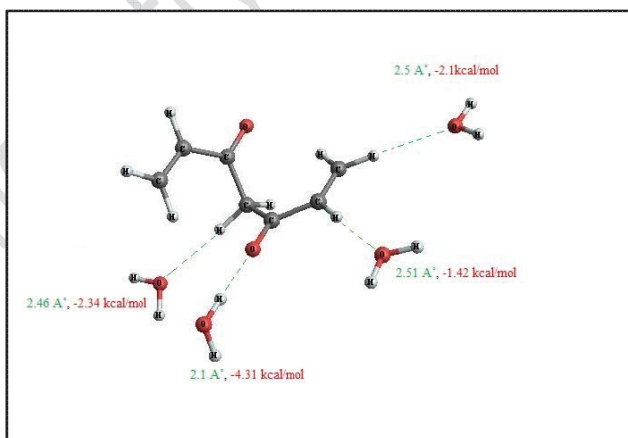


Figure 3. Interaction sites of (c) with water molecules.

Table 1. Force constants [$\text{kcal mol}^{-1} \text{\AA}^{-2}$, $\text{kcal mol}^{-1} \text{rad}^{-2}$].

Bond	CGenFF	MP2/6-31G(d)	Angle	CGenFF	MP2/6-31G(d)
ZC3-ZC2	300	327.21	ZH1-ZC1-ZC2	50	61.9
ZH3-ZC4	365	378.02	ZH3-ZC4-ZC3	45	68
ZH2-ZC3	360.5	364.21	ZC3-ZC2-ZC1	—	158.93



ZC2-ZC1-ZC2

71.2

QM target data were produced and iterative procedure was performed until convergence obtained. Figure 3 shows complexes of hydrogen bond donors and acceptors of 1,6-heptadiene-3,5-dione with single water which were used to produce charge optimization target data. Optimized interaction distances and scaled interaction energies at the HF/6-31G(d) level are listed as target data.

Conclusion:

CHARMM-compatible parameters were developed for Curcumin. Our parameters provide a new set of FF parameters that can be used in classical simulations.

References:

- [1] Subash C. Gupta, *et al*, *Nat. Prod. Rep.*, **28** (2011) 1937.
- [2] K. Vanommeslaeghe, *et al*, *J. Comput. Chem.*, **31** (2010) 671.



Theoretical investigation on Tautomerism and NBO Analysis of 3-hydroxyl-1,2,5-thiadiazole Derivatives: Solvent and Substitute Effects

Mohsen Hajibeygi^{1*}, Meisam Shabanian², Hassan Moghanian³, Azin Mohamadi²

¹Department of Chemistry, Varamin-Pishva Branch, Islamic Azad University, Varamin, Iran

²Young Researchers Club, Arak Branch, Islamic Azad University, Arak, Iran

³Department of Chemistry, Dezful Branch, Islamic Azad University, Dezful, Iran

E-mail: mhajibeygi@iauvaramin.ac.ir

KeyWords: 1,2,5-Thiadiazole, Tautomerism, DFT study, Solvent effect, NBO analysis

Introduction:

Tautomerism has been extensively studied experimentally and theoretically because it is one of the fundamental processes in (bio) organic chemistry that corresponds to most of the important condensation reactions [1-2]. Also, understanding the relative stabilities of heterocyclic tautomers and any subsequent conversions between tautomeric forms is very vital for both structural chemists and biologists. For example, tautomerism in keto-enol [3], imine-enamine [4] pyrimidines [5] and many other systems have been studied for past two decades. Therefore, compounds containing different tautomers can be the subject of interest by theoretical chemists.

Methods:

All calculations were carried out on a Pentium personal computer by means of GAUSSIAN03 program package.

Results and discussion:

Density functional calculations at the B₃LYP/6-311++G(d,p) level were employed to determine the stability, tautomerism and substitute effect for 1,2,5-Thiadiazole, a widely used skin-whitening, antibrowning, and antibacterial agent and its derivatives (4-NO₂, 4-CN, 4-F,



4-H, 4-CH₃, 4-OH, 4-NH₂), in the gas phase and solution using PCM model. Some selected IR frequencies, molecular parameters, NBO analysis and dipole moment results in the gas phase and in four different solvents (benzene, Tetrahydrofuran (THF), Dimethyl sulfoxide (DMSO) and H₂O) were extracted. In the gas phase when the substituents change from withdrawing groups to electron donating groups, NH form becomes more stable than OH form, but an exception can be seen in F substituent because fluorine can be a resonance donating group. The major difference between OH and NH form in gas phase was found for 4-cyano-3-hydroxy-1,2,5-thiadiazole with 4.70 kcal mol⁻¹.

Conclusions:

B3LYP/6-311++G(d,p) level has been applied to study the tautomerism in 3-hydroxy-1,2,5-thiadiazole with different substituents in position 4 in the gas phase and also in four different solvents. The following points emerge from the present study: In the gas phase the relative energies of the tautomers relate to the nature of substituents. In 4-amino-3-hydroxy-1,2,5-thiadiazole derivative with strong electron releasing groups, the NH tautomer was more stable than OH tautomer. In the solution if the polarity of solvents increased, NH isomers were observed to be more stable. The dipole moments of all compounds have relationship with the nature of substituents and solvents. With increase of the polarity of solvents the dipole moments of OH and NH tautomers were increased.

References:

- [1] Tavakol, H.; Esfandyari, M.; Taheri, S.; Heydari, *Spectrochim. Acta A Mol. Biomol. Spectrosc.* **2011**, 79, 574-582.
- [2] Koch, A.; Kleinpeter, E. *J. Mol. Model.* **1997**, 3, 375 – 381.
- [3] Hocquet, A.; Toro-Labbé, A.; Chermette, H. *J. Mol. Struct.* **2004**, 686, 213-218.
- [4] Dines T. J.; Onoh, H. *Spectrochim. Acta A Mol. Biomol. Spectrosc.* **2006**, 64, 891-900.
- [5] Hasanein, A.; Senior, S. A. *Int. J. Quantum Chem.* **2011**, 111, 3993–4010.



A DFT Study of Solvation Effects and NBO Analysis on the Tautomerism of 3-substituted 1H-pyrazol-5(4H)-one

Mohsen Hajibeygi^{1*}, Majid Khodaei-Tehrani², Meisam Shabani³,

¹Department of Chemistry, Varamin-Pishva Branch, Islamic Azad University, Varamin, Iran

²Department of Chemistry, Arak Branch, Islamic Azad University, Arak, Iran

³Young Researchers Club, Arak Branch, Islamic Azad University, Arak, Iran

E-mail: mhajibeygi@iauvaramin.ac.ir

KeyWords: 3-Substituted 1H-pyrazol-5(4H)-one, DFT study, Tautomerism, Dipole moment.

Introduction:

Heteroaromatic compounds have attracted considerable attention in the design of biologically active molecules and advanced organic materials [1]. Hence, a practical method for the preparation of such compounds is of great interest in synthetic organic chemistry. Pyrazole and its derivatives, a class of well known nitrogen containing heterocyclic compounds, occupy an important position in medicinal and pesticide chemistry with having a wide range of bioactivities such as antimicrobial [2], anticancer [3], anti-inflammatory [4], antidepressant, anticonvulsant [5] etc. In this article we studied tautomerism of five 3-substituted 1H-pyrazol-5(4H)-one ring in the gas phase and 3 solution using polarisable continuum method (PCM) at the B3LYP/6-31++G(d,p) level of theory.

Methods:

All calculations were carried out on a Pentium personal computer by means of GAUSSIAN03 program package.

Results and discussion:

The effect of solvent polarity on the tautomeric equilibria of 3-substituted 1H-pyrazol-5(4H)-one ring is studied by density functional theory calculation (B3LYP/6-31++G(d,p)) level for



predominant tautomeric forms of 1H-pyrazol-5(4H)-one derivatives (3-H, 3-CH₃, 3-NH₂, 3-Br, 3-CF₃) in the gas phase and selected solvents (benzene (non-polar solvent), DMSO (aprotic polar solvent) and water (protic solvent)). More stable is related to 3-Br substitute in gas phase and selected solvents. In addition variation of dipole moments and charges on atoms in the solvents are studied. In all tautomers, 3-bromo-1H-pyrazol-5(4H)-one moiety is more stable than the other substitute in gas phase and solution. Due to present of electron withdraw groups in 3-Br and 3-CF₃ substituted tautomers, these substitutes are more stable than the other compounds.

Conclusions:

In all tautomers, 3-bromo-1H-pyrazol-5(4H)-one moiety is more stable than the other substitute in gas phase and solution. The order of stability of 3-substituted 1H-pyrazol-5(4H)-one derivatives in gas phase is Br > CF₃ > NH₂ > CH₃ > H. The dipole moments of all compounds are affected by solvent. With increase of the polarity of solvents the dipole moments of the tautomers were increased. In all tautomers, were showed a special increase in dipole moment with increase polarity of solvent. The charges on all five positions were affected by substituents and solvents.

References:

- [1] Haino, T., Tanaka, M., Ikeda, K., Kubo, K., Mori, A., Fukazawa, Y. 2004. *Tet. Lett.*, 45, 2277.
- [2] Boyne, M., Stratton, C., Johnson, F., Tonge, P. 2006. *ACS Chem. Biol.*, 1, 43.
- [3] Magedov, I. V., Manpadi, M., Van slambrouck, S., Steelant, W. F. A., Rozhkova, E., Przheval'skii, N. M., Rogelj, S., Kornienko, J. 2007. *Med. Chem.*, 50, 5183.
- [4] Rovnyak, G. C., Millonig, R. C., Schwartz, J., Shu, V., 1982. *J. Med. Chem.*, 25, 1482.
- [5] Rajendra, P. Y., Lakshmana, R. A., Prasoon, L., Murali, K., Ravi, K. P. 2005. *Bioorg. Med. Chem. Lett.*, 15, 5030.



A computational ^{27}Al and ^{15}N NMR Characterization of Al_nN_n clusters with $n = 12, 16, 28, 36$ and 48

M. Saeedi, M. Anafcheh, R. Ghafouri, N. L. Hadipour*

Department of Chemistry, Tarbiat Modares University, Tehran, Iran

m_saeedi67@yahoo.com

Keywords: AlN nanocage, NMR, DFT.

Numerous efforts have been devoted recently to the study of possible fullerene-like structures constructed of other elements rather than carbon. Especially, clusters of Groups III–V have emerged as a choice for the next generation materials for applications in the microelectronic and light-emitting diodes [1]. Theoretical studies predicted [2] that the fullerene-like cages Al_nN_n may be magic clusters having inherent special stability. Wang et al. [3] suggested these clusters as ideal materials for hydrogen storage applications under ambient thermodynamic conditions.

NMR parameters such as chemical shielding (CS) tensors, either measured experimentally or reproduced reliably by performing high-level quantum chemical calculations provide highly valuable information about electrostatic environment around the nucleus, which feels subtle changes by any perturbations. This work aims at analyzing geometrical and electronic characteristic of Al_nN_n nanocages ($n = 12, 16, 28, 36$ and 48) on the basis of calculated ^{15}N and ^{27}Al NMR parameters, which might be a useful guidance for the experimental studies, see Fig.1.

Computational Method :

Geometries of all systems were fully optimized at the level of B3LYP/6-31+G* via Gaussian 98 package of program. The gauge including atomic orbital (GIAO) approach was applied to calculate chemical shielding. The calculated CSI tensors in the principal axes system (PAS) ($\sigma_{33} > \sigma_{22} > \sigma_{11}$) were used for converting data to measurable NMR parameters: chemical

shielding isotropic (CSI), using $\text{CSI (ppm)} = 1/3(\sigma_{11} + \sigma_{22} + \sigma_{33})$ and $\text{CSA (ppm)} = \sigma_{33} - (\sigma_{11} + \sigma_{22}) / 2$.

1. ²⁷Al NMR parameters:

For illustration, the calculated ²⁷Al chemical shielding isotropy (CSI, CSA) parameters have been depicted versus the number of Al atoms for considered models in Fig. 2. As seen the ²⁷Al CSI values of the Al_nN_n cages divide the electrostatic environment of the aluminium nuclei into few layers and in each layer the CSI values are the same. Meanwhile, there are three local structures, AL₁, AL₂, and AL₃, around the aluminium nuclei in AL₂₈N₂₈, AL₃₆N₃₆, AL₄₈N₄₈, illustrated in Fig. 2. Based on the obtained results, the calculated isotropic chemical shieldings of aluminium sites with the three local structures are found to be in the order of CSI (AL₃) > CSI (AL₂) > CSI (AL₁). Parallel to the CSI parameters, similar CSA parameters are anticipated in each layer due to equivalent electrostatic properties of the corresponding nuclei. Unlike ²⁷Al CSI values, layers of ²⁷Al CSA do not show any regular pattern in the orientation of electronic densities with raising the number of ALN units in the heterofullerenes.

2. ¹⁵N NMR parameters

According to the ¹⁵N NMR parameters, CSI and CSA parameters of the nitrogen nuclei in the ALN-substituted fullerenes are also divided into layers. However, slight differences in the values of CSI layers clarify diminutive diversity in the electron densities of the various layers for the nitrogen nuclei. In addition, there is an increasing tendency in the CSA values of the three local structures, CSA(N₁) > CSA (N₂) > CSA (N₃). Scuseria et al. [4] observed similar trends for the nitrogen chemical shifts of BN cages using DFT.

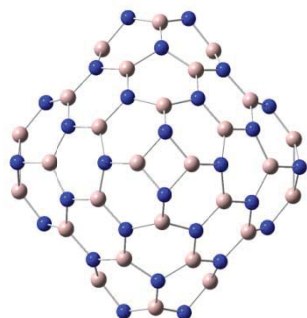


Fig. 1. Optimized structure of Al₄₈N₄₈

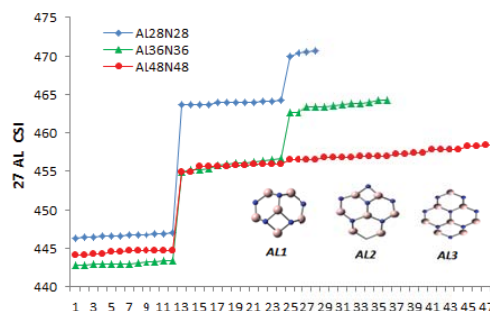


Fig. 2. ²⁷Al NMR CSI

Conclusion:

It was interestingly found that the isotropic chemical shielding parameters (CSI, CSA) of the Al_nN_n nanocages divide the electrostatic environments around N/Al nuclei into few layers each of which is related to the nuclei with similar isotropic chemical shielding. The difference in isotropic chemical shielding of local structure in the AlN cages could be due to changes in the electrostatic environment around the N/Al nuclei, originating from the curvature of AlN cages.

References:

- [1] A.K. Kandalam, M.A. Blanco, R. Pandey, J Phys Chem B 106 (2002) 1945-1953.
- [2] A. Costales, A.K. Kandalam, R. Franco, R. Pandey, J Phys Chem B 106 (2002) 1940-1944.
- [3] Q. Wang, Q. Sun, P. Jena, Y. Kawazoe, ACS Nano 3 (2009) 621-626.
- [4] V. Barone, A. Koller, G.E. Scuseria, J. Phys. Chem. A (2006) 110, 10844-10847.



A theoretical study on the reaction mechanism of NH₃ with OH radical.

S. Asgharzade ^{*a}, M. Vahedpour ^a, M. Asgarzade ^b

^a Department of Chemistry, Zanjan University, Zanjan, Iran.

^b Pasteur Institute of Iran, Tehran, Iran.

Email: Somaie.asgarzade@yahoo.com

Keywords: Hydroxyl, Ammonia, Reaction mechanisms, Quantum chemical method.

Introduction:

Ammonia is the third most abundant nitrogen species in the terrestrial atmosphere and it plays a critical role in both homogeneous and heterogeneous atmospheric reaction. Being the dominant basic gas in the atmosphere, ammonia partially neutralizes atmospheric acids in precipitation. However, possibly as much as 50% of atmospheric ammonia is oxidized in the gas phase. The most important oxidizing species in the air is the hydroxyl radical. It is extremely reactive and able to oxidize most of the chemical compounds that found in the troposphere. The hydroxyl radical is known as the detergent of the atmosphere [1].

The purpose of this work by means of computational methods based on quantum theories to carry out a detail of potential energy surfaces (PES) for the reaction of NH₃ and OH with the aim of clarifying the reaction mechanism.

Theoretical methods:

The geometries of the reactants, complexes, products and transition states involved in the reaction are optimized using density functional theory at the spin unrestricted B3LYP with the 6-311++G(3df,3pd) bases set. To obtain more reliable relative energy, a higher level of electronic correlation method, CCSD (T)/6-311++G (3df, 3pd)//B3LYP/6-311++G (3df, 3pd), are employed in the single point energy calculation to improve the accuracy of energetic information on minimum energy path. Additionally, intrinsic reaction coordinate (IRC) was performed to examine connections between the all species involved the reaction. CCSD

method is used to calculate the T1 diagnostic values for the structures. All the calculations were performed with the GAUSSSIAN 03 program [2].

Result and discussion:

The interaction between nitrogen atoms of ammonia (NH_3) and oxygen atom of OH radical produces two pre-reactive van der Waals stable complexes with no barrier with the energy lower than the original reactant. With decomposition of these complexes, four possible product channels have been found. The first channel is production of NH_2 and H_2O products and the other channels are production of P2 ($\text{H}_2\text{NO}+\text{H}_2$), P3 ($\text{HNOH}+\text{H}_2$) and P4 ($\text{H}_2\text{ON}+\text{H}_2$) via corresponding transition states and the intermediates, respectively. The total energies and relative energies of all species at the B3LYP/6-311++G (3df, 3pd), under atmospheric pressure and 298.15 K, are shown in figure 1. All energies are corrected by basis set superposition error. The results show that production of $\text{NH}_2+\text{H}_2\text{O}$ is the main reaction channel with $\Delta G = -79.224$ kcal/mol. So, this product channel is spontaneous in gas phase at atmospheric pressure and 298.15K. Because of low energy of P1 production channel transition state (TS1 with the energy barrier of 0.350 kcal/mol), it is the most feasible channel in comparison with the other product channels.

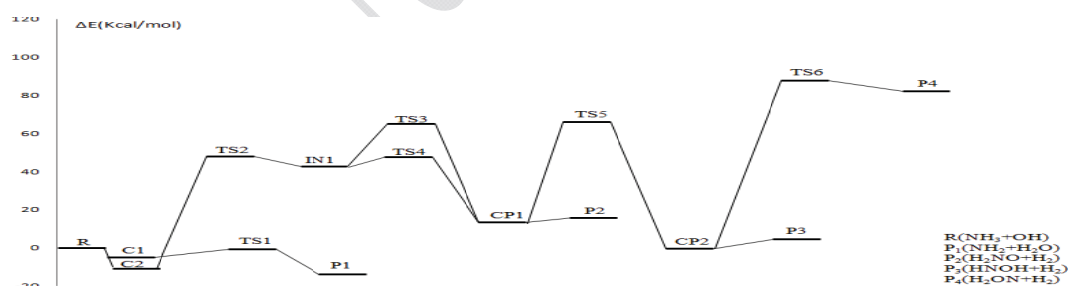


Figure.1. potential energy profiles of the $\text{NH}_3 + \text{OH}$ reaction at B3LYP level.

Conclusion:

The theoretical study carried out in this work lead to the following conclusions:

1. In the present work, the mechanism of NH_3 and OH reaction are suggested using the computational methods.



2. Four kind of product, P1, P2, P3, and P4 are obtained which P1 as the most stable with the lower transition state energy (-3.230 kcal/mol) the main product in both thermodynamic and kinetic approaches.

Reference:

- [1] S. Salimian, R.K. Hanson and C.H. Kruger, *INTERN. J. Chem. Kinetics* 16 (1984) 725.
- [2] Frisch et al; "GAUSSIAN 03, Revision B.03, Gaussian"; Inc., Pittsburgh, PA; 2003.

Complexation of cryptand(222) with Li^+ and K^+ : AIM and NBO analyses

R. Behjatmanesh-Ardakani^a, A. Soleimanipour^{a*}

^aDepartment of chemistry, Payame Noor University, PO BOX 19395-3697 Tehran, IRAN

*Email: akram.soleimanipour@yahoo.com

Key words: DFT, Binding energy, Cryptand, AIM, NBO

Introduction:

In recent years, DFT [1] studies of complexation of crown ethers with alkali-metal cations have been extended because of their unique properties such as ion selectivity. In this research, cryptand(222) complexations with Li^+ and K^+ are studied theoretically. The structures are as follows:

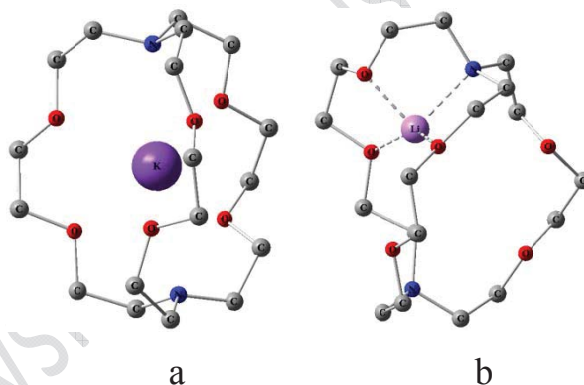


Fig 1. Configurations of complexes of studied cryptand with K^+ (a) and Li^+ (b). Hydrogen atoms have not been shown for clarity.

Methods:

B3LYP/6-311G level of theory was used for all calculations. The natural bond orbital (NBO) analysis [2] was performed to characterize the second-order interaction energy. The atoms in molecules (AIM) [3] was utilized to describe the binding characteristic between donors and acceptors.

Result and Discussion:

Zero point and BSSE corrected binding energies ($\Delta E_{bind}^{ZPE+BSSE}$) for complexes of cryptand with Li^+ and K^+ are equal to -120.0483 and -85.0685, respectively.

Some of the results of the AIM theory that have been carried out with AIM2000 package [4], are shown in Table 1.

Table 1: Some of the topological properties of the complexes.

Bonds	$\rho(r)$	$\nabla^2(\rho)$	$V(r)$	$G(r)$	$H(r)$	$\frac{ V }{2G}$
<u>L-Li⁺</u>						
Li ⁺ -O ₁₅	3.0219×10^{-2}	23.4352×10^{-2}	-3.6806×10^{-2}	4.7697×10^{-2}	1.0891×10^{-2}	3.8583×10^{-1}
Li ⁺ -O ₁₇	2.8044×10^{-2}	20.5608×10^{-2}	-3.2863×10^{-2}	4.2133×10^{-2}	0.9269×10^{-2}	3.8999×10^{-1}
<u>L-K⁺</u>						
K ⁺ -O ₁₅	1.7355×10^{-2}	8.7028×10^{-2}	-1.5047×10^{-2}	1.8402×10^{-2}	0.3355×10^{-2}	4.0884×10^{-1}
K ⁺ -O ₁₆	1.6553×10^{-2}	8.1236×10^{-2}	-1.4114×10^{-2}	1.7211×10^{-2}	0.3097×10^{-2}	4.1003×10^{-1}

For NBO, second-order interaction energies, HOMO and LUMO hybridization and charge transfer (Qt) between donor (Cryptand) and acceptor (cation) have been analyzed. Charge transfer for Li^+ and K^+ are equal to 0.4013 and 0.2629, respectively. The NBO analysis was carried out by NBO 3.1 included in Gaussian 09 program [5].

Conclusion:

Comparing of complexes binding energies shows that with increasing alkali-metal cations size, the interaction of cryptand(222) with alkali-ion decreases. Results of AIM show that there are critical points between donor-acceptor atoms with high electron density. This shows strong interactions between ligand and cations. In addition, NBO results confirm the AIM data.

References:

- [1] I.N. Levine; "Physical Chemistry" ; McGraw-Hill, New York, 6th edition, 2009.
- [2] E.M. Sproviero; G.Burton; "Stereolectronic Interactions and Molecular Properties. An NBO-Based Study of Uracil" ; J. Phys. Chem; 107, 5544-5554, 2003.



- [3] K.S. Diao et al.; "A DFT study on the metal binding selectivity of 12-crown-4 and its heterocyclic analogs" ; J. Mol. Struct. (Theochem); 901, 157-162, 2009.
- [4] F. Beigler-Konig et al.; "AIM2000- A program to analyse and visualize atoms in molecules"; J. Comp. Chem. 22, 545, 2001.
- [5] M.J. Frisch et al.; Gaussian 09, Revision A.02.

15th Physical Chemistry Conference



AIM, NBO and HOMO-LUMO Analysis of 1,1'-(Ethane-1,2-diyl)dipyridinium bis(iodate) (EDB) by Density Functional Method

M. Izadyar, M. Gholizadeh, M. Khavani,

Department of Chemistry, Faculty of sciences, Ferdowsi University of Mashhad, Mashhad, Iran

khavanim@yahoo.com

Keywords: Natural Bond Orbital (NBO); HOMO-LUMO energy; DFT; EDB; Hydrogen; AIM

Introduction:

There are two crystallographically independent iodate anions for the salt of 1,1'-(Ethane-1,2-diyl)dipyridinium bis(iodate) as shown in figures 1 and 2, in which I atoms are in a trigonal-pyramidal environment [1]. Two pyridine rings adopt an anti-conformation with respect to each other; the angle between these two rings is 3.84 degrees and, C—H...O hydrogen bonds between the cations and anions lead to the formation of layers arranged parallel to the ab plane. As a part of a research program which devoted to the study of structural and physicochemical properties of oxidative reagents by the theoretical procedures with the aim of the analysis of their properties from the molecular point of view, we decided to perform a comprehensive examination of NBO, HOMO-LUMO and AIM analysis of the new oxidant of EDB.

Computational Methods:

All calculations were performed with the Gaussian 09 software as it has been reported that the B3LYP method of the DFT calculation can reproduce good geometrical structures [2]. The structures for the studied molecules were fully optimized and characterized as true minima by the absence of imaginary frequencies. In order to obtain the exact energy of a particular structure, B3LYP method was used with large basis set of LANL2DZ Vibrational frequencies

were determined to provide an estimation of the zero point vibrational energies (ZPVE). The natural bond orbital (NBO) analysis was applied to determine the atomic charges. The atom in molecule (AIM) theory is a method provides a vigorous and unambiguous criterion to determine which atoms are bonded and which atoms are separated in the system. As a part of this study is the hydrogen bond investigations between O \cdots H atoms, AIM analysis at the B3LYP/LANL2DZ is of importance.

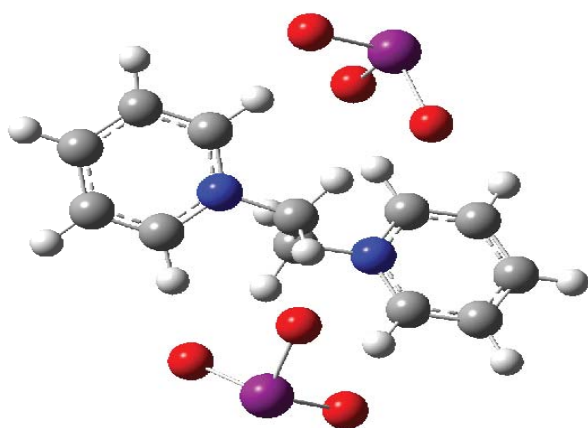


Figure 1. Optimized structure of 1,1'-(Ethane-1,2-diyl)dipyridinium bis(iodate)

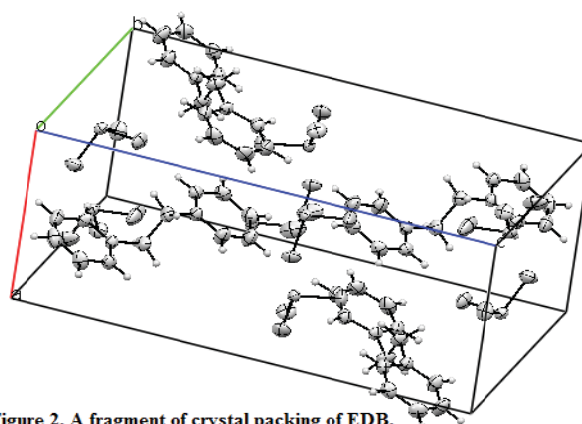


Figure 2. A fragment of crystal packing of EDB.

Results and Discussion:

The energy of several highest occupied and the lowest unoccupied molecular orbitals of EDB was obtained. Among the highest occupied MOs the largest numbers constitute σ orbitals of pyridine ring with a contribution from the O and I atoms. The lowest unoccupied MOs can be represented as a combination of σ^* ring, σ^*C-C , $\sigma^*C=N$, σ^*O-I , with the predominant involvement of the former corporate. Natural population analysis was carried out for EDB. Negative characters for N and O atoms in the N-C(H) \cdots O-I conjunction and positive character for H atom confirms the hydrogen bonding between two (three) molecules. Computed values of the NBO charges for N, O and H is reported -0.91, -1.2, and +0.51, respectively, positive character for H atom induces that to be attracted by O atom. This is due to a nearly large value of negative charges density around the oxygen atom. Atoms in molecules properties for electronic charge density of atoms and its Laplacian ($L(r)$) were



calculated for the main bonds which possess some degrees of hydrogen bond formation in this structure. From AIM data it can be confirmed that the hydrogen bonds have been formed between $\text{N-C(H)} \cdots \text{O-I}$. Bond distances for the hydrogen bonds in all compounds are about 2\AA , which is accordance to other reported data [1]. Charge density of ρ and L values for $\text{N-C}_{\text{ring}}(\text{H}) \cdots \text{O-I}$ are greater than $\text{NC}_{\text{ethyl}}(\text{H}) \cdots \text{O-I}$ at the bond critical points in EDB. Accordingly on can conclude that this type of hydrogen bond ($\text{N-C}_{\text{ring}}(\text{H}) \cdots \text{OI}$) is stronger than the other ($\text{N-C}_{\text{ring}}(\text{H}) \cdots \text{OI}$).

References:

- [1] M. Gholizadeh, M. Pourayoubi, M. Kia, B. Notash, *Acta Cryst., E*, 67 (2011) 06714.
- [2] Gaussian, Inc., Wallingford CT, Gaussian 09, Revision A (2009).

A Charge Density Analysis of Protein-Ligand Binding in the active site of FPPS enzyme

M. H. Karimi-Jafari^a, R. Firouzi^{b,*}

^a Department of bioinformatics, Institute of Biochemistry and Biophysics, University of Tehran, Tehran, Iran

^b Chemistry & Chemical Engineering Research Center of Iran (CCERCI) P. O. Box 14335-186, Tehran, Iran

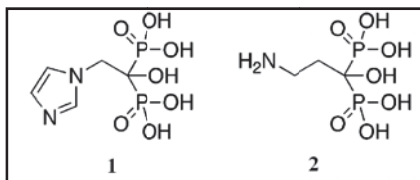
Email: firouzi.chemist@yahoo.com and RFirouzi@ccerci.ac.ir

Key words: bisphosphonates, FPPS enzyme, Protein-Ligand interaction, QTAIM

Introduction:

Nitrogen-containing Bisphosphonates (N-BP), such as zoledronate (**1**), and pamidronate (**2**), are an important class of drug molecules that are currently used to treat a variety of bone resorption diseases, such as osteoporosis, Paget's disease, and hypercalcemia due to malignancy [1].

N-BPs act by inhibiting the enzyme farnesyl pyrophosphate synthase (FPPS) within osteoclasts, the cells responsible for bone resorption. It has been shown former has about 100-fold higher bone resorption activity than latter. Here, we conducted QTAIM [2] calculations for these famous drug and their surrounding residues using the DFT methods to compare their potency as FPPS inhibitors on the basis of their interactions with FPPS.



Computational details:

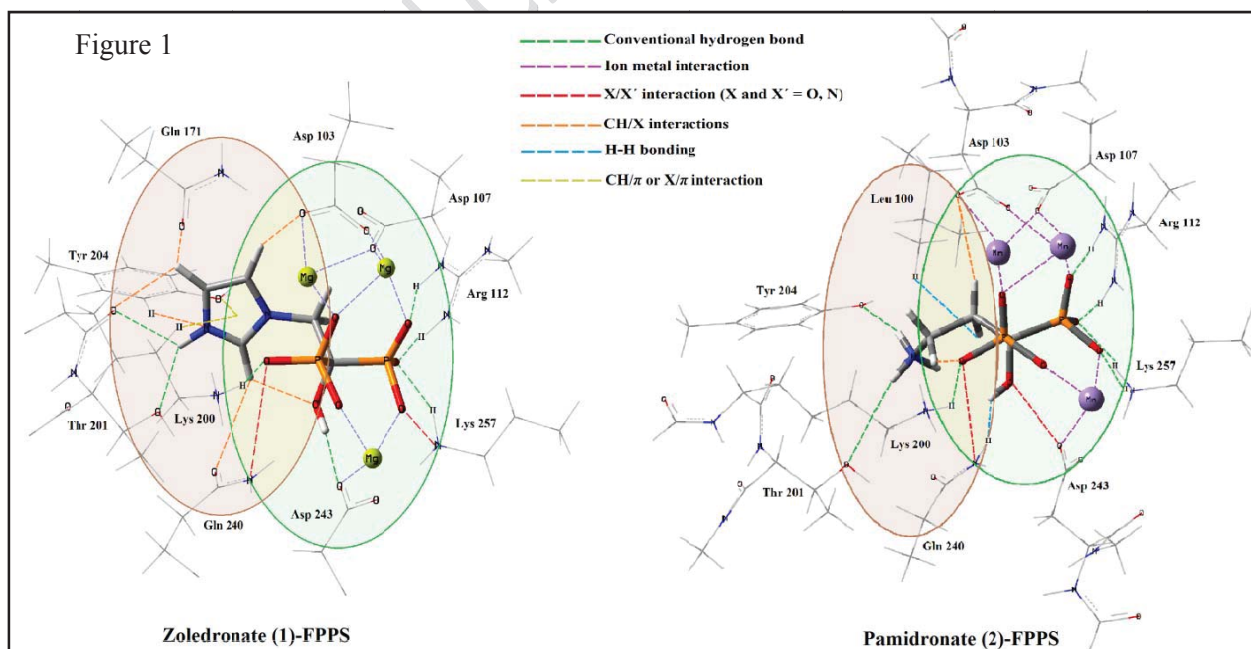
Crystal structures of all complexes were obtained from Protein Data Bank and a computationally tractable model was extracted from the complex structures by cutting all residues within 4.5 Å of the ligand. Dangling bonds in the N and C terminals of selected

residues were capped by CH₃-CO- and -NH-CH₃ fragments, respectively. Addition and energy minimization of hydrogen atoms was conducted using PM6. The wavefunction of optimized complexes were obtained using 6-31+G* basis set at B3LYP and M06-2X. Different computational tasks in this study were performed by VMD-1.9, MATHEMATICA8, REDUCE-3.14, MOPAC-2009, Gamess, and AIM2000 programs.

Result and discussion:

Figure 1 presents the interactions between N-BPs and their surrounding residues with colored dashed line, on the basis of QTAIM calculations. Some interactions belong to side chain of N-BPs and residues (located in a light brown oval) and others are interactions of the phosphonate groups (shown in a light green oval).

In the same pattern, the phosphonate groups of both of the N-BPs coordinate via metal ions with the aspartate-rich region of the active site, whereas side chain of zoledronate make more non-covalent bonds. In addition, since higher values of $\rho(r_c)$ indicate stronger bonds for the same pair of atoms, most interactions of zoledronate are stronger than similar interactions of pamidronate.





Conclusion:

Results of QTAIM calculations for two N-BPs and their surrounding residues showed that: (1) the presence of phosphonate groups is responsible for interaction with the molecular target, (2) the high potency of zoledronate might be a result of the presence the heterocyclic side chain, since number and strength of interactions of zoledronate and FPPS are more than those of pamidronate and FPPS.

The QTAIM approach is a promising tool for providing deeper insight into interaction between drugs and receptors. In particular, some weak interactions like CH/ π and CH/O are difficult to treat in the MM method and structural indicators [3].

References:

- [1] Frank H. Ebetino et al.; "The relationship between the chemistry and biological activity of the bisphosphonates"; Bone 49, 20–33, 2011
- [2] R.F.W. Bader, Atoms in Molecules: A Quantum Theory; Clarendon Press: Oxford, 1990.
- [3] K. Ohno et al.; "Computational Insights into Binding of Bisphosphates to Farnesyl Pyrophosphate Synthase"; Current Medicinal Chemistry, 18, 220-233, 2011.